Novel Lossen rearrangement and derived non-isocyanate polyurethanes (NIPUs)

Zur Erlangung des akademischen Grades eines

DOKTORS DER NATURWISSENSCHAFTEN

(Dr. rer. nat.)

von der KIT-Fakultät für Chemie und Biowissenschaften

des Karlsruher Instituts für Technologie (KIT)

genehmigte

DISSERTATION

von

M.Sc. Luca Filippi

Dekan: Prof. Dr. Manfred Wilhelm

1. Referent: Prof Dr. Michael A.R. Meier

2. Referent: Prof. Dr. Patrick Théato

Tag der mündlichen Prüfung: 20.10.2021

"Chemists do not usually stutter. It would be very awkward if they did, seeing that they have at times to get out such words as methylethylamylophenylium."

Sir Williams Crookes (1839 – 1919)

Declaration of Authorship

Die vorliegende Arbeit wurde von März 2018 bis September 2021 unter Anleitung von Prof. Dr. Michael A. R. Meier am Karlsruher Instituts für Technologie (KIT) angefertigt.

Hiermit versichere ich, dass ich die Arbeit selbstständig angefertigt, nur die angegebenen Quellen und Hilfsmittel benutzt und mich keiner unzulässigen Hilfe Dritter bedient habe. Insbesondere habe ich wörtlich oder sinngemäß aus anderen Werken übernommene Inhalte als solche kenntlich gemacht. Die Satzung des Karlsruher Instituts für Technologie (KIT) zur Sicherung wissenschaftlicher Praxis habe ich beachtet. Des Weiteren erkläre ich, dass ich mich derzeit in keinem laufenden Promotionsverfahren befinde, und auch keine vorausgegangenen Promotionsversuche unternommen habe. Die elektronische Version der Arbeit stimmt mit der schriftlichen Version überein und die Primärdaten sind gemäß Abs. A (6) der Regeln zur Sicherung guter wissenschaftlicher Praxis des KIT beim Institut abgegeben und archiviert.

_____   _____

Ort, Datum   Unterschrift

Acknowledgements

I would like to thank everyone that was part of my life during these last eight years, from the start of my studies as bachelor student and until now. I had an amazing time and met so many new friendly and interesting people that it is hard to believe that my time here in Karlsruhe is almost over.

First of all, I would like to thank you, Mike, for accepting me in your group since my master thesis and for giving me the opportunity to do my PhD here. I will never forget your friendly aura and your incredible support during the times of great chemical uncertainty. Already knowing that your door is always open is a source of trust and assurance, not only for me, but for the whole group. In addition, I am grateful for being able to visit Switzerland for a stay abroad at the Adolphe Merkle Institute in Fribourg. Thank you for your all the teachings you have given me, these lessons will not be forgotten.

Dear AK Meier, it has been an honor to work alongside a group of colleagues like you. Not even once I have felt to be treated unjustly, instead, I am amazed how well a group can be so united and work so well together. The parties and group trips were always a highlight for me, and I was glad to see that even after all the lockdowns, the will to celebrate all together remained firm. All in all, you are not just colleagues to me, you are friends.

To 409, the green hippie lab: Julian, Eren, Anja, Pia and Kenny, you were amazing lab mates with many hours of talking, gossiping and fun making during lab time or during the daily coffee breaks. I am convinced that although at the start of my PhD you all hated my metal music, deep in your hearts you now also enjoy it, even if you don't want to admit it. Dani and Jonas, I will never forget all the sophisticated jokes and the amazing Friday playlist blasting from 410. During these years I learned a lot about typical German music, commonly known as Schlager. Kevin, Philipp, Clara and Caitlyn, thank you for still being nice and friendly to me after all the smelly centrifuge vials I brought to you in 408. To Lab 103 and all its members, namely Michi, Roman, Maxi, Federico and Dennis: even if our labs were distant, our hearts were and are still close, keep up the good work!

Finally, special thanks to Julian's lab ghetto blaster: thank you for your service during these years, your sacrifice will not be forgotten.

Special thanks to Beate, Jürgen, Erika und Reiner, with their infinite kindness and hospitality. With you I feel as a member of your family, not just a stranger.

Thank you, Sophie, for your unconditional support, love and for the amazing last four years together. I don't know what I would do without you.

To my family, composed of lots of uncles, aunts, grandparents and cousins, which are all supporting me from Italy, checking in on me regularly. Greatest thanks to the very close family. Andrea, your comments and jokes never fail to make me laugh, and I know that I can count on you whatever the situation is. Mamma, there are no words that can describe how I feel. You, Andrea and papà taught me so much and made me to the man I am today. There is no way I can ever repay you for your infinite love, patience and support since the day I was born. I just wish papà was here to witness this moment. Papà, I hope you are proud of me. I miss you every day of my life.

Zusammenfassung

Die moderne Gesellschaft ist zur Aufrechterhaltung ihrer Wirtschaft und ihres Energieverbrauchs stark von fossilen Brennstoffen abhängig. Die weltweiten Vorräte an diesen Ressourcen gehen jedoch schnell zur Neige und haben große Auswirkungen auf die Umwelt. Daher werden für die nahe Zukunft erneuerbare und nachhaltige Technologien benötigt. Der Einfang, die Speicherung und Nutzung von CO_2, dem Hauptprodukt der Verbrennung fossiler Brennstoffe und Hauptverursacher der globalen Erwärmung, sowie die Nutzung erneuerbarer Rohstoffe sind daher von hoher Relevanz, insbesondere im Bereich der chemischen Forschung. Im ersten Teil dieser Arbeit wird die Verwendung von Kohlendioxid als Ersatz für teure und toxische Säurechloride zur Aktivierung von Hydroxamsäuren während der Lossen-Umlagerung diskutiert. Hierbei erfolgte die *O*-Acetylierung der Hydroxamsäure ohne Acylchloride, sondern durch Addition von CO_2 an die deprotonierte Hydroxylgruppe der Säure in einem CO_2-schaltbaren ionischen Flüssigkeitssystem (SWIL). Die Analyse der mechanistischen Aspekte der Reaktion erfolgte mittels Gaschromatographie (GC), kernmagnetischer Resonanzspektroskopie (NMR) und Online-Infrarot-Spektroskopie (IR). Im zweiten Teil dieser Arbeit wurde die Lossen-Umlagerung auch für die Synthese von erneuerbaren Carbamat-Dien-Monomeren für die Synthese von Nicht-Isocyanat-Polyurethanen (NIPUs) über Thiol-En-Polymerisation eingesetzt. Die Vorteile dieser Technik liegen nicht nur im nachhaltigeren Verfahren, sondern auch in der Nutzung der Nebenprodukte für den gleichen Zweck. Die anschließende Thiol-En-Polymerisation von nachwachsenden Carbamat- und Harnstoff-Dienen mit sowohl erneuerbaren als auch kommerziell erhältlichen Dithiolen führte zur Bildung von NIPUs mit interessanten und einstellbaren Eigenschaften. Das vorgeschlagene System ermöglicht auch die Herstellung von statistischen- und Block-Copolymeren, wodurch die Kombination von Monomereigenschaften in ein und demselben Makromolekül ermöglicht wird. Diese Fähigkeit wurde durch die Kombination verschiedener NIPU-Eigenschaften ausgenutzt, um Materialien zu erhalten, die für die Beibehaltung einer bestimmten Form und für die anschließende Analyse ihrer Zugfestigkeit durch Spannungs-Dehnungs-Experimente geeignet sind. Besonders interessante Ergebnisse lieferten NIPUs auf der Basis von Limonen und 10-Undecenoat, deren E-Modul und gummiartige Konsistenz ein großes Potenzial für Anwendungen als Elastomermaterial zeigten. Zusätzlich wurde das E-Modul des Limonen-basierten NIPU durch Zugabe von modifizierten

Cellulose Nanokristalle (CNCs) erhöht. Schließlich konnten die vorgeschlagenen Thiol-En-Polymere durch H_2O_2-Oxidation der Sulfidbindungen auf einfache und nachhaltige Weise nachmodifiziert werden, was zu entsprechenden Polysulfonen mit verbesserten thermischen Eigenschaften führte.

Abstract

Modern society strongly depends on fossil fuels to sustain its economy and energy consumption. However, the global deposits of these resources are depleting fast and have a major impact on the environment. This indicates that renewable and sustainable technologies are needed for the near future. Therefore, the capture, storage and utilization of CO_2, the main product of fossil fuel burning and the major cause for global warming, as well as the utilization of renewable feedstock are of high relevance, especially in the field of chemical research.

In the first part of this work, the use of carbon dioxide as replacement of expensive and toxic acid chlorides for the protection of hydroxamic acids during the Lossen rearrangement has been performed. More specifically, the *O*-acetylation of the hydroxamic acid occurred without an acyl chloride, but *via* addition of CO_2 to the deprotonated hydroxylic group of the acid in a CO_2-switchable ionic liquid system (SWIL). The analysis of mechanistical aspects of the reaction were carried out *via* gas chromatography (GC), nuclear magnetic resonance (NMR) spectroscopy and online infrared (IR) spectroscopy for monitoring.

In the second section of this thesis, the Lossen rearrangement was also employed for the synthesis of renewable carbamate diene monomers for the synthesis of non-isocyanate-based polyurethanes *via* thiol-ene polymerization. The advantages of this technique lie not only in the sustainable procedure, but also in the usage of side-products for the same purpose. The subsequent thiol-ene polymerization of carbamate and urea dienes with both renewable and commercially available dithiols led to the formation of NIPUs with interesting and tunable properties. The proposed system also allows for the preparation of random and block copolymers, enabling the combination of monomer properties in the same macromolecule. This ability was exploited by associating different NIPU characteristics in order to prepare materials suitable for maintaining their shape and for subsequent analysis of their tensile strength *via* stress-strain experiments. Especially interesting results were delivered by limonene- and 10-undecenoate-based NIPUs, whose E-modulus and rubber-like consistency showed great potential for applications as elastomeric material. Additionally, the E-modulus of the limonene-based NIPU was increased by addition of modified cellulose nanocrystals (CNCs). Lastly, the proposed thiol-ene polymers were modified by H_2O_2 oxidation of the sulfide

linkages in a facile and sustainable fashion, yielding the respective polysulfones with increased thermal transitions.

Table of contents

1 <u>Introduction</u>

Modern society currently depends on fossil fuel consumption for its energy demands. Although the dependence on these resources increases each year, fossil fuel deposits are rapidly declining. Additionally, the emissions derived from energy production, especially from CO_2, have increased the total greenhouse gas (GHG) concentration in the atmosphere to almost 500 ppm, compared to the pre-industrial level (280 ppm).[1] The alarming rate, at which the environment is affected by resource depletion, global warming and pollution has awakened the interest for the development of sustainable processes and the usage of renewable feedstock for industry. In the chemical and engineering field, P. Anastas[2] introduced the now well established "12 principles of Green Chemistry" in 1998 as a guideline for the design of sustainable procedures. The advances made by Green Chemistry over the last decades have reached a significant progress, however, all the steps made so far are still not sufficient to make a difference. Many sustainable technologies are still under development, as well as not efficient enough and often not well funded to achieve a sufficient reduction in CO_2 levels. Therefore, exploring all possibilities for sustainable methods is of utmost importance.

The use of biomass as feedstock[3] for chemical synthesis, for instance from carbohydrates, lignin or fatty acids, is an excellent way to exploit natures resources for everyday commodity materials to fine chemicals. Another example are CO_2 capture technologies, which are being intensively employed to reduce GHG emissions, for instance from exhaust streams.[4] Additionally, next to storage, the obtained CO_2 can be converted into everyday materials like polycarbonates in the polymer field.[5] Another important class of polymers, namely polyurethanes (PUs), are also produced in large quantities and distributed worldwide in many forms for a wide range of applications.[6] The scope of this polymeric class includes packaging, furniture, coatings, and insulation materials, which will be discussed in **section 2.5**. However, their industrial production requires the use of isocyanates, which are not only harmful for human health, but are also produced from the reaction of amines with the highly toxic phosgene,[7] a gaseous substance that was employed as chemical weapon during World War 1. Since then, multiple pathways were described to avoid isocyanates, creating the new class of non-isocyanate polyurethanes (NIPUs), for instance rearrangement, transesterification, ring-opening polymerization (ROP) or polyaddition.[8] Especially the polyaddition of *bis*(cyclic

Introduction

carbonates) with amines was proven to yield polyhydroxyurethanes *via* sustainable starting materials.[9] However, this method possesses the major disadvantages of requiring high temperatures and mostly reaching low conversions. Although the number of novel approaches for the preparation of NIPUs published over the last decades increased almost exponentially, an optimal procedure in the view of both sustainability and efficiency has not been developed to this day.

Sustainability, and the related Green Chemistry, are topics of great importance, indicating the way to a future with less pollution and a safe environment. However, this field is still not developed enough, requiring more attention not only from scientists, but from every person. Through the cooperation of society as a whole and the change sustainability has to offer on many aspects of our life, a path to a better future can be achieved.

2 <u>Theoretical background</u>

2.1 Renewability and climate change

In the last decades, the topic of climate change has gained great importance and many organizations have been founded to study and fight against its major problem: global warming. Global warming is a long lasting effect caused by many economic and environmental factors, and is therefore difficult to predict with precision. Nonetheless, the primary effects have already started to show, such as an increased rate of natural disasters, longer summers and higher overall temperatures.[10]

CO_2 has often been declared the main cause for climate change.[11] As the main greenhouse gas, CO_2 is present in the atmosphere in a concentration of 411 ppm (2019), much more than the value of 280 ppm as determined before the industrial revolution.[12] CO_2 is therefore the biggest contributor to the CO_2 equivalent (CO_2e) of all greenhouse gases (GHGs), with around 80% out of a total of 500 ppm in 2019 (all GHG combined).[13] The CO_2e is calculated by multiplying the amount of the GHG (e.g. hydrofluorocarbons, sulfur hexafluoride SF_6, etc.) by its global warming potential (GWP) in respect to CO_2 (GWP_{CO2} = 1).[14] For instance, SF_6 possesses a GWP of 22,800. This CO_2e increase has been deemed responsible for a temperature increase between 1-2 °C worldwide. Scientists have calculated that a temperature stabilization is still possible in the range of 430 to 550 ppm, between which the probability of major risks can be strongly reduced or even avoided. Although considering the step of over 250 years from the 1750s and now, one has to keep in mind that, since the beginning of the industrial revolution in 1750, the dependence on fossil fuel resources has been increasing almost exponentially until today, and is likely to rise even further in the future.[1] It has been calculated that carbon emissions have risen by at least 80% from 1970 to 2004,[1] with a further annual CO_2e gain of around 2 ppm during the early 2010s. More recently, the CO_2e changed from 407.4 ppm in 2018 to 414.7 ppm in 2019. Considering these aspects, the upper limit will be reached in around 30 years if no countermeasures are taken soon. Surpassing 550 ppm of CO_2e will lead to an over 50% chance for the temperature to increase by over 5 °C by the end of the century.[15] **Figure 1** shows the 5-95% range of the estimate temperature increase at different CO_2e levels at equilibrium points.[16]

Theoretical background

CO$_2$e	0 °C	1 °C	2 °C	3 °C	4 °C	5 °C	6 °C
400 ppm		←———————→					
450 ppm		←————————————→					
550 ppm			←——————————————————→				
650 ppm			←———————————————————————→			
750 ppm			←————————————————————————————————→		
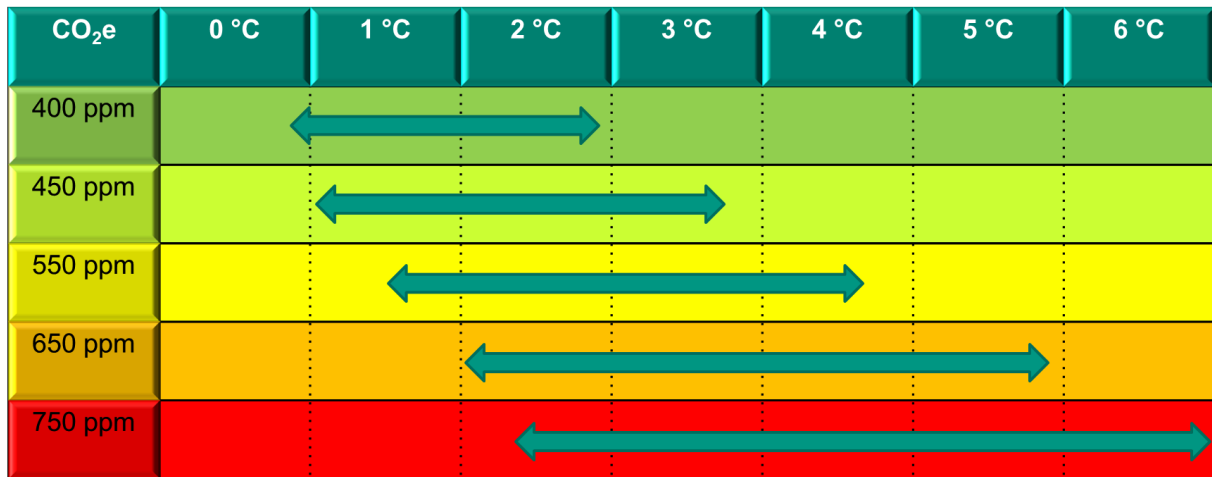
Figure 1 Range of temperatures projected at stabilization levels between 400 ppm and 750 ppm CO$_2$e at equilibrium, relative to pre-industrial revolution times (taken from the Stern review 2007).[1]

The increase of CO$_2$e is caused by human activities and technology, as confirmed by analysis of carbon isotope abundance in atmospheric CO$_2$. A decrease in the concentration of ^{13}C and ^{14}C nuclei detected in the air implies an artificial conversion of fossil fuels, since these species are less common than in naturally produced CO$_2$. Additionally, the atmospheric O$_2$ to N$_2$ ratio drops further as carbon bonds to oxygen virtually irreversibly.[17]

Carbon-based emissions are represented in the chart in **Figure 2**. Power production represents the main source, followed by transportation and industry. Nonetheless, also non-energy emissions have a fundamental role in the overall picture, with a total amount of 35%.
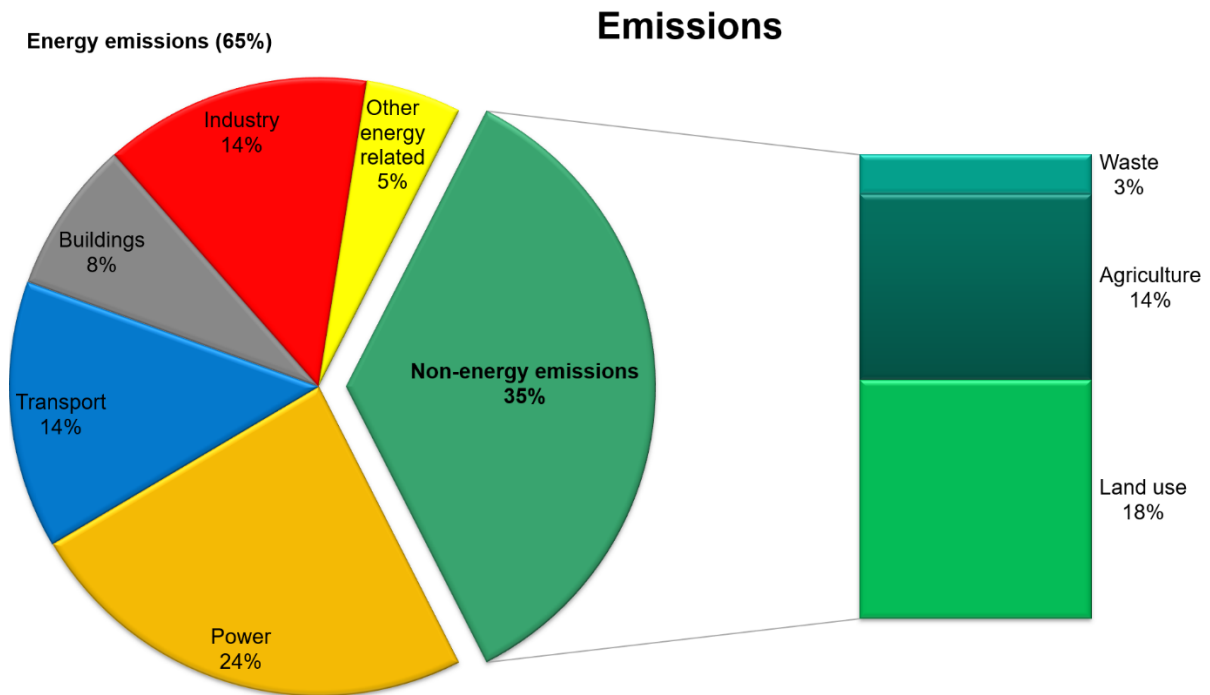
Figure 2 Pie chart of the total emission percentage of energy and non-energy nature (2000, adapted from the Stern Review 2007) [1]

Energy emissions consist essentially of CO_2, with few exceptions in the industrial and other energy-related fields, while non-energy emissions are represented both by CO_2 in land use and other emissions in agriculture and waste. The total amount produced in 2000 adds up to 42 Gt CO_2e.[1] For instance, deforestation is a great contributor to global warming, belonging to the non-emission block. With 13 million hectares of forests cut down every year, the ability of trees to perform photosynthesis becomes more and more restricted. Especially tropical deforestation causes almost 20% of the global greenhouse gas (GHG) emissions.[18] Therefore, less and less CO_2 can be transformed into O_2 by trees and plants, ultimately increasing the atmospheric CO_2e.

Summarizing the paragraphs above, the main causes for climate change derive from the creation of greenhouse gases, cutting of forests, energy creation and transportation. Additionally, growing economies in particular tend to invest in fossil fuel technologies and infrastructures, as cheap alternative to more renewable, but more expensive options. None

of the points mentioned above show immediate consequences, but have been shown to lead to severe results.

To stabilize the CO_2e between 500 and 550 ppm, economists have predicted the necessity of investment of 1% of the global gross domestic product (GDP) for a long-term plan.[1] Ignoring countermeasures and planning for the next few decades will lead to consequences requiring at least 5% of GDP annually to contrast the effects of global warming, according to estimations.[1] For instance, an increased wind speed of hurricanes of around 10-15% induced by higher ocean temperatures will double the repair costs of the affected areas, especially in the USA.[19] In 2003, the heatwave in Europe resulted in a financial damage of around 15 billion US dollars and the death of 35,000 people.[20]

Therefore, the topic of renewability and sustainability, as well as the development of "greener" technologies is of utmost importance in the current and upcoming decades and should not be ignored or underestimated. Especially decreasing CO_2 concentration through its capture,[21] storage[22] and utilization[23] are viable possibilities to reduce pollution in the atmosphere and for the continued use of carbon without harming the environment.[24] Meanwhile, the importance of the renewability and sustainability field will simultaneously create many business opportunities worth billions of dollars in the direction of low-carbon goods and services as well as technologies independent on fossil fuels, which have been employed for centuries as energy source, and are slowly but steadily approaching complete depletion.

2.2 Green Chemistry and Renewability

The concept of "Green Chemistry" emerged in the early 90s, as the causes of pollution resulting from the rapidly expanding industry became more significant and resource shortage gained major importance. **Figure 3** reflects the growing interest on this topic over the last two decades.
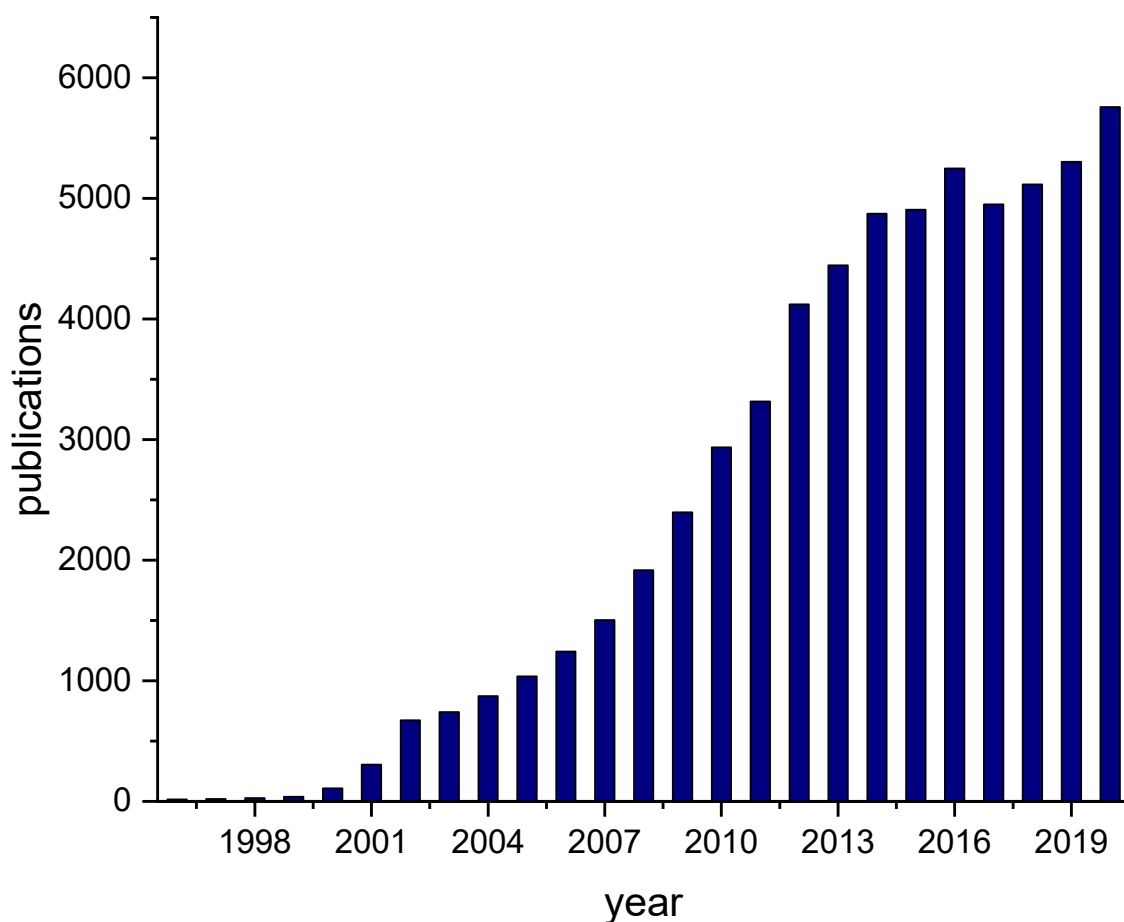
Figure 3 Publications per year under research topic "Green Chemistry" as entered (SciFinder-n, retrieved 06.07.2021).

The term *Green Chemistry* was first defined by P.T. Anastas and J.C. Warner in 1998[2] and applies both to chemistry as well as to chemical engineering. These 12 principles describe ideal processes that focus on the synthesis of biodegradable and harmless materials from non-hazardous chemicals, while also minimizing or avoiding the generation of waste:

1. **Prevention.** Preventing waste is better than treating or cleaning up waste after it is created.

2. **Atom economy.** Synthetic methods should try to maximize the incorporation of all materials used in the process into the final product. This means that less waste will be generated as a result.[25]

3. **Less hazardous chemical syntheses.** Synthetic methods should avoid using or generating substances that are toxic to humans and/or the environment.

4. **Designing safer chemicals.** Chemical products should be designed to achieve their desired function while being as non-toxic as possible.[26]

5. **Safer solvents and auxiliaries.** Auxiliary substances should be avoided wherever possible and be as non-hazardous as possible when they must be used.

6. **Design for energy efficiency.** Energy requirements should be minimized and processes should be conducted at ambient temperature and pressure, whenever possible.

7. **Use of renewable feedstocks.** Whenever it is practical to do so, renewable feedstocks or raw materials are preferable over non-renewable ones.

8. **Reduce derivatives.** Unnecessary generation of derivatives—such as the use of protecting groups—should be minimized or avoided, if possible, as such steps require additional reagents and may generate additional waste.[27]

9. **Catalysis.** Catalytic reagents that can be used in small quantities to repeat a reaction are superior to stoichiometric reagents (ones that are consumed in a reaction).[28]

10. **Design for degradation.** Chemical products should be designed so that they do not pollute the environment. When their function is complete, they should break down into non-harmful products.

11. **Real-time analysis for pollution prevention.** Analytical methodologies need to be further developed to permit real-time in-process monitoring and control before hazardous substances form.

12. **Inherently safer chemistry for accident prevention.** Whenever possible, the substances in a process and the forms of those substances should be chosen to minimize risks such as explosions, fires, and accidental releases.

Since following all 12 principles simultaneously is challenging, these rules were designed to serve as guidelines for chemists and chemical engineers to pursue the goal of sustainable chemistry for syntheses and processes.[29]

The first bullet point in the list above delineates the minimalization of waste or its complete prevention. For an easy and universal comparison of processes and overview over side product formation, the "Environmental Factor" (E-Factor) was introduced in 1992 by R.A. Sheldon.[30] The formula of the E-factor is simply the mass of waste divided by the mass of product, for which an ideal value of zero is possible. Some typical values in industrial processes are summarized in **Table 1**. The high E-factors in pharmaceutical industry trace back to the multiple reaction steps and the resulting large need for solvents during purification.

Table 1 E-factors in the chemical industry.

Industry segment	Product tonnage [tons per year]	E-Factor [kg waste/kg product]
Oil refining	10^6-10^8	< 0.1
Bulk chemicals	10^4-10^6	< 1-5
Fine chemicals	10^2-10^4	5-50
Pharmaceuticals	10-10^3	25-100

It is noted that often "Green Chemistry" is wrongly considered as a synonym of sustainable chemistry.[31] To resolve this misunderstanding, one must consider the origin of the term sustainability, which was formerly used to describe the balance between the felling and growing of trees by lumberjacks, gradually evolving to the present day in economic, environmental and social aspects.[32] Since these three categories are difficult to merge in one definition, sustainability remains more like an idea with a broader scope with no fixed limits, while the twelve principles of Anastas and Warner clearly describe all sides and boundaries of Green Chemistry. Economic aspects include stability and growth of the market, as well as secured prosperity for next generations. Social sustainability aims to ensure that education, health systems and personal safety are ensured at present and for posterity. Meanwhile, the ecological branch focuses on the regeneration of resources employed in every kind of process. Since chemistry aiming for non-hazardous and recyclable materials from renewable resources is strongly connected to this last category, Green Chemistry is ultimately considered as a subgroup of ecological sustainability.

The other main focus of this work, which is described by the bullet point 7 of the list of the 12 principles of "Green chemistry", is the employment of renewable feedstock for chemical syntheses. By definition, a renewable resource is a resource that, after being partially consumed or depleted, will be able to replenish itself by natural means at a faster rate than its depletion.[33]

Focusing on renewable raw material feedstock, biomass is a widely known source with an annual production of 150 billion tons worldwide.[34] Biomass consists of any organic material derived from plants and animals, for instance wood from trees or ethanol from plants.[35] Additionally, other naturally formed molecules and polymers are readily available just after extraction from their natural sources by physical methods, such as polysaccharides,

triglycerides and natural rubber, but also products like fatty acids and disaccharides, which are obtained after one-step biochemical modifications.[36] This way, materials in the scale of millions of tons per year are obtained without the need of complex synthetic steps. Cellulose, the most abundant organic polymer on earth is naturally produced in a scale of trillions of tons *p.a.*, making this polysaccharide a virtually inexhaustible source of raw material.[37] Also, industry has started to employ biomass as feedstock as it is inexpensive, vastly available and can offer a wide range of chemicals. An overview of some of the components of biomass is given in **Figure 4**.
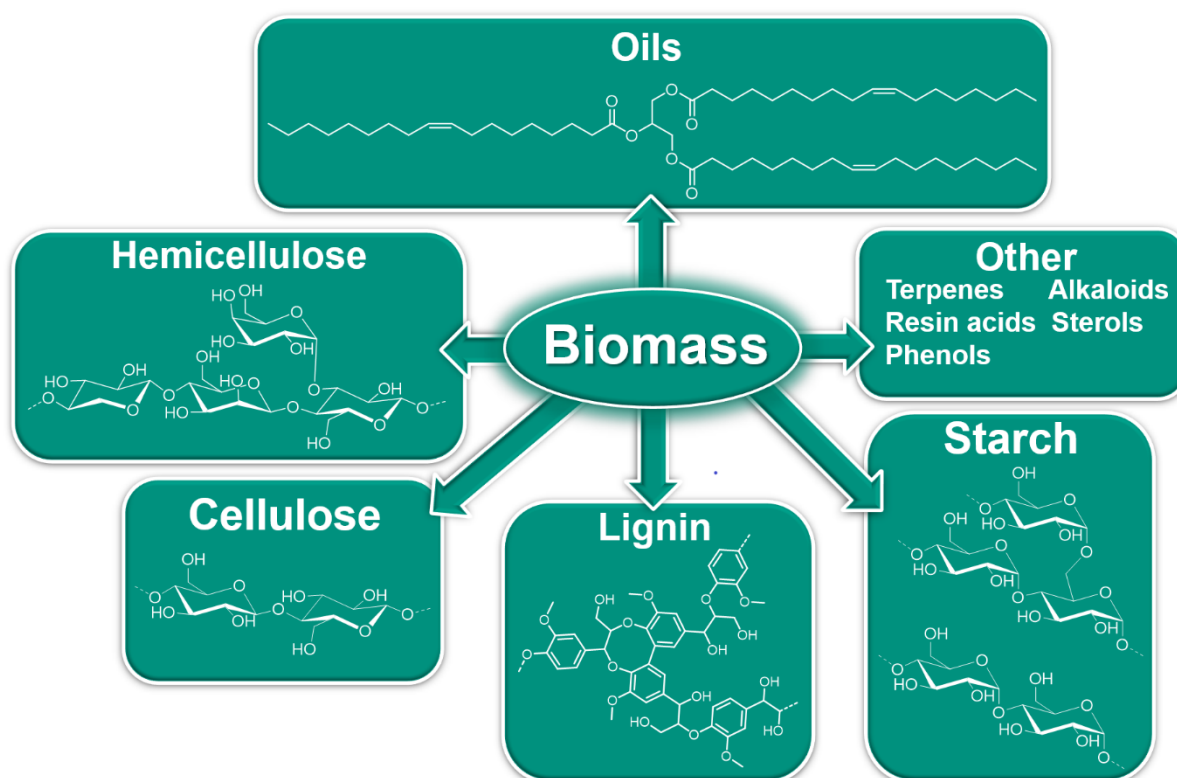
Figure 4 Main components of biomass.[38]

The main categories of biomass components are lignin, oils and cellulosic materials like starch, cellulose and hemicellulose.[39] However, as mentioned before, these components can be easily transformed into other interesting compounds, either by chemical or biochemical modification. The concept of a biorefinery is therefore to be introduced, as it describes the process of the conversion of biomass into many fine chemicals and molecules.[40]

Both cellulose and hemicellulose constitute a great percentage of the biomass obtained from wood, with a mass range between 55 and 80%. However, lignocellulose has to be treated before isolating the pure sugar-based biopolymers, mostly by catalytic hydrolysis leading to

the depolymerization of the polysaccharides. After this step, lignin can be easily separated with the help of ionic liquids, which are able to disrupt the network between lignin and hemicellulose, while simultaneously solubilizing cellulose.[41] This is currently the most common non-industrial separation method, without the risk of compromising the structure of the carbohydrates.[42] After lignin removal, the remaining sugars are subjected to different refinery methods: catalytic hydrodeoxygenation and aqueous phase reforming convert the saccharides to biofuels and other chemicals, for instance to hydrocarbons or biohydrogen. Classical fermentation produces mostly alcohols, like bioethanol, and the dehydration of sugars often yields furfurals, which can also be employed as fuels and are of great importance in the chemical industry.[43] Cellulose and hemicelluloses are exposed to hydrolysis, liquefaction, gasification, pyrolysis and/or hydrogenation in order to obtain fine chemicals with chain lengths between C1 and C6, as shown in **Figure 5**.
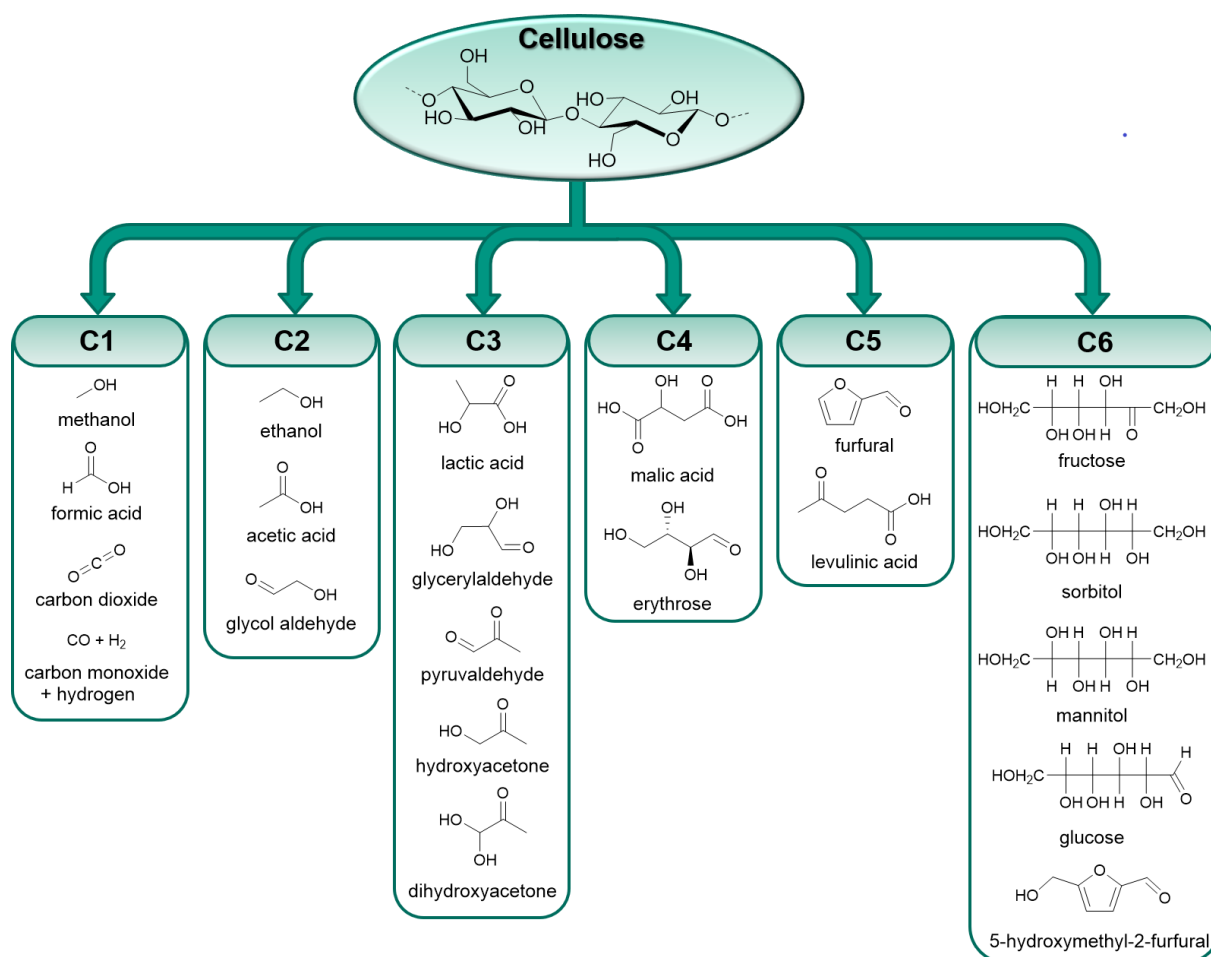

Figure 5 Fine chemicals with different chain lengths (C_1-C_6) obtained from biomass derived cellulose (adapted from [44]).

Theoretical background

Observing the figure above, the importance of biorefineries and their development becomes clear as a tool for the sustainable acquisition of a great variety of different structures. For this reason, many different methodologies are being developed in order to optimize these processes and to increase their efficiency.[45]

Meanwhile, lignin represents around 30% of lignocellulosic biomass, an amount making it worth being exploited to its full potential. Additionally, it is the second most abundant organic substance after cellulose.[46] Structurally, this source of raw materials is composed of phenylpropanoids, giving lignin the advantage of being a biodegradable material rich in chemical functionalities, while simultaneously showing UV-blocking, antioxidant and reinforcing properties. The three most common building blocks of lignin are depicted in **Figure 6**.
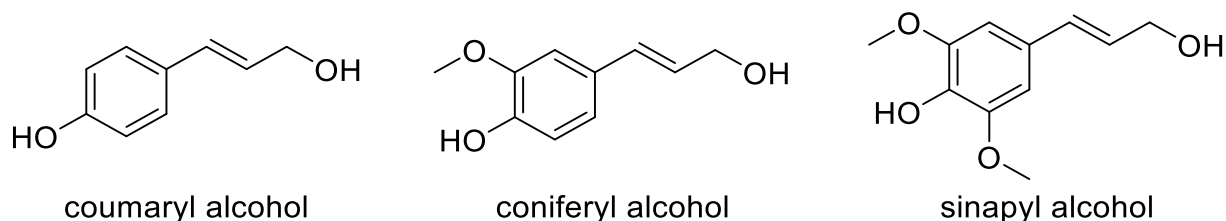

| coumaryl alcohol | coniferyl alcohol | sinapyl alcohol |

Figure 6 The major components of lignin, coumaryl, coniferyl and sinapyl alcohol, all of which belong to the phenol subclass.

As aromatic compounds are mostly extracted from petroleum in modern industry, similar phenolic molecules can be isolated by exploiting the chemical structure of lignin. However, currently, 98% of the yearly produced lignin is burned, since it is mostly seen as a byproduct, for instance in the paper industry.[46] The unique potential of this material is therefore lost.

With the importance gain of the topic of green chemistry and sustainability, many scientists started developing new routes for the processing of lignin in order to obtain chemically interesting phenolic compounds. This task is, however, not simple as the three alcohols shown in **Figure 6** are not only linked together in different ratios, but also form an extremely robust 3D network, which that is resistant to most chemical agents.[47] Already known methods under harsh conditions (up to 500 °C and 200 bar) are also undesirable, as the energy consumption is not only unsustainable, but also very expensive. The Rinaldi group found two catalysts to reduce emissions and optimize the reaction conditions. Thanks to this renewed process, lignin degradation was achieved below 40 bar and at 150 °C, yielding a mixture of chemicals easier

12

to separate, since the main issue concerning temperature-related side reactions was avoided during the treatment of lignin.[48] Following nature's example, novel methods make use of white rot fungi, through their enzymatic oxidative decomposition.[49] These fungi are named after the kind of wood-decay caused, as the cellulosic fractions of wood are left undigested, leading to a bright and soft rot residue.[50] The effectiveness of these fungi has been tested under laboratory conditions and, although slow when compared to burning, the decomposition of lignin proceeds to full conversion, enabling the isolation of many different functional groups and aromatic species.[51] Under the detected compounds, phenolic compounds like vanillin, coniferyl aldehyde, veratric acid and many more were identified.[52]

The other big class of noteworthy resources obtained from biomass are plant oils. Mostly obtained as viscous liquids, the main component of oils is the triglyceride unit (**Figure 4**). A triglyceride is a triester of glycerol and three fatty acids, which are carboxylic acids with long aliphatic chains found as both saturated and unsaturated species. The most common fatty acids found in nature are listed in **Table 2**.

Table 2 A few examples of the most common fatty acids and the respective saturation levels

Name	Carbon atoms	unsaturation	type
Lauric acid	12	-	-
Palmitic acid	16	-	-
Stearic acid	18	-	-
Arachidic acid	20	-	-
Palmitoleic acid	16	1	*cis*-Δ^9
Oleic acid	18	1	*cis*-Δ^9
Elaidic acid	18	1	*trans*-Δ^9
Linoleic acid	18	2	*cis, cis*-Δ^9,Δ^{12}
Linolenic acid	18	3	*cis, cis, cis*-$\Delta^9,\Delta^{12},\Delta^{15}$
Erucic acid	22	1	*cis*-Δ^{13}

Additionally, most of the naturally occurring fatty acids are not only unbranched, but also possess an even number of carbon atoms. Two exceptions are found in dairy products, namely pentadecanoic (C_{15}-chain) and heptadecanoic acid (C_{17}-chain).[53] It is worth mentioning that,

depending on the oil source, different types and ratios of fatty acids are attached to the glycerol. As an example, the compositions of fatty acids in vegetable oils are listed in **Table 3**.

Table 3 Examples of the most common vegetable oils and the percentual amount (mass) of saturated, unsaturated and polyunsaturated fatty acids.

Name	Saturated fatty acids [%]	Monounsaturated fatty acids [%]	Polyunsaturated fatty acids [%]
Sunflower oil	10.3	19.5	65.7
Palm oil	49.3	37.0	9.3
Soybean oil	15.6	22.8	57.7
Canola oil	7.4	63.3	28.1
Walnut oil	9.1	22.8	63.3
Olive oil	13.8	73.0	10.5
Corn oil	12.9	27.6	54.7
Castor oil	1.8	94	3.8
Coconut oil	82.5	6.3	1.7

As clearly shown in the table above, the diversity of fatty acids obtained from oils is great and should be therefore exploited as the yearly production of vegetable oil almost reached 210 million metric tons worldwide in the last year.[54] Another source of oils are lipids derived from animals, which can be divided into rendered fats, fish oils and milk fats. These three categories also greatly differ in their fatty acid compositions.[55] Rendered fats are, for instance, a byproduct of the meat industry and they consist of mostly saturated fatty acids, while oil extracted from fish, either as byproduct from the fishing industry or from fish explicitly caught for the oil production, contain a great amount of polyunsaturated fatty acids (> 3 double bonds). Dairy products, on the other hand, yield many short chain fatty acids, with most of them being between C_4 and C_{10}. An overview is given by **Table 4**.[56]

Table 4 Fatty acid content of some animal oils compared to the vegetable soy oil. All values are represented in percentages of the overall mass.

Fatty acid	Soy [%]	Whale [%]	Chicken fat [%]	Pork lard [%]	Beef tallow [%]
Myristic (C_{14}, saturated)	-	4-8	1	0.5-2.5	1.4-6.3
Palmitic (C_{16}, saturated)	10	7-12	25	20-32	20-37
Stearic (C_{18}, saturated)	5	1-3	6	5-24	6-40
Palmitoleic (C_{16}, monounsaturated)	-	7-18	8	1.7-5	0.7-8.8
Oleic (C_{18}, monounsaturated)	20	28-32	41	35-62	26-50
Linoleic (C_{18}, polyunsaturated)	50	1-2	18	3-16	0.5-5

Industrially, fatty acids are isolated by hydrolysis of the triglycerides, and glycerol is removed by distillation during the process.[57] Another useful treatment is the transesterification of the triglycerides with alcohols like methanol, yielding valuable fatty acid esters (FAMEs). As methyl esters are very reactive, these compounds are both employable as chemicals for further modification and can also be used as biofuels. Two advantages are known for the utilization of FAMEs as biofuels compared to the respective triglycerides: on the one hand the much lower viscosity of the esters and on the other hand the lack of many toxic byproducts formed by the thermal degradation of glycerol (*e.g.* acrolein). Ethanol, or the greener bioethanol, represent an additional candidate alcohol for transesterification, as ethyl alcohol is less toxic and volatile than the methyl alcohol counterpart.[58]

Conclusively, renewable resources can be obtained from multiple sources in large quantities. Depending on the treatment, the variability of the isolated chemicals and fuels, as well as the production of green energy, possess great potential, which has to be exploited in the following decades. It is especially important to research every aspect and process involved in each step from biomass towards the desired product, since fossil fuels and petrol are not present in infinite amounts on earth. Additionally, oil deposits are being depleted at higher rates by the continuously increasing energetic demand. Therefore, alternative routes starting from renewable feedstock are of utmost importance. The 12 principles of "Green Chemistry" introduced by Anastas are a useful tool for chemists and engineers for the design of new processes, a topic which is expected to gain even further importance during the next years.

2.3 CO$_2$ switchable solvent systems and materials

In the chemical field, especially in organic chemistry, it is common that a synthesis comprises multiple steps and purifications. During these "post-synthesis" actions, it is highly probable that the solvent used in one step is unsuitable for the following one. Therefore, the solvent has to be removed and replaced with an optimal alternative before being able to proceed. The extra steps mentioned not only extend the overall duration of the procedure and increase the cost in required laboratory materials and equipment, but also result in a large environmental impact caused by the energy demand and the formation of additional waste.[59] It has been proposed that utilizing a solvent system capable of changing its physicochemical properties, i.e. to optimize its suitability for different reaction steps, is highly desirable, particularly when such a switch takes place on account of changes in the pressure or temperature.[59] Unfortunately, such a scenario is not achievable for common organic solvents. Alternatives are supercritical fluids[60] and CO$_2$/organic mixtures,[61] with the main drawback of the necessary switch being achievable only under harsh conditions (e.g. above 40 bar pressure). An observation on the behavior of 1-hexanol and 1,8-diazabiciclo[5.4.0]undec-7-ene (DBU) in the presence of CO$_2$ by Jessop *et al.* in 2005[62] led to the development of a switchable solvent system under mild conditions and the subsequent discovery of its revolutionary potential for organic and polymer chemistry. The non-ionic liquid consisting of a base and an alcohol was reversibly converted to an ionic system in the form of a liquid salt by exposure to an atmospheric pressure of CO$_2$ (**Scheme 1**). Formally, the base deprotonated the alcohol, which subsequently, as an alcoholate, underwent a nucleophilic attack on the weakly electrophilic carbon of the CO$_2$. The resulting carbonate anion and its charge were stabilized by the remaining protonated base. It is worth mentioning that this addition even occurred at room temperature, increasing the sustainability of the proposed system.[62] Returning the now ionic solvent to its original state was achieved by bubbling inert gas through the mixture for 15 minutes.
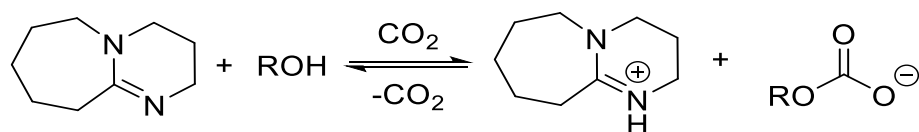
Scheme 1 Reversible non-polar to polar solvent system with an alcohol and DBU.

Polarity changes are either measured by ^{1}H NMR spectroscopy or *via* solvatochromic methods, *i.e.* by comparing the spectra of the same solvent in its ionic and non-ionic state. Additionally, the alcohol component should be chosen wisely, as specific salts like bicarbonates[63] and methyl carbonates[64] are not suitable solvents because of their solid state at standard conditions.

A practical demonstration of the effectiveness of the CO_2 switchable solvent system is depicted in **Figure 7**. In this scenario, DBU, alcohol, and decane are mixed in a flask or beaker. Afterwards, the mixture is exposed to CO_2 by bubbling for a few minutes. The newly formed highly polar ionic liquid separates from decane resulting in two distinct phases, facilitating solvent removal without requiring evaporation or more complex procedures. The triggered immiscibility is a promising alternative to rotary evaporation in the lab, but offers even greater advantages on industrial scale, mainly for separation procedures *via* extraction.
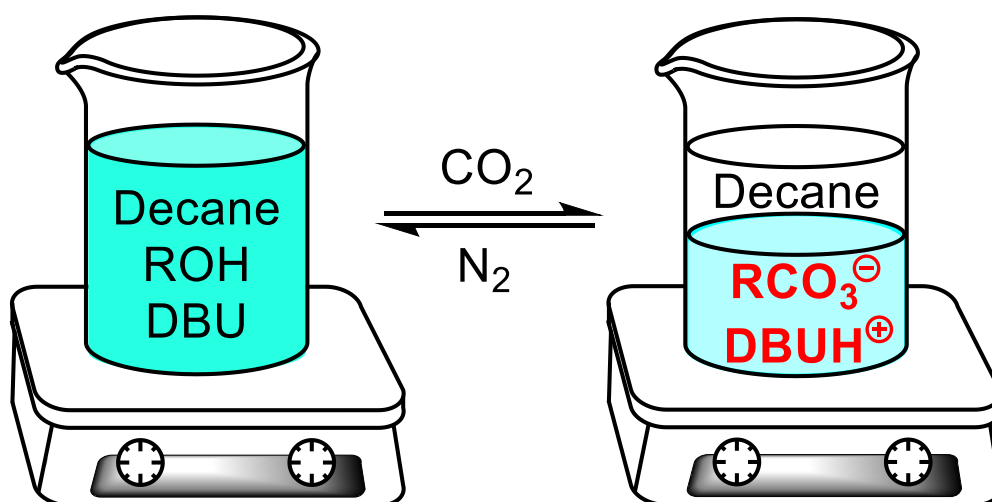

Figure 7 CO_2 and N_2 as a switch for miscibility and immiscibility, respectively, between decane and an alcohol.[62]

Heldebrandt *et al.*[65] have calculated the gravimetric uptake of different alcohol/base systems in 2008. For instance, the 1-hexanol/DBU system is capable of capturing 1.30 mol of CO_2 for each DBU equivalent. This confirms the involvement of physisorption of CO_2 to the solvent, additionally to the expected chemisorption. This value is about 30% higher than for a monoethanolamine solution, a standard mixture for CO_2 capture.[66] Studies have also been performed on amino– alcohol/DBU based systems, which show an increased CO_2 uptake when compared to their respective aqueous solutions.[67]

Two groups of switchable solvents based on CO_2 have been defined: switchable polarity solvents (SPS) and switchable hydrophilicity solvents (SHS).[59] Even though both categories seem to be very similar, their main difference is that SHSs are bound to their influence on water, while SPSs are focused on polarity effects and have an organic nucleophile as the main component. For example, **Figure 7** represents a typical SPS. A third group, "Switchable Water" (SW), will also be introduced in chapter2.3.3.

2.3.1 Switchable polarity solvents (SPS)

As mentioned before, it is common knowledge that for multiple reaction steps there is only a small chance that the same solvent is adequate for all steps, especially in organic chemistry. Therefore, a solvent possessing the ability to switch polarity on command (in this case exposure to CO_2) is highly desirable.

SPSs change their polarity based on the addition of CO_2 and are often composed of a nucleophilic component and an organic base. Amines and alcohols are the most used nucleophiles. Alcohols were the first example presented by Jessop and co-workers and show greater polarity range than amines.[68] However, they present a major issue as these systems have the crucial disadvantage of being highly water sensitive. All components need to be dried before usage, as bicarbonate salts are thermodynamically more stable than carbonate salts under mild conditions. Fortunately, this counts only if bicarbonate is not wanted, which is not the case for SHSs or SW (see **chapter 2.3.2** and **2.3.3**). In contrast, amines are highly selective towards CO_2 and the respective carbamate salts thermodynamically stable even at higher temperatures.[69] As for the base, guanidine- and amidine-based SPSs have often been reported in the literature and are highly efficient because of their basicity and readiness to form salts. Nonetheless, most of the representatives of these two categories are expensive and too basic to be appropriate for use as a solvent for reactive components (such as acids and alkyl halides).[70] A possible solution to this problem are single-component SPSs.[71] The first reported example was an SPS containing secondary amines, which possess the right properties to be both a nucleophile and a base. Nonetheless, as many carbamate salts are solid, they are not suitable for single-component SPSs, while anilines have been shown to be inert towards CO_2 in the absence of catalysts.[72]

These systems are not limited to phase separation, but are also employed for triggered precipitation or solubilization of organic compounds. As SPSs can be employed both as reaction solvents and extraction media, their attractiveness in organic and polymer chemistry has greatly increased since their discovery. For instance, polymerization of styrene has been performed in the presence of switchable compounds with low polarity.[73] By bubbling CO_2 through the mixture, the precipitation of pure poly(styrene) was achieved because of the polarity increase of the medium. The polymer was then removed by simple filtration. Other examples of reactions in SPSs include Michael additions, Claisen-Schmidt condensations, and even air sensitive Heck reactions.[74] As for extractions, a few notable examples were developed and have to be mentioned. One is the extraction of lipids from algae, which is currently performed with hexane and yields around 7.8% from freeze-dried samples. When employing the 1-octanol/DBU SPS for the same task, a yield of 16% by weight was isolated.[75] The SPS system was also employed in the extraction of soy oil from soybeans with benzylamine or an alcohol as nucleophilic component.[76]

The focus on facile recycling and the ability to reduce the amount of solvent and reduction of purification steps has been proposed to bring great economic advantages in large scale processes in the industry.[77]

Deeply connected to the field of green chemistry is the functionalization of cellulose, the most abundant natural polymer found on earth.[37] Cellulose is not only available in large quantities, but is also biocompatible and biodegradable,[78] making it one of the best known and favorite polymeric materials for green chemists. Changing the properties of the polysaccharide, for instance by reducing the hydrogen bonding *via* hydroxy group transformation (e.g. to esters[79]), is of utmost importance, as this material can afterwards be further processed when its crystallinity and insolubility are reduced. Additionally, depending on the functionalization chosen, cellulose properties can be tuned for the desired applications. However, cellulose remains insoluble in most organic solvents and in water, inhibiting potential functionalization of the saccharide backbone. Ionic liquids represented virtually the only solution to this drawback for a long time,[80] albeit at the expense of sustainability. Recently, two CO_2-based alternative routes were described, as published simultaneously by two different working groups, namely the Xie[81] and Zhang[82] groups. Even if the reactivity of CO_2 with alcohols

under basic conditions was exploited in the same manner, one example features a non-derivative pathway, while the second method is of derivative nature, as shown in **Scheme 2**.
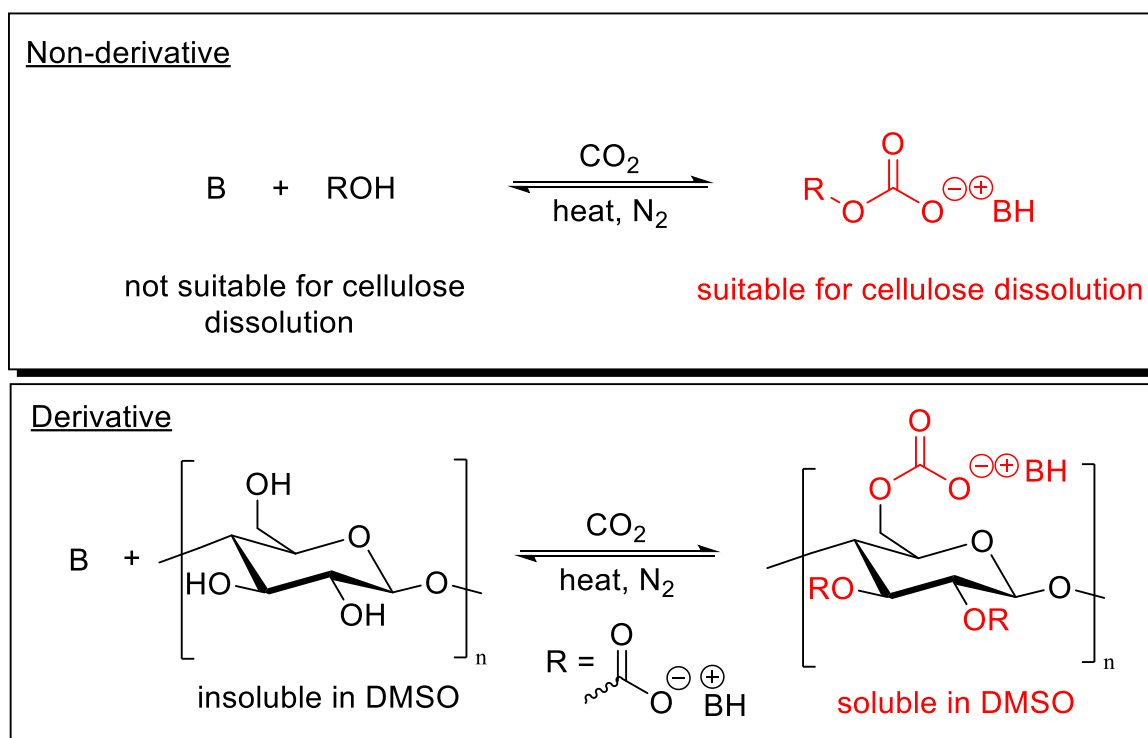
Scheme 2 Non-derivative approach (top): formation of reversible ionic liquid suitable for cellulose dissolution. Derivative approach (bottom): CO_2 addition to the deprotonated hydroxy groups of the polysaccharide, forming DMSO-soluble cellulose carbonate salts.

The non-derivative approach changes the properties of the solvent by increasing its polarity, allowing the solubilization of cellulose as a suitable ionic liquid, while the derivative strategy is based on the generation of DMSO-soluble cellulose carbonates by *in situ* functionalization of the saccharide hydroxyl groups with CO_2.[83]

While SPSs have been widely used, particularly when polymers with problematic solubility, such as cellulose, are considered, they lack the interaction with water that is often needed in SHS systems.

2.3.2 Switchable hydrophilicity solvents (SHS)

Simply described, an SHS consists of two separate layers of a hydrophobic base and water. Through bubbling or exposure of CO_2, the biphasic system changes into a homogeneous solution. The chemical addition of CO_2 to water is followed by the protonation of the base,

forming a water-soluble bicarbonate salt. Identical to the SPS, the gas can be removed *via* heating, sonication, or bubbling of inert gases like N_2 or Ar. The polarity range of a typical SHS, in this case the system $BuN=C(Bu)NBu_2/H_2O$, was measured with Nile red dye and compared with a few examples of SPS systems (**Figure 8**). It is worth mentioning that Nile red is a dye whose fluorescence changed based on the polarity of its environment.[84] This uncharged compound does, for instance, becomes red upon exposure to solvents like ethanol, while turning yellow upon being dissolved in unpolar media like hydrocarbons.

solvents	λ_{max}	SHS	NHEtBu	Diamine	MeHNCH$_2$Ph	TMBG / MeOH	DBU / PrOH	Me-TBD / acidic alcohol
	570 nm	●						●
Ethylene glycol								
	560 nm							
Methanol	550 nm					●	●	●
DMF	540 nm				●		●	
Chloroform								
Acetonitrile Acetone	530 nm		●	●		●		
Toluene	520 nm			●	●			
	510 nm	●	●					
Ether								
	500 nm							
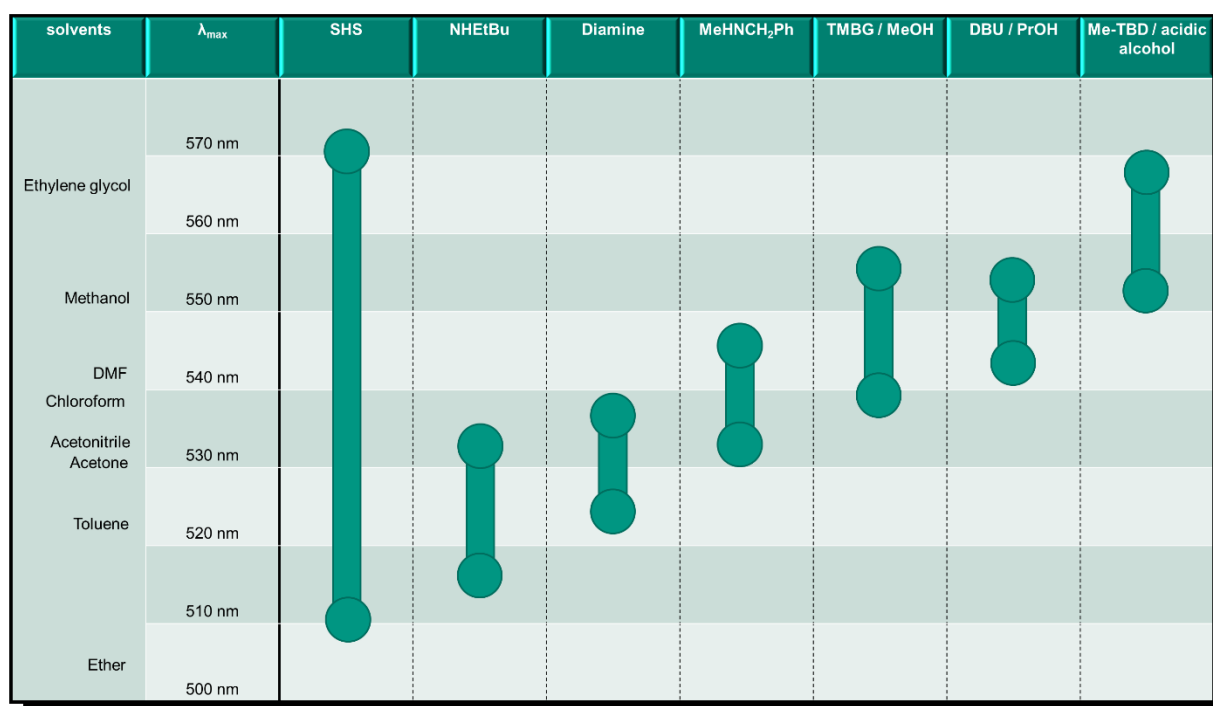
Figure 8 Range of polarity change of a typical SHS and different SPS systems measured with Nile red dye and compared to the polarity of common organic solvents.[59]

The scheme shown above confirms the much larger polarity change upon switching an SHS. One must note that, if the hydrophobic component is too basic, the application as an SHS becomes disadvantageous since the respective CO_2-based salt is highly stable. Thus, the release of CO_2 requires large amounts of energy, mostly in form of heat. Also, in most procedures, the solvent needs to be removed to isolate the product. This occurs mostly through distillation, which requires volatile liquids for satisfying efficiency and energy consumption. As SHSs separate from the product upon being triggered by CO_2 addition or removal, the choice of SHS does not rely on the need for volatility. This method was employed for extractions from renewable feedstocks, such as the recovery of soy oil from flakes[85] or bio oils from algae.[86]. Additionally, poly(styrene) was successfully recycled with different

SHSs.[87] A particular SHS system was developed by Ohno *et al*. based on tertabutylphosphonium *N*-trifluoromethane sulfonylleucine.[88] This compound behaves oppositely to the Jessop system because of its water miscibility under neutral conditions. While increasing acidity through the addition of CO_2, the carboxylate group is protonated, causing a phase separation between the ionic liquid and water.

The dependance on water of SHSs is of great use for tuning properties to cause miscibility and immiscibility with water on command, however, other systems are also known to make use of the increased polarity in aqueous media, such as switchable water (SW).

2.3.3 Switchable water (SW)

Distillation of water for a reaction workup is more expensive and energy consuming than for most organic solvents.[89] An efficient method in organic chemistry to separate polar organic compounds from water is to add salt to the mixture ("salting out"), thus increasing the ionic strength and forcing precipitation or phase separation.[90] Unfortunately, this method is irreversible and requires costly treatment for water recycling. For this purpose, a solvent possessing tunable polarity without having to change solvents or "salting-out" is desirable. Considering these premises, the switchable solvent system has been chosen as a suitable alternative.[91] Similar to SHSs, the system needs a base, this time with hydrophilic properties. Fitting for this task are many amines, resulting in a single layer of low ionic strength. The bubbling of CO_2 has the same chemical effect as on SHSs with the only difference being the dependance on aqueous media. In SW, the high ionic strength resulting from the formation of bicarbonate salt leads other organic compounds to become water-insoluble, thus facilitating the process and increasing separation efficiency.

The simplicity of this system has put it in the centre of a debate as to whether it encompasses a category of its own or whether it is a subgroup of SHSs. In this work, to the two were separated in two chapters to avoid possible misunderstandings.

All CO_2 switchable solvent systems have shown great advantages over common organic solvents for synthetic purposes. Therefore, the incorporation of such properties has been researched for materials and polymers, as will be described by a few major examples in the next subsections.

2.3.4 Other applications in CO₂ switchability

Many more applications have been investigated and published since 2005. As switchability does not capture CO_2 but rather entails its controlled addition and release that is responsible for changing the properties of a chemical substance, four important categories of specially designed switchable compounds arose next to the solvent system: catalysts, surfactants, polymers, and initiators.

2.3.4.1 Catalysts

Homogeneous catalysts often present higher activity and selectivity than their heterogeneous counterparts, but have the limitation of difficult separation from the product or solvent after the reaction.[92] Therefore, a few examples of switchable catalysts have recently been developed. One example is the aqueous extraction of a catalyst with terminal tertiary amines on phosphine ligands.[93] In the presence of CO_2, the protonated amine groups act as counter ion for a water-soluble bicarbonate salt enabling straightforward catalyst separation from organic media after the reaction. Another similar approach was published by Desset *et al.* in 2009,[94] employing switchable solubility for a catalyst bearing a PPh_3 ligand with amidine groups with a rhodium core for the hydroformylation of alkenes. The polarity increase caused by the chemisorption of CO_2 to the amidines allowed for a facile extraction with water from the organic reaction mixture. Of course, CO_2 switchability of catalysts is not restricted to its solubility in water. König *et al.* designed a catalytic system able to activate or deactivate the benzamidine in the aldol reaction between acetophenone and 4-nitrobenzaldehyde.[95] Benzamidine in its polar form is unable to catalyze the reaction, a state that can easily be reversed with heat or bubbling of inert gas when desired.

The reversible miscibility of catalysts to achieve homogeneous conditions has been proven to be of major importance for many reactions. The CO_2 is not only able to create a water-soluble catalytic system, but has also been employed for effective catalyst activation and deactivation.

2.3.4.2 Surfactants

Surfactants are essential to form polymeric emulsions and to stabilize latexes. Such materials have a broad scope, however, after completion of the preparation, excess surfactant removal is challenging, since often traces of surfactant can be found in the isolated polymer, even after

many purification steps. Depending on the residual amount, the properties of the polymer are also influenced.[96] Additionally, for applications that require dry polymer powders, the latexes have to be destabilized, which typically occurs by the addition of salt, base, or acid, depending on the employed surfactant type.[97] The advantage of having a switchable surfactant, therefore, lies in the simplicity of the reversible stabilization of latexes without the need for additives. A review about switchable surfactants was published by Brown *et al.*[98] in 2013 also describing acid/base,[99] redox-[100] and light-[101] based systems as triggers. CO_2 as a trigger presents the additional advantages of low toxicity and cost. At first, long alkyl chain amidines and amines[102] were chosen as suitable CO_2-switchable surfactants, as the hydrophobic tail and hydrophilic (active) head possessed ideal properties for bicarbonate salt formation. Poly(styrene) and poly(methyl methacrylate) (PMMA) were successfully synthesized in aqueous media aided by these surfactants.[103] The colloidal stability was then tested by multiple cycles of aggregation and redispersion of the latexes. The authors confirmed that if not only the surfactant, but also the initiator is switchable by CO_2, the best redispersion was observed. A detailed representation is given in **Figure 9**.
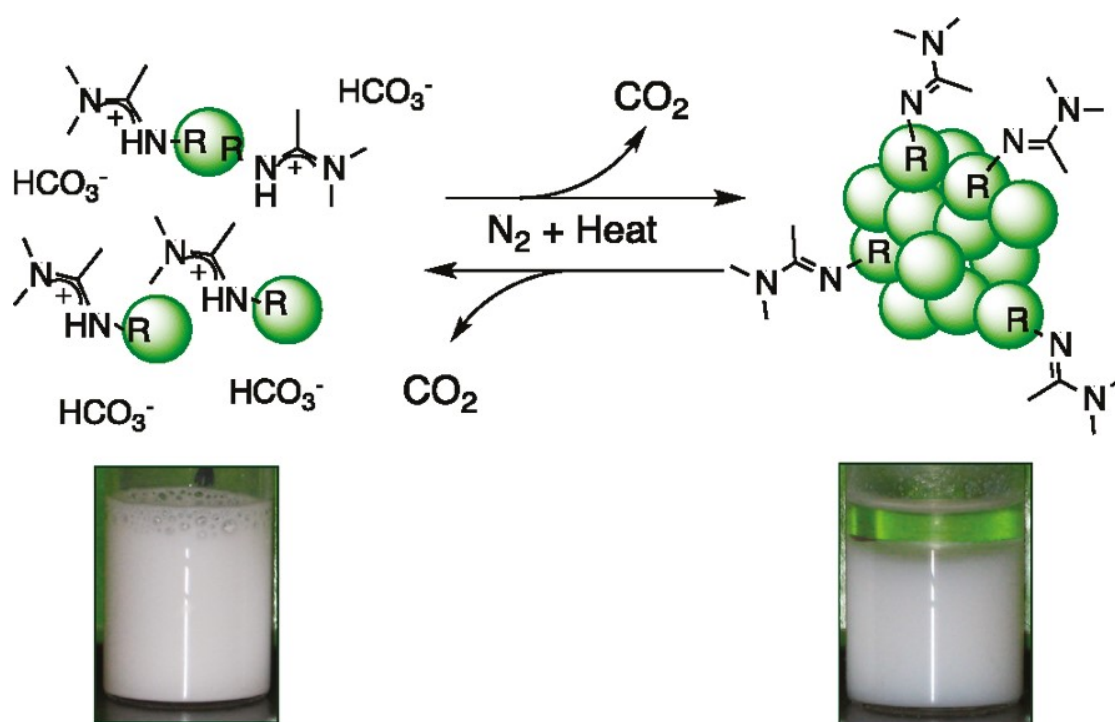
Figure 9 Typical dispersion (left) and agglomeration (right) when the surfactants are active and inactive, respectively. Reprinted with permission from *M. Mihara, P. Jessop, M. Cunningham,* Macromolecules *2011,* 44*, 3688-3693*.[103] Copyright (2021) American Chemical Society (ACS).

Imidazolium[104] groups have also been reported to be ideal as surfactant heads (**Scheme 3**), as they are less basic and thus easier to switch off, while simultaneously possessing lower protonation heats. Even if switchable surfactants mostly concern latexes for polymerizations, other applications are important as well. For instance, single walled carbon nanotubes were dispersed and coagulated multiple times by usage of a compound bearing an amidine group and a pyrene tail.[105] The latter were attached to the nanotubes *via* π-π interactions, while the head was in charge of solubility changes. Through formation of the corresponding bicarbonate salt, the nanorods were dispersed in water, while switching back to the neutral form caused precipitation.
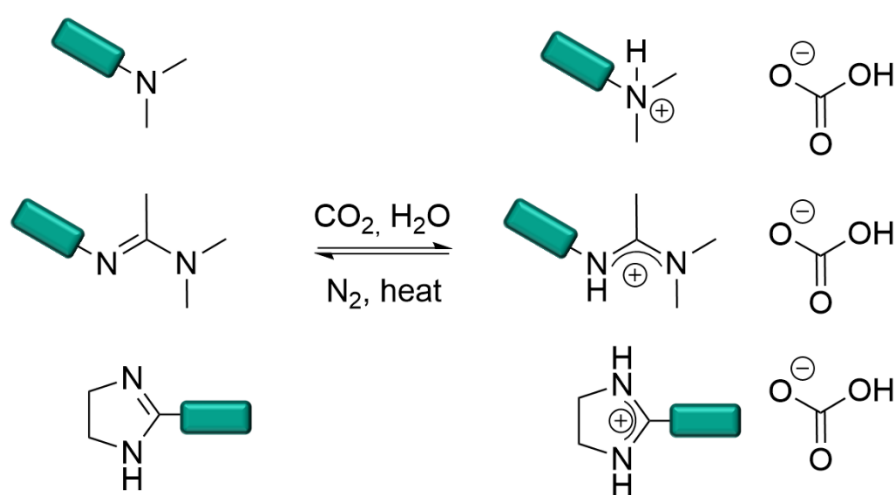
Scheme 3 Most common CO_2 switchable surfactant classes in their inactive (left) and active (right) state.

Subsequently, the Jessop group tested different head groups and their influence on basicity, solubility, and heat of protonation.[106] The authors determined that even if switchable surfactants are useful for many applications, one must keep in mind that this kind of surfactants are not disadvantage-free. The greatest problem derives from the degree of protonation, which can only be partially controlled. Since the surfactant is only active in its protonated form, the particle size and solids content are affected by every parameter that changes the degree of protonation, such as temperature, local environment, and the dissociation constant of the conjugate acids, as well as the effective dispersion of CO_2 in water.[107] Besides that, stability problems caused by surfactant migration on the surface remain a problem, like for non-switchable surfactants, since they are not covalently bound to the particle.

Even if switchable surfactants show the above mentioned disadvantages, these materials clearly possess an even greater potential in the polymer field by offering a potentially greener stabilization of latexes, both under environmental and economical aspects.

2.3.4.3 Switchable polymers

Switchability has also been added to polymeric materials. For this purpose, one approach is to employ already switchable monomers for radical polymerization. In the last decades, two molecules in particular have been employed in a lot for this purpose: diethylaminoethyl methacrylate (DEAEMA) and dimethylaminoethyl methacrylate (DMAEMA) (**Figure 10**). Before recognizing the importance of CO_2 addition with regards to reversibility, polymers based on these monomers were used on account of their pH responsive properties.[108]

DEAEMA   DMAEMA

DMAPMAm   DMAPMA
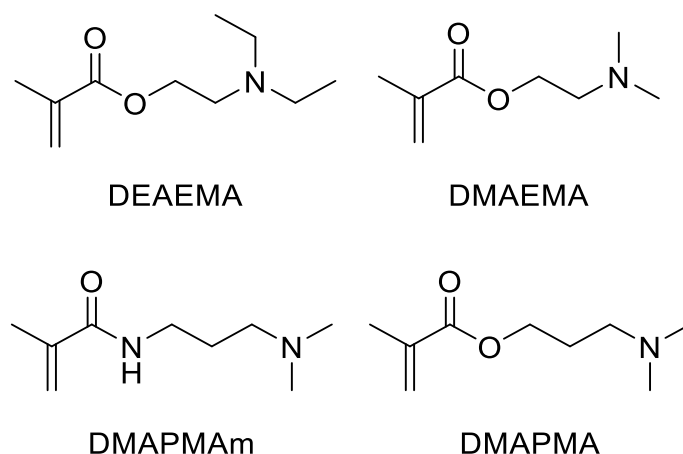
Figure 10 Structure of the most common CO_2 switchable monomers.

These compounds possess tertiary amines: diethyl and dimethyl amines, which possess similar structures, nonetheless they differ in their water-solubility properties thus influencing their application.[107] DEAEMA and DEAPMA are hydrophobic, while their respective methyl amine monomers are hydrophilic. The choice of monomer depends on different factors, including the precipitation solvent. For instance, precipitation of PDEAEMA with hexane is more difficult than for PDMAEMA, when both polymers exhibit the same molecular weight.[109] Although both polymers have shown satisfactory properties for potential applications, such as biocompatibility, the respective monomers are prone to hydrolysis. Under basic conditions, the two methacrylates decomposed into methacrylic acid and dialkylaminoethanol.[107] Therefore, another monomer has been introduced: the hydrophilic

N-[3-(Dimethylamino)propyl]methacrylamide DMAPMAm is, unlike the aforementioned (meth)acrylates, an acrylamide featuring a higher water resistance.

Polymerization techniques employed are based on radicals, both the free radical (FRP) and the reversible deactivation (RDRP) variant. Since control of molecular weight and dispersity are important for polymer properties, only a few examples in FRP are of great importance.[110] The RDRP method, despite being more expensive and slower than FRP, offers advantages other than molecular weight and dispersity control, such as the possibility to synthesize block copolymers. Atom transfer radical polymerization (ATRP),[111] reversible addition-fragmentation chain transfer (RAFT) polymerization[112] and nitroxide mediated polymerization (NMP)[113] are some RDRPs that have been employed in the synthesis of switchable polymers triggered by CO_2. The use of switchable monomers has been thoroughly studied but is not strictly necessary to achieve the desired properties. Responsive functionalities can, for example, also be introduced *via* post-polymerization modification.[114] For instance, the Wang group[114b] synthesized poly(*p*-azidomethylstyrene) by substitution of the side chains of poly(p-chloromethylstyrene) with sodium azide. Afterwards, the azide groups were "clicked" *via* 1,3-dipolar cycloaddition to *N*'-propargyl-*N*,*N*-dimethylacetamidine (PDAA), a compound capable to undergo CO_2 switchability.

Applications for switchable polymers range over a vast field and the most important examples are briefly described in the next subsections.

2.3.4.3.1 Switchable surfaces

Polymers are often employed as surface materials for many purposes such as coatings and biomaterials. The most common synthetic pathways are represented by different grafting approaches.

The first polymeric brushes featuring CO_2-switchability were prepared by Zhao and coworkers[115] polymerizing DEAEMA *via* ATRP on gold or silicon surfaces. The synthesized surface was then employed in controlled protein adsorption and release, depending on the state of the switch of the polymeric chain. In the hydrated form (hydrophilic, CO_2 bubbling), the chains extended, while they collapsed upon becoming dehydrated (hydrophobic, N_2 bubbling). This new method revolutionized the controlled release of substrates, as previous

approaches using pH (acid/base) as a switch always resulted in salt accumulation and contamination.[115]

Interesting properties derived from switchable surfaces have also been reported for nanoparticles (NPs). To control the dispersibility of NPs, CO_2 switchability has been confirmed to be a reliable method. For instance, PDEAEMA covalently bound to gold NPs showed reversible transitions upon exposure of CO_2 and N_2 gas in aqueous media, facilitating the recycling and increasing catalytic activity when compared to unmodified Au NPs.[116] The decrease of catalytic effectiveness of the unmodified Au NPs was reported to be caused by irreversible agglomeration of the NPs, an effect that could be mitigated by CO_2-switchability. In another publication, magnetic NPs were coated with silica and the surface was modified with methyl acrylate units. Afterwards, DMAEMA was polymerized in the presence of the coated NPs.[117] After confirming switchable contraction and expansion of the polymeric shell of the NPs, release experiments were conducted. Using doxorubicin (DOX) as payload, the functionalized NPs demonstrated a time-controllable dosage upon CO_2 exposure. DOX is a common drug against breast cancer,[118] bladder cancer,[119] lymphoma[120] or Kaposi's sarcoma.[121] Upon exposure to CO_2, the release rate increased because of the swollen surface-bound polymer chains. Additionally, these NPs indicated good biocompatibility and possessed low cytotoxicity, thus showing promise for *in vivo* experiments.

Similar gold based NPs have also been employed for reversible water/organic phase exchange.[122] In this approach, NPs gained switchable hydrophilicity. This gain does not only apply to particles with metal or silica cores, but also to pure organic conjugated polymer nanoparticles (CPNPs).[123] Wang *et al.*[124] reported the reversible emulsification during Pickering interfacial catalysis. Silica coated Fe_3O_4-based NPs (Fe_3O_4@SiO_2) surface-functionalized with amine-based polymers were employed as switchable stabilizing agents in water-in-oil Pickering emulsion systems, while simultaneously offering reactive sites for the Anelli system for the oxidation of alcohols. By employing these NPs, the authors showed a three-fold increase in the catalytic activity. Additionally, the disintegration of the emulsions was easily achieved by bubbling of CO_2, and recovery of the NPs was performed *via* magnetic separation. Zhang *et al.*[125] prepared silica NPs and mixed them with a cheap and commercially available surfactant, *N,N*-dimethyl-*N*-dodecylamine, in order to test the efficiency for switchable oil-in-water emulsification purposes. Upon CO_2 exposure, the

surfactant became cationic and was adsorbed on the particle surface. This caused stabilization of the emulsion, which was destabilized at the desired time through N_2 bubbling.

The combination of surface materials with CO_2 switchability is therefore of great importance for the above-mentioned reasons, especially when combined with NPs, whose properties are greatly reflected by their surface and surface to volume ratio.

2.3.4.3.2 Forward osmosis desalination

Another interesting application for switchable polymers with practical benefits has been reported in the context of osmosis.

Forward osmosis desalination is a method to purify salt or wastewater *via* extraction through a semipermeable membrane into a concentrated aqueous solution of an easily removable salt.[126] This draw solution causes high osmotic pressure, attracting the water from the waste. In 2012, Jessop *et al.*[127] patented a CO_2 switchable draw solution system in which a polymer bicarbonate salt was produced *via* CO_2 addition. A system based on PDEAEMA as draw solute was published shortly after by the Hu group in 2013 (**Figure 11**).[128]

Theoretical background
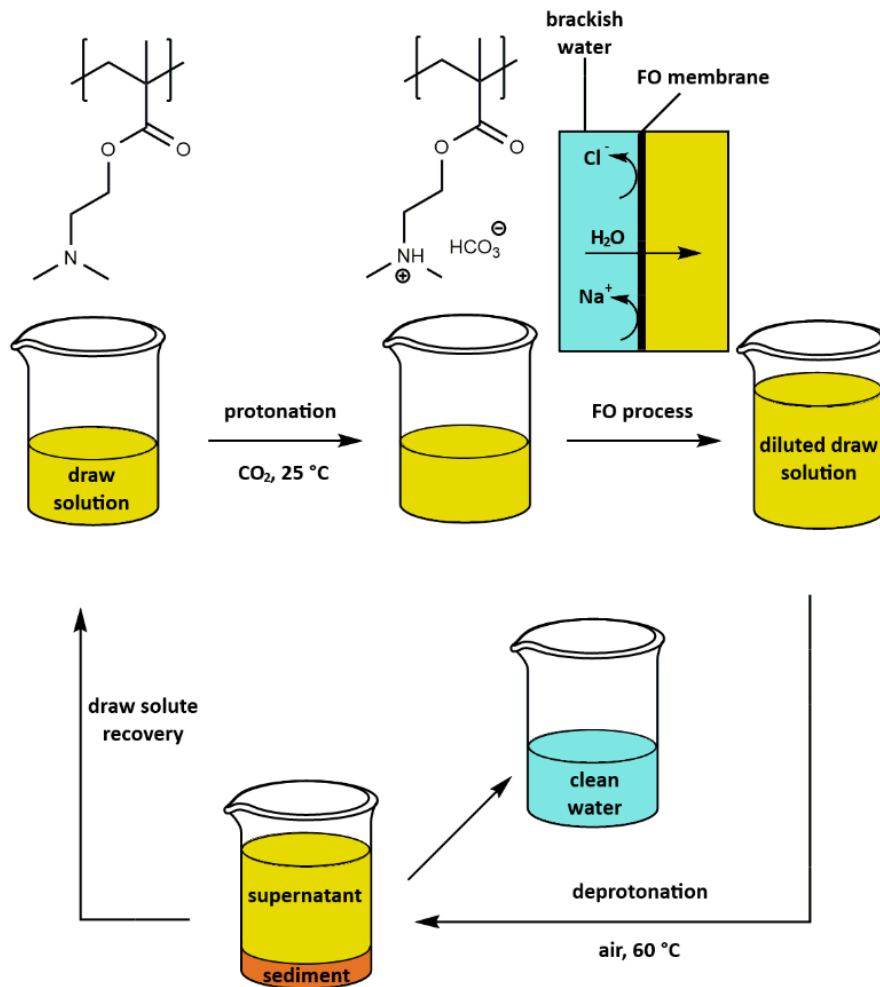
Figure 11 Schematic representation of forward osmosis desalination with CO_2 responsive polymers (PDEAEMA). Adapted from Ref.[128] with permission from the Royal Society of Chemistry.

After osmosis, simple bubbling of nitrogen gas caused the polymer to precipitate from the aqueous solution. PDEAEMA in particular showed promising properties, such as low toxicity, low back diffusion, and did not degrade the membrane. Using the same polymer, Jiang and co-workers[129] synthesized a pipe-like device, whose both ends were covered in PDEAEMA brushes. These brushes were reversibly activated upon CO_2 bubbling, thus opening or closing the channel entrances on command. It must be noted that this system finds applications not only in forward osmosis desalination, but also in sample filtration.

Forward osmosis desalination and the respective membranes will require more attention in the next years, especially with the increasing need for water. Their development and combination to CO_2 switchability is therefore expected to be of great help in the mitigation of the effects of global warming.

2.3.4.4 Switchable initiators

As already mentioned in chapter 2.3.4.2, switchable initiators have also been reported as a means to control their activity or solubility upon triggering with an external stimulus. The two most common of such molecules are VA-061 and VA-044, which are the base and the hydrochloride of the same compound (**Figure 12**). VA-044 only becomes CO_2 switchable after neutralization with a base. The mechanism behind the initiation step is not of switchable nature, but identical to the degradation mechanism of typical azo initiators like AIBN.[130] The difference between both mentioned VA-initiators and AIBN is the residual groups next to the N=N double bond.
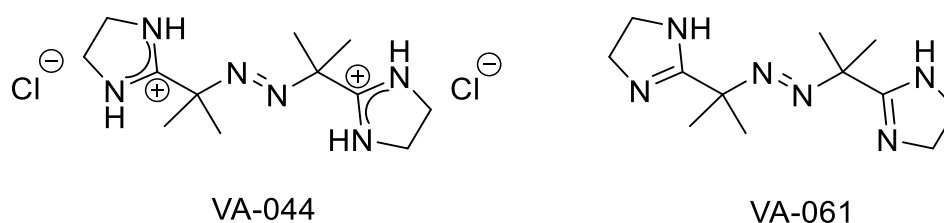
Figure 12 Structures of VA-044 and VA-061.

The remaining imidazole rings then act as surfactant, causing agglomeration in the deactivated state (neutral form). By CO_2 exposure in aqueous media, the basic imidazoles are protonated and form a salt with bicarbonate anions, thus creating a repelling effect between the latexes, and followingly causing their redispersion in water. As the 10 h half-life decomposition temperature of VA-061 is just 61 °C, reactions and polymerizations can be initiated easily under a CO_2 atmosphere, for instance the during surfactant-free polymerization of polystyrene in water described by Su *et al.*[131] However, many other polymerization require higher temperatures, which are not suitable for these compounds. The degradation of the initiator is favored by heat; however, it was already mentioned that also decreases or even reverses the addition of CO_2 to the nucleophilic compounds. This effect causes a diminished stabilization of the latexes, resulting in the formation of bigger polymer aggregates and lower polymer efficiency.[107]

While CO_2 switchable initiators clearly facilitate several polymerizations while being simultaneously being able to stabilize emulsions, the CO_2 employed for this process is ultimately released again into the environment. Therefore, in the next subsection, a few examples for the capture of CO_2 will be discussed.

2.3.4.5 CO$_2$ capture

Connected to the rising greenhouse gas concentration in the atmosphere, CO$_2$ capturing is a concept gaining great importance.[132] Therefore, new systems are developed to covalently bind CO$_2$ into materials reversibly. Many of them feature polymers or copolymers with DMAEMA,[133] but also representatives with acrylamides or amidines,[134] all of which are able to bind CO$_2$ under mild conditions. Zhou and co-workers produced porous polymer networks for CO$_2$ capturing on amines, increasing the capture efficiency even at low pressure. SPS system are also being employed for the same purpose. These systems especially designed for CO$_2$ capture were named CO$_2$-Binding Organic Liquids (CO$_2$BOLs), and typically consist of compound groups such as alkanolguanidines, alkanolamidines or various amines.[68],[135] While the mentioned examples are being used for flue gas applications, capture from high pressure streams is not ensured because of the required heating for sorbent regeneration. The Heldebrant group therefore introduced an SPS capable of releasing CO$_2$ upon pressure drops.[136] The proposed system showed to successfully capture the gas both chemically and physically, however with the disadvantage of possessing low CO$_2$-selectivity in mixed gas streams.

Conclusively, this chapter has given a broad overview of the major CO$_2$ switchable solvent systems (SPS, SHS and SW), as well as the most common materials, which have been combined with CO$_2$ switchability. Additionally, many applications examples were given to describe the huge advantages offered by this system and the vast potential of still researchable areas.

2.4 Hydroxamic acids and the Lossen Rearrangement

2.4.1 Hydroxamic acids

The first synthetic route to hydroxamic acids was developed by Heinrick Lossen in 1869 using ethyl oxalate and hydroxylamine to form oxalohydroxamic acid.[137]

The standard synthetic procedure for the synthesis of hydroxamic acids is the reaction of carboxylic acids or esters with N,O-bisprotected hydroxylamine in aprotic solvents at low temperatures and in the presence of a base.[138] The use of protected hydroxyl amines leads to the need of long and intensive deprotection steps, resulting in the major drawback of this method: great yield loss. Another synthesis pathway also features a carboxylic acid, which is

first converted into an anhydride and then added to a hydroxylamine solution in methanol. The required workup is, however, rather time consuming, while purification *via* column chromatography is commonly required.[139]

As for their chemical properties, this compound class "hydroxamic acid" already suggests acidic properties, however, compared to their carboxylic acid counterparts ($pK_a \approx 4$), hydroxyamides possess higher pK_a values ($pK_a \approx 9$), making them weaker acids. The chemical properties of hydroxamic acids are not only dependent on the pK_a, but also on the keto-iminol tautomerism. **Figure 13** shows hydroxamate ions formed under basic conditions.[140]
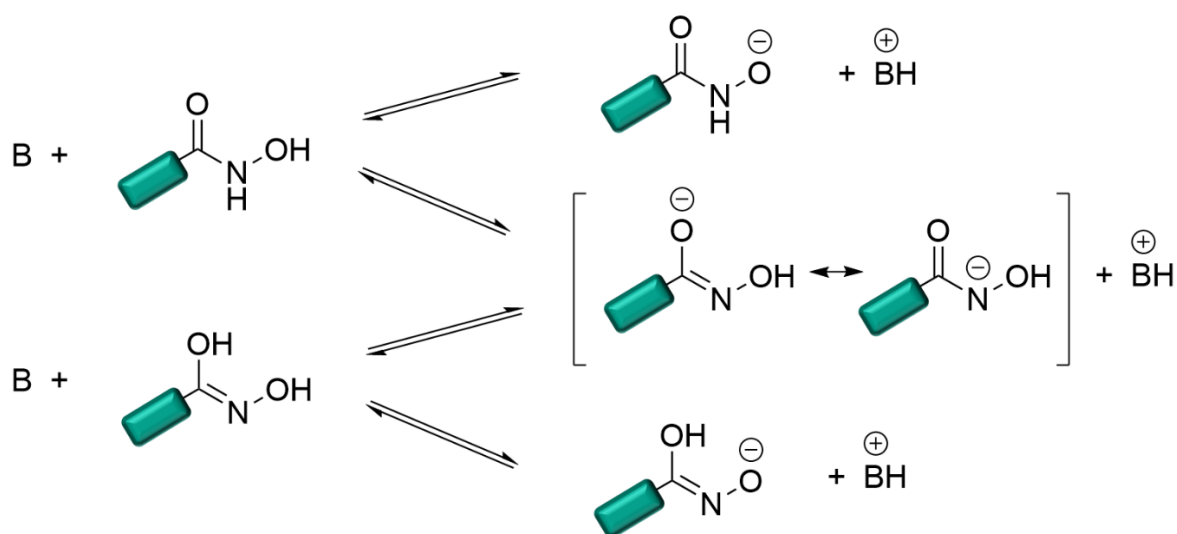
Figure 13 The four possible anions of hydroxamic acids.[141]

In biochemistry and coordination chemistry, the excellent behavior of hydroxamic acids as bidentate ligands is exploited, especially in combination with metals like lead or iron.[142] Specific types of hydroxamates exhibit high affinity to iron, thus earning the name siderophores.[143] The meaning of the latter term derives from the Greek word for "iron carrier", and the respective representatives are defined as the strongest ferric binding agents.[144] These compounds are able to render even the most chemically resistant and insoluble $Fe^{II/III}$-based blends and ores soluble. This is an ability, which was observed to be employed by the metabolism of microbes grown under iron-deficient conditions in order to assimilate iron from mostly indigestible sources like ores.[145] The separated iron ions bound to hydroxamates can thus be transported into the cell, where the metal is assimilated by the host organism. The same capability has been applied for antifungal[146] and antibacterial[147] purposes as the metabolic integration of iron after its removal from the complex also led to

cell apoptosis. Siderophores find numerous applications also in the medical field, for instance for therapy of Cooley's anemia, also known as β-thalassemia.[148] The patient is required to undergo numerous and constant blood transfusions caused by the lack of a β-protein in Hemoglobin (Hb). However, the large amount of blood transfers often leads to an excessive iron concentration in the bloodstream resulting in fatal organ failure. To prevent this, siderophores, such as hydroxamates, are added in the blood bags in order to reduce and stabilize the metal quantities in the blood.

The numerous aforementioned advantages of hydroxamic acids are, however, not the only properties of this interesting compound class. *N*-hydroxyamides and hydroxamates have also been widely exploited in the chemical field, especially as starting materials for the Lossen rearrangement.

2.4.2 Lossen rearrangement

In 1872, Wilhelm Clemens Lossen isolated phenyl isocyanate after heating benzoyl benzohydroxamate at a temperature above its melting point.[149] After identifying the product as a new substance, the rearrangement was named after him. With this method, not only isocyanates are accessible, but also ureas and carbamates. Since hydroxamic acids alone are not reactive enough, their O-acetylated derivatives are often used as reactants.[150] Mostly acid chlorides are used to yield O-acetylated hydroxamic acids, which are then eliminated as anions after the rearrangement (**Scheme 4**). Reports showed that also other rearrangements are possible, for example carbodiimidazoles,[151] dimethyl carbonate,[152] sulfonic bromides,[153] as well as O-sulfonylating compounds[154] as activating agents for hydroxamic acids.

R_1 = OMe, Cl R_2= Cl, OAc
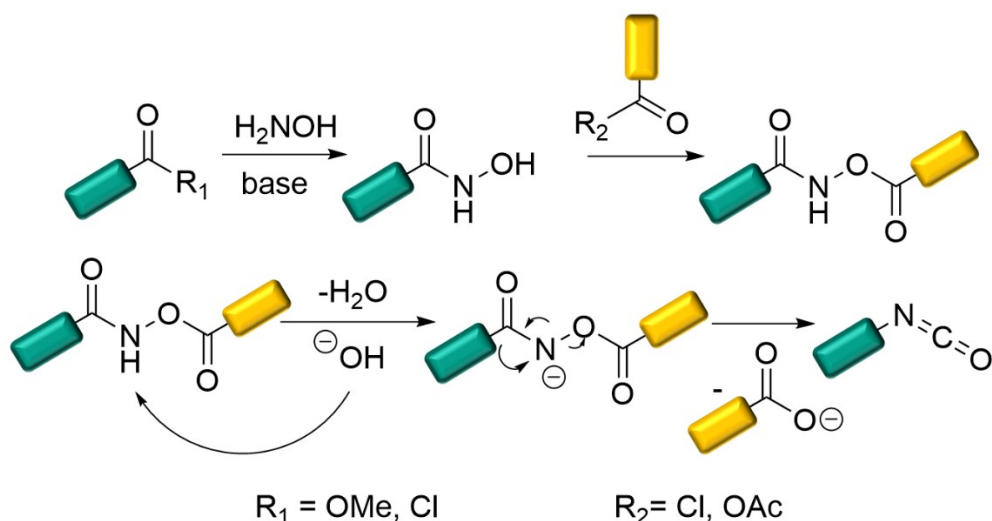
Scheme 4 Synthesis of hydroxamic acid derivatives and subsequent Lossen rearrangement.[149]

In 1974, it was commonly known that a hydroxamic acid rearranges in strongly alkaline solutions.[155] However, Honda and coworkers[156] only recently confirmed a self-propagating mechanism for the Lossen rearrangement, whereby the activating agents are reduced to catalytic amounts of a base. The authors declared that two hydroxamic acid molecules can protect each other under basic conditions, forming the isocyanate, which in return possesses the ability to protect another hydroxamic acid. An example is given in **chapter 4.1.3.**

Scheme 4 shows that through the Lossen rearrangement, isocyanates are obtained *in situ*. Other routes towards isocyanates, like the Curtius or Hofmann rearrangement (**Scheme 5**), are also known, as well as the phosgenation of amines, dehydrogenation of formamides,[157] the carbonylation (oxidative) of amines[158] and (reductive) of nitro compounds[159] and oxidation of isonitriles.[160] Compared to the other synthetic routes for isocyanates, the Lossen rearrangement is the one that received the least attention because of the marginally lower reactivity of hydroxamic acids.
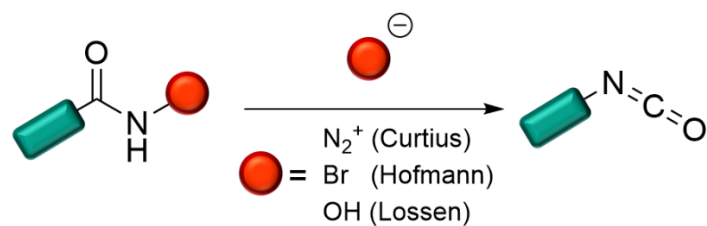
Scheme 5 General mechanism for the Curtius, Hofmann and Lossen rearrangements.[141]

In other methods to synthesize isocyanates, however, the components are typically neither renewable nor sustainable and most of them are also toxic. For instance, the Curtius rearrangement makes use of azides, respectively, which have been proven to be toxic.[161] Some azides are also explosive.[162] Meanwhile, the Hofmann variant requires the extremely harmful bromine.[163] In this work, we concentrated on the Lossen reaction because hydroxamic acids can be produced renewably and more sustainably and are not dangerous for the human health, a characteristic that defines this route possibly as the safest of the three rearrangements.

2.4.2.1 Products of the Lossen rearrangement

Isocyanates are known for their decomposition upon exposure to water.[164] The nucleophilic addition H_2O forms a highly unstable carbamic acid, which releases CO_2, ultimately yielding an amine (**Scheme 6**).
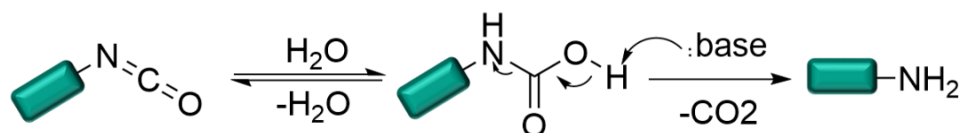
Scheme 6 Hydrolysis of isocyanates to amines.[141]

Isocyanates with aromatic substituents are more prone to degradation than their aliphatic counterparts with an aromatic amine obtained within minutes, compared to hours for aliphatic amines, respectively. This instability towards water is exploited when the amine is the desired product.[165]

Water is not the only nucleophile known to react with isocyanates. Alcohols and amines are also added to the electrophilic carbon of the isocyanate yielding carbamates and ureas, respectively. (**Scheme 7**).
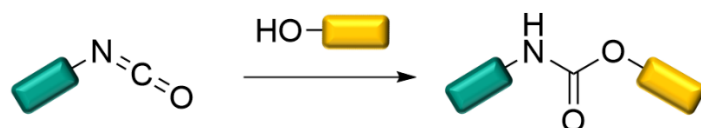
Scheme 7 Synthesis of carbamates from isocyanates.

Two industrially important representatives of carbamates are carbaryl or aldicarb. These two molecules have been widely employed as insecticides, since the active component is able to

deactivate the acetylcholine esterase, thus inhibiting neurotransmission in insects.[166] Meanwhile, other compounds, like fenoxycarb, find application as an insect growth regulator (IGR). IGRs hinder insects from reaching maturity, thus inhibiting their reproduction and thus also limiting the life cycle of the organism.[167] Strong carbamate-based insecticides work as nerve agents upon inhalation or dermal exposure and have also been considered for chemical weapon testing.[168] Similar compounds have also been reported to target melatonin receptors in humans, which could lead do disrupted sleep-wake cycles and to a decrease in blood pressure regulation.[169]

Ureas are molecules composed of a symmetric, weakly electrophilic amide functional group, enabling strong hydrogen bonding and the ability to activate numerous other functionalities, such as carbonyl-, sulfoxide-, or nitro-containing molecules.[170] On industrial scale, ureas find application as herbicides for general weed control in agriculture,[171] the first example being N,N-dimethyl-N'-(4-chlorophenyl)-urea, introduced by the company DuPont in 1952. Similarly important is the usage of urea derivatives as pharmaceuticals, as ureas are waste products of many living organisms,[172] but also show a large spectrum of biological activities.[173] For instance, specific aromatic and heterocyclic ureas were shown to be efficient in cancer treatment.[174] Moreover, also in the medical field, first treatments against human immunodeficiency virus (HIV) were tested with urethanes, for example with the drug Darunavir.[175]

In industry, the reactivity of isocyanates towards alcohols is of great importance for the synthesis of polyurethanes (PU, **Scheme 8**), a material that is typically sought as a foam, a rigid solid, or a highly elastomeric solid and therefore finds use in many different applications.
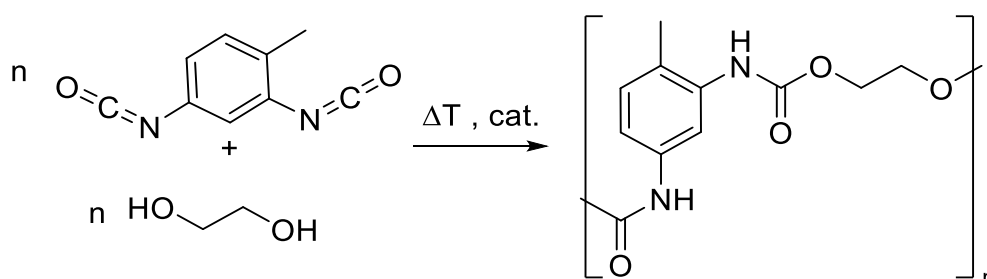
Scheme 8 Schematic synthesis of polyurethanes from toluene diisocyanate (TDI) and ethylene glycol.[176]

Further information about polyurethanes can be found in the **chapter 2.5**.

Conclusively, the Lossen rearrangement has been proven to provide a useful pathway towards interesting chemical compounds, such as ureas, carbamates and amines, through the *in situ* formation of isocyanates, a reactive functional group exploited for many applications, such as the synthesis of polyurethanes. However, this rearrangement is also hindered by some side reactions, which will be shortly discussed in the next paragraph.

2.4.2.2   Anomalous behavior in the Lossen rearrangement

The Lossen rearrangement is focused on producing isocyanates and the aforementioned derivatives. However, interesting side reactions have been reported in the literature. For instance, during the heating of benzoyllactohydroxamate in water, only three substances were isolated, namely acetaldehyde, ethyl alcohol and dibenzoyl urea, next to carbon dioxide and ammonia.[177] H. Yale explained this unexpected behavior as a side reaction based on the dissociation of the reactant to the acetaldehyde and benzoyl fulminate.[155] The latter compound is then suspected to rearrange towards an isocyanate, thus forming the urea. The authors also tested benzoyl glycolohydroxamate under the same conditions in combination with isoamyl alcohol. Unlike the previous example, the isolated products were formaldehyde and isoamyl allophanate.[178] The established mechanism was predicted and confirmed to feature the dissociation of the hydroxamate to cyanic acid and formaldehyde. Similar molecules with hydroxy groups in the α-position exposed to Lossen rearrangement conditions confirmed the hypothesis as the formation of cyanic acid was always accompanied by the isolation of ketones or aldehydes (**Scheme 9**).
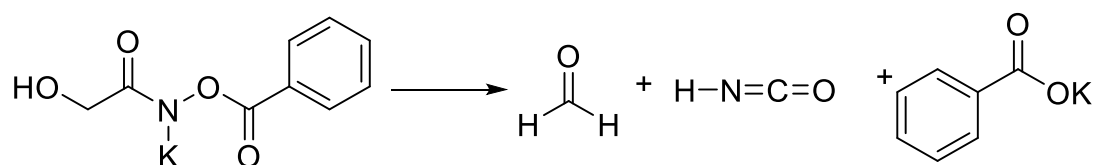
Scheme 9 Side reaction of the Lossen rearrangement over formaldehyde and cyanic acid as dissociation product.[155]

Another interesting experimental result was observed by Gastaldi after treating α-benzoylformohydroxamic acid oxime with phosphorus pentachloride in dry ether.[179] Instead of detecting the desired rearrangement product, which was the isocyanate, a different hydroxamic acid was isolated, namely phenyl cabamyl formohydroxamic acid. The authors

concluded that a Beckmann-type rearrangement is favored if the employed *N*-hydroxyamide possesses an additional oxime group, leaving the hydroxamic functionality untouched.

Lastly, different types of hydroxamates have been confirmed to be unable to undergo a Lossen rearrangement. Examples include arylsulfon-,[180] carbamyl-,[181] thiocarbamamyl-[182] and thiobenzo- [183] hydroxamic acids and their derivatives.

Although this paragraph described reported examples of an anomalous and unexpected behavior during the Lossen rearrangement, the numerous advantages provided by this reaction still dominate its drawbacks. The preparation of isocyanates is currently of great importance for the chemical and polymer field, especially during the last decades. In the following chapter, the use of isocyanates will be discussed further on a major polymer class: the polyurethanes (PUs).

2.5 Polyurethanes and Non-isocyanate polyurethanes (NIPUs)

2.5.1 Polyurethanes

Polyurethanes (PUs) are polymers composed of carbamate linkages, typically synthesized by the polyaddition of polyisocyanates with polyols (**Scheme 10**). This polyaddition reaction was discovered by Otto Bayer in 1937 at IG Farben and published in 1947.[184] This new class of materials showed various interesting properties, offering many advantages compared to the already known polymeric materials at the time, like increased flexibility and coating efficiency. Already during World War II, PUs in form of fibers and foams were employed as aircraft coatings[185] and their importance grew further, especially after commercialization of polyisocyanates in 1952.[186] A few years later, polyether polyols were introduced to the market by DuPont, closely followed by Dow Chemicals and BASF. Afterwards, many other chemical industries started their own polyurethane production, building the foundation of a commercial sector that is still growing, even in 2020.[187]
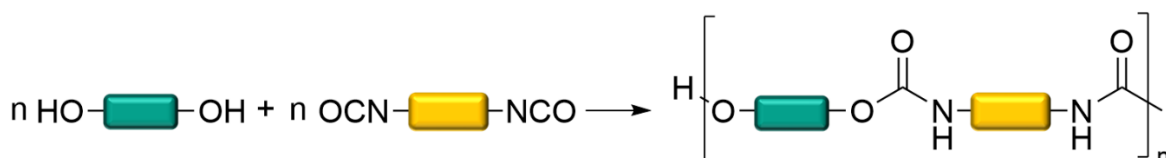
Scheme 10 standard synthesis of linear polyurethane.

Thermoplastic PUs (TPUs) are a category of interest as their broad range of properties also include a good processability.[188] These materials are usually crystalline block copolymers consisting of hard (mostly a rigid diisocyanate linked by a short polyol) and soft (in which the long polyol is dominant) segments. Most examples possess appropriate hydrolytic stability for outdoor uses as well as high impact resistance and good flexibility.[6] They exhibit different attributes depending on side groups, monomers, crosslinking degree and additives in the resin blend.[189] Additionally, the presence of water influences the crystallinity of the polyurethane, since the isocyanate decay caused by water leads to the formation of urea linkages instead of carbamates. Because of the lower solubility, these functionalities mostly tend to separate into hard segment phases.

As, however, the properties of PUs greatly derive from the employed monomers and can thus be optimized through different monomer combinations, they will be further discussed in the paragraphs regarding polyisocyanates and polyols (**chapter 2.5.2**).

Additionally, the polymer can be obtained as a foam,[190] either by the formation of CO_2 as side product due to traces of water, or because of the boiling of volatile substances (so called "blowing agents"), like chlorinated alkanes or hydrocarbons, present in the mixture during the step-growth reaction. Two types of foam are known: the "closed-shell"[191] and the "open-shell",[192] depending if the bubbles in the polyurethane retained their shape or burst open.[193] Rigid foams are the result of the first scenario, while softer and more elastic materials originate from the allowed airflow[194] of the "open-shell" model. These two models are not only observed in the presence of blowing agents, but also when certain surfactants are mixed in the blend. Depending on the design of the surfactant, the "open-"[195] or "closed-cell"[196] content can be maximized through stabilization of the respective cell type. In applications based on non-foams, the surfactants act as wetting and antifoaming agents, as well as for the elimination of surface imperfections. Foams are the most widespread form of PU as they make up around 67% of the whole polyurethane market.[190] The highly crosslinked rigid foams are mostly applied as noise and thermal insulation materials in buildings,[197] while the flexible foams, whose properties depend on the soft segments, are more suitable for furniture and packaging.[198]

In the industrial process, two (or more) liquid streams are converged, namely the isocyanate component and the polyol blend. The polyol blend also consists of, other than the reactant

and the catalyst, chain extenders, fillers, surfactants, stabilizers (UV, hydrolysis), pigments and crosslinkers, depending on the desired properties.[199]

Commonly used catalysts are tertiary amines, for instance DABCO or dimethylethanolamine, which increase the nucleophilicity of the alcohol functionality, but also Lewis acids like dibutyltin dilaurate, that enhance the electrophilicity of the isocyanate.[200]

It is worth mentioning that, although PUs are non-hazardous, chemically inert and are non-carcinogenic and nontoxic, they are still flammable. The polymer can be ignited by open flame and its fumes contain carbon monoxide, as well as hydrogen cyanide.[201] Therefore, most of commercially available products are enriched with flame retardants like diphenyl cresyl phosphate and dimethyl propyl phosphonate. Other additives include UV stabilizers,[202] for instance benzophenones and benzotriazoles or cyanoacetate esters, organic and inorganic colorants[203] such as diazo dyes and titanium dioxide, respectively, as well as hydrolysis stabilizers like carbodiimides, epoxides phenyliminooxazolidines.[204] Additionally, oxidation stabilizers are added to prevent core scorching, defined as darkening of the material caused by oxidative processes, mostly mediated by high temperatures.[205] The most common compounds are thioethers, alkylated anilines and sterically hindered phenols.[206]

Meanwhile, stronger materials can be obtained *via* isocyanurates (**Scheme 11**), which were first synthesized by Hofmann in 1858[207] and characterized, much later, in 1965.[208] By employing specific catalysts, like phenol Mannich bases[209] or potassium acetate[210] and an excess isocyanate, the trimeric rings provide a robust structure, which is then reflected in the overall rigidity of the polyurethane. Including isocyanurate in polyurethane foams does not only increase the toughness, but also makes the material more resistant to heat.[211] For instance, Ball *et al.*[211] showed that an isocyanurate foam with 20% isocyanate linkages exhibited a 5% weight loss around 280 °C, while temperatures for MDI- and TDI-based polyurethanes possessed a $T_{d5\%}$ at 220 °C and 240 °C. Decreasing the urethane content led to $T_{d5\%}$ of up to 340 °C. An overview on the mechanical properties of poly(urethane-isocyanurates) elastomers was published in 2002 by Samborska-Skowron and Balas.[212] The authors described the almost linear decrease in Young's modulus from 32 MPa to 3.5 MPa, based on a isocyanurate concentration of 540 mol/m^3 compared to the pure polyurethane.
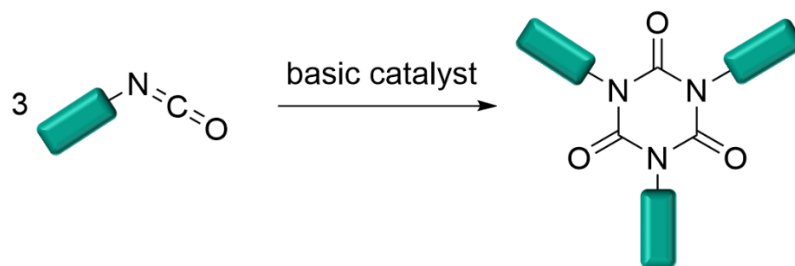
Scheme 11 Schematic representation of isocyanurate formation under basic catalysis.

2.5.2 Polyisocyanates and polyols

The choice of monomer is of vital importance to the overall traits of the final products. The isocyanate component can be divided into the aromatic and aliphatic subclass. Nowadays, over 90% of commercially available PU is produced as elastomers, thermosets, adhesives and plastics, and is composed of purely aromatic polyisocyanates,[189] as their mechanical properties and reactivity are superior compared to their aliphatic counterparts.[213] This statement is nonetheless not aimed to underestimate the significance of the latter group. Instead, aliphatic polyisocyanates exhibit a greater UV and heat resistance, making them especially suitable as coatings.[214]

Compared to polyisocyanates, polyols (**Figure 14**) are also separated into different subgroups, but their chemical composition and molecular weight impose an even greater influence on the final material properties.[215] The first category, polyether polyols, are mainly produced from oxiranes,[216] with the first and most important building blocks being ethylene or propylene oxide (EO and PO), resulting in very cheap materials with high hydrolytic stability. In addition, the resulting PUs exhibit high flexibility and performance at low temperature. However, at higher temperatures, the PU tends to degrade due to oxidation with atmospheric oxygen.[217] Poly(THF) is another important representative employed during the synthesis of polyurethanes, used as soft segment to increase chain mobility of the material.[218]

The second group is represented by polyester polyols, which are synthesized by polycondensation of polyols and dicarboxylic acids or anhydrides.[219] Contrary to ether-based polyols, esters are resistant both to heat and UV irradiation, and are thus suitable as paints and coating materials.[214] Their outstanding thermal stability also allows for employment as flame retarding foams, but most polyester polyols are obtained in glassy/crystalline states or as highly viscous substances, a major disadvantage in the industrial production, as the chain

mobility is lowered, thus slowing the reaction.[220] This is a major issue, since only high conversions yield high molecular weights in step growth polymerizations. Polycaprolactone polyols are also featured in this category, even if their synthesis differs from polycondensation.[221] Even if the production costs are higher, the reaction conditions of the lactone ring-opening are significantly milder and result in lower dispersities, defined functionality and higher reproducibility.[189] The polyesters obtained *via* this method show lower viscosities and enhanced hydrolytic stability than other typical polymers, like adipate polyesters polyols.[222] Combined with their excellent resistance to outdoor conditions, like heat, oxidation and UV irradiation, these macromolecules offer outstanding properties in many desirable applications.

Finally, polycarbonates with terminal hydroxyl groups have been thoroughly researched in the literature as polyol component. These compounds are obtained either by transesterification of commercially available carbonates (usually dimethyl carbonate or diphenyl carbonate) with glycols or *via* copolymerization of oxiranes with CO_2.[223] They exhibit uniquely high tear and tensile strength, for instance a PU composed of polypropylene carbonate exhibits Young's moduli around 300 MPa compared to 10 MPa for pure polypropylene oxide polyols.[224] Meanwhile, the chemical stability against hydrolysis, as well as their resistance towards fuels, oils and light irradiation of the respective NIPU is also significant. Alagi *et al*. demonstrated that the carbonate polyols exhibit lower corrosion current densities (I_{corr} in solution $1.852E^{-8}$ in NaOH and $1.412E^{-6}$ in HCl) than the respective polyether polyols (I_{corr} in solution $5.826E^{-8}$ in NaOH and $3.105E^{-6}$ in HCl).[224] The concentration of each medium was reported to be 3.5 wt%, and the unit for I_{corr} is A/cm^2. However, the production of polycarbonates results in a more expensive process than for the first two categories. The higher viscosities of these polyols also reduce the attractiveness for the industry, as the need to contrast the low chain mobility has to occur at high temperatures and inert atmosphere.[225]

Polyols

polyether
(from propylene oxide)

polycarbonate
(from ethylene oxide)

polyester
(from adipic acid and butanediol)
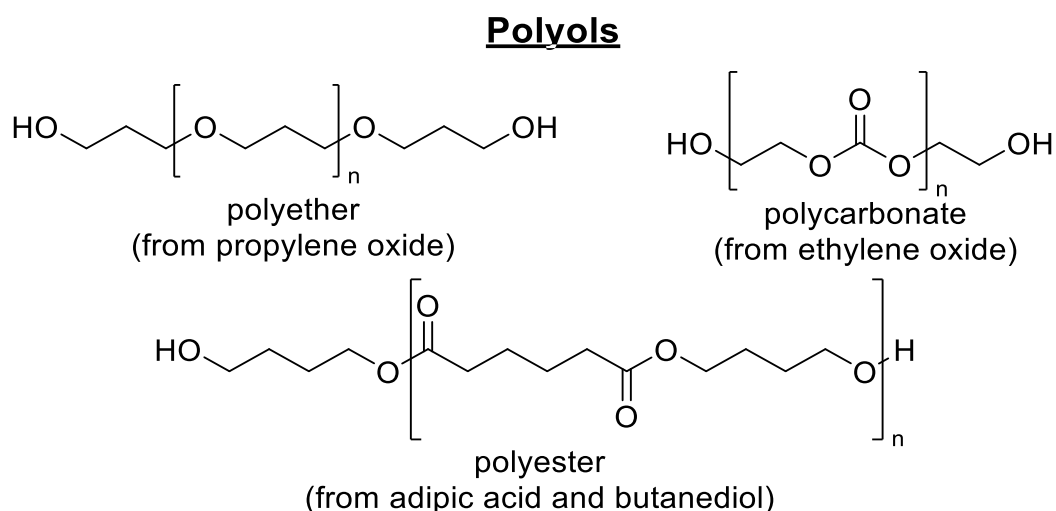
Figure 14 Most common polyol classes employed for polyurethane synthesis.

The variation and combination of building blocks result in properties that are responsible for the versatility of PUs, thus allowing for tailored design towards desired materials. Examples include construction materials,[226] high performance adhesives,[227] furniture coatings,[228] and hard plastic parts,[229] with an increase of the annual demand from 16 million (2016) to 20 million tons (2017)[189] worldwide.

2.5.3 Non-isocyanate polyurethanes (NIPUs)

Despite the non-toxic nature of the final PUs, isocyanates, one of their main components, are known to cause substantial damage to the human health, both *via* respiratory[230] as well as dermal[231] exposure, leading to conditions ranging from asthma and respiratory sensitization to hypersensitivity pneumonitis, all of which may be fatal. Additionally, the industrial preparation of isocyanates requires the use of highly toxic phosgene, a gaseous substance which was employed during World War I as chemical weapon.[232] Exposure through inhalation can lead to pulmonary edema, heart failure, chronic bronchitis and emphysema.[233] Its odor can be detected starting from 0.4 ppm, a concentration four times higher than it is safe to inhale, and no antidote exists so far.[16] Due to these severe effects on the human body, phosgene was banned by the Geneva protocol in 1925. Thus, it is obvious that the development of milder and more sustainable synthetic routes towards PUs have become of great interest by many research groups.[234] A representation of the increasing importance of PU synthesis alternatives is given in **Figure 15**.
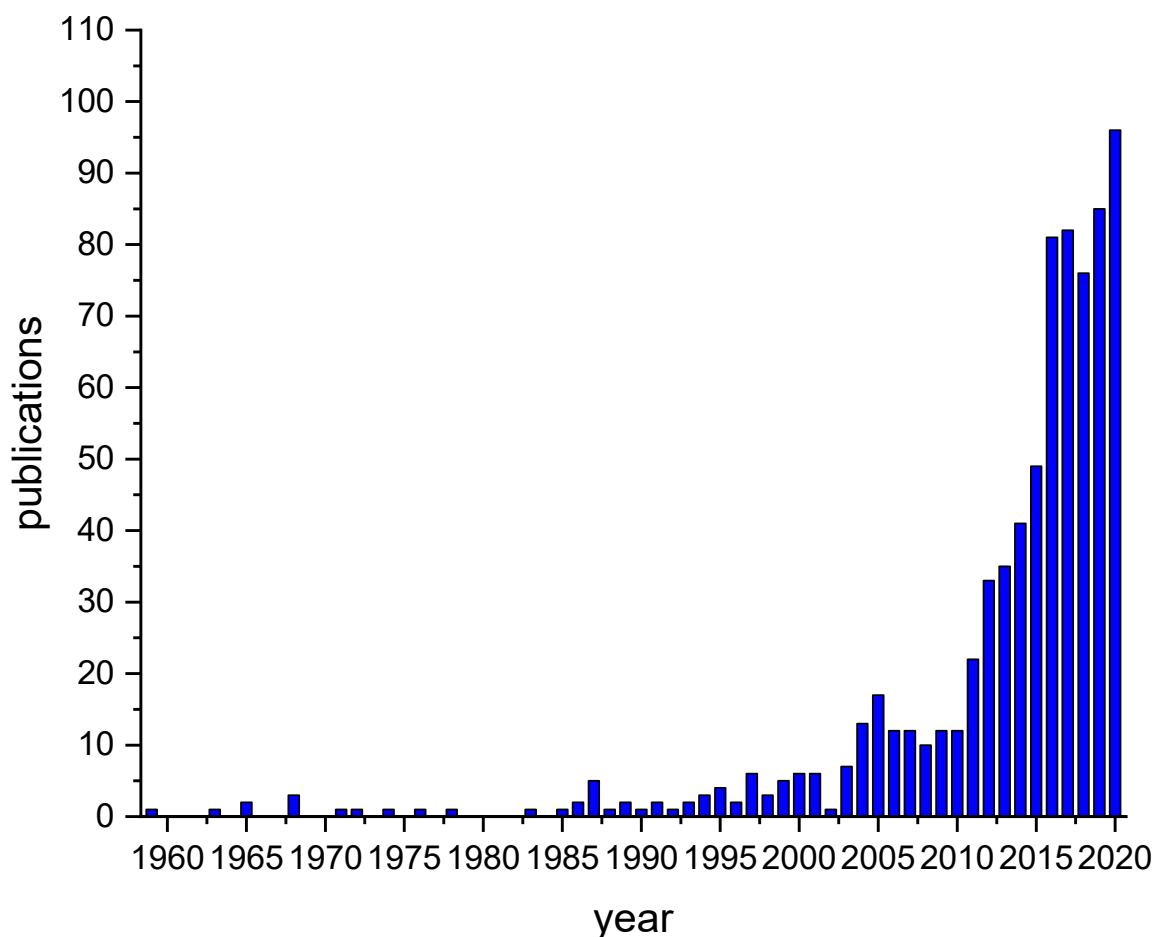
Figure 15 Number of publications per year containing the concept "non-isocyanate polyurethane" from 1959 to 2020 (Scifinder search "non-isocyanate polyurethane", retrieved on 05.02.2021).

The same polymer class has therefore been divided into two different subgroups depending on the synthetic employment of isocyanates or of substitutes thereof. The newly defined "non-isocyanate polyurethanes" (NIPUs) have been prepared in multiple ways, shortly described in **Figure 16**.
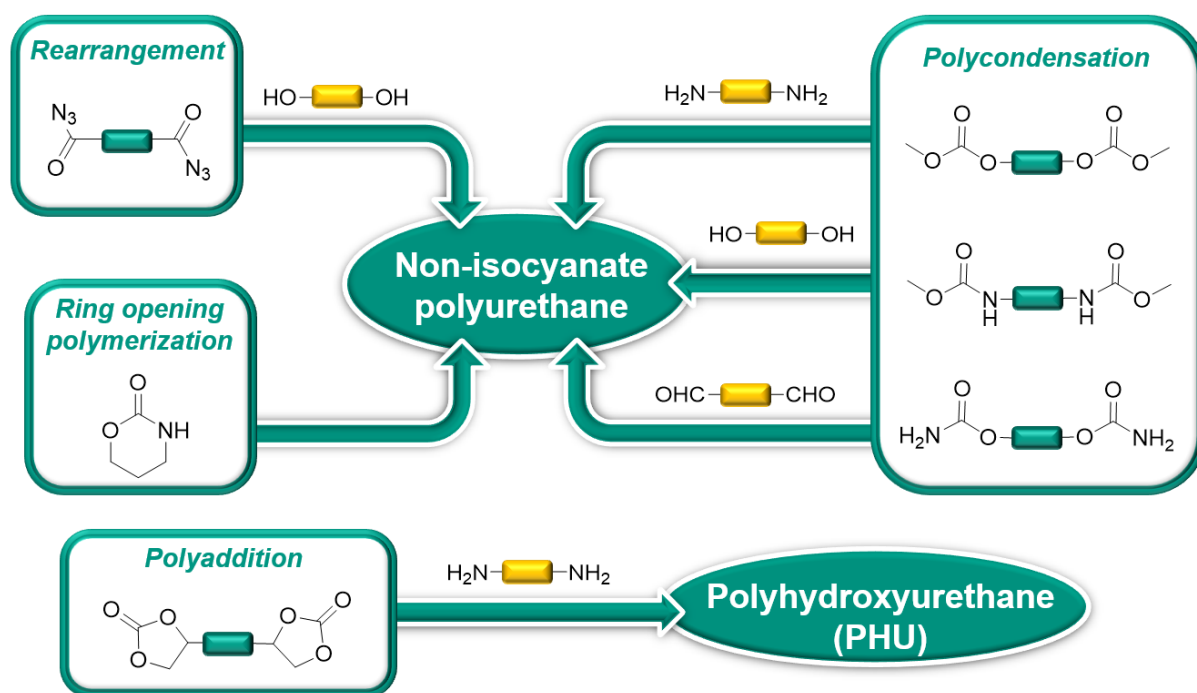
Figure 16 Schematic representation of reported routes towards non-isocyanate polyurethanes (NIPUs) and polyhydroxyurethanes (PHU) (adapted from[234c]).

The polycondensation route of polychloroformates[235] and polycarbonates[236] with polyamines or of polycarbamates[237] and polycarbamoyl chloride with polyols are well known, but it possesses the drawback to require the use of phosgene at some stage during their synthesis. Additionally, these pathways possess drawbacks for industrial applications, because of the formation of side products like hydrogen chloride during the polycondensation. A more sustainable approach was published by the Meier group, in which carbamate precursors for NIPUs were prepared from renewable materials, namely from castor oil *via* the Lossen rearrangement.[238] From ricinoleic acid, two *bis*(methyl carbamates) were obtained in satisfactory yields around 70%, which formed polyurethanes with molecular weights up to 25 kDa in combination with four renewable diols of different chain lengths. The same group was also able to produce fully sustainable NIPUs from the polycondensation of limonene-derived methyl carbamates and diols.[239] These NIPUs were obtained by first functionalizing limonene to a diol or *bis*(methyl carbamates) *via* thiol-ene reaction, as depicted in **Scheme 12**.
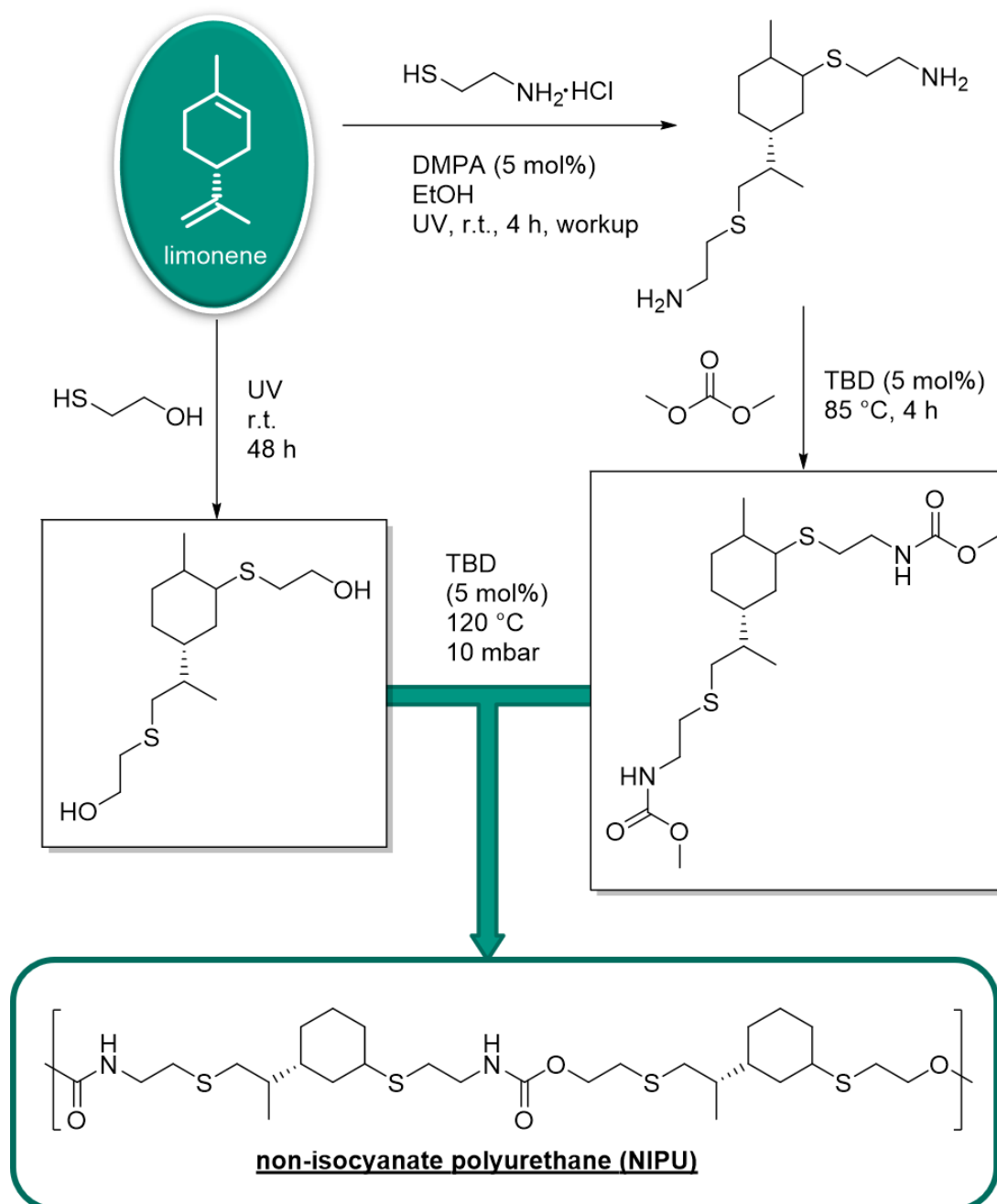
Scheme 12 Schematic synthesis of limonene-based NIPUs. In the first step, the terpene is subjected to thiol-ene functionalization to obtain either the diamine or diol. The diamine is further reacted with DMC to yield the respective *bis*(methyl carbamate). The polycondensation of diol and *bis*(methyl carbamate) ultimately leads to polyurethane formation (adapted from [239] and [240]).

The obtained polymers possessed molecular weights up to 13 kDa and showed amorphous to semicrystalline structures, as confirmed by DSC analysis. The same approach was also employed for the production of limonene-based polyamides.

Theoretical background

Interestingly, NIPUs have also been prepared *via* ring-opening polymerization of 6- or 7-membered cyclic carbamates[241] or aziridines,[242] without any side products (**Scheme 13**).
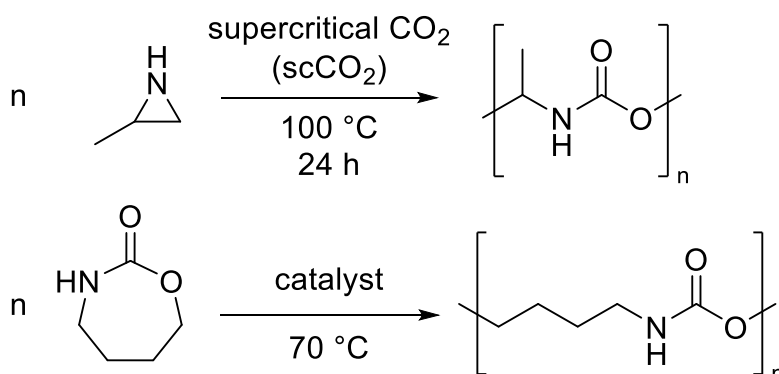
Scheme 13 Schematic representation of the ring-opening polymerization of aziridines and cyclic carbamates to form the respective NIPUs.

Suitable for the ring-opening polymerization (ROP) of cyclic carbamates are either acid[243] or organometallic catalysts.[244] Unfortunately, the reaction conditions are usually harsh and the starting materials are either toxic, like in the case of aziridines,[245] or industrially synthesized from phosgene (cyclic carbamates).[246] Related to the previous chapter, the three rearrangement approaches (Lossen, Curtius, Hofmann) have also been topic of discussion for the synthesis of NIPUs. As explained before, the Curtius and Hofmann reactions make use of toxic azides[247] and bromines, while the Lossen variant employs the more benign and stable hydroxamic acids. In all cases, an isocyanate is formed *in situ*, which then reacts with a polyol towards the formation of a polycarbamate.

The most sustainable pathway toward NIPUs is represented by the polyaddition of polyamines to polycyclic carbonates,[248] and will therefore be discussed more in detail. The required *bis* cyclic carbamates are readily prepared from renewable resources. For instance, glycerol carbonate has been esterified with a diacid[249] or acid chloride.[250] Another example includes the use of fatty acids, which are converted in the respective *bis* carbonates in a four-step procedure, including the epoxidation of terminal alkene functions and subsequent carbonation with CO_2.[251] Another interesting preparation procedure was first described in 2012 by Rokicki *et al.* featuring the carbonation of erythritol to the respective erythritol *bis*(carbonate) (EBC) with dimethyl carbonate under basic conditions.[252] However, the yield did not exceed 5% at that time as it was considered a side product of tetrahydrofuran derivatives. Other groups improved the reaction conditions by employing diphenyl carbonate

and a metal catalyst to isolate the product in the range of 80% to 90% yield after 19 h at 120 °C and 30 mbar.[253] Although the authors determined the impossibility to synthesize EBC efficiently from DMC, the Meier group published a much more sustainable route in DMC shortly after.[254] The reaction conditions were optimized to be performed at 60 °C at 350 mbar for just two hours in the presence of catalytic amounts of TBD (**Scheme 14**).
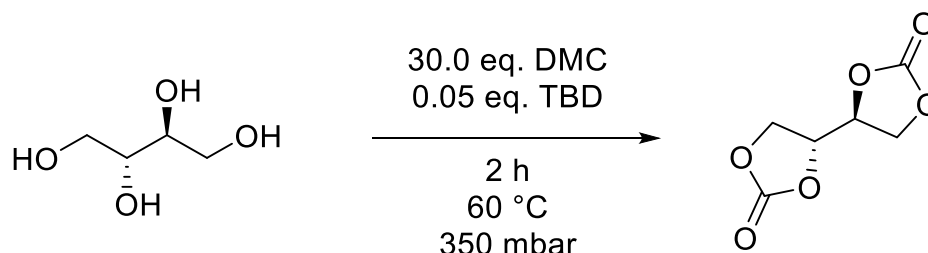
Scheme 14 Synthesis of erythritol bis(carbonate) from erythritol (adapted from [254]).

Interestingly, the reaction was performed in a rotary evaporator, while the product was obtained in 90% yield after simple filtration and the filtered residue was recycled up to 5 times by simply adding more erythritol.

The polyaddition of the *bis*(carbonates) with diamines occurs at high temperatures, typically around 100 °C, as kinetic studies have shown that the reaction accelerates with temperature.[255] The final polyhydroxyurethane (PHU) differs in properties from classical PUs, as the hydroxyl groups on the side chains are capable of undergoing intra- and intermolecular hydrogen bonding with the carbamate functionality, thus increasing the polarity and their hydrolytic stability.[256] It is also worth mentioning that the opening of the carbonate ring occurs in two directions leading to both primary and secondary alcohols (**Scheme 15**).
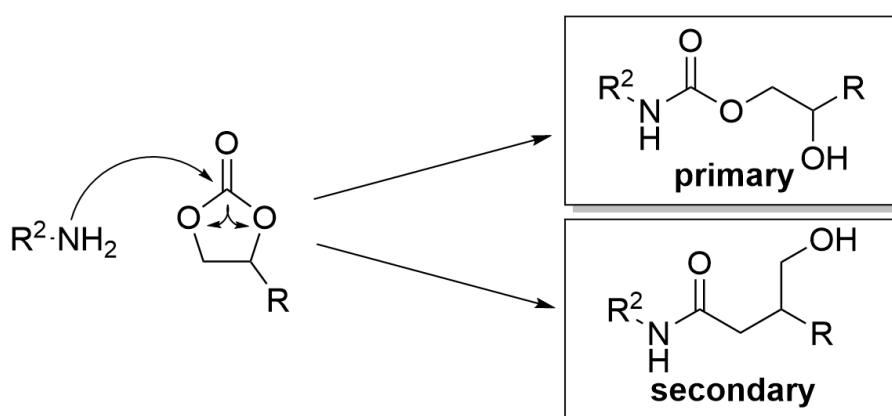
Scheme 15 Formation of primary or secondary alcohols after the nucleophile-mediated ring opening of a cyclic carbonate.

The formation of secondary alcohols is favored and the ratio of isomers was shown to be dependent on the solvent, alkyl chain length and EWGs at the carbonate,[257] rather than being driven by temperature.[258] For instance, in DMSO, the percentage of primary hydroxyl groups was higher than in toluene. Although this polyaddition is the most sustainable polymerization of all listed examples, it is limited by the low reactivity of the cyclic carbonate, which often leads to low molecular weight polymers. It has been speculated that this behavior derives from the hydrogen bonding between amine and cyclic carbonate.[259]

Due to environmental regulations and issues, the recycling of polyurethanes has gained increasing attention,[260] albeit it is not an easy task due to the stability and resistance of many of the produced PU types. However, some techniques have been reported and are divided in four categories: mechanical recycling, chemical, as well as thermochemical processing and energy recovery.[261] The first group describes the physical treatment of PUs, such as compression and injection molding, as well as regrinding. Meanwhile, chemical and thermochemical processing focus on the treatment of PUs for the generation of chemical feedstock making use of methods like glycolysis, hydrolysis, fractionation, aminolysis, hydrogenation or pyrolysis, in which polyols are reobtained and recycled for further uses.[262] The energy recovery is achieved by combustion of the PU and related production of heat, fuels and oils.[263]

In conclusion, polyurethanes have been shown to possess great versatility and tunability *via* many parameters, such as choice of monomers, additives, polymerization method, crosslinking degree and the presence of urea or isocyanurates in the material. Additionally, numerous methods have been developed for the formation of PUs, with or without the use of isocyanates, and the isolated materials are obtained in the desired forms, e.g. foams. The advantages listed in this chapter and the wide range of applications covering many fields therefore set this polymer class as one of the most important representatives in polymer chemistry.

2.6 Thiol-Ene "Click" Reaction

2.6.1 "Click" chemistry

The term "click chemistry" was introduced by K.B. Sharpless in 1998, but was first fully evaluated three years later by Sharpless, Kolb and Finn.[264] The idea was born from the observation that, in nature, a large number of molecules possess great affinity for carbon (**C**)-heteroatom (**X**) bond formations, rather than carbon-carbon bonding. Additionally, the spontaneity of these natural formation processes is what captured the attention of researchers. The most common examples are macromolecules connected by **C-X-C** bonds, such as proteins (**X**=N) or polysaccharides (**X**=O), originating from the condensation of smaller molecules. Therefore, the aim of this particular type of chemistry, *i.e.* "click"-chemistry, is to reproduce similar linkages in the laboratory. To officially establish their concept, Sharpless *et al.*[264] published the prerequisites for a "click" reaction as follows:

1. Modular, wide scope
2. High yields
3. Generation of only inoffensive by-products, which can be easily removed without chromatographic purification methods
4. Stereospecific reaction (but not necessarily enantioselective)
5. Simple reaction conditions (e.g. insensitivity to oxygen or water)
6. Readily available starting materials and reagents
7. Avoidance of solvent or the employment of solvents which are benign (e.g. water) or readily removable
8. Simple product isolation

The driving force is of thermodynamic nature. Values for the Gibbs free energy are usually lower than −84 kJ/mol, which often lead to a single reaction product and near quantitative yields.[264] Therefore, this field of organic reactions has gained the attention of many researchers, increasing the number of publications to a total of over 18,500 at the end of 2020, with a peak in the year 2014 (**Figure 17**).
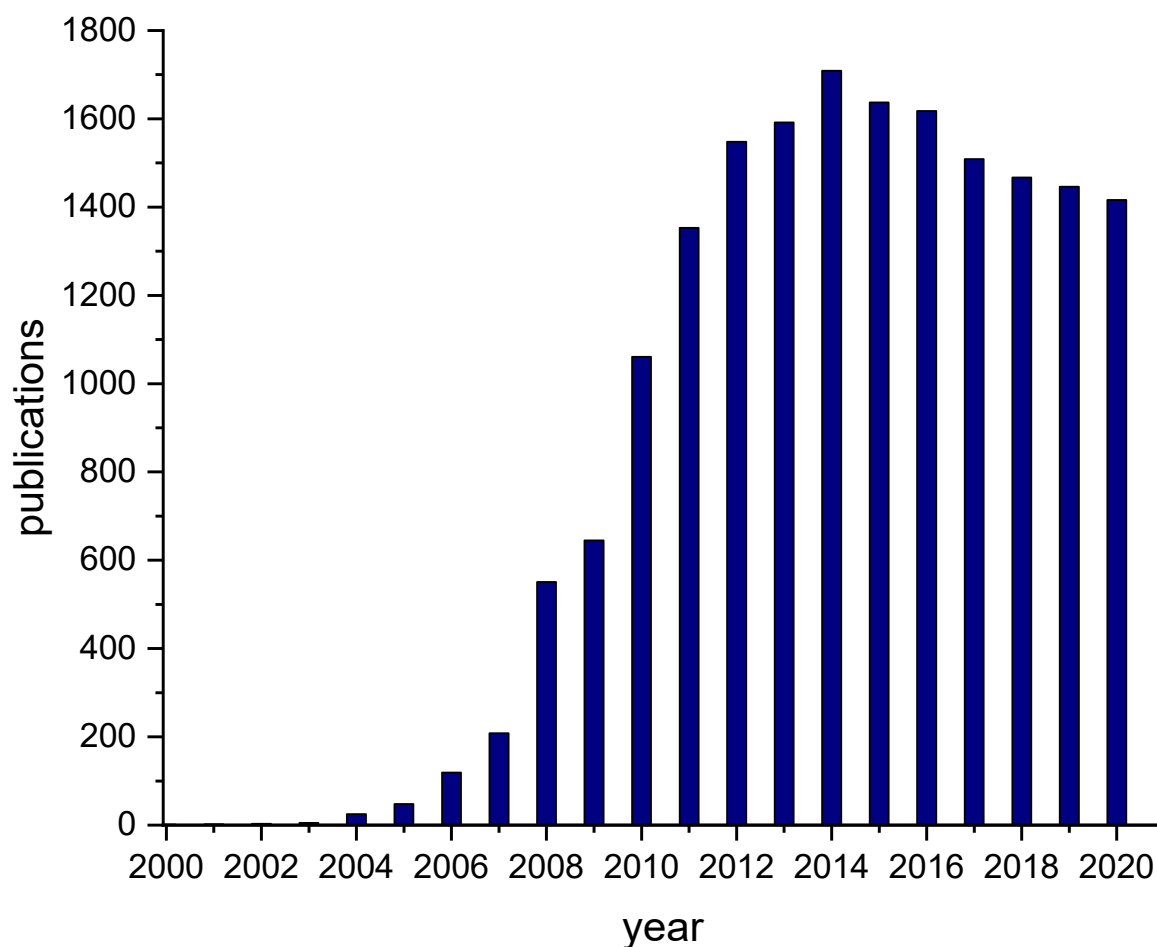
Figure 17 Publications containing the concept "click chemistry" over the last decades (Scifinder-n search "click chemistry", retrieved on 07.07.2021).

Four major classes of "click" reactions have been established and are schematically shown in **Figure 18**:

1. Cycloadditions
2. Nucleophilic ring-opening reactions
3. Additions to C-C double bonds
4. Non-aldol carbonyl reactions

The first category[265] features the 1,3-Huisgen dipolar cycloaddition[266] as its most renowned example, but also includes hetero-Diels-Alder reactions.[267] Meanwhile, nucleophilic ring-opening reactions make use of the strain of an electrophile, such as aziridines[268] or epoxides,[269] to force ring-opening *via* a nucleophile. Additions on unsaturated carbons[270] are fundamental in "click chemistry", since olefins are easily accessible, cheap and come with a wide variety of different functional groups. The oxidative addition on the double bond creates a stable, but also reactive intermediate, like an epoxide,[271] which can be further

functionalized. Lastly, carbonyl-type chemistry, centered around the partial positive charge at the carbonyl carbon and its susceptibility towards nucleophilic attacks entails reactions such as the formation of urea,[272] amides[273] and heterocycles.[274] The reason behind the exclusion of aldol reactions from "click" reactions is the low thermodynamic driving force, which requires long reaction times and in most cases a *push*, such as the addition of a basic or acidic catalyst, to achieve high yields.
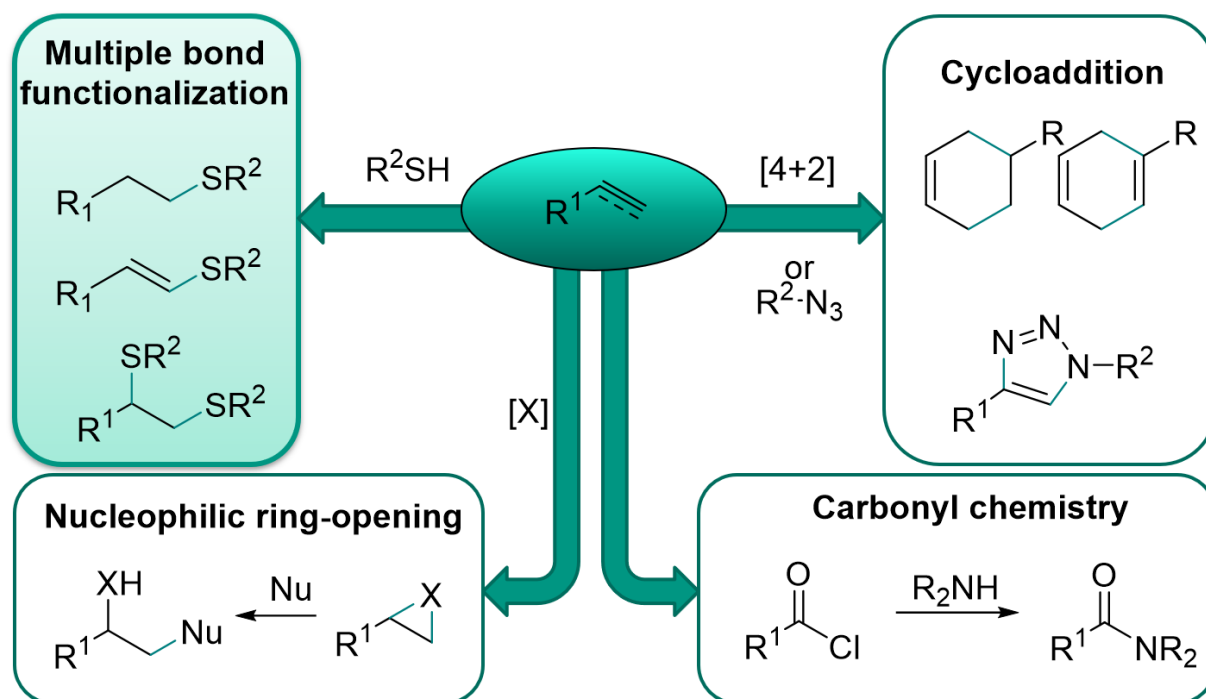
Figure 18 Common "click" reactions.[275]

Different types of "click" chemistry and their basic features have been introduced in this chapter. The next section will focus on one category, namely the multiple bond functionalization, more specifically *via* the thiol-ene reaction.

2.6.2 The thiol-ene reaction

An aspect of the work described in this thesis is concerned with thiol-ene chemistry, a reaction which will be introduced here and is schematically depicted in **Scheme 16**. The organic reaction between an alkene and a thiol is called "thiol-ene". Although it was first described in 1905,[276] its use as an important reaction only became evident in the last few decades after the introduction of the concept of "click chemistry".
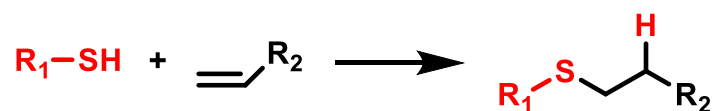
Scheme 16 Schematic representation of the thiol-ene reaction.

The number of relevant publications per year are shown in **Figure 19** (research topic "thiol-ene" in SciFinder). The rise in interest since the 1990s is based on the properties of this reaction, including the fast addition rate, high yields and regioselectivity.[277] For such characteristics, next to the large thermodynamic driving force, the thiol-ene reaction is also considered a "click" reaction.[278] Especially the light-mediated variant is a topic of extensive research, as it carries both the advantages of photoinduction, which is the activation at specific times and locations, and of "click" reactions.[279]
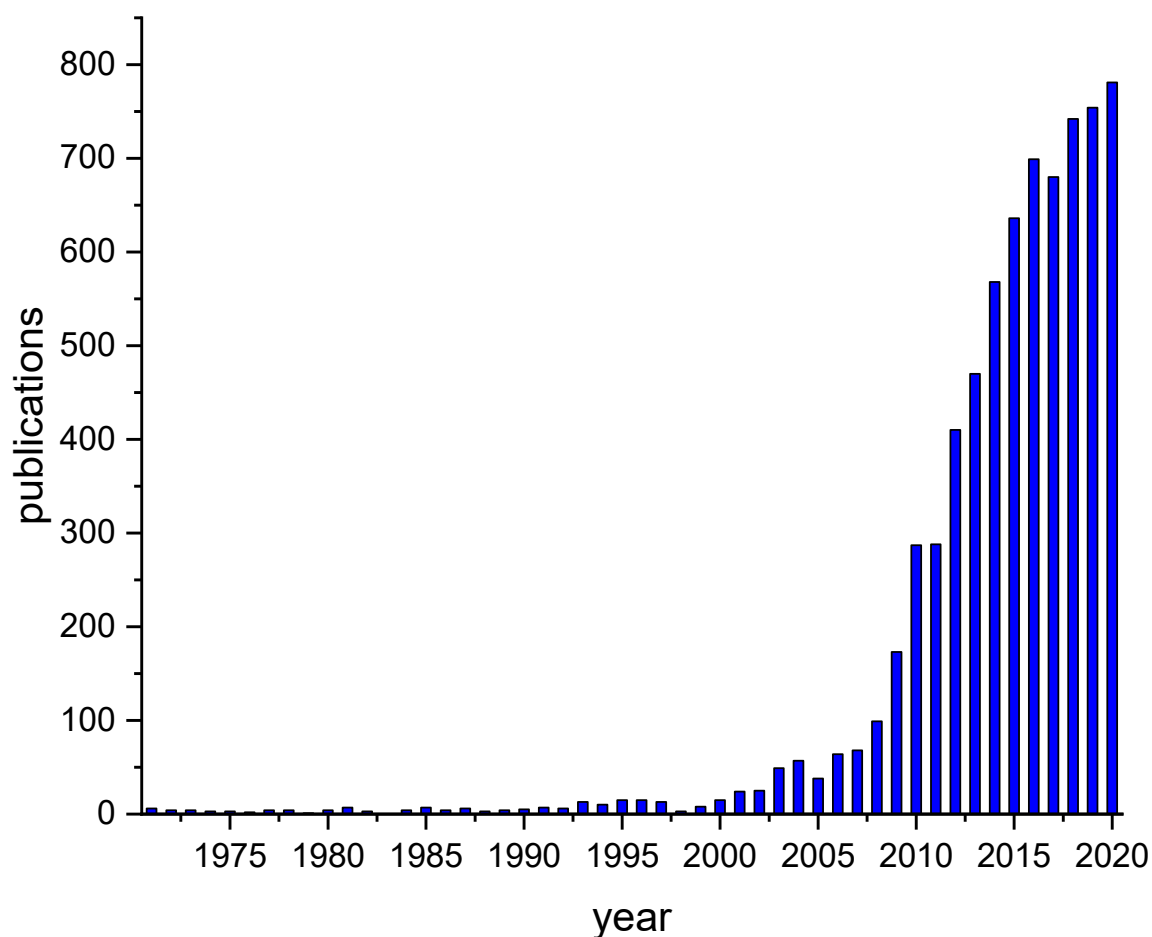
Figure 19 Publications per year containing the concept "thiol-ene" (Scifinder search "thiol ene", retrieved on 05.02.2021).

The thiol-ene reaction has been shown to proceed *via* two different mechanisms:

1. Radical addition[275]

In this category, radicals are formed in the first step of the reaction. This can be achieved by light or heat, as well as in the presence of a radical initiator, such as azobisisobutyronitrile (AIBN) or 2,2-dimethoxy-2-phenylacetophenone (DMPA). The thiyl radical (**Scheme 17**) reacts with the double bond in an anti-Markovnikov addition, forming the more stable carbon-centered radical. Finally, a hydrogen radical is removed *via* chain transfer from another thiol, which can continue the reaction with another alkene.

k_{ct} = chain transfer rate constant
k_p = propagation rate constant
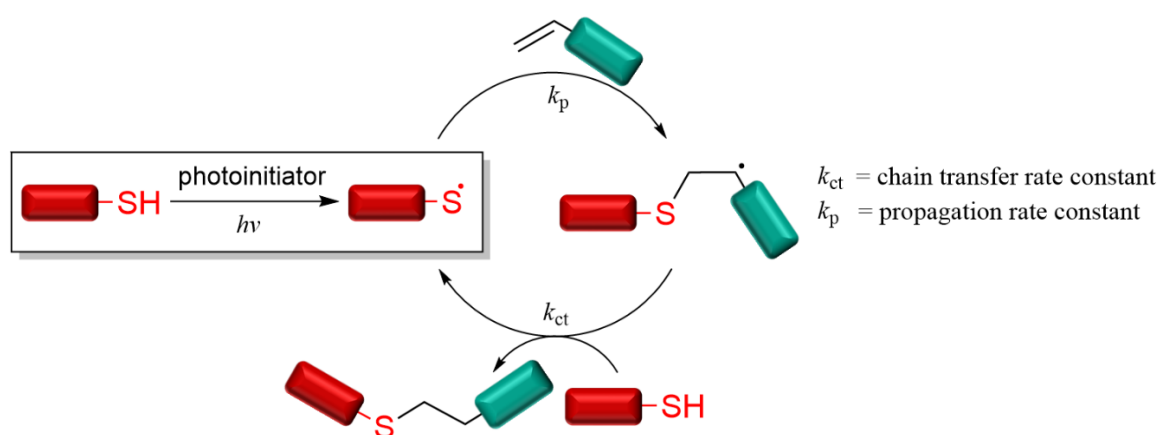
Scheme 17 Mechanism of free-radical addition pathway for the thiol-ene reaction.[280]

The reactivity depends on the employed starting materials. Beginning from the three most employed categories of thiol compounds, which are thiol glycolate esters, thiol propionate esters and alkyl thiols, Hoyle *et al.*[279] described that the first two groups lead to weakened sulfur-hydrogen bonds through hydrogen bonding with the carbonyl oxygen atom, thus increasing the overall reaction rate. In the same publication, the authors state that addition rates to 1-heptene were 6 times lower for 1-pentanethiol compared to methyl mercaptopropionate. Although in most synthetic procedures only primary thiols are employed, secondary or tertiary ones have advantages, like milder odor and lower risk of spontaneously reacting without light stimulus, confirming the prediction that the reaction rate decreases with higher substitution.[281] An overview on reactivities of thiol groups towards different -ene moieties in apolar and polar media are described in reviews by Renaud *et al.*[282] and by Karl Griesbaum.[283]

Theoretical background

The effect of the -ene component has been thoroughly analyzed by computational and kinetic methods by B.H. Northrop.[284] Unreactive species are molecules with conjugated double bonds, which are stabilized by resonance, and -enes with groups that increase the stability of the carbon-centered radical, such as acrylates or styrenes. The reactivity increases with the electron density at the double bond. Additions to norbornenes are exceptionally fast, compared to all previous examples. There, the reason behind the high tendency to form a C-S-bond is the combination of high electron density and alleviation of ring strain. Therefore, the predicted order of reactivity with methyl mercaptan is as follows (**Figure 20**):

norbornene > vinyl silane > allyl ether > vinyl ether > fumarate

> propene > maleimide > methacrylate > crotonate > styrene

> acrylonitrile > butadiene
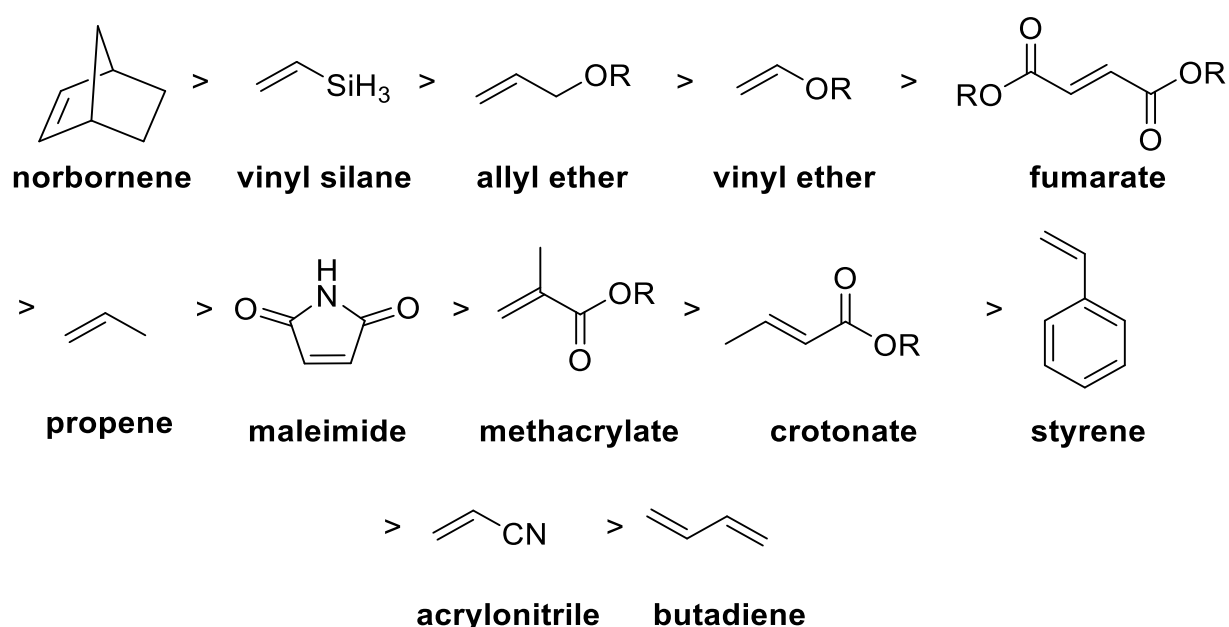
Figure 20 Most common examples of -ene compounds listed by decreasing predicted reactivity towards the thiol-ene reaction (adapted from[284]).

Furthermore, the position of the double bond in the alkene is an important factor in the reactivity. Using the reactivity of a terminal alkene (n-hexene) as reference, trans-2-hexene and trans-3-hexene were shown to possess an 8- and 18-fold lower affinity towards addition, resulting mostly from steric hindrance. The proposed reactivities were confirmed by experimental data from other studies on the same topic,[285] as well as from the two reviews mentioned before.[282,283]

The radical mechanism shows many advantages in the addition of thiols to alkenes, such as high reaction rates and the possibility for photoinitiation. However, this system cannot always be employed, for instance when radical coupling is to be avoided. An alternative, the Michael-Addition mechanism, is therefore described in the next paragraph.

2. Michael-Addition

The second pathway to a thiol-ene reaction is the Michael-Addition, which was first reported by Allen *et al*. in 1964.[286] The main difference lies in the anionic species that suffers no penalty of early chain termination through coupling. This advantage is especially useful in polymerizations, thus allowing to reach high molecular weights without by-products. Specific reactions, like the end-group functionalization of polymers, as well as the conjugation of polymers under low concentration conditions, have been confirmed to proceed without the generation of side reactions, for instance through disulfide formation.[277]

The Michael reaction is catalyzed by a base or a nucleophile resulting in the same product as the radical addition.[287] Many catalysts have therefore been tested in order to efficiently shift the equilibrium towards the adduct. Common examples include the usage of weak bases like triethylamine (Et$_3$N) or nucleophiles like methoxide salts or phosphines. However, further systems have been analyzed, for instance the use of iodine,[288] Lewis acids like gadolinium triflates[289] or even ionic liquids.[290] Nonetheless, the base- and nucleophile-mediated pathways were confirmed to procure the highest efficacy as catalysts. The schematic representation of basic and nucleophilic initiation is shown in **Scheme 18**.[291] It is noted that primary amines catalyze the reaction in a nucleophilic way, rather than acting as bases.[275]
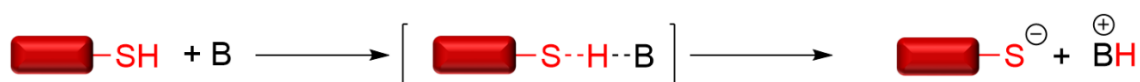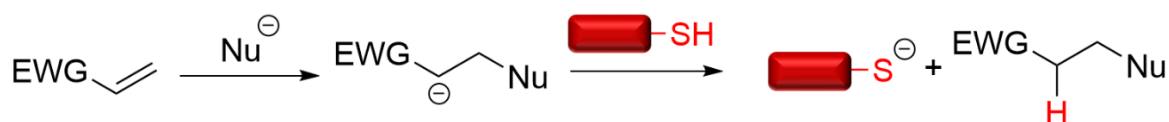
Scheme 18 The most common initiation pathways for the thio-Michael addition: base mediated (top), and nucleophile mediated (bottom). Adapted from [291].

The reactivity of dithiols for both the base and nucleophile mediated Michael addition is highly dependent on the pK_a of the thio component.[292] The lower the pK_a value, the more the thiol is prone to deprotonate and form the required thiolate. Alkyl thiols (pK_a = 10–11) are therefore

one of the most inert thiol species, while thioglycolates, thiopropionates or even cysteine (pK_a *ca*. 8) are more reactive in a thio-Michael addition.

The electron deficiency of the -ene component is another factor influencing the kinetics of the addition as it facilitates a nucleophilic attack. Typically, -enes such as acrylates or maleimides,[293] in combination with amines[294] or alkyl phosphines[295] are chosen. Nonetheless, the free-radical variant is often preferred because of the shorter reaction times, as well as more facile synthesis procedures.

After discussing the mechanisms of both radical and Michael addition, as well as the respective properties and advantages, the possible applications will be discussed next.

The overall stability toward oxygen, simplicity of reaction kinetics and conditions as well as high control over the activation step has also captured the attention of polymer chemists,[275] as these advantages unlock the facile synthesis of more complex structures. Many thiol-ene dendrimers,[296] including glycodendrimers,[297] have, for example, been reported in the literature, in addition to new photocuring procedures for thermosets[298] and semicrystalline materials.[299] As the number of different isolated polymeric structures increases based on the variation of thiols and alkenes, so does the number of possible applications. Currently, the scope ranges from high energy absorbing materials to adhesives and optical components.[275] Furthermore, thiol-ene chemistry has been applied for the preparation of materials with interesting mechanical properties from dienes and dithiols.

Typically, thiol-ene based polymers possess glass transition temperatures (T_g) between −30 and 60 °C and many of the studied materials also show high impact capacity.[300] The material properties do not originate from the C-S bond itself, but rather from the monomer type. Especially favored for providing high-impact resistance are monomers containing bisphenol A,[299] which enhances the energy absorption, when combined to urethane functionalities,[301] which increase the elastomeric properties of a material *via* hydrogen bonding. These materials promise great potential in personal protection gear, but also as dental devices. For example, in the field of dentistry, studies have determined that carbamate-containing materials synthesized *via* thiol-ene show higher impact attenuation at intraoral temperatures than the commercially available Polyshok™, which is commonly used for dental prosthetics, while simultaneously possessing greater water permeability and lower tear strength and hardness.[302] Furthermore, the rapidly formed networks, derived from the fast reaction rates

of the thiol-ene reaction, showed higher homogeneity compared to traditional photopolymerizations.[303]

Meanwhile, adhesives synthesized *via* thiol-ene reaction have also been reported. Most adhesives are based on acrylates or methacrylates, which suffer from the main drawback of forming heterogeneous networks and oxygen inhibition of their curing processes.[304] The thiol-ene reaction, however, does not exhibit such disadvantages.[305] For instance, the Patton group synthesized crosslinked thiol-ene networks in the presence of dopamine acrylamide, ultimately forming a sticky polymer.[306] The same group also reported novel polymeric materials with good adhesive properties based on clove oil derivatives, such as eugenol.[307] Interestingly, thiol-ene networks have also been exploited as anthracene-based adhesives, which showed reversible binding upon irradiation at different wavelengths.[308]

In bioorganic functionalization, examples where thiol-ene chemistry has been used include glycodendrimers and glycopolymers, e.g. by "clicking" trehalose units to RAFT polymers,[309] but also sugar-containing networks were efficiently polymerized, for instance *via* thiol-ene polymerization of sucrose dienes with different dithiols.[310] Cysteine, as the only amino acid containing a thiol group, was also employed as thio-component during bioorganic functionalization.[311] As cysteine is a component in many peptides, functionalization[312] and incorporation of peptides in synthetic hydrogels[313] *via* thiol-ene reactions and polymerizations has been well reported. Of utmost importance is the application of such materials in drug delivery, while simultaneously taking advantage of the low toxicity and biocompatibility of peptides. In 2007, Wittrock *et al*. conjugated *via* thiol-ene the core of bovine serum albumin to glycopeptide antigens to work as a vaccine carriers.[314] Different drug delivery systems have also been developed, e.g. micellar systems by Lou *et al.*[315] that were obtained by functionalizing a butadiene-styrene copolymer with thiol-containing saccharide units. This method is attractive in medical science since these glycopolymers are easily accessible in high yields and show high affinity to lectins during biological recognition events.[316] The importance of this affinity lies in ability of lectins to bind to cell walls and trigger biochemical reactions,[317] while simultaneously exhibiting antibiotic properties on bacteria. For example, polyhedral silsequioxanes were coupled with thiol-terminated saccharides with spacers of different lengths.[318] The resulting material demonstrated efficient binding of lectins and receptor inhibiting properties of cell surface biological

processes like infections and inflammations. Hubbel *et al.* developed hydrogels for controlled drug release between 2001[319] and 2005,[320] followed by many others like Giammona *et al.* in 2008 who presented a thiol-ene network based on vinyl sulfone–derivatized insulin for controlled release of 2-methoxyestradiol, a known anti-cancer agent.[321]

The most common applications of thiol-ene products are in electrooptics, resulting from the facile incorporation of sulfur and its high refractive index (η_D) in organic materials.[322] Apart from the requirement for high content of sulfur, substrates for these materials lack long carbon chains or functionalities, like esters, as they tend to lower the η_D.[323] This effect is caused by the low atomic refraction of the common organic components carbon, oxygen, nitrogen and hydrogen compared to sulfur.[324] Therefore, many groups have focused on the use of thiol-epoxides and thiol-halides as substrates.[275] In these cases, apart from the desirable optical properties, the advantageous processing of the resulting materials was also enabled by the highly efficient thiol-ene reaction.

Liquid crystals are another class of materials where thiol-ene chemistry has proven highly advantageous. Such materials are very sought-after because of their particular properties: they are transparent in visible light,[325] possess switchable birefringence by change from isotropic to anisotropic phases through application of e.g. electrical fields[326] and, more importantly, electro-optic performances[327], that remain intact even if the material is deformed.[328] Further applications for liquid crystals range from dielectric layers[329] to optical waveguides[330] and many more.[331]

The "click" properties and further mechanistical aspects of the thiol-ene reaction were discussed in this chapter. In conclusion, this reaction possesses many attractive characteristics for both organic and especially polymer chemistry, proving to be advantageous for its fast reaction rates, high selectivity and homogeneity of the obtained polymeric materials. The versatility of the thiol-ene provides a useful tool for the tailored design of materials, allowing for a wide range of applications such as adhesives, high impact materials and glycopolymers.

3 <u>Aim of this work</u>

In the introduction and theoretical background, the importance of sustainability for various chemical processes and especially for polymers, compounds that have tainted our world for decades, was discussed. Therefore, the aims of this work were inspired on the principles of Green Chemistry, a subgroup of sustainability.

The goal of this thesis is the preparative investigation and evaluation of novel sustainable procedures bound to the Lossen rearrangement and further applications in the field of polymer chemistry. The thesis is divided into two main topics:

1. The introduction of a CO_2-based modification of the Lossen rearrangement, including the optimization of reaction parameters for the synthesis of amines, carbamates and ureas and application of gas chromatography (GC), nuclear magnetic resonance (NMR) spectroscopy and infrared (IR) spectroscopy for reaction monitoring.

2. The sustainable synthesis and characterization of non-isocyanate polyurethanes (NIPUs) *via* the highly efficient thiol-ene polymerization. This topic is divided in five sections:

    a) The preparation of diene carbamates and ureas from fatty acid derivatives *via* the Lossen rearrangement and the synthesis of dithiols from renewable feedstock.

    b) The optimization of the molecular weight (M_n) for the thiol-ene polymerization of diene monomers and both renewable and commercially-available dithiols, as well as the analysis of thermal properties *via* differential scanning calorimetry (DSC).

    c) The preparation of random copolymers *via* multi-component polymerization of different dienes and dithiols as well as the formation of block copolymers by thiol-ene "click" reaction of end group–functionalized prepolymers and the evaluation of their thermal properties in order to produce macromolecules with combined properties.

    d) The sustainable post-polymerization modification of polysulfides *via* the straightforward oxidation with hydrogen peroxide to the respective polysulfones.

e) The preparation of specific thermally processable random copolymers and the evaluation of mechanical properties (Young's modulus) by stress-strain experiments.

The CO_2 based Lossen rearrangement was found to proceed under different mechanisms than proposed in the past, as determined by online IR monitoring. Meanwhile, the renewable preparation of NIPUs *via* thiol-ene polymerization led to the formation of materials with tunable thermal and mechanical properties, opening new doors for future applications.

4 Results and discussion

4.1 The CO$_2$-based Lossen rearrangement

4.1.1 Introduction

In this chapter, by employing the well established Lossen rearrangement, the aim is to test a more sustainable variant by replacing toxic activating reagents for hydroxamic acids in favor of CO$_2$. The experimental methods, the results and evaluation, as well as the outlook for this reaction will be discussed in the following chapter.

In the Lossen rearrangement, a hydroxamic acid is employed that is readily synthesized in one step from methyl esters or acid chlorides with hydroxylamine under basic conditions (e.g. potassium hydroxide).[332] It is worth mentioning that the approach featuring the methyl esters is preferred in view of sustainability, as these compounds can be readily obtained in high yields from the respective carboxylic acid with methanol and result in less waste and use less toxic chemicals as for the acid chloride route. Besides the Lossen approach, two similar rearrangements are known in organic chemistry,[333] all of which possess the same building block, namely an amide function, but a different leaving group that forms an isocyanate *via* a nitrene. In the Curtius variant (see **chapter 2.4.2**), the very reactive azide next to the carbonyl reacts upon heating by the energetically favored release of nitrogen. The remaining unstable nitrene readily rearranges to an isocyanate. In the Hofmann rearrangement, an amide is functionalized with Br$_2$ to a *N*-bromoamide providing a bromide anion as strong leaving group. Comparing these three rearrangement approaches, the stability of the starting material is the main difference.[334] Hydroxamic acids, being much more stable than azides and *N*-bromoamides against heating and light irradiation, do not undergo a spontaneous Lossen reaction, even at high temperatures, but have to be priorly activated. One possibility is to employ salts of hydroxamic acids, namely hydroxamates, but these need temperatures above 100 ˚C. Furthermore, industry and other large scale productions usually convert hydroxamic acids with *O*-acyl, *O*-sulfonyl or *O*-phosphoryl groups in order to create a better leaving group that releases as carboxyl, sulfonate or phosphate group, respectively. The problem of this method is the general toxicity of the functional groups of the agents used for activation; for instance acid chlorides, sulfuryl chlorides and phosphoryl chlorides. Especially phosphoryl

chlorides have been confirmed to need special precautions due to their toxic and strongly corrosive properties.[335]

Taking a closer look at the structure of hydroxamic acids, one notices the presence of two acidic protons. The transformation with acid chlorides increases the reactivity of the hydroxamate by forming a better leaving group, while the deprotonation of the amide functionality facilitates a rearrangement.[336] Following this line of thought, the idea was to employ CO_2 as activating group in cooperation with a base, in a system similar to the "switchable ionic liquids" described by Jessop *et al.* in 2005 (Scheme 1a).[62] In the first step, the base (DBU) deprotonates *N*-hydroxyamide forming a hydroxamate salt. Subsequently, the weakly electrophilic CO_2 molecule attaches to the nucleophilic hydroxamate, possibly forming the intermediate **A** (**Scheme 19b**).
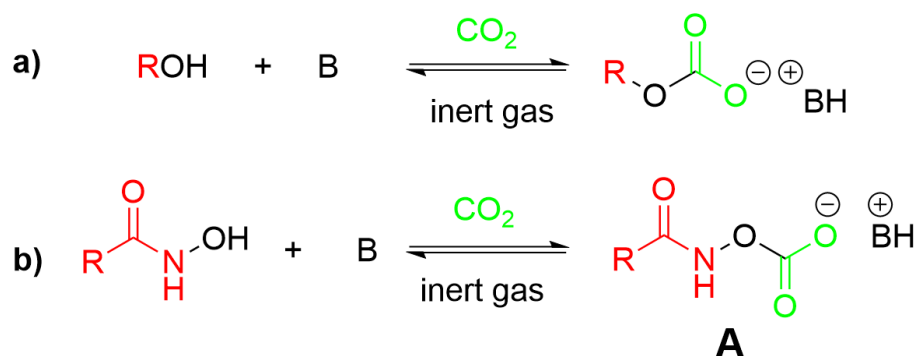
Scheme 19 a.) Schematic representation of the formation of a carbamate salt with DBU and an alcohol introduced by Jessop *et al*. **b.)** formation of intermediate **A** with the same approach using a hydroxamic acid instead of an alcohol.

Afterwards, it was hypothesized that upon subsequent heating, the rearrangement should take place leading to the isocyanate (**Scheme 20**). The presence of water in the reaction mixture hydrolyses the formed isocyanate to an unstable carbamic acid, which readily decomposes into the more thermodynamically stable amine and CO_2. As a consequence, a second common side reaction takes place, since the highly reactive isocyanate also reacts with its hydrolysis product, an amine. Therefore, next to the amine, ureas are synthesized in moderate yields.[152] Although the formed isocyanate is isolated by performing the reaction and work-up in the absence of water, or rather avoiding long time exposure to larger amounts of water,[141] typically *in situ* conversion/capture is commonly applied in an isocyanate-

forming rearrangement by using nucleophiles, like alcohols. This way, carbamates (or urethanes) are isolated.[337]
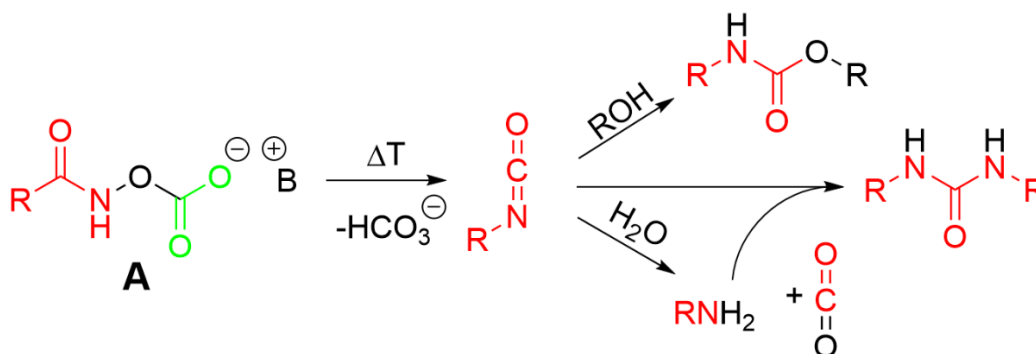
Scheme 20 Rearrangement of intermediate **A** and possible subsequent nucleophilic additions of the formed isocyanate with alcohol and water.

Another point to keep in mind is the difference in reactivity between aliphatic and aromatic compounds. The partial negative charge at the nitrogen atom is delocalized if a suitable π-system is present, thus increasing the partial positive charge at the carbonyl carbon. Aliphatic compounds, therefore, take longer times to rearrange under standard reaction conditions (around 20 h), while aromatic molecules are converted into their products around three times faster.[338] Also, aromatic hydroxamic acids do not form ureas or carbamates under basic conditions, but only anilines and derivatives are isolated from their Lossen rearrangement.[152] One of the reasons is related to the formation of the hydrogen carbonate, which is the anion of the adduct of water and CO_2. The influence of heat and partial re-protonation leads to decarboxylation, thus producing water in the reaction mixture. Secondly, anilines are weak nucleophiles, therefore showing a reduced affinity to the isocyanate. However, aromatic hydroxamic acid would lead to more reactive intermediates that would benefit the overall reaction.[338]

Here, a library of 19 hydroxamic acids was synthesized containing aliphatic and aromatic moieties, as well as five dihydroxamic acids, to obtain detailed information on the influence of the moieties of hydroxamic acids in a Lossen rearrangement with CO_2 (**Figure 21**). In addition, the focus was put on renewable starting materials. For instance oleic acid, the most abundant fatty acid representative, but also other less known components, like erucic acid obtained from rapeseed oil,[339] or capric acid found in coconut oil, were used, while keeping the scope of the library as diverse as possible. It is noted that some hydroxamic acids do not

Results and discussion

have a sustainable origin, but were synthesized to expand the library and assist with drawing conclusions (for instance, adamantly hydroxamic acid **1l**). All compounds were synthesized from the respective methyl esters, which were obtained *via* sulfuric acid (H_2SO_4)-catalyzed esterification from the respective acid in methanol.
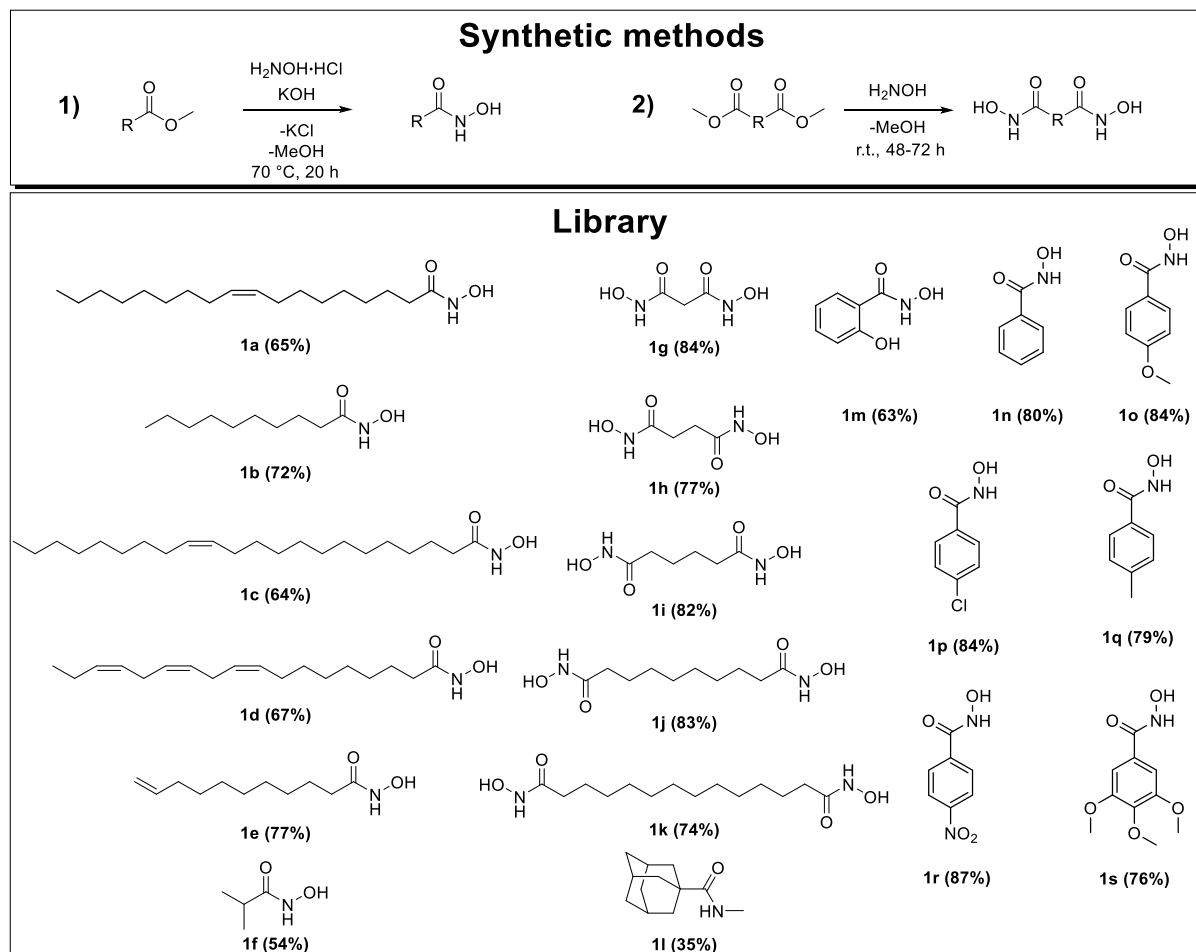
Figure 21 Synthetic procedures and library of synthesized hydroxamic acids with corresponding yields.

While the yields for aromatic starting materials ranged between 63-87%, their aliphatic counterparts behaved differently, depending on chain structure. Methyl esters bearing longer alkyl chains were isolated as *N*-hydroxyamides with similar yields above, *i.e.* 64-77%. More problematic were shorter alkyl chains, with less hydroxamic acid isolated the shorter the aliphatic group. Chains shorter than isopropyl were not isolated. The reason behind this behavior was likely the standard purification method, which employs extraction with ethyl acetate (EA) and washing with water. Even though hydroxamic acids are highly polar and prone to form hydrogen bonding, possessing an apolar chain still results in greater solubility in the organic phase rather than in the aqueous one. This seems reasonable since they can also form hydrogen bonding in organic media among themselves and, in this case, also with

66

the solvent resulting in no obvious thermodynamical penalty compared to aqueous phase.[340] Therefore, if a shorter tail is chosen, solubility in water becomes dominant, leading to large yield losses. In the case of **1f** and **1l**, the increased steric hindrance derived from the isopropyl and adamantly structures are also expected to cause a yield reduction. The procedure containing hydroxylamine solution, employed for diesters, led to the highest yields. The reason behind this behavior is likely the fact that the dihydroxamic acids were simply precipitated by addition of an antisolvent and directly filtered off, while the mono hydroxamic acids were purified by aqueous workup and recrystallization, thus leading to losses in yield.

In the following chapter, the respective subgroups of the library are discussed in more detail. In general, first confirmation of the presence of hydroxamic acids was achieved through simple visual observation, as the hydroxamic acids are obtained as crystalline substances, unlike the respective liquid methyl esters. All compounds were fully characterized by proton and carbon NMR spectroscopy and high-resolution mass spectrometry (HRMS). In a typical NMR spectrum (**1a**), the disappearance of the methyl ester signal at around 3.7 ppm is clearly depicted, while two other distinct broad peaks in the range between 8 and 11 ppm, that belong to the acidic protons of the hydroxamate moiety, are observable in **Figure 22**.
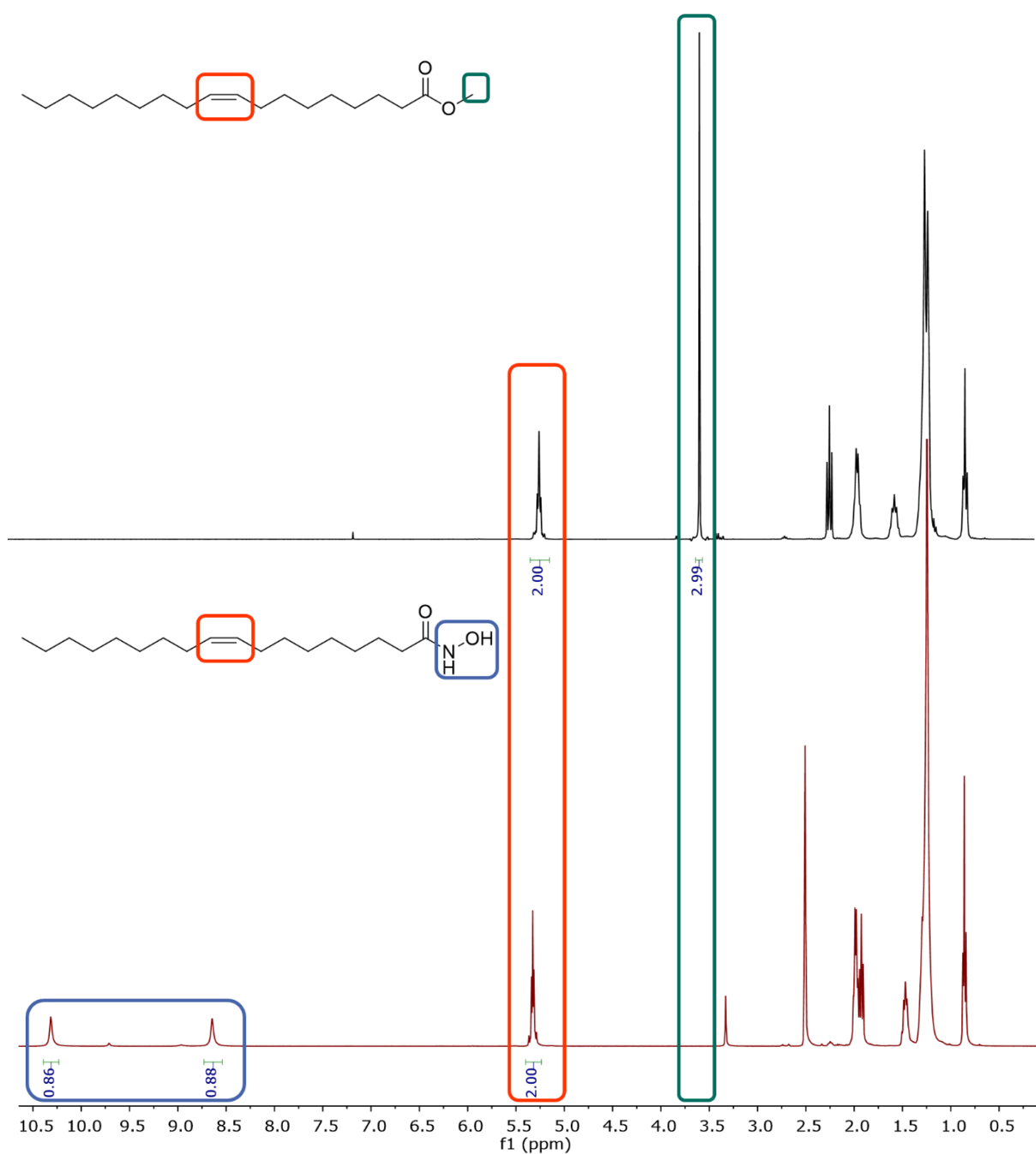
Figure 22 ^{1}H NMR spectra of methyl oleate (top, measured in CDCl$_3$ with a residual peak at 7.26 ppm) and the respective hydroxamic acid **1a** (bottom, measured in DMSO-d$_6$ with a residual peak at 2.5 ppm and respective water signal at 3.3 ppm).

The methyl ester peak at 3.7 ppm is replaced by the acidic amide and hydroxyl protons at 8.7 and 10.4 ppm, while the other signals remain nearly identical. Exception is the small shift of the CH$_2$ group next to the carbonyl function, due to the changing from an ester to an amide.

The preparation of both aliphatic and aromatic hydroxamic acids with hydroxylamine was performed and the resulting compounds **1a**–**1s** were isolated in moderate to high yields. In the next section, the CO_2-based Lossen rearrangement is first discussed on the aliphatic *N*-hydroxyamides.

4.1.2 Aliphatic compounds

The first compounds prepared for the Lossen rearrangement were methyl esters derived from sustainable materials. However, also shorter chain hydroxamic acids and dihydroxamic acids were synthesized to cover a broader spectrum of application (**Figure 21**).

A major issue in the Lossen test reactions was first represented by the insufficient solubility of many compounds in DMSO. Especially hydroxamic acids possessing long alkyl chains and diacids were problematic, as only very dilute conditions were achieved. An approach featuring a reaction in suspension with **1c** in DMSO was unsuccessful. The premature addition of the base, in this case DBU, only partially improved the homogeneity of the reaction mixture. However, increasing the temperature (up to 70 °C) led to sufficient solubility in most cases. Still, DMSO was the best solvent choice for several reasons and was used for most reactions. The first reason is that DMSO was the best medium for dissolving such polar groups, with a few exceptions that were mostly caused by long unpolar aliphatic side chains of several starting materials. Secondly, DMSO is non-toxic, "green" and possesses a high boiling point, making it suitable for high temperature conditions.

For the first test Lossen rearrangement reaction, the two compounds **1e** and **1a** with 10-undecenoic and oleic chains were chosen as renewable substrates. Before the start of every reaction, the DMSO mixture containing 1.00 eq. hydroxamic acid and 1.00 eq. base was exposed to atmospheric CO_2 pressure (balloon) for 15 minutes to ensure the formation of the intermediate. Afterwards, the reaction flask was heated to the desired temperature for 24 h, while CO_2 was added *via* balloon (**Scheme 21**).

Results and discussion
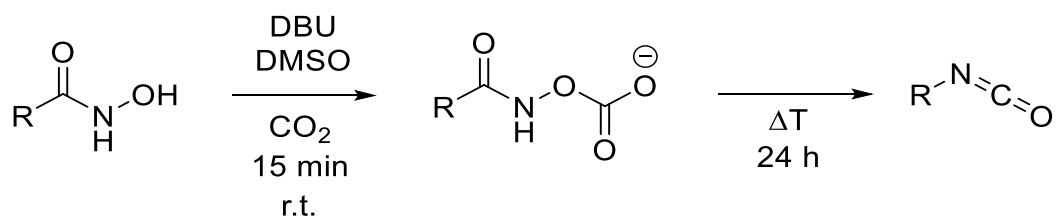
Scheme 21 Reaction procedure for the CO_2 based Lossen rearrangement.

After the cooling of the reaction mixture, formation of colorless solid was observed in both cases, which was easily filtered off. After analysis *via* ^{1}H NMR, ^{13}C NMR and IR spectroscopy, as well as HRMS, the powder was determined to be the respective symmetrical urea (compounds **9** and **10**). The presence of the urea moiety was a strong indirect indication of the *in situ* formation of the isocyanate and its degradation to the respective amine, as shown in **Scheme 20**. However, as the yield was low (*ca.* 10%), the filtrate was worked up further to isolate further possible products. Subsequent addition of water to the filtrate and extraction with different organic solvents was performed and the residue obtained after evaporation of the solvent was used for thin layer chromatography (TLC) analysis for first indication of the obtained mixture. Although the TLCs did not show clear spots (Seebach reagent and potassium permanganate used for staining), column chromatography was performed with cyclohexane:ethyl acetate mixtures. However, none of the two obtained fractions (R_f = 0.52 and R_f = 0.40 in CH:EA (2:1)) contained the respective product (isocyanate or amine) of the Lossen rearrangement. The starting material and the base were partially recycled by flushing the column with ethyl acetate, however, multiple steps, including redistillation of the DBU, were necessary for this purpose. Since the isocyanate was not obtained, it was decided to change the reaction parameters based on the urea yield. The temperature was varied between 70 and 110 °C, the concentration was increased from 0.1 to 3 mol/L, and different reaction times were tested in the range of 8 and 72 h. Additionally, different organic and inorganic bases were employed, including 1,8-diazabicyclo(5.4.0)undec-7-ene (DBU), 1,5,7-triazabicyclo(4.4.0)dec-5-ene (TBD), 1,5-diazabicyclo(4.3.0)non-5-ene (DBN), K_2CO_3 and 1,4-diazabicyclo[2.2.2]octane (DABCO). DBU equivalents between 0.50 eq and 2.00 eq. were also tested. However, urea yields did not surpass 12% for any of these conditions. A possible explanation was speculated to be the degradation of the CO_2 intermediate after the temperature increase, leading to low yields. No bubbling was noticed during the reaction, probably because of the high stirring rates. The CO_2 atmosphere was therefore kept for up to

8 h by continuously renewing the CO_2 balloons shifting the equilibrium to the intermediate **A**. No improvement was detected, thus the pressure was increased by working with a Berghof 300 mL pressure vessel. The pressure was set to the desired value (5 – 30 bar) and the reaction mixture was allowed to stir overnight at the chosen temperature. Even after 72 h under the described conditions, the urea yield remained under 15%. The possible formation of water through the hydrogen carbonate or the presence of water in DBU and DMSO were hypothesized to lead to a "dying" effect by the isocyanate. The isocyanate, therefore, degraded faster to the amine with high concentrations of water before another amine was able to capture it by forming the urea. However, this explanation does not explain why the amine yields were too low to be isolated, even if over 50% of unreacted hydroxamic acid was recycled afterwards.

Therefore, a different approach included the capture of the *in situ* isocyanate with an alcohol (2.00 eq., respective to the hydroxamic acid) as nucleophile. Three alcohols were chosen: methanol, ethanol and butanol. Methanol, despite its higher nucleophilicity, however, was eliminated as its boiling point is lower than the applied temperatures. Ethanol and 1-butanol evaporate at around 80 and 120 °C, allowing for test reactions at higher temperatures. However, after workup and column chromatography, no carbamate was isolated or detected by NMR spectroscopy or GC-MS, while the urea yield remained stable around 12%. This behavior may be explained through the strong nucleophilic character of water and amines, therefore consuming the isocyanate before being able to undergo an addition with the alcohol component. The alcohol also forms adducts with CO_2 producing a weakly nucleophilic carbonate anion, which is less reactive than water. Following this line of thought, water was employed as an additive to avoid urea formation in favor of an increase of the amine formation. On the contrary, the mentioned addition did not shift the equilibrium towards the amine, but rather helped the formation of bicarbonate salt already in the early stages of the reaction. The bicarbonate ion utilizes the protonated base as counterion, thus inhibiting the Lossen rearrangement completely. However, in most cases, much of the unreacted hydroxamic acid (up to 50%) was recycled by extraction and crystallization out of ethyl acetate or ethyl acetate/cyclohexane mixtures. The capture of the isocyanate with an amine was not attempted, as side reactions, *i.e.* formation of a carbamate salt with CO_2 are expected to occur.

Results and discussion

For the reasons mentioned above, it was decided to abandon the further optimization of the reaction conditions to study the reaction mechanism more in detail. First, to capture the intermediate **A**, the hydroxamic acid was mixed with DBU in DMSO and exposed to CO_2 followed by the addition of methyl iodide. As a second electrophile, benzyl bromide, was also tested to capture the intermediate. However, the captured intermediate **A** (respective methyl or benzyl ester) was not detected by neither GC-MS nor NMR spectroscopy (**Scheme 22**) after extractions with different organic solvents, and thus its formation, the intermediate was not detected. The reason for the unsuccessful activation of **A** was not possible. However, the strong electrophiles possibly interact with the base, thus leading to the decarboxylation of the now destabilized intermediate before capture occurred.
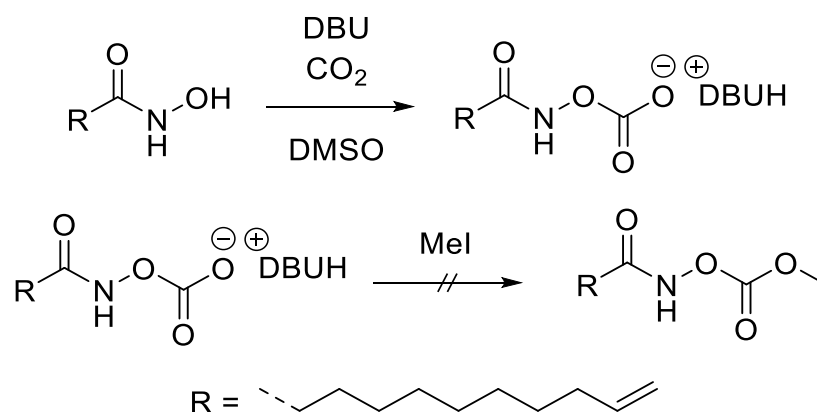
Scheme 22 Schematic representation of the formation and attempted capture of the CO_2-intermediate with methyl iodide as electrophile. Capturing with benzyl bromide was hypothesized to follow the same reaction path.

To fully understand the mechanism, further screening methods were performed. As a model system, a mixture composed of DBU, DMSO-d_6 and *N*-hydroxyisobutyrate **1f** was chosen to be able to monitor the reaction process *via* NMR spectroscopy. **1f** showed good solubility in DMSO at room temperature and possesses a structure, which is easily further analyzed *via* GC or GC-MS. However, after exposure to CO_2, the solution changed to a cloudy mixture in which a colorless solid precipitated. The precipitate was confirmed by NMR spectroscopy to be the bicarbonate salt of DBU, a very stable compound which ultimately consumed most of the added base. With water being the consequence of this side reaction, further reactions were performed in anhydrous DMSO. At the desired intervals, ^{1}H NMR spectroscopy samples were taken and diluted with DMSO-d_6. However, the monitoring yielded unsatisfactory resolution, since the signals of remaining non-deuterated DMSO, DBU and water dominated a significant

72

range of the spectrum. Especially the shifting of the 2.3 ppm signal belonging to the CH_2 group adjacent to the amide carbonyl (hydroxamate) to 3.2 ppm of a rearranged amide (urea) was obstructed by those residual signals. In case of amine formation, the same alkyl group next to the NH_2 function also overlapped with the base, hindering a possible evaluation. This disadvantage was observed with most organic superbases, such as TBD, DABCO, and DBN, other than DBU. Inorganic bases such as K_2CO_3 was anticipated to partially improve the mentioned issues exhibiting no proton signals, however, a related signal broadening in the whole spectrum made the integration ineffective due to extensive overlapping of neighboring peaks (e.g. **Figure 23**).
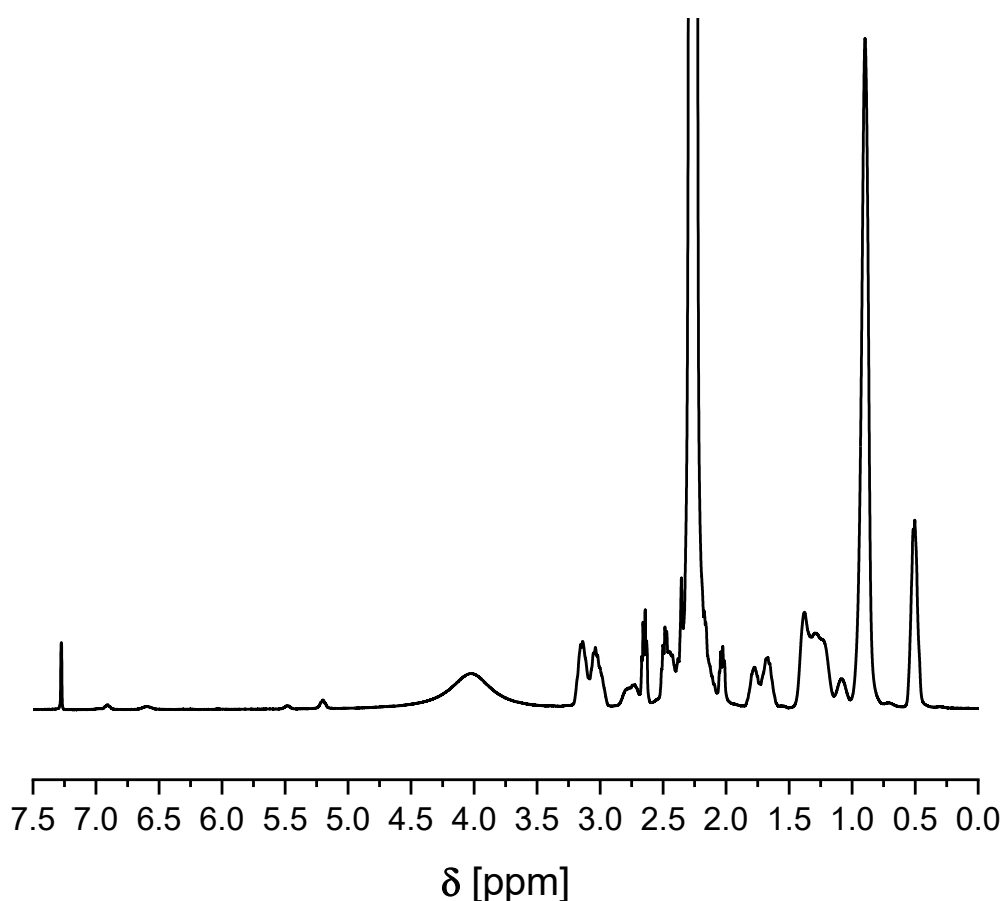
Figure 23 Typical spectrum of a reaction mixture of the CO_2-based Lossen rearrangement containing **1c** and DBU in DMSO. The CH_2 group next to the amide functionality (expected at ca. 3.15 ppm) is masked by DBU, while the amide (expected at ca. 4.5 ppm) overlaps with the broad water signal, which is shifted toward higher ppm values because of the acidifying influence of CO_2.

The amide proton, in many cases the only signal visible, was impossible to be used as a quantitative handle as the span of the broad peak was found to vary across measurements

Results and discussion

due to minor baseline fluctuations and other minor peaks overlapping. It was speculated that the basicity of the reaction solution leads to such peak broadening that disappearance of the amide signals was possible. Therefore, quantitative screening could not be performed by NMR analyses.

As an alternative, gas chromatography (GC) was tested for monitoring. The hydroxamic acid **1f** was initially chosen for its low molecular weight, thus improving detectability in the chromatogram, and for the isopropyl group, which is easy to evaluate in mass spectra, while it offers greater steric hindrance, thus leading to a rise in dwell time for the isocyanate. For these reasons, it was supposed to better the detection of the isocyanate moiety. For quantitative calculation of the yield obtained in *via* GC, a calibration curve is crucial. Thus, one was produced using six prepared samples containing **2f** and an internal standard (IS), namely tetradecane (**Figure 24**).[341] The standard was chosen because of its miscibility in ethyl acetate and high boiling point.

Equation	y = a + b*x
Weight	No Weighting
Intercept	0 ± --
Slope	1.17531 ± 0.02604
R-Square (COD)	0.99755
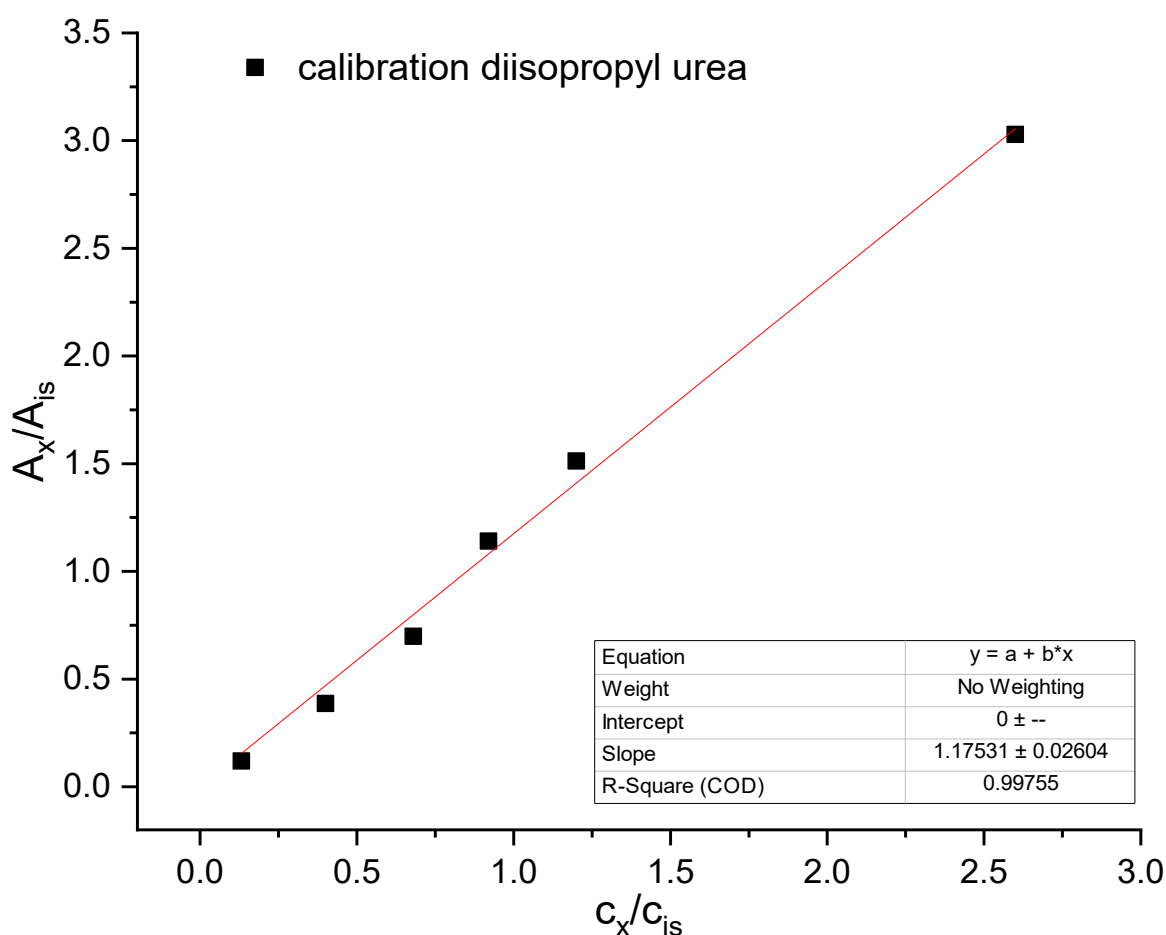
Figure 24 Calibration curve for diisopropyl urea **2f** with tetradecane as internal standard for GC measurements. The response factor R_f equals to the slope of the curve (linear fit).

Each sample contained the same amount of internal standard and an increasing amount of diisopropyl urea. The different ratio detected in the GC was afterwards calculated with the following formula (**Equation 1**):

Equation 1

$$R_f = \frac{(A_x c_{is})}{(A_{is} c_x)}$$

$A_{x/is}$ = area of the sample/internal standard peak

$C_{x/is}$ = concentration of the sample/internal standard

R_f = response factor

It is worth mentioning that the intercept for the linear fit was set to zero, as absence of product leads to no signal. The response factor is used to measure the relative chromatographic response of the analyte compared to the mass spectral response of the internal standard, with which it is possible to determine the yield by integration of the product and internal standard peak in the GC chromatogram according to **equation 2**:

Equation 2

$$c_x = \frac{A_x c_{is}}{A_{is} R_f}$$

However, the previously chosen system could not be analyzed directly, as DMSO is known to cause many problems in GC columns and detectors, such as clogging.[342] For this reason, the reaction parameters were changed to enable GC screening. First, the solvent was changed to EA for easier sample preparation and the temperature was adjusted to 70 °C to avoid boiling of the reaction mixture. Additionally, the concentration was reduced from a range of 2 mol/L to 5 mol/L to values below 1 mol/L, since even the most soluble aliphatic hydroxamic acids were rather insoluble in EA. After the addition of DBU, the first sample was taken (t_0). Subsequently, the reaction mixture was exposed to a CO_2 atmosphere and the temperature set to the desired value, and the samples were extracted at increasing intervals. In **Figure 25**, the monitored reaction was performed in a concentration of 0.4 mol/L with 1.00 eq. of DBU at 70 °C.

Results and discussion
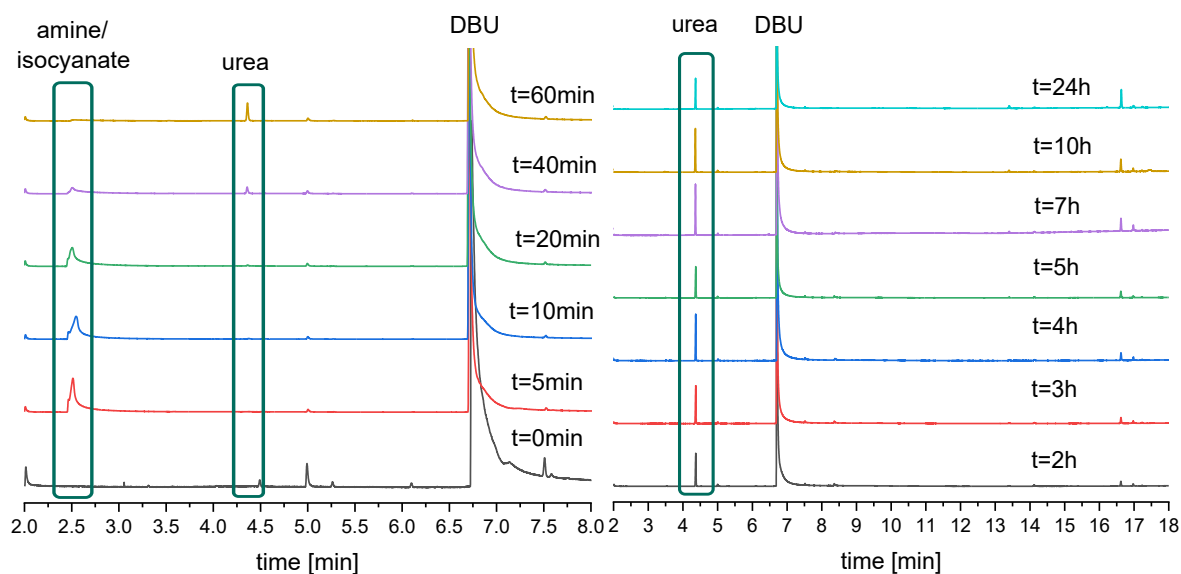
Figure 25 GC screening of the CO_2-protected Lossen rearrangement of *N*-hydroxy isobutyramide **1f**. The reaction was performed under diluted conditions in EA (c = 0.40 mol/L) at 70 °C with 1.00 eq. DBU.

Two close signals were detectable after the first sample (5 minutes) in the region of 2.5 min of retention time and were assigned to the amine and isocyanate products, after confirmation by GC-MS analysis: the same samples also measured *via* GC-MS and comparison of chromatograms and mass spectra with isopropylamine was carried out. From the initial results, the chromatograms suggested fast reaction towards the isocyanate and the amine, since already after 5 minutes the amine/isocyanate signals indicated maximum intensity, which subsequently decreased over time. Meanwhile, starting from the 20 min sample, another signal around 4.3 min was observed, which was shown *via* GC-MS to belong to diisopropyl urea. This transition clearly shows that both amine and isocyanate directly begin to be transformed to their respective adduct. Interestingly, after this initial phase the 2.5 min signals disappeared, while the urea peak continued to increase, further suggesting a continuous *in situ* generation of isocyanate and subsequent conversion. After a reaction time of two hours, the urea yield remained stable with slight fluctuations, while more signals in the range of 16 to 17 min appeared. However, these peaks could not be assigned to any known compound, even after GC-MS analysis. The result of the yield calculation is shown in **Table 5**.

Table 5 GC calculated yields of diisopropylurea during the Lossen rearrangement of *N*-hydroxyisobutyramide **1f**.

Time [min]	yield [%]
40	2
60	5
120	13
180	14
240	19
420	16
1440	14

A maximum in yield was obtained after four hours of reaction time under the described conditions. As no amine or isocyanate were detected after 60 minutes, no attempt to isolate further products was attempted. The observed GC yields are in good agreement with the isolated yields.

The same GC screening was performed with compound **1e**. The respective amine was found to exhibit a retention time of around 4.8 minutes (**Figure 26**) and the mass was determined by GC-MS. It is worth mentioning beforehand that the retention times are shifted between GC and GC-MS, as the instruments do not possess the same columns.
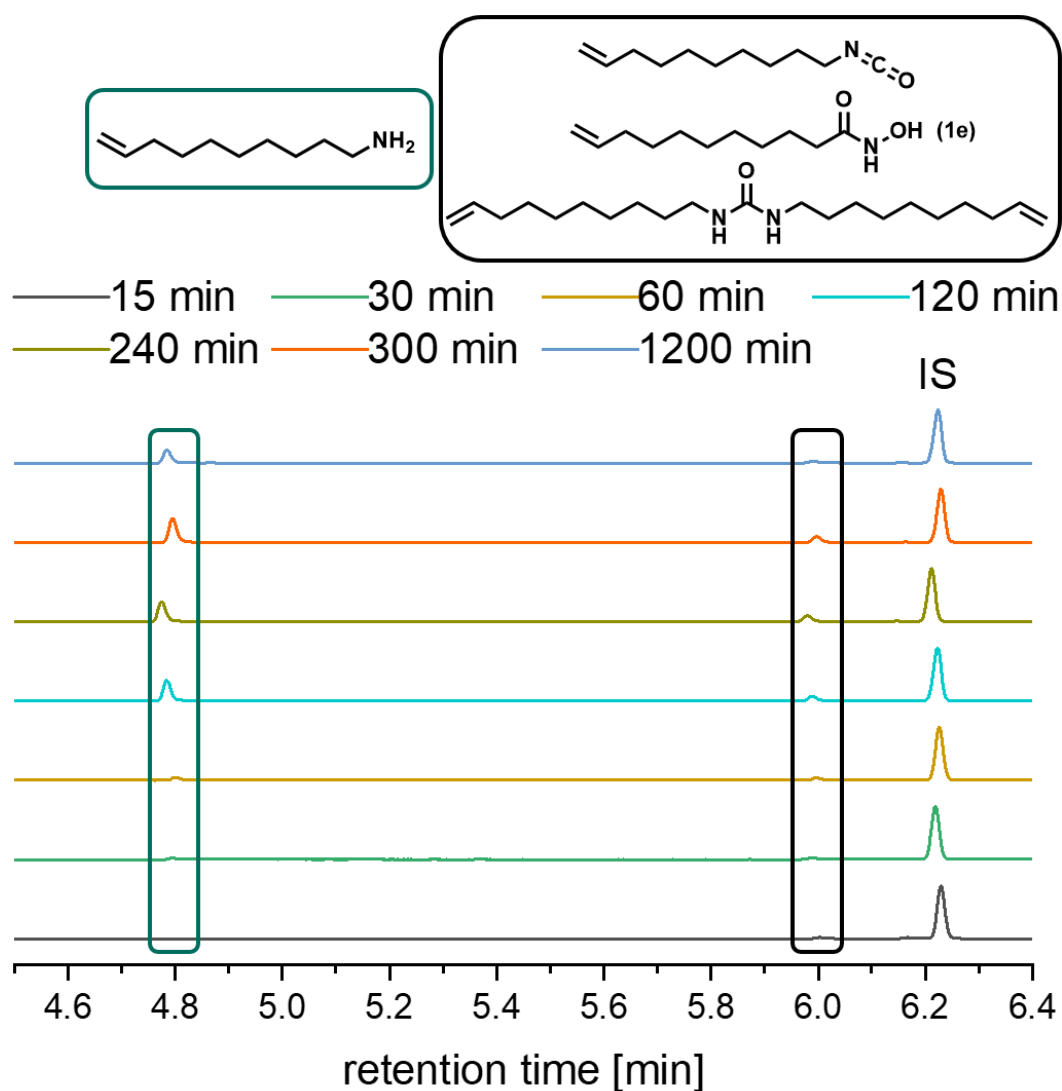
Figure 26 GC screening of the amine and urea of **1e**. The signal intensities were normalized to the standard peak (IS, tetradecane).

During this GC screening, another peak was observed at around 6.0 min, which, based on the mass fragmentation data in the GC-MS (peak in chromatogram at 6.5 min), was ascribed to be the isocyanate. However, the same signal appeared for both the urea and the hydroxamic acid of **1e** (**Figure 27**), which also exhibited the same fragmentation pattern in the GC-MS. As the isocyanate was not isolated, the retention time in GC and GC-MS, as well the mass spectrum in GC-MS was not confirmed for this compound. Another possibility is that the isocyanate is not stable under GC conditions or that the urea decomposes to an isocyanate during the GC heating process.
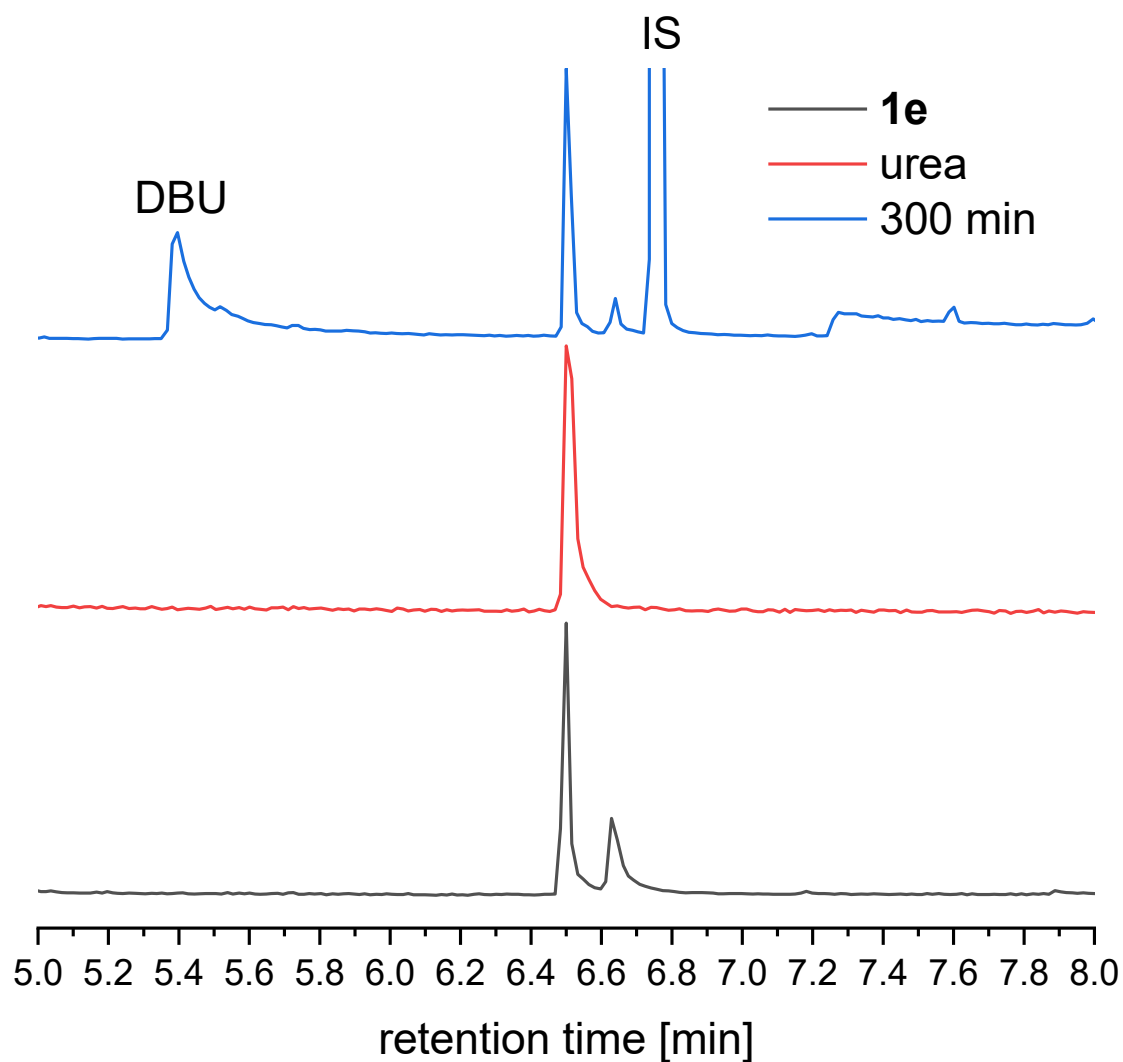
Figure 27 GC-MS chromatograms of **1e** (black), the corresponding urea (red), and the crude reaction mixture after 5 h. The signal intensity was normalized to the 6.5 min peak, belonging to both **1e** and urea. The internal standard employed was tetradecane (IS). The mass spectra of the signals at 6.5 min were identical for each measurement.

The same behavior was also observed for another fatty acid component, namely *N*-hydroxyoleamide **1a**. A clear difference was not visible between the three possible species. In **Figure 26**, the GC signal at 6.0 min has its peak after 4 to 5 hours, steadily decreasing afterwards. Similarly, the amine yield maximum (signal at 4.8 min) is at 5 hours, since the amine is strictly bound to the isocyanate, more specifically to its hydrolysis. The 6.0 min signal (hydroxamic acid) was present in the chromatogram at t_0 albeit its intensity was weak. The additional increase in intensity, therefore, relates to the concentration increase of isocyanate, urea or both. It was assumed that the urea is not consumed or degraded during the reaction since there is no reasonable reaction partner present and ureas do not decompose at the

applied temperatures,[343] therefore the decrease of the peak intensity was ascribed to isocyanate consumption. Furthermore, due to their low intensity, the small peaks carry characteristically large measurement error values. The presence of three overlapping species in the chromatogram makes the calculation of the urea yield inaccurate, even with a calibration. Additionally, as the amine was not possible to be isolated *via* the proposed approach, a calibration was not performed and the yield was not calculated. Similar assumptions can be also made for the rearrangement of **1f** where the urea yield decreased after 4 hours. Although improbable that all substances behave like **1a** and **1e** in GC screenings, the large inconsistency observed was a significant drawback for this monitoring method. Meanwhile, dihydroxamic acids could not be screened via GC because of solubility issues in ethyl acetate and methanol. It is also worth mentioning that the dialkyl ureas were hardly soluble in either ethyl acetate or methanol, increasing the measurement error and the difficulty of this screening method.

Therefore, GC monitoring of the reaction leads to insufficient resolution of the reaction progress and instead other characterization techniques, for instance liquid chromatography (LC) and/or suitable heating methods and columns, have to be established to obtain reasonable data.

Exhibiting many issues during the Lossen rearrangement, such as solubility and low yields, aliphatic components were discarded and the focus was shifted towards aromatic hydroxamic acids **1m**-**1s**. It was anticipated that the higher reactivity in the rearrangement could lead to a better insight of the reaction progress.

4.1.3 Aromatic compounds

4.1.3.1 GC screenings

The seven aromatic hydroxamic acids synthesized for the screening of the CO_2 catalyzed Lossen rearrangement are shown in **Figure 21**. To facilitate the characterization and monitoring, the aromatic moieties were chosen to be simple, containing only functional groups, which were to be expected to be inert under the applied conditions, with the exception of **1m** that bears an OH group and was chosen for the purpose of isocyanate capture.

For the aromatic compounds **1m-s**, no sustainable precursors were used because of the unavailability of suitable compounds. Though not as sustainable as the fatty acid–based hydroxamic acids, the aromatic counterparts all produced the expected products when subjected to the same reaction conditions, as explained in the chapter before (Chapter **4.1.2**). Applying the same reaction conditions for the Lossen rearrangement, the aromatic compounds did not yield the respective ureas as described above but the amines, *i.e.* aniline derivatives. As a proof of concept, the isolation of methyl carbamates by work-up was attempted several times by addition of methanol to the reaction mixture. This approach was, as expected, unsuccessful in every case, as methyl carbamates of anilines are supposedly not stable under basic conditions.[152],[344] The increased formation of amine compounds was explained by the higher reactivity of the isocyanate, as mentioned at the end of the previous section. Furthermore, the following reaction toward the urea compound is more inhibited because of the lower stability of aromatic ureas under basic conditions and heat[344] and the weaker nucleophilic character of anilines compared to aliphatic amines.
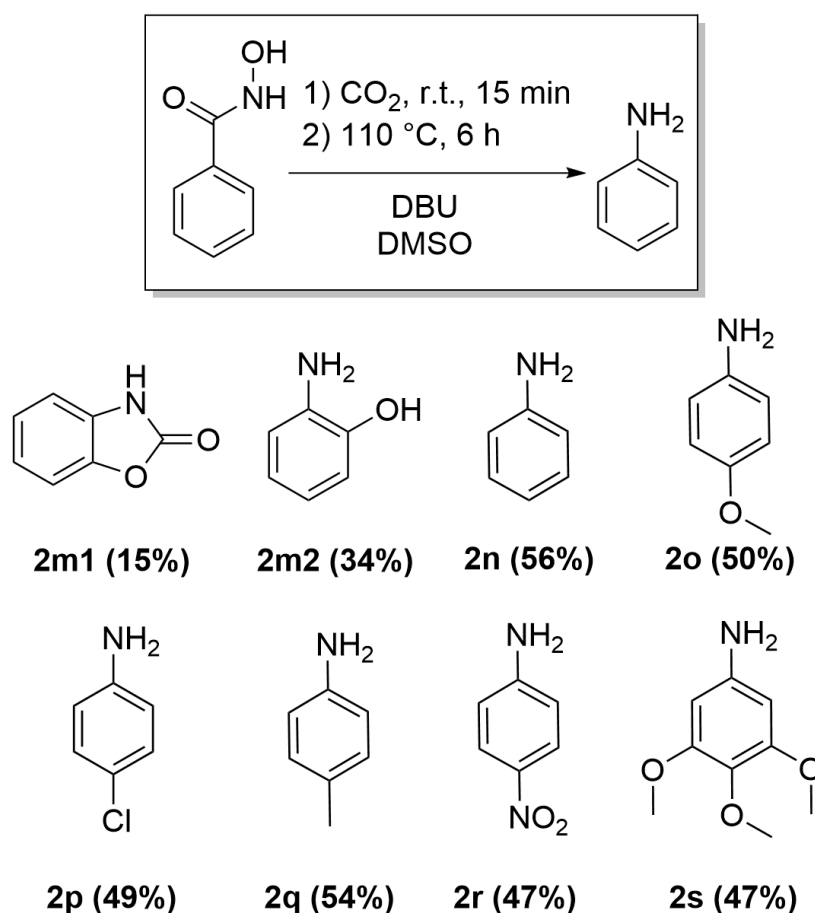
Figure 28 Structures and yields of products **2m-s** of aromatic hydroxamic acids after the CO_2-protected Lossen rearrangement. The yields refer to the optimized conditions discussed in this chapter.

Results and discussion

It is evident from the above listed isolated yields, ranging from 34% to 56%, that the different functionalities on the benzene ring have minimal effect on the Lossen rearrangement of the hydroxamic acids. For instance, trimethoxyaniline **2s**, possessing three methoxy substituents with positive mesomeric (+M) effect, was isolated with a yield slightly lower than *p*-toluidine **2r**, with substituents with -M effect. In the literature, the higher reactivity of aromatic hydroxamic acids with electron-donating groups in *para*- and *meta*-positions have been reported to be good substrates for the classical Lossen rearrangement,[345] which justifies the higher yield of **2q** compared to **2r**, although the effect is small. In the same publication, the authors also describe the increased efficiency of the presence of *ortho*-substituents toward the rearrangement, independently of the nature of the side group (electron-donating or -withdrawing). Therefore, the Lossen rearrangement of salicylhydroxamic acid bearing a hydroxy group in the 2-position is worth mentioning. Due to the vicinity of the alcohol to the in situ formed isocyanate, the aromatic nature of the two functionalities and the presence of an *ortho* substituent, carbamate **2m1** was indeed obtained during the reaction in a yield of 15%, providing indirect proof for isocyanate formation This explains why compound **1m** has the lowest yield of the aniline derivatives (34%, 49% taking the carbamate yield into account) (**Scheme 23**). Berndt *et al.*[346] studied the influence of steric hindrance on aryl hydroxamic acids, concluding that the reaction rate is slowed down with sterically demanding substituents. This effect is observable on the yield of **2n**, derived from the lack of side groups of compound **1n**.
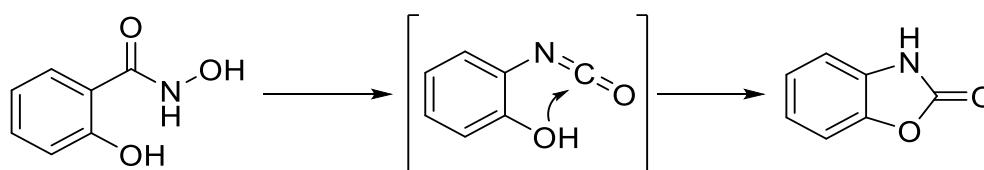
Scheme 23 Formation of benzo[d]oxazol-2(3H)-one **2m1** during the Lossen rearrangement of salicylhydroxamic acid **1m**.

As the only example, next to the respective amine product, a cyclic carbamate was isolated after column chromatography, however, the yields were low. Nonetheless, this method shows that the synthesis of anilines is possible *via* the CO_2-based Lossen rearrangement. Additionally, the formation of cyclic carbamates was confirmed and the isocyanate intermediate thus indirectly confirmed. This increases the sustainability for such compounds, as they are usually produced from phosgene (see **chapter 2.5.3**).

Therefore, as a subsequent step, the reaction was screened *via* GC in the same fashion as aliphatic *N*-hydroxyamides to optimize the yield. *N*-Hydroxybenzamide **1n** was chosen as the model compound, since it would lead to unsubstituted aniline, which is easily detectable by GC and is expected to resemble in reactivity to those of the synthesized aromatic compounds. The reaction conditions were therefore adjusted. The solvent was changed to ethyl acetate from DMSO to enable the measurement and the reaction temperature was reduced to 70 °C from 90 °C. Additionally, the concentration was lowered to ensure dissolution of all components. Most of the selected examples were nonetheless heated to at least 40 °C to produce a clear solution. The samples were taken at the following times: 5, 10, 20, 40, 60, 120, 180, 240 and 300 minutes (**Figure 29**).

Afterwards, the chromatograms were evaluated by integration of the product and standard (tetradecane) signals. Analogously to **chapter 4.1.2**, a calibration was performed beforehand for each aniline.
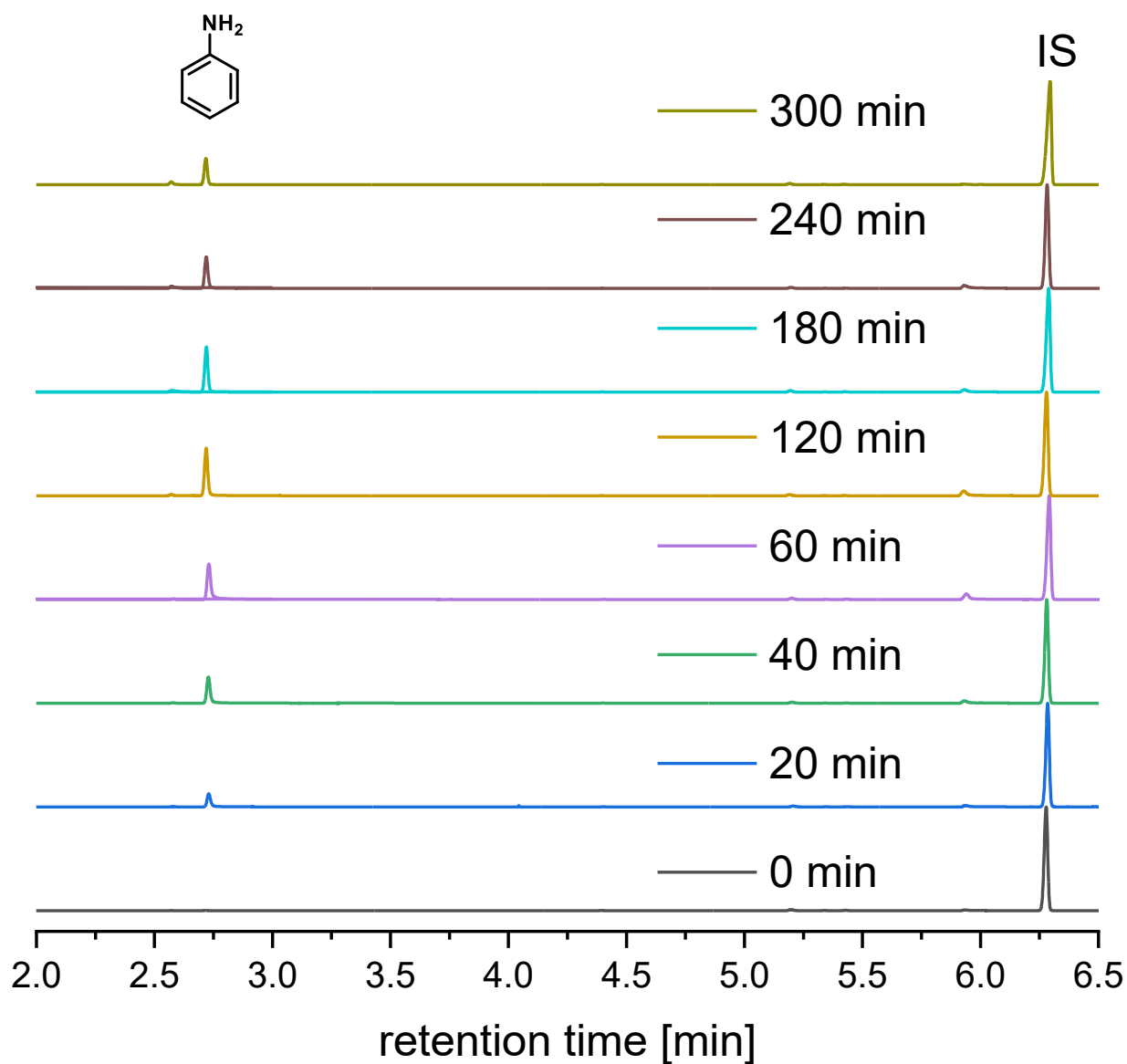
Figure 29 GC screening of the aniline signal during the CO_2 catalyzed Lossen rearrangement of *N*-hydroxybenzamide **1n**.

Table 6 Yields of the GC screening of the Lossen rearrangement of *N*-hydroxybenyamide **1n**.

Time [min]	Yield [%][a)	Time [min]	Yield [%][a)
0	0	120	22
20	7	180	19
40	14	240	15
60	20	300	9

a) Conditions: 0.4 mol/L in EA, 70 °C, 1.00 eq DBU, the yield was determined *via* internal standard (IS) integration.

The yield reached a maximum of 22% after 2 h, decreasing afterwards to 9% after 5 h. This result was not expected as the Lossen rearrangement supposedly reaches its maximum yield after two hours at 90 °C, at least in a self-propagated reaction mechanism.[156] Two explanations are possible: the first is that although the maximal yield is obtained in early stages, prolonged heating in ethyl acetate causes side reactions with the aniline, while the second is, analogously to **1a** and **1e**, that the isocyanate signal overlaps with the aniline. The second explanation is plausible as after comparing the chromatograms aniline and phenyl isocyanate, the retention times were similar (**Figure 30**).

Results and discussion
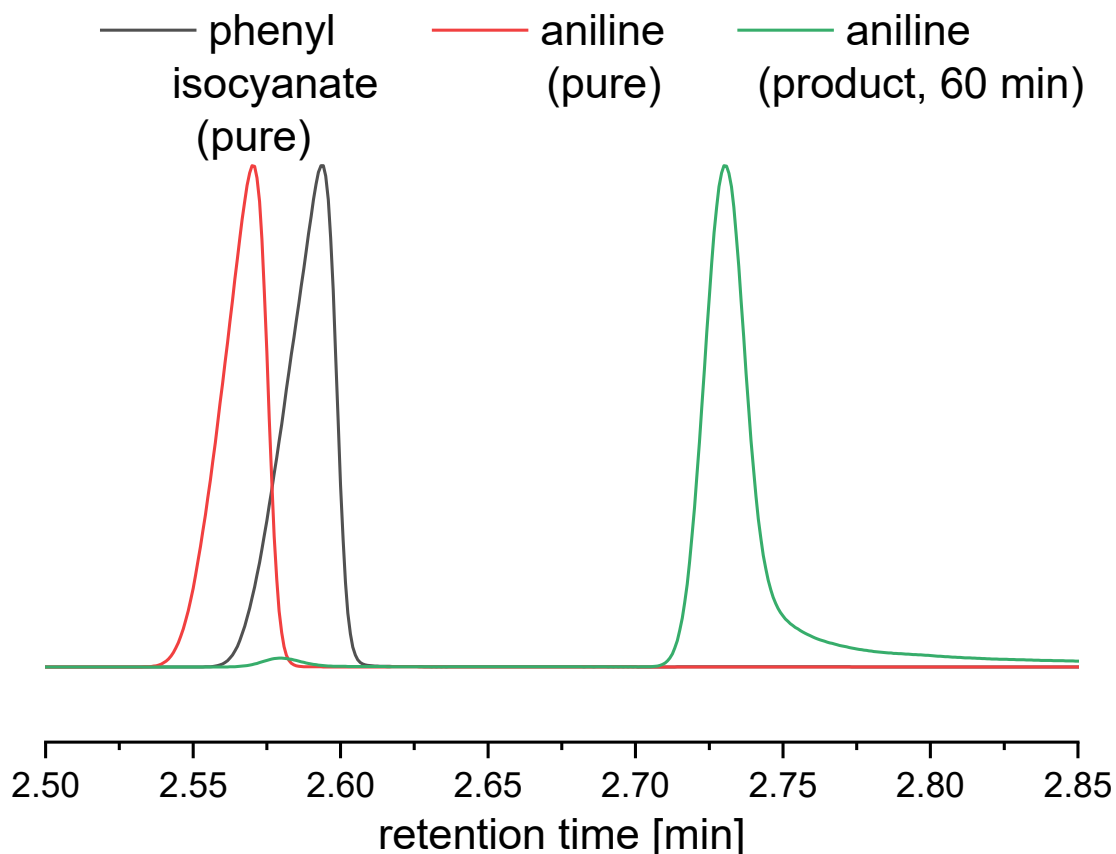
Figure 30 GC chromatograms of phenyl isocyanate (black), aniline (red) and aniline after 60 min reaction at 70 °C in EA in the presence of 1.00 eq. DBU (green).

However, the signal for aniline during the reaction was at around 2.73 minutes (retention time (aniline) = 2.56 min). This behavior is expected to originate from the basicity of the solution as DBU is a strong base capable of deprotonating aniline. Aniline therefore requires more time to pass the GC column, leading to higher retention. The isocyanate does not deprotonate and therefore is not expected to undergo a shift on the x-axis. Additionally, the green trace shows the presence of a small peak at the same location as the black trace, which confirms that the isocyanate is present in small concentrations in the reaction mixture and that its degradation proceeds with high rates. Lastly, the decrease in aniline yield after 2 h is expected to be caused by side reactions, for instance by undergoing amidation with ethyl acetate over prolonged times. However, the determination of side products was not possible *via* GC-MS, as the fragments in the mass spectra were not consistent with aromatic moieties.

Subsequently, the screening was performed with compounds **1q** and **1s**. Interestingly, a product signal (determined by GC-MS) was detected in the t_0 sample for both *N*-hydroxy-3,4,5-trimethoxybenzamide **1s** and *N*-hydroxy-4-methylbenzamide **1q**. The same vial was

86

subsequently measured *via* GC-MS to give further insights into the nature of the peaks. The mass spectrum confirmed the presence of both aniline and/or isocyanates before the addition of CO_2 at low temperatures. Therefore, it was decided to run a GC-MS sample of the starting material. This step was avoided after hydroxamic acid synthesis as the procedure had been previously reported and the only analytical methods performed were NMR and IR spectroscopy.[152] The evaluation showed an almost identical chromatogram as the t_0 measurement. The main difference consisted in the mass spectrum of the signal at 8.7 min, whereby the fragmentation pattern suggested the presence of isocyanate instead of aniline (**Figure 31**).
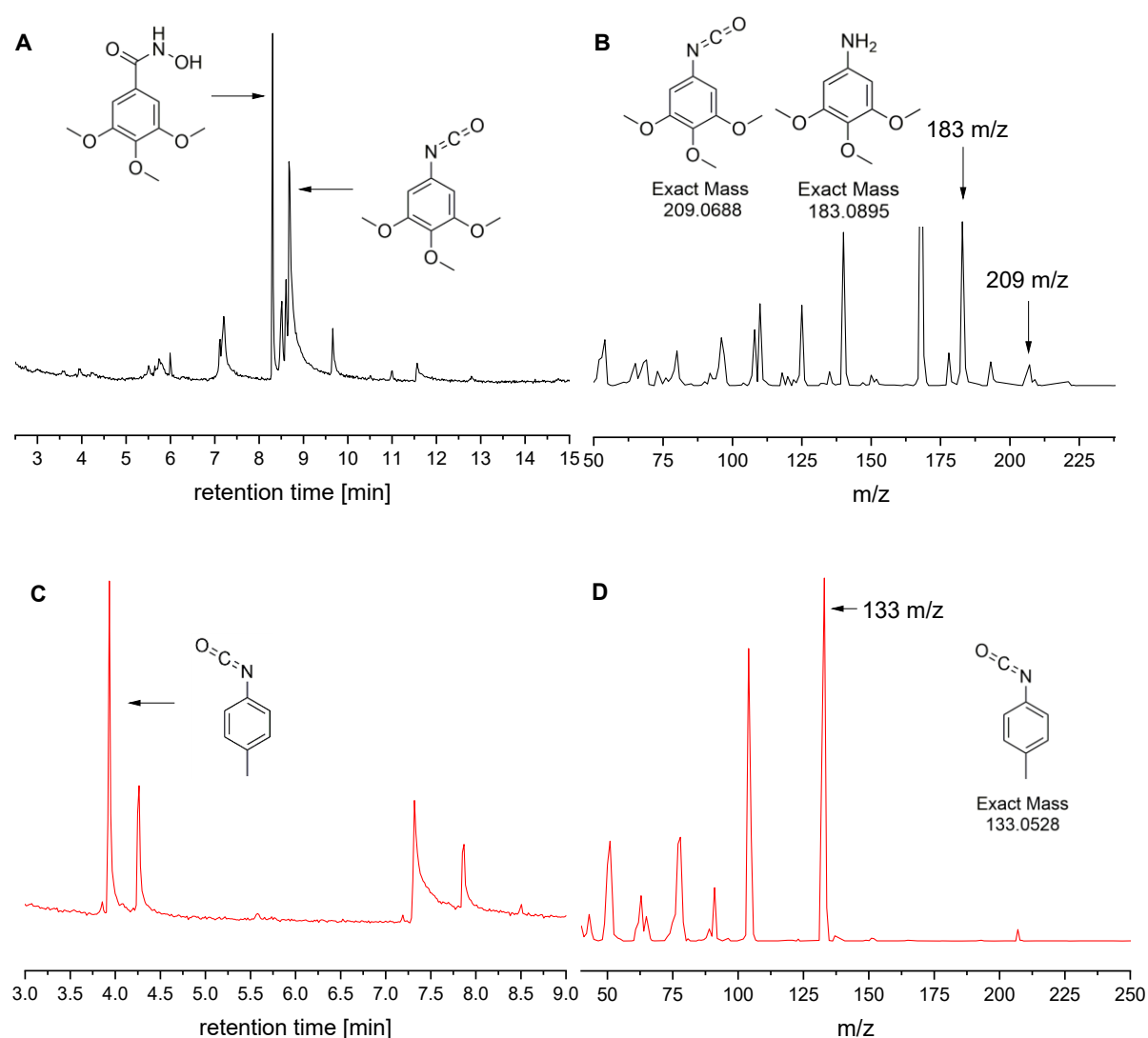
Figure 31 GC-MS results for *N*-hydroxy-3,4,5-trimethoxybenzamide **1s** (black) and *N*-hydroxy-4-methylbenzamide **1q** (red). The MS spectra of 1-isocyanato-3,4,5-trimethoxybenzene (**B**) and 1-isocyanato-4-methylbenzene (**D**) correspond to the peak with a retention time of 8.7 (**A**) and 4.0 min (**C**), respectively, and suggest that the eluting molecules are the respective isocyanates.

Results and discussion

Consequently, the isocyanate is expected to have already formed during the synthesis of the hydroxamic acid. This hypothesis is highly plausible, as the nucleophilic attack on the methyl ester is base-catalyzed and performed under reflux conditions, parameters that are similar to the Lossen rearrangement. Since the usual work-up was performed by recrystallization, the aniline derivatives were not removed, since they also exhibit low solubility in EA. In a previous publication, in 2016, by Honda *et al*.,[156] the authors proposed the self-propagated Lossen rearrangement under basic conditions, in which the reaction starts by formation of catalytic amounts of isocyanate after a first rearrangement of self-protected hydroxamic acid. This is shown for **1q** in **Scheme 24**.
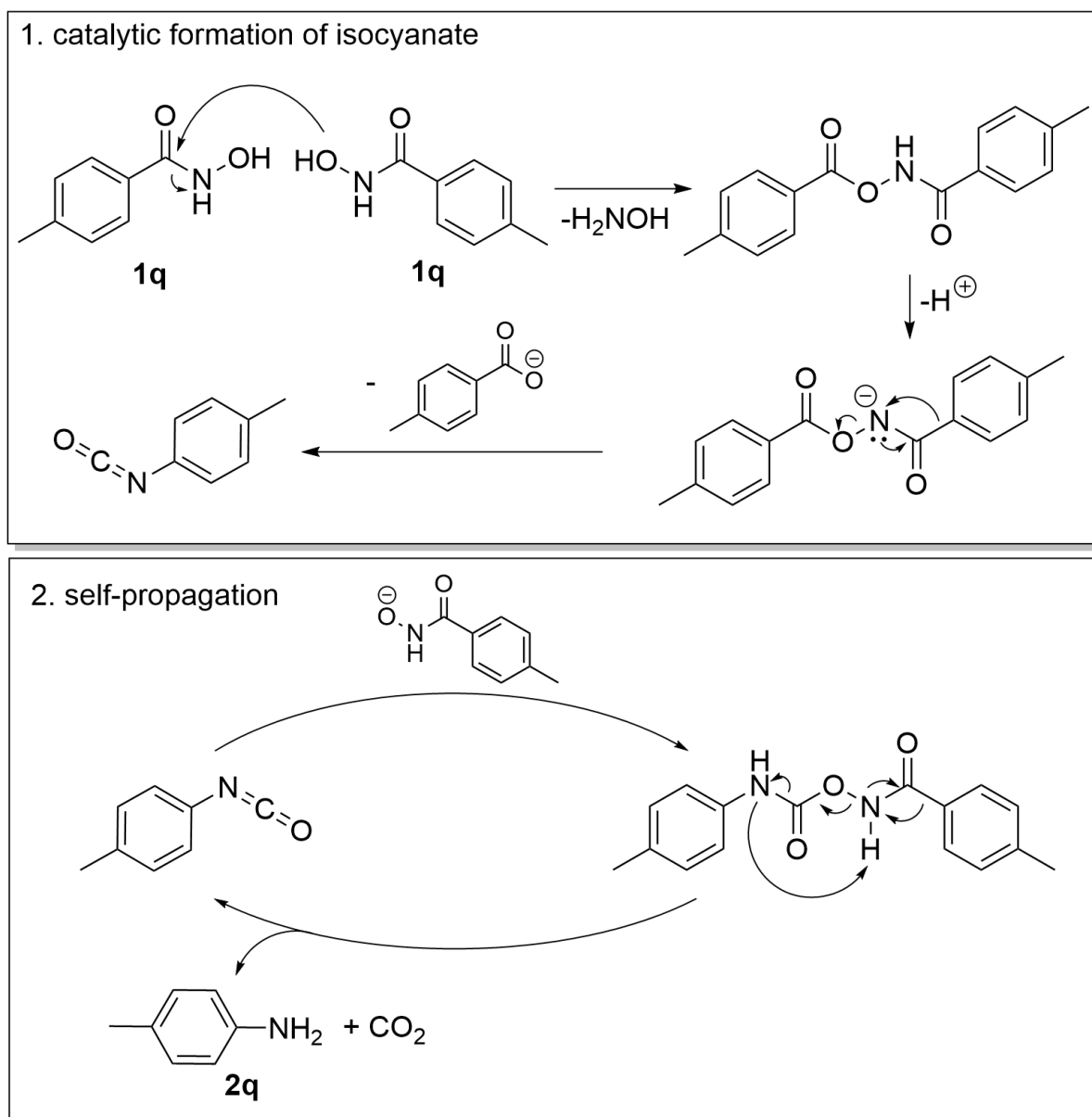
Scheme 24 Mechanism of the self-propagative Lossen rearrangement after an initial self-condensation step proposed by Honda *et al.* with *p*-toluidine **2q** as final product.

The first step occurs only in catalytic amounts, therefore the chance that the expelled hydroxylamine performs side-reaction is small. Beside this self-propagating aniline formation, it is also plausible that both tested hydroxamic acids (**1q** und **1s**) are not stable under GC conditions (temperature up to 300 °C) and therefore fragmenting and/or rearranging during the chromatographic analysis cannot be ruled out. In either case, these examples produce unreliable results, thus being unsuitable for screening *via* the proposed method.

Conclusively, a satisfactory screening could not be performed *via* GC, as the activating effect of CO_2 on the Lossen rearrangement was not quantified. The results and calculated yields were

tainted from the presence of aniline and phenyl isocyanate moieties already present in the mixture before addition of CO_2 or the degradation of the aromatic components during the GC analysis. Additionally, the screening parameters, including the need for a certain temperature to dissolve the starting material in ethyl acetate, only partially reflect the properties of the DMSO/CO_2 switchable solvent system. Therefore, an alternative is proposed in the next subsection to avoid the mentioned issues.

4.1.3.2 NMR screening

After initial problems with the GC monitoring, ^{1}H NMR spectroscopy proved to be an efficient monitoring analysis. Compared to aliphatic hydroxamic acids, the aromatic compounds possess the advantage of typical structural signals located at higher ppm values, far from solvent residual peaks and interference from the organic bases (see chapter **4.1.2**).

The model system was designed to employ dry chemicals to avoid the formation of bicarbonate salt. In a standard procedure, the hydroxamic acid and the analytical standard were dissolved in anhydrous DMSO, followed by the addition of DBU. The t_0 sample was taken before and after exposure to CO_2 ($t_0(CO_2)$). Afterwards, samples were taken at the desired times and diluted with DMSO-d_6. The internal standard, in this case 1,3,5-trimethoxybenzene, was chosen since its signals do not overlap with those of other reaction components, as well as of intermediates and products (signal of standard at 3.8 (s) and 6.1 ppm (s)). In **Figure 32**, a typical screening spectrum is shown for the Lossen rearrangement of *N*-hydroxybenzamide **1n**.
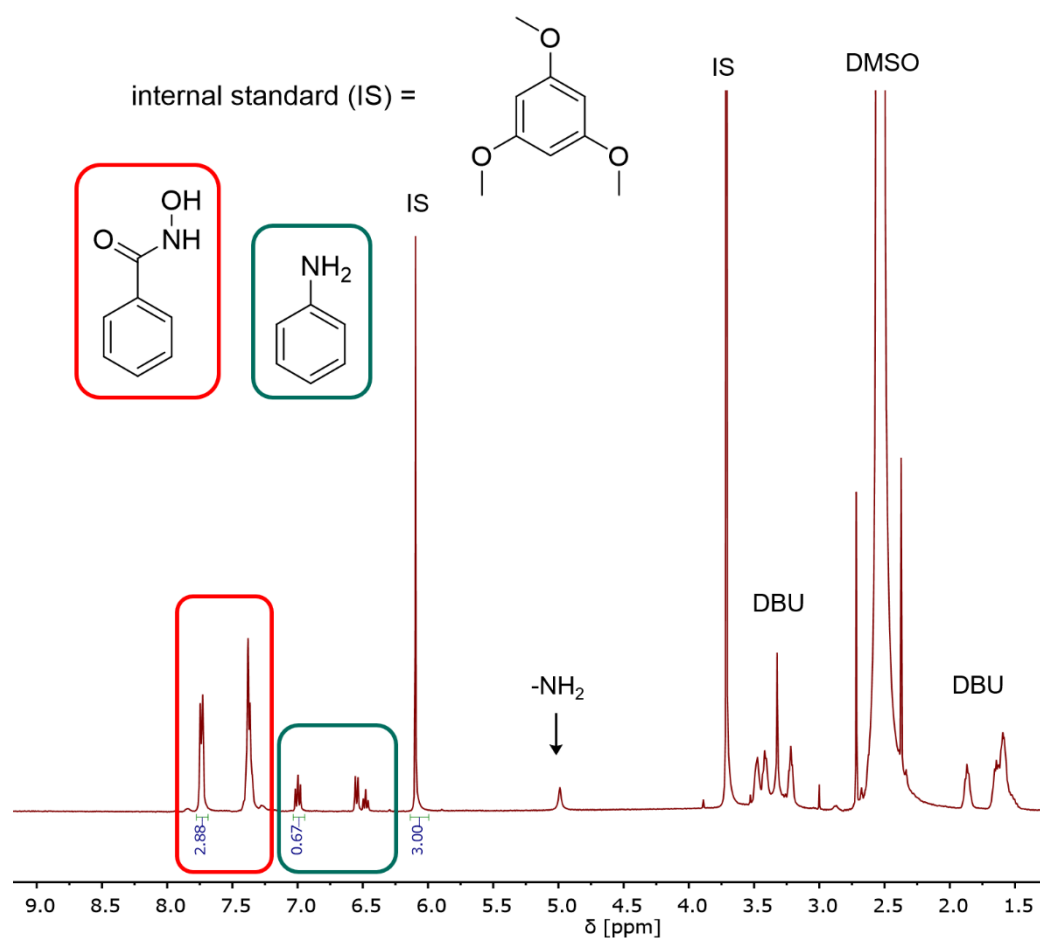
Figure 32 Typical NMR spectrum from the screening of the CO_2 based Lossen rearrangement of *N*-hydroxybenzamide **1n** in the presence of DBU and DMSO.

It is noted that the single broad acidic signal of the hydroxamic acid functionality under basic conditions differs to the sharp signals in a slightly acidic environment and, therefore, the baseline error for the amine protons of the aniline (*ca*. 5 ppm) increases. As the reaction progressed, the mixed broad OH/NH signal of the hydroxamic acid shifted towards lower ppm values: from *ca*. 9 ppm to 4 ppm after 20 h, a behavior indicating increasing basicity with time, which is explained by the transformation of hydroxamic acid to a weakly basic aniline. A similar effect is observed directly after the introduction of CO_2, since the broad signal shifts from 9.12 ppm to 9.37 ppm, indicating a minor acidification of the reaction mixture (**Figure 33 A**). However, the presence and shift of the mentioned peak prevented the uniform integration of the same peaks for the whole reaction. For instance, the amine signal at 5 ppm was compared to the internal standard up to 5 hours (**Figure 33, B**), while the benzene ring proton signals were only integrated after.

Results and discussion
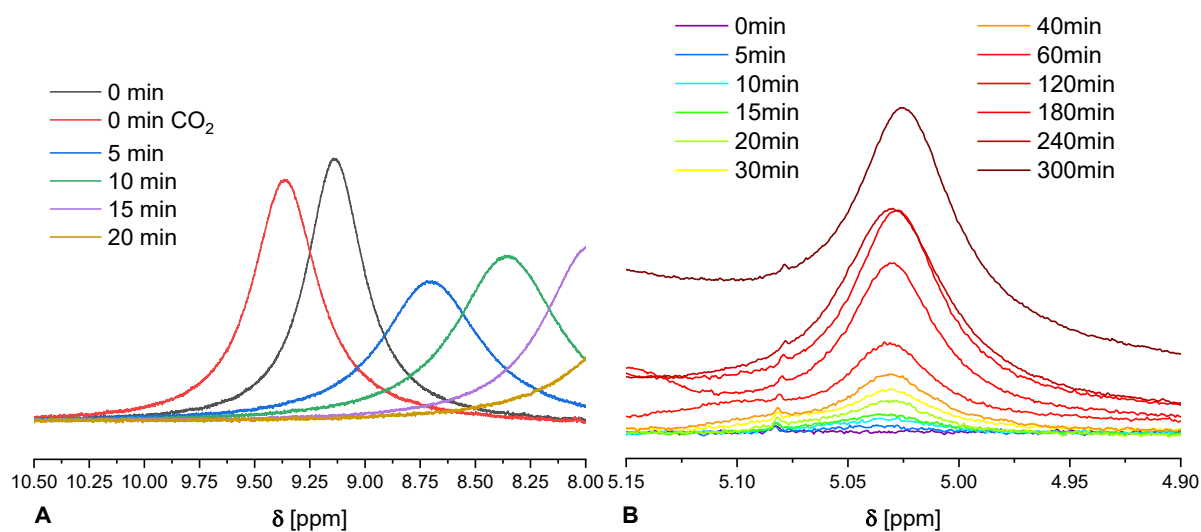
Figure 33 A: Gradual upfield shift of the acidic protons signals caused by the decrease in acidity of the system. **B**: The signal at 5 ppm of the aniline **2n** protons increasing in intensity with time.

Table 7 Yield over time calculated from ^{1}H NMR spectra for the CO_2 based Lossen rearrangement. Conditions: 1.00 mol/L in DMSO, 100 °C, 1.00 eq. **1n**, 1.00 eq. DBU, CO_2 (atm).

Time [min]	Yield [%][a]	Time [min]	Yield [%][a]
0	0	60	10
5	0	120	17
10	1	180	29
15	2	240	32
20	3	300	32
30	5	360	33
40	7	480	34

a) Yield was determined using IS (3,4,5-trimethoxybenzene).

Therefore, the yield was calculated by integrating both the aromatic region and the aniline protons and comparing them to the signals of the IS, which was set to the same integral determined prior by the t_0 sample (**Table 7**). ^{1}H NMR screening reactions were exclusively conducted on the system based on the same hydroxamic acid, namely *N*-hydroxybenzamide **1n**, under different reaction parameters. For instance, the temperature range was increased from 70 to 110 °C in 10 K steps. The results indicated an optimal temperature of 110 °C, which is higher than what was reported in literature (90 °C). At 70 °C, no conversion was observed, even after 6 hours (**Table 8**).

Table 8 Yields of **2n** in a CO_2 based Lossen rearrangement after 6 h at different temperatures.

T [°C]	Yield [%]
70	-
80	10
90	18
100	33
110	60
120	56

This result confirms the inadequacy of GC screenings, where the reaction was performed at 70 °C under more dilute conditions in a non-optimal system and thus presumably led to the formation of aniline **2n**, in low yield. One possible explanation discussed at the end of chapter 4.1.3.1, the fact that *N*-hydroxybenzamides are not stable under GC conditions, was therefore supported by the ^{1}H NMR spectroscopy findings.

By observing the obtained yields, the low efficiency of the reaction becomes clear, especially when compared to already published procedures. Honda *et al*. reported a 96% isolated yield of aniline in a DBU promoted Lossen rearrangement at 90 °C for 2 h, in which the base was employed in catalytic amounts.[156] The mechanism of the reaction has already been shown in **Scheme 24**. Though the reaction conditions described in this work were adjusted to enable suitable monitoring (higher dilution, equimolar amount of base), the overall yield did not surpass 60% after 6 h at 110 °C. Further parameter optimization is therefore unlikely to reach the same yield as that reported in literature. As the only difference in the mechanistic pathway is the exposure to CO_2, two explanations are possible. The first one is based on the equilibrium in the last step of the Lossen rearrangement: the addition of water to the isocyanate leads to the formation of the carbamic acid, a highly unstable compound which quickly degrades to amine and CO_2. Performing the rearrangement under CO_2 atmosphere could promote a shift in the equilibrium toward the carbamic acid. However, the formation of the carbamic acid is energetically unfavorable and this class is usually unstable at atmospheric pressure. In addition, aromatic amines are known to be inert toward CO_2.[71] A pressure slightly over 1 bar is therefore improbable to cause a retrogression of the reaction course. Meanwhile, the second possibility focuses on the base. DBU is a weakly nucleophilic guanidine base, therefore able to actively bond electrophiles such as CO_2 in a covalent manner, an addition reported

multiple times in the literature.[63b],[347] As the equilibrium between the guanidine and its adduct is dependent on the temperature and pressure, the presence of CO_2 could cause a decrease in concentration of free base in the reaction mixture, thus partially preventing the reaction. Furthermore, further optimization of the reaction conditions (like solvent, stoichiometry, concentration, additives, etc.) could lead to a reasonable increase in yield, although screening is challenging since the conditions do not match those of the ^{1}H NMR monitoring. However, since optimizations are time-consuming and are not likely to reach the same yields as reported in literature, no further adjustments on the synthetic parameters were performed.

As a final part of this project, the influence of CO_2 on the Lossen rearrangement was studied to determine the difference in mechanistical pathways between the proposed method and a classical Lossen rearrangement, which will be shortly discussed in the next subsection.

4.1.4 IR screening

As discussed in the previous chapters, the impossibility to determine the mechanistic details on the rearrangement of hydroxamic acids, as well as to confirm the presence of intermediate **A**, led to a temporary halt of the project. To gain further insights, a new approach based on online IR spectroscopy was chosen to overcome the deficiencies of both NMR spectroscopy and GC. The monitoring setup consisted of a 130 mL pressure reactor coupled to a MettlerToledo® online IR detector, as described in **section 5.1.7.** This system was designed for easy detection of typical vibrational signals, such as carbonyls expected from intermediate **A**, under harsh conditions, thus enabling the detection of a possible intermediate at CO_2 pressures up to 130 bar and at temperatures ranging from −80 to 180° C. Additionally, a vertical window was installed for a visual check on the homogeneity of the mixture on the chosen conditions.

In a typical reaction, the hydroxamic acid and DBU were dissolved in DMSO and the reaction status was monitored every 30 seconds. A typical 3D spectrum is shown in **Figure 34**.
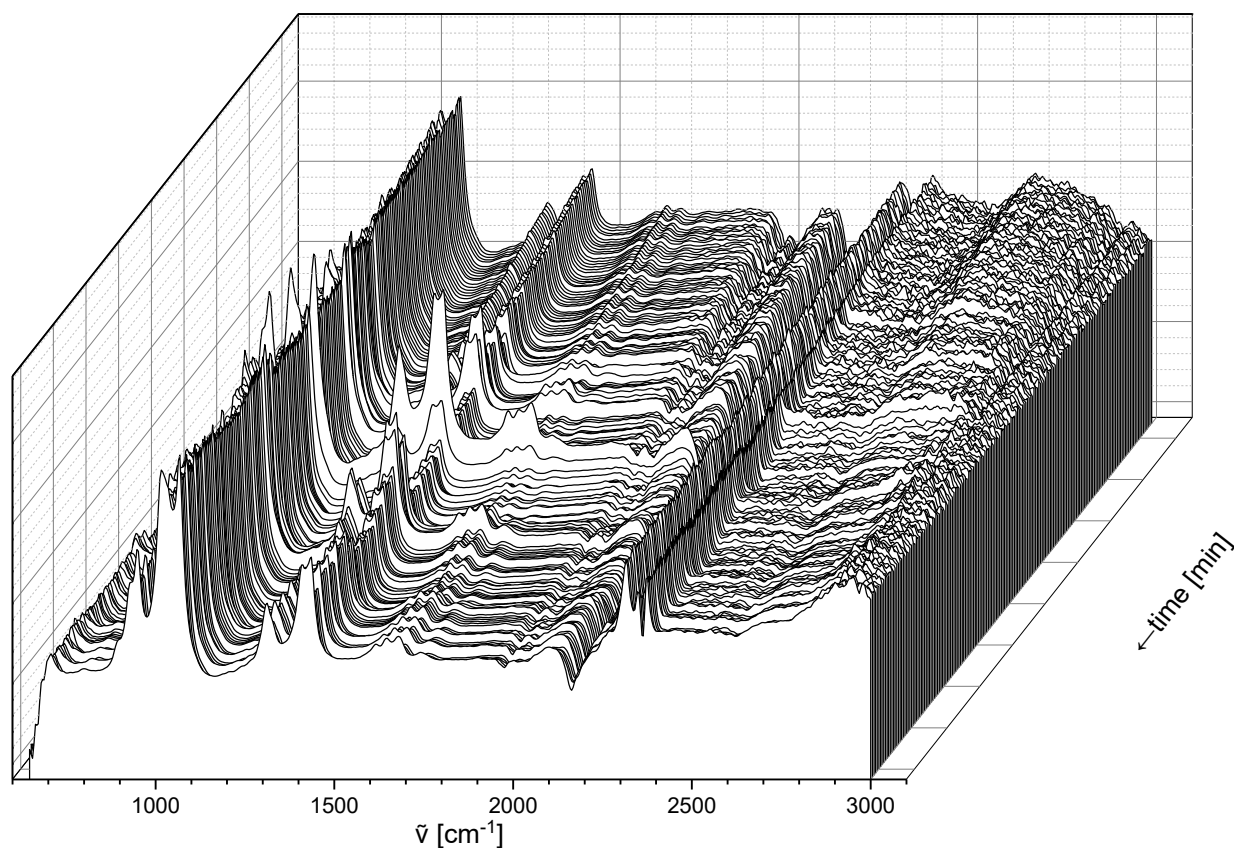
Figure 34 3D absorbance plot over reaction time of the mixture containing hydroxamic acid **1e** and DBU in DMSO, after exposure to 10 bar of CO_2 at 40 °C.

The differing IR signal intensities, especially in the central regions of the plot, are caused by temperature fluctuations resulting from external factors such as during temperature stabilization after fast heating. The advantage of online monitoring becomes clear as one measurement is taken in intervals to check for changes in the spectrum. This method allows for the screening of many parameters at once, which is difficult *via* offline screenings. In this case, after the addition of CO_2, a new signal was detected around 1725 cm^{-1}, and is seen in the last scan (front) of the 3D plot.

The 2D plot of the reaction mixture composed of hydroxamic acid and DBU in DMSO at 10 bar CO_2 pressure and 40 °C is shown in **Figure 35**.
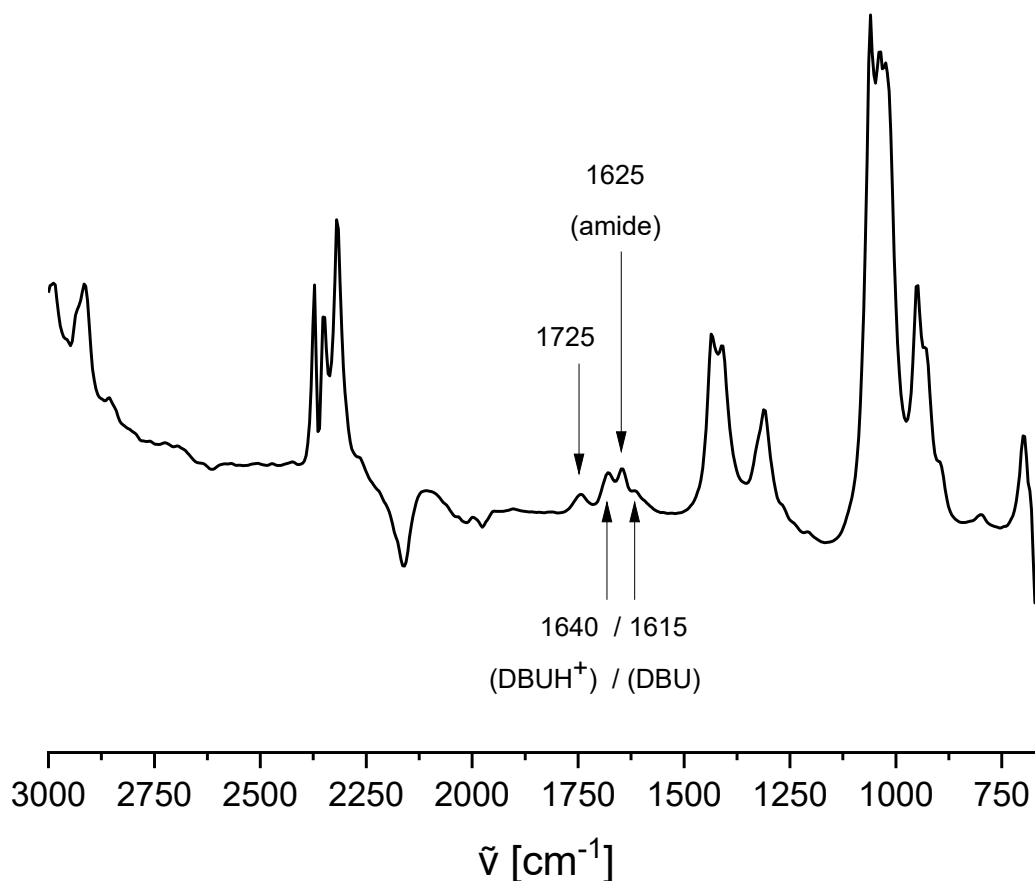
Figure 35 2D IR spectrum of the reaction mixture containing hydroxamic acid **1e** and DBU in DMSO, after exposure to 10 bar of CO_2 at 40 °C.

After the addition of CO_2, a low intensity signal in the region of carbonyls (1725 cm^{-1}) appeared. The signal does not belong to either DBU in its neutral or protonated form (1615 and 1640 cm^{-1}, respectively)[348] or the hydroxamic acid (1625 cm^{-1}). However, the experiment was not repeated a second time due to technical- and time-related issues. In the future, further attempts for a full characterization of this species will be performed. The intermediate was thus not be further identified, however, IR spectroscopy under harsh conditions clearly pointed to the change in chemical properties upon CO_2 exposure. In the future, the employment of online IR technology should be fully exploited for further insights in this project, but also for many other potential procedures requiring CO_2.

4.1.5 Conclusion and outlook

Conclusively, this chapter described the synthesis of hydroxamic acids from renewable materials and aromatic compounds and their subsequent CO_2-mediated Lossen rearrangement. The optimization of the rearrangement conditions with aliphatic hydroxamic

acids was followed by NMR spectroscopy and GC screening methods giving further insights on the mechanistical aspects of the procedure and the related encountered issues.

From the information gained with the mentioned compounds, an improvement was made by employing aromatic hydroxamic acids. Aliphatic hydroxamic acids did not react in the proposed rearrangement under the employed conditions. The respective aniline products were synthesized under the optimized conditions determined by both GC and by ^{1}H NMR spectroscopy screening. Especially the second option proved extremely helpful, with facile evaluation by simple integration of typical aromatic signals and comparison with an inert standard, namely 1,3,5-trimethoxybenzene. The employed techniques increased aniline yields, for instance for aniline **2n** from around 10% to 60%. Even if reported literature yields are higher than with the proposed CO_2-based system, further optimization of the reaction conditions is still possible. Crucially, this method represents a "greener" procedure for the preparation of anilines.

Furthermore, preliminary online IR analysis indicated the formation of a new species upon CO_2 exposure at pressures higher than atmospheric, possibly originating from a CO_2-hydroxamate intermediate. Therefore, it is likely that the mechanism of the described Lossen rearrangement proceeds differently than the pathway introduced by Honda *et al*. in 2016. Following research on this topic should focus on the use of online IR techniques for two reasons: to find the optimal conditions for the intermediate formation, to capture the adduct of CO_2 and the hydroxamic acid with an electrophile such as methyl iodide, and to monitor the course of the reaction by examining the carbonyl regions between 1600 and 1800 cm^{-1}. The last point will include an improvement of the reaction conditions for the synthesis of the desired product, which is either an amine, urea or carbamate. As the described reactor system can withstand even harsh temperatures and extreme pressure, for laboratory scales, great variation of parameters can be performed highlighting the great potential of the proposed system. Additionally, theoretical calculations are anticipated to help understand the reaction mechanism and pinpoint the optimal conditions.

4.2 Thiol-ene Polymerization

4.2.1 Monomers

In the previous chapter, the Lossen rearrangement was introduced on the basis of amine and urea synthesis, *via* a CO_2 based mechanism. In this section, the Lossen rearrangement will be employed for another purpose.

In a publication of the Meier group in 2013, a more sustainable variant of the Lossen rearrangement was published. Kreye *et al.*[152] employed dialkyl carbonates as solvent and reactant in cooperation with alkyl alcohols as trapping agents. With this method, alkyl carbamates were isolated in yields up to 85%, especially methyl carbamates.[152] As mentioned in the previous chapter, aromatic compounds only led to the formation of anilines also in this case. Therefore, the use of diallyl carbonate and allyl alcohol in the Lossen rearrangement is of particular interest. A rearrangement in such a system leads to a terminal allyl double bond (**Scheme 25**), which offers a variety of possible applications for further functionalization.
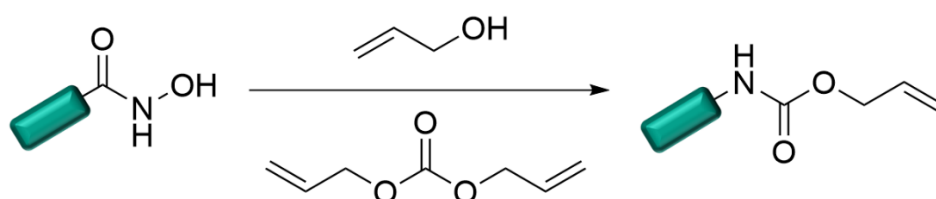
Scheme 25 Lossen rearrangement performed in diallyl carbonate with allyl alcohol as trapping agent.

Terminal double bonds are not only interesting for the easy conversion into other groups *via* epoxidation, addition and hydroxylation reactions, but also for polymerization. For example, the conversion of the unsaturated moiety to a polyethylene backbone–based polymer with carbamate side chains is possible (e.g. vinyl carbamates, **Scheme 26**, **A**),[349] whereas such carbamates are currently typically introduced by post-polymerization functionalization of polyols with toxic isocyanates (**Scheme 26**, **B**).[350]
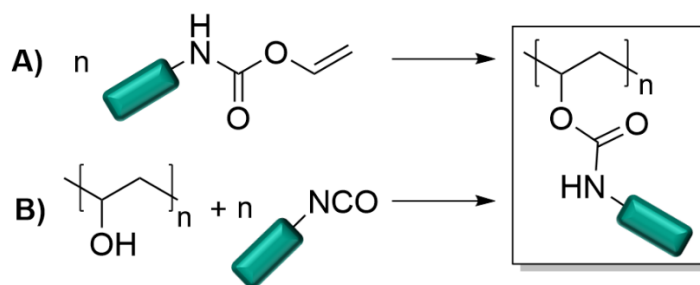
Scheme 26 Two different approaches for the preparation of polymers with carbamate side chains.[349],[350]

Another possible conversion is the formation of a polyurethane backbone, which is industrially produced *via* polyaddition of diisocyanates and dialcohols.[184] To be able to form non-isocyanate-based polyurethanes (NIPU), a different kind of polymerizable monomer is needed. For example, the Lossen rearrangement of an hydroxamic acid with terminal double bond allows for the preparation of carbamates with two terminal alkene groups. Afterwards, two polymerization methods are possible: either acyclic diene metathesis (ADMET)[351] or thiol-ene polyaddition. The first method requires only the carbamate as monomer, but depends on a metal catalyst and, to achieve high molecular weights, the polymerization has to be performed under vacuum or under constant inert gas stream to remove the ethylene formed during the condensation (**Scheme 27**).[352]
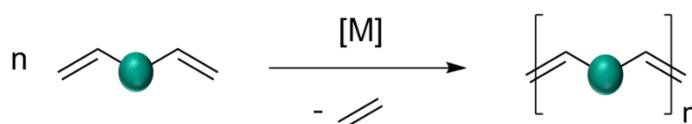
Scheme 27 Schematic representation of the ADMET-polymerization of dienes.

Polymer properties derive only from the functionality of the diene. The thiol-ene method requires a dithiol as second component and offers high selectivity, fast reaction times, no necessity for a catalyst and the polymer properties are influenced by the choice of both dithiol and diene, and their additional functionalities.[275] Furthermore, as already mentioned in **chapter 2.6.2**, polymers with high sulfur content tend to display promising optical properties. Considering the advantages and disadvantages of both methods, the thiol-ene polymerization was deemed advantageous, both from a synthetic and applications point of view (**Scheme 28**).

Results and discussion
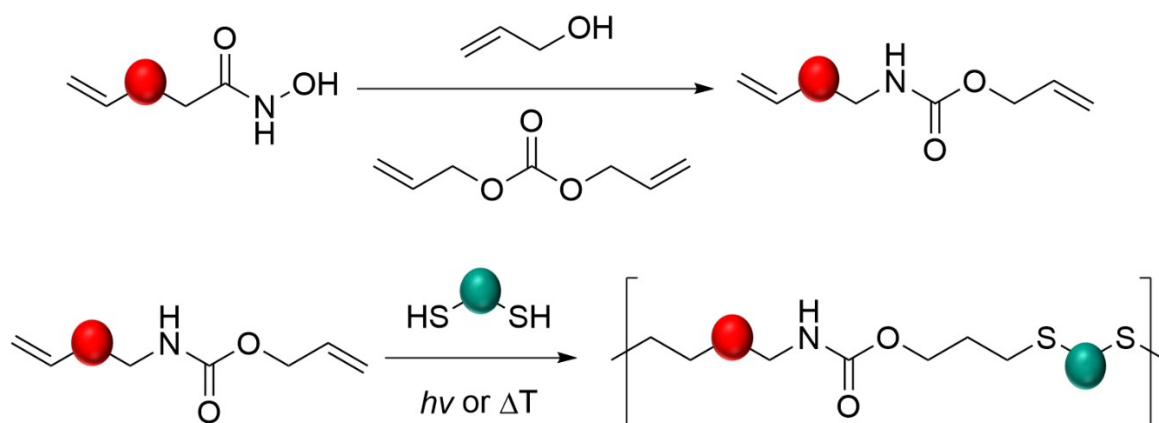
Scheme 28 Schematic representation of the formation of carbamates with two terminal double bonds *via* the Lossen rearrangement (above) and subsequent thiol-ene copolymerization with a dithiol (below).

As mentioned in **chapter 2.4.2**, the Lossen rearrangement of hydroxamic acids leads to carbamates, while side reactions yield further useful products. The main side reaction results in the formation of urea compounds, which are generated through the addition of the *in situ* formed isocyanate and its hydrolyzed form, the amine.[353]

The aim of this chapter was therefore to perform the Lossen rearrangemement of unsaturated fatty hydroxamic acids in the presence of diallyl carbonate and allyl alcohol in order to isolate both carbamate and urea, which possess two terminal double bonds. The double bonds present on each side of the functionality then allow these compounds to be used as monomers in the thiol-ene polymerization. A general observation was, that the urea precipitated after cooling of the crude reaction mixture. Simple filtration and drying of the white precipitate yields clean urea. The advantage of the formation of polymerizable products and side products, which are also readily separable after the rearrangement, increases the importance of the Lossen reaction and opens new opportunities in the polymer field. Another interesting compound has been detected during the column chromatography at a high retardation factor (R_F) in TLC of *ca*. 0.87, which is the respective allyl ester, as determined by NMR spectroscopy, presumably formed through transesterification of the hydroxamic acid with the present allyl alcohol (**Scheme 29**).
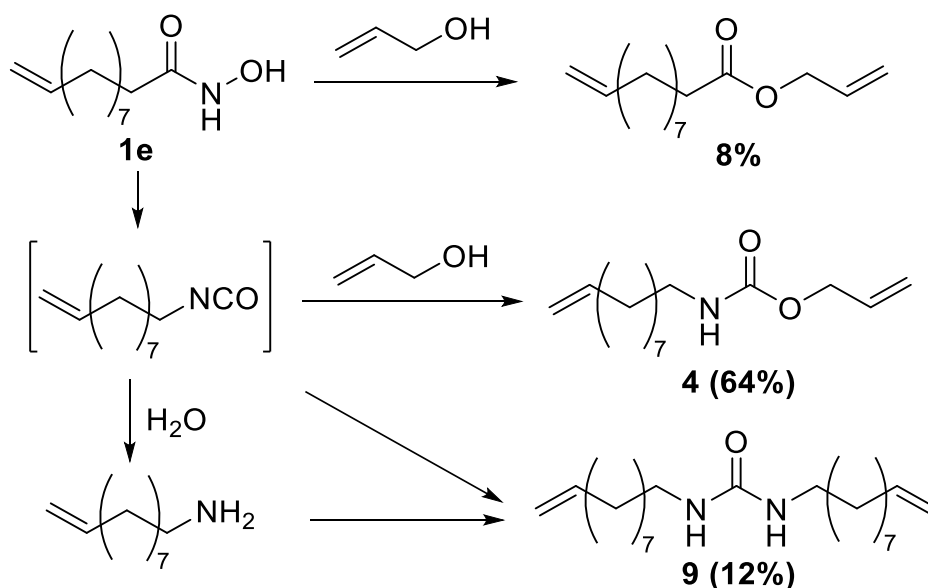
Scheme 29 Formation of products, intermediates and side products during the Lossen rearrangement based on the model compound *N*-hydroxy-10-undeceneamide **1e**.

However, the fraction containing allyl undecenoate was found to be contaminated by diallyl carbonate (DAC), as identified by NMR spectroscopy. Weakly dependent on the eluent mixture, DAC yielded broad bands on the TLC that overlapped with the spot of the ester and thus isolation of pure allyl undecenoate was not possible. After integration of the signals observed in the corresponding ^{1}H NMR spectra and subsequent subtraction of DAC from the yield, it was decided not to perform a second column chromatography, as it would result in waste of materials, considering the low amount of ester side product (8%) (**Scheme 29**). The carbamate (R_F = 0.4) was isolated in 64% yield and was not contaminated by DAC because of the large difference in R_F value.

The same procedure was applied to different fatty hydroxamic acids (**Figure 36**). For instance, the respective carbamate and urea obtained from *N*-hydroxyoleamide (**1a**) were isolated in moderate yields (40% urethane **5** and 3% urea **10**). More problematic were molecules with longer alkyl chains, like the hydroxamic acid synthesized from erucic acid **1c**. The C$_{22}$ residue bearing one unsaturated double bond was found to be insoluble in diallyl carbonate, even under the influence of heat. The introduction of DMSO as cosolvent also proved to be unsuccessful.

In a similar approach, the same reaction was then attempted with five hydroxamic acids produced from diesters (**1g-h**) (**Figure 21**). In the case of the sebacate **1j** and

tetradecanedioate **1k** staring materials, even the addition of DMSO as cosolvent did not dissolve the compounds in diallyl carbonate. The rearrangement took place nonetheless, leading to a white solid after filtration of the reaction mixture. The precipitate was analyzed *via* mass spectrometry, where both the carbamate and the urea (**7a+b**) were detected. The two molecules were impossible to separate by recrystallization or column chromatography because of solubility issues. The Lossen rearrangement of **1j** was repeated at 160 °C, a temperature at which the dihydroxamic acid became soluble. The result, however, did not change, as the white solid forming upon cooling to room temperature could not be purified because of the same issues as in the previous attempts. In contrast, the shorter *N*-hydroxyamides of maleic and succinic diesters were soluble. TLC suggested the presence of both carbamate products based on the appearance of new spots, however, upon isolating the fractions by column chromatography in DCM:EA (85:15) and removing the solvent *via* distillation, the amount of solid obtained was insufficient for any kind of analysis (<1 mg from a 0.5 g batch). Therefore, the respective carbamates were not isolated.

Meanwhile, the Lossen rearrangement of adipoyl dihydroxamic acid **1i** produced the bis allyl carbamate **6** in moderate to low yields (**Figure 36**). Despite the low yield, its employment as a diene component in the thiol-ene polymerization, as will be discussed in **chapter 4.2.8**, was carried out.

Furthermore, a shorter chain carbamate diene was synthesized to enable determination of a trend if a property change was observed after the polymerization. Therefore, *N*-allyl allylcarbamate **3** was synthesized from diallyl carbonate and allyl amine. The reaction proceeded slowly as the reaction temperature was limited by the boiling point of allylamine. The conversion was monitored by GC until the DAC signal disappeared. After purification, the carbamate was polymerized as described in **chapter 4.2.7**.
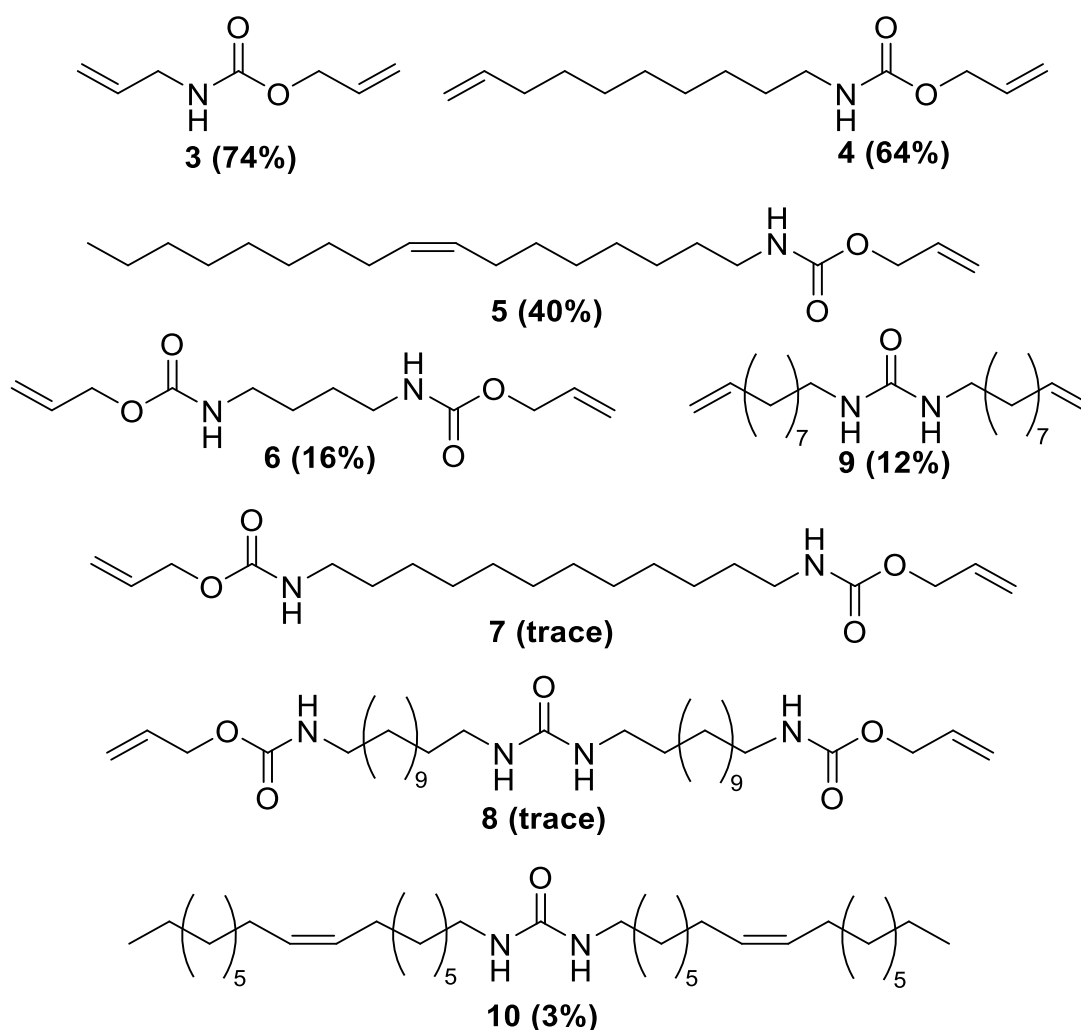
Figure 36 Structures and yields of the synthesized dienes. All compounds, except **3**, were obtained *via* the Lossen rearrangement. Carbamates **7** and urea **8** were detected by FAB-MS, the compounds were, however, not isolated.

With several carbamate containing dienes in hand, the focus was turned to the preparation of the second monomer for the thiol ene polymerization, namely the dithiols. Most of the employed dithiols were commercially available, however, since this work is focused on the employment of renewable materials, three dithiols were synthesized following an already known procedure (**Scheme 30**).[354] For this purpose, (*R*)-(+)-limonene and 1,4-cylohexadiene were chosen as starting materials.
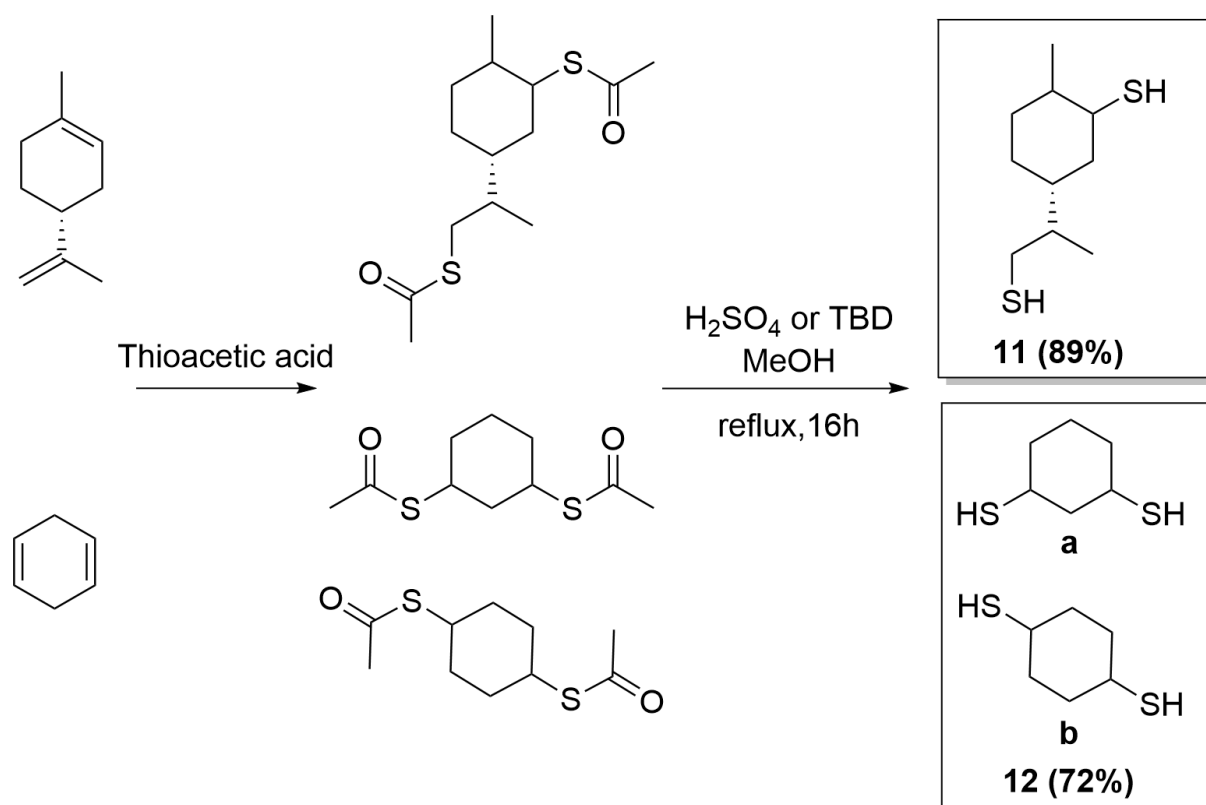
Scheme 30 Schematic representation of the synthetic procedure for the synthesis of dithiols from the respective renewable dienes in a two-step approach.

Limonene is abundant in citrus fruits and is extracted from the respective peel oil, while 1,4-cyclohexadiene is obtained as a product from the metathesis of plant oils with high linolenic acid content.[355] The procedure for the formation of the dithiols is based on a two-step synthesis. First, the diene is reacted with two equivalents of thioacetic acid to yield the dithioester in quantitative yields. The full conversion to the respective dithioester was confirmed by GC analysis in ethyl acetate (**Figure 37**). It is worth mentioning that the cyclohexanedithiol was obtained as a mixture of four different isomers, specifically the *cis-* and *trans*-isomers for both the 1,3- and the 1,4-products, respectively. Since the isomers were not possible to be separated by column chromatography, the mixture was used as isolated for future polymerizations.
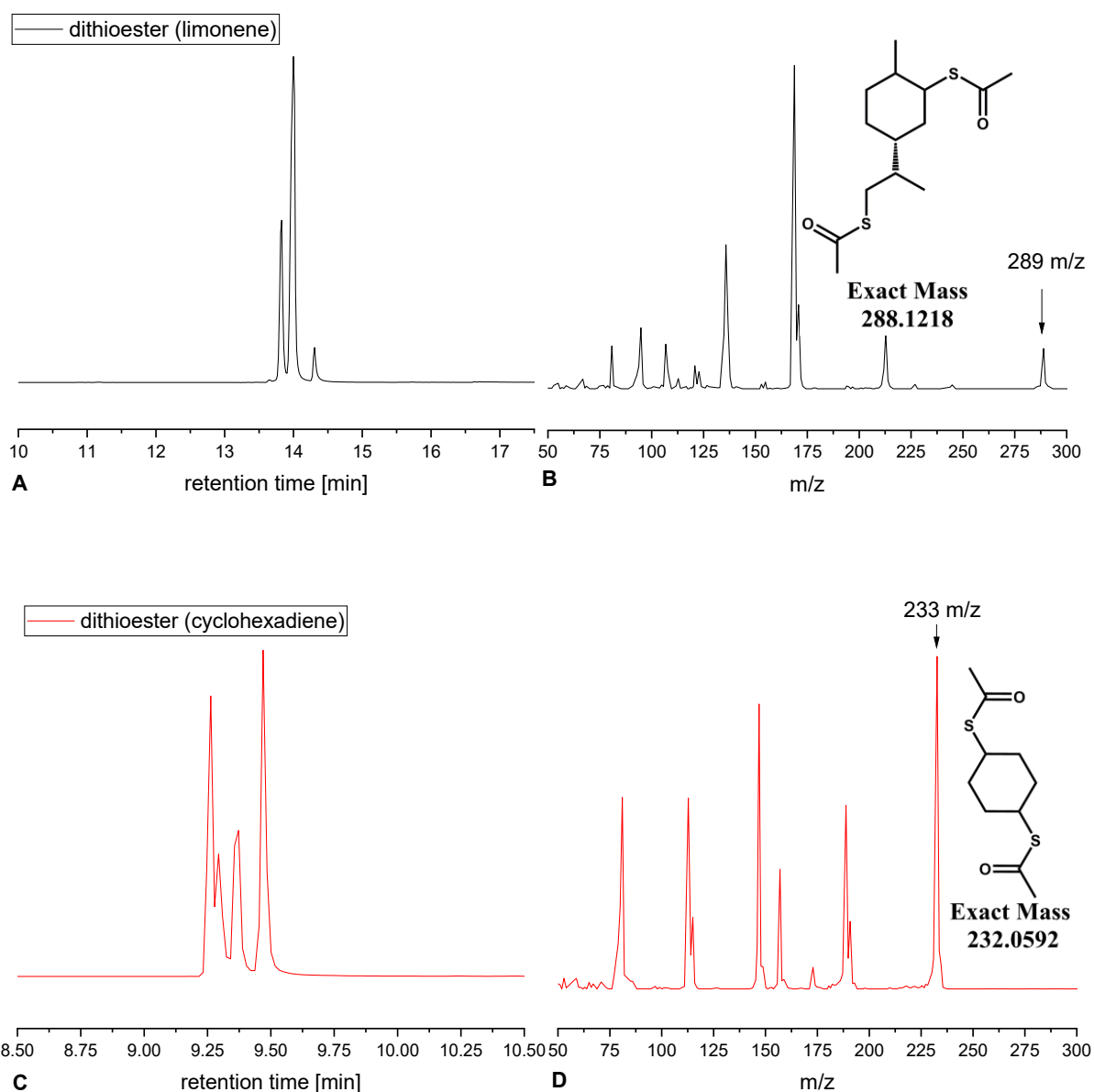
Figure 37 GC graphs of the dithioester intermediates and respective MS of limonene (**A**, **B**) and 1,4-cyclohexadiene (**C**, **D**).

The multiple signals in the chromatogram result from the different isomers after the addition of thioacetic acid to the diene functionalities (**Figure 38**). Llimonene possesses two *cis*- and *trans*-adducts (**A1-2**), however, another isomer is visible at a small intensity, which was assumed to belong to the sterically hindered **A3** (see **Figure 38**). In case of 1,4-cyclohexadiene, the four signals were attributed to the *cis*- (**B1**, **B3**) and *trans*-isomers (**B2**, **B4**) of the 1,3- and 1,4-dithioester products. The respective product masses were found by GC-MS, as also shown in **Figure 38**.
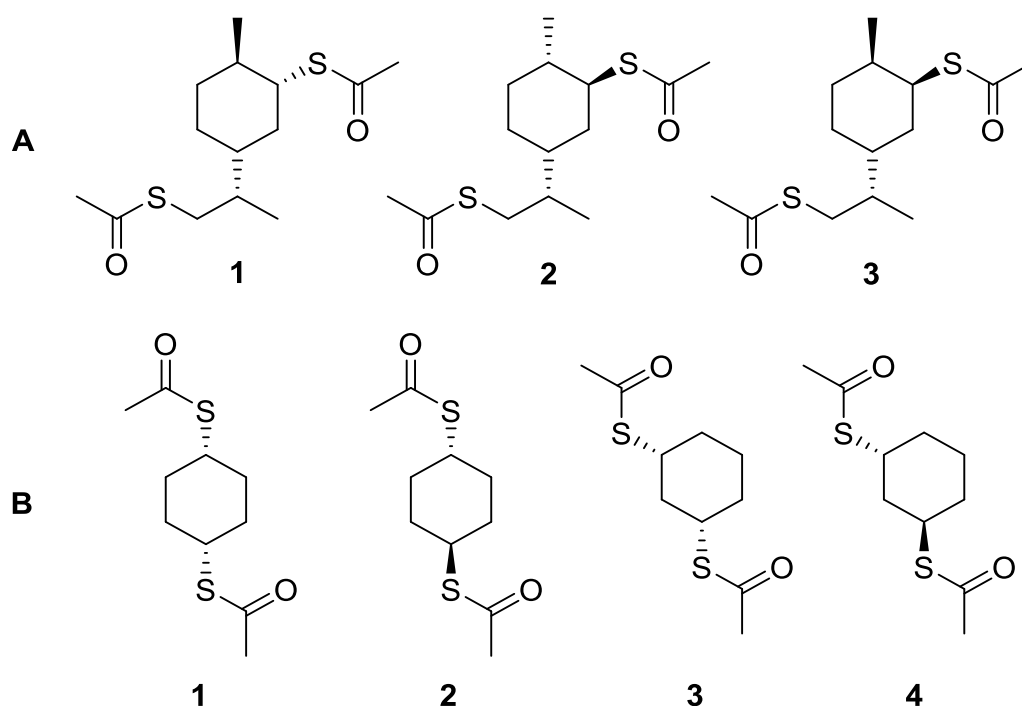
Figure 38 Isomers of the dithioesters prepared from limonene (A), and 1,4-cyclohexadiene (B).

Afterwards, the isolated dithioesters were transesterified with methanol in the presence of either TBD or H_2SO_4 as basic or acid catalyst, respectively. Subsequently, the resulting dithiols were analyzed *via* NMR and high-resolution mass spectrometry (HRMS) techniques (see **chapter 5.2.4**).

Another terpene, 1-isopropyl-4-methylcyclohexa-1,4-diene (γ-terpinene), was employed for the preparation of the respective dithiol (**Scheme 31**) and subsequent employment in the thiol-ene polymerization, however, only the monothioester was observed *via* GC-MS.
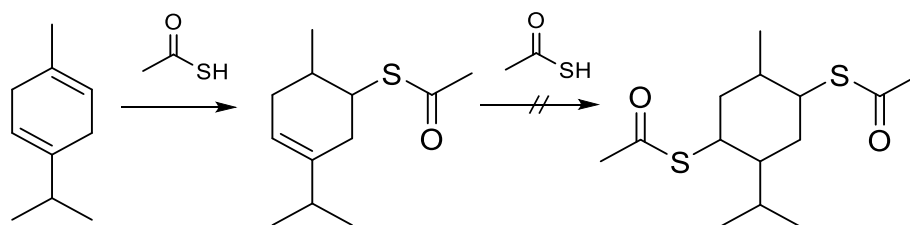
Scheme 31 Schematic representation of the synthesis of a dithioester from γ-terpinene.

An attempt or prepare the dithioester by increasing the equivalents of thioacetic acid was unsuccessful, as the outcome did not change. This behavior was hypothesized to be the result

of the steric hindrance of the isopropyl group, hindering the addition of thioacetic acid to the unsaturated substrate.

With suitable renewable diene and thiol monomers in hand, their polymerization in a classical thiol-ene fashion was sought: the diene and dithiol were mixed at room temperature (r.t.) in tetrahydrofuran (THF) in a 1:1 ratio, followed by the addition of a suitable photoinitiator and subsequent exposure to ultraviolet (UV) light (365 nm) for the desired time. The crude mixtures were analyzed *via* size exclusion chromatography in hexafluoroisopropanol (HFIP-SEC) to determine the molecular weight and dispersity of the polyurethane, as well as the presence of impurities. After purification by precipitation in cold methanol from a concentrated THF solution and drying under vacuum, the polymers were compared with the diene *via* IR (**Figure 39**) and NMR spectroscopy (**Figure 40**).
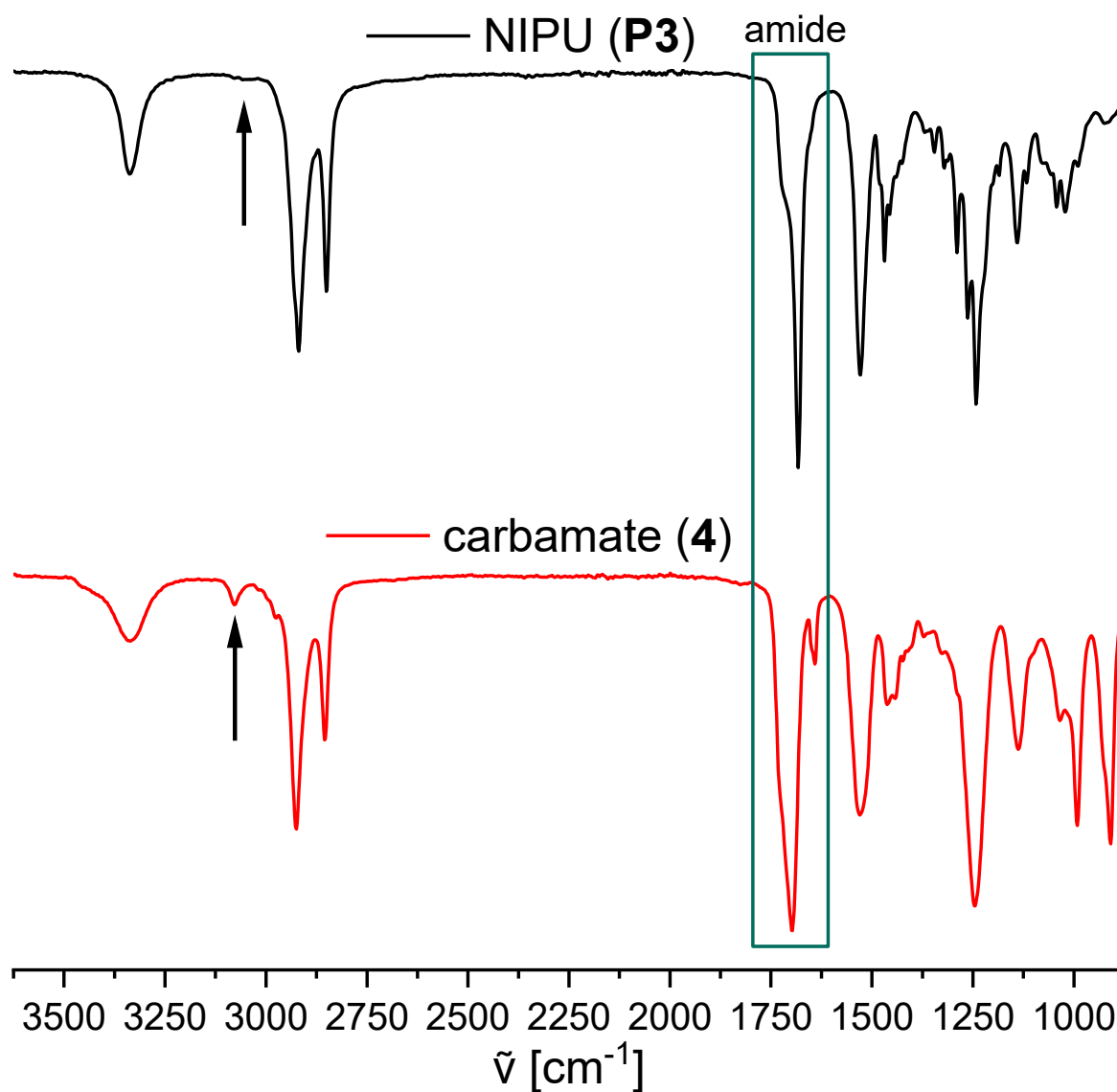
Figure 39 IR spectra of the carbamate monomer **4** (red) and the respective polyurethane **P3** (black).

In **Figure 39**, the arrow indicates the double bond signal, which almost disappears after the polymerization, indicating the conversion of the terminal double bonds of the carbamate **4**. Meanwhile, the amide carbonyl signal at 1700 cm^{-1} belonging to the carbamate functionality remains unchanged after the polymerization.
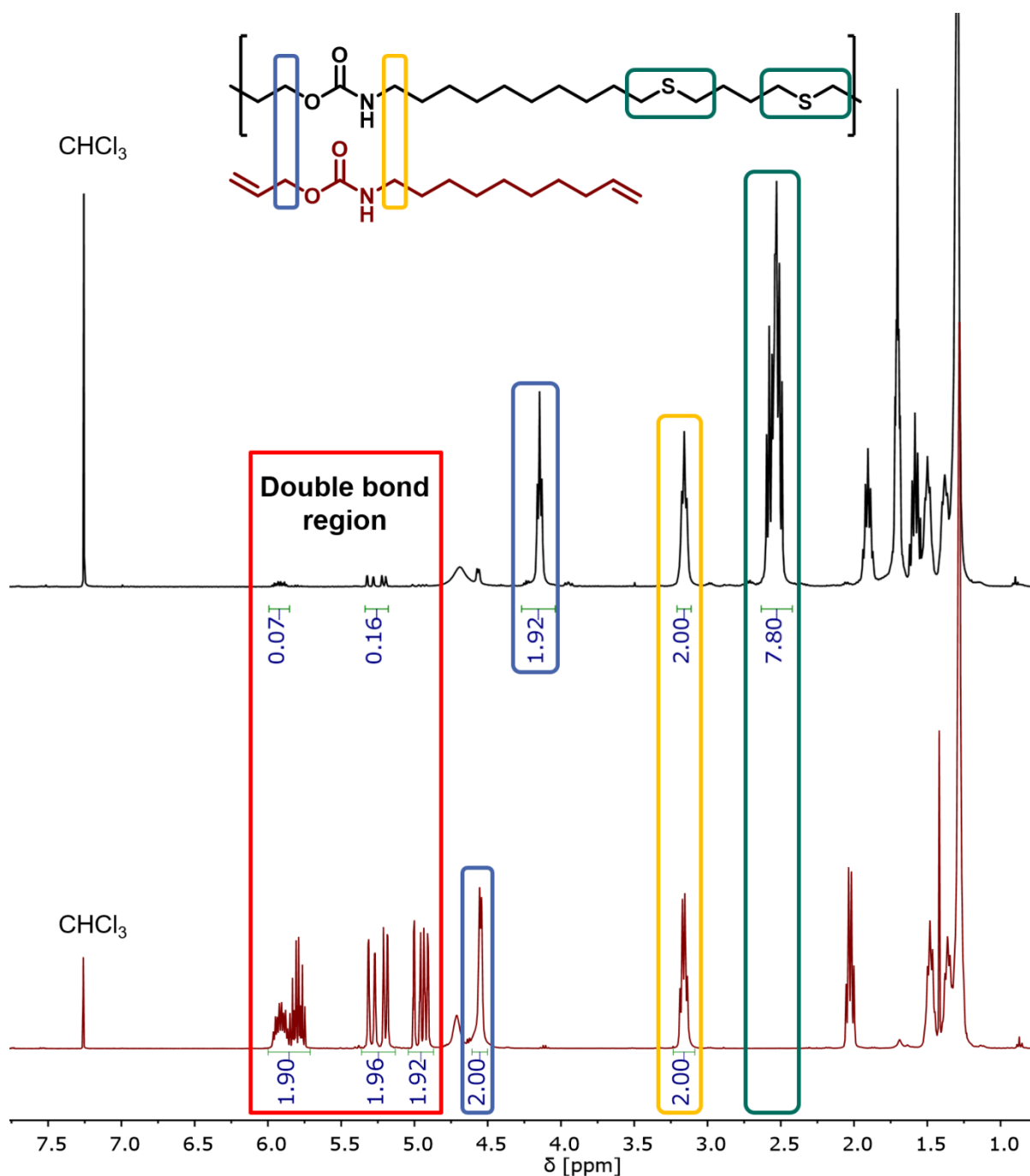
Figure 40 ^{1}H NMR spectra of the carbamate monomer **4** (red) and the respective NIPU **P3** (black).

In **Figure 40**, the difference in ^{1}H NMR between the carbamate monomer and the respective NIPU is observed by means of three different signals. The increase of intensity after polymerization in the double bond region (red box) is caused by the unsaturated terminal functionalities of the diene being converted to thioethers, whose signals are visible in the region between 2.4 and 2.6 ppm (green box). Additionally, the CH$_2$-group in the blue box shifts towards lower ppm values (from 4.6 to 4.1 ppm) as a thiol is added to the allyl group. Meanwhile, the alkyl group in the vicinity of the amide functionality (yellow box) remains

unaffected by the polymerization, thus possessing a signal at 3.1 ppm in both the monomer and respective polymer.

As the focus of this work was to create sustainable procedures, the utilization of the mentioned urea side-products is a highly desirable possibility. Consequently, the urea dienes were polymerized in a similar manner. As urea exhibits stronger hydrogen bonding than the corresponding carbamate,[356] the use of THF as solvent is not suitable. Therefore, chloroform, as the only suitable solvent for ureas **9** and **10** at room temperature, was employed.

In the next subchapters, the optimization of the reaction conditions for the carbamate monomers is discussed.

4.2.2 Effect of time

The parameter of time was investigated as follows: the 1:1 monomer mixture composed of carbamate **4** and different dithiols was dissolved in THF at a concentration of 5 mol/L. Afterwards, the initiator 2,2-dimethoxy-2-phenylacetophenone (DMPA) was added and the mixture was stirred for 3 hours at room temperature under UV irradiation (365 nm). In most cases, the formation of a solid was observed within the first two hours, completely inhibiting magnetic stirring. In order to investigate the parameter of time in detail, the polymerization was thus performed under more dilute conditions (**Table 9**) to ensure full solubility of the NIPU throughout the experiment. Already after one hour, the molecular weight exceeded 7 kg/mol, while only a small increase throughout the subsequent measurements, with a M_n value of 8.5 kg/mol after four hours. The reaction mixture was then allowed to stir overnight. **Entry 5** was measured after 18 h reaction time, when a rise of about 3 kg/mol was obtained after further reaction of 12 hours. Therefore, it was decided to not change the reaction time (3 h) further. The SEC traces are depicted in **Figure 41**.

Table 9 Effect of time on the thiol-ene polymerization.

entry	Reaction time [h]	M_n [g/mol] [b]	$Đ_M$ [b]
1	1	7,450	1.97
2	2	7,900	1.96
3	3	8,100	1.90
4	4	8,500	1.93
5	18	11,350	1.79

[a]   Conditions: 0.40 mol/L in THF, r.t., 1.00 eq. **4**, 1.00 eq. 1,4-butanedithiol, DMPA

[b]   HFIP-SEC calibrated with poly(methyl methacrylate) (PMMA) standards
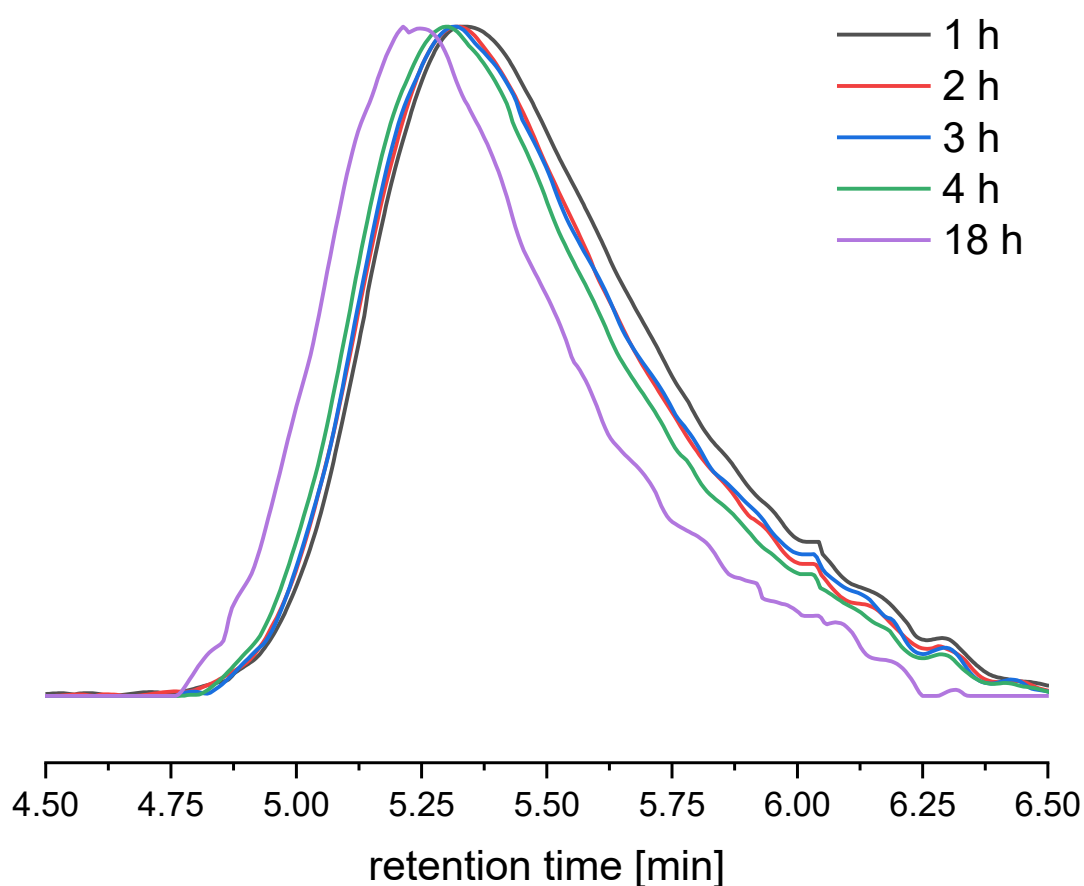
Figure 41 SEC traces of the polymerization of carbamate **4** with 1,4-butanedithiol. The samples were taken at 1, 2, 3, 4 and 18 hours from the beginning of the reaction and measured *via* HFIP-SEC.

In the case of carbamate **5**, which was expected to be less reactive because of the disubstituted double bond instead of being a terminal alkene, the reaction time was first set to 6 h. After HFIP-SEC analysis of the crude mixture, only low molecular oligomers were detected in the chromatogram and the mixture was further exposed to UV light overnight. However, the M_n values did not increase over 2 kg/mol even after multiple experiments to

confirm the reproducibility of the procedure. This behavior is dictated by the decreasing reactivity with the degree of substitution at the double bond, as already discussed in **chapter 2.6.2**.

4.2.3 Effect of initiation

As mentioned in previous chapters, the thiol-ene reaction is induced either by light or heat. Two different irradiation wavelengths are usually used for thiol-ene reaction and many other photoreactions: 254 nm and 365 nm. For this purpose, DMPA was chosen as photoinitiator (absorption maximum (λ_{max}) 310-390 nm). Additionally, for the heat-based initiation, azobisisobutyronitrile (AIBN) is a commonly employed material, as it produces radicals starting from 40 °C.[357] In **Table 10**, the comparison of the mentioned initiation methods is shown in the system consisting of carbamate **4** and 1,4-butanedithiol as a 5 mol/L solution in THF. The molecular weights and dispersities were determined by HFIP-GPC.

Table 10 M_n and $Đ_M$ values for different types of initiation for polymer **P3**.

entry	initiation[a]	M_n [g/mol] [b]	$Đ_M$ [b]
1	UV (254 nm)	10,900	2.51
2	UV (365 nm)	26,600	1.87
3	Heat (50 °C)	1,700	1.37

a) Conditions: 5.00 mol/L in THF, 3 h, r.t., 1.00 eq. **4**, 1.00 eq. 1,4-butanedithiol, DMPA (UV), AIBN (heat)

b) HFIP-SEC calibrated with PMMA standards

Initial experiments employing 254 nm UV irradiation yielded low M_n products, a result that was ascribed to the glass vial employed for the reaction as UV light (254 nm) is partially absorbed by normal glassware, which consist of around 80% of silica. In comparison, quartz glass possesses greater transmission (99.9%) at the same wavelength.[358] Therefore, all subsequent tests at 254 nm were performed in a quartz glass flask. However, the molecular weight of the resulting polyurethanes did not exceed 11 kg/mol, whilst resulting in broader dispersity. This behavior is explained by the λ_{max} of DMPA, which lies in the region between 310 nm and 390 nm.[359] Therefore, at 254 nm, radicals are not formed in high amounts, as DMPA does not degrade efficiently. In the next step, DMPA was replaced by azobisisobutyronitrile (AIBN) in order to provide an initiation by heat. A temperature of 50 °C

was chosen and kept for the desired time, as higher temperatures are expected to lead to evaporation of the solvent. However, as seen from **entry 3**, only oligomers were formed during the polymerization. Although the decomposition of AIBN starts at 40 °C,[357] the temperature was insufficient for producing an adequate amount of radicals in three hours, as it possesses a half-life time of 10 h at 60 °C. As this last mentioned method did not supply satisfactory results, further reactions were carried out exclusively under the influence of UV irradiation at 365 nm.

4.2.4 Effect of concentration

After evaluating suitable initiation conditions (UV, 365 nm), the following series of experiments focused on the choice for the optimal concentration, as step-growth polymerizations are highly dependent on the concentration and are therefore often conducted in bulk.[360] The chosen system featured the thiol-ene polymerization of carbamate **4** and 1,4-butanedithiol in THF. Tested values ranged from 0.1 mol/L solutions to bulk polymerizations and the respective values are shown in **Table 11**.

Table 11 Effect of concentration on M_n and $Đ_M$ of **P3**.

entry	c [mol/L]	M_n [g/mol] [a)]	$Đ_M$ [a)]
1	bulk	13,200	1.75
2	5	26,600	1.87
3	2.5	17,900	1.88
4	1	9,750	1.59
5	0.5	11,900	1.87
6	0.1	5,600	2.32

[a)] Conditions: THF, 1.00 eq. **4**, 1.00 eq. 1,4-butanedithiol, DMPA, 365 nm, r.t., 3 h

[b)] HFIP-SEC calibrated with PMMA standards

For every entry, the formation of a solid was observed during the reaction. Nonetheless, a trend was observed as the molecular weight of the isolated product increased with concentration, with a maximum at 5 mol/L. This result was expected as polyadditions are known to proceed faster under concentrated conditions.[360] However, bulk conditions were less efficient with the M_n reaching a value of 13 kg/mol. The most plausible explanation is similar to the problem occurring during most laboratory or industrial step-growth

polymerizations: the increasing viscosity.[225] In this case, the rapid solid formation and the absence of a solvent, like THF, is presumed to lower the diffusion greatly. Between **entries 4** and **5**, a discrepancy is noted as the higher concentration resulted in a lower molecular weight. The reason was not determined albeit it is likely that the real M_n value was in the standard deviation range of the SEC instrument, especially since the SEC columns were designed for high molecular weights and because of the high dispersities. However, since the polymerization in a 5 mol/L solution in THF led to the most promising results, this concentration was chosen for all further thiol-ene reactions with carbamates.

4.2.5 Choice of solvents

Continuing with a DMPA-photoinitiated procedure in a 5 mol/L solution, the next parameter to optimize was the choice of solvent. The optimization was performed with common organic solvents like chloroform ($CHCl_3$) and THF,[361] as well as greener variants to increase the sustainability of the process (**Table 12**). Possible renewable choices are γ-valerolactone (GVL), γ-butyrolactone (GBL), dimethyl carbonate, DMSO, cyrene and methyl tetrahydrofuran (Me-THF). Me-THF and GVL can both be synthesized from levulinic acid,[362] which can in turn be obtained from hexoses isolated from cellulosic biomass, thus making their sourcing sustainable.[363] Me-THF exhibits a far lower toxicity than THF, as well as higher boiling point, rendering it an optimal solvent for pharmaceutical product synthesis.[364] Meanwhile, cyrene has been shown to be an excellent alternative for solvents like *N,N*-dimethylformamide (DMF) and *N*-methyl-2-pyrrolidone (NMP), as it is fully biodegradable and originates from levoglucosenone, a material obtained from lignocellulosic biomass.[365] Finally, DMSO and dimethyl carbonate are known for their low toxicity and mild synthetic conditions.[366] The last example is synthesized by acidic esterification of gamma hydroxybutyric acid to form the simplest lactone, GBL. One last attempt was made with a new solvent called PolarClean®. It was recently commercialized by the company Solvay[367] showing many advantages like wide polarity range, low vapor pressure, excellent eco-friendliness as well as virtually non-existing flammability.[367] For the aforementioned reasons, PolarClean®, with the main component being methyl 4-(dimethylcarbamoyl)-2-methylbutanoate, was included in the following list.[367]

Carbamate **4** and 1,4-butanedithiol were polymerized in a 5.00 mol/L solution in the chosen solvent, under UV irradiation (365 nm) and at room temperature for 3 h.

Table 12 Molecular weights and $Đ_M$ of **P3** in different solvents.

entry	solvent[a]	M_n [g/mol] [b]	$Đ_M$ [b]
1	Cyrene	Oligomers	-
2	Dimethyl carbonate	3,200	2.70
3	GBL	5,200	2.73
4	GVL	5,400	2.70
5	DMSO	6,900	2.00
6	PolarClean®	10,600	1.87
7	Me-THF	12,650	1.77
8	CHCl$_3$	22,000	1.69
9	THF	26,600	1.87

[a] Conditions: 5.00 mol/L, 1.00 eq. compound **4**, 1.00 eq. 1,4-butanedithiol, DMPA, 365 nm, r.t., 3 h

[b] HFIP-SEC calibrated with PMMA standards

Classical solvents employed for polymerizations, like CHCl$_3$ or THF, showed an increased effectiveness compared to the more sustainable representatives, leading to molecular weights above 20 kg/mol. However, the greener alternatives resulted in a range between 3 kg/mol and 12 kg/mol. Lactones, carbonates and sulfoxides were found to poorly dissolve the resulting polymer, as a few minutes after the beginning of the reaction, insoluble solid formation was observed, hindering stirring of the mixture and ultimately leading to low molecular weights and larger dispersities. Promising results were delivered by both Me-THF and PolarClean®, surpassing 10 kg/mol with a dispersity value below 2 allowing for a greener procedure compared to ethers and chlorinated solvents. Nonetheless, the best conditions regarding solubilization and M_n of the resulting NIPUs were applied for further syntheses. Thus, THF was chosen as solvent for future investigations.

4.2.6 Monomer choice

Up to this point, the analyzed NIPU was composed of carbamate **4** and 1,4-butanedithiol. However, polymer properties prepared *via* thiol-ene polymerization do not originate from the urethane only, as the dithiol monomer possesses a decisive influence on structure and

material properties. Therefore, the influence of the dithiol moiety on molecular weight and thermal transitions was analyzed next by SEC and DSC. At first, linear aliphatic monomers were compared, based on their respective chain length to evaluate the changes in melting point with longer linkers. The results are shown in **Table 13**. With increasing length, the molecular weight rapidly increases up to 34 kg/mol for a C_6 chain (**P4**), while the molecular weight decreased again for even longer spacers. The volatility of 1,2-ethanedithiol and 1,3-propanedithiol was ascribed to be the issue behind the low molecular weight of **P1** and **P2**, being 8 kg/mol and 7.5 kg/mol, respectively, by disrupting the stoichiometry between diene and dithiol due to evaporation. Another reason for these values was deemed to be the inhomogeneous reaction mixture caused by the increased polarity of the two.

Meanwhile, reaction mixtures of C_4, C_6 and C_8 dithiols were homogeneous. A longer chain dithiol, 1,10-decanedithiol, formed an inhomogeneous mixture after the addition to THF. The same assumption can be made with the corresponding polymers, as THF, especially under concentrated conditions, is expected to be unable to dissolve the more polar **P1** or the unpolar **P6** efficiently. These polymers supposedly start to precipitate early during the reaction upon reaching certain molecular weights, inhibiting further additions to the macromolecule. Therefore, the synthetic procedure of **P6** was repeated in CHCl$_3$, leading to a fourfold increase in molecular weight and confirming the assumptions regarding the solubility of monomers and polymers. The dispersities are in range of 1.5-2.3, near the expected value of 2 for step-growth polymerizations.[360]

Table 13 Molecular weights and $Đ_M$ of polymers of **4** with different alkyl dithiols.

Polymer	Dithiol[a)	M_n [g/mol][b)	$Đ_M$[b)	T_g [°C]	T_m [°C]
P1	1,2-ethane	8,000	1.50	-	80.4
P2	1,3-propane	7,200	2.29	-	65.4
P3	1,4-butane	26,600	1.87	-	73.3
P4	1,6-hexane	33,900	2.73	-	66.5
P5	1,8-octane	15,250	1.90	-	83.1
P6	1,10-decane	5,550	2.29	-	84.6
	1,10-decane[c)	21,550	2.00		

a)   Conditions: 5.00 mol/L in THF, 3 h, r.t., 1.00 eq. compound **4**, 1.00 eq. dithiol, DMPA, 365 nm

b)   HFIP-SEC calibrated with PMMA standards

c)   Reaction in $CHCl_3$

The thermal properties of the polymers listed above were assessed by DSC and were found similar for every entry, showing melting points in the range of 65–80 °C. One exception in the melting trend is seen in **Table 13**, as **P4** exhibits a lower T_m than **P3** and **P5** although showing higher molecular weights. This behavior is expected to be caused by the broader dispersity of **P4** ($Đ_M$ = 2.7) compared to **P3** and **P5** ($Đ_M$ *ca.* 1.9). Such temperatures do not enable the usage of the polymers for high temperature applications, e.g. for electrical encapsulation or in automotive industry,[368] where materials are required to remain rigid at temperatures over 100 °C. Nonetheless, low T_m values allow facile processability, especially when a material can be molded into a defined shape. In polymer industry, where often a single batch is in the ton scale, the energy consumption and the related costs for the processing are greatly reduced for low melting materials.
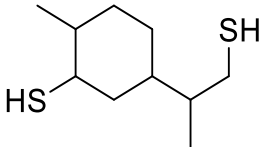
After evaluating the influence of the chain length on both molecular weight, dispersity, and melting point, more bulky dithiols were employed to study the effect of steric hindrance not only on the molecular characteristics but also on the morphology of the resulting polymers. The results are shown in **Table 14**. Three different dithiols were chosen for this purpose: limonene- (**11**) and cyclohexene dithiol (**12 a** and **b**) were employed for their renewable sources and for the presence of a bulky cyclohexane ring in both monomer structures, while 2,3-butanedithiol was chosen to analyze the effect of steric hindrance on NIPU properties caused by two methyl side chains. NIPUs **P7** and **P9** led to high M_n values, up to 21 kg/mol,

while the cyclohexane-based **P8** resulted in low molecular weight chains, slightly above 6 kg/mol, even after 18 hours reaction time. In the latter case, the issue was partially caused by the low solubility of the monomer in THF. However, traces of residual cyclohexane from column chromatography had been detected in the NMR spectrum of the dithiol **12**. The presence of cyclohexane could not be avoided, since high yield loss was experienced during prolonged rotary evaporation due to the high volatility of the 1,3- and 1,4-cyclohexane dithiol monomers. It is worth mentioning that the cyclohexane impurity was subtracted from **12** by NMR spectroscopy, however, the cyclohexane signal overlapped with the dithiol compound (see experimental **12**), increasing the calculation error for the polymerization batch. Followingly, the presence of cyclohexane in the monomer mixture is expected to disrupt the 1:1 ratio of monomers, thus causing the low molecular weight. Nevertheless, the yield and M_n of the obtained polymers proved to be enough for further analysis *via* NMR spectroscopy (experimental section, **chapter 5.3**) and DSC (**Table 14**). In the future, the purification of dithiol **12** is suggested to be performed *via* column chromatography with lower boiling solvents (e.g. pentane), to avoid both yield losses and the presence of impurities.

The difference in thermal behavior of **P7**-**P9** compared to their unsubstituted alkyl chain counterparts represented in **Table 14** was observable after precipitation as the obtained substances were not colorless powdery solids but rather liquids with high viscosity and transparency. The introduction of side chains was expected to inhibit the formation of intermolecular hydrogen bonds, thus hindering the formation of crystalline regions. The viscous liquid character of these polymers suggests that the glass transition temperatures of the synthesized materials are below room temperature.[369] Indeed, **P7-9** were viscous while DSC indicated glass transitions ranging from −30 to −15 °C. Simultaneously, no T_ms were detected, suggesting the presence of pronounced amorphous domains.

Table 14 Molecular weights and $Đ_M$s of polymers of **4** with different bulky dithiols.

Polymer[a]	Dithiol	M_n [g/mol][b]	$Đ_M$[b]	T_g [°C]	T_m [°C]
P7	Limonene **11**[c]	21,150	2.08	−22.9	-
P8	1,3- and 1,4-Cyclohexane **12**[d]	6,150	2.00	−14.6	-
P9	2,3-Butane	15,650	1.88	−28.8	-

[a] Conditions: 5.00 mol/L in THF, 3 h, r.t., 1.00 eq. compound **4**, 1.00 eq. dithiol, DMPA, 365 nm

[b] HFIP-SEC calibrated with PMMA standards

[c] Reaction in bulk

[d] 18 h

After observing the changes brought by variation of the employed monomers, it was decided to attempt the same polymerization with additional dithiols: differing in functionalities as side groups or with functional groups integrated in the main chain (**Table 15**). For the first category, two polymers were prepared (**P10** and **P11**). The monomer 2-aminobutane-1,4-dithiol hydrochloride was dissolved in the presence of DMSO as the salt could not be dissolved in pure THF. Additionally, the respective polymer **P10** was precipitated in diethyl ether instead of methanol because of the increased solubility in the alcohol derived by the increased polarity given by the ionic nature of the monomer. Nonetheless, **P10** was isolated with a satisfactory M_n value of almost 14 kg/mol. The white powder, however, did not show any thermal transitions in the measured temperature range (−80 − 180 °C). This effect most probably resulted from the strong interactions of the amino hydrochloride salt *via* hydrogen bonding. Although suspected that the T_m of **P10** was above 180 °C, the measurement was not repeated at higher temperatures, as urethane linkages are known to decompose above 180 °C.[201] In the future, TGA measurements will be performed in order to analyze the degradation temperature of **P10**. By using 2,3-dihydroxybutane-1,4-dithiol as dithiol monomer, the introduction of polar groups showed an increase in melting point of **P11** (98 °C) of almost 30 °C compared to **P3** (73 °C) at similar molecular weights and with the same chain length (C₄), caused by the increased hydrogen bonding between polymeric chains. By means of these results, it was confirmed that introducing functionalities in the dithiol side chains is an

effective method to achieve distinct variations in thermal properties, mostly derived by the polarity of the side groups.

As for the second category, the introduction of functionalities in the polymer backbone was attempted with dithiols with different linkers. The aromatic dithiol of **P12** only formed short oligomers, as expected due to the stabilization offered by the π-system: the thiyl radical exhibits lower reactivity, since it is stabilized by three mesomeric resonance structures of the aromatic species, including the thioketone.[283] In the case of ethers, the degree of polymerization remained in the same range for each monomer (**P13-15**) with the molecular weight increasing proportionally to the length of the dithiol to up to 20 kg/mol. By changing from oxygen to sulfur-based ethers, the molecular weight dropped to a maximum value of 5 kg/mol (**P16**) since an early precipitation (*ca.* 1 min) from the reaction mixture was caused by the lower polarity of the thioether dithiol. Therefore, no further experiments were performed with thioethers. It is worth mentioning that the already described polymers of **Table 15** were colorless solids, independently of the molecular weight. In contrast, diester dithiols yielded transparent liquid polymers (**P17**, **P18**) with a viscosity similar to the bulky side chain based NIPUs listed in **Table 14**. However, even if the mixture could not be stirred further, M_n values did not exceed the low value of 9 kg/mol, probably because of solubility issues of the polyester urethane.

Table 15 Molecular weights and $Đ_M$ of polymers of **4** with dithiols bearing different functional groups.

entry	Dithiol[a)	M_n [g/mol][b)	$Đ_M$[b)	T_g [°C]	T_m [°C]
P10	2-amino-1,4-butane-hydrochloride	13,550	1.67	-	-
P11	dithioerythritol	23,000	1.99	−8.0	98.2
P12	1,3-mercaptobenzene	oligomers	-	-	-
P13	2,2'-oxybis(ethane-1-thiol)	6,550	1.86	−41.0	63.7
P14	3,6-dioxa,1,8-octane	12,550	1.78	-	46.3
P15	10,10'-(hexane-1,6-diylbis(oxy))bis(decane-1-thiol)	20,000	1.86	-	62.3
P16	2,2'-thiobis(ethane-1-thiol)	5,450	2.30	-	94.8
P17	butane-1,4-diyl bis(2-mercaptoacetate)	5,550	2.11	−54.5	−0.6 39.8
P18	ethane-1,2-diyl bis(3-mercaptopropanoate)	8,600	2.11	−25.7	22.0 49.5

[a) Conditions: 5.00 mol/L in THF, 3 h, r.t., 1.00 eq. compound **4**, 1.00 eq. dithiol, DMPA, 365 nm

[b) HFIP-SEC calibrated with PMMA standards

The introduction of functionalities to the backbone shows great promise for the tuning of polymer properties. Esters, for instance, confirmed the possibility to prepare viscous NIPUs with crystalline domains (**P17**, **P18**), compared to the amorphous **P7**-**P9**, while thioethers were found to greatly increase the melting point even at lower molecular weights.

This section described the effect of different dithiols employed during the thiol-ene polymerization on molecular weight, dispersity and thermal properties. The influence of the dithiol moiety greatly influenced these attributes, especially by introduction of functionalities like esters or bulky structures in the polymer backbone. To give further comparison, the influence of other carbamates will be discussed in the following section.

4.2.7 Allyl carbamate 3 based NIPUs

As already mentioned in **chapter 4.2.1**, *N*-allyl allylcarbamate **3** was prepared in a condensation reaction between diallyl carbamate and allylamine. After the optimization of the reaction conditions and thorough testing with different dithiol monomers, most of the already shown dithiol monomers were copolymerized with the shorter carbamate **3** in order to investigate the influence of the chain length of the dithiol on the synthesis of polyurethanes (**P19**-**P27**). An overview is given in **Table 16**.

Table 16 Molecular weights and $Đ_M$ of polymers of *N*-allyl allylcarbamate **3** with different dithiols.

entry	Dithiol[a]	M_n [g/mol][b]	$Đ_M$[b]	T_g [°C]	T_m [°C]
P19	1,2-ethane	12,300	5.81	−13.6	69.0
P20	1,4-butane	16,000	1.94	-	56.3
P21	1,6-hexane	30,500	2.27	-	63.1
P22	2,3-butane	7,500	1.69	−12.4	
P23	limonene **11**	2,100	3.64	1.4	-
P24	dithioerythritol	10,400	1.34	3.1	-
P25	3,6-dioxa,1,8-octane	9,350	1.30	−49.9	-
P26	2,2′-thiobis(ethane-1-thiol)	3,800	2.43	-	91.6
P27	butane-1,4-diyl bis(2-mercaptoacetate)	8,000	1.90	−41.9	-

a)　Conditions: 5.00 mol/L in THF, 3 h, r.t., 1.00 eq. **3**, 1.00 eq. dithiol, DMPA, 365 nm

b)　HFIP-SEC calibrated with PMMA standards

The shorter carbamate monomer, allyl allylcarbamate **3**, produced NIPUs similar to polymers based on allyl dec-9-en-1-ylcarbamate (**4**). However, the overall molecular weights appeared to be lower than for **4**, for instance comparing the 1,4-butanedithiol-based **P3** (26 kg/mol) and **P20** (16 kg/mol), or the 2,3-butanedithiol-based **P9** (16 kg/mol) and **P22** (7.5 kg/mol). The possible cause between the decreased M_n values lies in the more polar nature of carbamate **3**, since it leads to increased hydrogen bonding with increasing molecular weight, thus causing precipitation of the polymer at lower M_n values than **4**.

The thermal properties of **P19**-**21** and **P26** resembled the values for the carbamate **4** based NIPUs with small variations. The use of a C_{10} (**4**) or a C_3 (**3**) carbamate chain did not influence the T_m values significantly as these thermal transitions appear to slightly shift towards lower temperatures compared to **4**. This effect is, however, most likely determined by the overall smaller chain length obtained under the same polymerization conditions.[370] For instance, for **P21** (C_6)**,** possessing a longer spacer than **P20** (C_4), the T_m increased from **P20** (T_m = 56 °C) to **P21** (T_m = 63 °C), caused by an increase of the M_n from 16 kg/mol to 30 kg/mol, respectively. More interesting is the increase of all glass transition temperatures for polymers bearing side chains or NIPUs prepared with bulky dithiols (**P22**-**24**, **P27**). Analogously to the effect on the melting point, lower T_gs are expected with lower M_n values. However, the polarity increase

appears to be dominant in this case as the T_gs measured *via* DSC show an increase of the T_g between 10 °C and 30 °C. **P22** (T_g = −12 °C) and **P23** (T_g = 1 °C), for example, exhibit a glass transition 17 °C and 24 °C higher than the respective **4**-based **P9** (T_g = −29 °C) and **P7** (T_g = −23 °C).

By shortening the carbamate, it was observed that **P25,** prepared with 3,6-dioxa-1,8-octanedithiol, exhibited thermal transitions more similar to polyethylene oxide (PEO) than of PUs, with a T_g around −50 °C, compared to −52 °C for PEO.[371] However, no melting point was observed in DSC for this polymer, contrary to the allyl dec-9-en-1-ylcarbamate (**4**) based **P14** (T_m = 46 °C). Deeper analysis of the thermal properties will be performed in future, as the cause of these changes are not completely clear.

Another main difference caused by the chain length variation between carbamates **3** and **4** is represented by **P19**. All described macromolecules with linear alkyl chains exhibited only T_ms in the measured temperature ranges. However, this polyurethane exhibited also a T_g around −13 °C, as visible by DSC analysis. This behavior is supposedly caused by the broad dispersity ($Đ_M$ = 5.8), compared to the dispersities of **P1**-**P6** ($Đ_M$ *ca.* 2). However, as DSC analysis proved to be inadequate for T_g detection of **P1**-**P6**, these NIPUs require different analytical methods in future, such as thermomechanical analysis (TMA) or dynamic mechanical analysis (DMA).

Conclusively, the use of a shorter carbamate (**3**) resulted in an overall increase of polarity in the respective polymers, which led to lower molecular weights caused by the lower solubility of the macromolecules in THF. The lower M_n values likely led to lower melting transitions in the polymers **P19-21** and **P26**, however, the polarity increase proved to be dominant against the M_n reduction, increasing the glass transition temperatures of NIPUs **P19**-**25** and **P27** by up to 30 °C. Additionally, **P19** and **P25** exhibited interesting thermal transitions, varying greatly from the respective carbamate **4** based NIPUs (**P1** and **P14**). These thermal properties will be analyzed in future with analytic techniques different from DSC.

Another type of carbamate-based diene was prepared for the thiol-ene polymerization, whose polymerization will be described in the next section.

4.2.8 Dicarbamate 6 based NIPUs

In order to broaden the range of the compared carbamates **3** and **4**, the focus was subsequently shifted to the synthesis of dicarbamates starting from diesters or diacids followed by the Lossen rearrangement in diallyl carbonate and allyl alcohol.

The *bis*-allylcarbamate **6** was, contrary to **3** and **4**, a colorless solid which was partially soluble in THF. Thus, CHCl$_3$ was used as solvent under more diluted conditions of 1.00 mol/L. The results of SEC and thermal analysis are shown in **Table 17**.

Table 17 SEC and DSC data of polymers obtained by polymerizing compound **6** with different dithiols.

entry	Dithiol[a]	M_n [g/mol][b]	$Đ_M$[b]	T_g [°C]	T_m [°C]
P28	1,4-butane	2,500	4.73		
P28[c]	1,4-butane	12,100	3.20	-	133.1
P29	limonene **11**	3,300	3.47	4.5	-
P30	2,3-butane	8,600	2.57	−0.7	-
P31	butane-1,4-diyl bis(2-mercaptoacetate)	9,050	3.42	−24.2	-
P32	10,10'-(hexane-1,6-diylbis(oxy))bis(decane-1-thiol)	6,400	4.00	-	115.1

[a]   Conditions: 1.00 mol/L in CHCl$_3$, 18 h, r.t., 1.00 eq. **6**, 1.00 eq. dithiol, DMPA, 365 nm

[b]   HFIP-SEC calibrated with PMMA standards

[c]   DMSO instead of CHCl$_3$

The first two experiments (**P28**, **P29**) produced polymers with molecular weights below 4 kg/mol. The formation of solid was observed at early stages of the reaction, which was attributed to either the high polarity of the diene or the opposite effect deriving from the employed dithiols and the resulting solubility issues. Therefore, ester- and ether-based dithiols were applied for the following experiments only slightly increasing the M_n values to a maximum of 9 kg/mol. By repeating the synthesis of **P28** in the more polar solvent DMSO, the molecular weight was increased by a factor of approximately 5, thus confirming the assumption that the polymerization in CHCl$_3$ is hindered by the high polarity of the carbamate moiety instead of the dithiol.

All thermal transitions were found shifted toward higher temperatures, compared to polymers synthesized from **3** and **4**. For instance, **P28** exhibited a melting point at 133 °C, 60 °C above that of **P3** and 85 °C more that of **P20**, while all T_gs increased in the range of 20 to 25 °C. Notably, when **6** was employed, instead of monocarbamates, the resulting polymers that exhibited glass transitions had a different appearance: while **P7** and **P9** were viscous colorless substances, the analogous macromolecules **P29** and **P30** were similar to elastic rubbers. All effects on the thermal and morphological properties were likely caused by the fact that the diene **6** possesses twice the number of functional groups capable of hydrogen bonding, compared to **3** and **4**, thus increasing the interactions between chains of the material. However, the low yield during the synthesis of **6** hindered the usage of polymers **P29** for tensile testing, where several grams of material are required for each sample.

The Lossen rearrangement in the presence of diallyl carbonate and allyl alcohol was performed also on the hydroxamic acids derived from malonic, succinic, sebacic and tetradecanedioic methyl esters. As previously mentioned in **chapter 4.1.2**, the products of the rearrangement of **1j** and **1k** (**Figure 21**), the dihydroxamic acids of sebacic acid and tetradecanedioic acid, were isolated only as mixtures containing many different products, including the dicarbamate and urea. The polymerization of the crude diene mixture of **7** and **8** was attempted *via* thiol-ene. However, only oligomers were detected by SEC analysis.

As three types of carbamates and the related NIPUs have been analyzed and compared, the focus was shifted to the polymerization of the side product of the monomer synthesis: the ureas.

4.2.9 Ureas

As mentioned at the beginning of this chapter, the urea compounds **9** and **10**, obtained as side products from the Lossen rearrangement, also possess two polymerizable double bonds. Therefore, the same approach used for carbamate **4** was tested with the isolated 1,3-di(dec-9-en-1-yl)urea **9** as model compound. However, two parameters were varied before attempting the thiol-ene polymerization. First, urea **9** is insoluble in THF at room temperature, therefore, CHCl₃ was chosen as solvent instead. Second, although the monomer was dissolved in chloroform at 25 °C, the maximal concentration achievable was lower than that of the carbamate concentration in THF (5 mol/L). By testing different concentrations for the urea **9**,

the maximum concentration for complete dissolution at room temperature was found to be 0.83 mol/L. In addition, the influence of different solvents on the polymerization was investigated under elevated temperatures to improve monomer solubility (**Table 18**). DMSO and PolarClean® represent appropriate replacements for $CHCl_3$ at 50 °C (**entries 2** and **3**) regarding monomer solubility, however, the obtained molecular weights and broader dispersities were attributed to low molecular weight oligomers rather than polymers. Therefore, all subsequent experiments were performed at room temperature in $CHCl_3$ as in **entry 1**.

Table 18 Results of the copolymerization of urea **9** in different solvents.

entry	T [°C]	solvent[a]	M_n [g/mol] [b]	$Đ_M$ [b]
1	r.t.	$CHCl_3$	5,750	2.24
2	50	PolarClean	-	-
3	50	DMSO	-	-

[a] Conditions: 0.83 mol/L, 1.00 eq. compound **9**, 1.00 eq. 1,4-butanedithiol, 365 nm, DMPA, 3 h.

[b] HFIP-SEC calibrated with PMMA standards

Next, different dithiol monomers were employed for the thiol-ene polymerization. Among the employed dithiols, commercially available examples based on linear alkyl chains as well as the renewable and bulkier limonene dithiol **11** were mixed with urea **9** in $CHCl_3$ in the presence of the initiator DMPA. Already at the early stages of the reaction (<5 min), the mixture showed some turbidity followed by formation of precipitate over the following 3 to 6 hours. The HFIP-SEC and DSC results are shown in **Table 19**.

Results and discussion

Table 19 Results of the copolymerization of urea **9** with different dithiols.

entry	Dithiol[a]	M_n [g/mol] [b]	$Đ_M$ [b]	T_g [°C]	T_m [°C]
P33	1,2-ethane	7,150	2.02	-	142.3
P34	1,4-butane	5,750	2.24	-	137.4
P35	1,6-hexane	4,850	2.32	-	136.3
P36	1,10-decane	6,500	1.59	-	132.8
P37	limonene **11**	7,400	2.13	-	67.5
P38	1,3- and 1,4-cyclohexane **12**	1,800	4.2	-	122.1
P39	2,3-butane	5,850	2.15	-	81.6
P40	butane-1,4-diyl bis(2-mercaptoacetate)	3,950	2.14	-	119.7

a) Conditions: 0.83 mol/L in CHCl$_3$, 1.00 eq compound **9**, 1.00 eq dithiol, 365 nm, DMPA, r.t., 3 h.

b) HFIP-SEC calibrated with PMMA standards

The measurements were performed after purification by washing with CHCl$_3$ in order to remove low molecular oligomers, as the polyureas were not soluble in most common organic solvents and were therefore not purified by precipitation. The washing and the low M_n are also possibly the main reasons for the lower polyurea yields listed in **chapter 5.3** (Experimental section) compared to the respective polyurethanes. In this case, the molecular weights were found to be dictated by the diene monomer as the isolated polymers all showed comparable M_n values, independently of the employed dithiol. The only exception was **P38**, which, analogously to **P8**, was synthesized from cyclohexane dithiol **12**. The reason for the low molecular weight below 2 kg/mol was once again the presence of cyclohexane in the monomer mixture, thus lowering the dithiol/diene ratio.

The tendency of urea moieties for hydrogen bonding was suspected to be the reason behind the overall lower M_n values compared to the respective NIPUs. CHCl$_3$ and other solvents, like MeOH and DMSO, have limited capacity to antagonize and thus reduce the hydrogen bonding between the polymeric chains, limiting the maximum molecular weight to a value below 10 kg/mol through early precipitation, even if a bulky linker, like limonene (**Table 19, entry 4**), is employed. As for the thermal properties, all synthesized polymers exhibited melting points, while a T_g was not observable. Compared to the respective linear alkyl NIPUs **P1–6**, the polyureas **P33–36** had melting points above 100 °C, typically around 50–70 °C more than their

128

NIPU counterparts. As an example, the 1,4-butanedithiol-based **P34** (T_m = 137 °C, M_n = 5,750 g/mol) requires 64 °C more than **P3** (T_m = 137 °C, M_n = 26,600 g/mol) in order to melt, although possessing a much lower molecular weight. The last four entries of **Table 19** (**P37–40**) were prepared with the same dithiols employed for NIPUs **P7–9** (**Table 14**) and **P17** (**Table 15**), whose thermal properties were characterized by low glass transitions, leading to their unique viscosity. Meanwhile, the respective polyureas **P37–40** were obtained as colorless solids exhibiting only moderate to high melting temperatures. For instance, the limonene-based **P37** exhibited a T_m at 67 °C, while the respective **P7** a T_g at −29 °C without melting. This behavior was explained by the increased hydrogen bonding derived from the second NH-unit of the urea functionality. Urea **10**, derived from *N*-hydroxyoleamide **1a**, was polymerized by the same reaction conditions for comparative purposes. However, analogously to its respective carbamate **5**, only oligomers were obtained and the diene was not employed for further polymerizations.

The thiol-ene polymerization of urea dienes for the synthesis of polyureas overall yielded relatively high-melting polymeric materials. In the next subsections, the influence of urea content in NIPUs on molecular weight and thermal properties will be investigated and discussed.

4.2.10 Diene based copolymers

As already mentioned in **chapter 2.5.1** of the theoretical background, in some cases, commercially available polyurethanes contain not only carbamate units, but also urea linkages (poly(urea-urethanes)). Depending on the amount of urea functionalities, the polymer exhibits different thermal and mechanical properties.[372] Industrially, the selective urea linkage formation in a polyurethane is achieved by water addition prior to polymerization causing partial degradation of the isocyanates to amines.[373] In this work, the same kind of copolymers were synthesized, however, the urea and carbamate diene ratio was adjusted directly by mixing the exact quantity of the desired monomer to the reaction mixture. As a model system, a mixture of 0.9 eq. of carbamate and 0.1 eq of urea in $CHCl_3$ was chosen (**Scheme 32**).
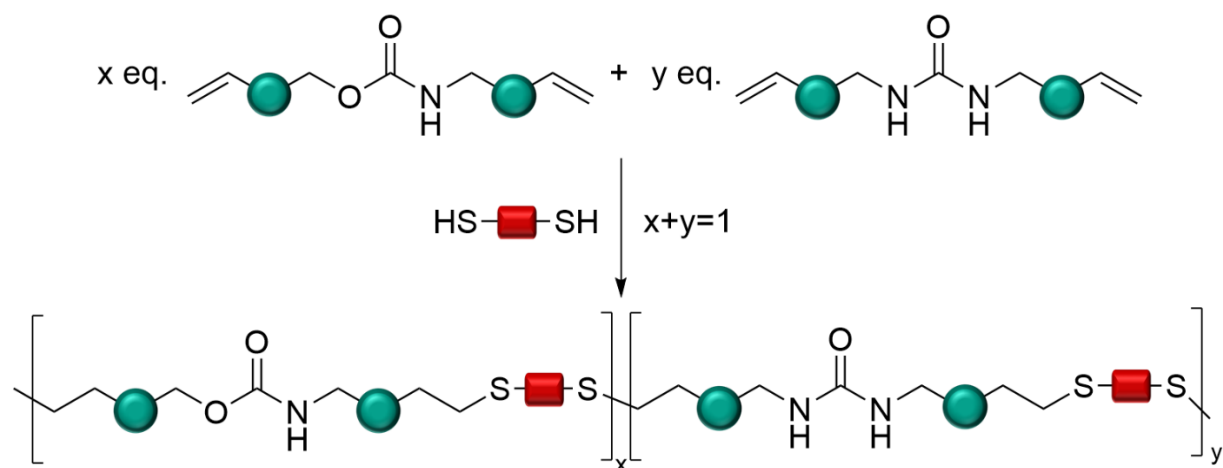
Scheme 32 Schematic synthesis of copolymers consisting of both carbamate and urea dienes.

Being completely soluble at room temperature, the monomers were polymerized with 1,4-butanedithiol in the presence of DMPA under UV irradiation (365 nm) for 8 hours. Different concentrations were tested for the aforementioned reaction and the HFIP-SEC results are shown in **Table 20**.

Table 20 Concentration effects on the three-component polymerization of carbamate **4** and urea **9** with 1,4-butanedithiol (**P41**).

entry	c [mol/L][a]	M_n [g/mol] [b]	$Đ_M$ [b]
1	3.33	4,650	1.87
2	2.5	15,850	1.98
3	1.67	21,250	1.87
4	1	-	-

[a] Conditions: CHCl₃, 0.10 eq urea **9**, 0.90 eq carbamate **4**, 1.00 eq 1,4-butanedithiol, 365 nm, DMPA, r.t., 8 h.

[b] HFIP-SEC calibrated with PMMA standards

At a concentration of 3.33 mol/L, the urea was not dissolved completely leading to a slightly turbid solution. The resulting low molecular weight is therefore possibly caused by the early precipitation of the polymer from the chloroform. Subsequently, dilution of the reaction mixture led to a great increase of M_n, with a maximum of 21 kg/mol at a concentration of 1.67 mol/L. However, decreasing the concentration even further lowered the molecular

weight, leading to the formation of only low molecular oligomers (**Table 20 entry 4**). This decrease is supposedly caused by the low reaction rate under diluted conditions.

Further, different monomer ratios were tested for the same system. The carbamate molar percentage was decreased in 0.10 eq. steps to a final value of 0.60 eq. (**Table 21**). At 0.5 eq. and lower, the respective urea fraction was not fully dissolved at room temperature. The HFIP-SEC results shown in **Table 21** indicate that the molecular weights rapidly drop below 5 kg/mol with decreasing carbamate. The early precipitation of polymer above a certain urea content may be responsible for this behavior, as the solvent was not able to break the urea hydrogen bonds after a certain threshold. Afterwards, the thermal properties were analyzed *via* DSC to determine the influence of increased hydrogen bonding during the copolymerization.

Table 21 Changes in the molar ratio between urea **9** and carbamate **4** monomer and the respective effect on molecular weight and thermal properties.

entry[a]	carbamate 4 (eq.)	M_n [g/mol] [b]	$Đ_M$ [b]	T_g [°C]	T_m [°C]
1	0.9	21,250	1.87	-	87.2
2	0.8	9,300	1.68	-	92.2
3	0.7	3,600	3.09	-	92.5
4	0.6	4,950	3.50	-	101.5/139.4

[a]   Conditions: 1.67 mol/L in CHCl$_3$, x eq. **4**, (1-x) eq. **9**, 1.00 eq. 1,4-butanedithiol (1.00 eq), 365 nm, DMPA, r.t., 8 h.

[b]   HFIP-SEC calibrated with PMMA standards

The effect of hydrogen bonding was observed by the increase of the melting temperature with the decreasing concentration of the carbamate. The T_ms increase to up to 140 °C in the case of **entry 4**, where 0.4 eq. of the urea monomer was applied as the diene component. However, a double melting transition is observable in this case, most probably caused by phase separation of the highly crystalline urea segments from the more amorphous carbamate region. The small difference in melting temperature between **entry 2** and **3** is caused by the low molecular weight of the polymer composed of 0.3 eq. urea **9**.

Since this work lays its focus on sustainability and the synthesis of both carbamate and urea includes purification by column chromatography, an attempt at polymerizing the crude

product was performed. Following the procedure explained in detail in **chapter 5.2** of the experimental section, the solid urea was filtered off and the reaction mixture was freed from the solvent by evaporation after complete conversion of the hydroxamic acid starting material. In this case, the solvent was evaporated prior to urea filtration, leaving a crude product consisting of both monomers, namely allyl dec-9-en-1-ylcarbamate **4** and 1,3-di(dec-9-en-1-yl)urea **9**. After confirming a ratio of around 7:3 between carbamate and urea by NMR analysis, the crude mixture was directly polymerized *via* thiol-ene polymerization, leading to a NIPU with a molecular weight of 6 kg/mol. This value was compared to **Table 20 entry 3**, where the copolymer was prepared with a similar diene ratio. The approach from the crude produced a lower yield, possibly because of the not completely precise diene content, as further species undetectable by NMR spectroscopy may have skewed the required mass for the polymerization. However, the procedure for the preparation of poly(urea-urethane)s directly from the crude reaction mixture of the Lossen rearrangement clearly demonstrated its effectiveness in producing polymers. Additionally, this approach represents a highly sustainable alternative by avoiding distillation and excessive purification steps, like column chromatography, thus preventing high energy consumption and large amounts of waste. As an additional proof for the efficiency of this copolymerization method, a NIPU consisting of 0.9 eq. carbamate **4** and 0.1 eq. urea **9** was synthesized with limonene dithiol **11**. The obtained polymer **P42** was analyzed via HFIP-SEC and DSC, showing a M_n value of 10 kg/mol and a dispersity of around 2.1, typical for step-growth polymerizations. Additionally, the obtained thermal transition, a T_g at −19.2 °C, was found to be slightly higher than for the pure carbamate polymer (**P7**, T_g = −22.9 °C).

The thiol-ene copolymerization of more types of dienes proved to be successful, yielding polymers with tunable properties. In the next subsection, another approach for three or more components will be discussed.

4.2.11 Dithiol based copolymers

The copolymerization of carbamate and urea dienes led to the formation of NIPUs with increased thermal transition, showing that the properties of all monomers are transferred to the resulting polymer. The same principle as with diene-based copolymers is applicable for

producing copolymers with more than one dithiol monomer, as depicted in **Scheme 33**.
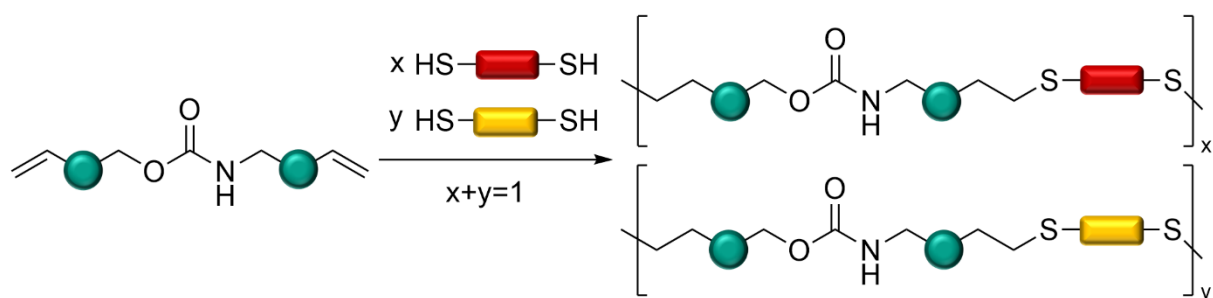
Scheme 33 Schematic synthesis of polyurethane copolymers prepared with two different dithiols in a one pot reaction.

Only one carbamate species was employed for the polymerization in the presence of two different dithiols. For instance, monomer **4** was mixed with 1,4-butanedithiol and 1,10-decanedithiol in a 1:1 ratio in order to investigate how the thermal properties are affected (**Table 22**, **P46**).

Results and discussion

Table 22 HFIP-SEC and DSC results for the polymerization of carbamate **4** with a mixture of two different dithiols (1:1).

entry	Diene[a)]	dithiol	M_n [g/mol] [b)]	$Đ_M$ [b)]	T_g [°C]	T_m [°C]
P43	4	1,4-butane limonene **11**	10,650	2.29	−27.7	-
P44	4	1,4-butane 2,3-butane	9,250	1.74	−39.0	37.4
P45	4	1,4-butane ethane-1,2-diyl bis(3-mercaptopropanoate)	9,450	1.91	−42.9	62.6
P46	4	1,4-butane 1,10-decane	13,900	1.97	-	74.3
P47	3	1,4-butane limonene **11**	10700	1.55	−20.2	-
P48	4	1,2-ethane limonene	2,200	1.88	−30.5	71.9/78.4
P49	4	1,8-octane limonene **11**	4,100	2.09	−28.6	44.7
P50	4 9	1,4-butane limonene **11**	4,550	1.97	−31.6	60.9

a) Conditions: 1.00 eq. diene, 0.50 eq. dithiol 1, 0.50 eq. dithiol 2, 5 mol/L in THF, 10 h, 365 nm, DMPA, r.t.

b) HFIP-SEC calibrated with PMMA standards

The obtained NIPU **P46** showed one thermal transition, similar to the 1,4-butanedithiol based **P3**, with a melting point around 74 °C. This analysis clearly shows that the shorter dithiol has a larger influence on the overall properties of the macromolecule. It is noted that there is a chance that one dithiol possesses a higher reactivity, thus being incorporated in a non-statistical distribution. However, ^{1}H NMR analysis confirmed an almost identical presence of both species, as evaluated on the basis of **P45**. **P45** was chosen as the key signals of the ester (red box), the alkyl groups of 1,4-butanedithiol (green box) and the N-CH$_2$ (yellow box) signals do not overlap with any other group (see **Figure 42**).

134
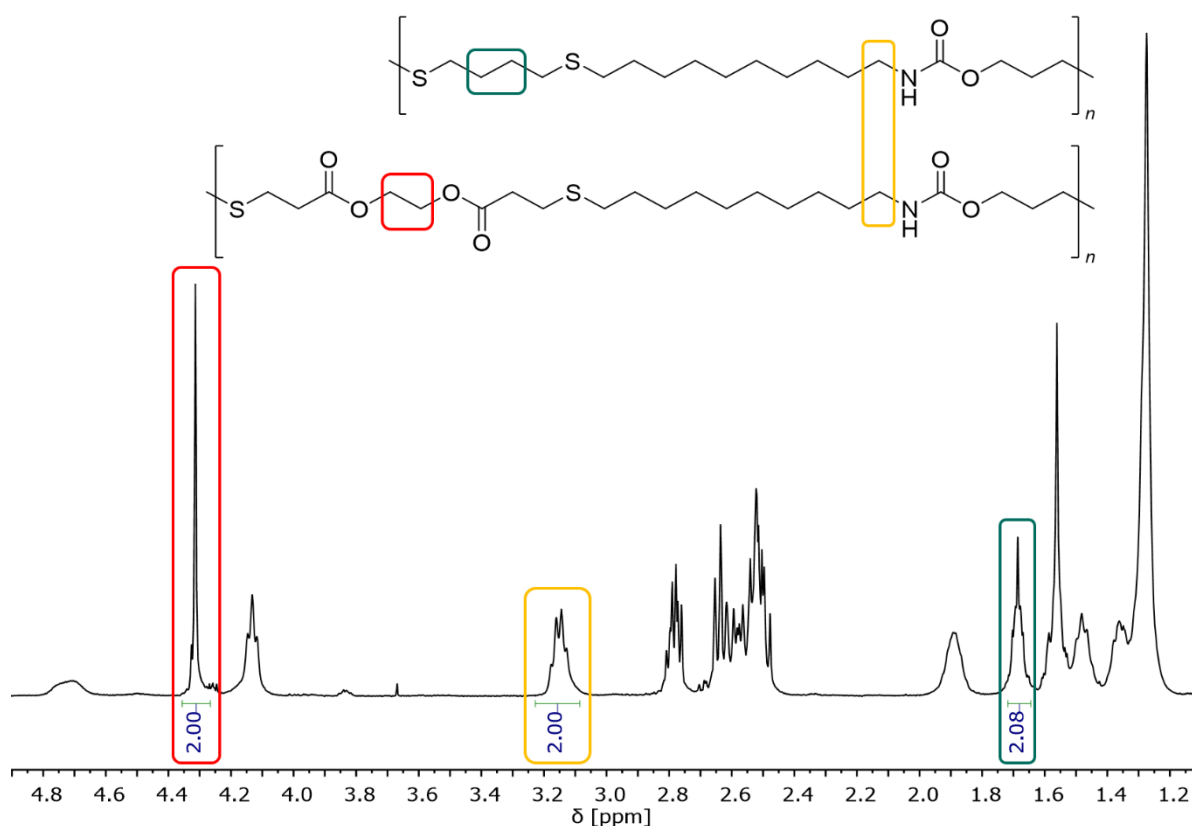
Figure 42 ^{1}H NMR spectrum of **P45** and integrated values of specific signals belonging to carbamate **4** (3.15 ppm), 1,4-butanedithiol (1.67 ppm) and ethane-1,2-diyl *bis*(3-mercaptopropanoate) (4.32 ppm).

As previously discussed in **chapter 4.2.6**, viscous polymers like **P7** or **P9** exhibit low glass transitions without melting, while all NIPUs produced from linear dithiols **P1–6** exhibit a melting point, without any observable T_g. The aim of the copolymerization is therefore the combination of different thermal transitions, which depend on the employed dithiol, in one polymer. Therefore, first experiments were performed by adding a 1:1 ratio of 1,4-butanedithiol and limonene dithiol to carbamate **4** under the optimized reaction conditions (**P43**). The polymer reached a molecular weight of around 10 kg/mol and the thermal properties were analyzed by DSC.

NIPU **P43** shows the presence of a T_g around −28 °C (**Table 23**, **entry 1**), a glass transition similar to the related **P7**. However, the material did not exhibit any melting transition in the measured range. Most likely, the steric hindrance caused by the limonene is able to suppress crystallization thus forming a mostly amorphous polymeric material. The same reaction was repeated with carbamate **3** to yield **P47**. Also for this NIPU, only a glass transition was observed. By copolymerizing two alkyl dithiols with different chain lengths, namely a C$_4$ and a

Results and discussion

C_{10}, (**P46**) additionally confirmed the dominance of one monomer over the other, since the onset point of the PU melting curve corresponded to **P3** rather than to **P6**.

In order to fully understand the behavior of this copolymer, four NIPUs with different monomer ratios were prepared exclusively for thermal analysis. **P43** was chosen as model compound as it includes the renewable limonene dithiol **11** and because the various thermal transitions are typically within the measured temperature range. The data is presented in **Table 23** below.

Table 23 Thermal transitions of copolymer **P43** with different monomer ratios of limonene dithiol **11**.

entry	limonene dithiol [eq.]	T_g [°C]	T_m [°C]
1[c)]	0.50	−27.7	-
2	0.40	−45.4	69.3/77.5
3	0.30	−48.1	66.7/78.2
4	0.20	-	71.6
5	0.10	-	77.9

[a)] Conditions: 5 mol/L in THF, 3 h, r.t., 1.00 eq **4**, DMPA, 365 nm

[b)] **P43** (**Table *22***), 10 h

Interestingly, the single T_gs and T_ms of **Table 23 entries 1**, **4** and **5** differ from those in entries **2** and **3**. This was probably caused by the shorter reaction times compared to **entry 1** (10 h, **Table 22**, **P43**), leading to lower molecular weights. Additionally, the **entries 2** and **3** exhibited a double melting, supposedly caused by phase separation.[374]

For further comparison, another polymer was prepared by adding the 1,4- and 2,3-isomers of butanedithiol starting again from a 1:1 ratio (**Table 22**, **P44**). Differently to the previous example, both T_m and T_g were observed under the measurement conditions. Similarly, all other random copolymers (**P45**, **P48** and **P49**) showed transitions ascribed to both dithiols. The molar composition and resulting thermal properties of these copolymers were not investigated like the limonene based NIPU, as they are less interesting from the point of view of renewability and the 1:1 ratio gave satisfactory results, thus not requiring changes in synthetic procedure.

One last copolymer (**P50**) was prepared from two different dienes (0.90 eq. carbamate **4** and 0.10 eq. urea **9**) in the presence of 1,4-butanedithiol and limonene dithiol **11**. The resulting

136

macromolecule melted at around 60 °C, confirming that the limonene structure was responsible for the missing crystallinity of **P43**, thus resulting in the lack of melting. By increasing the hydrogen bonding by just replacing 0.10 eq. of carbamate with urea, the T_m was observed at 61 °C by DSC analysis (**Table 22**, **P50**).

Random copolymers are of high importance for the tuneability of NIPU properties. This copolymerization offers the possibility for the tuning of T_gs and T_ms in desired ranges by varying the monomer ratios, as well as by interchanging different diene and dithiol compounds. The consistency of the resulting material is also affected by the inclusion of more than two monomers. For instance, **P43** possesses a texture that resembles a combination of its respective homopolymers, more specifically the viscous character of **P7** and the solidity of **P3**. However, their exact structure cannot be determined *via* NMR spectroscopy, especially regarding the statistical arranging of the dithiols, owing to the potential difference in reactivity of the respective monomers. A solution is proposed in the next paragraph.

4.2.12 Block copolymers

A solution to the issue mentioned above is the synthesis of block copolymers, which are composed of two or more different homopolymers, in a two-step procedure (**Scheme 34**). First, two separate NIPUs with the desired properties are prepared under optimized reaction conditions (**chapters 4.2.2** - **4.2.5**). At the end of the reaction, an excess of diene or dithiol is added to the prepared NIPUs in order to assure the presence of either alkene or thiol end groups. In the second step, the two end group-functionalized homopolymers are mixed in a suitable solvent and subjected to polymerization conditions. This way, they are linked on each end forming the desired multiblock copolymer.
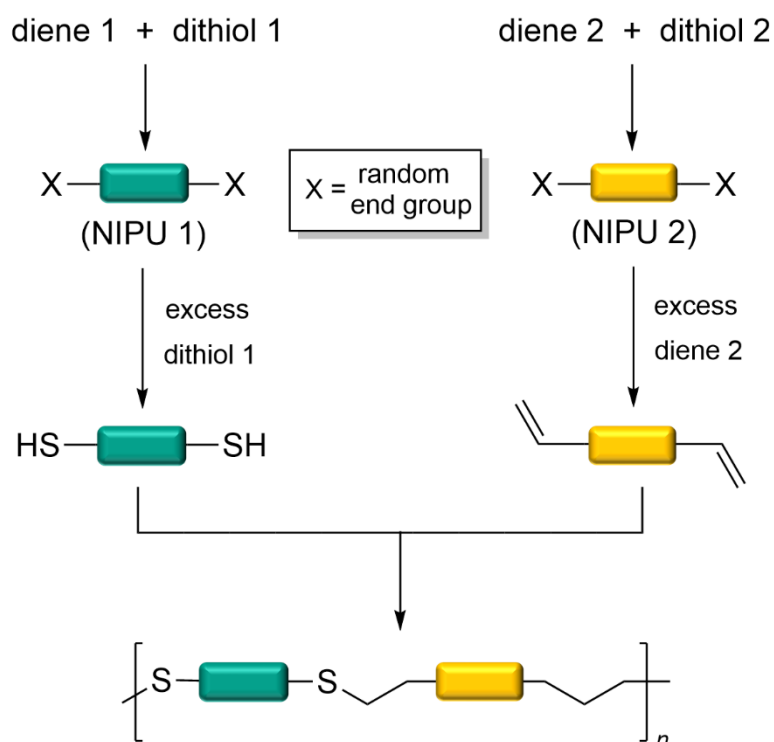
Scheme 34 Schematic of the preparation of block copolymers *via* thiol-ene polymerization of end group-functionalized homopolymers.

A model system with the first NIPU being based on carbamate **4** and limonene dithiol **11** and the second NIPU based on carbamate **4** and 1,4-butanedithiol was chosen because of the efficiency of the monomers, the greatly differing thermal transitions of the two prepolymers and the renewability of monomer **4**. To confirm the successful preparation of a block copolymer, the two prepolymers were first analyzed *via* SEC, NMR spectroscopy and DSC separately to determine their molecular and thermal characteristics after end-group modification. Afterwards, the two NIPUs were reacted with each other and the obtained solid was analyzed in the same fashion and under the same criteria. The obtained data on molecular weight of the block copolymers are listed in **Table 24**.

Table 24 SEC data for the synthesized block copolymers of **BP43-45**.

Entry[a]	Block 1	Block 2	M_n [g/mol] [b]	$Đ_M$ [b]
BP43	**P3**	**P7**	10,450	1.77
BP44	**P3**	**P9**	6,600	2.24
BP45	**P3**	**P18**	13,150	1.87

a)   Conditions: THF, 24 h, r.t., DMPA, 365 nm

b)   HFIP-SEC calibrated with PMMA standards

The prepolymers and block copolymers were analyzed by HFIP-SEC to ensure the successful conjoining of the blocks. In **Figure 43**, the two end group- functionalized prepolymers **P3** (green) and **P18** (blue) were superimposed with the trace of the block copolymer **BP45** (orange).
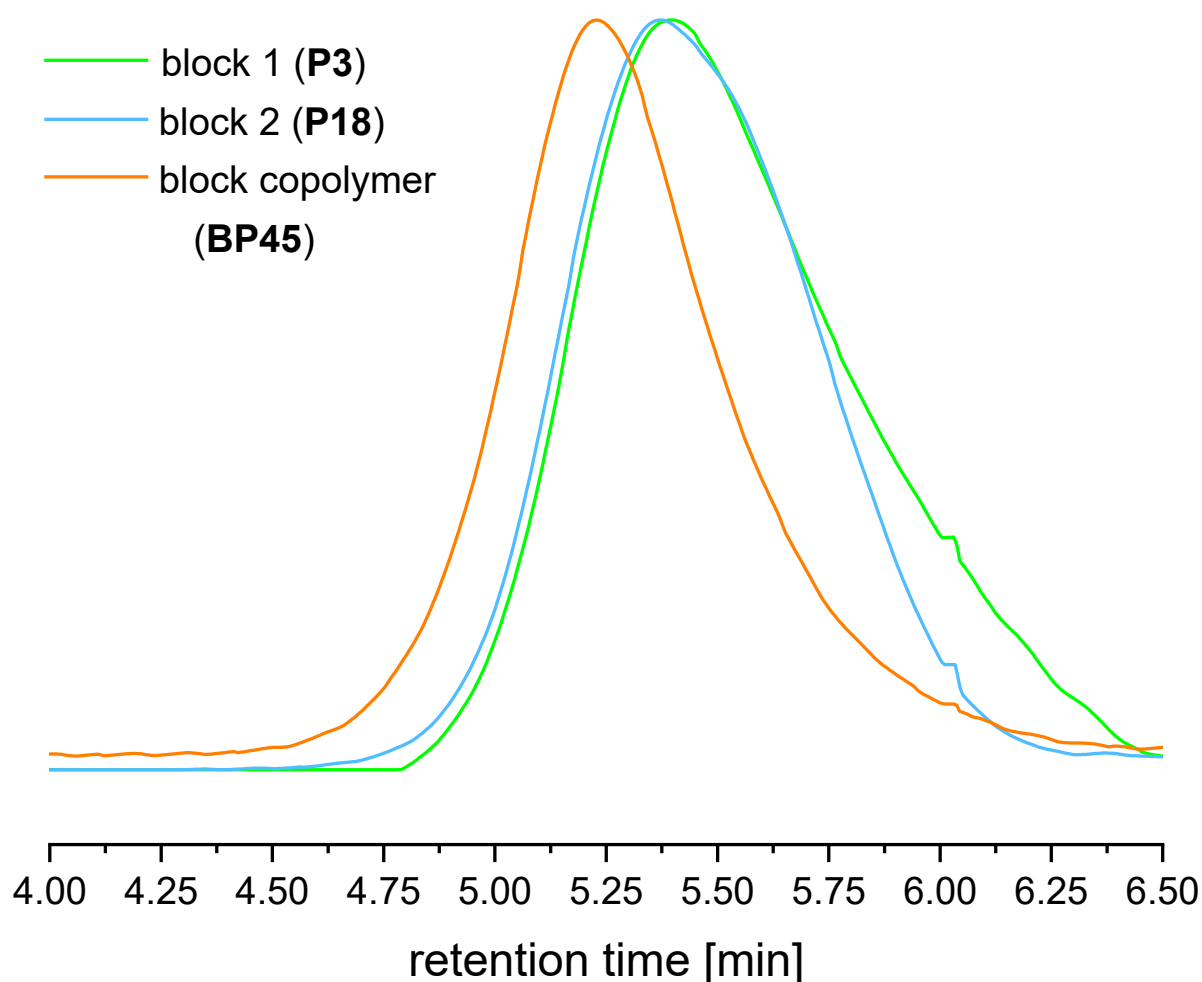
Figure 43 SEC chromatograms of block 1 (**P3**, green), block 2 (**P18**, blue) and the respective block copolymer **BP45** (orange).

139

Results and discussion

The SEC chromatograms indicate coupling of the polymers, as the curve shifts to lower retention times,. It is worth mentioning that the decrease of the prepolymers signals is not a result of the workup as the purification of the block copolymer was performed by precipitation in methanol, which is the same Solvent used for the precipitation of the respective prepolymers. However, SEC is unable to confirm the absence of small amounts of unreacted prepolymers in the final product, as the dispersity of the block copolymer is large and the peak overlaps with potential residual peaks of the prepolymers. Therefore, additional to SEC, the polymers were subjected to DOSY NMR to check for multiple species in the polymer. This technique distinguishes the ^{1}H NMR signals of different compounds in a mixture based on their diffusion coefficients. DOSY therefore permits the identification of residual unreacted end group-functionalized prepolymers in the block copolymer sample by separating overlapping NMR signals in a 2D spectrum.[375]
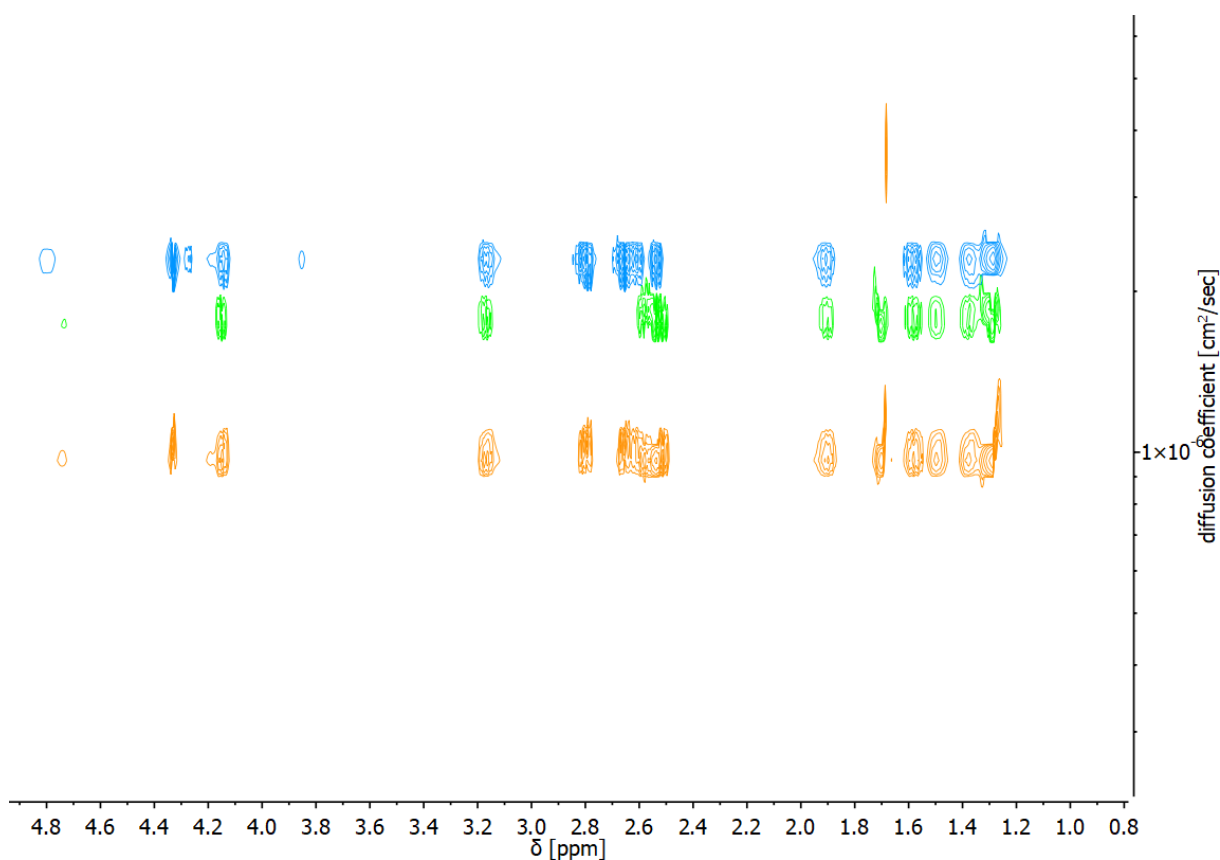
Figure 44 DOSY NMR of block 1 (**P3**, green), block 2 (**P18**, blue) and the respective block copolymer (**BP45**, orange) obtained after copolymerizing the two polymers *via* thiol-ene reaction.

In **Figure 44**, the orange trace for the block copolymer **BP45** (described in **Table 24**, **entry 3**) was superimposed with the DOSY spectra of block 1 (green, **P3**) and block 2 (blue, **P18**), both

140

employed for its synthesis. All species exhibit different diffusion coefficients indicating that **P3** has been successfully reacted with **P18** to yield the block copolymer **BP45**.

Afterwards, the thermal properties of the synthesized block copolymers were analyzed *via* DSC. In **Table 25**, the DSC data is listed for block-copolymers **BP43**-**45**, while the thermal data of the blocks **P3**, **P7**, **P9** and **P18** is shown in **Table 26**.

Table 25 DSC data for the synthesized block copolymers of **BP43-45**.

entry	Block 1	Block 2	T_g [°C]	T_m [°C]
BP43	**P3**	**P7**	−28.1	57.7
BP44	**P3**	**P9**	−32.6	80.5
				25.8
BP45	**P3**	**P18**	−36.1	52.2
				64.5

Table 26 DSC data and monomer composition of the individual blocks employed for the synthesis of block copolymers.

entry	diene	dithiol	T_g [°C]	T_m [°C]
P3	**4**	1,4-butane	-	73.3
P7	**4**	limonene **11**	−22.9	-
P9	**4**	2,3-butane	−28.8	-
P18	**4**	ethane-1,2-diyl bis(3-mercaptopropanoate)	−25.7	22.0 / 49.5

From the data in the two tables above, the T_gs and T_ms of each block are also exhibited by the respective block copolymer. As a visual example, in **Figure 45**, the DSC trace of **BP43** was compared to the respective random copolymer **P43**, as well as to the thermal transitions of its prepolymers **P3** and **P7**.
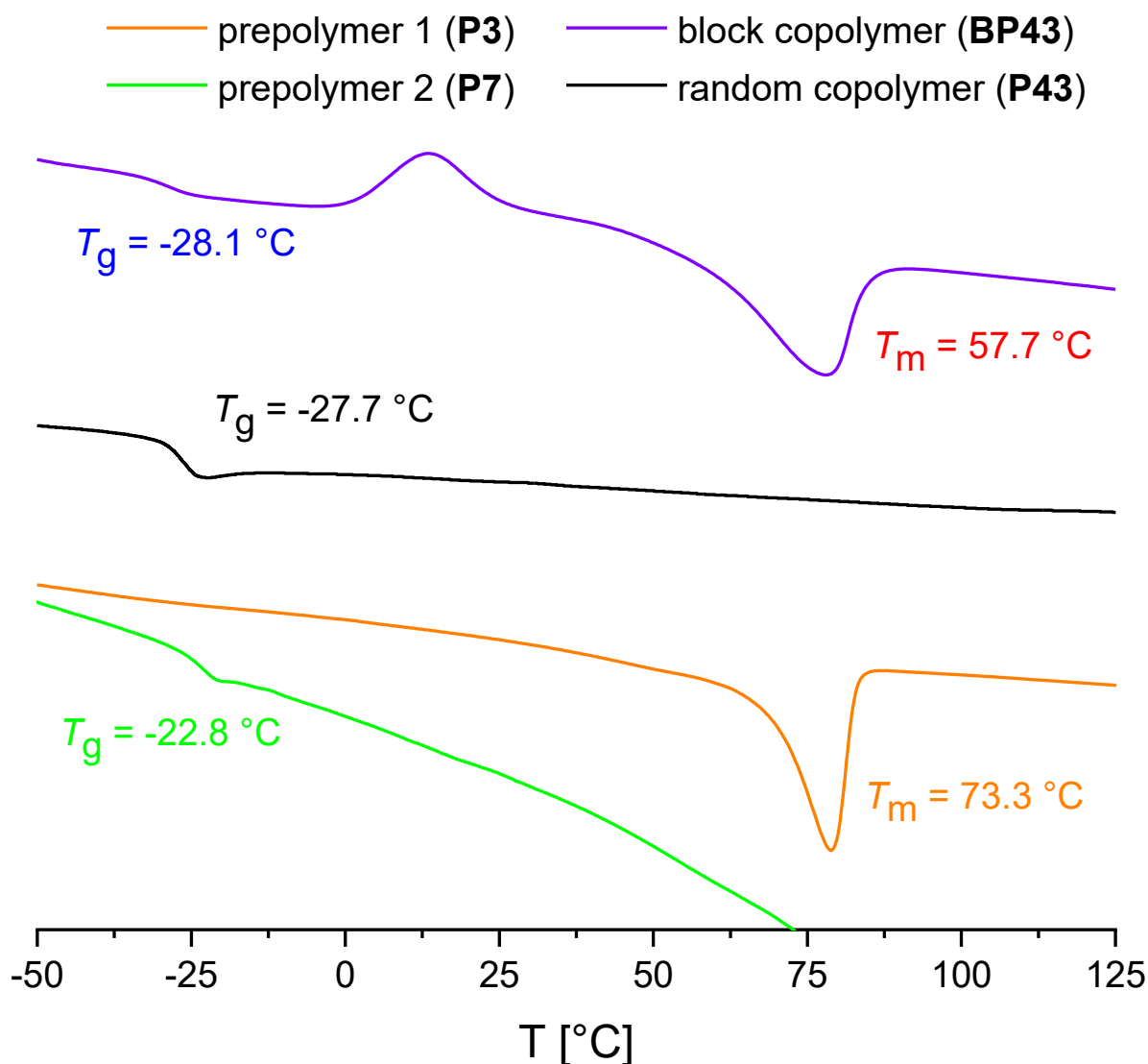
Figure 45 DSC trace of the block copolymer (purple) **BP43**, showing both transitions of **P7** (green, T_g) and **P3** (orange, T_m), compared to the T_g of the random copolymer **P43** (black).

An exothermic transition observed at around 12 °C (**Figure 45**) derives from cold crystallization, which occurs during fast heating rates.[376] Even with a dithiol ratio of 1:1, a melting point at around 70 °C belonging to the linear NIPU **P3** is clearly observed, along the already known glass transition temperature of *ca.* −30 °C. In this case, as the block copolymer is composed of two distinct units, the individual properties of the polymer blocks are still distinguishable, while the characteristics of a random copolymer are dictated by the local environment and statistical nature of interactions.[377] **BP44** also inherited the thermal transitions of the respective prepolymers, showing a T_g at −37 °C (derived from **P9**) and a T_m at 81 °C (derived from **P3**). **BP45** even exhibits three distinct melting points, two of which

belong to the **P18** block (T_m = 26 °C and 52 °C) and the other to **P3** (T_m = 65 °C). Additionally, the T_g of **P18** (T_m = −26 °C) was also detected by DSC.

In conclusion, the thiol-ene polymerization was determined to be a useful tool for the preparation of end group-functionalized homopolymers and the subsequent transformation into block copolymers. This method also proves to be able to provide better thermal property transfer of the individual monomers than the synthesis of random copolymers. The T_gs and T_ms of each block were efficiently transferred to the final product, allowing for the combination of desired thermal properties. Additionally, the simple and straightforward preparation of random- and multiblock copolymers can also be exploited for the tuning of mechanical properties. This topic will be however described in **chapter 4.2.15**.

In previous chapters, the structure and properties of the NIPUs were determined to be influenced by both diene and dithiol components. However, the synthesis of NIPUs *via* thiol-ene polymerization also leads to the formation of sulfide linkages, opening an opportunity for post-polymerization oxidation of the thioether, as will be discussed in the next section.

4.2.13 Post Polymerization modification (Oxidation)

The post polymerization modification or functionalization of isolated polymers is interesting in the view of material properties for application purposes. For instance, a PMMA surface treated with calcium phosphate or substituted with alkoxysilanes led to improved adhesive properties. After modification, these materials possessed properties suitable for application as corneal substitutes in medicine.[378] For the NIPUs and polyureas reported in all previous sections of this chapter (**chapter 4.2**), the functionalization by substitution is more difficult because of the unavailability of commercial dithiols with ester side chains. However, another possibility is described in this chapter.

An optimal modification suitable for both NIPUs and polyureas prepared *via* thiol-ene polymerization is based on the main structural similarity represented by the thioether linkages. Previously reported by Meier *et al.*[354] in 2014, similar polysulfides derived from renewable materials were oxidized to yield the respective polysulfones, with water as the only side product. As the procedure proved to be straightforward and efficient, the herein reported polymers (**Table 27**) were subjected to the same conditions. After polymer dissolution in THF

and addition of a 30% H_2O_2 solution, the reaction mixture was stirred for 24 h at 65 °C (**Scheme 35**) and subsequently precipitated in a water-methanol mixture (3:7, volume ratio). The dried products were then first analyzed *via* IR spectroscopy to qualitatively observe changes in the chain structures. As shown in **Figure 46**, new signals arose after the reaction at around 1230 and 1100 cm^{-1}, typically assigned to sulfone functionalities, both belonging to the S=O stretching vibration.
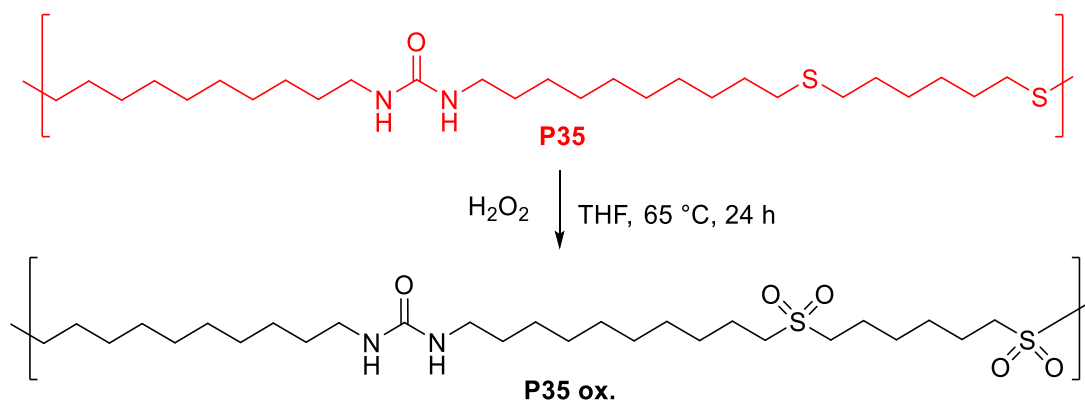
Scheme 35 Oxidation of polysulfides to polysulfones with H_2O_2. As an example, polyurea **P35** and the respective oxidized **P35 ox.** were chosen.
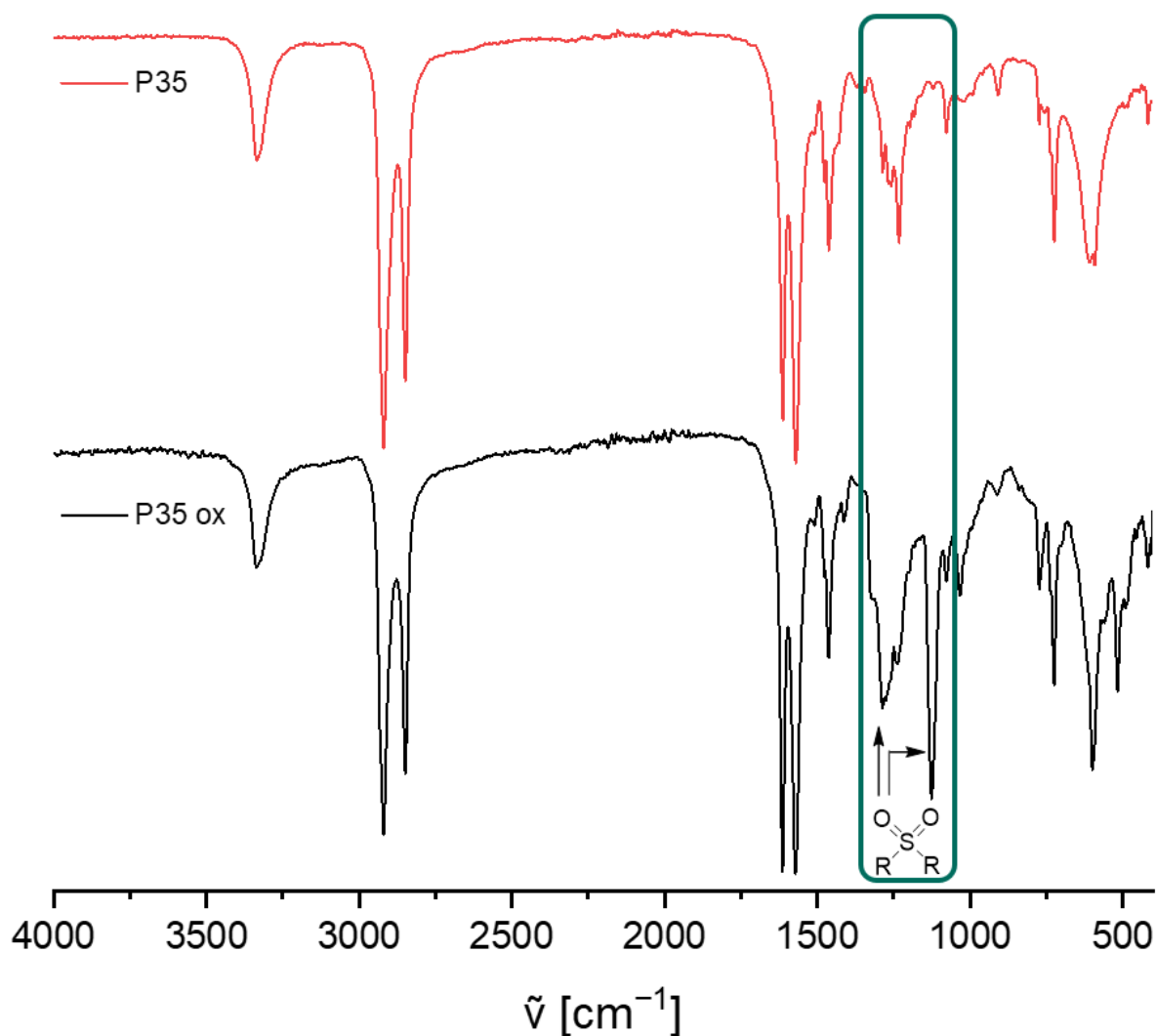
Figure 46 Comparison between the IR spectra of the unmodified (**P35**, red) and oxidized (**P35 ox.**, black) polyurea. At the signals at 1,230 cm^{-1} and 1,100 cm^{-1} are ascribed to the sulfone moiety.

It is worth mentioning that, although polyureas **P35-37** were not soluble in THF even at the reaction temperatures of 65 °C, the desired oxidized polymer was still obtained.

Afterwards, the polysulfones were tested for solubility in common deuterated solvents to allow NMR analysis. Unfortunately, none of the polysulfones could be dissolved, except for **P7 ox.**, which was measured in CDCl$_3$ at highly diluted concentrations. The higher solubility of **P7 ox.** in chloroform compared to the other polymers may result from the bulkier nature of the limonene dithiol–based NIPU. The compared spectra of sulfide and sulfone are shown in **Figure 47.**

Results and discussion
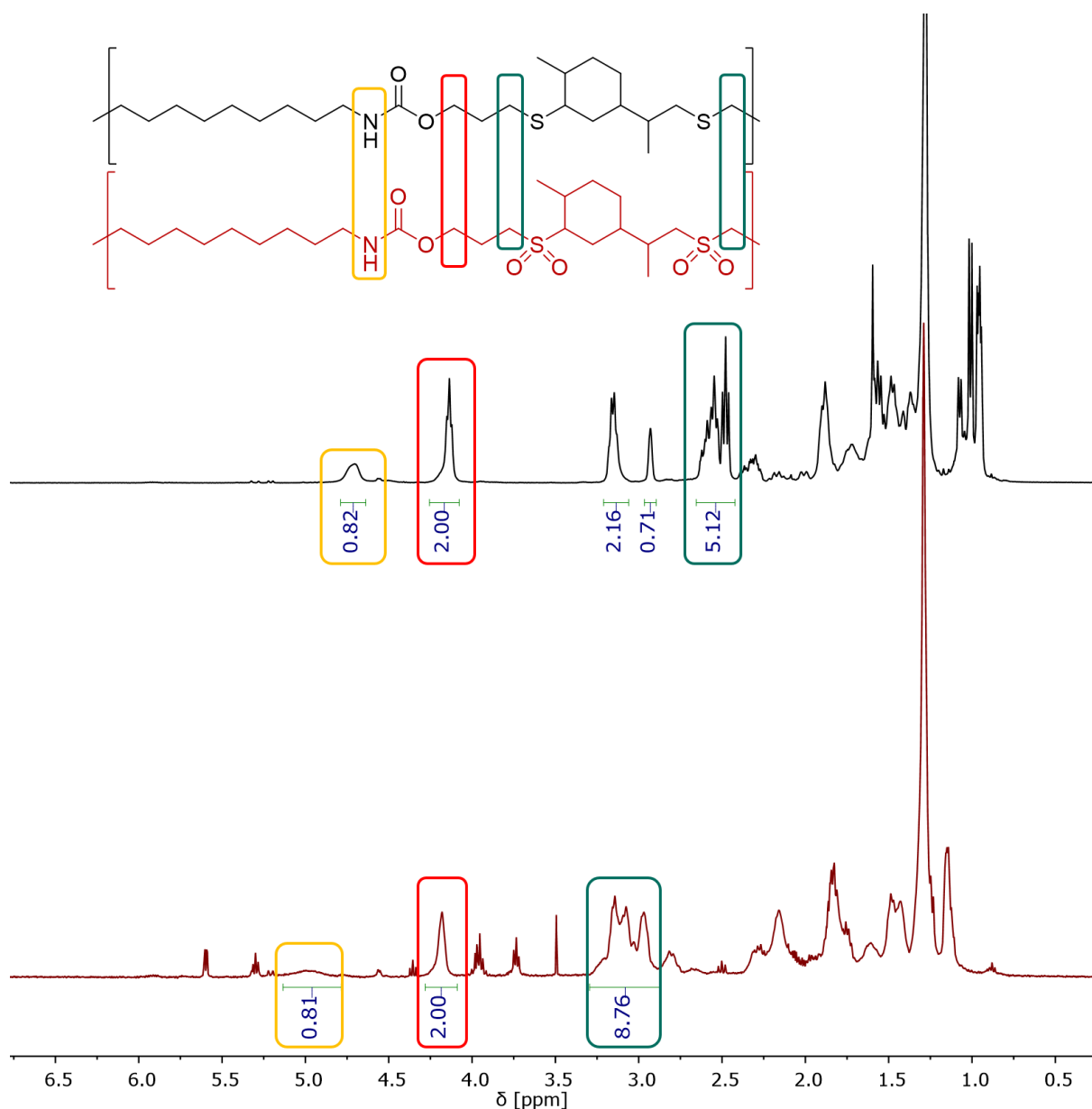
Figure 47 ^{1}H NMR spectrum of polysulfide NIPU (**P7**, black) and the respective oxidized polysulfone NIPU (**P7 ox.**, red).

Figure 47 suggests that the modification was near quantitative as the proton signals of the methylene groups adjacent to the sulfide linkage at 2.42 ppm are small. Furthermore, the new signals at 2.8-3.1 ppm are attributed to the new oxidized species as expected from a sulfone. Also, the methyl groups, which previously ranged in a multiplet from 0.8 to 1.05 ppm, shifted uniformly toward a single peak at 1.07 ppm. The urea proton shifted from 4.65 to 4.97 ppm, showing significant broadening. Therefore, the method was successful, as confirmed by both IR and NMR spectroscopy. The use of the more polar DMSO for both synthesis and NMR analysis was avoided. The reason for not performing the reaction in DMSO is because this

146

solvent is also readily oxidized by H_2O_2 to the respective dimethylsulfone, which is a solid. As for NMR analysis, none of the polysulfones were soluble in deuterated DMSO. Additionally, the residual solvent signal at 2.5 ppm overlaps with the alkyl signals adjacent to the sulfide, thus covering traces of unoxidized thioether in the polysulfone.

In the next step, both molecular weight and molecular weight distributions were determined *via* SEC for all prepared polysulfones. Since the oxidized polymers were insoluble in THF, HFIP (0.1 wt% potassium trifuoroacetate) was chosen as solvent. The results are shown in **Table 27**.

Table 27 Molecular weight and dispersities of the polysulfides before and after oxidation with H_2O_2.

entry	diene	dithiol	M_n [g/mol] [a]	$Đ_M$ [a]
P2	4	1,3 propane	7,200	2.29
P2 ox			4,600	2.50
P3	4	1,4-butane	11,850	1.82
P3 ox			3,800	2.69
P4	4	1,6- hexane	3,550	1.90
P4 ox			1,200	3.12
P7	4	limonene **11**	5,800	1.77
P7 ox			7,400	1.56
P9	4	2,3-butane	11,300	2.05
P9 ox			6,000	1.72
P14	4	3,6-dioxa,1,8-octane	9,850	1.48
P14 ox			21,000	1.20
P15	4	10,10'-(hexane-1,6-diylbis(oxy))bis(decane-1-thiol)	32,900	2.18
P15 ox			9,400	1.94
P21	3	1,6-hexane	5,700	2.09
P21 ox			1,450	2.59
P35	9	1,6-hexane	4,850	2.32
P35 ox			2,050	3.52
P36	9	1,10-decane	5,550	2.29
P36 ox			3,500	2.14
P37	9	limonene **11**	6,450	2.46
P37 ox			5,000	2.53
P43	4	1,4-butane	10,650	2.29
P43 ox		limonene **11**	17,250	1.52
P44	4	1,4-butane	9,250	1.74
P44 ox		2,3-butane	6,050	1.79
P45	4	1,4-butane	9,450	1.92
P45 ox		Butane-1,4-diyl bis(2-mercaptoacetate)	2,700	1.78

[a] HFIP-SEC calibrated with PMMA standards

Using the same calibration as with polysulfides, polysulfones exhibited lower apparent molecular weights in most cases, despite the anticipated increase due the oxidation process. This behavior was explained by the stronger interactions caused by the sulfone moiety: in the polysulfone, the additional oxygen atoms can provide both inter- and intramolecular dipole-dipole interactions between chains. The sulfone macromolecules are expected to exhibit increased attraction compared to the respective sulfides, ultimately leading to smaller hydrodynamic radii and therefore retention times on the SEC setup that correspond to low M_n values. The only contradicting examples are limonene-bearing NIPUs (**P7 ox. and P43 ox.**). The synthesis and post polymerization modification of the limonene-based polyurethane was repeated to ensure the reproducibility of the experiment and the SEC evaluation. In both cases, the molecular weight and the dispersity exhibited opposite behavior compared to the linear sulfone NIPUs as the M_n value increased, for instance from approximately 6 kg/mol to 7.5 kg/mol and the dispersity decreased from 1.8 to 1.6 for **P7**. The bulkier structure of the limonene is assumed to partially disrupt the dipole interactions because of the steric hindrance of the terpene moiety leading to the detection of an expected weight gain after the oxidation.

Lastly, the study of the thermal properties of the polymers was performed *via* DSC. In **Table** *28* the melting and glass transition temperatures of the polysulfones are directly compared to their sulfide counterparts.

Results and discussion

Table 28 T_gs and T_ms before and after the oxidation of polysulfides with H_2O_2.

Entry [a]	T_g [°C]	T_m [°C]
P2	-	65.4
P2 ox	-	187.7
P3	-	73.3
P3 ox	-	163.5
P4	-	64.8
P4 ox	-	154.8
P7	−22.9	-
P7 ox	41.3	-
P9	-30.0	-
P9 ox	30.0	-
P14	-	46.3
P14 ox.	−34.1	-
P15	-	62.3
P15 ox	-	128.9
P21	-	63.1
P21 ox	-	152.5
P35	-	136.3
P35 ox		151.8 /179.2
P36	-	124.6
P36 ox	126.5	162.9
P37	-	63.8
P37 ox	-	129.5
P43	−27.7	-
P43 ox	33.4	148.7
P44	−39.0	37.4
P44 ox	-	153.3
P45	−42.9	62.6
P45 ox	50.2	152.1

[a] Conditions: 5.00 eq. H_2O_2 (30% aqueous solution), THF, 24 h, 65 °C.

Based on the results listed in **Table 28**, significant changes in thermal transitions were observed, with polysulfones exhibiting values greatly surpassing their polysulfide counterparts. For instance, **P3**, a linear NIPU melting at 73 °C before oxidation, exhibited a melting point of 164 °C after oxidation (**Figure 48**).
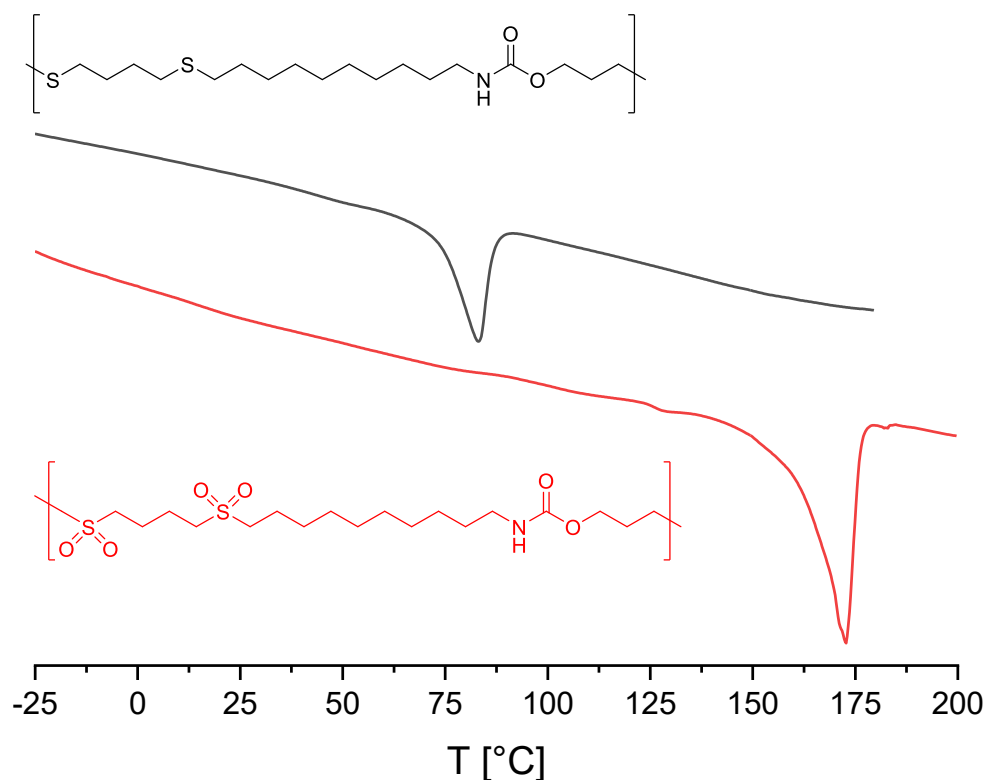
Figure 48 DSC trace of the polysulfide **P3** (black, above) and the respective polysulfone **P3 ox.** (red).

NIPUs prepared with sterically more demanding dithiols, like limonene or 2,3-butanedithiol, formed viscous materials with T_gs below 0 °C (−23 and −30 °C, respectively). These polysulfides exhibited much lower transitions compared to the oxidized polysulfone NIPUs, with new glass transition temperatures being around 60 °C higher. The same effect was observed for all other examples. When comparing the oxidation of **P43**-**45**, the modification had different impacts on each polymer. **P45** showed an expected increase for both T_g and T_m of 90 °C. However, in **P43**, the glass transition was dominant in the DSC, which was not the case in its oxidized form, for which a melting transition at around 150 °C was observed. For **P44**, the opposite effect was observed: the sulfide copolymer composed of the 1,4- and 2,3- isomers of butanedithiol possessed a distinctive T_g at −39 °C and a T_m at 37 °C, while only a higher T_m of 153 °C was observed for the respective polysulfone. This suggests that the oxidation and increase of polarity of the species by additional dipole-dipole interactions can weaken the intensity of the

glass transition in favor of the melting transition. This is likely caused by the higher crystallinity percentage in the polysulfone, since melting transitions are a property of crystalline regions while glass transitions of amorphous domains. In order to confirm this hypothesis, additional analytical methods to detect the glass transitions, e.g. TMA and DMA, will be employed in future.

An exception is **P14** as it behaves in an opposite fashion compared to all other polymers, both in SEC and DSC experiments. First, the molecular weight increased by oxidation, however, it was determined that the dipole interactions tend to lower the hydrodynamic radius of the polysulfone compared to the polysulfide. One would assume that the ethylene glycol structure might be the reason for this behavior, however, the thermal properties also changed dramatically upon oxidation. In **P14 ox.** a T_g was observed at around -35 °C, while a melting transition was not detected. Two possible explanations are a that either the NIPU was both oxidized, as suggested by IR spectroscopy (see experimental section, **chapter 5**), and further modified *via* an unknown reaction pathway that cannot be identified by IR alone, or the melting point increased to temperatures above the measurement settings (200 °C). In a publication of Zhang *et al.* in 2003, the authors reported that dipole interactions with PEG-based resins cause physical crosslinking, decreasing the mobility of the chains.[379] The formation of crosslinking is therefore a plausible explanation for the second option, although this hypothesis was not proven. Unfortunately, as **P14 ox.** was insoluble in all common deuterated solvents, NMR analysis was not performed. Alternative analytical methods will be attempted in future, such as solid state NMR or high temperature NMR spectroscopy. Additionally, **P14 ox.** exhibits the texture of a colorless solid, however, as no T_m was detected *via* DSC, the degree of crystallinity is suggested to be determined *via* small angle- or wide angle X-ray scattering (SAXS or WAXS).

Dicarbamate NIPUs **P28**-**32** were not soluble in THF and could therefore not be oxidized. Utilizing DMSO as solvent or co-solvent was also impossible as the hydrogen peroxide would also transform the sulfoxide to dimethyl sulfone. Therefore, polymers prepared from dicarbamate **6** were not utilized in this chapter.

Conclusively, the oxidation of polysulfides to polysulfones is a straightforward and green method for the post-polymerization modification of NIPUs. The efficient conversion with water as the only waste product makes it an optimal procedure for property tunability. In the

future, the partial oxidation of the polysulfide NIPUs is expected to make even further properties accessible, based on the average composition between sulfide, sulfoxide and sulfone species. The thermal properties were tuned in ranges of more than 90 °C, independently of the transition type, thus enabling possible applications at high temperatures. With this method, polysulfide T_gs similar to poly(vinylidene fluoride) (PVDF, T_g = -40 °C), plasticized poly(vinyl chloride) (PVC, T_g = -50 °C) or poly(propylene) (PP, T_g = -10 °C) were increased to values resembling those of poly(butylene terephthalate) (PBT, T_g = 55 °C), poly(amide 11) (PA, T_g = 35 °C) or poly(methyl pentene) (PMP, T_g = 20 °C) in polysulfones, all of which are valuable commodity polymers.

4.2.14 Film casting

As previously mentioned (**chapter 2.5.1**), polyurethanes find applications in many fields, such as foams and insulation materials. However, the main differences between industrially produced polyurethanes and the polymers described in this work is the absence of networks obtained *via* crosslinking and the presence of thioether linkages herein. In this chapter, a few approaches have been tested to obtain films or different shapes from the synthesized NIPUs for further applications and to evaluate material properties.

First, solution casting[380] was investigated because of the simplicity of this method, and **P3** was chosen as a model compound for its good solubility in THF and chloroform. The sample was dissolved in THF or chloroform, and solvent casting was applied on a glass plate. The solution was subsequently heated in a vacuum oven until the solvent had completely evaporated. Although almost no bubbles were observed in the final film, the material adhered to the surface of the glass causing numerous fractures during its removal (**Figure 49 A**). Therefore, the casting was repeated in a Teflon™ dish. However, the obtained films were inhomogeneous and the evaporating solvent caused bubbles in the final film. The most homogeneous films were obtained by heating the Teflon™ dish in an oil bath in the fumehood. Most likely, the slightly decreased vapor pressure was optimal for the solution casting. However, it was difficult to align the dish horizontally, hence, the obtained film possessed one thicker side that also presented bubbles (**Figure 49 B** and **C**).

Results and discussion
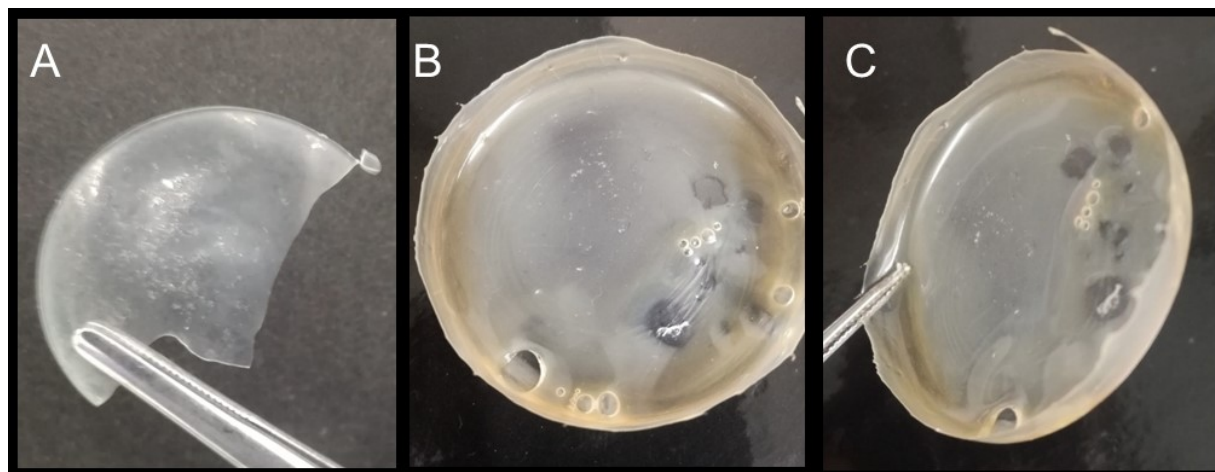
Figure 49 Results of solvent casting of NIPU **P3**. **A**: on glass. **B** and **C**: on a Teflon™ dish and heating in a vacuum.

To mitigate these issues, the pure polymer was ground into a fine powder and distributed evenly on a Teflon™ dish and was then heated in an oven around 10 °C above the melting temperature (at 85 °C) for approximately 1 h. The material was given time to spread evenly across the dish. However, the final film was not homogeneous and bubbles were observed on the surface. In another attempt, a vacuum oven was employed to avoid bubble formation, because of the reduced pressure. Although the obtained film was more even, it was still too inhomogeneous for mechanical testing. After cooling, the residual material was rather brittle (**Figure 50**) leading to the conclusion that solvents like chloroform or THF are able to act as plasticizers, thus yielding a film suitable for mechanical testing. Without any plasticizing agent, the final material was only isolated as a brittle opaque disc. Similarly, NIPUs synthesized with different monomers led to similar outcomes.
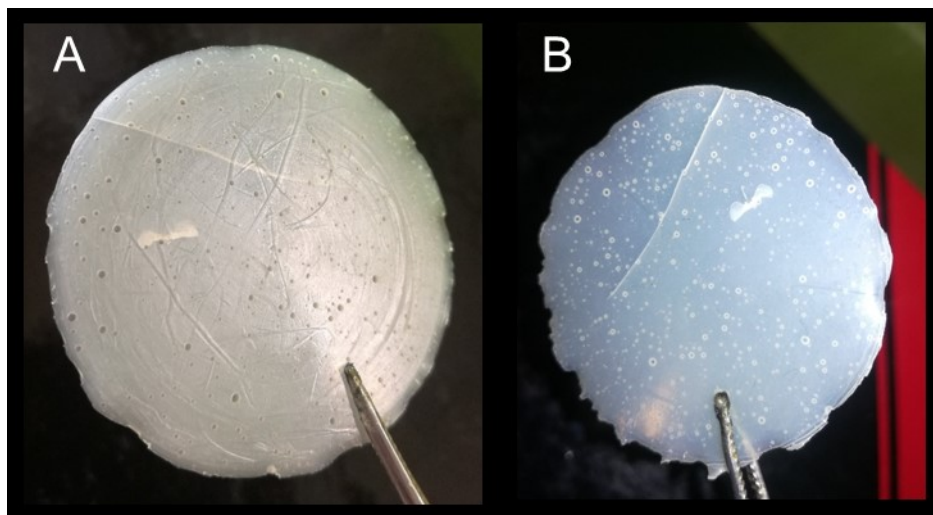
Figure 50 Disc obtained after melt casting polymer **P3** in the absence of solvent (**A**). The same disk was kept near a light source to show the partial transparency of the sample (**B**).

The use of a hot press was considered for this task, however, the resulting material (**P3**) was expected to exhibit high brittleness as with the melt-casting. An exception were the polyurethanes produced from bulkier dithiols: NIPUs from limonene dithiol **11** and 2,3-butanedithiol, for instance, possess side groups bulky enough to prevent crystallization. The respective polymers were, therefore, highly viscous and transparent, showing almost adhesive properties, with a highly sticky consistency. In **chapter 4.2.11** and **4.2.12,** it was shown that if a NIPU is synthesized from both a linear and a bulky dithiol, the thermal transitions of both components are identified in the DSC. Therefore, it was assumed that the same copolymers or block copolymers exhibit rubber-like mechanical properties by combining the hard segments of **P3** and the soft segments of the limonene-based **P7**.[186] To investigate the mechanical properties, the casting of films of rectangular shape was performed utilizing a hot press (**Figure 51**).

Figure 51 Digital image of a hot-pressed NIPU copolymer (**P43**).

The samples were heated for 15 minutes at 10 °C above their melting temperature, to be subsequently pressed at 2 bar for 2 minutes at the same temperature and subsequently for around 1 hour while cooling. Qualitatively, the samples of **P44** and **45** were both rubbery with an opaque yellowish appearance, probably because of initial degradation derived by the long exposure to heat. A difference in processability between random and block copolymers was not observed, therefore, only the synthetically more simple copolymers were employed for further testing to preserve valuable samples for future assessments. The hot pressed film of the limonene-based NIPU **P43** was more elastic and more transparent than all other samples. The high elasticity is a sign of the glass transition being near room temperature, and the transparent character is explained by the reduced crystallinity derived from the sterically demanding limonene structure.

For the evaluation of the mechanical properties of the hot pressed polymers, stress-strain testing was conducted to analyze the elasticity of the new materials.

4.2.15 Tensile testing

The six copolymers chosen for their mechanical testing are shown in **Figure 52**. Additionally, the copolymer **P43** was tested with both a 50% and 40% molar percentage of limonene for a better understanding of the mechanical behavior of the synthesized NIPUs.
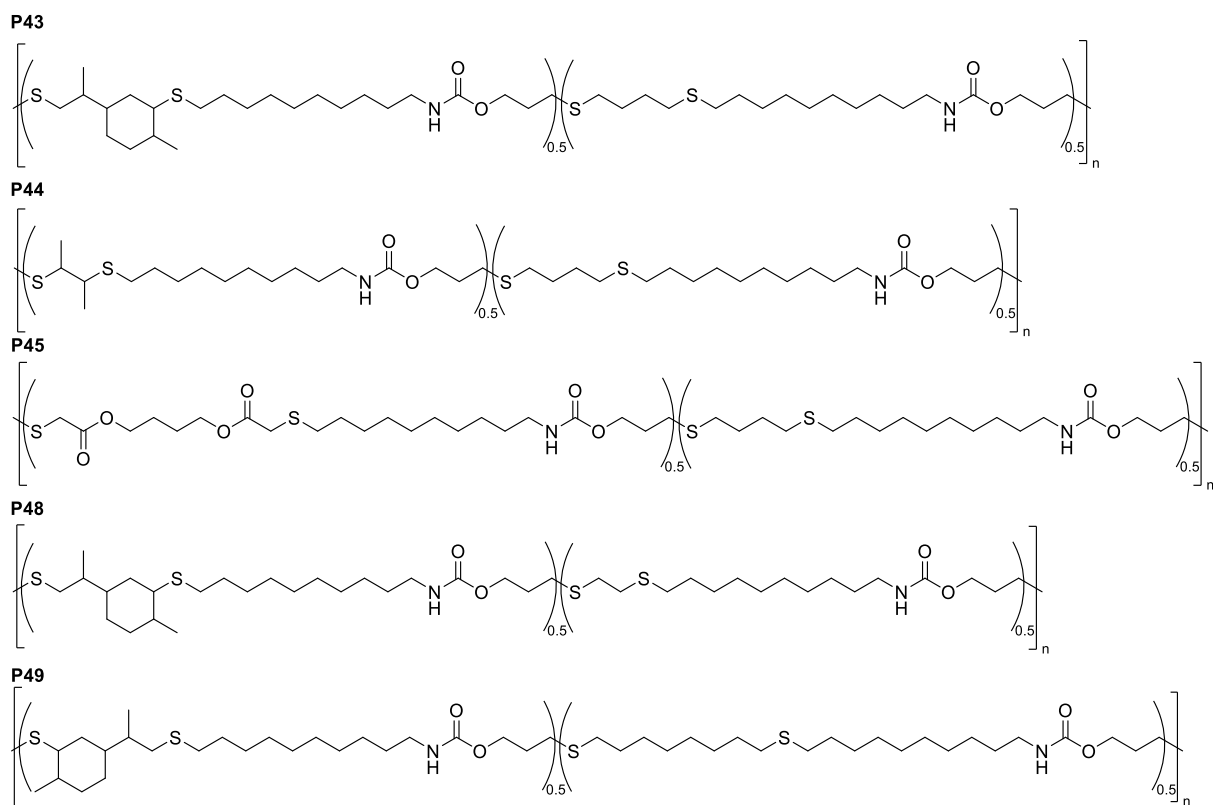
Figure 52 The five thiol-based NIPU copolymers employed for tensile testing.

As mentioned in the previous chapter, **P44** was qualitatively harder than the more elastic **P43**. However, one major problem was encountered at the beginning of the tensile testing as the specimen proved to be problematic during clamping. Only a few data points were obtained from each measurement, as the sample either slipped or was fractured by the clamp during further tightening. Meanwhile, copolymer **P43** was clamped and measured without issues.

A typical stress-strain diagram of **P43** is shown in **Figure 53**.

Results and discussion
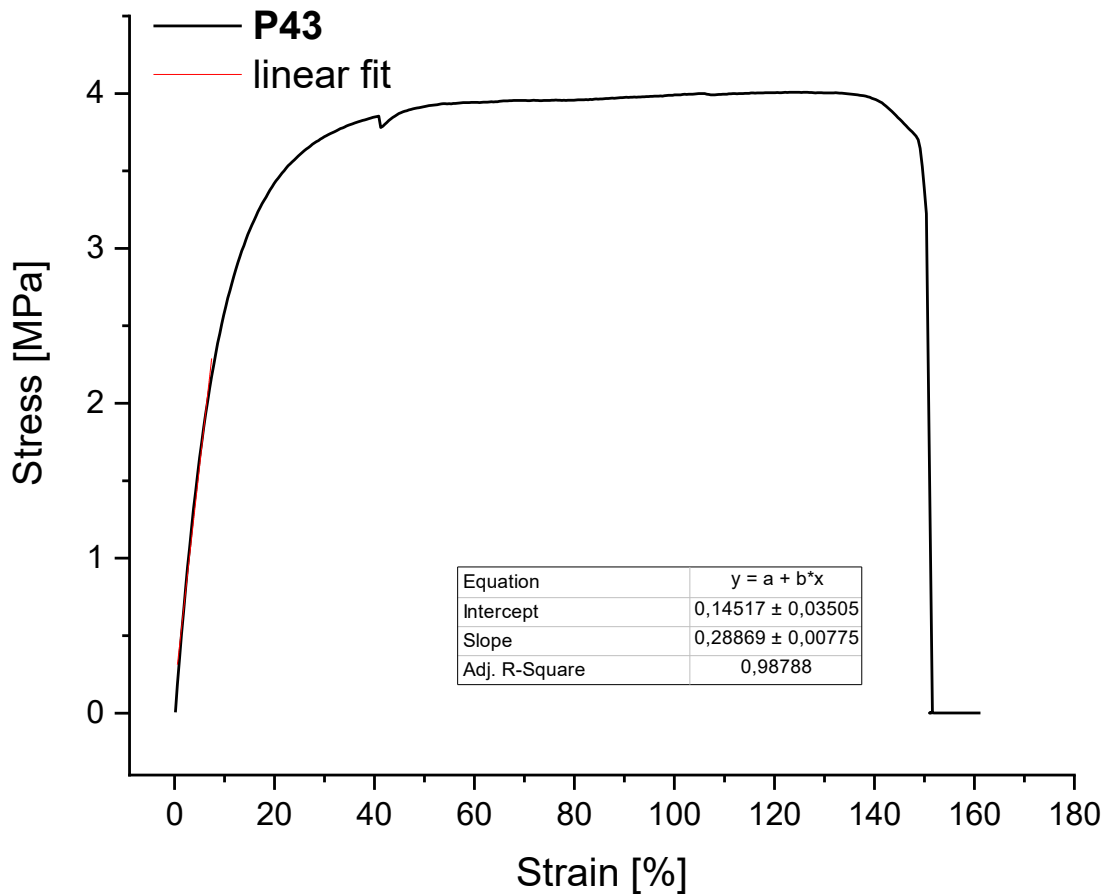
Figure 53 Typical stress-strain diagram for **P43**. The E modulus was calculated from the slope of the linear fit of the initial region.

The axis values were calculated with the following formulas (**Equation 3**, **Equation 4**):[381]

Equation 3

$$stress\ [MPa] = \frac{F\ [N]}{A\ [cm^2]}$$

Equation 4

$$strain = \frac{l - l_0}{l_0}\ \text{x}\ 100\%$$

In **Equation 3** and **Equation 4**, F represents the applied force, A the surface area of the sample, l and l_0 the sample length at each timepoint and at the start of the experiment, respectively. The stress-strain plot provides the Young modulus as the slope of the initial linear region.[381] From the diagram, it was argued that the material behaves like a thermoplastic,[382] with a curve progression similar to that of low density polyethylene (LDPE) at room temperature. PUs exhibit the same behavior at low weight percentages of hard segments.[383] Large elongations

158

already at low applied force are also typical of polymers with broad amorphous regions and a T_g lower than room temperature,[384] as DSC measurements already confirmed for this NIPU copolymer. This behavior derives from the mobility of the polymeric chains in the amorphous domains. In summary, the maximal elongation of 300% was reached for the random copolymer **P43** at a force of 53 N, with an average Young's modulus of 30 MPa.

Results and discussion
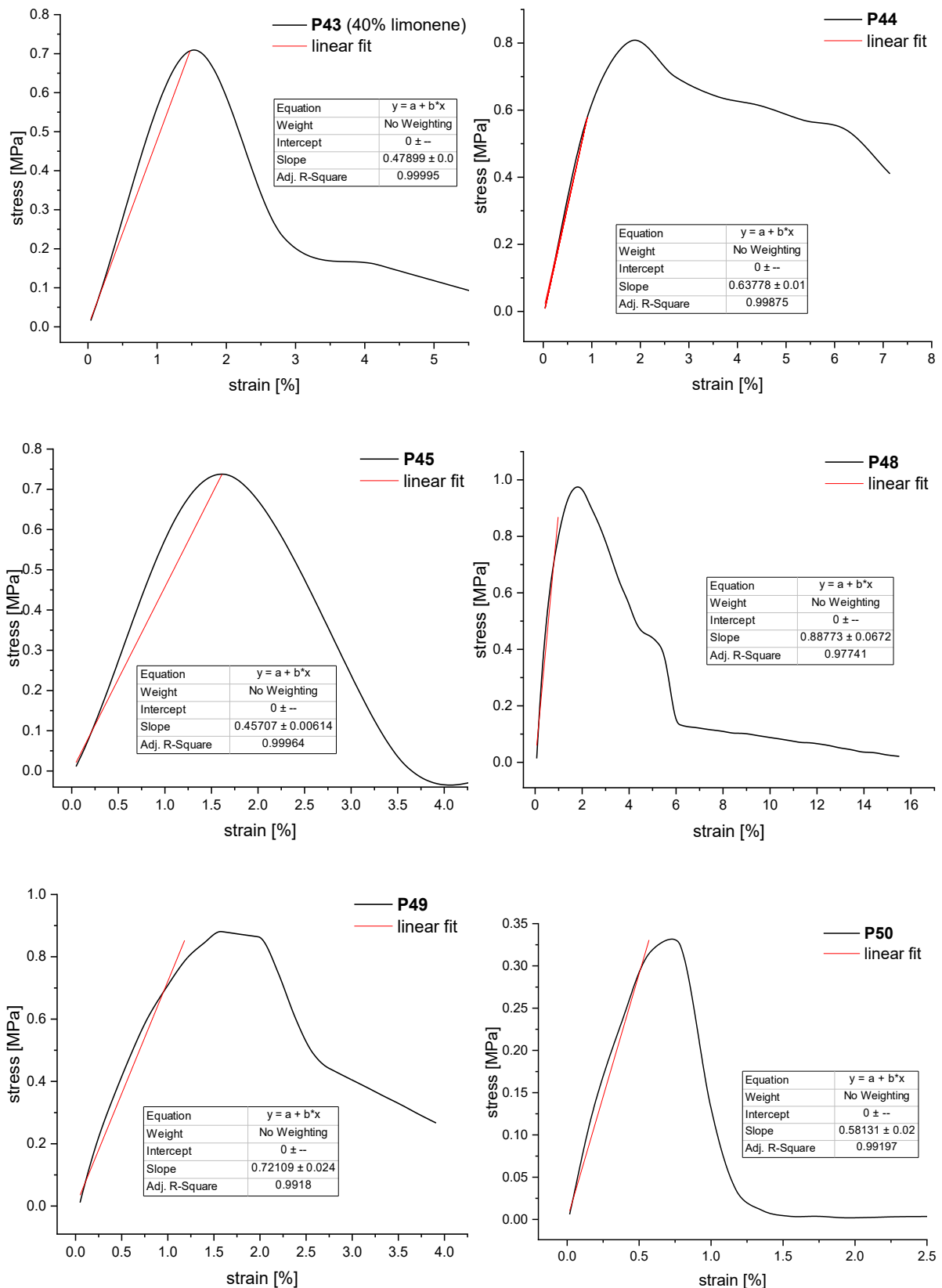
Figure 54 Stress-strain diagrams for **P43-45** and **P48-50**. Some diagrams were plotted with a smoothing option because of the low amount of data points in the initial region (e.g. **P45** with two suitable data points). The linear fit was performed on the experimental data points and not on the smoothened plot.

The other random copolymers were analyzed under the same conditions as **P43**. However, as mentioned before, the samples were more brittle than the elastic limonene-based NIPU. **P44** and **P45** showed maximal elongations around 2% before the polymer sample broke. It is worth mentioning that the samples did not break in the middle but rather at the clamping position. The obtained results until that point have been used for preliminary E modulus calculation (**Figure 54**). However, the inaccuracy of the obtained data is expected to be high since the weakening caused by the clamp most likely results in a lower Young's modulus.

Nonetheless, a difference in the stress-strain slope between **P44** and **P45** was observed. The average Young´s modulus of 2,3-butanedithiol based NIPU was 63 MPa while changing the second dithiol component to butane-1,4-diyl bis(2-mercaptoacetate) led to a lowered Young's modulus of around 45 MPa. This behavior was attributed to the longer backbone chain of the diester monomer compared to the C_2 chain of the 2,3-butane structure. Furthermore, the polarity increase endowed by the carbonyl groups of **P45** as well as the related higher probability of the carbamate to build hydrogen bonds between polymer chains contributed less to tensile strength than shorter linkers between urethane functionalities.

To give further comparison, **P43** was subjected to tensile testing with a limonene content of 40% instead of 50% in order to determine if the material was toughened by reducing the soft segment percentage of the NIPU, while simultaneously retaining the stability of the previously measured **P43** (50 mol% limonene). The hot-pressed sample, which was already optically similar to **P44** and **P45**, was found to possess the same brittleness as the other two copolymers with an average E modulus of 48 MPa. Although the measurements ended prematurely due to the issue with the clamping, this material was more resistant towards elongation when compared to **P43** with a 1:1 molar composition of limonene and 1,4-butanedithiol. Since a change of 10% molar content caused such a pronounced change in morphology, **P43** should be analyzed further on mechanical properties in future, especially in the range of limonene dithiol percentage between 40 and 50%.

Furthermore, to determine the influence of the chain length of the repeating unit of the NIPU, **P48** and **P49** were prepared in which the 1,4-butanedithiol component in **P43** was switched to 1,2-ethane- and 1,8-octanedithiol, respectively. Both materials were less elastic than **P43** leading to similar brittleness as did **P44** and **P45**. Only a few data points were collected before the samples were fractured by the clamp. Nonetheless, the average E moduli differed from

Results and discussion

each other. **P48**, bearing the ethane chain, resulted in an average tensile modulus of 74 MPa, more than twice as resistant to elongation than **P43** (30 MPa). The increase was expected as the carbamate functionalities are closer to each other in shorter repeating units. However, **P49** also resulted in a Young's modulus of around 64 MPa surpassing the value for **P43**. This behavior was explained by the lowered influence of the limonene structure on the suppression of hydrogen bonding induced crystallization in a longer repeating unit, thus making the material more rigid.

With a C_8 linker, an increase of interactions between carbamate groups is achieved, as the bulky terpene probably does not possess the required steric hindrance to block hydrogen bonding over a long repeating unit. This assumption is valid only for the already reported 1:1 ratios between dithiols, as this effect is most likely tunable by increasing the limonene content in **P49**. Under the described polymerization conditions, 1,4-butanedithiol offers the optimal chain length in which the amorphous and crystalline regions, or rather the ratio between hard and soft segments, are balanced in order to form an elastic material. Therefore, this system will have to be analyzed thoroughly in the future by varying the monomer ratios of **P48** and **P49**. Additionally, experiments should include the synthesis of a random copolymer with 1,6-hexanedithiol, possessing a different chain length between the 1,4-butane- and 1,8-octanedithiol.

One last attempt to increase the resistance against elongation of the flexible **P43** is described by the stress-strain diagrams of **P50**. This random copolymer was prepared by adding two different dithiols in the initial polymerization mixture as well as two different dienes. For this purpose, it was decided to include 0.10 eq. of urea **9** in combination to 0.90 eq. of carbamate **4** to induce stronger hydrogen bonding interactions between polymer chains. However, preliminary results suggested a 10% molar concentration of urea to cause the formation of a material too brittle for tensile testing. After calculation of the slope of the initial region of the stress-strain diagrams, an average Young's modulus of 66 MPa, a value similar to **P49,** was determined. The molar composition of **P50** is therefore to be adjusted to contain less than 0.1 eq. of urea as diene component in order to avoid the material to become too brittle for further applications.

Conclusively, seven different random copolymers were analyzed *via* stress-strain experiments to determine the respective tensile modulus to gain further insights on material properties for

162

further application. A 1:1 dithiol ratio was determined to be optimal for the preparation of the rubber-like NIPU **P43** produced from carbamate **4**, 1,4-butanedithiol and limonene dithiol **11**, which showed properties of a typical elastic material.

Under the same polymerization conditions, polymers **P44**, **P45** and **P48**-**50** were too brittle to be employed as elastic materials, showing E moduli between 45 and 80 MPa. Lowering the limonene content to 40% or exchanging 10% of carbamate **4** with urea **9** led to similar results, with the material breaking at low strains. However, the investigated materials show great potential for the development of tunable materials with a variety of promising properties, just by varying monomers and their molar composition as suggested in the previous paragraphs.

However, apart from elasticity, for many applications it is desirable for the elastomer to exhibit a high tensile strength. A strong PU material is defined by its hard segments, more specifically on the hydrogen bonds and the crystallinity, however, often at the cost of brittleness, as seen with the random copolymers **P44**, **P45** and **P48**-**50**. In brittle samples it is common to add plasticizer to make the material more ductile by increasing the elasticity. In the same way, additives such as the bioderived cellulose nanocrystals (CNCs) present an opportunity to increase the tensile strength in rubbery materials, as **P43** will be described in the subsequent section.

4.2.16 Cellulose nanocrystals (CNCs) as additives

Material properties are readily tuned by including different types of, for example plasticizers, flame retardants and many others, as explained in the theoretical background in **chapter 2.5.1**. For an elastic material, it is common to employ additives that offer strengthening. For this work, cellulose nanocrystals (CNCs) were explored. CNCs are obtained from the acid hydrolysis of cellulosic feedstock such as cotton, thus making them a renewable candidate additive. Additionally, it has been shown that the presence of CNCs in polymeric composites leads to an increased rigidity of the final material, increasing the Young's modulus in an almost linear fashion with the added CNC weight percentage.[385] However, most composites are limited to low CNC weight fractions as the percolation threshold [386] is easily exceeded causing the CNCs to agglomerate and form crystalline domains ultimately leading to brittle materials.[385],[387]

Results and discussion

Another advantage of the mentioned composites is the fact that, through dissolution of the polymer, the CNCs can be separated from the polymer and reused. However, for common polymeric materials, melting or dissolution are needed for processing, two methods which often cause phase separation and aggregation of the CNCs. This ultimately causes brittleness and introduces inhomogeneities in the processed material. In this line of thought, if the CNCs are covalently connected to the NIPUs, the overall strength should not decrease even after heating or after more cycles of solvent casting. Therefore, in a thiol-ene polymerization, CNCs modified with side chains bearing double bonds, for instance with unsaturated fatty acids, represent an optimal option for the binding of the crystals to the polymer.

During a three-month visit at the Adolphe Merkle Institute (AMI) in Fribourg, one of the projects included the modification of CNCs with fatty acids. The CNCs were provided by the Weder group and prepared by acid hydrolysis with sulfuric acid. The procedure was furthermore inspired by a previous publication from our group featuring the modification of cellulose with high oleic sunflower oil (HOSO).[388] The main component of the oil, the triglyceride, was transesterified under basic conditions to yield the cellulosic ester of oleic acid.[388] However, as the CNCs rod-like structure was to be maintained, they were not dissolved but first sonicated in distilled water in order to perform a solvent exchange from water to ethanol, from ethanol to acetone and from acetone to the oil. The solvent exchange procedure reduced the agglomeration of the nanocrystals compared to direct addition to the triglyceride.

After the solvent exchange, the initial synthetic conditions applied for transesterification of CNCs with oils were similar to the above-mentioned publications,[388] with 1.00 eq. base at 115 °C for 24 h, without DMSO and CO_2. The two employed oils were HOSO and epoxidized soybean oil (ESBO). ESBO was chosen for further possible post-modifications not involving double bonds, for instance the ring-opening of the oxiranes with different nucleophiles (curing). After the reaction, the crude product was purified *via* multiple washing steps with different organic solvents, like acetone and ethyl acetate. The IR spectrum of the dried solid suggested the presence of residual DBU (1,640 cm^{-1}) on the cellulose and traces of carbonyl species at *ca*. 1,730 cm^{-1} (**Figure 55, B**). The product was additionally washed with ethanol five times, leading to the disappearance of both the DBU and carbonyl signals, confirming that transesterification did not occur.
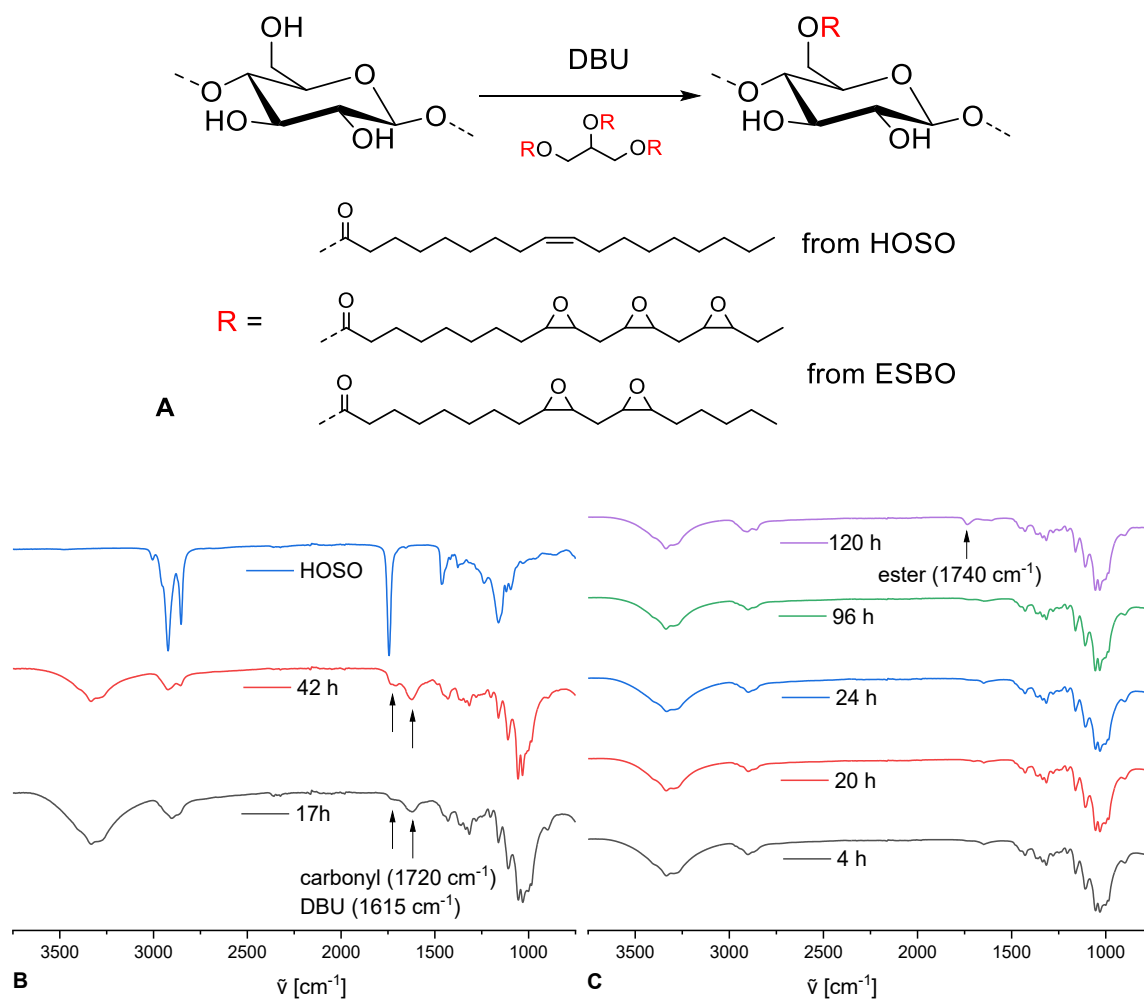
Figure 55 Schematic representation of CNC-modification with triglycerides with DBU as catalyst (**A**). IR spectra at different reaction times with the saccharide ester signals highlighted (**B**). IR spectra of the purified products at different reaction times. The addition of 2.00 eq. of DBU was performed after 96 h (**C**).

The low intensity of the carbonyls indicated the inefficiency of this method as also the variation of the reaction conditions, like temperature (100-130 °C), reaction time (12-120 h) and CNC concentration (2-5 wt%) did not improve the carbonyl intensity, based on IR measurements. A small enhancement in DS was achieved by increasing the equivalents of base as seen in **Figure 55** (**C**). During the reaction, two equivalents of DBU were added after 96 h (green trace), leading to a more distinct carbonyl signal in the next sample (purple trace). However, after evaluation of the elemental analysis (**Equation 6**), the degree of substitution (DS) was calculated to be low (<0.1).

DS determination was performed *via* elemental analysis.[389] The utilized formula for DS calculation is shown below (**Equation 5**, **Equation 6**):

Results and discussion

Equation 5

$$C = \frac{12.011 \times (6 + \sum DS_i n_i)}{12.011 \times (6 + \sum DS_i n_i) + 1.008 \times (10 + \sum 2 \times DS_i(n_i - 1)) + 15.999 \times (5 + \sum DS_i)}$$

Equation 6

$$DS = \frac{5.13766 - 11.5592 \times C}{0.996863 \times C - 0.856277 \times n + nC}$$

The values for **C** and **n** are given by the carbon content and the amount of carbon atoms of the substituent of the elemental analysis, respectively. **Equation 5** is the formula for the carbon content of a sample and is valid for the modification to one or more different ester types (n_i). However, if only one acid is used during the esterification (i= 1), then the equation is solved to yield **Equation 6**.

Performing the reaction with ESBO did not change the result for the modification of CNCs. Epoxide signals were also not detected during IR measurement, indicating a poor conversion or/and the instability of oxirane rings towards the reaction conditions. The calculated DS was similar as for the approach with HOSO (*ca*. 0.08).

Since neither conversion nor DS showed any signs of improvement after increasing time (144 h) and base equivalents (5.00 eq.) even further, the transesterification was attempted by directly using the methyl ester of a fatty acid. For this purpose, methyl-10-undecenoate was chosen as model compound, since the terminal double bond offers a higher reactivity compared to disubstituted unsaturated bonds, for instance for thiol-ene modifications. IR results showed again low reactivity of the methyl ester towards the transesterification of the CNCs, even with a 10-fold excess of carbonyl compound. The route was therefore abandoned in favor of a traditional esterification.

The model compound chosen was 10-undecenoic acid, because of its sustainable source, as it is obtained by pyrolysis of ricinoleic acid. A first approach included a classical esterification under acidic conditions. The reaction was monitored *via* IR spectroscopy. Even after numerous days and optimization of the parameters, such as temperature (90-115 °C) and concentration (1.5-5 wt%), as well as an optimization of the workup procedure, the ester signal was only visible at low intensities indicating that low DSs were obtained.

As a last alternative, a modified procedure from Ushanov *et al*.[390] was attempted, in which freeze-dried CNCs were added to a mixture consisting of *p*-tosyl chloride and undecenoic acid

followed by the subsequent addition of pyridine (**Scheme 36**). The reaction mixture was stirred for 2 hours at 50 °C under nitrogen atmosphere.
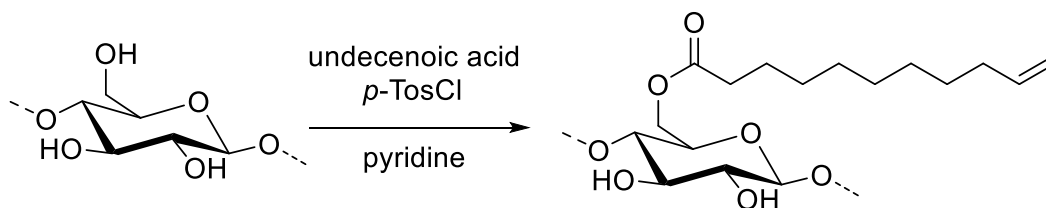
Scheme 36 Schematic representation of the functionalization of CNCs with 10-undecenoic acid.

The work up consisting of multiple washing steps with ethanol and water was fortified by an additional Soxhlet extraction in ethanol. The obtained powder was analyzed qualitatively by IR after drying *in vacuo* (**Figure 56**).
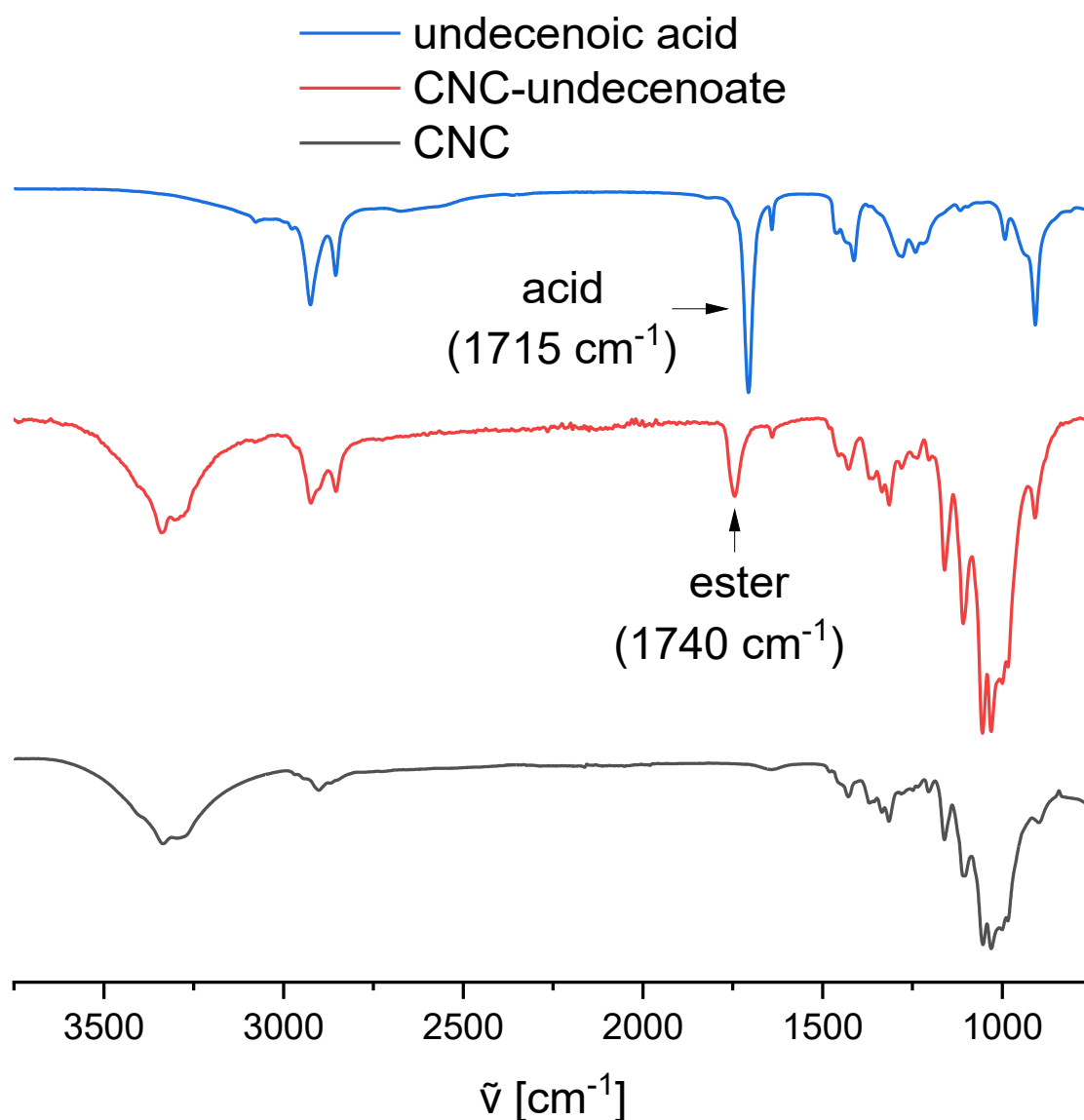
Figure 56 IR spectra of 10- undecanoic acid (blue), the pure CNCs (black) and of the 10-undecenoic acid–modified CNCs (red).

The DS of the undecenoate-functionalized CNCs was calculated to be 0.12, with a maximum possible value of less than 1[391] as two of the three hydroxyl groups of CNCs are oriented inside the structure of the nanocrystals and the OH groups on the surface are partially sulfonated. The sulfonated groups are formed during the synthesis of the CNCs, more specifically during the acid hydrolysis of cellulose with sulfuric acid.[392] Nonetheless, the properties of the modified CNC-undecenoate largely vary from the pure CNCs, even with low amounts of side chains. First, CNC-undecenoate nanocrystals were found to be hydrophobic as they were impossible to redisperse in water, even after extensive sonication. THF, however, was able to produce a dispersion in just a few minutes of sonication. The resulting mixture

was stable for *ca.* 10 to 15 minutes before some sedimentation was observed. *Via* this method, it is therefore possible to covalently bind these modified CNCs to a NIPU in a one-pot thiol-ene polymerization, without the risk of causing phase separation or agglomeration of the CNCs. Thus, after the end of the visit at the Adolphe Merkle Institute, the CNC-NIPU composites were prepared *via* thiol-ene polymerization.

The NIPU was synthesized in the same manner as previously described in **chapter 4.2.11**. The undecenoate-modified CNCs were mixed with carbamate **4** before the addition of DMPA and dithiols in form of a THF suspension (**Scheme 37**).
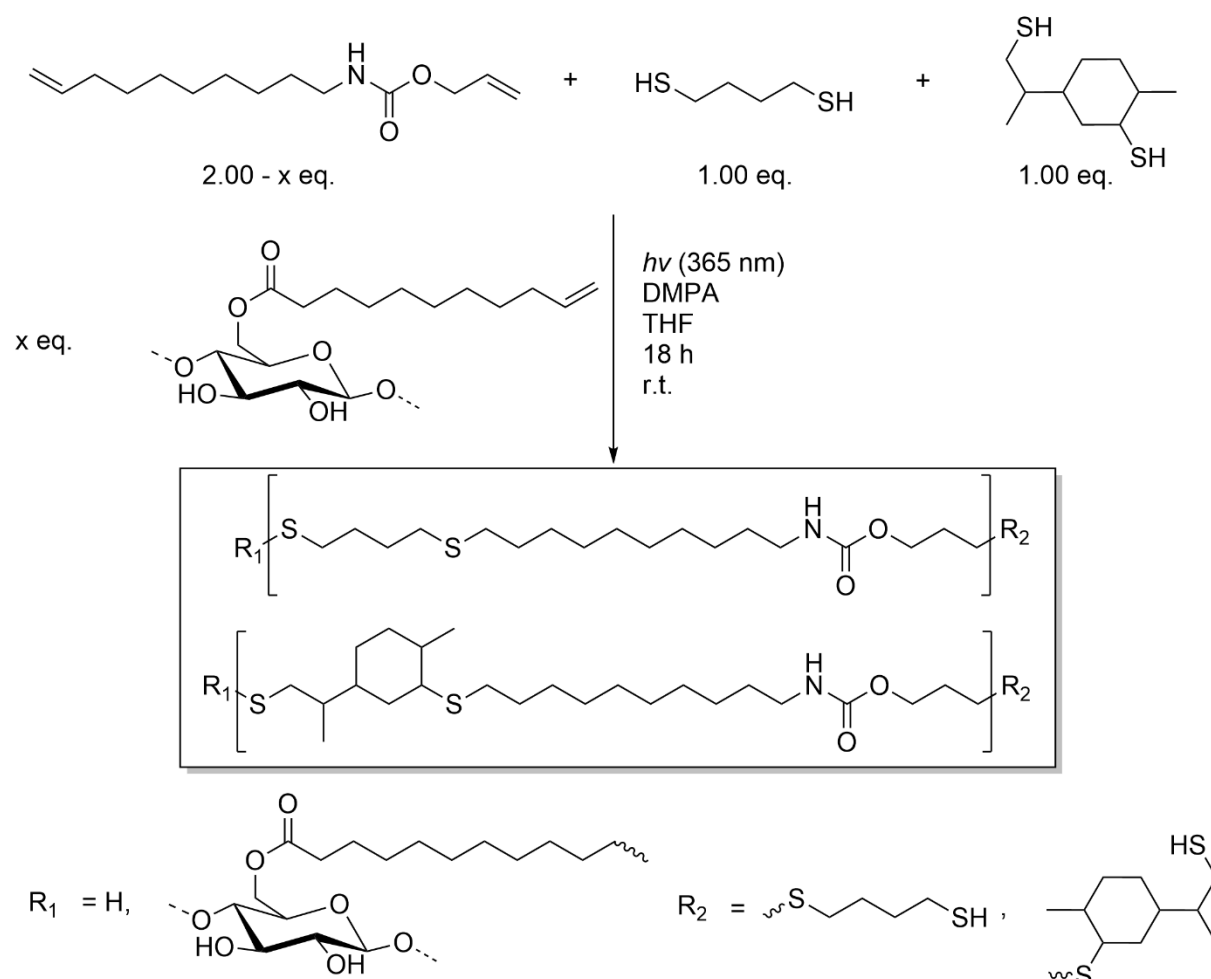
Scheme 37 Synthetic pathway for the synthesis of the random NIPU copolymer **P43** with different amounts of modified CNCs as covalently bonded additives.

Afterwards, the reaction mixture was allowed to react overnight to ensure high conversions. CNC concentrations of 1.5, 3 and 5 wt% were chosen with the goal to evaluate the mechanical properties of the composites. As the CNCs are not soluble in any solvent but are instead dispersed, solvent-based analytical methods like NMR spectroscopy and SEC were not

performed since it does not offer any insights on the conversion of the modified CNCs. IR spectroscopy and DSC analysis of the composites did not show any difference compared to the pure **P43** copolymer, supposedly because of the low CNC concentration (max. 5 wt%).

After workup and subsequent drying, the materials were hot pressed at 85 °C and subjected to tensile testing under the same conditions as the respective NIPU counterpart (random copolymer **P43**) (**Figure 57**).

It is worth mentioning that the opaque rectangular shapes containing CNCs were qualitatively more rigid than the counterpart without additives but also less flexible.
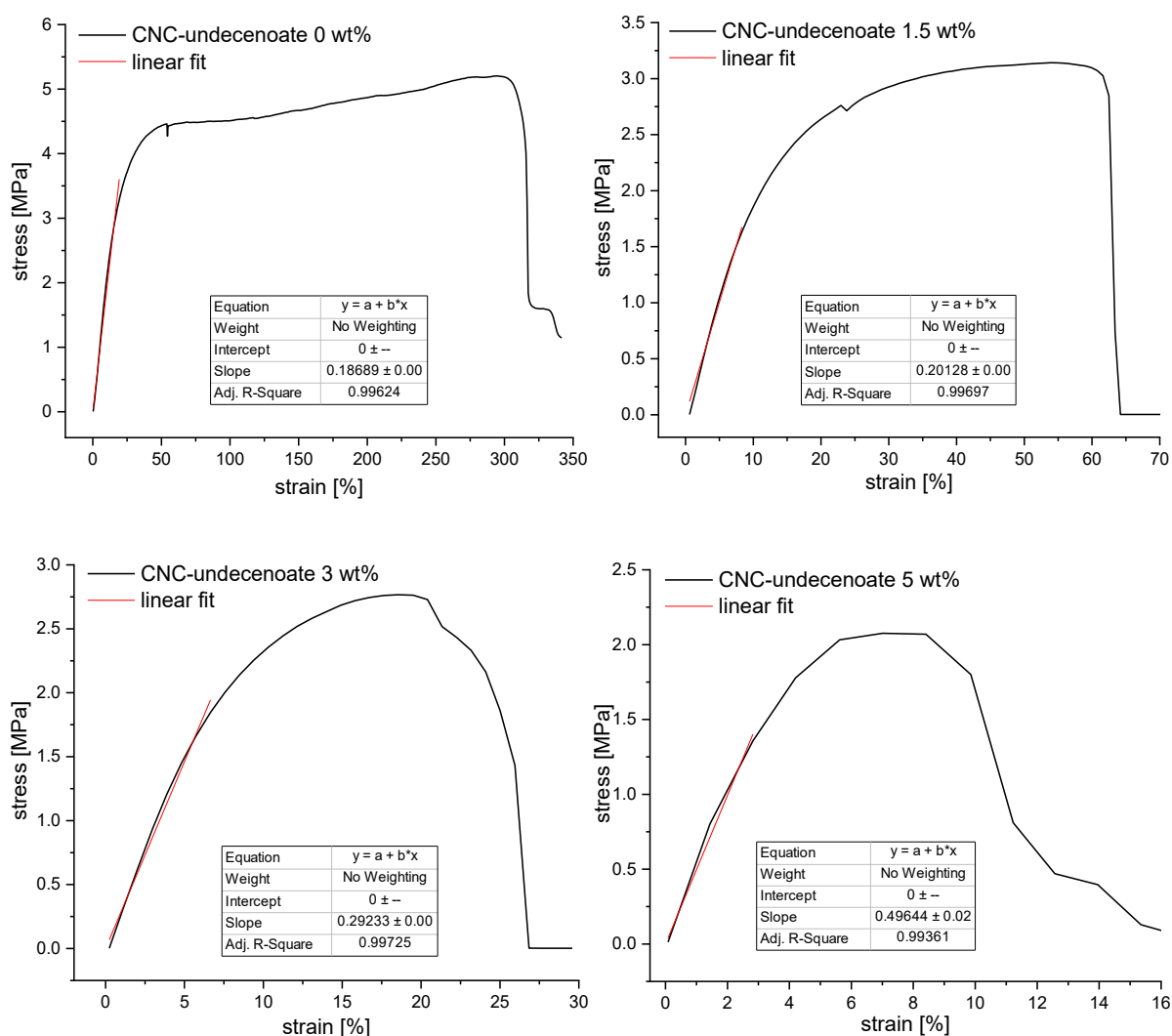
Figure 57 Stress strain diagrams for 0, 1.5, 3, and 5 wt% CNC-undecenoate in copolymer **P43**.
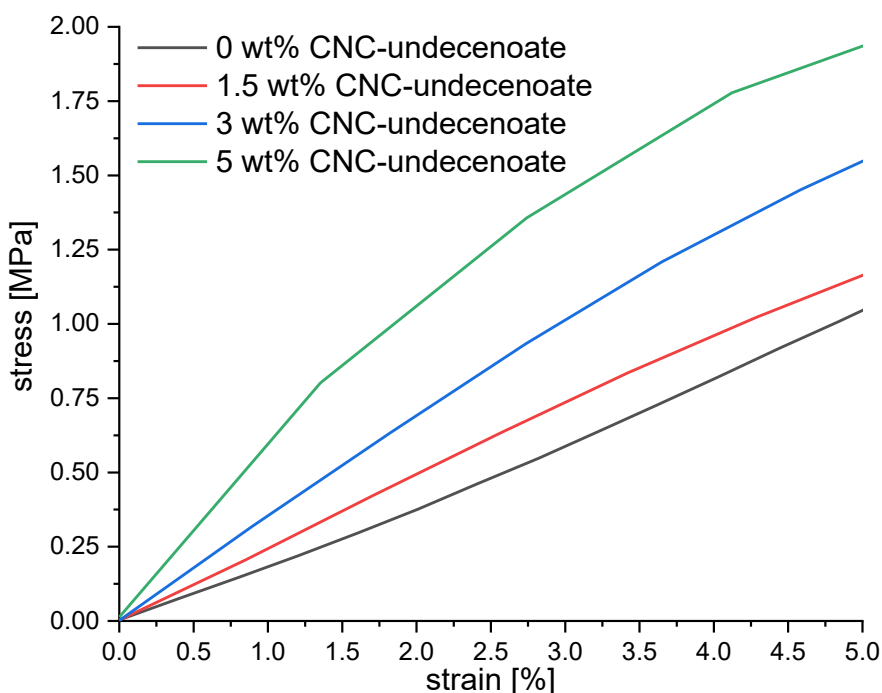
Figure 58 Comparison of the initial region for all tested CNC-undecenoate-containing **P43** composites.

Results showed a shortening of the elongation at break, decreasing from around 300% to just 8% (**Figure 57**). Simultaneously, the E modulus calculated form the slope of the initial region of the plot increased (**Table 29**, **Figure 58**). This behavior was anticipated on the basis of previously published works on the CNC-induced strengthening of materials.[393]

Table 29 E modulus and max. elongation at break of **P43** composites with different concentrations of modified CNCs.

CNCs [wt%]	E modulus [MPa]	Elongation at break [%]
-	20	300
1.50	23	65
3.00	33	27
5.00	50	8

Conclusively, 10-undecenoic acid–modified CNCs with a DS of 0.12 were prepared and used as covalent additives in the limonene-based random copolymer **P43**. Results showed that by increasing the concentration from 1.5 to 5 wt% of CNC-undecenoate led to a decrease of the maximal elongation, while simultaneously increasing the E modulus of the copolymer. Therefore, this approach represents a good method for the strengthening of rubber-like materials in a straightforward way with renewable additives derived from cellulose.

4.2.17 Conclusions and outlook

The first sections of this chapter described the sustainable synthesis of carbamate dienes *via* the one-pot TBD-catalyzed Lossen rearrangement of fatty hydroxamic acids, like 10-undecenoic and oleic acid, in the presence of diallyl carbonate and allyl alcohol. The advantage of this method lies not only in the efficiency of the procedure, but also in the simple isolation of the respective useful diene byproducts, the symmetric ureas. In order to produce fully renewable polyurethanes *via* thiol-ene polymerization, dithiols from renewable materials, like limonene and 1,4-cyclohexadiene, were synthesized in a two-step pathway and isolated in high yields (70-95%).

Afterwards, an optimization of the reaction conditions was performed for the system composed of carbamate **4** and 1,4-butanedithiol in order to achieve high molecular weights. It was found that the maximum molecular weight was obtained in a 5 mol/L system in THF at room temperature under UV irradiation (365 nm). The same parameters were used for the photopolymerization of carbamate dienes with both renewable and commercially available dithiols. The obtained NIPUs were analyzed by HFIP-SEC and DSC. The linear dithiols led to NIPUs with melting points ranging from 60 °C to 100 °C, while more bulky monomers like limonene dithiol **11** formed transparent viscous NIPUs with glass transition temperatures below -10 °C. Further thermal property tuning was achieved by employing dithiols with additional functionalities, like ethers, alcohols and esters. For instance, NIPUs including esters in the backbone exhibited T_gs around -50 °C, while the polar alcohols raised the melting temperature of the macromolecule by *ca*. 30 °C *via* increased hydrogen bonding.

Another approach was presented by preparing and polymerizing more polar non-fatty acid–based carbamate dienes, like the bis-allylcarbamate **6** and allylcarbamate **3** with the already discussed dithiol monomers, confirming the efficient property variation by exchanging the diene component. The thermal data was compared, resulting T_gs and T_ms were higher by a range of 40 °C to 70 °C when **6** was employed, due to increased hydrogen bonding interactions derived from the second carbamate unit. NIPUs consisting of **3** showed higher transitions (T_g and T_m) than polymers derived from **4**, caused by the higher polarity of the shorter carbamate **3**. Polarity also led to overall lower molecular weights since the more polar NIPUs precipitated early from the reaction solvent, THF.

The aforementioned urea side product **9**, which also possesses terminal alkene groups on each side of the moiety, was also polymerized in a similar fashion. The more polar urea led to polyureas with M_n values up to 10 kg/mol, whose detected melting temperatures were in the region between 115 °C and 150 °C, depending on the employed linear dithiol. The use of sterically hindered terpene dithiols or more sterically demanding alkyl chains led to T_ms below 100 °C.

In order to showcase the straightforward nature of the experimental setup, mixtures of monomers were prepared and led to copolymers. Therefore, diene-based copolymers were prepared by mixing two dienes in the same pot, combining the properties of both components into one macromolecule. The same approach was also applied for dithiol-based NIPU copolymers, where polymers exhibiting both glass and melting transitions were obtained. This combination was exploited to create copolymer NIPUs exhibiting a range of physical properties between the powdery polymers **P1**-**6** and the viscous NIPUs obtained from bulky dithiols (**P7**-**9**) or ether dithiols (**P17**, **P18**), leading to flexible polymeric materials. The six copolymers **P43**-**45** and **P48**-**50** were successfully hot-pressed and the E-moduli were calculated after tensile testing. Especially **P43**, composed of carbamate **4**, and an equimolar ratio of 1,4-butane- and limonene dithiol **11**, demonstrated interesting elastic properties with great potential for applications requiring elastic rubber-like materials. Undecenoate-modified CNCs were introduced in four different concentrations as covalent additives in the same random copolymer, increasing the E-modulus of **P43**, while simultaneously reducing the maximal elongation.

During the thermal analysis of the random copolymers consisting of two different thiol monomers, it was observed that transitions derived from one dithiol monomer were dominant, thus hindering the detection of T_gs or T_ms of the second dithiol. For instance, **P43**, which consists of repeating units of **P3** and **P7**, exhibited only the T_g typical of **P7** during DSC analysis. In order to determine the influence of both dithiol species in the copolymers, a straightforward approach was tested by synthesizing block copolymers. Three different block copolymers (**BP43**-**45**) were produced by thiol-ene "click" reaction of two polymers, which were previously end group-functionalized with either thiol or alkene groups. The synthetic efficiency of this method was confirmed by SEC and DOSY-NMR, while and the thermal transitions of all prepared block copolymers **BP43**-**45** were analyzed *via* DSC. The DSC traces

proved the presence of all expected transitions derived from the respective integrated blocks, more specifically the thermal properties of **P3** ($T_m = 73.3\,°C$) and **P7** ($T_g = -22.9\,°C$) in **BP43** ($T_g = -28.1\,°C$, $T_m = 57.7\,°C$), of **P3** and **P9** ($T_g = -28.8\,°C$) in **BP44** ($T_g = -32.6\,°C$, $T_m = 80.5\,°C$). and of **P3** and **P18** ($T_g = -25.7\,°C$, $T_m = 22.0$, $49.5°C$) for **BP45** ($T_g = -36.1\,°C$, $T_m = 25.8$, 52.2, $64.5\,°C$).

Lastly, the post-polymerization modification of NIPUs and polyureas was achieved *via* the facile oxidation with H_2O_2 in THF. The transition from polysulfides to polysulfones was verified by IR and ^{1}H NMR spectroscopy and the increase of all thermal transitions caused by additional dipole-dipole interactions was confirmed *via* DSC analysis.

Subsequent research on thiol-ene derived NIPUs, as well as on NIPU random and block copolymers, can be performed in a wide range of parameters based on the employed monomers and their ratios to get the desired composition between hard and soft segments. For instance, the use of more sterically demanding dithiols is promising for the preparation of the soft segments of the NIPU, while more polar dithiols and dienes are optimal for the specific design of hard segments. In addition, after the optimization of the NIPU compositions for suitable polymer properties, the thermomechanical analysis of the resulting materials by rheology and DMA is considered important. By analyzing the influence of frequency and temperature on the mechanical properties of the synthesized NIPUs, a comparison between these prepared materials and other known commodity polymers will be made in order to introduce fully renewable sourced NIPUs with widely tunable properties in the market, while simultaneously providing a replacement to toxic alternatives.

While the efficiency of additives was confirmed by introducing CNCs in the polymer, many other additive classes exist and are expected to tune the NIPU properties even further, such as plasticizers or fillers. For instance, the use of plasticizers was not explored in this work. However, plasticized NIPUs, especially polymers with hard segment dominance, are expected to exhibit interesting mechanical and thermal properties.

To conclude, the thiol-ene polymerization of sustainable carbamate and urea dienes in combination with dithiols derived from either renewable feedstock or from commercially available sources was confirmed to constitute a stable and flexible polymerization method for the formation of NIPUs and polyureas. The advantages of the proposed procedure include the main benefits of the "click" properties of the thiol-ene reaction as well as the facile adjustment

of properties by synthesizing random and block copolymers and the possibility for "green" post-polymerization modifications in order to further tune the polymer properties.

Results and discussion

5   Experimental section

5.1 Experimental section – CO$_2$-catalyzed Lossen rearrangement

5.1.1 Materials

Succinic acid (99%, Acros Organics), Stearic acid (95%, Sigma-Aldrich), Oleic acid (90%, Sigma-Aldrich), 10-undecenoic acid (98%, Sigma-Aldrich), adamantane carboxylic acid (98%, Acros Organics), methyl caprate (98%, Acros Organics), methyl isobutyrate (99%, Sigma-Aldrich), methyl erucate (90%, CRODA), methyl benzoate (99%, Sigma-Aldrich), dimethyl sebacate (99%, Sigma-Aldrich), dimethyl adipate (99%, Sigma-Aldrich), dimethyl tetradecanedioate (98%, TCI), methyl-*p*-anisate (99%, Sigma-Aldrich), methyl-4-chlorobenzoate (99%, Sigma-Aldrich), methyl-*p*-toluate (99%, Sigma-Aldrich), methyl-3,4,5-trimethoxybenzoate (98%, Sigma-Aldrich), methyl salicylate (99%, Sigma-Aldrich), methyl-4-nitrobenzoate (99%, Sigma-Aldrich), dimethyl malonate (98%, Sigma-Aldrich), methyl linolenate (70-80%, Sigma-Aldrich), acetic acid (glacial 96%, ROTH), potassium hydroxide (Bernd Kraft GmbH), TBD (98%, TCI), DABCO (99%, Sigma-Aldrich), DBN (98%, abcr), DBU (98%, TCI), K$_2$CO$_3$ (99%, Sigma-Aldrich), hydroxylamine hydrochloride (97%, ACROS Organics), hydroxylamine solution (50 wt% in H$_2$O, abcr), DMSO (Acros Organics, anhydrous; Fisher Scientific, 99.9%), cyclohexane and ethyl acetate were used in above technical grade.

5.1.2 Analytical methods

Thin layer chromatography (TLC)-identifications of reactants and products were performed on silica gel coated aluminum foil (silica gel 60, F254 with fluorescence indicator) from Aldrich. Compounds were visualized by Seebach reagent (mixture of phosphomolybdic acid, cerium(IV)-sulfate, water and sulfuric acid) or potassium permanganate staining solution (mixture of potassium permanganate, potassium carbonate, sodium hydroxide and water).

High Resolution Electron ionization (HR-EI) and **fast atom-bombardment (FAB)** mass spectra were recorded on a Finnigan MAT 95 instrument.

Electrospray-Ionisation Mass Spectrometry (ESI-MS) mass spectra were recorded on a Q Exactive (Orbitrap) mass spectrometer (Thermo Fisher Scientific, San Jose, CA, USA) equipped

with an atmospheric pressure ionisation source operating in the nebuliser assisted electrospray mode. The protonated molecular ion is expressed by the term: $[M + H]^+$.

^{1}H and ^{13}C NMR spectra were recorded on BRUKER Avance DPX spectrometer with a 5-mm dual proton/carbon probe (400 MHz). All spectra were measured at ambient temperature. The chemical shift for ^{1}H NMR spectra was reported in parts per million (ppm) and referenced to characteristic solvent signals of partly deuterated solvents e.g. $CDCl_3$ at 7.26 ppm. ^{13}C NMR spectra were reported in ppm relative to characteristic signals of partly deuterated solvents, e.g. the centroid peak of the $CDCl_3$ triplet at 77.2 ppm. The spin multiplicity and corresponding signal patterns were abbreviated as follows: s = singlet, d = doublet, t = triplet, q = quartet, quint. = p, sext. = h, m = multiplet and br = broad signal. Coupling constants J were noted in Hz.

Gas chromatography (GC) was performed on a Bruker 430 GC instrument equipped with capillary column FactorFourTM VF-5 ms (30.0 m × 0.25 mm × 0.25 μm), using flame ionization detection (FID). The oven temperature program was: initial temperature 95 °C, hold for 1 min, ramp at 15 °C min^{-1} to 220 °C, hold for 4 min, ramp at 15 °C min^{-1} to 300 °C, hold for 2 min, ramp at 15 °C min^{-1} to 325 °C, hold for 3 min. Measurements were performed in split-split mode using nitrogen as the carrier gas (flow rate 30 mL min^{-1}).

Gas Chromatography – Mass Spectrometry (GC-MS) electron impact (EI) measurements were performed on the following system: a Varian 431 GC instrument with a capillary column FactorFour VF-5 ms (30 m × 0.25 mm × 0.25 mm) and a Varian 210 ion trap mass detector. Scans were performed from 40 to 650 m/z at rate of 1.0 scans s^{-1}. The oven temperature program was: initial temperature 95 °C, hold for 1 min, ramp at 15 °C min^{-1} to 220 °C, hold for 4 min, ramp at 15 °C min^{-1} to 300 °C, hold for 2 min. The injector transfer line temperature was set to 250 °C. Measurements were performed in the split – split mode (split ratio 50:1) using helium as carrier gas (flow rate 1.0 mL min^{-1}).

Online infrared (IR) spectroscopy screening was performed with a React IR 702 detector (MettlerToledo) and a DST 6.35 x 1.5 m DiComp probe coupled to a Parr 130 mL pressure vessel. The spectra were recorded at a rate of 2 spectra min^{-1} in a range of 650-3000 cm^{-1}. The temperature was set *via* a Parr temperature controller of the type LTR 2500.

5.1.3 General procedure for the synthesis of methyl esters

The carboxylic acid (1.00 eq.) was dissolved in methanol (10.0 − 20.0 eq.), following the addition of catalytic amounts of sulfuric acid (0.10 eq.). Afterwards the reaction mixture was heated to reflux for at least six hours. The solution was allowed to cool down to room temperature and $NaHCO_3$ was added until the solution reached pH 7. The formed salt was filtered off and the solution was evaporated under reduced pressure. The residue was dissolved in ethyl acetate and washed thrice with saturated $NaHCO_3$ solution. The organic phase was subsequently washed with water and brine and dried over Na_2SO_4. The crude product was further purified by flash column chromatography (cyclohexane/EA 4:1) over basic aluminium oxide.

Experimental section

Methyl-10-undecenoate
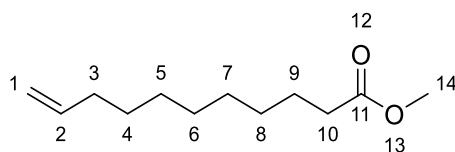
The esterification of 10-undecenoic acid (1.00 eq.) with excess methanol catalyzed by H_2SO_4 (0.10 eq.) led to the formation of methyl-10-undecenoate as light-yellow liquid (88%).

^{1}H NMR (CDCl$_3$, 400 MHz) δ= 1.22 – 1.40 (m, 10 H, 5 CH$_2^{4-8}$), 1.60 (p., J = 7.2 Hz, 2 H, CH$_2^9$), 2.02 (q, J = 6.2 Hz, 2 H, CH$_2^3$), 2.28 (t, J = 7.4 Hz, 2 H, CH$_2^{10}$), 3.65 (s, 3 H, CH$_3^{14}$),4.87 – 5.02 (m, 2 H, CH$_2^1$), 5.79 (tdd, J = 17.0 Hz, 10.4 Hz, 6.6 Hz, 1 H, CH^2) ppm.

^{13}C NMR (CDCl3, 100 MHz) δ = 24.9 (CH$_2^9$), 28.8 (CH$_2^4$), 29.0 (CH$_2^{5-8}$), 29.1 (CH$_2^{5-8}$), 29.1 (CH$_2^{5-8}$), 29.2 (CH$_2^{5-8}$), 33.7 (CH$_2^{10}$), 34.0 (CH$_2^3$), 51.4 (CH$_3^{14}$),114.1 (CH$_2^1$), 139.1 (CH^2), 174.2 (CO^{11}) ppm.

HRMS-EI-MS of C$_{12}$H$_{22}$O$_2$ [M+H]$^+$ calculated: 198.1614, found 198.1617.
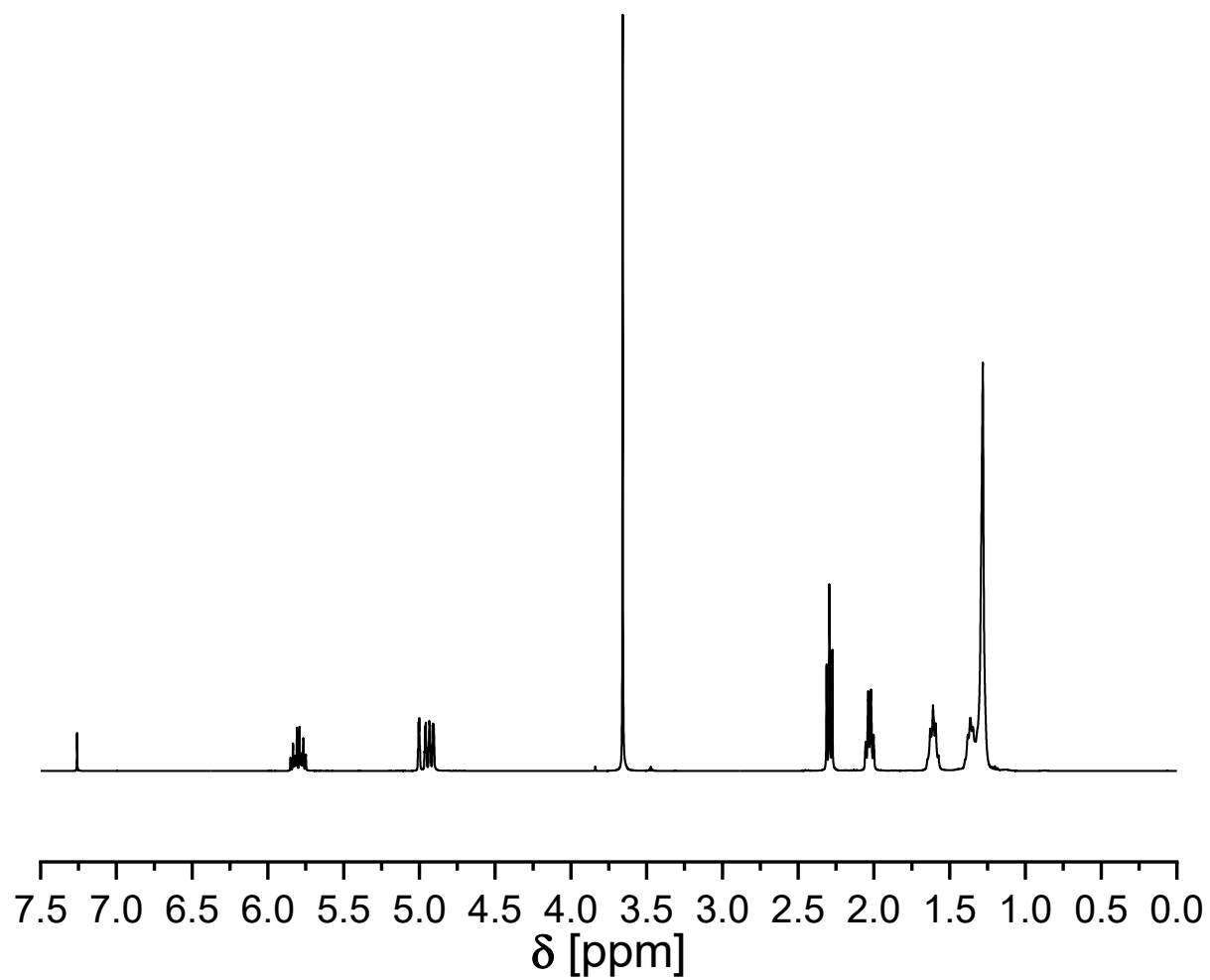
Figure 59 ^{1}H NMR spectrum of methyl-10-undecenoate (CDCl$_3$, 400 MHz).

Methyl stearate

The esterification of stearic acid (1.00 eq.) with excess methanol catalyzed by H_2SO_4 (0.10 eq.) led to the formation of methyl stearate as white solid (94%).

^{1}H NMR (CDCl$_3$, 400 MHz) δ= 0.80 (t, *J* = 7.1 Hz, 3H, CH$_3{}^1$), 1.14 – 1.26 (m, 28H, CH$_2{}^{2-15}$), 1.55 (p., *J* = 7.4, 7.0 Hz, 2H, CH$_2{}^{16)}$, 2.23 (t, *J* = 7.5 Hz, 2H, CH$_2{}^{17}$), 3.60 (s, 3H, CH$_3{}^{21}$) ppm.

^{13}C NMR (CDCl$_3$, 100 MHz) δ= 14.1 (CH$_3{}^1$), 22.7 (CH$_2{}^2$), 24.9 (CH$_2{}^{16}$), 27.1 (CH^{8,11}), 27.2 (CH^{8,11}), 29.2 (CH$_2{}^{4-15}$), 29.3 (CH$_2{}^{4-15}$), 29.4 (CH$_2{}^{4-15}$), 29.5 (CH$_2{}^{4-15}$),29.6 (CH$_2{}^{4-15}$), 29.7 (CH$_2{}^{4-15}$), 29.7 (CH$_2{}^{4-15}$), 29.7 (CH$_2{}^{4-15}$), 31.9 (CH$_2{}^3$), 34.1 (CH$_2{}^{17}$), 51.4 (CH$_3{}^{21}$), 174.3 (CO^{18}) ppm.

HRMS-EI-MS of C$_{19}$H$_{38}$O$_2$ [M+H]$^+$ calculated: 298.2866, found 298.2868.
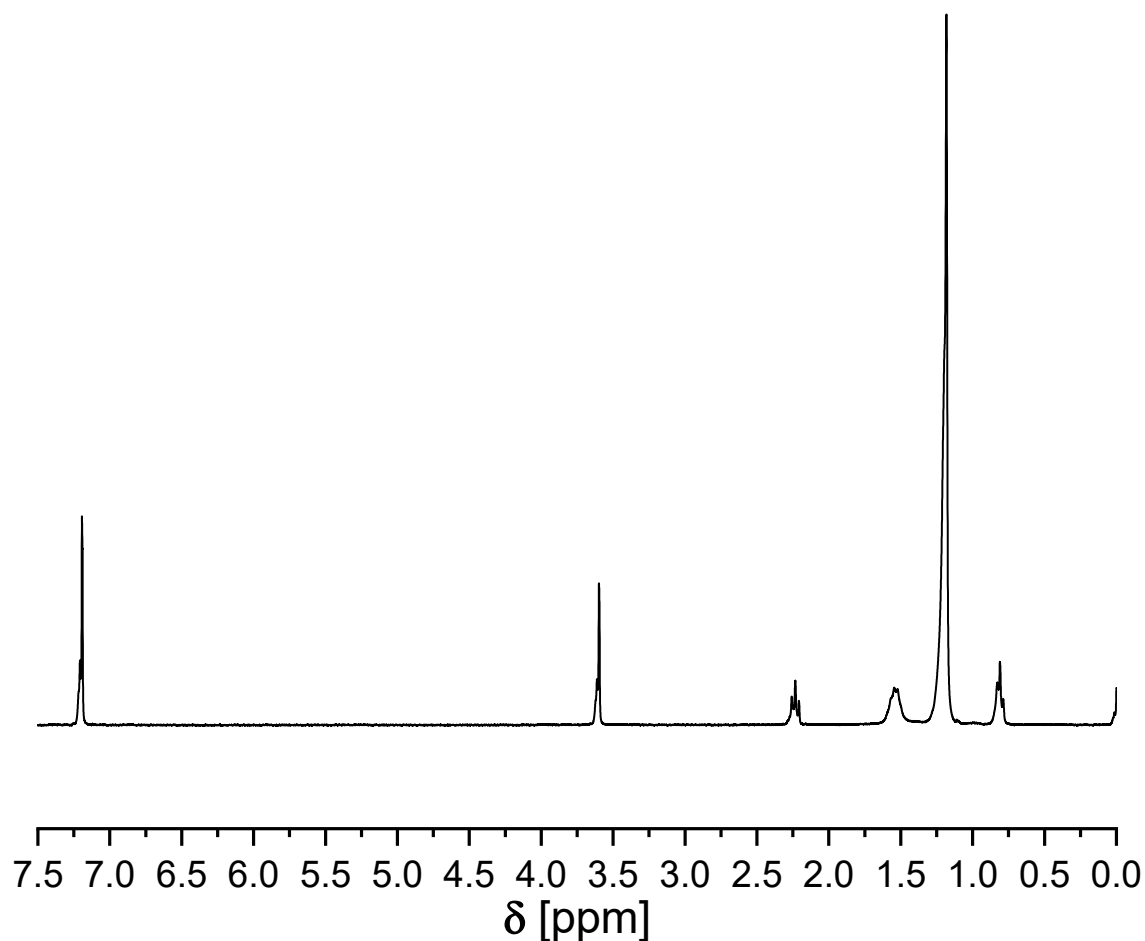
Figure 60 ^{1}H NMR spectrum of methyl stearate (CDCl$_3$, 400 MHz).

Methyl-adamantane-1-carboxylate
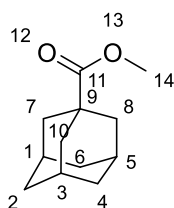
The esterification of adamantane-1-carboxylic acid (1.00 eq.) with excess methanol catalyzed by H_2SO_4 (0.10 eq.) led to the formation of methyl-adamantane-1-carboxylate as colorless solid (78%).

^{1}H NMR (CDCl$_3$, 300 MHz) δ= 1.69 (t, J = 15.2 Hz, 6H, CH$_2$^{2,4,6}), 1.86, (d, J = 3.0 Hz, 6H, CH$_2$^{7,8,10}), 1.99 (p., J = 3.3 Hz, 3.1 Hz, 3H, CH^{1,3,5}), 3.62 (s, 3H, CH$_3$^{14}) ppm.

^{13}C NMR (CDCl$_3$, 75 MHz) δ= 27.9 (CH^{1,3,5}), 36.5 (CH$_2$^{2,4,6}), 38.9 (CH$_2$^{7,8,10}), 40.7 (C^9), 51.5 (CH$_3$^{14}), 178.2 (CO^{18}) ppm.

HRMS-EI-MS of C$_{12}$H$_{18}$O$_2$ [M]$^+$ calculated: 194.1301, found 194.1300.
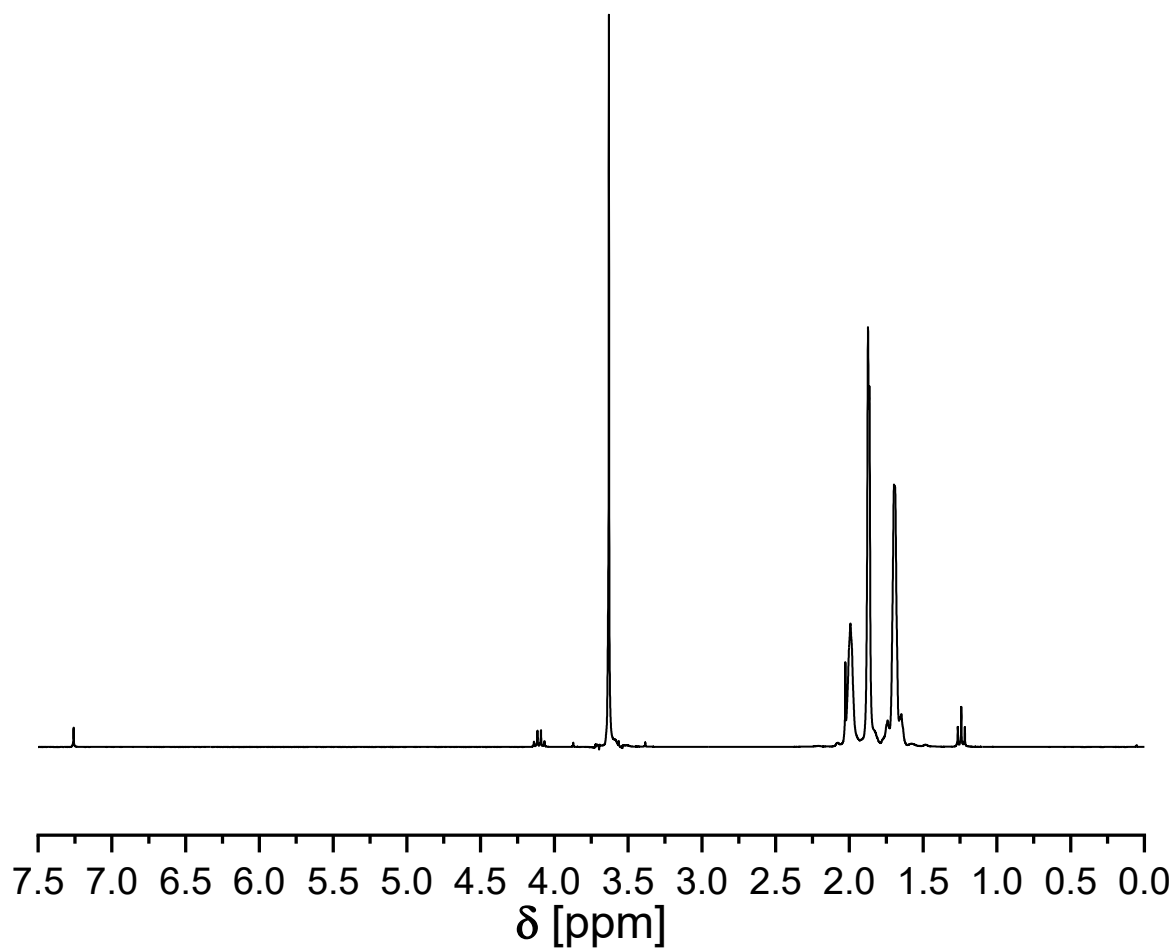
Figure 61 ^{1}H NMR spectrum of methyl-adamantane-1-carboxylate (CDCl$_3$, 400 MHz).

Methyl oleate
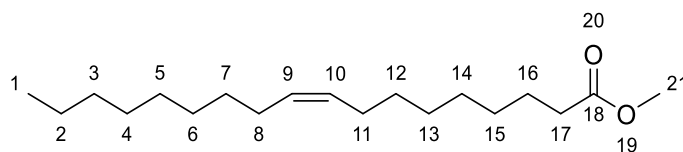
The esterification of oleic acid with excess methanol catalyzed by H_2SO_4 (0.10 eq) led to the formation of methyl oleate as colorless liquid (92%).

^{1}H NMR (CDCl$_3$, 300 MHz) δ= 0.87 (t, *J* = 6.2 Hz, 3H, CH$_3^1$), 1.26, (m, 20H, CH$_2^{2-7,12-15}$), 1.59 (p., *J* = 7.2 Hz, 2H, CH$_2^{16}$), 1.97 (m, 4H, CH$_2^{8,11}$), 2.27 (t, *J* = 7.6 Hz, 2H, CH$_2^{17}$), 3.63 (s, 3H, CH$_3^{21}$), 5.31 (m, 2H, CH^{9,10}) ppm.

^{13}C NMR (CDCl$_3$, 75 MHz) δ= 14.1 (CH$_3^1$), 22.7 (CH$_2^2$), 24.9 (CH$_2^{16}$), 27.1 (CH^{8,11}), 27.2 (CH^{8,11}), 29.1-29.7 (CH$_2^{4-7,12-15}$), 31.9 (CH$_2^3$), 34.0 (CH$_2^{17}$), 51.5 (CH$_3^{21}$), 129.7 (CH^{9,10}), 129.9 (CH^{9,10}), 174.2 (CO^{18}) ppm.

HRMS-EI-MS of C$_{19}$H$_{36}$O$_2$ [M+H]$^+$ calculated: 296.2710, found 296.2709.
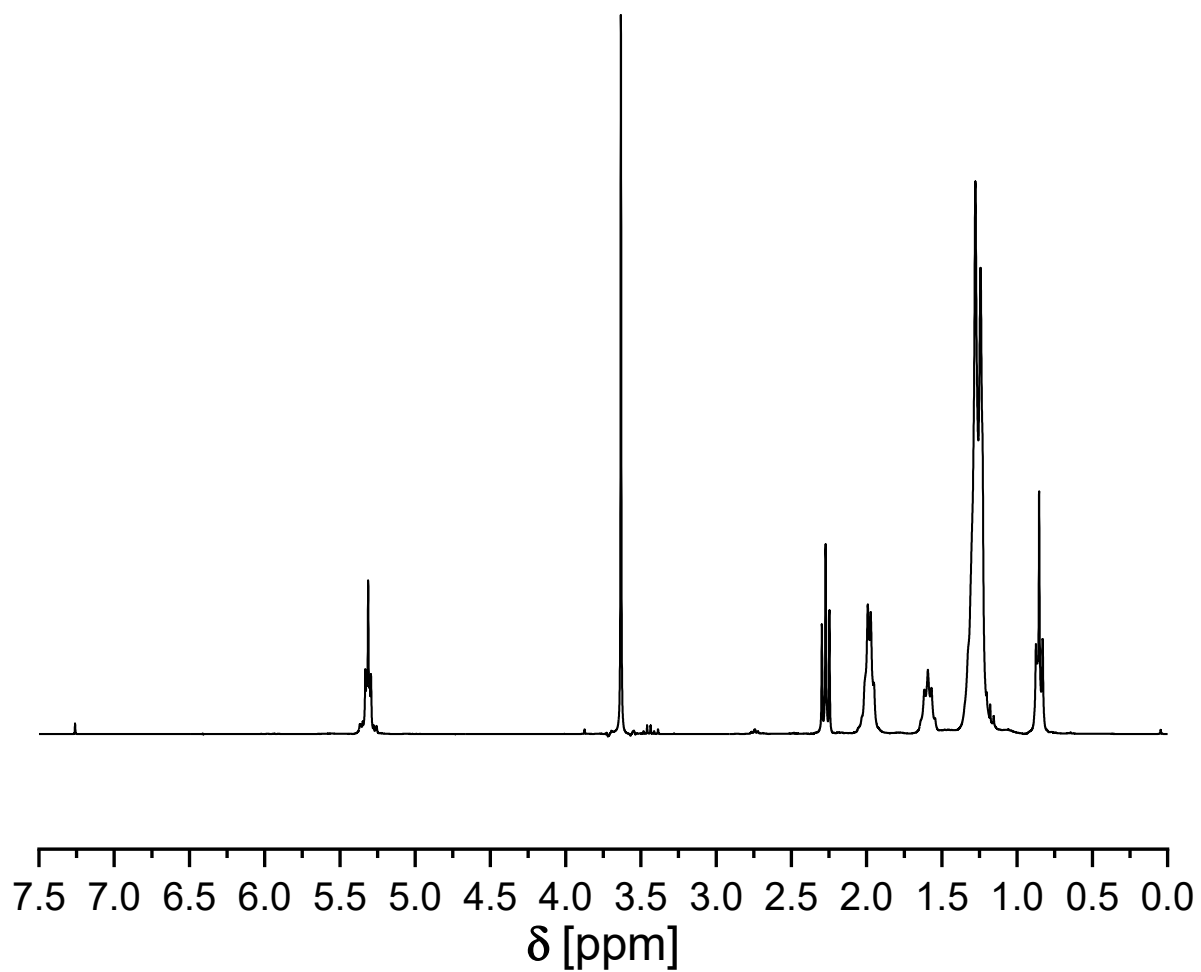
Figure 62 ^{1}H NMR spectrum of methyl oleate (CDCl$_3$, 400 MHz).

Dimethyl succinate
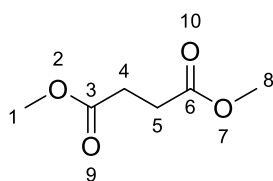
The esterification of succinic acid (1.00 eq.) with excess methanol catalyzed by H_2SO_4 (0.10 eq.) led to the formation of dimethyl succinate as colorless liquid (91%).

¹H NMR (CDCl$_3$, 400 MHz) δ= 2.59 (s, 4H, CH$_2$[4,5]), 3.65 (s, 6H, CH$_3$[1,8]) ppm.

¹³C NMR (CDCl$_3$, 100 MHz) δ= 28.8 (CH$_2$[4,5]), 52.8 (CH$_3$[1,8]), 172.7 (CO[3,6]) ppm.

ESI-MS of C$_6$H$_{11}$O$_4$ [M+H]$^+$ calculated: 147.0652, found 147.0651.
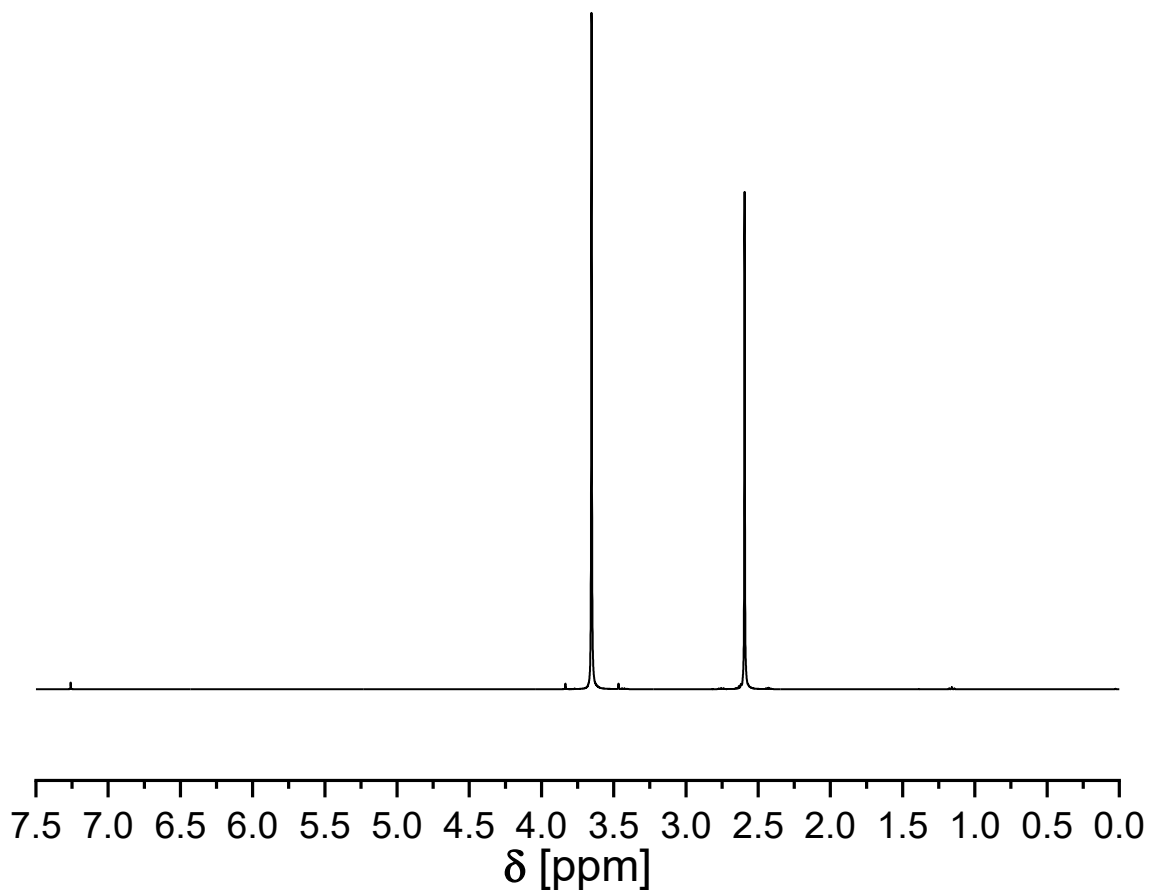
Figure 63 ¹H NMR spectrum of dimethyl succinate (CDCl$_3$, 400 MHz).

5.1.4 General procedure for the synthesis of hydroxamic acids

Most hydroxamic acids were prepared with the procedure from Kreye *et al.*[152]

The methyl esters (1.00 eq.) were suspended with hydroxylamine hydrochloride (3.00 eq.) in methanol. After the addition of potassium hydroxide (6.00 eq.), the reaction mixture was stirred for the selected amount of time under reflux conditions.

After full conversion was determined via GC, the reaction mixture was acidified with 25% acetic acid solution to pH 4. After removing all solvents under reduced pressure, the solid residue was dissolved in an ethyl acetate/water mixture (4:1). The organic layer was separated and dried over Na_2SO_4. The solvent was evaporated and the crude product recrystallized (from ethyl acetate/hexane mixtures).

In case of dimethyl succinate, malonate and adipate, the hydroxamic acid was prepared by mixing the diester in 2.10 eq. hydroxylamine solution (50 wt% in H_2O) and stirring for 48 h at room temperature. The product was then collected by filtration after the addition of an antisolvent (ethanol) or after crystallization at 4 °C.

N-Hydroxyoleamide **1a**
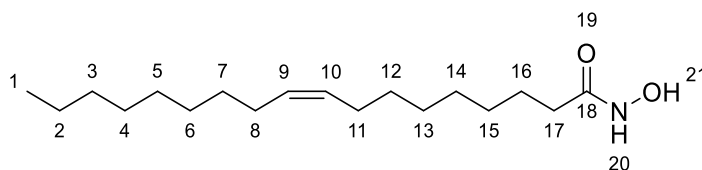
The reaction of methyl oleate (1.00 eq.) with hydroxylamine hydrochloride (3.00 eq.) and potassium hydroxide (6.00 eq.) for 20 h under reflux conditions led to the formation of pure *N*-hydroxyoleamide **1a** (65%) in form of a colorless crystalline solid. The crude product was purified by recrystallization from ethyl acetate/hexane (1:5).

^{1}H NMR (CDCl$_3$, 300 MHz) δ= 0.88 (t, J = 6.9 Hz, 3H, CH$_3^1$), 1.21-1.38 (m, 20H, CH$_2^{2-7,12-15}$), 1.62 (p., J = 7.4 Hz, 7.1 Hz, 2H, CH$_2^{16}$), 2.01 (dt, 8.9 Hz, 6.5 Hz, 6.1 Hz, 4H, CH$_2^{8,11}$), 2.13 (t, J = 7.7 Hz, 2H, CH$_2^{17}$), 5.34 (m, 2H, CH^{9,10}), 9.14 (s, br, 2H, NH^{20}, OH^{21}) ppm.

^{13}C NMR (CDCl$_3$, 75 MHz) δ = 14.1 (CH$_3^1$) ,22.7 (CH$_2^2$), 25.5 (CH$_2^{16}$), 27.2(CH$_2^{8,11}$), 29.1 (CH$_2^{4-7,12-15}$), 29.2 (CH$_2^{4-7,12-15}$), 29.2 (CH$_2^{4-7,12-15}$), 29.3 (CH$_2^{4-7,12-15}$), 29.3 (CH$_2^{4-7,12-15}$), 29.5 (CH$_2^{4-7,12-15}$), 29.7 (CH$_2^{4-7,12-15}$), 29.8 (CH$_2^{4-7,12-15}$), 31.9 (CH$_2^3$), 33.0 (CH$_2^{17}$), 129.7 (CH^{9,10}), 130.0 (CH^{9,10}), 172.1 (CO^{18}) ppm.

HRMS-EI-MS of C$_{18}$H$_{35}$NO$_2$ [M+H]$^+$ calculated: 298.2741, found 298.2741.
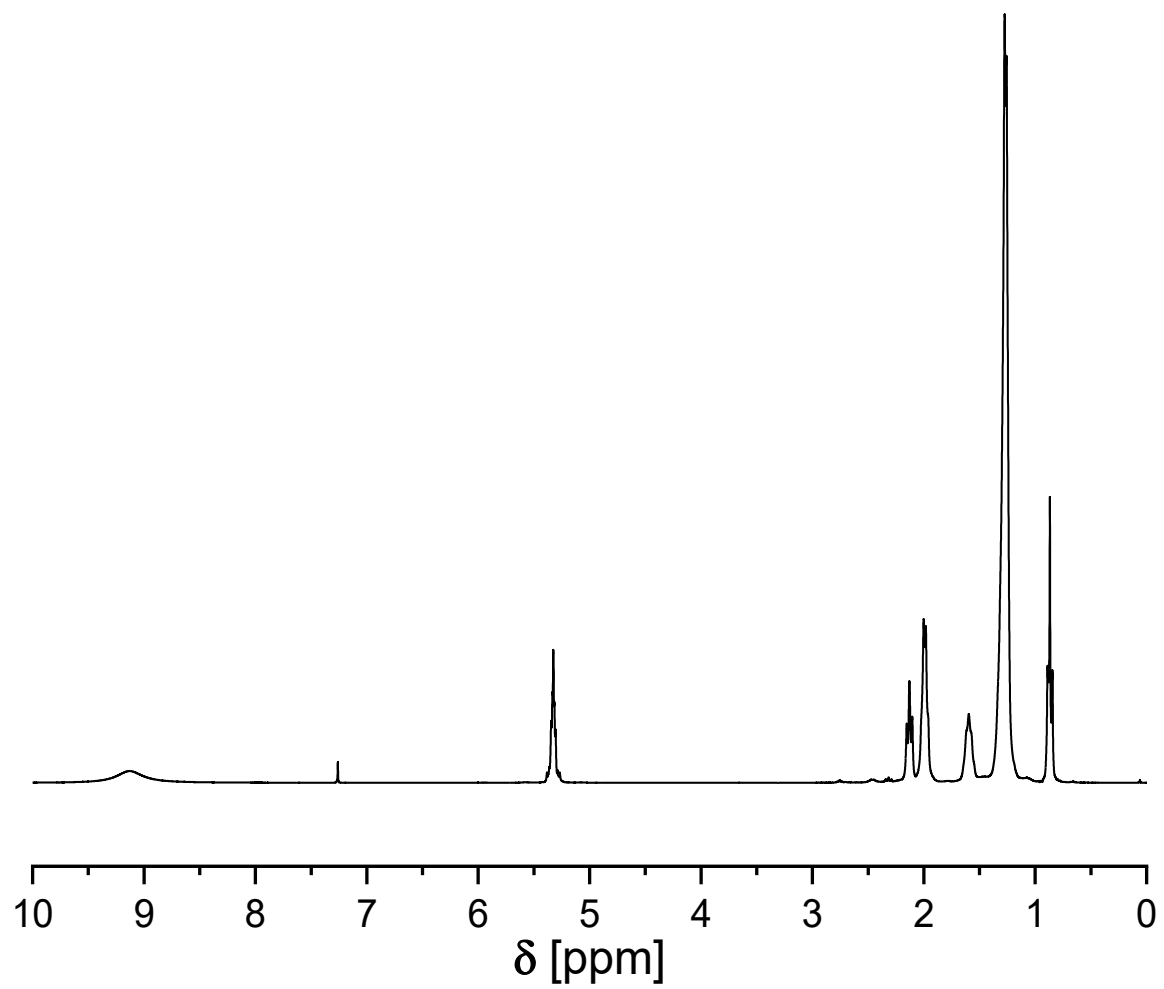
Figure 64 ^{1}H NMR spectrum of **1a** (CDCl$_3$, 400 MHz).

N-Hydroxydecanamide **1b**
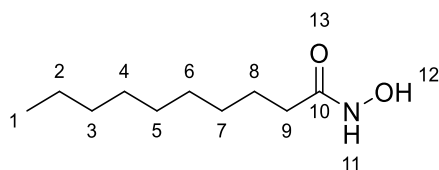
The reaction of methyl decanoate (1.00 eq.) with hydroxylamine hydrochloride (3.00 eq.) and potassium hydroxide (6.00 eq.) for 20 h under reflux conditions led to the formation of pure *N*-hydroxydecaneamide **1b** (72%) in form of a colorless crystalline solid. The crude product was purified by recrystallization from ethylacetate/hexane (1:5).

^{1}H NMR (DMSO-d_6, 300 MHz) δ= 0.84 (t, *J* = 6.9 Hz, 3H, CH_3^1), 1.23 (m, 12H, CH_2^{2-7}), 1.47 (p., *J* = 7.1 Hz, 6.6 Hz, 2H, CH_2^8), 1.92 (t, *J* = 7.6 Hz, 2H, CH_2^9), 8.77 (br, s, 1H, NH^{11}), 10.16 (br, s, 1H, OH^{12}) ppm.

^{13}C NMR (DMSO-d_6, 75 MHz) δ = 14.4 (CH_3^1), 22.6 (CH_2^2), 25.6 (CH_2^8), 29.1 (CH_2^{4-7}), 29.2 (CH_2^{4-7}), 29.2 (CH_2^{4-7}), 29.4 (CH_2^{4-7}), 31.8 (CH_2^3), 32.7 (CH_2^9), 169.5 (CO^{10}) ppm.

HRMS-EI-MS of $C_{10}H_{22}NO_2$ [M]$^+$ calculated: 188.1645, found 188.1643.
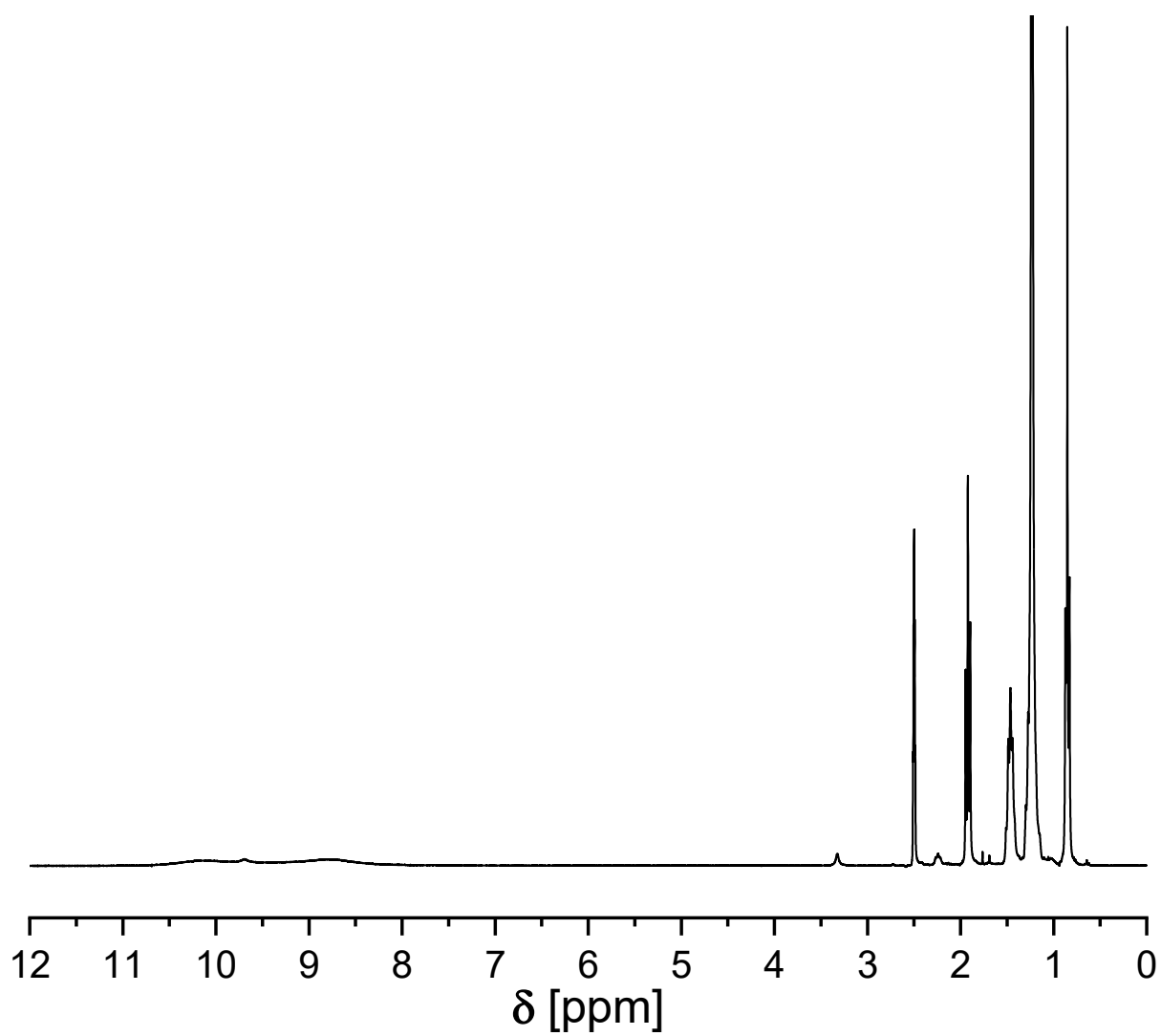
Figure 65 ^{1}H NMR spectrum of **1b** (DMSO-d_6, 300 MHz).

(Z)-N-Hydroxydocos-13-enamide **1c**
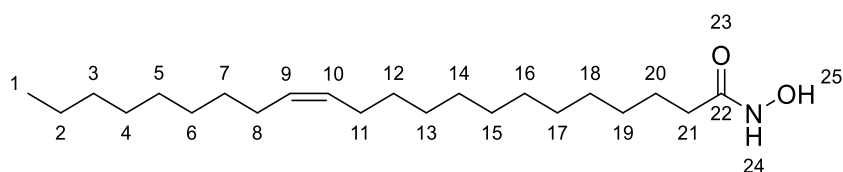
The reaction of methyl erucate (1.00 eq.) with hydroxylamine hydrochloride (3.00 eq.) and potassium hydroxide (6.00 eq.) for 20 h under reflux conditions led to the formation of pure (Z)-*N*-hydroxydocos-13-enamide **1c** (64%) in form of a colorless crystalline solid. The crude product was purified by recrystallization from ethylacetate/hexane (1:5).

^{1}H NMR (DMSO-d_6, 400 MHz) δ= 0.81 (t, J = 7.1 Hz, 3H, CH$_3^1$), 1.20 (m, 28H, CH$_2^{2-7,12-19}$), 1.55 (p, J = 7.2, 6.7 Hz, 2H, CH$_2^{20}$), 1.94 (dt, J = 9.9 Hz, 6.5, 5.6 Hz, 4H, CH$_2^{8,11}$), 2.06 (t, J = 7.7 Hz, 2H, CH$_2^{17}$), 5.26 – 5.30 (m, 2H, CH^{9,10}), 7.81 (br, s, 2H, NH^{24}, OH^{25}) ppm.

^{13}C NMR (DMSO-d$_6$, 100 MHz) δ= 14.1 (CH$_3^1$), 22.7 (CH$_2^2$), 25.4 (CH$_2^{20}$), 27.1 (CH^{8,11}), 27.2 (CH$_2^{8,11}$), 29.2 (CH$_2^{5-7,12-17}$), 29.3 (CH$_2^{5-7,12-17}$), 29.3 (CH$_2^{5-7,12-17}$), 29.5 (CH$_2^{5-7,12-17}$), 29.6 (CH$_2^{5-7,12-17}$), 29.7 (CH$_2^{5-7,12-17}$), 29.7 (CH$_2^{5-7,12-17}$), 29.8 (CH$_2^{5-7,12-17}$), 29.8 (CH$_2^{5-7,12-17}$), 31.9 (CH$_2^3$), 33.1 (CH$_2^{21}$), 129.9 (CH^{9,10}), 129.9 (CH^{9,10}), 171.8 (CO^{22}) ppm.

HRMS-EI-MS of C$_{22}$H$_{44}$NO$_2$ [M]$^+$ calculated: 354.3367, found 354.3367.
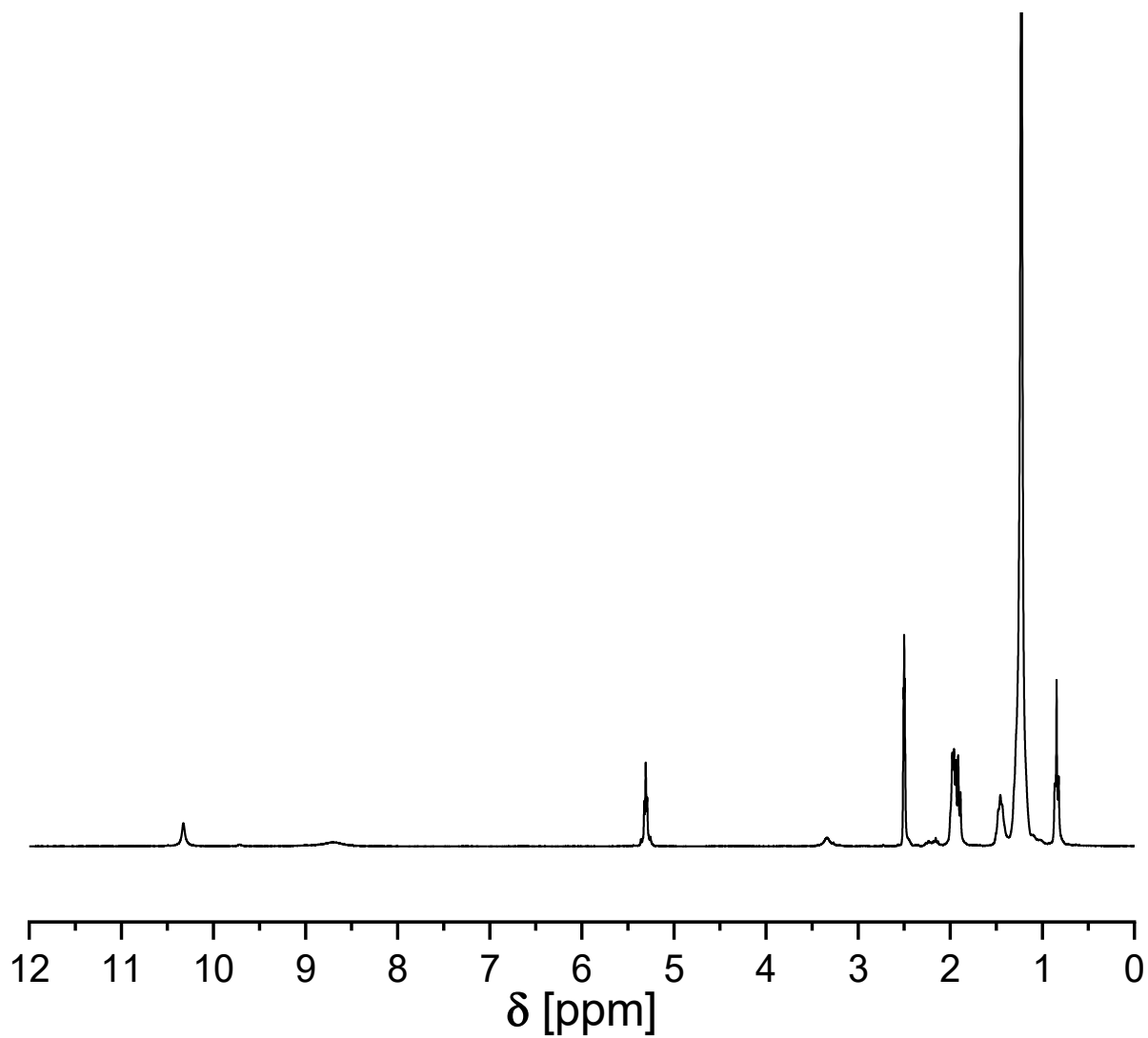
Figure 66 ^{1}H NMR spectrum of **1c** (DMSO-d_6, 400 MHz).

(9Z,12Z,15Z)-N-hydroxyoctadeca-9,12,15-trienamide **1d**
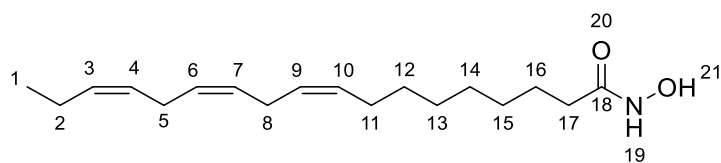
The reaction of methyl linolenate (1.00 eq.) with hydroxylamine hydrochloride (3.00 eq.) and potassium hydroxide (6.00 eq.) for 20 h under reflux conditions led to the formation of pure *(9Z,12Z,15Z)-N*-hydroxyoctadeca-9,12,15-trienamide **1d** (67%) in form of a yellow oil.

^{1}H NMR (CDCl$_3$, 400 MHz) δ= 0.89 (t, *J* = 6.8 Hz, 3H, CH$_3^1$), 0.97 (t, *J* = 7.4 Hz, 3H, CH$_3^1$), 1.31 (s, 8H, CH$_2^{12\text{-}15}$), 1.63 (p, *J* = 7.2 Hz, 2H, CH$_2^{16}$), 2.03 – 2.07 (m, 4H, CH$_2^{2,11}$), 2.34 (t, *J* = 7.5 Hz, 2H, CH$_2^{17}$), 2.78 – 2.82 (m, 4H, CH$_2^{5,8}$), 5.33 – 5.38 (m, 6H, CH^{3,4,6,7,9,10}), 9.01 (s, br, 2H, NH^{19}, OH^{21}) ppm.

^{13}C NMR (CDCl$_3$, 100 MHz) δ= 14.3 (C^1), 20.6 (C^2), 24.7 (C^{16}), 25.6 (C^{5,8}), 25.6 (C^{5,8}), 27.2 (C^{11}), 29.0 (C^{15}), 29.1 (C^{14}), 29.2 (C^{13}), 29.6 (C^{12}), 34.0 (C^{17}), 127.1 (C^9), 127.8 (C^4), 128.3 (C^{6,7}), 128.3 (C^{6,7}), 130.3 (C^{10}), 132.0 (C^3), 171.7 (C^{18}) ppm.

HRMS-EI-MS of C$_{18}$H$_{31}$O$_2$N [M+] calculated: 293.2349, found 293.2350.
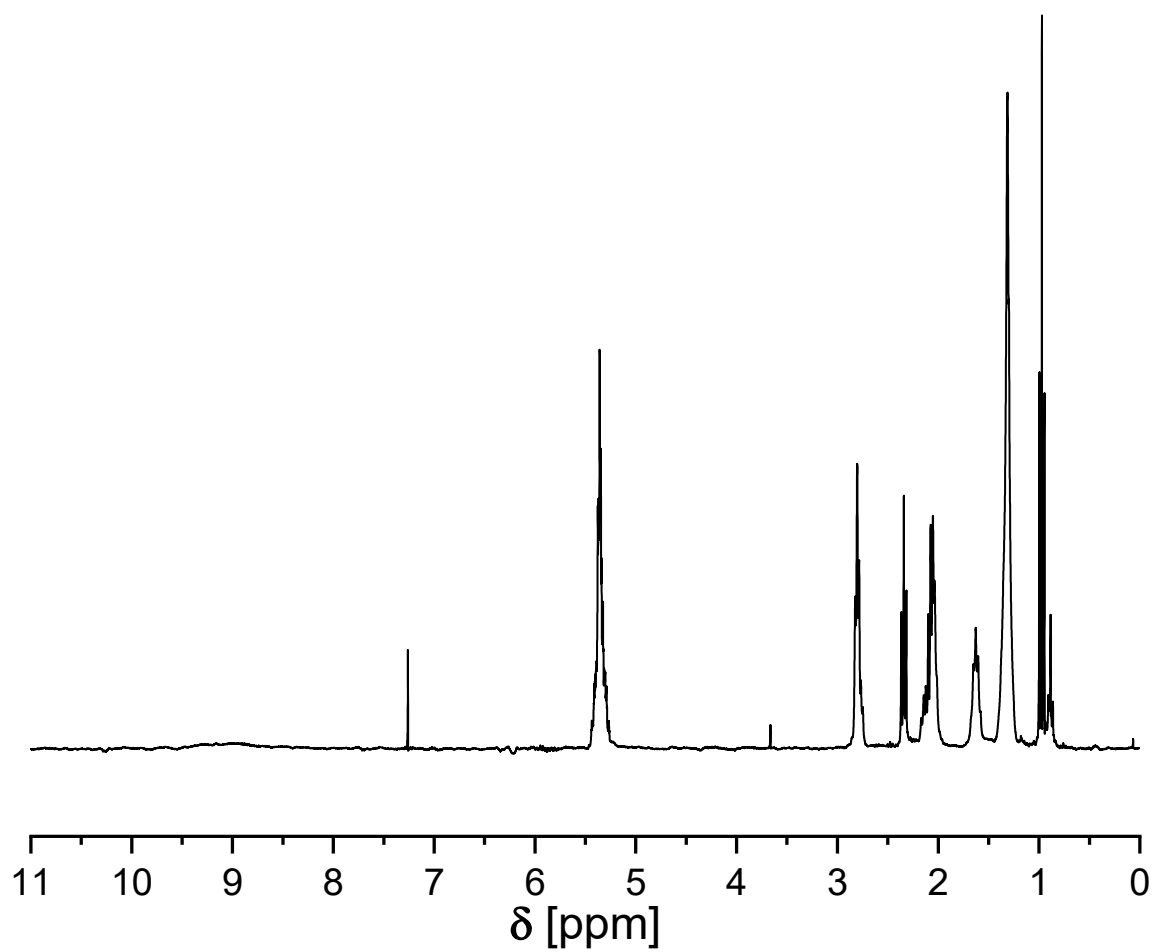
Figure 67 ^{1}H NMR spectrum of **1d** (CDCl$_3$, 400 MHz).

N-Hydroxyundec-10-enamide **1e**
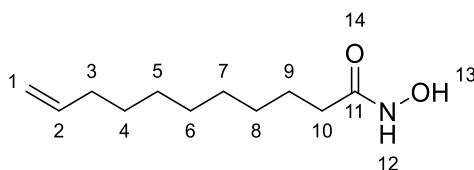
The reaction of methyl-10-undecenoate (1.00 eq.) with hydroxylamine hydrochloride (3.00 eq.) and potassium hydroxide (6.00 eq.) for 20 h under reflux conditions led to the formation of pure *N*-hydroxyundec-10-eneamide **1e** (77%) in form of a colorless crystalline solid. The crude product was purified by recrystallization from ethylacetate/hexane (1:5).

^{1}H NMR (CDCl$_3$, 400 MHz) δ= 1.22 − 1.40 (m, 10 H, 5 CH$_2$$^{4-8}$), 1.60 (p., J = 7.2 Hz, 2 H, CH$_2$^{9}), 2.02 (q, J = 6.2 Hz, 2 H, CH$_2$^{3}), 2.28 (t, J = 7.4 Hz, 2 H, CH$_2$^{10}), 4.87 − 5.02 (m, 2 H, CH$_2$^{1}), 5.79 (tdd, J = 17.0 Hz, 10.4 Hz, 6.6 Hz, 1 H, CH^2), 8.92 (br, s, 2H, NH^{12}, OH^{13}) ppm.

^{13}C NMR (CDCl$_3$, 100 MHz) δ = 25.5 (CH$_2$^{9}), 28.9 (CH$_2$$^{4-8}$), 29.1 (CH$_2$$^{4-8}$), 29.1 (CH$_2$$^{4-8}$), 29.3 (CH$_2$$^{4-8}$), 29.3 (CH$_2$$^{4-8}$), 33.0 (CH$_2$^{10}), 33.8 (CH$_2$^{3}), 51.4 (CH$_3$^{14}),114.2 (CH$_2$^{1}), 139.1 (CH^2), 172.0 (CO^{11}) ppm.

HRMS-EI-MS of C$_{11}$H$_{21}$NO$_2$ [M+H]$^+$ calculated: 200.1645, found 200.1647.
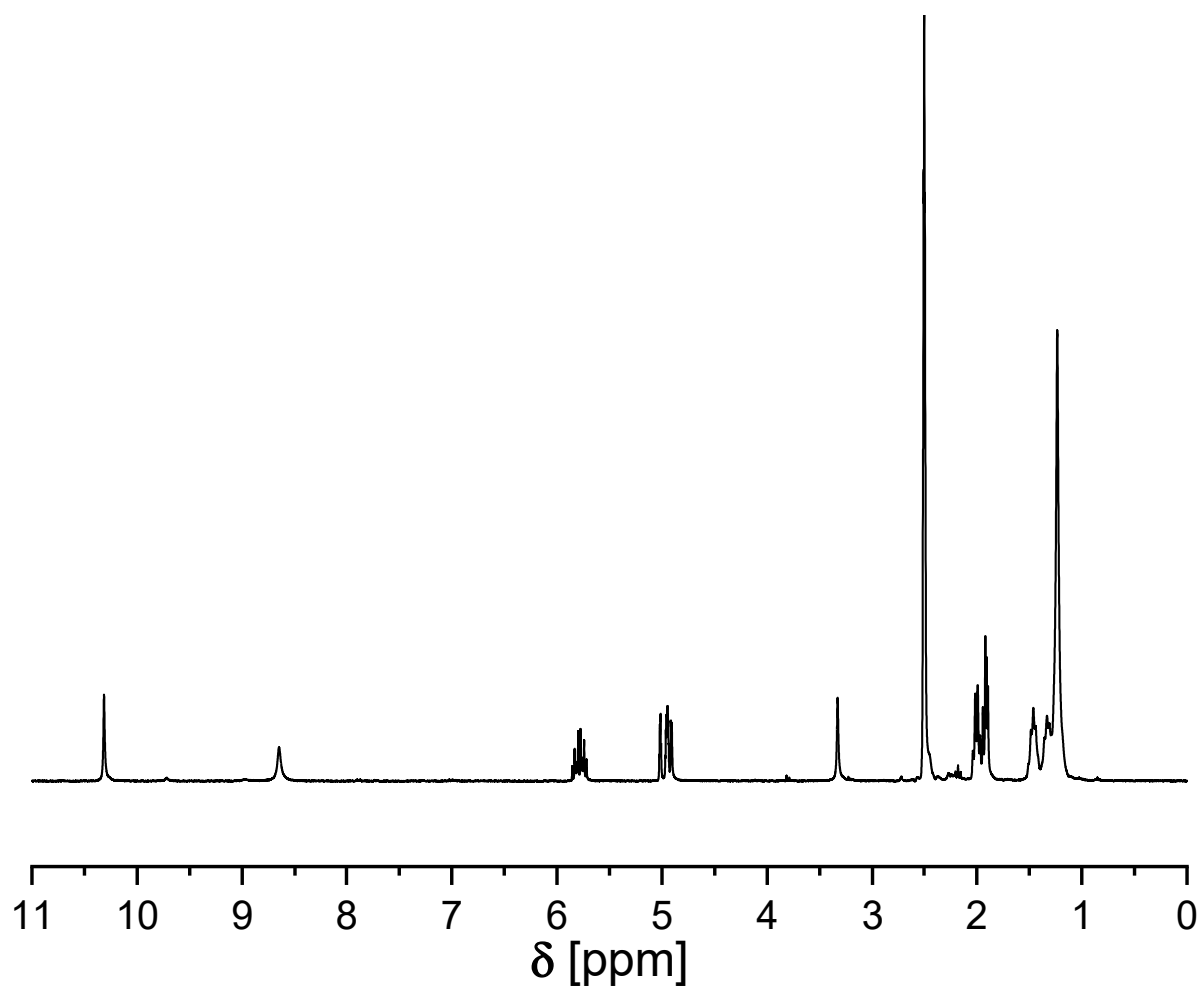
Figure 68 ^{1}H NMR spectrum of **1e** (CDCl$_3$, 400 MHz).

N-Hydroxyisobutyramide 1f
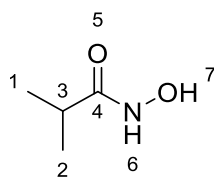
The reaction of methyl isobutyrate (1.00 eq.) with hydroxylamine hydrochloride (3.00 eq.) and potassium hydroxide (6.00 eq.) for 20 h under reflux conditions led to the formation of pure *N*-hydroxyisobutyramide **1f** (54%) in form of a colorless crystalline solid. The crude product was purified by crystallization from ethylacetate.

1H NMR (DMSO-d_6, 400 MHz) δ= 0.99 (d, *J* = 6.8 Hz, 6H, CH_3[1,2]), 2.22 (hept, *J* = 6.8 Hz, 1H, CH^3), 9.51 (br, s, 2H, NH^6, OH^7) ppm.

13C NMR (DMSO-d_6, 100 MHz) δ= 19.9 (CH_3[1,2]), 31.6 (CH^3), 173.6 (CO^4) ppm.

HRMS-EI-MS of $C_4H_9NO_2$ [M+H]$^+$ calculated: 103.0628, found 103.0628.
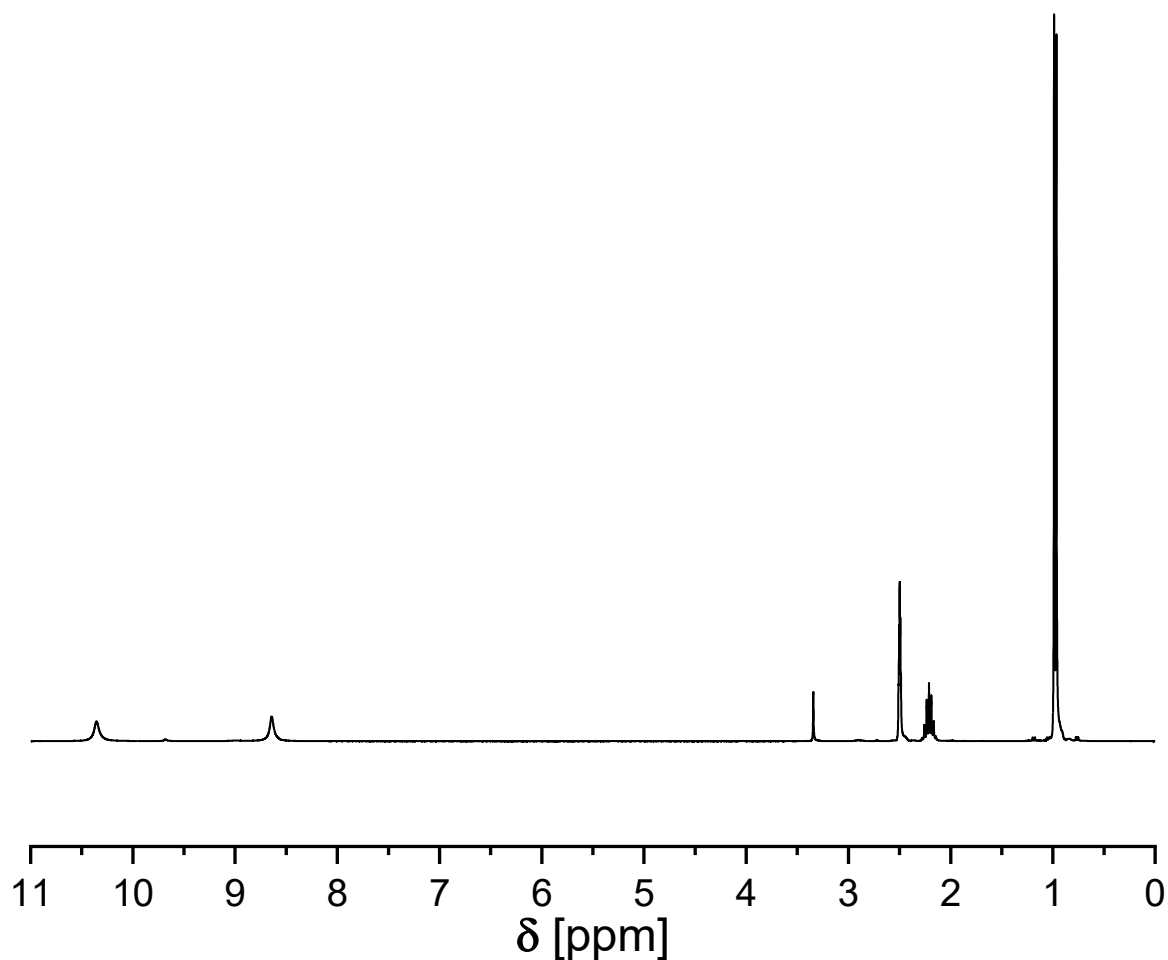
Figure 69 ¹H NMR spectrum of **1f** (DMSO-d_6, 400 MHz).

Experimental section

N^1,N^3-dihydroxymalonamide 1g
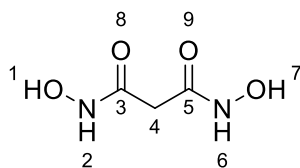
The reaction of dimethyl malonate (1.00 eq.) and hydroxylamine solution (50wt%, 6.00 eq.) led to the formation of N^1,N^3-dihydroxymalonamide **1g** in the form of a colorless crystalline solid (84%).

^{1}H NMR (DMSO-d_6, 400 MHz) δ= 2.75 (s, 2H, CH$_2^4$), 8.88 (br, s, 2H, NH^{2,6}), 10.47 (br, s, 2H, OH^{1,7}) ppm.

^{13}C NMR (DMSO-d_6, 100 MHz) δ= 38.7 (C^4), 163.8 (C^{3,5}) ppm.

HRMS-EI-MS of C$_3$H$_6$N$_2$O$_4$ [M+H]$^+$ calculated: 134.0322, found 134.0321.
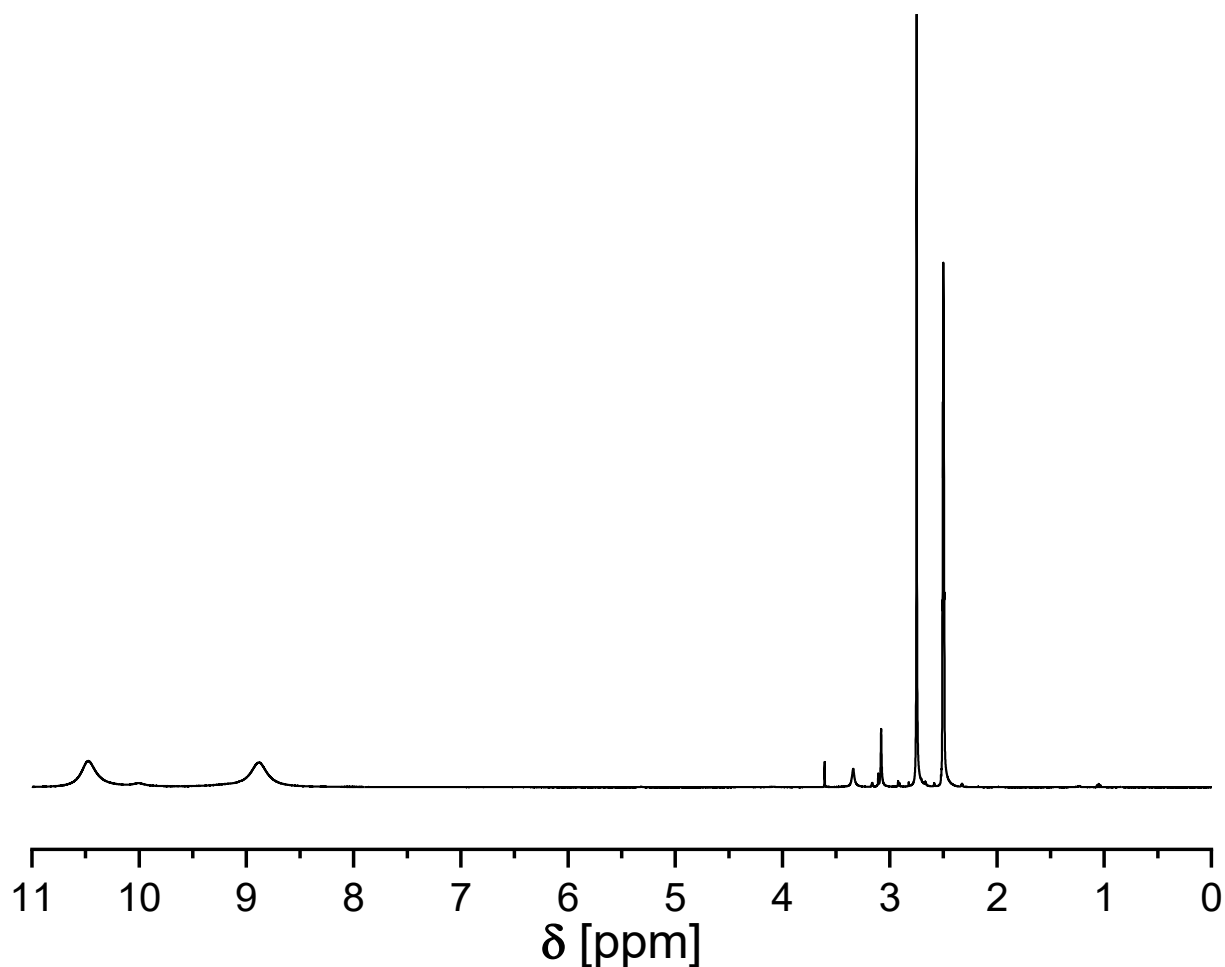
Figure 70 ^{1}H NMR spectrum of **1g** (DMSO-d_6, 400 MHz). The impurities at 3.61 and 3.16 ppm are the methyl ester and methanol, respectively.

N^1,N^4-dihydroxysuccinamide **1h**
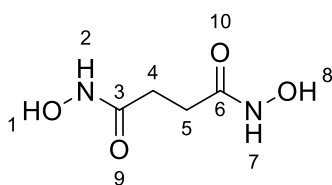
The reaction of dimethyl succinate (1.00 eq.) and hydroxylamine solution (50wt% in H$_2$O, 6.00 eq.) led to the formation of N^1,N^4-dihydroxysuccinamide **1h** in the form of a colorless crystalline solid (77%).

^{1}H NMR (DMSO-d_6, 400 MHz) δ= 2.18 (s, 4H, CH$_2^{4,5}$), 9.01 (s, br, 2H, NH^{2,17}), 10.37 (br, s, 2H, OH^{1,8}) ppm.

^{13}C NMR (DMSO-d_6, 100 MHz) δ= 28.2 (C^{4,5}), 168.6 (C^{3,6}) ppm.

ASAP-MS of C$_4$H$_9$N$_2$O$_4$ [M+H]$^+$ calculated: 149.0557, found 149.0556.
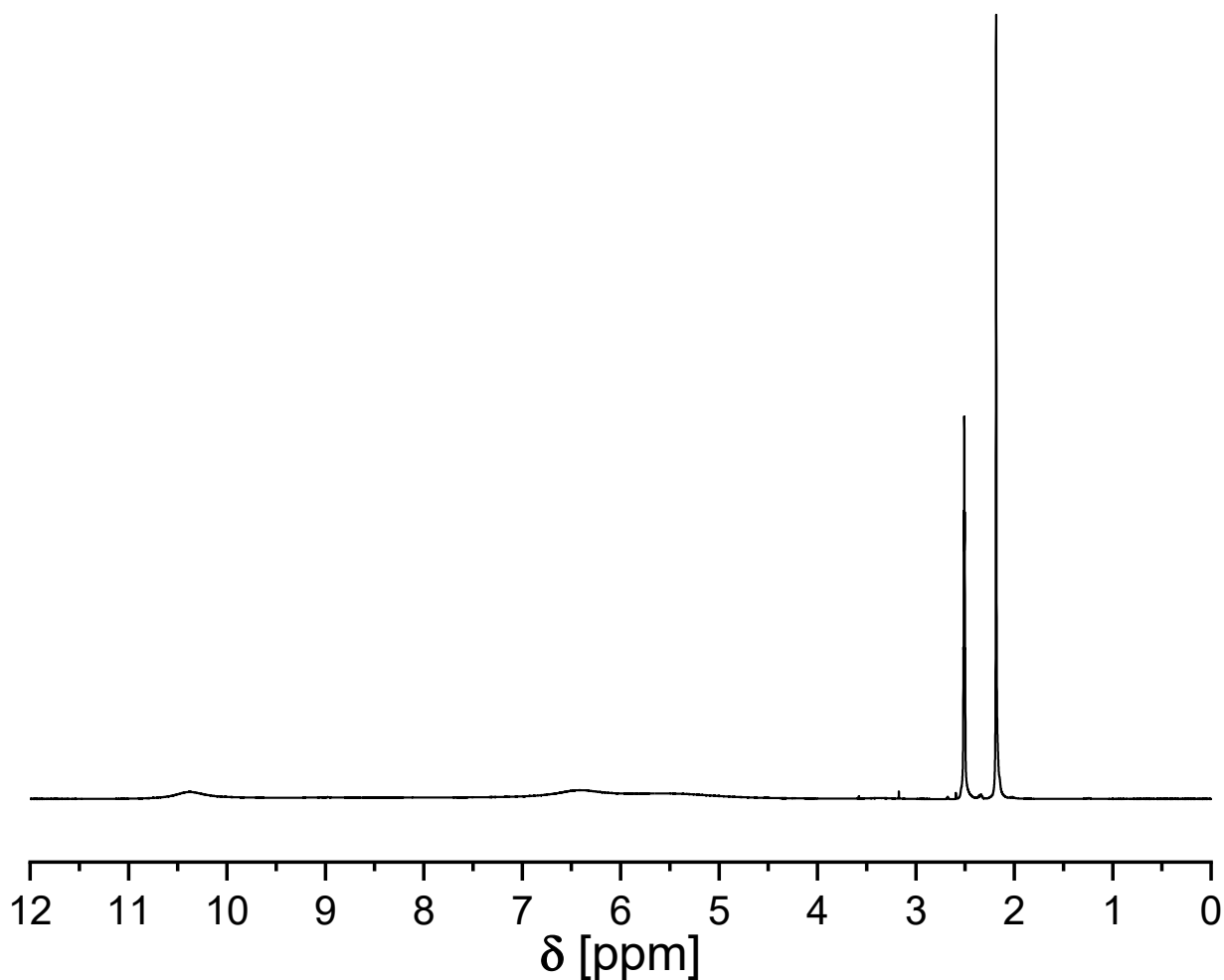
Figure 71 ^{1}H NMR spectrum of **1h** (DMSO-d_6, 400 MHz).

Experimental section

N^1,N^6-dihydroxyadipamide 1i
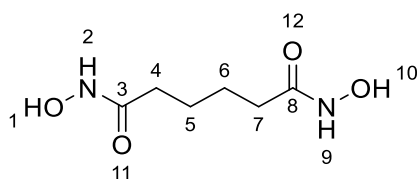
The reaction of dimethyl adipate (1.00 eq.) and hydroxylamine solution (50wt%, 6.00 eq.) led to the formation of N^1,N^6-dihydroxyadipamide **1i** in the form of a colorless crystalline solid (82%).

¹H NMR (400 MHz, DMSO-d_6) δ= 1.45 (p, *J* = 3.7 Hz, 4H), 1.93 (p, *J* = 3.7 Hz, 4H, CH$_2$^{4,7}), 8.66 (s, 2H, NH^{2,9}), 10.33 (s, 2H, OH^{1,10}) ppm.

¹³C NMR (100 MHz, DMSO-d_6) δ= 25.3 (CH$_2$^{5,6}), 32.6 (CH$_2$^{4,7}), 169.4 (C^{3,8}) ppm.

HRMS-EI-MS of $C_6H_{12}N_2O_4$ [M+H]$^+$ calculated: 176.0792, found 176.0790
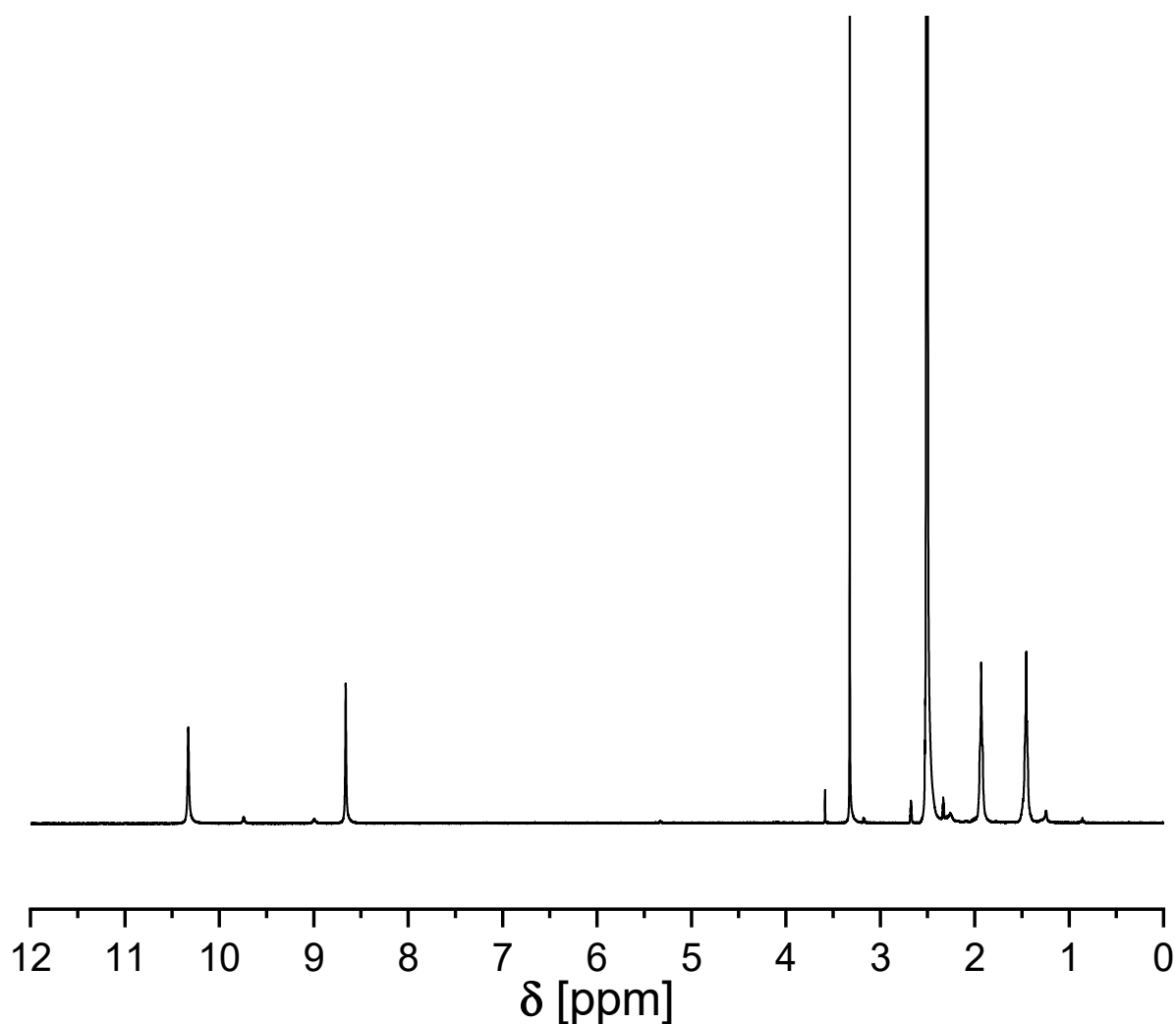
Figure 72 ¹H NMR spectrum of **1i** (DMSO-d_6, 400 MHz).

N^1,N^{10}-*Dihydroxydecanediamide* **1j**
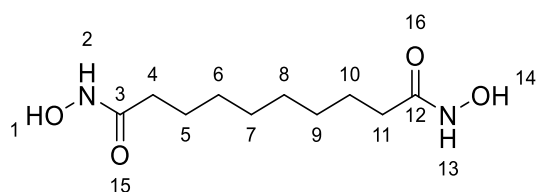
The reaction of dimethyl sebacate (1.00 eq.) with hydroxylamine hydrochloride (3.00 eq. for each ester group) and potassium hydroxide (6.00 eq. for each ester group) for 20 h under reflux conditions led to the formation of N^1,N^{10}-dihydroxydecanediamide **1j** (83%) in form of a colorless crystalline solid. The insoluble crystals in the ethyl acetate/water mixture were filtered and dried.

¹H NMR (DMSO-d_6, 400 MHz) δ= 1.19 – 1.25 (m, 8H, CH$_2^{6-9}$), 1.47 (p., J = 7.5 Hz, 6.5 Hz, 4H, CH$_2^{5,10}$), 1.92 (t, J = 7.4 Hz, 4H, CH$_2^{4,11}$), 9.07 (br, s, 2H, NH^{2,13}), 10.31 (br, s, 2H, OH^{1,14}) ppm.

¹³C NMR (DMSO-d_6, 100 MHz) δ = 25.6 (CH$_2^{5,10}$), 29.0 (CH$_2^{6-9}$), 29.1 (CH$_2^{6-9}$), 33.7 (CH2^{4,11}), 169.5 (CO^{3,12}) ppm.

HRMS-EI-MS of C$_{10}$H$_{20}$N$_2$O$_4$ [M]$^+$ calculated: 232.1418, found 232.1419.
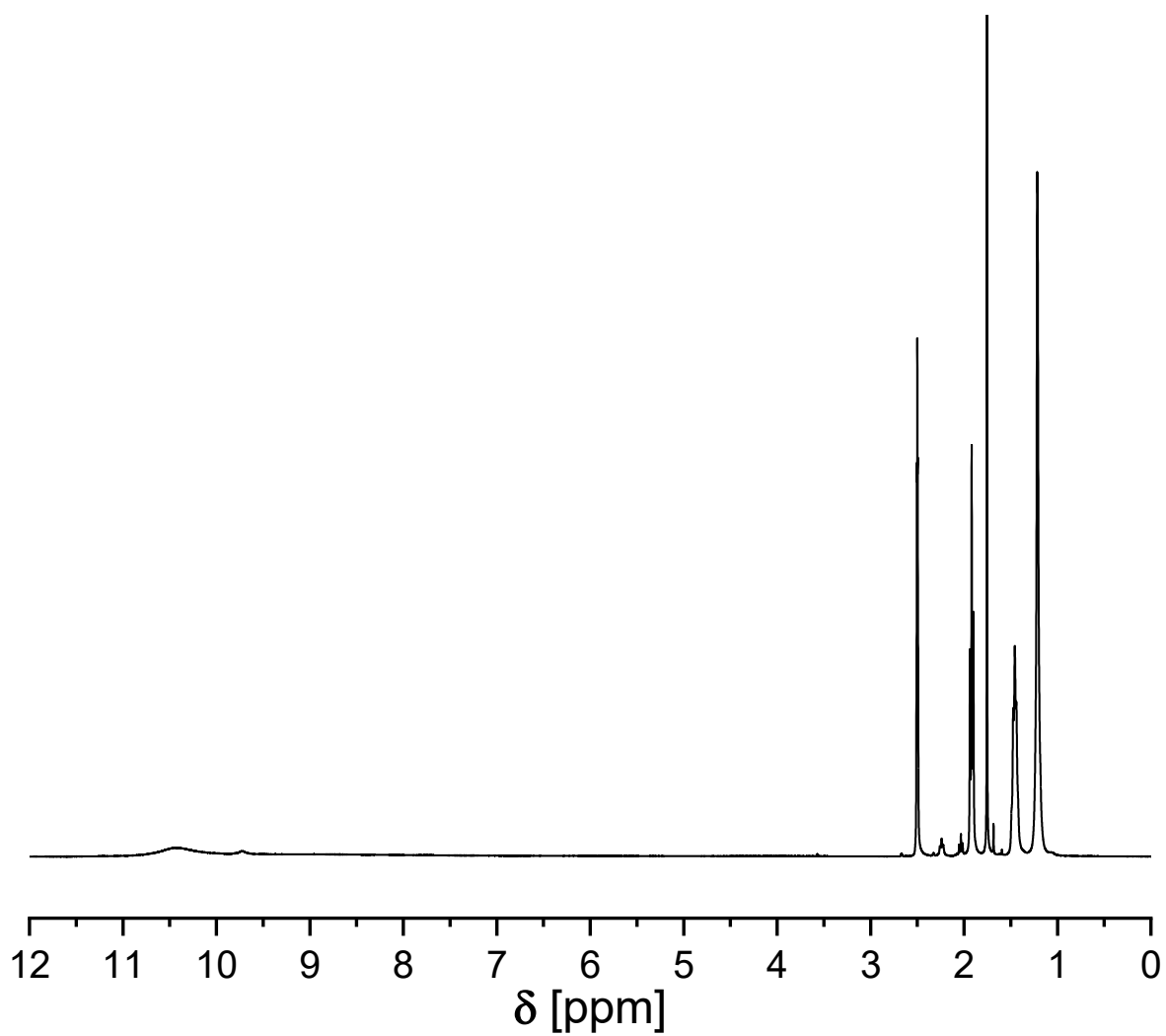
Figure 73 ^{1}H NMR spectrum of **1j** (DMSO-d_6, 400 MHz).

N^1,N^{14}-dihydroxytetradecanediamide **1k**
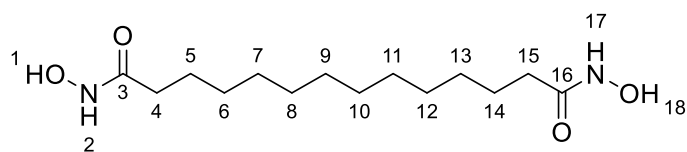
The reaction of dimethyl tetradecanedioate (1.00 eq.) with hydroxylamine hydrochloride (3.00 eq. for each ester group) and potassium hydroxide (6.00 eq. for each ester group) for 20 h under reflux conditions led to the formation of N^1,N^{14}-dihydroxytetradecanediamide **1k** (74%) in form of a colorless crystalline solid. The insoluble crystals in the ethyl acetate/water mixture were filtered and dried.

^{1}H NMR (DMSO-d_6, 400 MHz) δ= 1.24 (s, 16H, CH_2^{6-13}), 1.47 (p., *J* = 6.8 Hz, 4H, $CH_2^{5,14}$), 1.93 (t, *J* = 7.4 Hz, 4H, $CH_2^{4,15}$), 9.01 (br, s, 2H, $NH^{2,17}$), 10.33 (br, s, 2H, $OH^{1,18}$) ppm.

^{13}C NMR (DMSO-d_6, 100 MHz) δ= 25.6 ($CH_2^{5,14}$), 29.1 (CH_2^{6-13}), 29.1 (CH_2^{6-13}), 29.2 (CH_2^{6-13}), 29.3 (CH_2^{6-13}), 29.4 (CH_2^{6-13}), 29.5 (CH_2^{6-13}), 29.5 (CH_2^{6-13}), 32.7 ($CH2^{4,15}$, 169.6 ($CO^{3,16}$) ppm.

ASAP-MS of $C_{14}H_{29}N_2O_4$ [M+H]$^+$ calculated: 289.2122, found 289.2119.
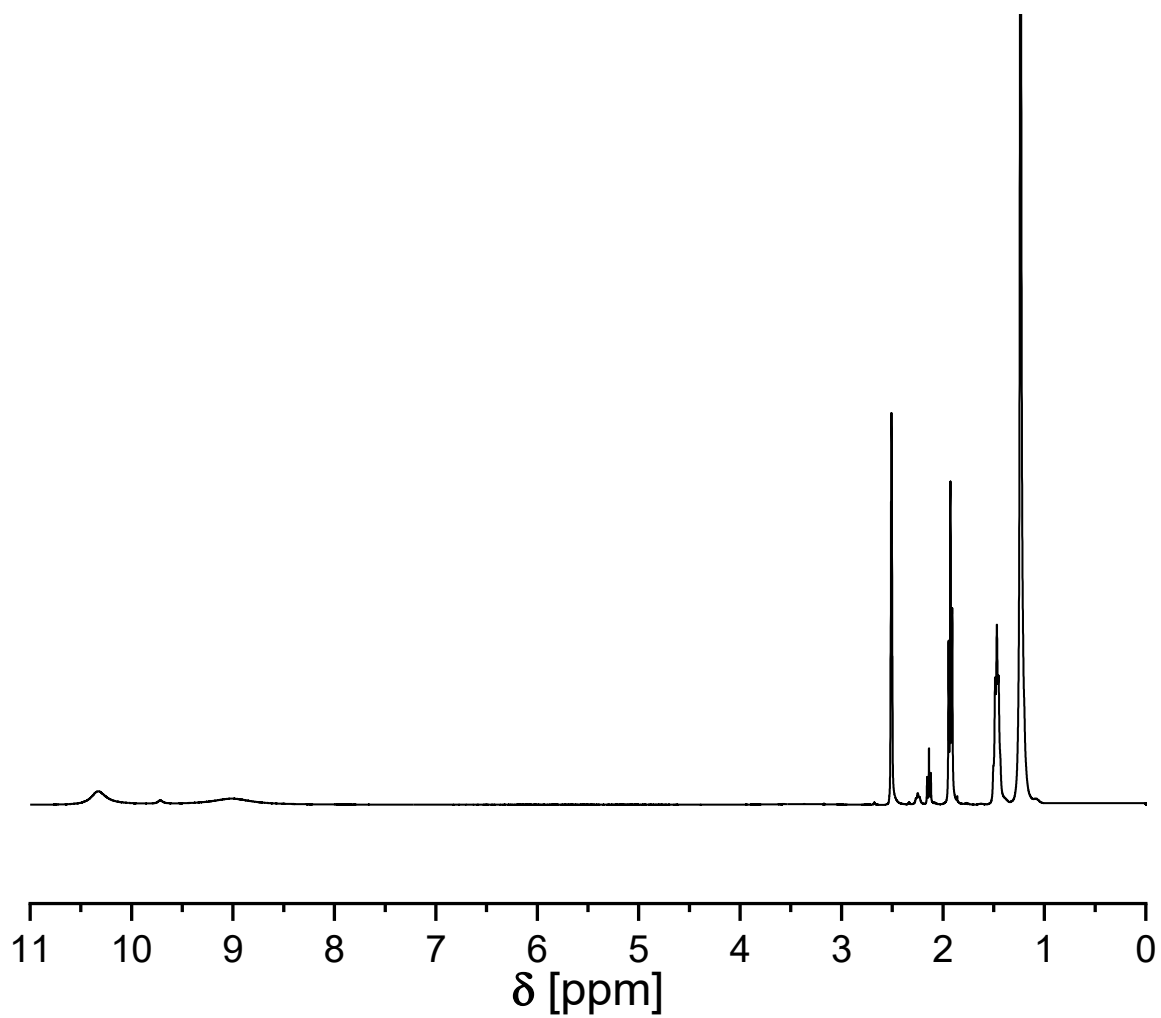
Figure 74 ^{1}H NMR spectrum of **1k** (DMSO-d_6, 400 MHz).

N-Hydroxyadamantane-1-carboxamide **1l**
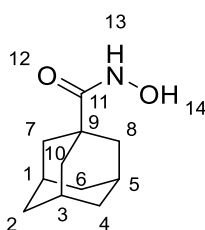
The reaction of methyl adamantane-1-carboxylate (1.00 eq.) with hydroxylamine hydrochloride (3.00 eq.) and potassium hydroxide (6.00 eq.) for 20 h under reflux conditions led to the formation of pure *N*-hydroxyadamantane-1-carboxamide **1l** (35%) in form of a colorless crystalline solid. The crude product was purified by recrystallization from ethyl acetate/hexane (1:5).

^{1}H NMR (CDCl$_3$, 400 MHz) δ= 1.71 (t, *J* = 14.9 Hz, 6H, CH$_2^{2,4,6}$), 1.91 (d, *J* = 2.6 Hz, 6H, CH$_2^{7,8,10}$), 2.03 (p., *J* = 3.2 Hz, 2.8 Hz, 3H, CH^{1,3,5}), 10.51 (br, s, 2H, NH^{13}, OH^{14}) ppm.

^{13}C NMR (CDCl$_3$, 100 MHz) δ = 27.9 (CH^{1,3,5}), 36.5 (CH$_2^{2,4,6}$), 39.0 (CH$_2^{7,8,10}$) 178.9 (CO^{11}) ppm. The peak for C^9 could not be attributed, as it overlaps with the DMSO signals around 40 ppm.

HRMS-EI-MS of C$_{11}$H$_{18}$NO$_2$ [M]$^+$ calculated: 196.1332, found 196.1331.
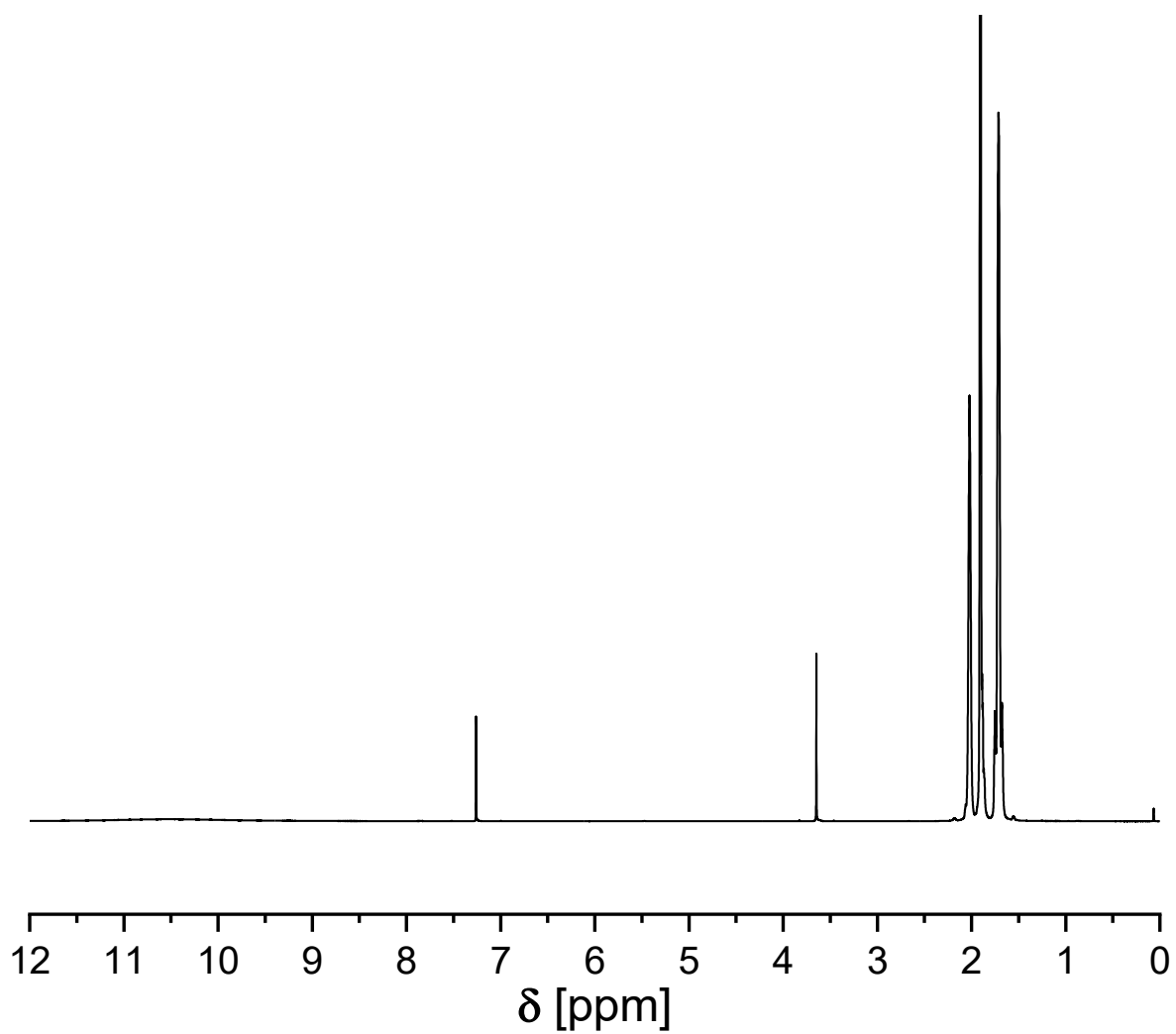
Figure 75 ^{1}H NMR spectrum of **1l** (CDCl$_3$, 400 MHz). The impurity at 3.6 ppm belongs to residual methyl ester.

N-Hydroxy-2-hydroxybenzamide **1m**
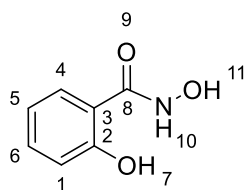
The reaction of methyl-salicylate (1.00 eq.) with hydroxylamine hydrochloride (3.00 eq.) and potassium hydroxide (6.00 eq.) for 20 h under reflux conditions led to the formation of pure salicyl hydroxamic acid **1m** (63%) in form of a colorless crystalline solid. The crude product was purified by crystallization in ethyl acetate.

^{1}H NMR (DMSO-d_6, 400 MHz) δ= 6.79 − 6.97 (m, 2H, CH^{1,5}), 7.37 (dt, *J*= 7.2 Hz, 1H, CH^6), 7.68 (dd, *J*= 8.0 Hz, 1.7 Hz, 1H, CH^4), 9.33 (s, 1H, NH^{10}), 11.44 (s, 1H, OH^{11}), 12.24 (s, 1H, OH^7) ppm.

^{13}C NMR (DMSO-d_6, 100 MHz) δ = 114.5 (CH^1), 117.8 (C^3), 119.2 (CH^5), 127.5 (CH^4), 133.8 (CH^6), 159.9 (C^2), 166.8 (CO^8) ppm.

HRMS-EI-MS of $C_7H_7NO_3$ [M+H]$^+$ calculated: 153.0420, found 153.0419.
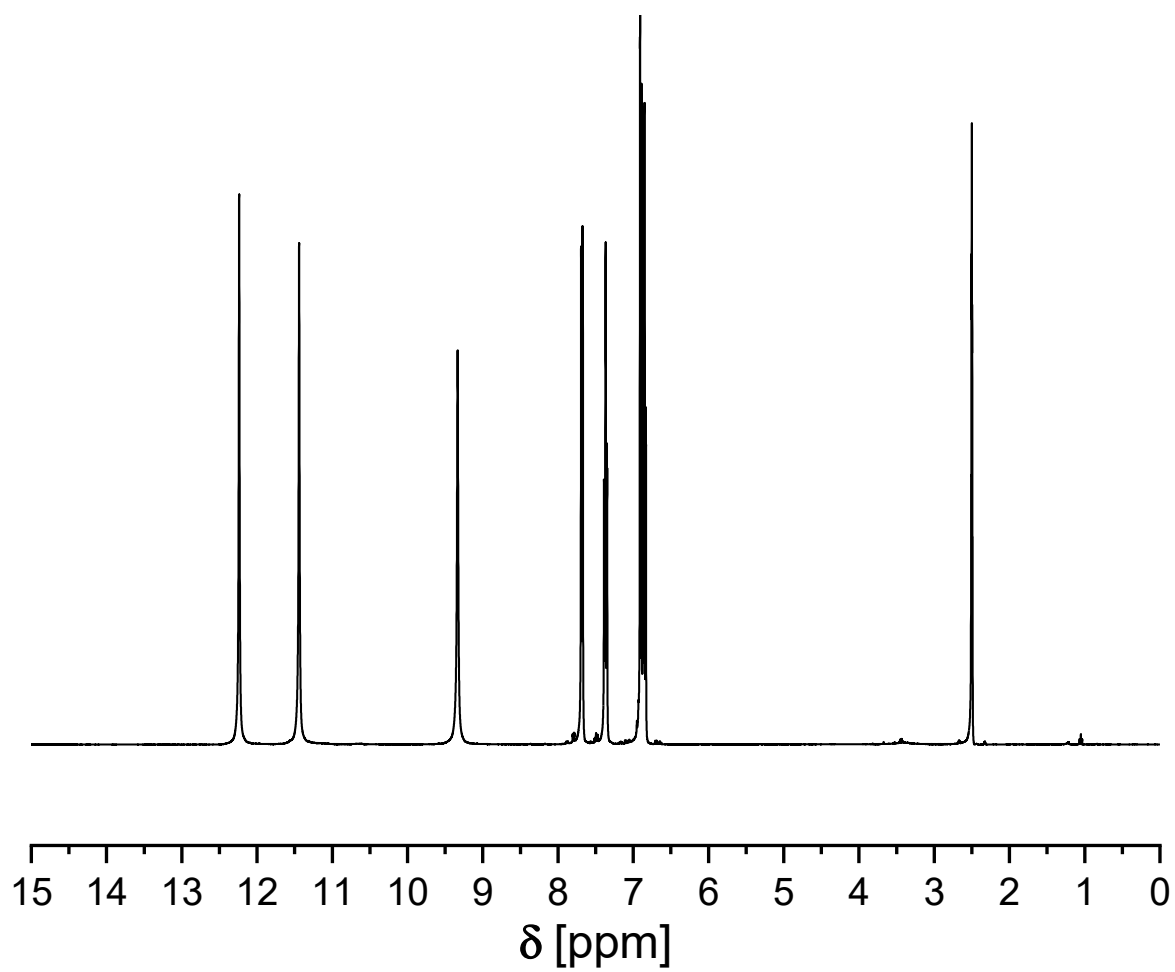
Figure 76 ^{1}H NMR spectrum of **1m** (DMSO-d_6, 400 MHz).

N-Hydroxybenzamide **1n**
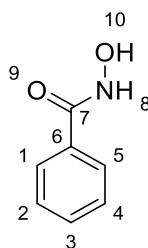
The reaction of methyl benzoate (1.00 eq.) with hydroxylamine hydrochloride (3.00 eq.) and potassium hydroxide (6.00 eq.) for 20 h under reflux conditions led to the formation of pure *N*-hydroxybenzamide **1n** (80%) in form of a colorless crystalline solid. The crude product was purified by recrystallization from ethyl acetate/hexane (1:1).

^{1}H NMR (DMSO-d_6, 400 MHz) δ= 7.42 – 7.47 (m, 2H, $CH^{2,4}$), 7.49 – 7.53 (m, 1H, CH^3), 7.75 – 7.78 (m, 2H, $CH^{1,5}$), 9.26 (br, s, 1H, NH^9), 11.24 (br, s, 1H, OH^{10}) ppm.

^{13}C NMR (DMSO-d_6, 100 MHz) δ= 127.3 ($CH^{1,5}$), 128.8 ($CH_2^{1,5}$), 131.6 (C^3), 133.3 (C^6), 164.6 (CO^7) ppm.

HRMS-EI-MS of $C_7H_7NO_2$ [M+H]$^+$ calculated: 137.0471, found 137.0470.
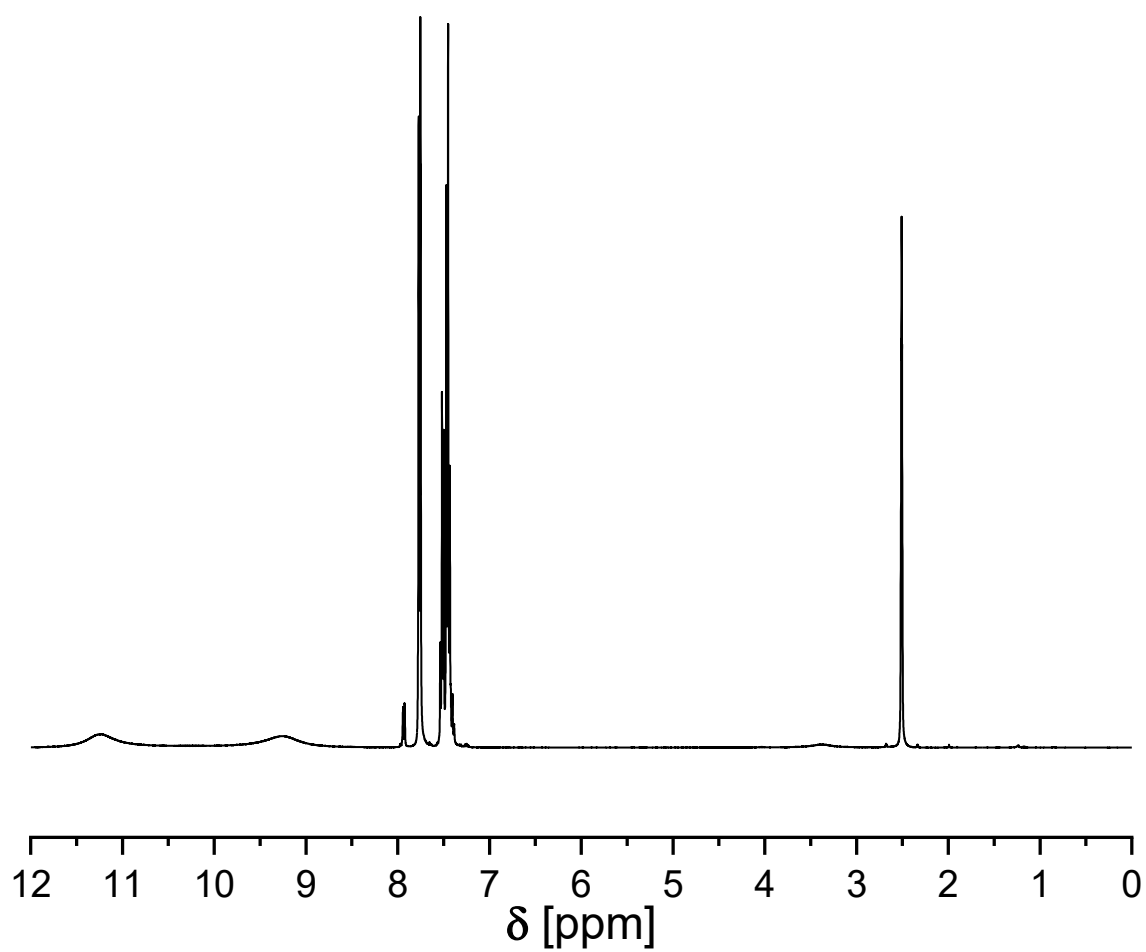
Figure 77 ^{1}H NMR spectrum of **1n** (DMSO-d_6, 400 MHz).

N-Hydroxy-4-methoxybenzamide 1o
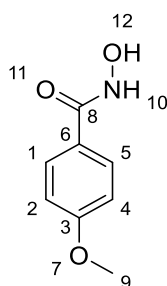
The reaction of methyl-4-methoxybenzoate (1.00 eq.) with hydroxylamine hydrochloride (3.00 eq.) and potassium hydroxide (6.00 eq.) for 20 h under reflux conditions led to the formation of pure *N*-hydroxy-4-methoxybenzamide **1o** (84%) in form of a colorless crystalline solid. The crude product was purified by crystallization in ethyl acetate.

^{1}H NMR (DMSO-d_6, 400 MHz) δ= 3.79 (s, 3H, $CH_3{}^9$), 6.98 (dt, J = 2.8 Hz, 8.9 Hz, 2H, $CH^{2,4}$), 7.73 (dt, J = 2.8 Hz, 8.9 Hz, 2 H, $CH^{1,5}$), 8.90 (s, br, 1H, NH^{10}), 11.07 (s, br, 1H, OH^{11}) ppm.

^{13}C NMR (DMSO-d_6, 100 MHz) δ= 55.8 ($CH_3{}^9$), 114.1($CH^{2,4}$), 125.4 (C^6), 129.1 ($CH_2{}^{1,5}$), 162.0 (CO^8), 164.5 (C^3) ppm.

HRMS-EI-MS of $C_8H_9NO_3$ [M+H]$^+$ calculated: 167.0577, found 167.0578.
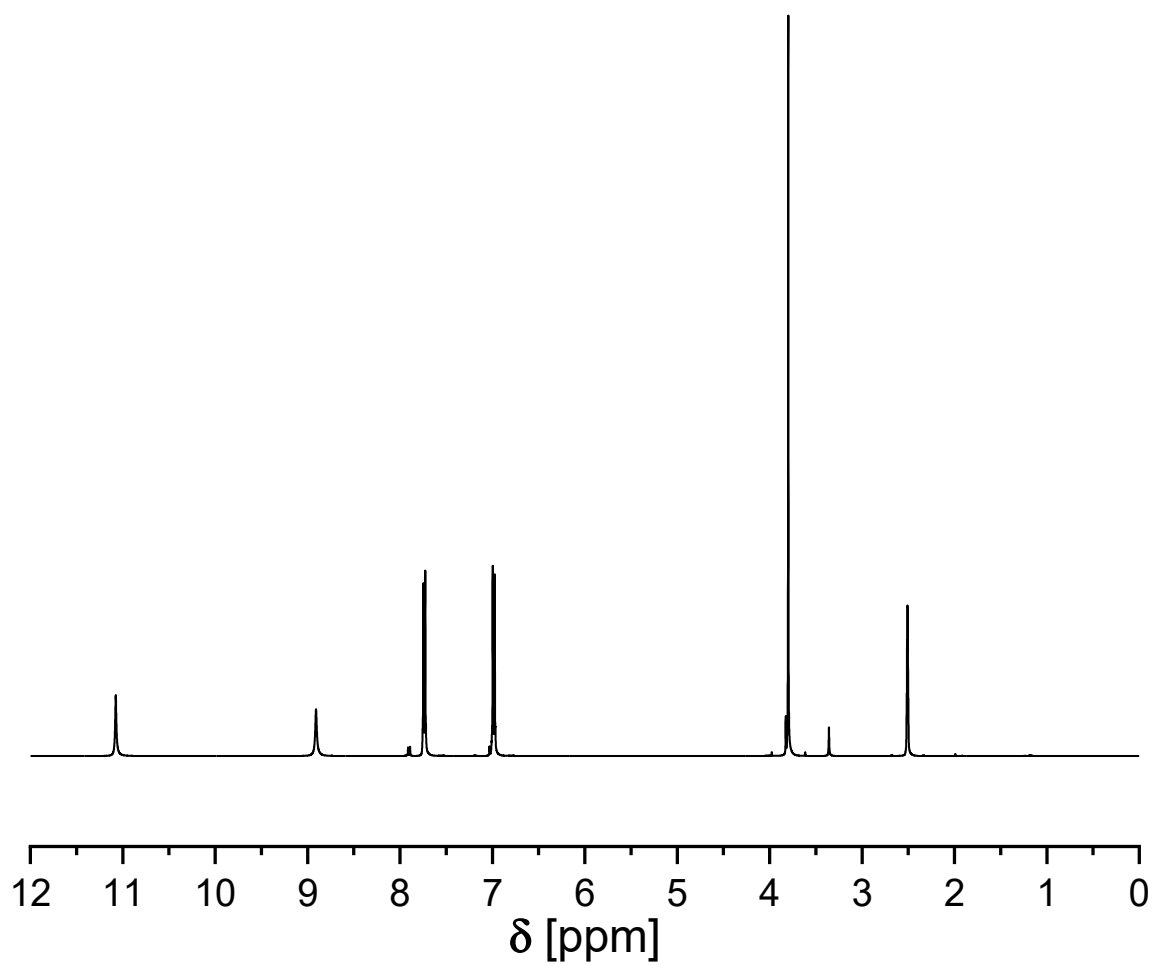
Figure 78 ^{1}H NMR spectrum of **1o** (DMSO-d_6, 400 MHz).

N-Hydroxy-4-chlorobenzamide **1p**
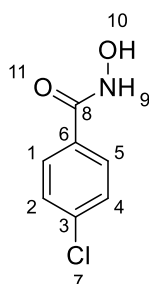
The reaction of methyl-4-chlorobenzoate (1.00 eq.) with hydroxylamine hydrochloride (3.00 eq.) and potassium hydroxide (6.00 eq.) for 20 h under reflux conditions led to the formation of pure *N*-hydroxy-4-chlorobenzamide **1p** (84%) in form of a colorless solid. The crude product was purified by crystallization in ethyl acetate.

^{1}H NMR (DMSO-d_6, 400 MHz) δ= 7.51 – 7.55 (m, 2H, CH^{2,4}), 7.74 – 7.78 (m, 2H, CH^{1,5}), 9.11 (br, s, 1H, NH^9), 11.30 (br, s, 1H, OH^{10}) ppm.

^{13}C NMR (DMSO-d_6, 100 MHz) δ= 129.0 (CH$_2$^{2,4}), 129.2 (CH^{1,5}), 132.0 (C^6), 136.4 (C^3), 163.6 (CO^8) ppm.

HRMS-EI-MS of C$_7$H$_6$NO$_2$^{35}Cl [M+H]$^+$ calculated: 171.0082, found 171.0080.
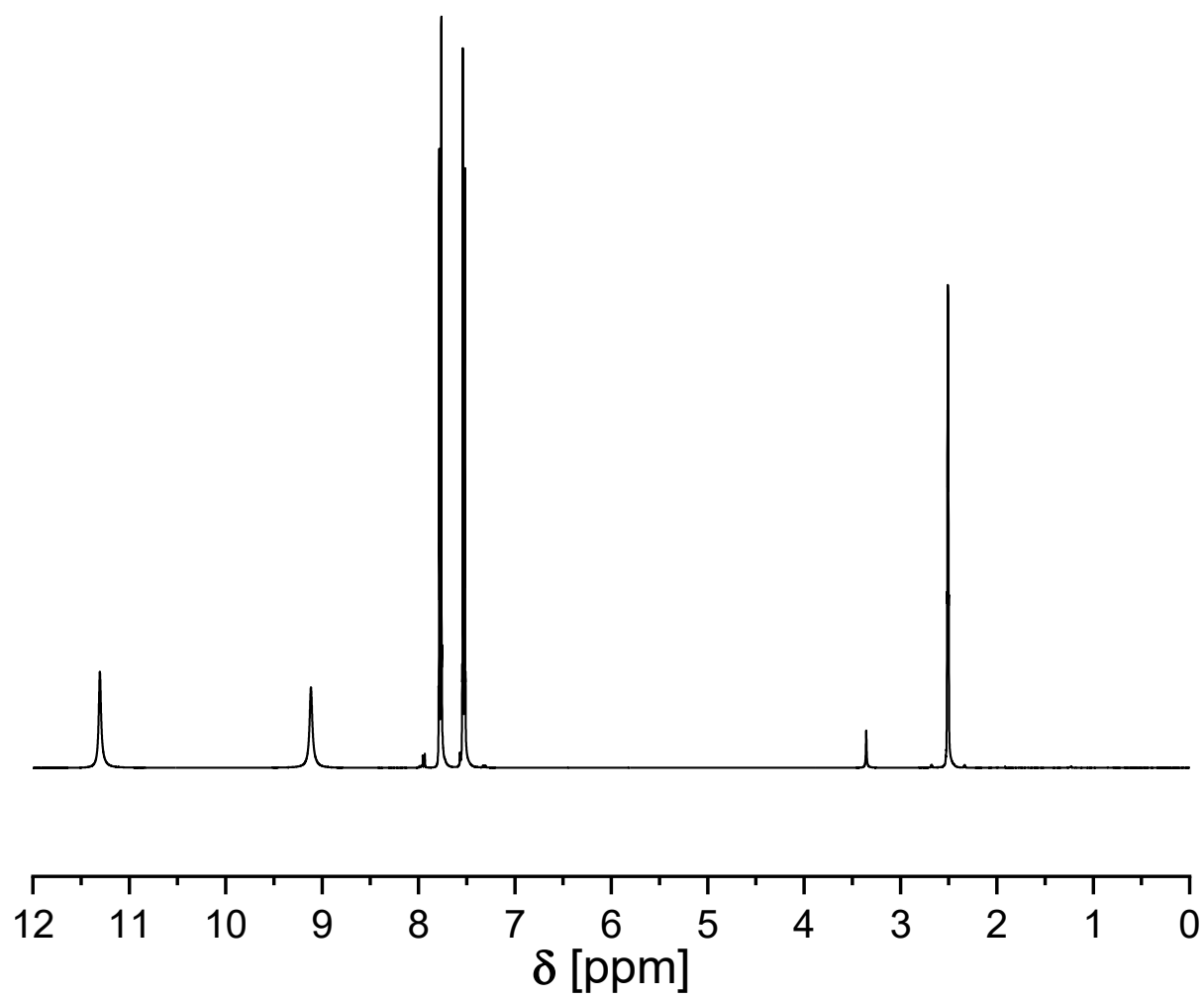
Figure 79 ^{1}H NMR spectrum of **1p** (DMSO-d_6, 400 MHz).

N-Hydroxy-4-methylbenzamide **1q**
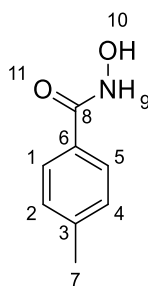
The reaction of methyl-4-methylbenzoate (1.00 eq.) with hydroxylamine hydrochloride (3.00 eq.) and potassium hydroxide (6.00 eq.) for 20 h under reflux conditions led to the formation of pure *N*-hydroxy-4-methylbenzamide **1q** (79%) in form of a colorless crystalline solid. The crude product was purified by crystallization in ethyl acetate.

^{1}H NMR (DMSO-d_6, 400 MHz) δ= 2.34 (s, 3H, $CH_3{}^7$), 7.23 – 7.27 (m, 2H, $CH^{2,4}$), 7.65 – 7.69 (m, 2H, $CH^{1,5}$), 9.13 (br, s, 1H, NH^9), 11.13 (br, s, 1H, OH^{10}) ppm.

^{13}C NMR (DMSO-d_6, 100 MHz) δ= 21.4 ($CH_3{}^7$), 127.3 ($CH^{1,5}$), 129.0 ($CH_2{}^{2,4}$), 130.4 (C^6), 141.4 (C^3), 164.6 (CO^8) ppm.

HRMS-EI-MS of $C_8H_9NO_2$ [M+H]$^+$ calculated: 151.0628, found 151.0628.
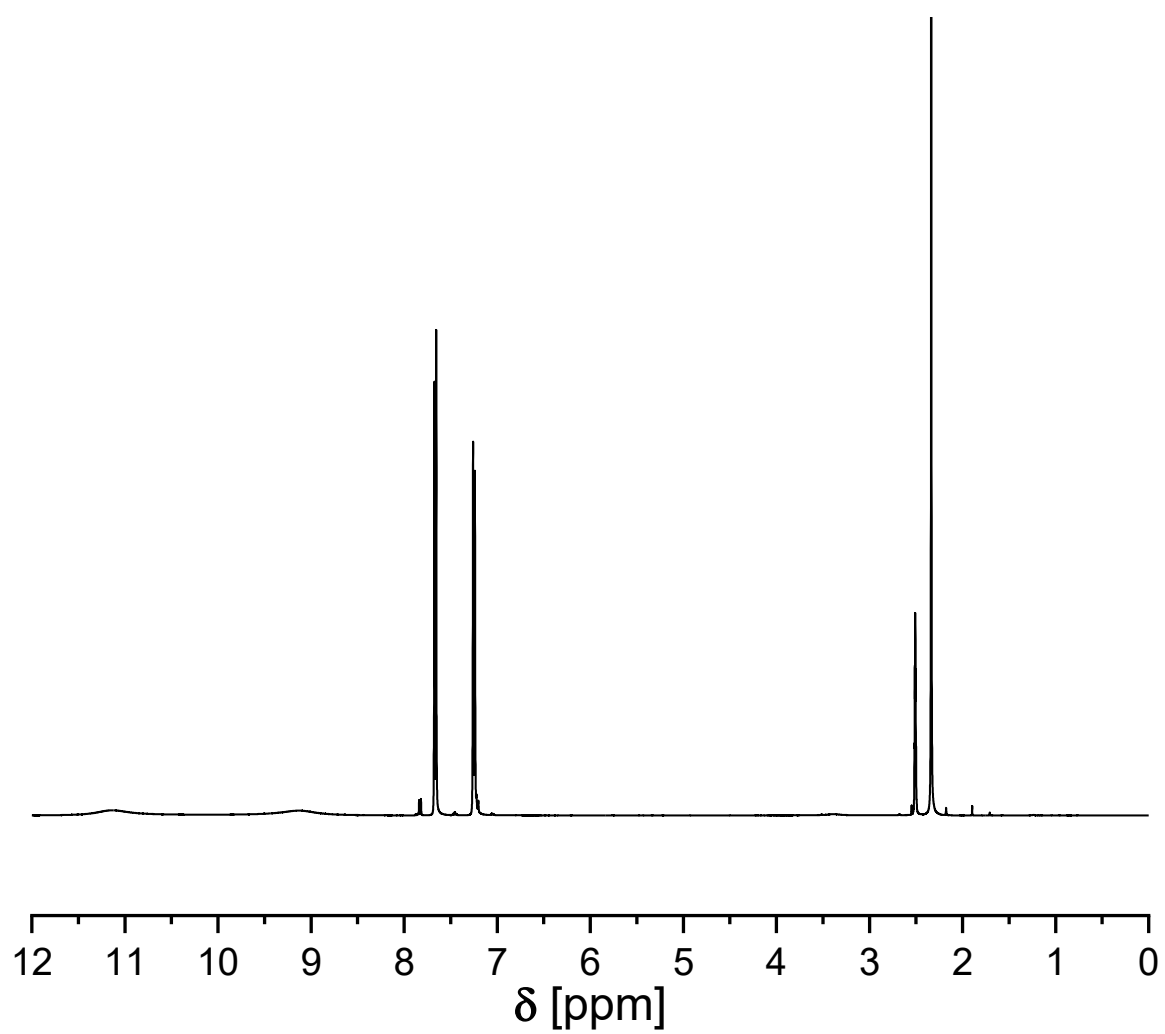
Figure 80 ^{1}H NMR spectrum of **1q** (DMSO-d_6, 400 MHz).

N-Hydroxy-4-nitrobenzamide **1r**
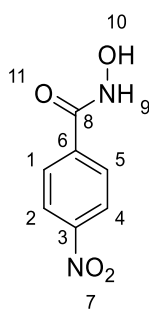
The reaction of methyl-4-nitrobenzoate (1.00 eq.) with hydroxylamine hydrochloride (3.00 eq.) and potassium hydroxide (6.00 eq.) for 20 h under reflux conditions led to the formation of pure *N*-hydroxy-4-nitrobenzamide **1r** (87%) in form of an orange solid. The crude product was purified by crystallization in ethyl acetate.

^{1}H NMR (DMSO-d_6, 400 MHz) δ= 7.95 (d, J = 8.2 Hz 2H, CH^{1,5}), 8.29 (d, J = 8.9 Hz, 2H, CH^{2,4}), 9.38 (br, s, 1H, NH^9), 11.56 (br, s, 1H, OH^{10}) ppm.

^{13}C NMR (DMSO-d_6, 100 MHz) δ= 123.6 (CH^{2,4}), 128.3 (CH^{1,5}), 138.5 (C^6), 148.9 (C^3), 162.1 (CO^8) ppm.

HRMS-EI-MS of $C_7H_7N_2O_4$ [M+H]$^+$ calculated: 182.0322, found 182.0324.
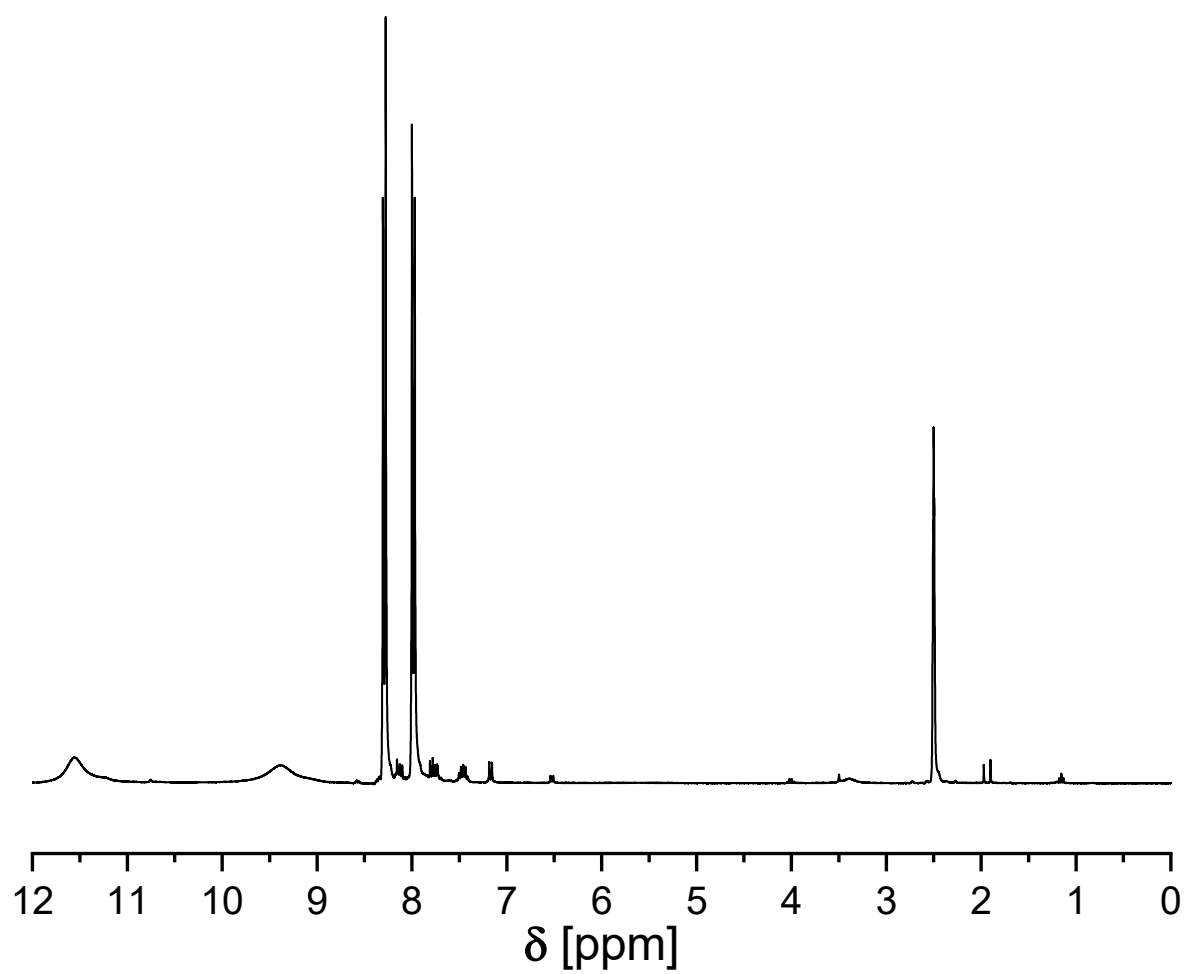
Figure 81 ^{1}H NMR spectrum of **1r** (DMSO-d_6, 400 MHz).

N-Hydroxy-3,4,5-trimethoxybenzamide **1s**
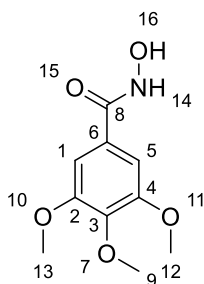
The reaction of methyl-3,4,5-trimethoxybenzoate (1.00 eq.) with hydroxylamine hydrochloride (3.00 eq.) and potassium hydroxide (6.00 eq.) for 20 h under reflux conditions led to the formation of pure *N*-hydroxy-3,4,5-trimethoxybenzamide **1s** (76%) in form of a colorless crystalline solid. The crude product was purified by crystallization in ethyl acetate.

^{1}H NMR (DMSO-d_6, 400 MHz) δ= 3.69 (s, 3H, CH$_3$^{9}), 3.81 (s, 6H, CH$_3$^{12,13}), 7.09 (s, 2H, CH^{1,5}), 7.65 – 7.69 (m, 2H, CH^{1,5}), 9.02 (s, 1H, NH^{14}), 11.17 (s, 1H, OH^{16}) ppm.

^{13}C NMR (DMSO-d_6, 100 MHz) δ= 56.4 (CH$_3$^{12,13}), 60.5 (CH$_3$^{9}), 104.8 (CH^{1,5}), 128.3 (C^6), 140.2 (C^3), 153.1 (C^{2,4}), 164.1 (CO^8) ppm.

HRMS-EI-MS of C$_{10}$H$_{13}$NO$_5$ [M+H]$^+$ calculated: 227.0788, found 277.0790.
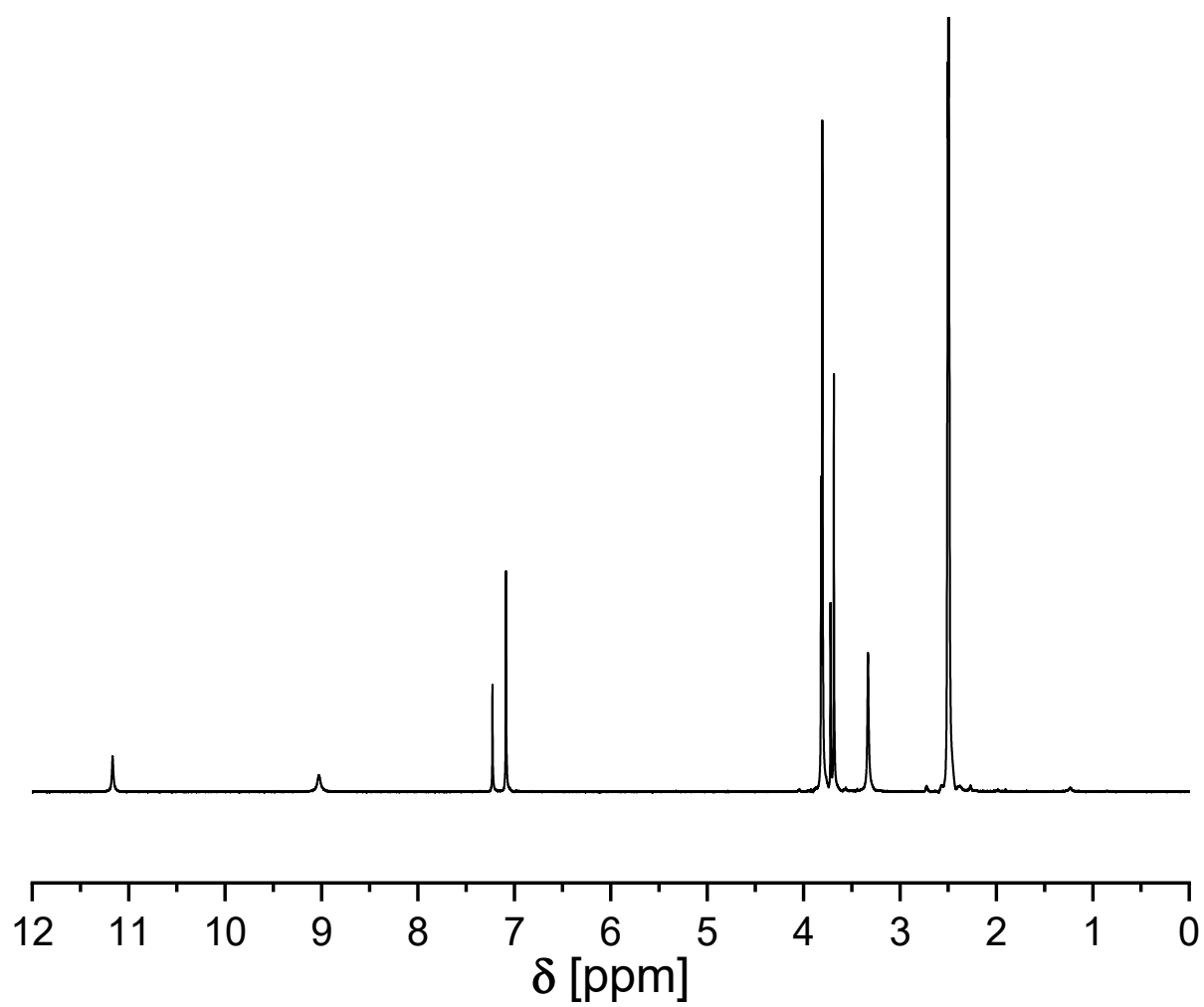
Figure 82 ^{1}H NMR spectrum of **1s** (DMSO-d$_6$, 400 MHz).

5.1.5 General procedure for the synthesis of ureas and anilines

Hydroxamic acids (1.00 eq.) were dissolved in dimethyl sulfoxide in a 20 mL vial. After the addition of DBU (1.00 eq.), the mixture was allowed to stir for 2 minutes at room temperature. Afterwards the vial was moved to a Parr reactor vessel (300 mL) and the selected pressure of 10 bar CO_2 was applied. After setting the temperature at 110 °C, the mixture was stirred for 18 h before releasing the gas.

Depending on the employed hydroxamic acid, the synthesis led to either ureas or anilines. Urea derivatives were isolated after column chromatography or filtration, anilines were extracted from the crude mixture and amines via flash column chromatography.

1,3-Di((Z)-heptadec-8-en-1-yl)urea **10**
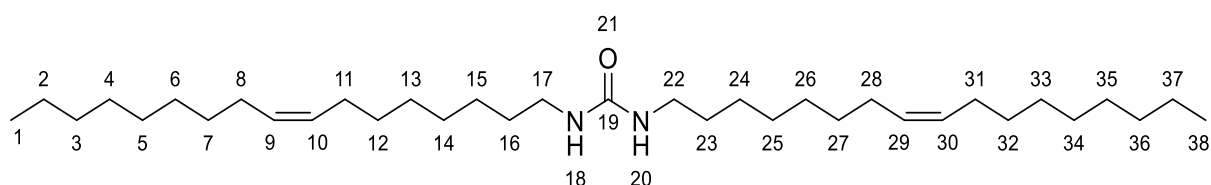
The CO_2 based Lossen rearrangement of *N*-hydroxy oleamide **1a** (1.00 eq) with DBU (1.00 eq) led to the formation of 1,3-Di((Z)-heptadec-8-en-1-yl)urea **10** as white solid (10%). The product was obtained by filtration from the reaction mixture.

The analytical data is found in **chapter 5.2.3**.

1,3-Di(dec-9-en-1-yl)urea **9**
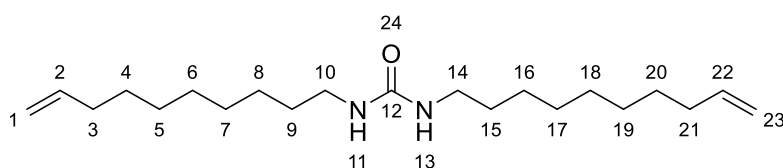
The CO_2 based Lossen rearrangement of *N*-hydroxy undeceneamide **1e** (1.00 eq) with DBU (1.00 eq) led to the formation of 1,3-Di(dec-9-en-1-yl)urea **9** as white solid (15%). The product was obtained by filtration from the reaction mixture.

The analytical data is found in **chapter 5.2.3**.

Experimental section

Diisopropylurea **2f**
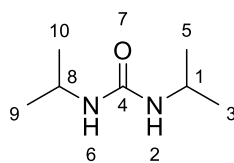
The CO_2 based Lossen rearrangement of *N*-hydroxy isobutyramide **1f** (1.00 eq) with DBU (1.00 eq) led to the formation of diisopropylurea **2f** as white solid (11%). The product was obtained by filtration from the reaction mixture.

¹H NMR (DMSO-*d₆*, 300 MHz) δ= 1.14 (d, *J* = 6.5 Hz, 12H, CH₃[3,5,9,10]), 3.84 (hept, *J* = 6.5 Hz, 6.6 Hz, 6.5 Hz, 2H, CH[1,8]), 4.26 (br, s, 2H, NH[2,6]) ppm.

¹³C NMR (DMSO-*d₆*, 75 MHz) δ= 23.8 (CH₃[3,4]), 41.1 (CH[1]), 157.3 (CO[4]) ppm.

HRMS-EI-MS of $C_7H_{17}N_2O$ [M+H]⁺ calculated: 144.1257, found 144.1256.
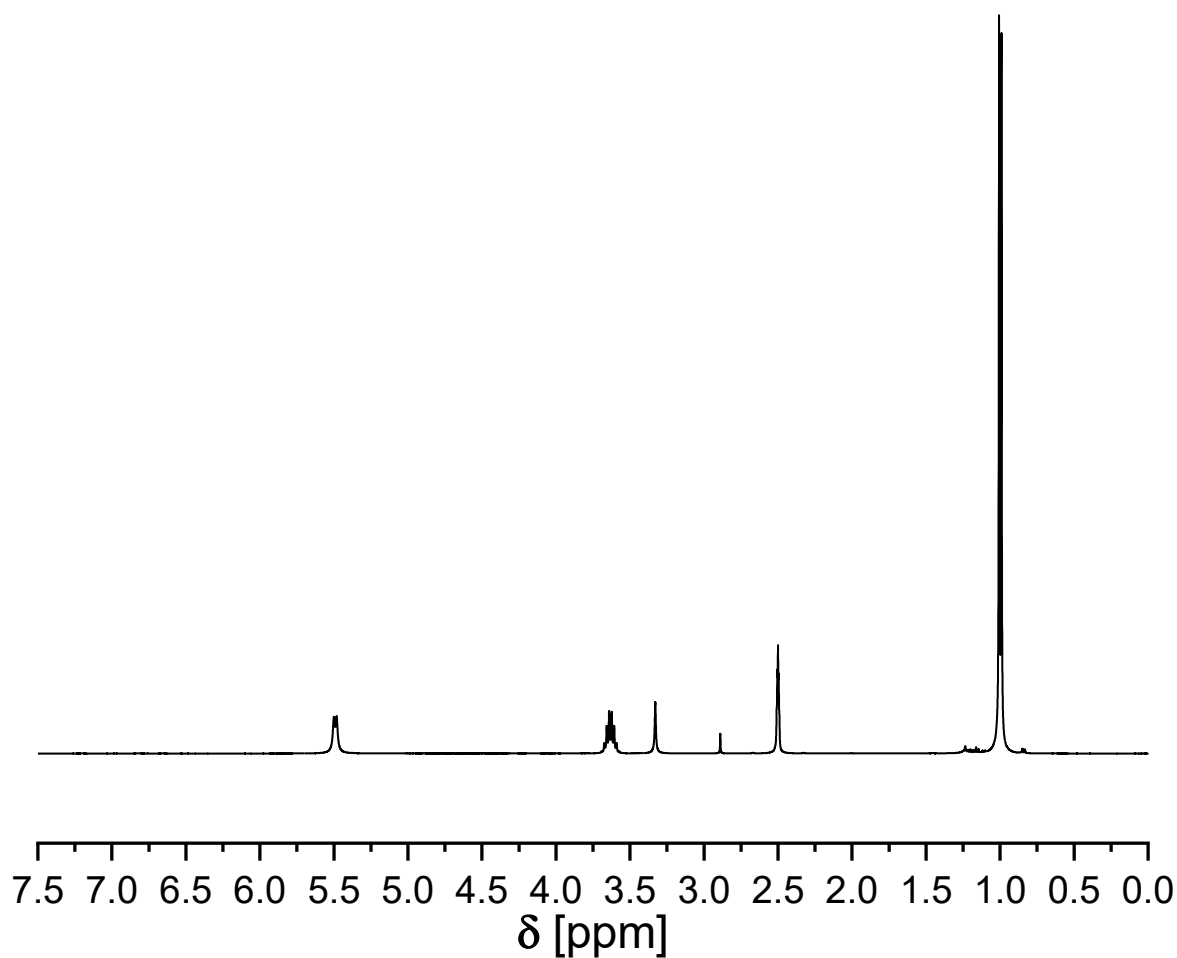
Figure 83 ¹H NMR spectrum of **2f** (DMSO-*d₆*, 300 MHz).

Benzo[d]oxazol-2(3H)-one **2m1**
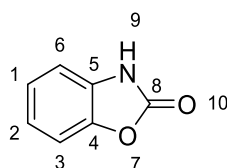
The CO_2 based Lossen rearrangement of salicylhydroxamic acid **1m** (1.00 eq.) with DBU (1.00 eq.) led to the formation of pure Benzo[d]oxazol-2(3H)-one **2m1** as light brown solid (15%). The crude was purified by column chromatography (ethyl acetate).

^{1}H NMR (DMSO-d_6, 500 MHz) δ= 7.07 – 7.10 (m, 2H, CH[1,2]), 7.13 – 7.16 (m, 1H, CH[6]), 7.26 – 7.30 (m, 1H, CH[3]), 11.61 (s, 1H, NH[9]) ppm.

^{13}C NMR (DMSO-d_6, 125 MHz) δ= 109.9 (CH[3,6]), 110.2 (CH[1,2]), 122.3 (CH[2]), 124.2 (CH[1]), 130.8 (CH[5]), 143.8 (CH[4]), 154.9 (CO[8]) ppm.

HRMS-EI-MS of $C_7H_5NO_2$ [M]$^+$ calculated: 135.0315, found 135.0314.
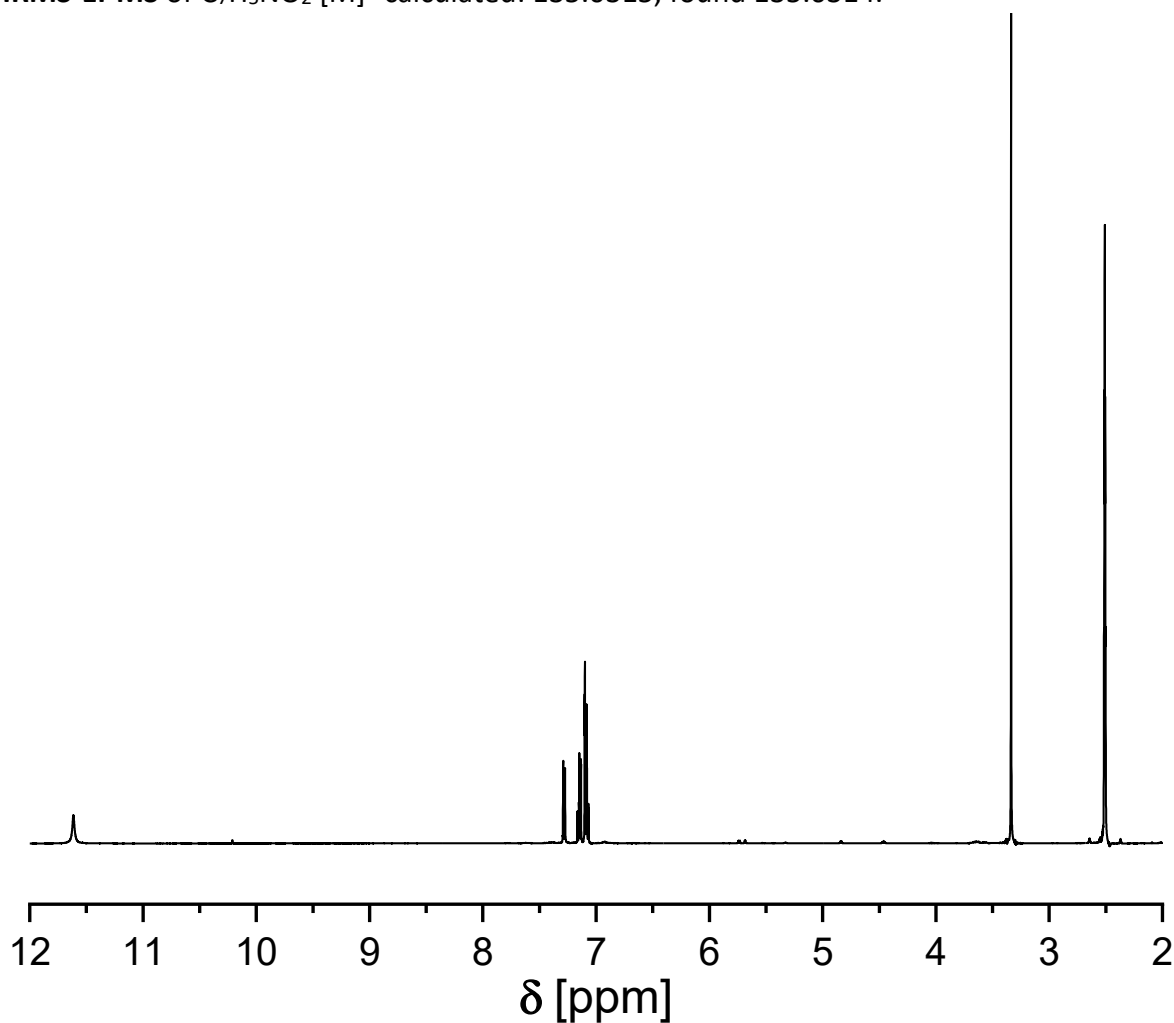
Figure 84 ^{1}H NMR spectrum of **2m1** (DMSO-d_6, 500 MHz).
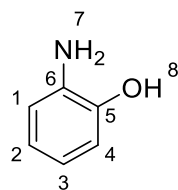
2-Hydroxyaniline **2m2**

The CO_2 based Lossen rearrangement of salicylhydroxamic acid **1m** (1.00 eq.) with DBU (1.00 eq.) led to the formation of pure 2-hydroxyaniline **2m2** as light-yellow solid (34%). The crude was purified by column chromatography (ethyl acetate).

^{1}H NMR (DMSO-d_6, 400 MHz) δ= 4.44 (s, 2 H, NH$_2$^{7}), 6.38 (td, *J* = 7.5 Hz, 1.9 Hz, 1H, CH^1), 6.49-6.59 (m, 2H, CH^{2,4}), 6.62 (dd, *J* = 7.8 Hz, 1.4 Hz 1H, CH^4), 8,90 (s, 1H, OH^8) ppm.

^{13}C NMR (DMSO-d_6, 100 MHz) δ = 115.6 (CH^{1,5}), 119.2 (C^3), 128.9 (CH^{2,4}), 148.2 (C^6) ppm.

HRMS-EI-MS of C_6H_8NO [M+H]$^+$ calculated: 109.0522, found 109.0523.
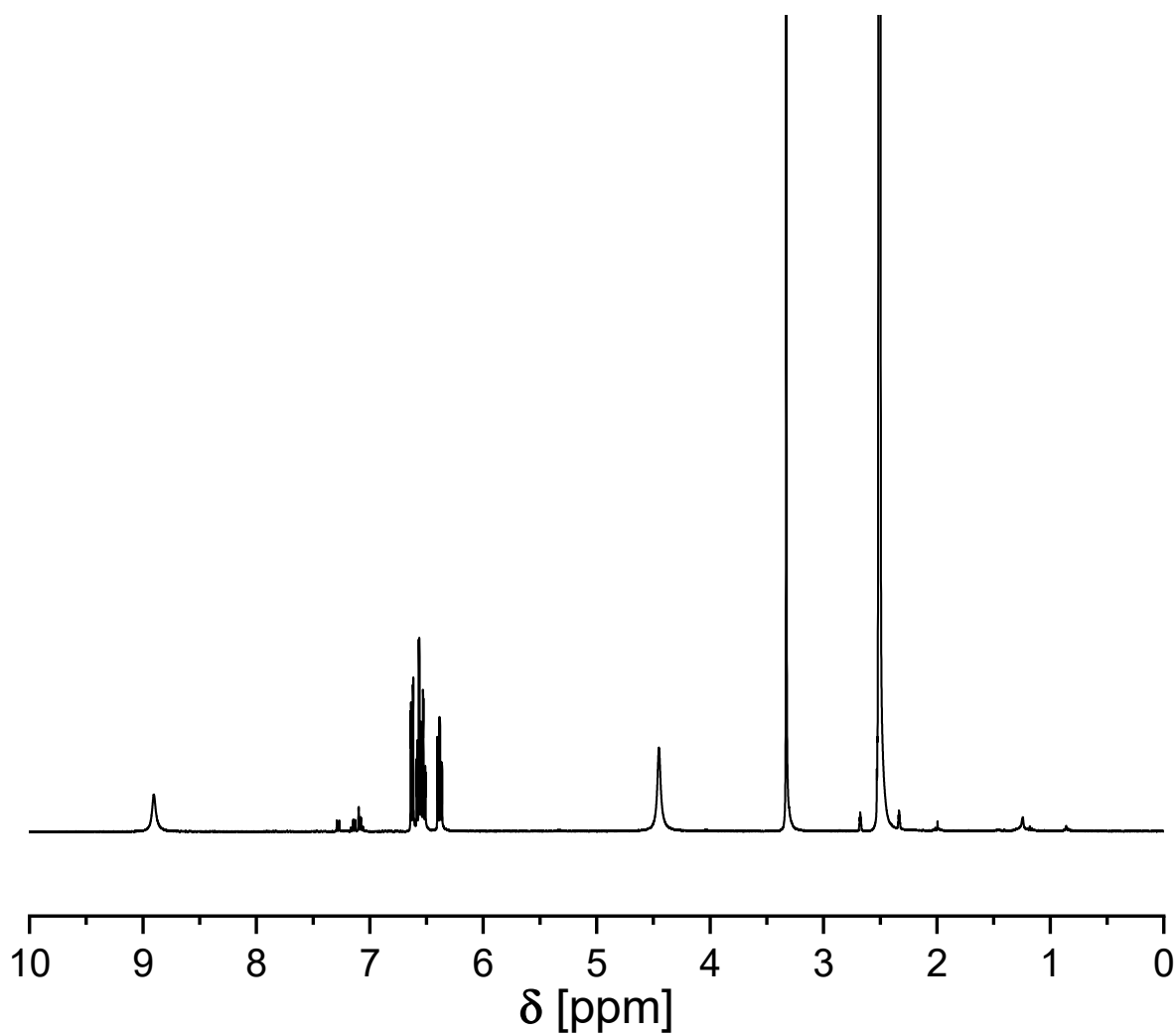
Figure 85 ^{1}H NMR spectrum of **2m2** (DMSO-d_6, 400 MHz).

Aniline **2n**
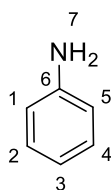
The CO_2 based Lossen rearrangement of *N*-hydroxybenzamide **1n** (1.00 eq.) with DBU (1.00 eq.) led to the formation of pure aniline **2n** as light-yellow liquid (56%). The crude was purified by column chromatography (cyclohexane/ethyl acetate 5:1 to 2:1).

^{1}H NMR (DMSO-d_6, 400 MHz) δ= 5.00 (s, 2H, NH$_2$^{7}), 6.55 (t, *J* = 7.1 Hz, 1H, CH^3), 6.63 –6.67 (m, 2H, CH$_2$^{2,4}), 7.04 – 7.09 (m, 2H, CH^{1,5}) ppm.

^{13}C NMR (DMSO-d_6, 100 MHz) δ= 114.4 (CH^{1,5}), 116.2 (C^3), 129.3 (CH^{2,4}), 149.1 (C^6) ppm.

HRMS-EI-MS of C_6H_8N [M+H]$^+$ calculated: 93.0573, found 93.0572.
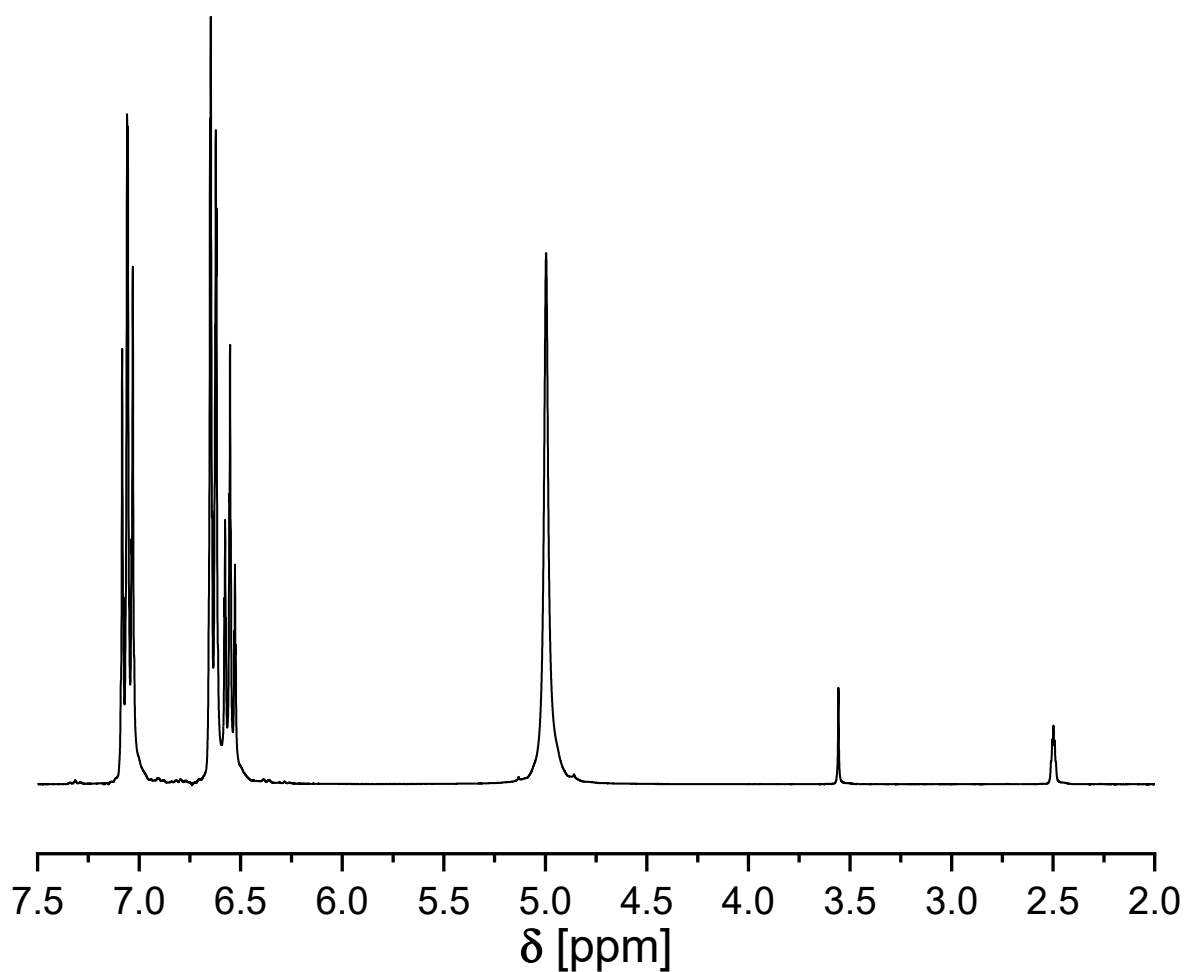
Figure 86 ^{1}H NMR spectrum of **2n** (DMSO-d_6, 400 MHz).

4-Methoxyaniline **2o**
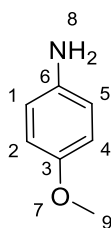
The CO_2 based Lossen rearrangement of *N*-hydroxy-4-methoxybenzamide **1o** (1.00 eq.) with DBU (1.00 eq.) led to the formation of pure 4-methoxyaniline **2o** as light yellow solid (50%). The crude was purified by column chromatography (cyclohexane/ethyl acetate 9:1 to 1:1).

^{1}H NMR (DMSO-d_6, 400 MHz) δ= 3.62 (s, 3H, CH_3^9), 4.58 (s, 2H, NH_2^8), 6.48 – 6.52 (m, 2H, $CH_2^{2,4}$), 6.62 –6.67 (m, 2 H, $CH_2^{1,5}$) ppm.

^{13}C NMR (DMSO-d_6, 100 MHz) δ= 55.8 (C^9), 115.0 ($C^{2,4}$), 115.4 ($C^{1,5}$), 142.8 (C^6), 151.1 (C^3) ppm.

HRMS-EI-MS of C_7H_9NO $[M]^+$ calculated: 123.0679, found 123.0680.
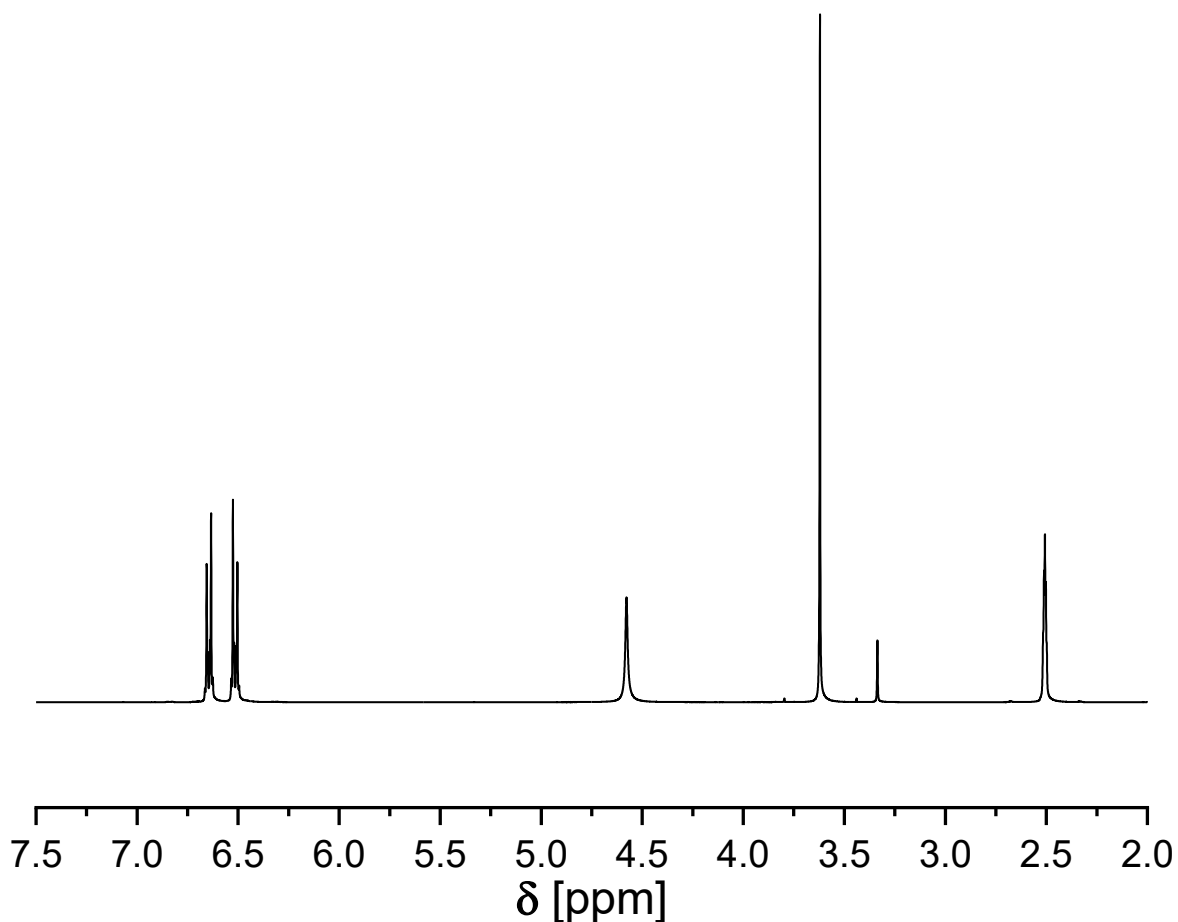
Figure 87 ^{1}H NMR spectrum of **2o** (DMSO-d_6, 400 MHz).

4-Chloroaniline **2p**
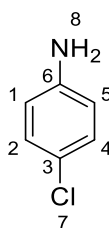
The CO_2 based Lossen rearrangement of *N*-hydroxy-4-chlorobenzamide **1p** (1.00 eq.) with DBU (1.00 eq.) led to the formation of pure 4-chloroaniline **2p** as white powder (49%). The crude was purified by column chromatography (cyclohexane/ethyl acetate 4:1 to 1:1).

^{1}H NMR (DMSO-d_6, 400 MHz) δ= 5.21 (br, s, 2H, NH$_2^8$), 6.52 – 6.56 (m, 2H, CH^{1,5}), 6.98 – 7.02 (m, 2H, CH^{2,4}) ppm.

^{13}C NMR (DMSO-d_6, 100 MHz) δ= 115.6 (CH^{1,5}), 119.2 (C^3), 128.9 (CH^{2,4}), 148.2 (C^6) ppm.

HRMS-EI-MS of C_6H_6NCl [M]$^+$ calculated: 127.0183, found 127.0182.
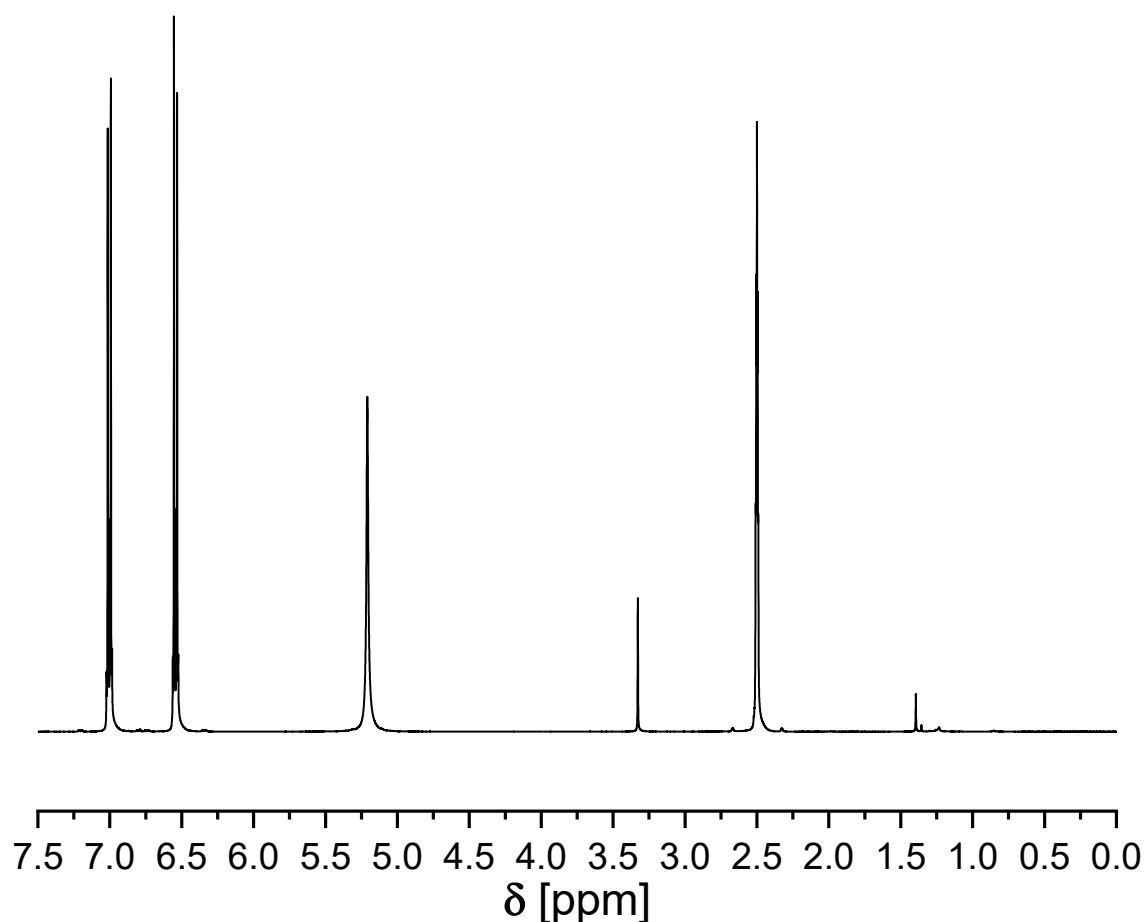
Figure 88 ^{1}H NMR spectrum of **2p** (DMSO-d_6, 400 MHz).

Experimental section

p-Toluidine **2q**
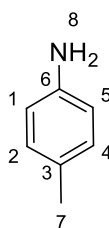
The CO_2 based Lossen rearrangement of *N*-hydroxy-4-methylbenzamide **1q** (1.00 eq.) with DBU (1.00 eq.) led to the formation of pure *p*-toluidine **2q** as light-yellow solid (54%). The crude was purified by column chromatography (cyclohexane/ethyl acetate 4:1 to 1:1).

¹H NMR (DMSO-d_6, 400 MHz) δ= 2.12 (s, 3H, CH$_3$[7]), 4.76 (s, 2H, NH$_2$[8]), 6.38 − 6.52 (m, 2H, CH[1,5]), 6.73 − 6.85 (m, 2H, CH[2,4]) ppm.

¹³C NMR (DMSO-d_6, 100 MHz) δ =20.6 (CH$_3$[7]), 114.9 (CH[1,5]), 124.4 (C[3]), 129.7(CH[2,4]), 146.5 (C[6]) ppm.

HRMS-EI-MS of C_7H_9N [M]⁺ calculated: 107.0730, found 107.0728.
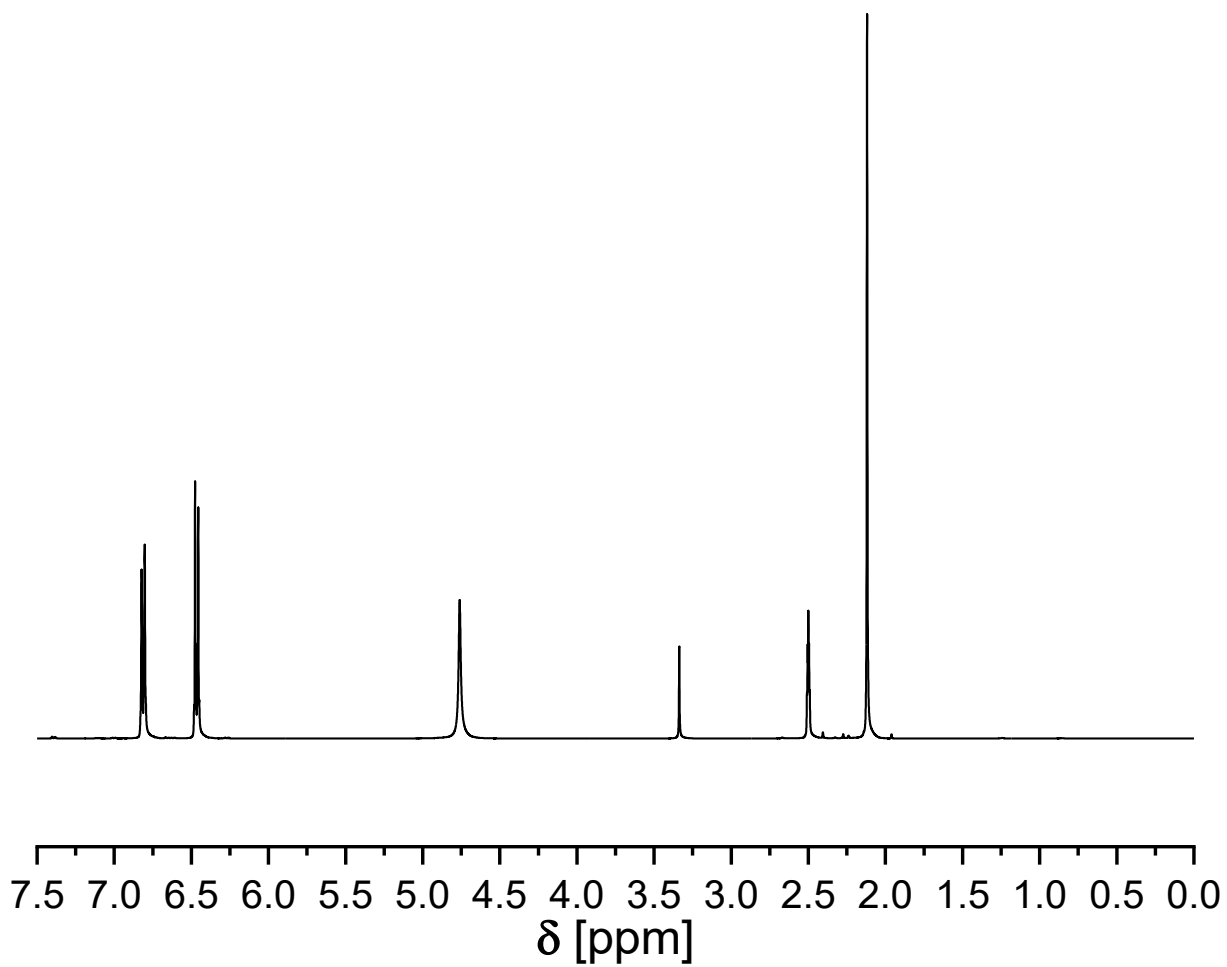
Figure 89 ^{1}H NMR spectrum of **2q** (DMSO-d$_6$, 400 MHz).

Experimental section

4-Nitroaniline **2r**
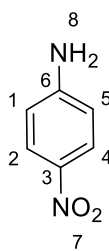
The CO_2 based Lossen rearrangement of *N*-hydroxy-4-nitrobenzamide **1r** (1.00 eq.) with DBU (1.00 eq.) led to the formation of pure 4-nitroaniline **2r** as yellow solid (47%). The crude was purified by column chromatography (cyclohexane/ethyl acetate 4:1 to 1:1).

¹H NMR (DMSO-d_6, 400 MHz) δ= 6.57 – 6.62 (m, 2H, CH^{1,5}), 6.68 (s, 2H, NH$_2^8$), 7.89 – 7.97 (m, 2H, CH^{2,4}) ppm.

¹³C NMR (DMSO-d_6, 100 MHz) δ=112.8 (CH^{1,5}), 126.8(CH^{2,4}), 136.1 (C^3), 156.2 (C^6) ppm.

HRMS-EI-MS of $C_6H_7N_2O_2$ [M+H]$^+$ calculated: 138.0424, found 138.0424.
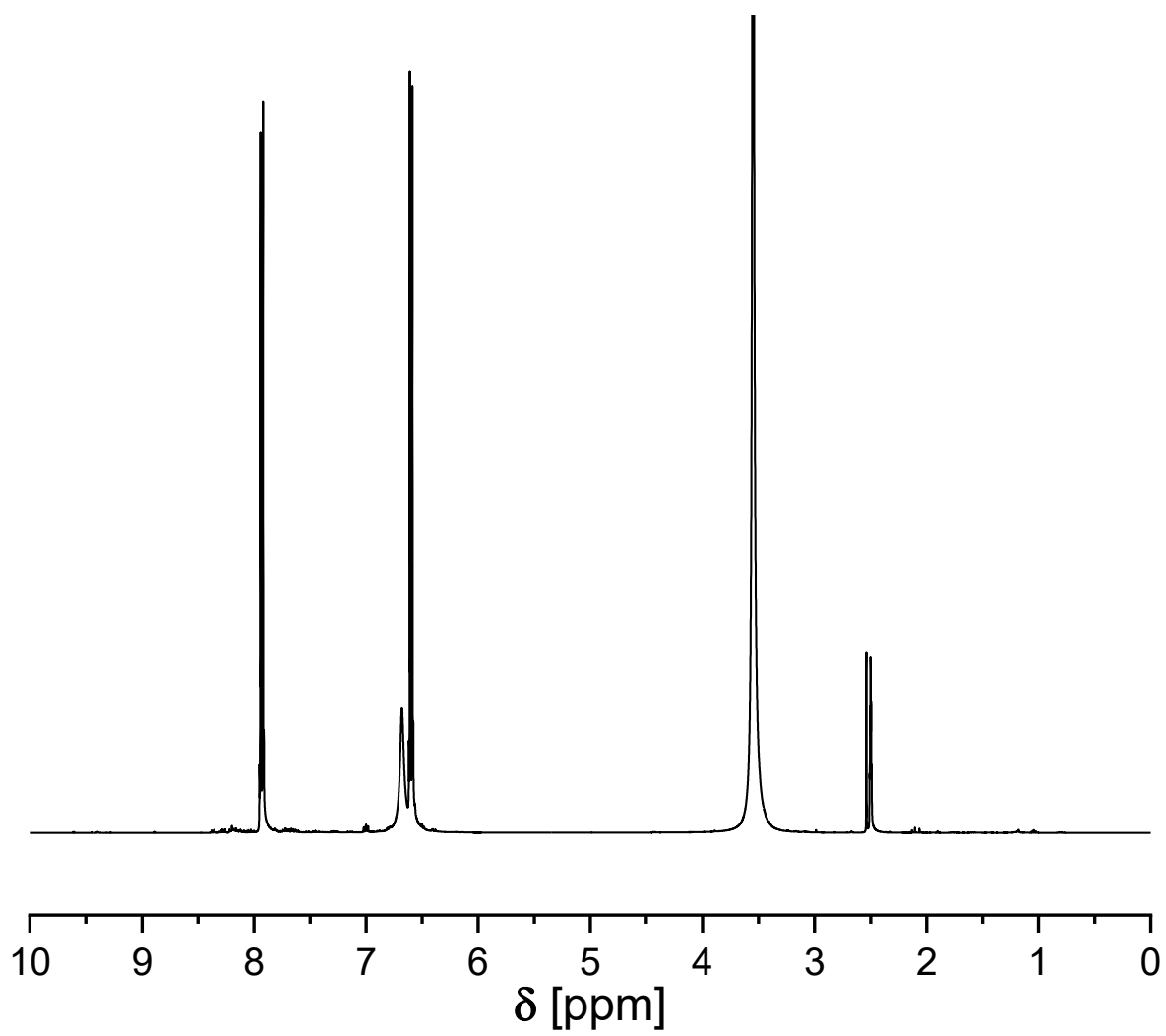
Figure 90 ^{1}H NMR spectrum of **2r** (DMSO-d_6, 400 MHz).

Experimental section

3,4,5-trimethoxyaniline 2s
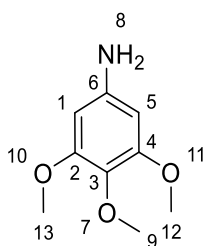
The CO_2 based Lossen rearrangement of *N*-hydroxy-3,4,5-trimethoxybenzamide **1s** (1.00 eq.) with DBU (1.00 eq.) led to the formation of pure 3,4,5-trimethoxyaniline **2s** as white solid (47%). The crude was purified by column chromatography (cyclohexane/ethyl acetate 4:1 to 1:2).

^{1}H NMR (DMSO-d_6, 400 MHz) δ= 3.34 (s, 3H, CH$_3{}^{9}$), 3.66 (s, 6H, CH$_3{}^{12,13}$), 4.85 (s, 2 H, NH$_2{}^{8}$), 5.87 (s, 2H, CH^{1,5}) ppm.

^{13}C NMR (DMSO-d_6, 100 MHz) δ= 55.8 (CH$_3{}^{12,13}$), 60.6 (CH$_3{}^{9}$), 92.0 (CH^{1,5}), 128.8 (C^3), 145.6 (C^6), 153.8 (C^{2,4}) ppm.

HRMS-EI-MS of $C_9H_{13}NO_3$ [M]$^+$ calculated: 183.0890, found 183.0890.
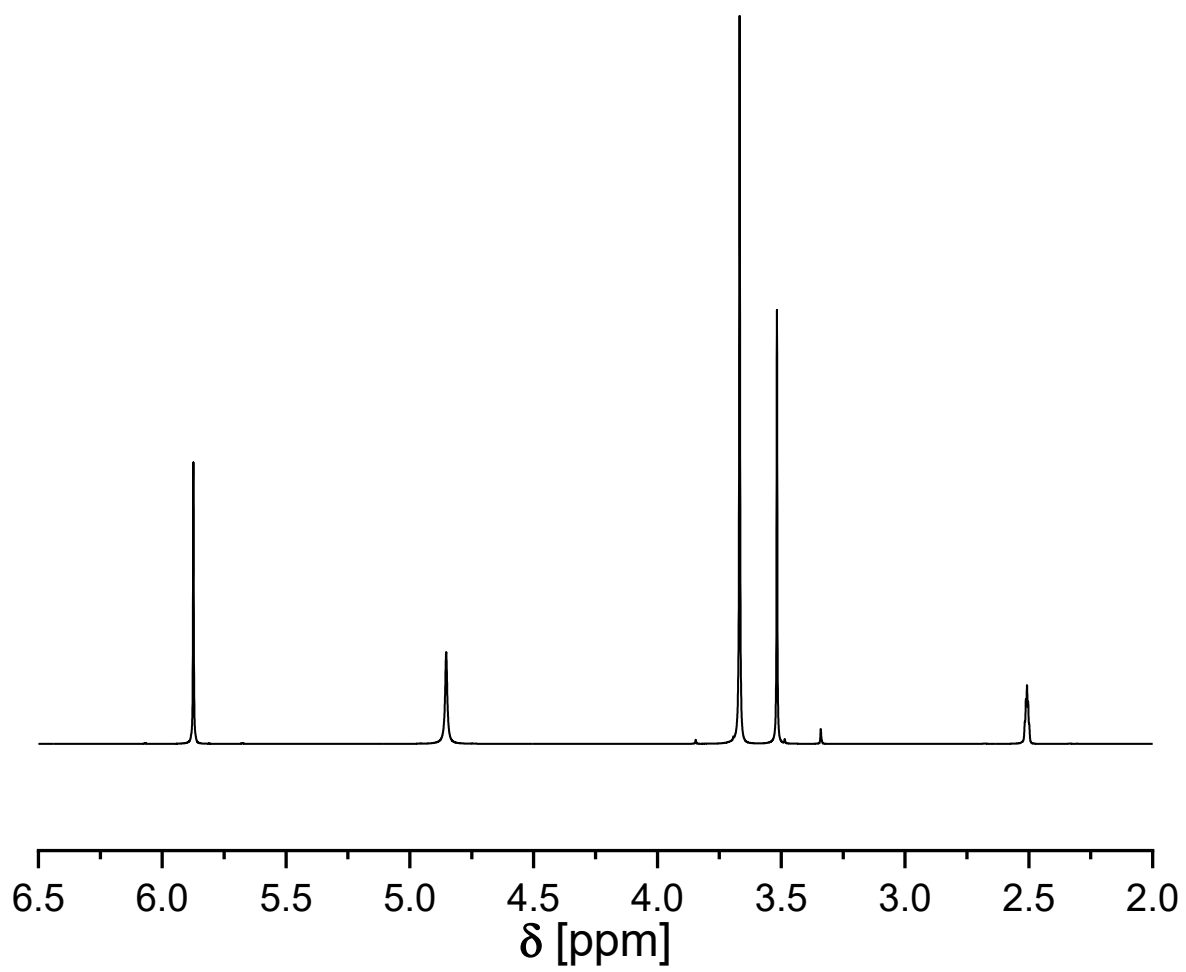
Figure 91 ^{1}H NMR spectrum of **2s** (DMSO-d_6, 400 MHz).

5.1.6 Calibration curves for GC analysis

Equation	y = a + b*x
Weight	No Weighting
Intercept	0 ± --
Slope	1.17531 ± 0.02604
R-Square (COD)	0.99755
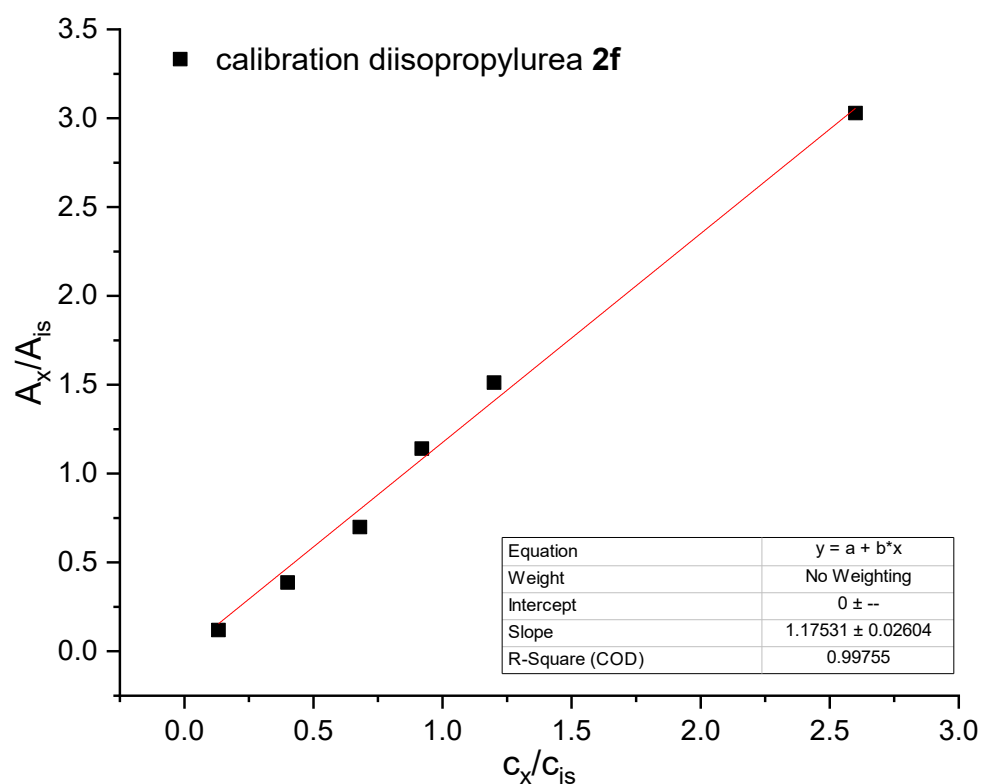
Figure 92 GC calibration curve for diisopropylurea **2f**.

Equation	y = a + b*x
Weight	No Weighting
Intercept	0 ± --
Slope	0,38263 ± 0,0049
Adj. R-Square	0.99915
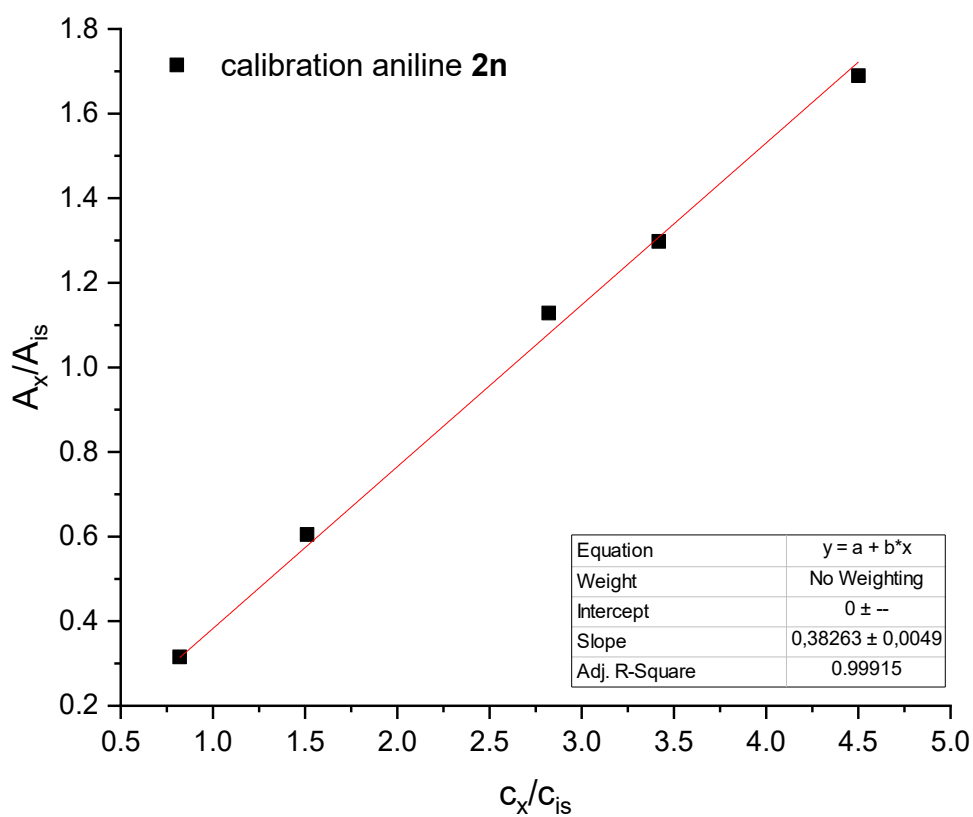
Figure 93 GC calibration curve for aniline **2n**.
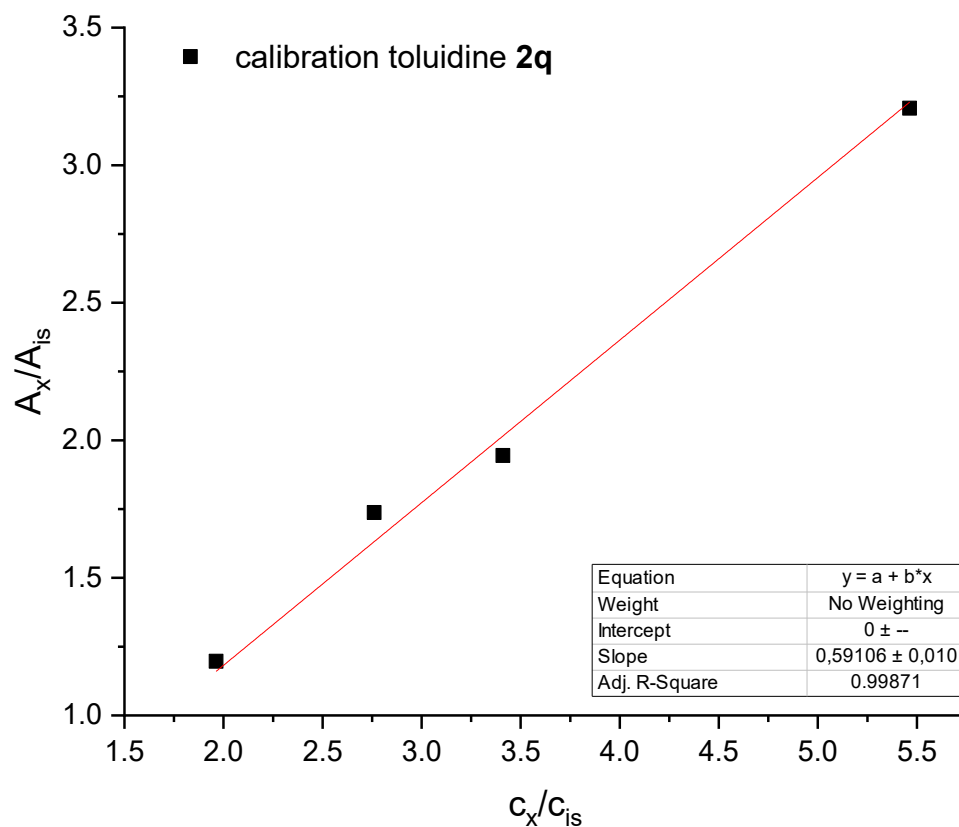
Figure 94 GC calibration curve for p-toluidine **2q**.

Equation	y = a + b*x
Weight	No Weighting
Intercept	0 ± --
Slope	0,59106 ± 0,010
Adj. R-Square	0.99871
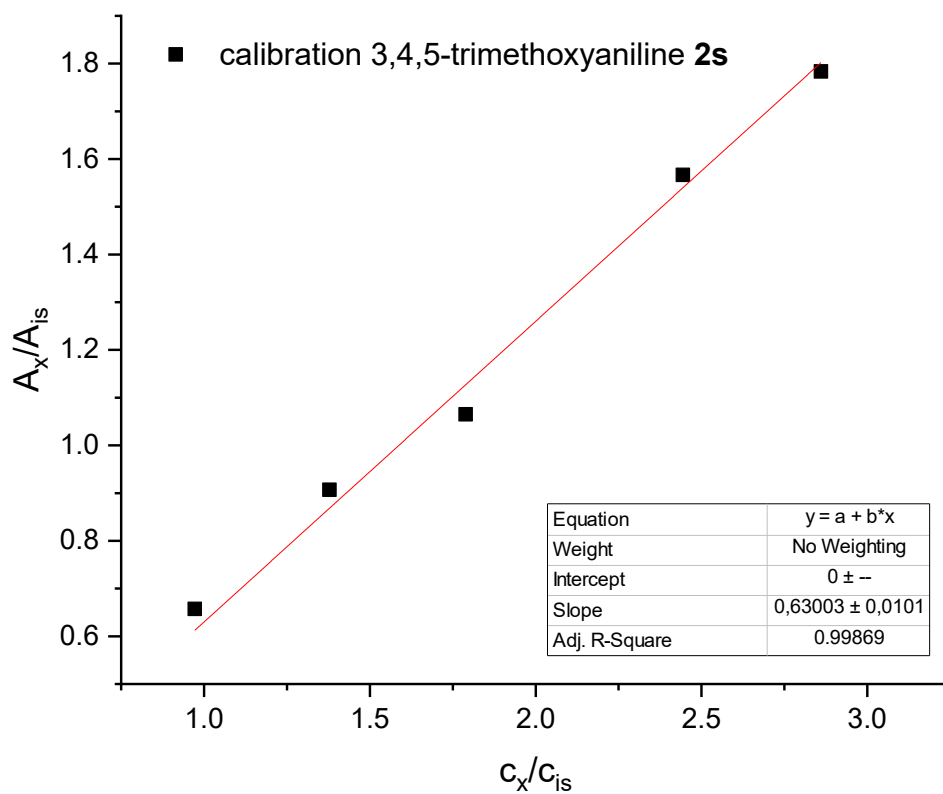
Figure 95 GC calibration curve for 3,4,5-trimethoxyaniline **2s**.

Equation	y = a + b*x
Weight	No Weighting
Intercept	0 ± --
Slope	0,63003 ± 0,0101
Adj. R-Square	0.99869

5.1.7 General procedure for online-IR experiments

The DST 6.35 x 1.5 m probe was first coupled with the Parr 130 mL pressure vessel and the measurement was started, followed by the addition of the solvent. Afterwards each component was added to the solvent separately in order for the detector to separate each spectrum. After the addition of all required chemicals, the pressure vessel was closed, and the desired CO_2 pressure (5-30 bar) was set. The pressure vessel was then heated to the required temperature and the reaction mixture is stirred for the desired time.

5.2 Experimental section -Diene and dithiol monomers

5.2.1 Materials

(+)-limonene (96%, ACROS Organics), allyl amine (98%, Alfa Aesar), gamma-terpinene (97%, Sigma-Aldrich), 1,4-cyclohexadiene (97%, ACROS Organics), thioacetic acid (97%, abcr GmbH), allyl alcohol (99%, ACROS Organics), 1,5,7-triazabicyclo[4.4.0]dec-5ene (TBD, 98%, Sigma-Aldrich), dimethyl carbonate (anhydrous, Sigma-Aldrich), gamma-valerolactone (99%, Sigma-Aldrich), dimethyl sulfoxide (99.9%, Fisher Chemical), cyclohexane and ethyl acetate were used in a purity above technical grade.

5.2.2 Additional analytical methods

Infrared (IR) spectra of all samples were recorded on a Bruker alpha-p instrument in a frequency range from 3998 to 374 cm^{-1} using ATR technology.

Diallyl carbonate
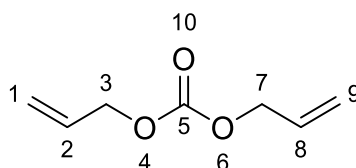
The transesterification of dimethyl carbonate (1.00 eq.) with allyl alcohol (2.10 eq.) catalyzed by TBD (0.20 eq) led to the formation of diallyl carbonate as a colorless liquid (60%).

^{1}H NMR (CDCl$_3$, 400 MHz) δ= 4.64 (dt, *J* = 5.8, 1.4 Hz, 4H, CH$_2$^{3,7}), 5.42 – 5.23 (m, 4H, CH$_2$^{1,9}), 5.94 (ddt, *J* = 17.3, 10.5, 5.8 Hz, 2H, CH^{2,8}) ppm.

^{13}C NMR (CDCl$_3$, 100 MHz) δ= 68.4 (C^{3,7}), 118.9 (C^{1,9}), 131.6 (C^{2,8}), 154.8 (C^5) ppm.

IR (ATR) ṽ = 3021, 2951, 1743 (carbonate), 1650, 1451, 1376, 1294, 1237, 1064, 963, 932, 790 cm^{-1}.

HRMS-EI [M+H$^+$] of C$_7$H$_{11}$O$_3$ calculated 143.0703, found: 143.0703.
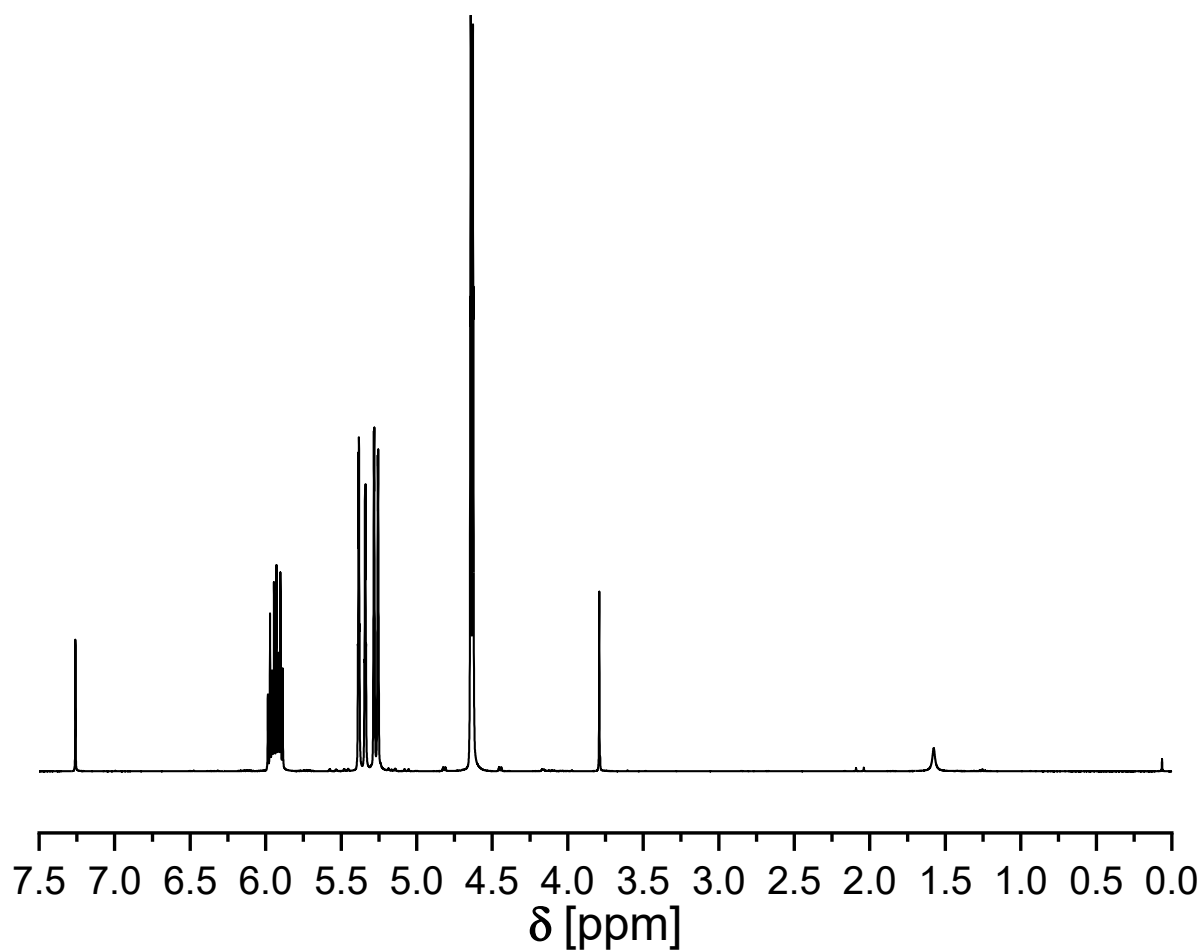
Figure 96 ^{1}H NMR spectrum of diallyl carbonate (CDCl$_3$, 400 MHz). The impurity at 3.79 ppm belongs to the residual methyl carbonate (0.12 integral, normalized).

Allyl allylcarbamate **3**
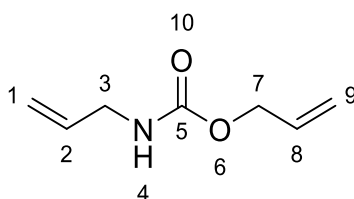
The reaction of diallyl carbonate (1.00 eq.) with allylamine (3.00 eq.) at 50 °C for 48 h led to the formation of *N*-allyl allylcarbamate **3** in form of a colorless liquid (75%).

^{1}H NMR (CDCl$_3$, 400 MHz) δ= 3.81 (t, *J* = 5.5 Hz, 2H, CH$_2^3$), 4.57 (d, *J* = 5.7 Hz, 2H, CH$_2^7$), 4.84 (br, s, 1H, NH^4), 5.10-5.33 (m, 4H, CH$_2^{1,9}$), 5.77 – 5.98 (m, 2H, CH^{2,8}) ppm.

^{13}C NMR (CDCl$_3$, 100 MHz) δ= 43.5 (C^3), 65.6 (C^7), 116.0 (C^9), 117.7 (C^1), 132.9 (C^2), 134.5 (C^8), 156.1 (C^5) ppm.

HRMS-EI-MS of C$_7$H$_{11}$NO$_2$ [M]$^+$ calculated: 141.0784, found 141.0786.

IR (ATR) ṽ = 3330.1, 3081.3, 2929.0, 1694.9 (amide), 1647.6, 1520.1, 1460.4, 1421.3, 1396.6, 1324.6, 1238.3, 1147.8, 1137.5, 1061.4, 1032.6, 987.3, 917.4, 777.5, 627.4, 547.1 cm^{-1}.
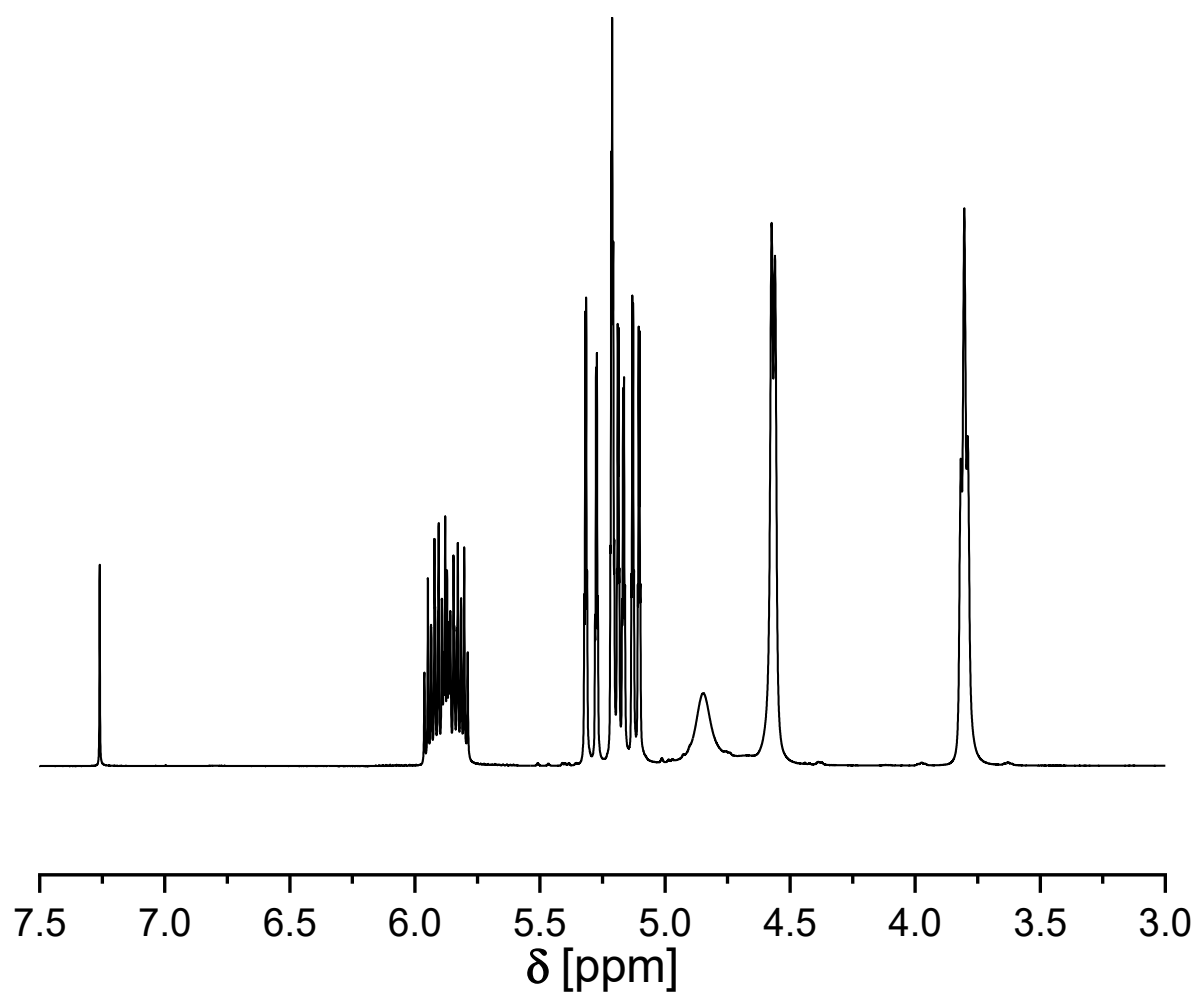
Figure 97 ^{1}H NMR spectrum of **3** (400 MHz, CDCl$_3$).

5.2.3 General procedure for the synthesis of carbamates and ureas *via* the Lossen rearrangement

The hydroxamic acid (1.00 eq.) was dissolved in diallyl carbonate (20.0 eq.) and allyl alcohol (2.00 eq.). After addition of TBD (0.20 eq.), the reaction mixture was stirred at 110 °C for 20 h. The mixture was allowed to cool down to ambient temperature. The urea, precipitated as white solid during the cooling, was filtered, washed with diallyl carbonate and acetonitrile, and dried in vacuo. The reaction mixture was freed from the solvent and unreacted allyl alcohol by vacuum distillation, and the residue is purified via flash column chromatography (CH/EA, 9:1). If a dihydroxamic acid was employed, DMSO was added as cosolvent and the equivalents for TBD (0.60 eq.) and allyl alcohol (4.00 eq.) were increased.

Experimental section

Allyl dec-9-enylcarbamate **4**
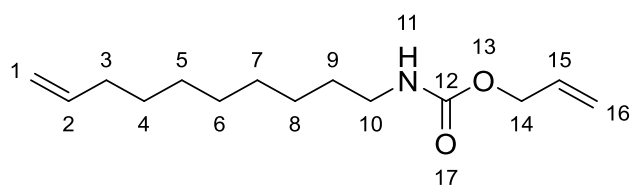
The Lossen Rearrangement of *N*-Hydroxyundeceneamide **1e** (1.00 eq.) in allyl alcohol (2.00 eq.) and diallyl carbonate catalyzed by TBD (0.20 eq.) led to the formation of allyl dec-9-enyl carbamate **4** as a colorless viscous liquid (64%).

^{1}H NMR (CDCl$_3$, 300 MHz) δ= 1.24-1.38 (m, 10H, CH$_2$$^{4-8}$), 1.48 (p, *J* = 6.5 Hz, 6.6 Hz, 2H, CH$_2$^{9}), 2.01 (q, *J* = 6.5 Hz, 2H, CH$_2$^{3}), 3.15 (q, *J* = 6.5 Hz, 2H, CH$_2$^{10}), 4.55 (d, *J* = 5.5 Hz, 2H, CH$_2$^{14}), 4.74 (br, s, 1H, NH^{11}), 4.85 − 5.01 (m, 2H, CH$_2$^{1}), 5.17 − 5.32 (m, 2H, CH$_2$^{16}), 5.79, (tdd, *J* = 16.9 Hz, 10.2 Hz, 6.5 Hz, 2H, CH^2), 5.91, (tdd, *J* = 16.3 Hz, 10.9 Hz, 5.9 Hz, 2H, CH^2) ppm.

^{13}C NMR (CDCl$_3$, 75 MHz) δ= 26.9 (CH$_2$^{8}), 28.9 (CH$_2$$^{4-7}$), 29.0 (CH$_2$$^{4-7}$), 29.2 (CH$_2$$^{4-7}$), 29.4 (CH$_2$$^{4-7}$), 30.0 (CH$_2$^{9}), 33.8 (CH$_2$^{3}), 41.1 (CH$_2$^{10}), 65.4 (CH$_2$^{14}), 114.2 (CH$_2$^{1}), 117.5 (CH$_2$^{16}), 133.1 (CH^{15}), 139.2 (CH^2), 156.3 (CO^{12}) ppm.

ESI-MS of C$_{14}$H$_{25}$NO$_2$ [M+H]$^+$ calculated: 240.1958, found 240.1952.

IR (ATR) ṽ = 3335.5, 2925.4, 2854.5, 1697.2 (amide), 1641.3, 1530.2, 1462.6, 1245.9, 1137.6, 991.8, 909.3, 776.9, 722.9, 634.8, 552.5 cm^{-1}.

Figure 98 ^{1}H NMR spectrum of **4** (400 MHz, CDCl$_3$).

Experimental section

Allyl (Z)-heptadec-8-en-1-ylcarbamate 5

The Lossen rearrangement of *N*-hydroxy oleamide **1a** (1.00 eq.) in diallyl carbonate and allyl alcohol (2.00 eq.) catalyzed by TBD (0.20 eq.) led to the formation of allyl (*Z*)-heptadec-8-en-1-ylcarbamate **5** as colorless oil (40%).

^{1}H NMR (CDCl$_3$, 400 MHz) δ= 0.88 (t, *J* = 7.1, 6.6 Hz, 3H, CH$_3$^{1}), 1.26 (m, 20H, CH$_2$$^{2-7,12-15}$), 1.48 (p, *J* = 7.0, 6.4 Hz, 2H, CH$_2$^{16}), 2.00 (q, *J* = 6.7, 6.4, 5.9 Hz, 4H, CH$_2$^{8,11}), 3.18 (q, *J* = 6.7 Hz, 2H, CH$_2$^{17}), 4.56 (d, *J* = 5.9 Hz, 2H, CH$_2$^{22}), 4.69 (br, s, 1H, NH^{18}), 5.18 – 5.39 (m, 4H, CH^{9,10}, CH$_2$^{24}), 5.92 (ddt, *J* = 16.2, 10.9, 5.6 Hz, 1H, CH^{23}) ppm.
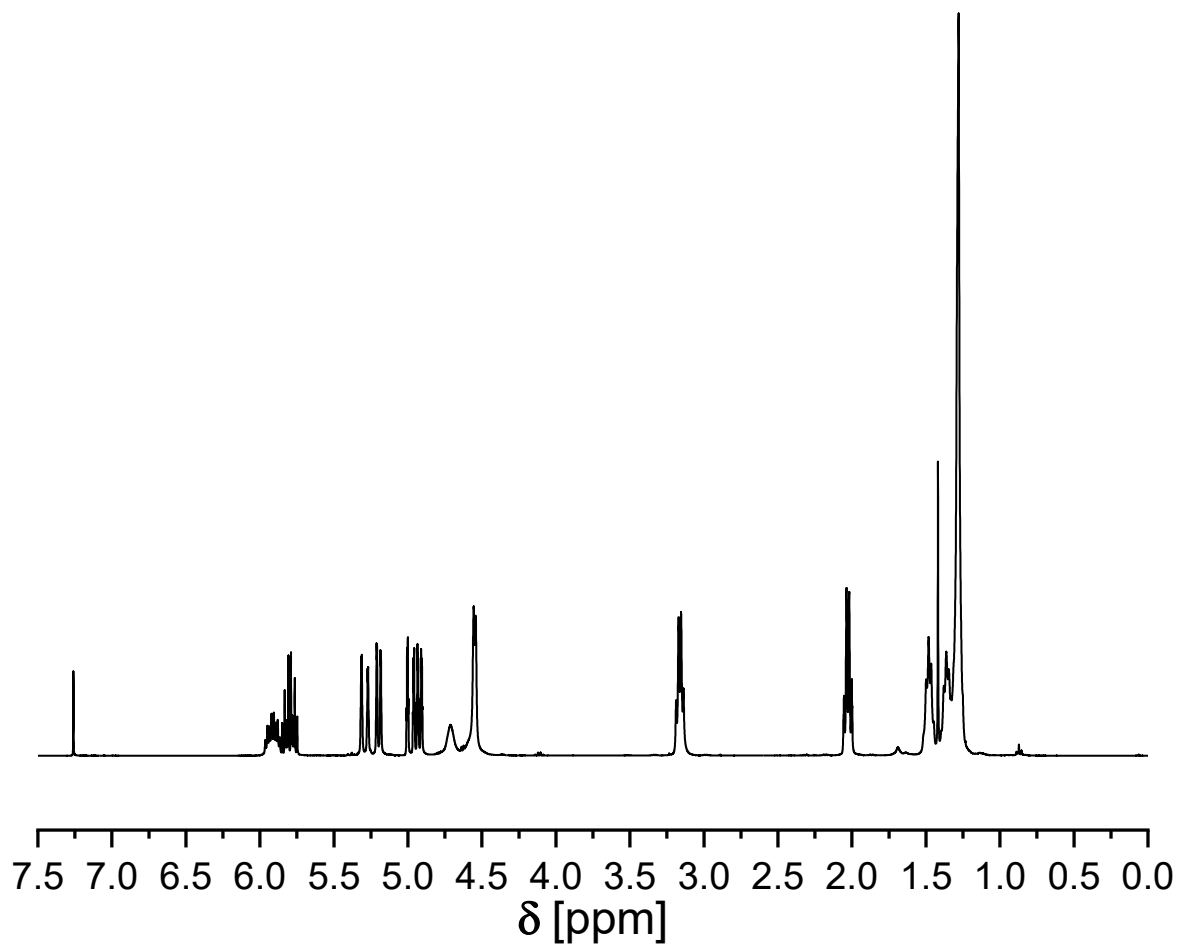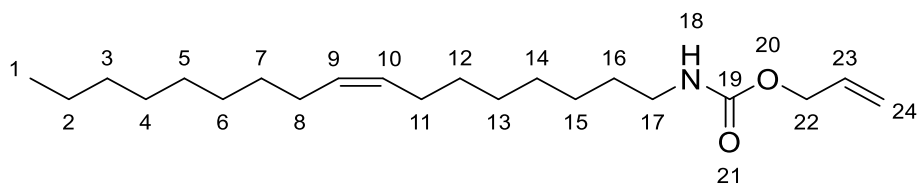
^{13}C NMR (CDCl$_3$, 100 MHz) δ= 14.1 (C^1), 22.7 (C^2), 26.7 (C^{15}), 27.2 (C^{8,11}), 27.2 (C^{8,11}), 29.2 (C^4), 29.3(C^{16}), 29.3 (C^{5,6}), 29.5(C^{14}), 29.7 (C^{13}), 29.8 (C^7), 30.2 (C^{12}), 31.9 (C^3), 41.1 (C^{17}), 65.4 (C^{22}), 117.6 (C^{24}), 129.7 (C^{9,10}), 130.0 (C^{9,10}), 133.1 (C^{23}), 156.2 (CO^{19}) ppm.

ESI-MS of C$_{21}$H$_{39}$NO$_2$ [M+H]$^+$ calculated: 338.3054, found 338.3051.

IR (ATR) ṽ = 3339.5, 2922.9, 2853.3, 1699.2 (amide), 1530.0, 1462.8, 1248.3, 1137.8, 992.0, 926.1, 776.3, 722.2 cm^{-1}.
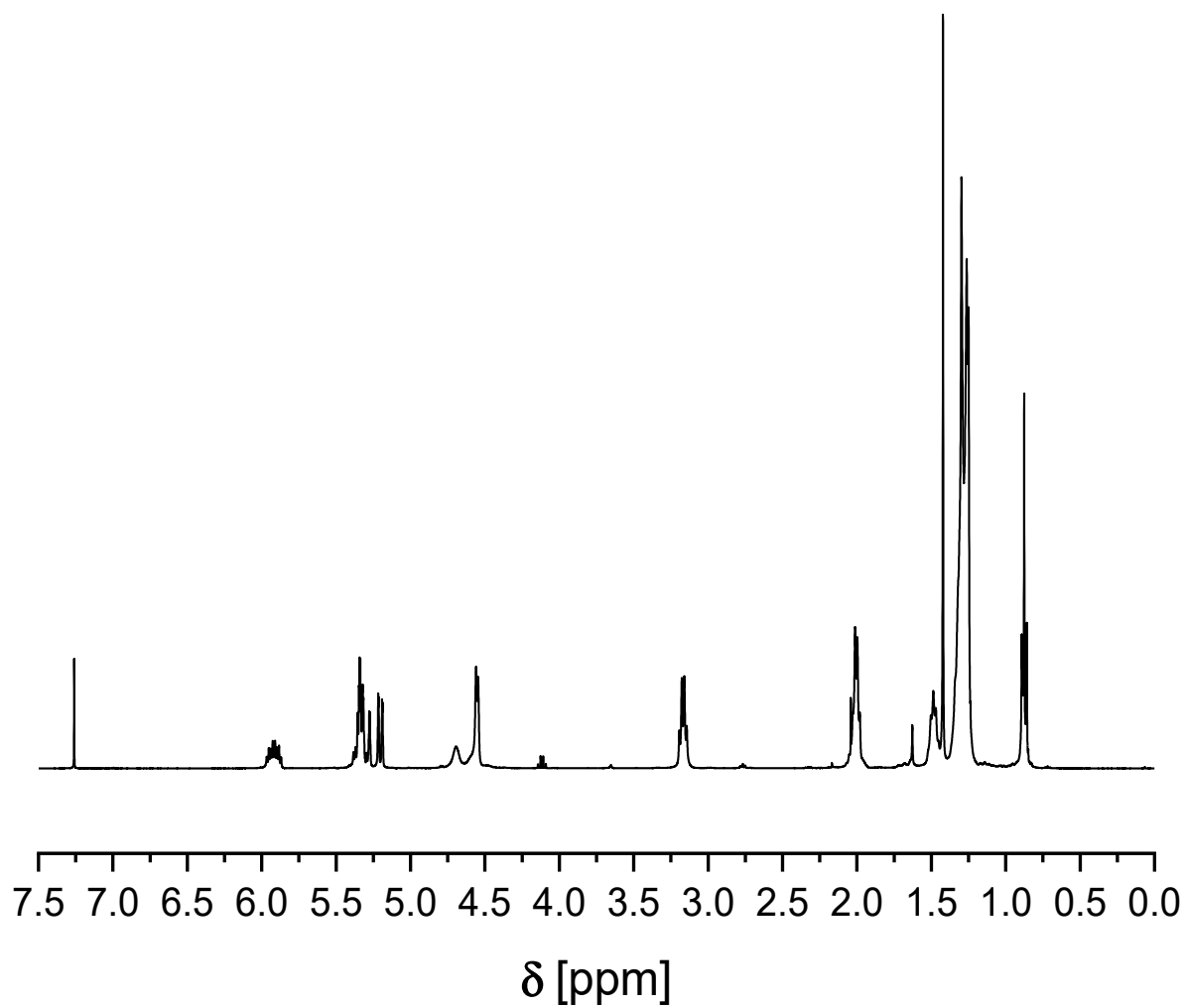
Figure 99 ^{1}H NMR spectrum of **5** (400 MHz, CDCl₃).

Experimental section

Diallyl butane-1,4-diyldicarbamate **6**
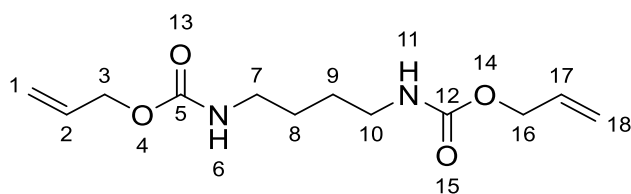
The Lossen Rearrangement of N^1,N^6-dihydroxyadipamide **1i** (1.00 eq.) in allyl alcohol (4.00 eq.) and diallyl carbonate catalyzed by TBD (0.60 eq.) led to the formation of diallyl butane-1,4-diyldicarbamate **6** as a colorless solid (15%).

^{1}H NMR (CDCl$_3$, 400 MHz) δ= 1.39 − 1.59 (m, 4H, CH$_2^{8,9}$), 3.20 (p, J = 5.6 Hz, 4H, CH$_2^{7,10}$), 4.55 (d, J = 5.7 Hz, 4H, CH$_2^{3,16}$), 4.77 (br, s, 2H, NH^{6,11}), 5.05 − 5.52 (m, 4H, CH$_2^{1,2,17,18}$), 5.92 (ddt, J = 16.4, 10.9, 5.6 Hz, 2H, CH^{3,17}) ppm.

^{13}C NMR (CDCl$_3$, 400 MHz) δ= 27.3 (C^{8,9}), 40.6 (C^{7,10}), 65.5 (C^{3,16}), 117.7 (C^{1,18}), 132.9 (C^{2,17}), 156.3 (C^{5,12}) ppm.

IR (ATR) ṽ = 3320.3, 2953.2, 2880.1, 1683.9 (amide), 1649.5, 1525.0, 1477.1, 1457.5, 1422.8, 1422.8, 1270.9, 1230.9, 1134.9, 1037.7, 989.4 cm^{-1}.

HRMS-EI-MS of C$_{12}$H$_{20}$N$_2$O$_4$ [M]$^+$ calculated: 256.1418, found 256.1420.
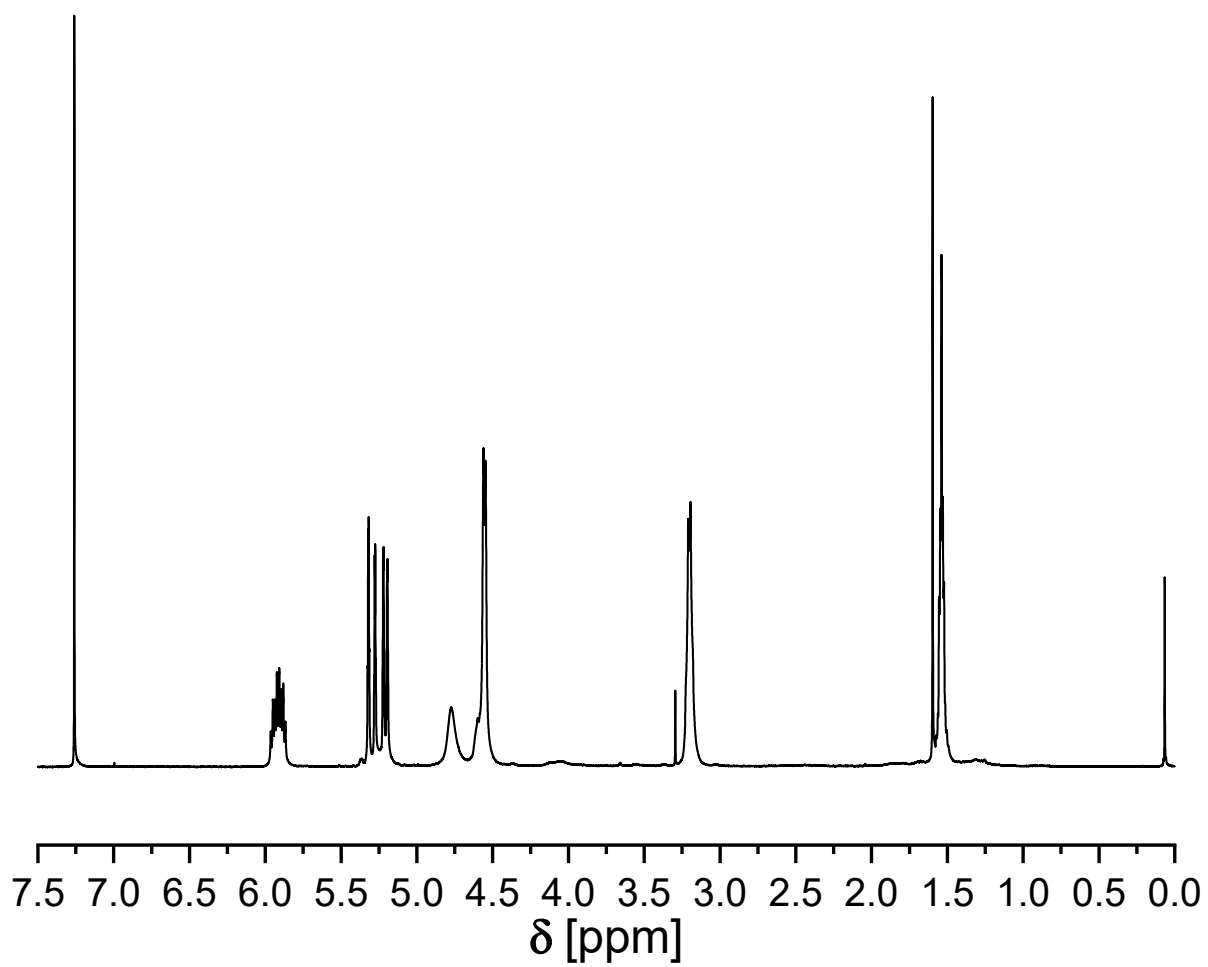
Figure 100 ^{1}H NMR spectrum of **6** (400 MHz, CDCl$_3$).

Diallyl dodecane-1,12-diyldicarbamate **7**
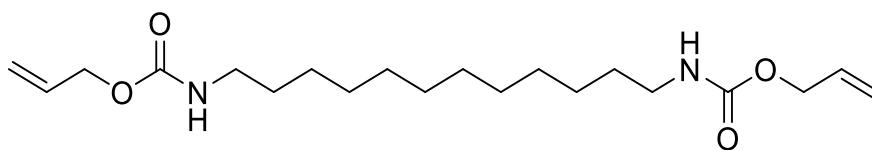
The product of the Lossen rearrangement of tetradecane dihydroxamic acid **1k** was identified by FAB-MS, however the bisallylcarbamate **7** was not isolated from the crude mixture. The urea side product **8** was also detected with the same method alongside the respective carbamate.

FAB-MS of $C_{20}H_{37}N_2O_4$ [M+H]$^+$ calculated: 369.2748, found 369.2750.
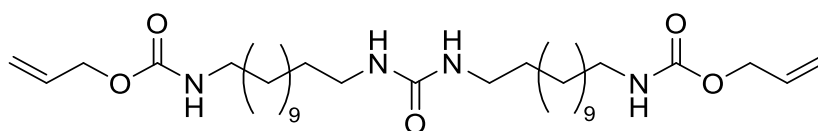
ESI-MS of $C_{33}H_{62}N_4O_5$ (M+H): calculated 595.4792, found 595.4792.

IR (ATR) $\tilde{v}$ = 3309.6, 2929.0, 2875.6, 2852.9, 1682.6 (amide, carbamate), 1622.9 (amide, urea), 1571.5, 1536.5, 1478.9, 1466.6, 1448.1, 1423.4, 1367.8, 1304.1, 1246.5, 1205.3, 1141.6, 1123.1, 1084.0, 1040.8, 1026.4, 987.3, 923.6, 781.6, 728.1, 701.4 cm^{-1}.
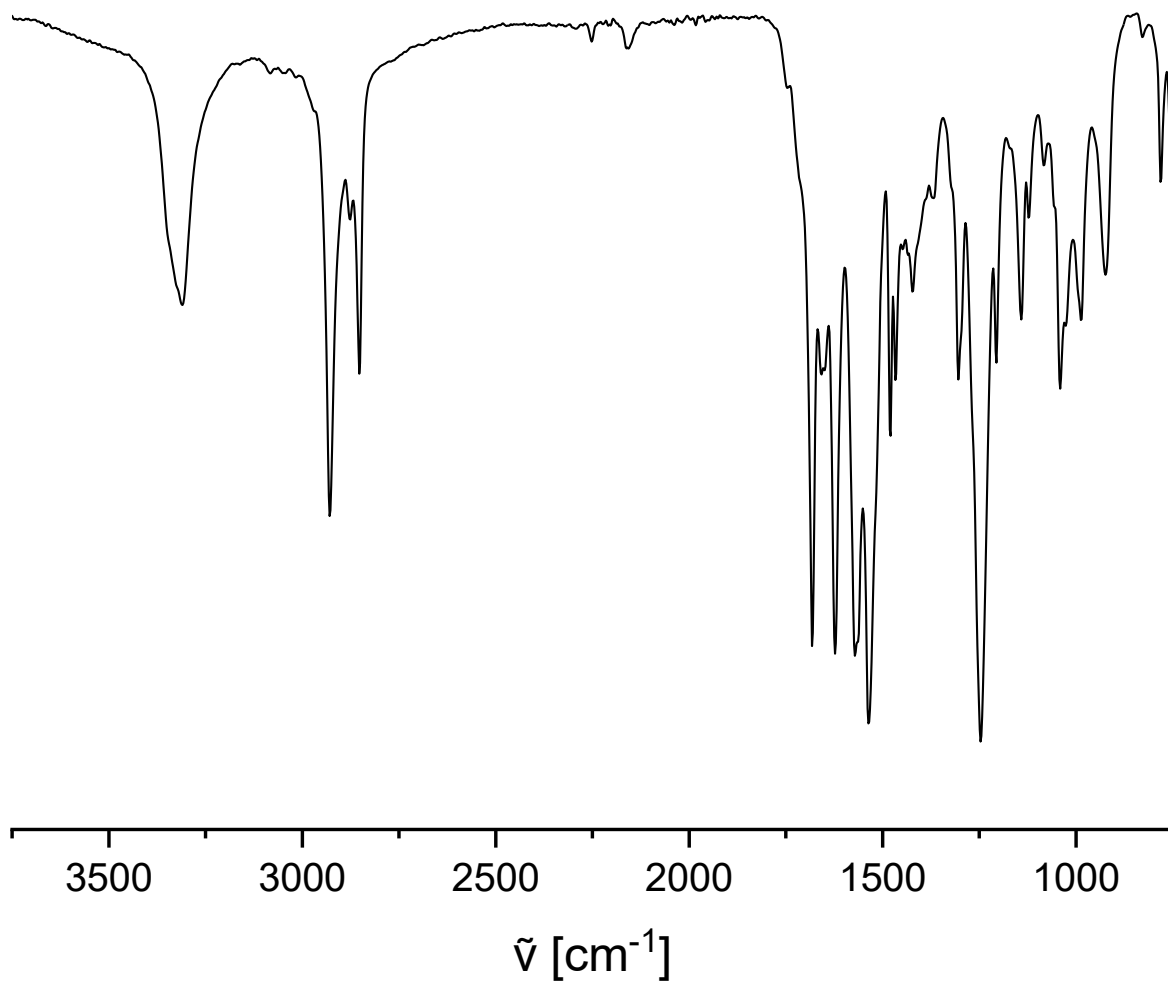
Figure 101 IR spectrum of the mixture containing both carbamate **7** and urea **8**. Both carbonyl species are clearly visible at ca.1680 and 1620 cm^{-1}, respectively.

Experimental section

1,3-Di(dec-9-en-1-yl)urea 9
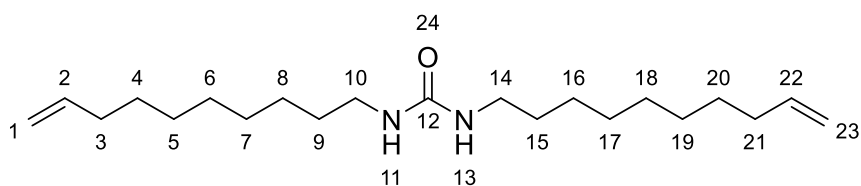
The side reaction of the Lossen rearrangement of *N*-Hydroxyundeceneamide **1e** (1.00 eq.) in allyl alcohol (2.00 eq.) and diallyl carbonate catalyzed by TBD (0.20 eq.) led to the formation of 1,3-di(dec-9-en-1-yl)urea **9** as a colorless solid (12%).

¹H NMR (CDCl₃, 300 MHz) δ= 1.24 − 1.40 (m, 20H, CH₂$^{4\text{-}8,16\text{-}20}$), 1.48 (p, *J* = 7.0 Hz, 6.6 Hz, 4H, CH₂^{9,15}), 2.02 (q, *J* = 6.8 Hz, 4H, CH₂^{3,21}), 3.14 (q, *J* = 7.2 Hz, 4H, CH₂^{10,14}), 4.37 (br, s, 2H, NH^{11,13}), 4.90 − 5.02 (m, 4H, CH₂^{1,23}), 5.75-5.86 (tdd, *J* = 16.9 Hz, 10.3 Hz, 6.8 Hz, 4H, CH₂^{2,22}) ppm.

¹³C NMR (CDCl₃, 75 MHz) δ= 27.0 (CH₂^{8,16}), 28.9 (CH₂$^{4\text{-}7,17\text{-}20}$), 29.1 (CH₂$^{4\text{-}7,17\text{-}20}$), 29.4 (CH₂$^{4\text{-}7,17\text{-}20}$), 29.4 (CH₂$^{4\text{-}7}$), 30.3 (CH₂^{9,15}), 33.8 (CH₂^{3,21}), 40.5 (CH₂^{10,14}), 114.2 (CH₂^{1,23}), 139.1 (CH^{2,22}), 158.6 (CO^{12}) ppm.

ESI-MS of C₂₁H₄₀N₂O [M+H]⁺ calculated: 337.3214, found 337.3205.

IR (ATR) ṽ = 3334.2, 2921.5, 2850.3, 1615.1 (amide), 1571.5, 1477.4, 1465.0, 1253.7, 1229.5, 1075.3, 990.8, 909.0, 723.3, 615.6 cm⁻¹.
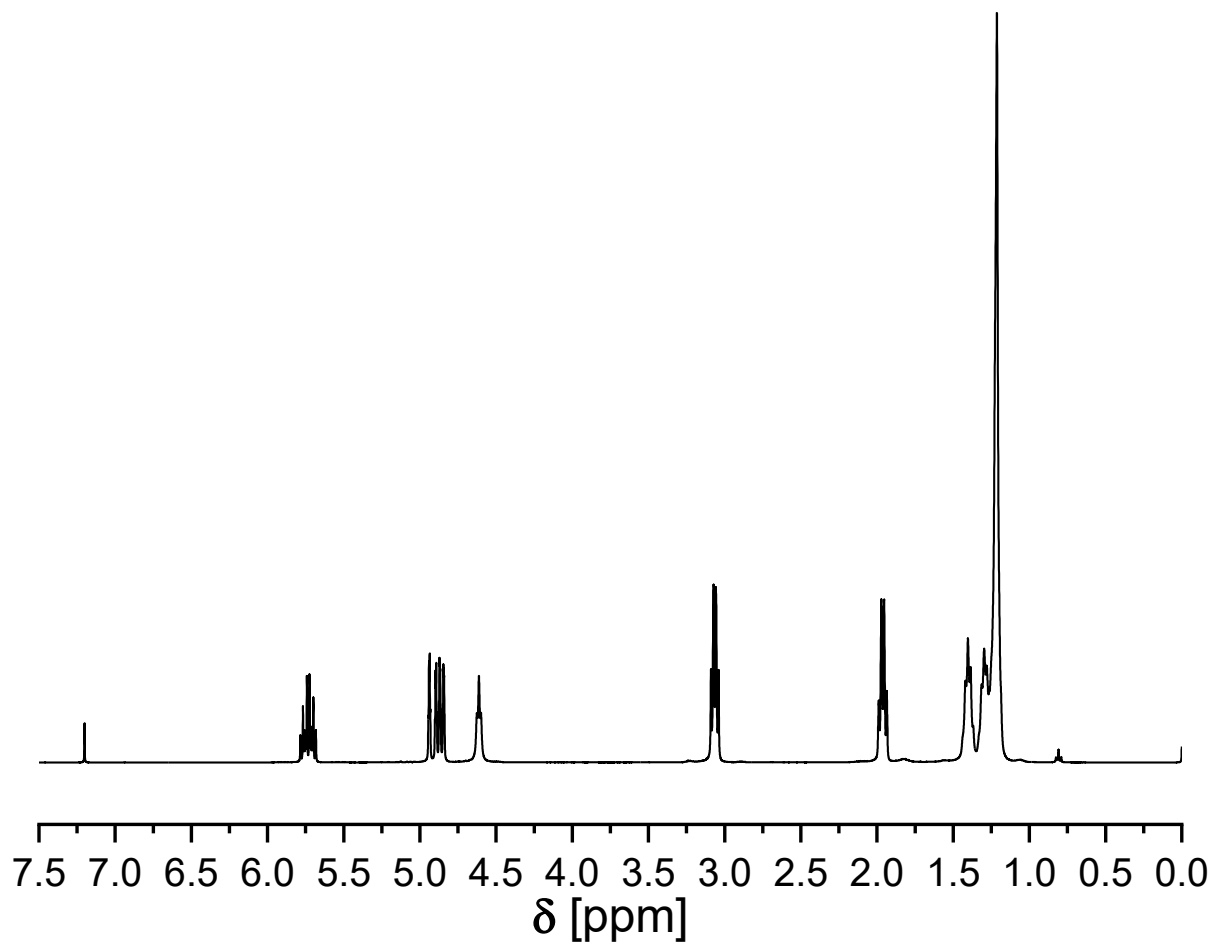
Figure 102 ^{1}H NMR spectrum of **9** (400 MHz, CDCl$_3$).

Experimental section

1,3-Di((Z)-heptadec-8-en-1-yl)urea 10
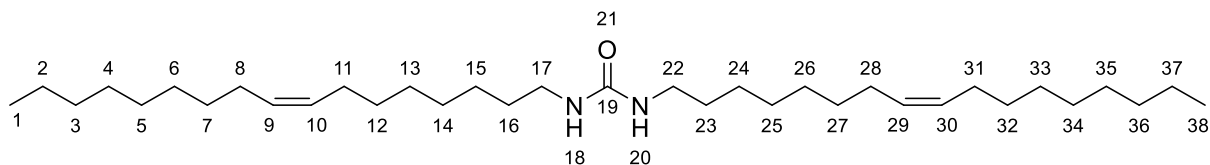
The side reaction of the Lossen rearrangement of *N*-hydroxy oleamide **1a** (1.00 eq.) in diallyl carbonate and allyl alcohol (2.00 eq.) catalyzed by TBD (0.20 eq.) led to the formation of di-((*Z*)-heptadec-8-en-1-yl)urea **10** as colorless solid (3%).

^{1}H NMR (CDCl$_3$, 400 MHz) δ= 0.88 (t, *J* = 7.0 Hz, 6H, CH$_3^{1,38}$), 1.24 – 1.30 (m 40H, CH$_2^{2-7,12-15,24-27,32-37}$), 1.48 (p, *J* = 7.1 Hz, 4H, CH$_2^{16,23}$), 2.00 (q, *J* = 6.7 Hz, 8H, CH$_2^{8,11,28,31}$), 3.14 (t, J = 7.2 Hz, 2H, CH$_2^{17,22}$), 4.24 (s, 1H, NH^{18,20}), 5.34 (m, 2H, CH^{9,10,29,30}) ppm.

^{13}C NMR (CDCl$_3$, 100 MHz) δ= 14.1 (C^{1,38}), 22.7 (C^{2,37}), 26.9 (C^{15,24}), 27.2 (C^{8,11,28,31}), 27.2 (C^{8,11,28,31}), 29.2 (C^{4,35}), 29.3 (C^{16,23}), 29.3 (C^{5,6,33,34}), 29.5 (C^{14,25}), 29.7 (C^{13,26}), 29.8 (C^{7,32}), 30.2 (C^{12,27}), 31.9 (C^{3,36}), 40.7 (C^{17,22}), 129.7 (C^{9,10,29,30}), 130.0 (C^{9,10,29,30}), 158.2 (CO^{19}) ppm.

IR (ATR) ṽ = 3325.0, 2919.5, 2849.3, 1611.6 (amide), 1578.9, 1459.3, 1379.0, 1261.1, 1233.7, 1051.8, 717.5, 619.8cm^{-1}.

ESI-MS of C$_{35}$H$_{68}$N$_2$O [M+H]$^+$ calculated: 533.5405, found 533.5404.
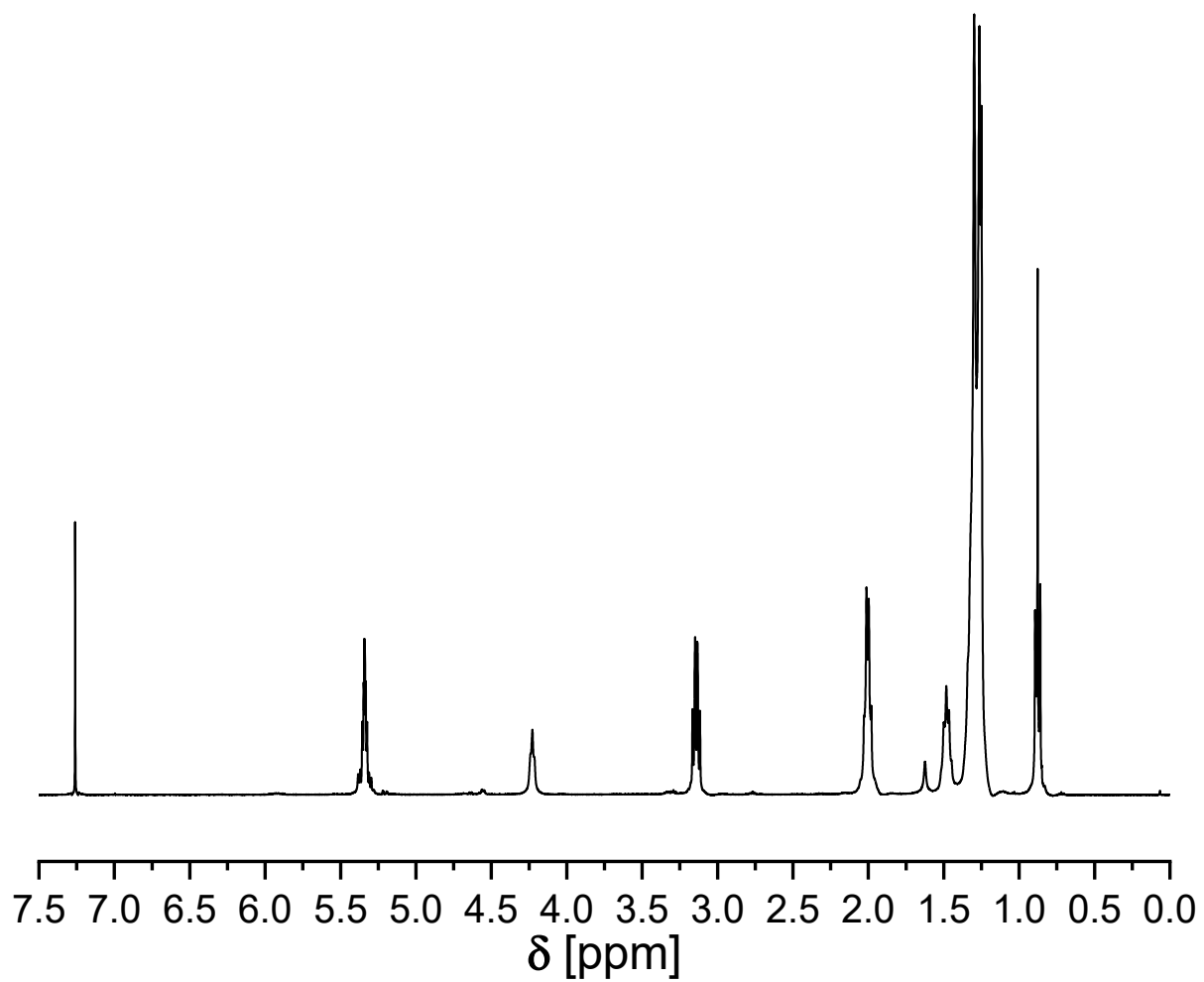
Figure 103 ^{1}H-NMR spectrum of **10** (400 MHz, CDCl$_3$).

5.2.4 General procedure for the synthesis of dithiols from dienes

Dithiols were synthesized in a modified procedure previously published by our group.[354] The diene component (1.00 eq.) was prepared in a round bottom flask, followed by the addition of thioacetic acid (2.50 eq.). The mixture was allowed to stir for 18 h at room temperature. Afterwards, excess of thioacetic acid was removed via rotary evaporation. Methanol (20.0 eq.) and H_2SO_4 (0.10 eq.) or TBD (0.20 eq.) were added to the dithioester and stirred under reflux conditions for 16 h. The solvent was evaporated under reduced pressure, and the crude product purified by flash column chromatography (CH/EA, 19:1).

Limonene dithiol **11**
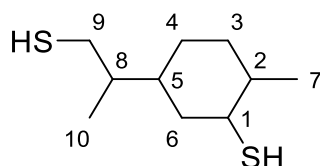
The reaction between limonene and thioacetic acid and subsequent transesterification with methanol catalyzed by TBD led to the formation of limonene dithiol **11** as colorless liquid (89%). The evaluation by NMR required the use of COSY and HSQC technique, since signal assignment is unambiguous, especially in the case of the carbon spectrum. In the proton spectrum, the use of CH_x groups in the brackets was omitted for clarity.

^{1}H NMR (CDCl$_3$, 400 MHz) δ= 0.89 − 0.98 (m, H^{10}, H^8, H^7, H^4), 1.06 (d, J = 6.5 Hz, H^7), 1.00 − 1.21 (m, H^2, H^4, H^5, H^6), 1.21 − 1.33 (m, H^4, SH), 1.34 − 1.52 (m, H^8, H^4), 1.53 − 1.60 (m, H^3), 1.61 − 1.73 (m, H^5, H^6), 1.74 − 1.88 (m, H^2, H^3), 1.99 (dd, J = 21.3, 8.0 Hz, H^3), 2.34 − 2.47 (m, H^1, H^9), 2.53 − 2.63 (m, H^9), 3.33 (h, J = 6.7, 3.4 Hz, H^1) ppm.

^{13}C NMR (CDCl$_3$, 100 MHz) δ= 15.3 (C^{10}), 15.3 (C^{10}), 15.4 (C^{10}), 20.5 (C^7), 20.5 (C^7), 20.8 (C^7), 20.8 (C^7), 27.8 (C^6), 28.0 (C^6), 28.2 (C^4), 28.3 (C^4), 29.3 (C^9), 29.4 (C^9), 29.6 (C^9), 30.3 (C^6), 30.4 (C^6), 32.9 (C, minor diast), 33.0 (C, minor diast), 33.7 (C^2), 33.9 (C^2), 34.3 (C, minor diast), 33.4 (C, minor diast), 35.3 (C^4), 35.4 (C^4), 35.9 (C, minor diast), 36.2 (C^5), 36.2 (C^5), 37.1 (C^3), 39.3 (C^3), 40.6 (C^8), 40.7 (C^8), 40.9 (C^2), 40.9 (C^2), 40.9 (C^3), 41.0 (C, minor diast), 41.1 (C, minor diast), 41.3 (C^5), 41.6 (C^8), 41.6 (C^8), 41.9 (C, minor diast), 41.9 (C, minor diast), 42.4 (C, minor diast), 42.5 (C, minor diast), 43.1 (C^3), 43.8 (C^1), 43.9 (C^1), 46.2 (C^1), 46.2 (C^1) ppm.

IR (ATR) ṽ = 2955.1, 2918.8, 2851.8, 2557.1 (thiol), 1452.2, 1375.5, 1292.1, 1251.6, 979.4, 938.4, 766.5, 719.4 cm^{-1}.

HRMS-EI-MS of C$_{10}$H$_{20}$S$_2$ [M]$^+$ calculated: 204.1001 found 204.1000.
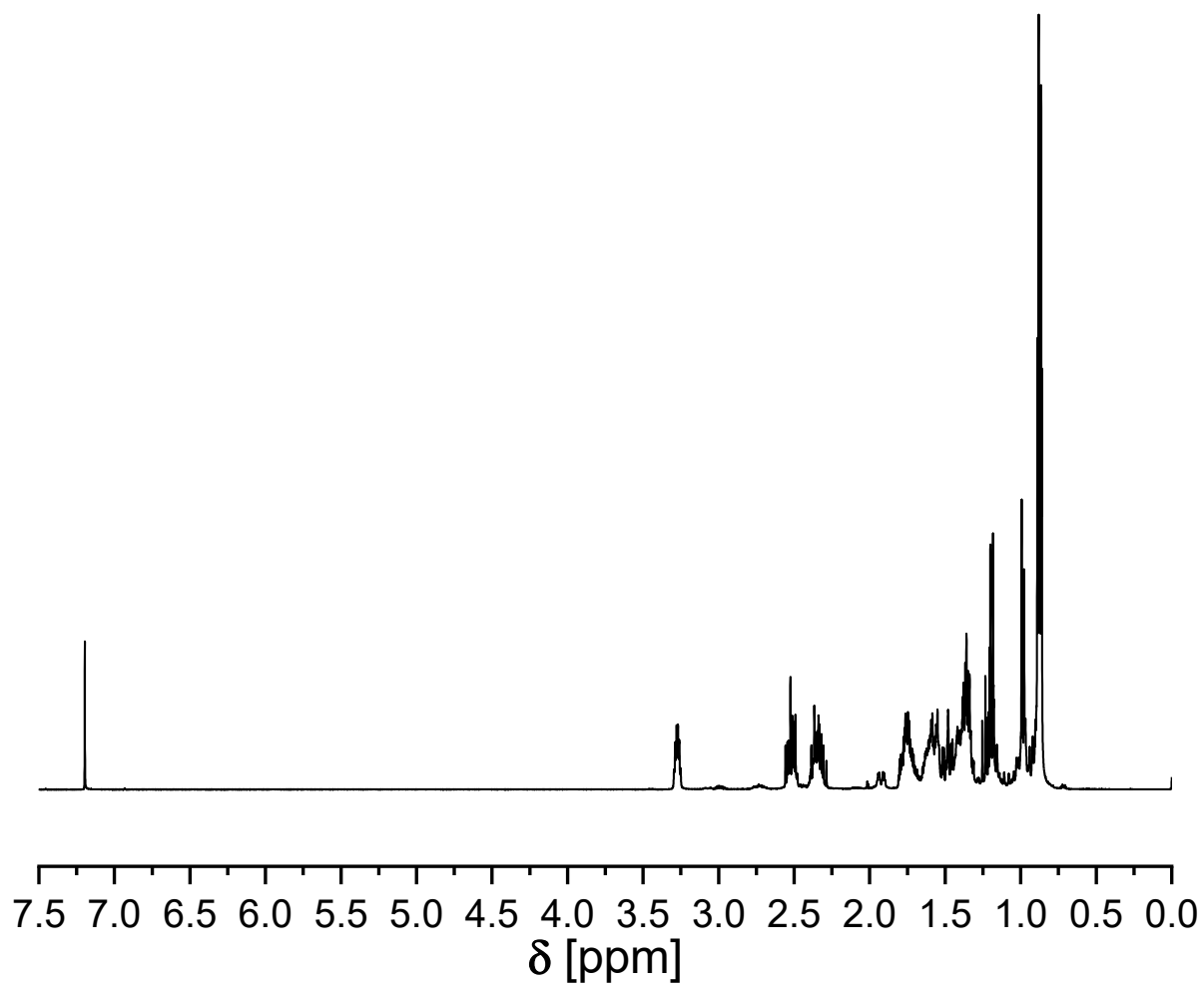
Figure 104 ^{1}H NMR spectrum of **11** (400 MHz, CDCl$_3$).

1,3- and 1,4-cyclohexanedithiol 12

12a   **12b**
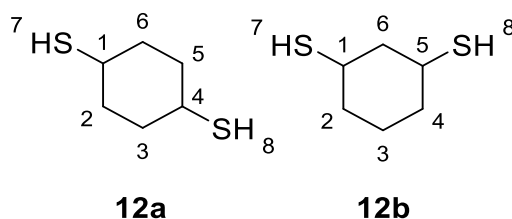
The reaction between 1,4-cyclohexadiene and thioacetic acid and subsequent cleavage of the thioester in methanol catalyzed by sulfuric acid led to the formation of a mixture of 1,3- and 1,4-cyclohexanedithiol **12** (ratio 1:2, 72%). Because of the high volatility of the product, the main impurity derives from residual solvent (cyclohexane) at 1.43 ppm. The spectrum can be compared to the literature of a mixture of cis- and trans-cyclohexane dithiol.[394]

^{1}H NMR (CDCl$_3$, 400 MHz) δ=1.21 – 1.65 (m, 2H, **12a**-CH$_2$^{2,3,5,6}; 4H, **12b**-CH$_2$^{2,4}), 1.47 – 1.59 (m, 2H, **12a**-SH^{7,8}; 2H, **12b**-SH^{7,8}), 1.65 – 2.15 (m, 6H, **12a**-CH$_2$^{2,3,5,6}; 4H, **12b**-CH$_2$^{2,4}), 3.19, 2.91, 2.63 (m, 2H, **12b**-CH^{1,4}), 3.40, 3.08, 2.75 (m, 2H, **12a**-CH^{1,4}) ppm.

^{13}C NMR (CDCl$_3$, 100 MHz) δ= 21.1 (**12b**-C^3), 33.2 (**12b**-C^{2,3,5,6}), 37.2 (**12b**-C^{1,5}), 38.1 (**12a**-C^{1,4}, **12b**-C^{2,4}), 45.4 (**12b**-C^6) ppm.

IR (ATR) ṽ = 2929.4, 2849.5, 2550.5 (thiol), 1443.8, 1343.7, 1274.3, 1182.5, 995.6, 893.8, 734.9, 568.9 cm^{-1}.

HRMS-EI-MS of C$_6$H$_{12}$S$_2$ [M]$^+$ calculated: 148.0375, found 148.0373.
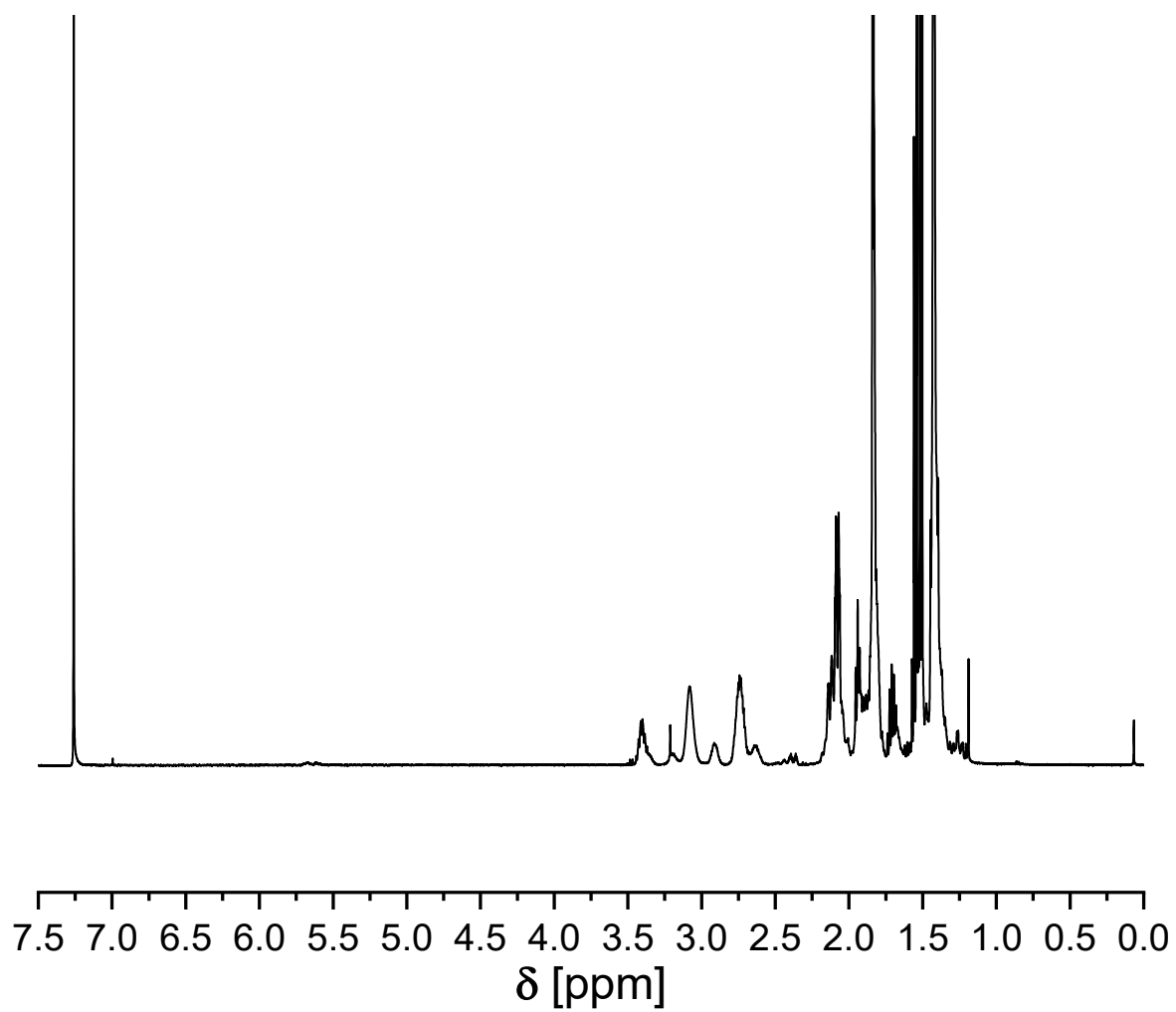
Figure 105 ^{1}H NMR spectrum of **12** (400 MHz, CDCl$_3$).

5.3 Experimental section – Non-isocyanate polyurethanes (NIPUs)

5.3.1 Materials

1,2-Ethanedithiol (98%, Fluka Analytical), 1,3-propanedithiol (97%, VWR), 1,4-butanedithiol (97%, SAFC), 1,6-hexanedithiol (97%, Alfa Aesar), 1,8-octanedithiol (97%, Sigma-Aldrich), 1,10-decanedithiol (98%, TCI), 2,3-butanedithiol (98%, TCI), dithioerythritol (99%, Acros Organics), 2,2'-oxybis(ethane-1-thiol) (95%, Sigma-Aldrich), 3,6-dioxa-1,8-octanedithiol (95%, TCI), (S)-2-aminobutane-1,4-dithiol hydrochloride (99%, Sigma-Aldrich), 1,3-benzenedithiol (99%, Sigma-Aldrich), 2,2-thiobis(ethane-1-thiol) (90%, Acros Organics), Butane-1,4-diyl bis(2-mercaptoacetate) (95%, TCI), ethane-1,4-diyl bis(2-mercaptoaetate) (97%, abcr), gamma-valerolactone (99%, Sigma-Aldrich), gamma-butyrolactone (99%, Sigma-Aldrich), Cyrene (Sigma-Aldrich), dimethyl sulfoxide (99.9%, Fisher Chemical), tetrahydrofuran (HPLC grade, VWR), chloroform (99.8%, Fisher Chemical), PolarClean (SOLVAY), 2-methyl tetrahydrofuran (99.5%, Sigma-Aldrich), 2,2-dimethoxy-2-phenylacetophenone (99%, Sigma-Aldrich), methanol (HPLC grade, VWR).

The dithiol 10,10'-(hexane-1,6-diylbis(oxy))bis(decane-1-thiol) was synthesized and characterized by Dr. Patrick-Kurt Dannecker, a previous PhD student of our group. The full characterization can be found in his doctoral thesis.[254]

5.3.2 Additional analytical methods

Size exclusion chromatography (SEC) measurements were performed on a Tosoh EcoSEC HLC-8320 SEC with 1,1,1,3,3,3-Hexafluoro-2-propanol (HFIP) containing 0.1 wt.% potassium trifluoroacetate as eluent. The solvent flow was 0.40 mL min^{-1} at 30 °C and the concentration of the samples was 1.00 mg mL^{-1}. The analysis was performed on a three-column system: PSS PFG Micro precolumn (3.0 × 0.46 cm, 10,000 Å), PSS PFG Micro (25.0 × 0.46 cm, 1000 Å) and PSS PFG Micro (25.0 × 0.46 cm, 100 Å). The system was calibrated with linear poly(methyl methacrylate) standards (Polymer Standard Service, Mp 102 – 981 kDa).

Differential scanning calorimetry (DSC) experiments were performed on two different instruments. The first was a DSC821e (Mettler Toledo) calorimeter using 40 μL aluminum crucibles under nitrogen atmosphere. The cycles were adjusted accordingly to the employed monomers. For macromolecules containing urea moieties or oxidized NIPUs three cycles

respectively of 25 – 125 °C, 125 – -50 °C and -50 – 200 °C were used. For NIPUs and thiol-based copolymers three cycles respectively of 25 – 125 °C, 125 – -80 °C and -80 – 180 °C were measured. Each measurement was performed with 3-7 mg sample. T_g and T_m values were recorded by taking the second heating curves.

The second instrument was a TA DSC 2500 with a in TA Tzero sample holder. The glass transition temperature T_g and melting temperature T_m were determined in the second heat run to eliminate possible interference from the polymer's thermal history. The heating rates and temperatures were kept as for the previous instrument.

5.3.3 General procedure for the thiol-ene polymerization

The desired amount of carbamate and/or urea was weighted in a 2 mL vial, followed by addition of solvent. The mixture was stirred until completely homogeneous. Afterwards, the initiator was added and stirred for a few seconds. The dithiol was added via Eppendorf pipette, and the vial was placed either between two handheld 6 W-UV lamps or in front of a single 13 W-UV lamp (365 nm). In the case of 254 nm polymerization, the reaction was performed in a quartz glass flask. The mixture was lastly allowed to stir at the required temperature for the desired time.

Purification of polymers varied depending on the solubility in THF. If the polymeric compound was soluble, it was dissolved in a small amount of THF and reprecipitated in cold methanol. The white solid was then collected by filtration or centrifugation and dried under reduced pressure.

In the case of insoluble products, the polymers were washed several times with $CHCl_3$ and dried in vacuo.

P1
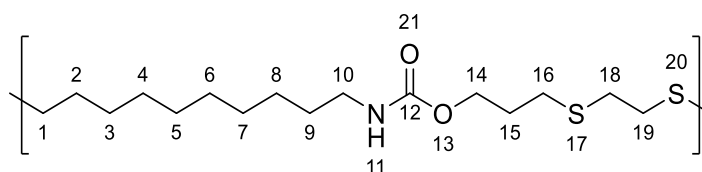
The thiol-ene polymerization of allyl dec-9-enyl carbamate **4** (1.00 eq.) and 1,2-ethanedithiol (1.00 eq.) led to the formation of **P1** as a colorless solid (88%).

^{1}H NMR (CDCl$_3$,400 MHz) δ= 1.15 – 1.36 (m, 12H, CH$_2^{3-8}$), 1.41 (q, J = 7.0 Hz, 2H, CH$_2^2$), 1.51 (p, J = 7.5 Hz, 2H, CH$_2^9$), 1.83 (p, J = 6.7 Hz, 2H, CH$_2^{15}$), 2.47 (t, J = 7.4 Hz, 2H, CH$_2^1$), 2.54 (t, J = 7.3 Hz, 2H, CH$_2^{16}$), 2.65 (t, J = 2.2 Hz, 4H, CH$_2^{18,19}$), 3.09 (q, J = 6.9 Hz, 2H, CH$_2^{10}$), 4.07 (t, J = 6.3 Hz, 2H, CH$_2^{14}$), 4.64 (br, d, J = 22.1 Hz 1H, NH^{11}) ppm.

IR (ATR) ṽ = 3319.8, 2918.8, 2848.8, 1682.6 (amide), 1536.5, 1466.6, 1437.8, 1320.5, 1260.9, 1246.5, 1205.3, 1143.6, 1061.4, 1024.3, 779.6, 721.0 cm^{-1}.
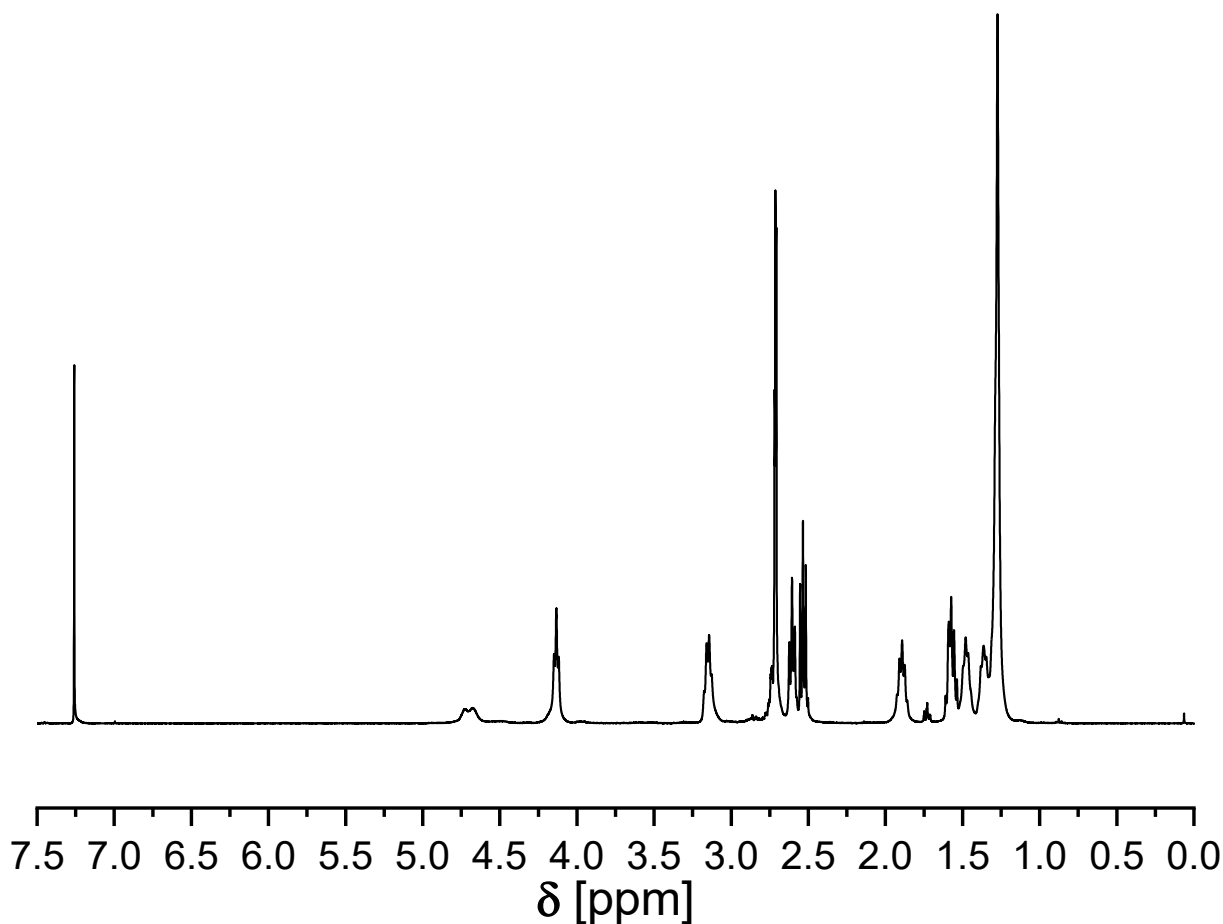
Figure 106 ^{1}H NMR spectrum of **P1** (400 MHz, CDCl$_3$).

P2
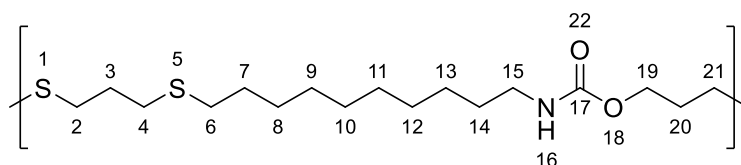
The thiol-ene polymerization of allyl dec-9-enyl carbamate **4** (1.00 eq.) and 1,3-propanedithiol (1.00 eq.) led to the formation of **P2** as a colorless solid (91%).

¹H NMR (CDCl$_3$, 400 MHz) δ= 1.20 − 1.42 (m, 12H, CH$_2$$^{8-13,}$), 1.48 (t, J = 7.4, 6.9 Hz, CH$_2$^{14}), 1.57 (p, J = 8.1, 7.7, 7.0, 6.7 Hz CH$_2$^{7}), 1.79 − 1.96 (m, 4H, CH$_2$^{3,20}), 2.45 − 2.66 (m, 8H, CH$_2$^{2,4,6,21}), 3.15 (q, J = 6.8 Hz, 2H, CH$_2$^{15}), 4.13 (t, J = 6.3 Hz, 2H, CH$_2$^{19}), 4.69 (br, s, 1H, NH^{16}) ppm.

IR (ATR) ṽ = 3324.8, 2920.5, 2850.7, 1682.1 (amide), 1535.0, 1468.9, 1289.6, 1244.4, 1142.4, 1078.7, 1039.2, 778.8, 720.8, 637.6 cm^{-1}.

Figure 107 ¹H NMR spectrum of **P2** (400 MHz, CDCl$_3$).

P3

The thiol-ene polymerization of allyl dec-9-enyl carbamate **4** (1.00 eq.) and 1,4-butanedithiol (1.00 eq.) led to the formation of **P3** as a colorless solid (90%).

^{1}H NMR (CDCl$_3$, 400 MHz) δ= 1.22 − 1.40 (m, 12H, CH$_2$$^{9\text{-}14}$), 1.47 (p, J = 6.8 Hz, 2H, CH$_2$^{15}), 1.55 (p, J = 7.7, 6.7 Hz, 2H, CH$_2$^{8}), 1.68 (p, J = 3.4 Hz, 4H, CH$_2$^{3,4}), 1.89 (p, J = 7.0, 6.6 Hz, 2H, CH$_2$^{21}), 2.45 − 2.59 (m, 8H, CH$_2$^{2,5,7,22}), 3.14 (t, J = 6.6 Hz, 2H, CH$_2$^{16}), 4.14 (t, J = 6.1 Hz, 2H, CH$_2$^{20}), 4.69 (br, s, 1H, NH^{17}) ppm.
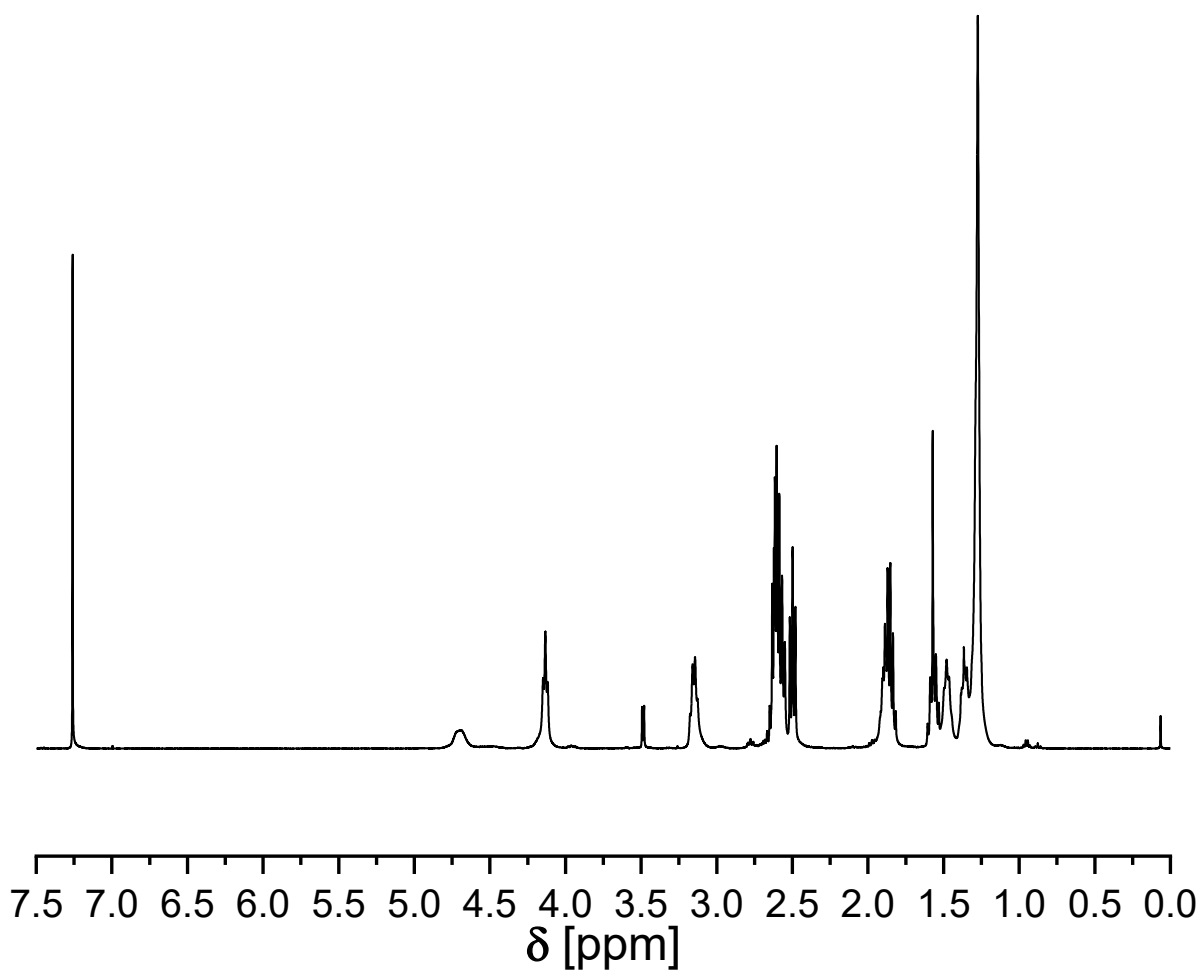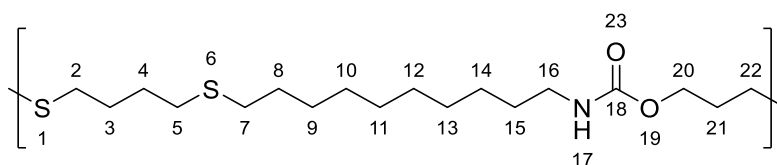
IR (ATR) ṽ = 3333.0, 2919.4, 2850.6, 1683.1 (amide), 1530.4, 1468.9, 1289.5, 1141.2, 1019.5, 779.4,721.2, 630.7 cm^{-1}.
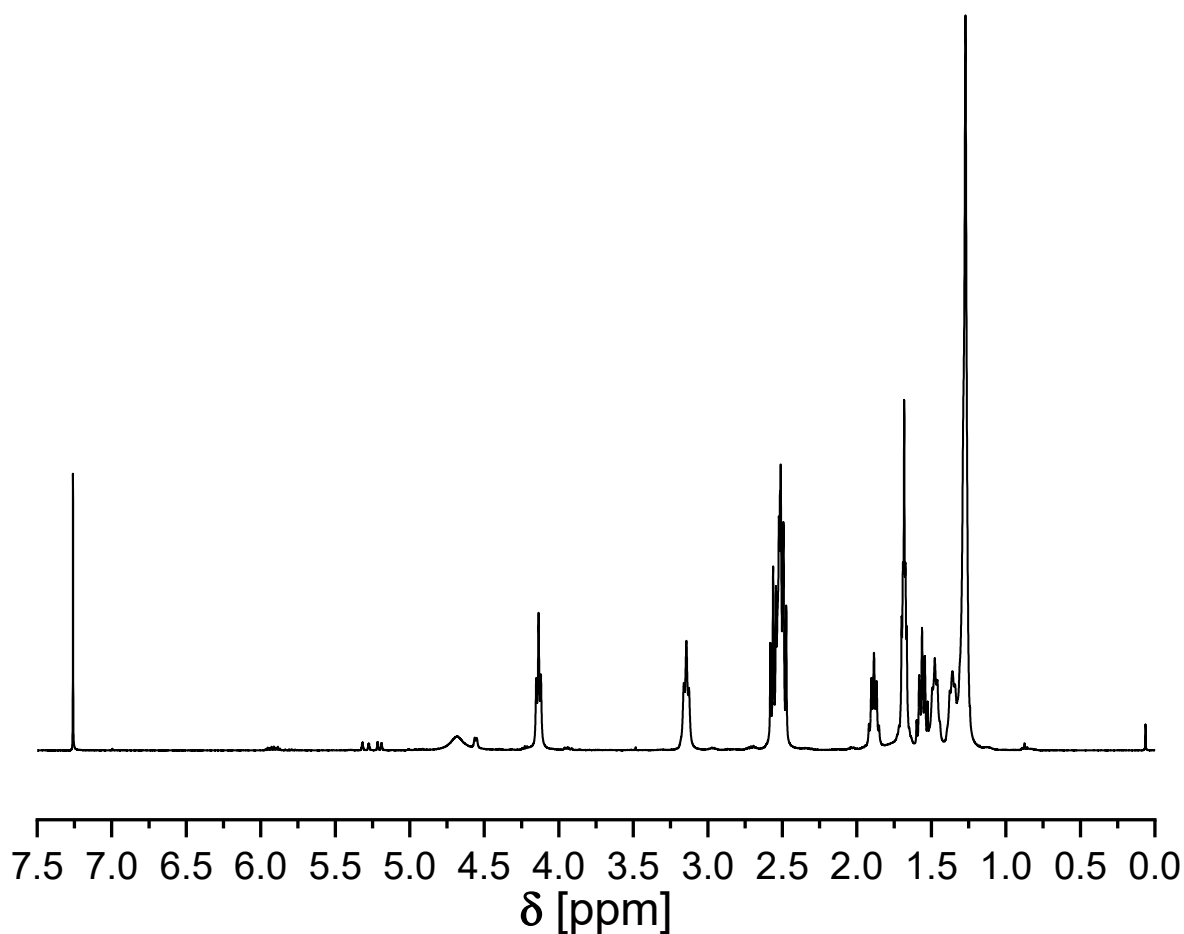
Figure 108 ^{1}H NMR spectrum of **P3** (400 MHz, CDCl$_3$).

Experimental section

P4
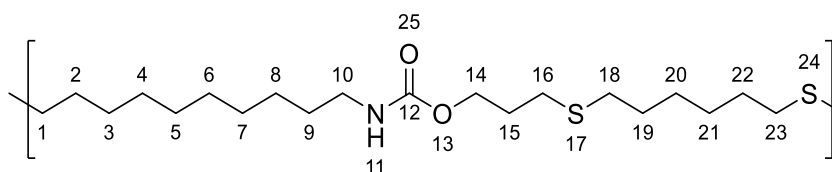
The thiol-ene polymerization of allyl dec-9-enyl carbamate **4** (1.00 eq.) and 1,6-hexanedithiol (1.00 eq.) led to the formation of **P4** as a colorless solid (94%).

^{1}H NMR (CDCl$_3$, 400 MHz) δ= 1.21 − 1.36 (m, 12H, CH$_2^{3-8}$), 1.38 (td, J = 10.2, 8.7, 5.1 Hz, 4H, CH$_2^{20,21}$), 1.47 (q, J = 7.1 Hz, 2H, CH$_2^2$), 1.58 (dq, J = 14.6, 7.2 Hz, 6H, CH$_2^{9,19,22}$), 1.87 (p, J = 6.3, 5.8 Hz, 2H, CH$_2^{15}$), 2.43 − 2.58 (m, 8H, CH$_2^{1,16,18,23}$), 3.14 (q, J = 6.8 Hz, 2H, CH$_2^{10}$), 4.14 (t, J = 6.1 Hz, 2H, CH$_2^{14}$), 4.68 (br, s, 1H, NH^{11}) ppm.

IR (ATR) ṽ = 3328.1, 2918.8, 2850.9, 1682.5 (amide), 1534.5, 1468.6, 1439.8, 1345.2, 1322.6, 1289.7, 1262.9, 1244.4, 1186.8, 1143.6, 1116.9, 1077.8, 1061.4, 1040.8, 1018.2, 779.6, 719.9 cm^{-1}.
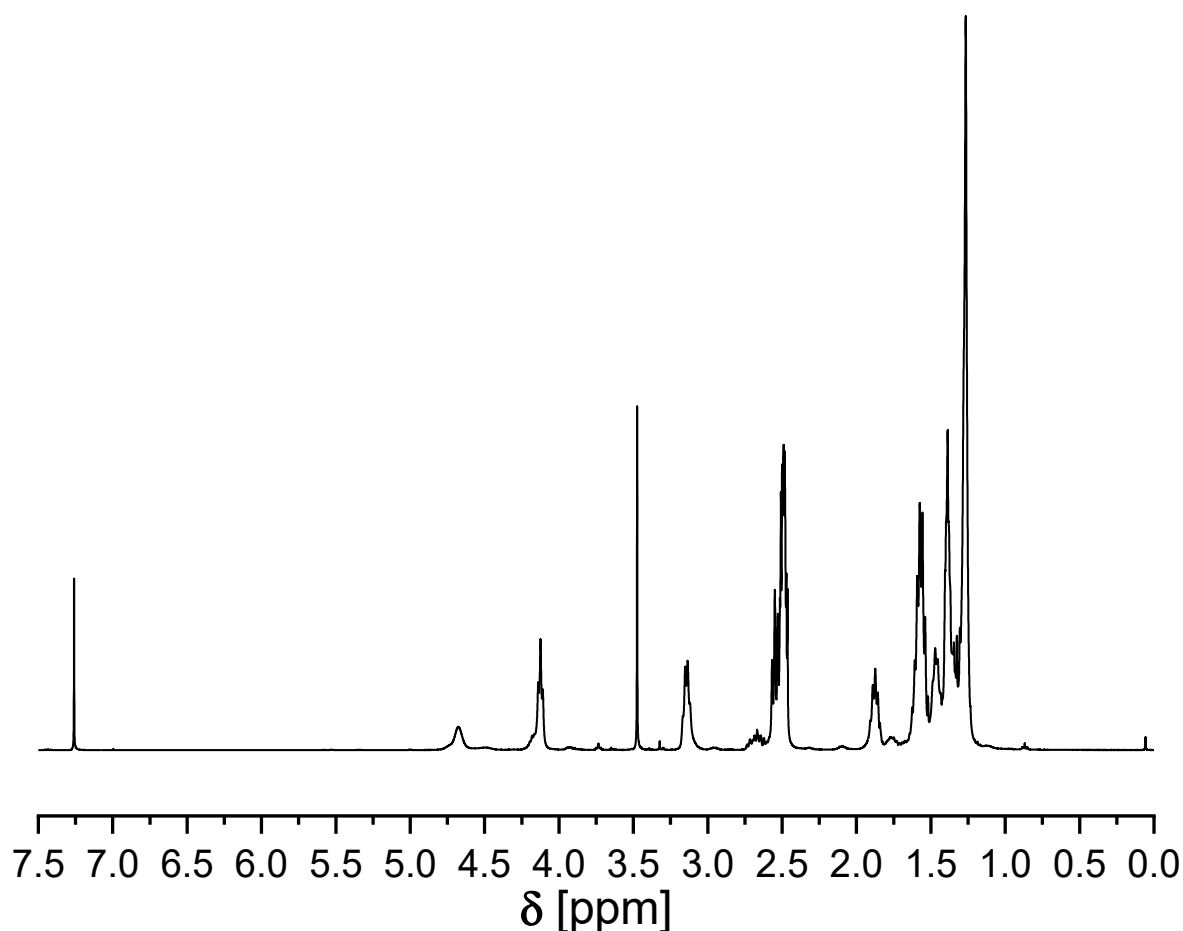
Figure 109 ^{1}H NMR spectrum of **P4** (400 MHz, CDCl$_3$). The impurity at 3.49 ppm derives from residual methanol.

P5
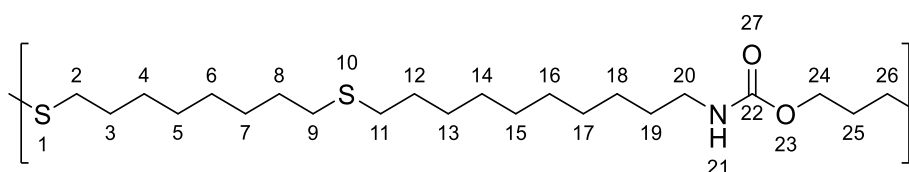
The thiol-ene polymerization of allyl dec-9-enyl carbamate **4** (1.00 eq.) and 1,8-octanedithiol (1.00 eq.) led to the formation of **P5** as a colorless solid (90%).

^{1}H NMR (CDCl$_3$, 400 MHz) δ= 1.25 − 1.35 (m, 20H, CH$_2{}^{3-7,13-18,}$), 1.48 (t, J = 6.8 Hz, CH$_2{}^{19}$), 1.57 (p, J = 7.6 Hz, 6H CH$_2{}^{3,8,12}$), 1.88 (p, J = 6.9Hz, 2H, CH$_2{}^{25}$), 2.50 (td, J = 7.4, 2.9 Hz, 6H, CH$_2{}^{2,9,11}$), 2.56 (t, J = 7.3 Hz, 2H, CH$_2{}^{26}$), 3.15 (q, J = 6.8 Hz, 2H, CH$_2{}^{20}$), 4.13 (t, J = 6.1 Hz, 2H, CH$_2{}^{24}$), 4.66 (br, s, 1H, NH^{21}) ppm.

IR (ATR) ṽ = 3328.1, 2918.8, 2850.9, 1684.6 (amide), 1536.5, 1468.6, 1322.7, 1289.7, 1265.0, 1244.4, 1141.6, 1075.8, 1040.8, 1022.3, 779.6, 719.1 cm^{-1}.
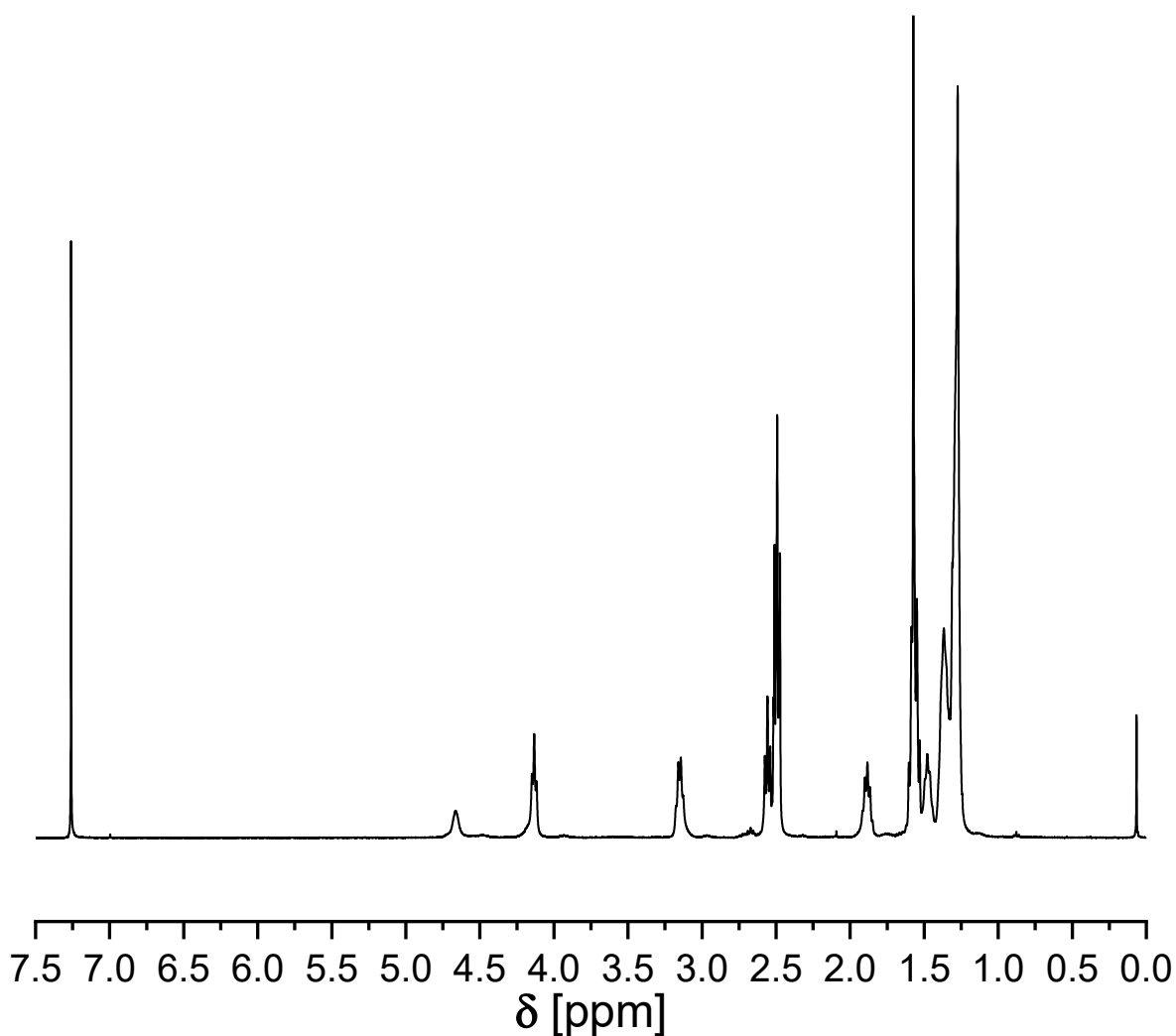
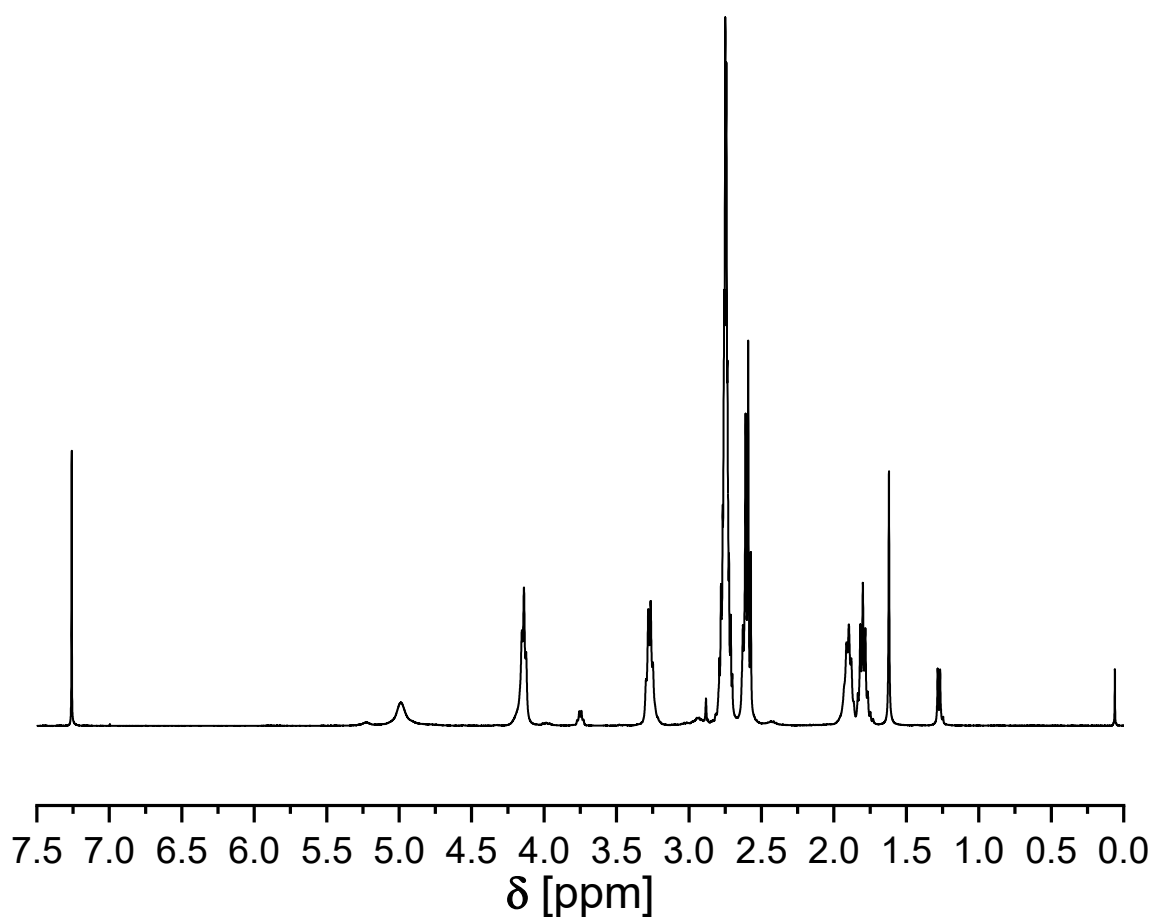**Figure 110** ^{1}H NMR spectrum of **P5** (400 MHz, CDCl$_3$).

P6
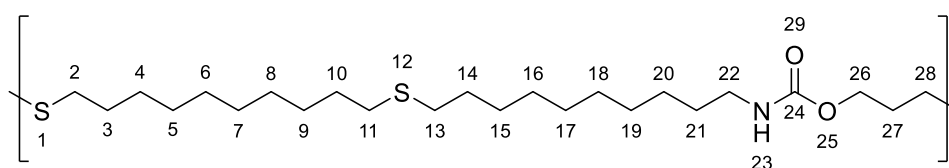
The thiol-ene polymerization of allyl dec-9-enyl carbamate **4** (1.00 eq.) and 1,10-decanedithiol (1.00 eq.) led to the formation of **P6** as a colorless solid (82%).

^{1}H NMR (CDCl$_3$, 400 MHz) δ= 1.18 − 1.41 (m, 24H, CH$_2$$^{4-9,15-20}$), 1.46 (p, J = 7.0, 6.4 Hz, 2H, CH$_2$^{21}), 1.58 (d, J = 7.4 Hz, 6H, CH$_2$^{3,10,14}), 1.88 (p, J = 6.7 Hz, 2H, CH$_2$^{27}), 2.50 (td, J = 7.5, 2.7 Hz, 6H, CH$_2$^{2,11,13}), 2.56 (t, J = 7.4 Hz, 2H, CH$_2$^{28}), 3.15 (q, J = 6.8 Hz, 2H, CH$_2$^{22}), 4.13 (t, J = 6.2 Hz, 2H, CH$_2$^{26}), 4.65 (br, s, 1H, NH^{23}) ppm.

IR (ATR) ṽ = 3328.2, 2919.0, 2850.3, 1685.8 (amide), 1535.9, 1468.7, 1345.4, 1289.0, 1245.7, 1142.4, 1021.8, 779.1, 719.5, 638.8 cm^{-1}.

Figure 111 ^{1}H NMR spectrum of **P6** (400 MHz, CDCl$_3$).

P7

The thiol-ene polymerization of allyl dec-9-enyl carbamate **4** (1.00 eq.) and limonene dithiol (1.00 eq.) led to the formation of **P7** as transparent, viscous substance (90%).

^{1}**H NMR** (CDCl$_3$, 400 MHz) δ= 0.91 – 1.12 (m, CH^{26}, CH$_2^{22}$, CH$_3^{25,27}$), 1.22 – 1.80 (m, CH$_2^{2-9,20-22}$, CH^{24,}), 1.89 (m, 2H, CH$_2^{15}$), 1.96 – 2.42 (m, CH$_2^{23}$, CH^{21,19}), 2.48 (t, J = 7.5 Hz, CH$_2^{16}$), 2.51 – 2.64 (m, CH$_2^{1,28}$), 2.93(br, s, CH^{19}), 3.14 (q, J = 6.9, 6.2 Hz, CH$_2^{10}$), 4.14 (t, J = 6.1, 5.4 Hz, CH$_2^{14}$), 4.71 (br, s, NH^{11}) ppm.

IR (ATR) ṽ = 3336.6, 2921.6, 2851.8, 1699.7 (amide), 1522.8, 1453.3, 1373.7, 1242.5, 1135.8, 1019.7, 910.4, 776.0, 730.3, 645.8 cm^{-1}.

Figure 112 ^{1}H NMR spectrum of **P7** (400 MHz, CDCl$_3$).

P8

The thiol-ene polymerization of allyl dec-9-enyl carbamate **4** (1.00 eq.) and a mixture of 1,3- and 1,4-cyclohexanedithiol (1.00 eq.) led to the formation of **P8** as a viscous substance (84%).

¹H NMR (CDCl$_3$, 400 MHz) δ= 1.17 − 1.42 (m, CH$_2^{3-8,}$), 1.48 (t, J = 7.3, 6.3 Hz, CH$_2^9$), 1.52 − 1.72 (m, CH$_2^{2,15}$), 1.50 − 2.20 (m, CH$_2^{,20,21,23,24,29,31}$), 2.46 − 2.64 (m, CH$_2^{1,16}$, CH^{19,22,26,28}), 2.83 (br, s, CH^{19,22,26,28}), 3.14 (q, J = 7.1 Hz, CH$_2^{10}$), 4.12 (t, J = 5.8 Hz, CH$_2^{14}$), 4.66 (br, s, NH^{11}) ppm.

IR (ATR) ṽ = 3330.1, 2924.6, 2851.2, 1721.4 (amide), 1530.0, 1447.2, 1243.1, 1136.1, 1066.6, 996.3, 905.8, 776.2 cm^{-1}.

Figure 113 ¹H-NMR spectrum of **P8** (400 MHz, CDCl$_3$).

P9

The thiol-ene polymerization of allyl dec-9-enyl carbamate **4** (1.00 eq.) and 2,3-butanedithiol (1.00 eq.) led to the formation of **P9** as a viscous substance (87%).

^{1}H NMR (CDCl$_3$, 400 MHz) δ= 1.18 – 1.42 (m, 18H, CH$_2$$^{9-14}$, CH$_3$^{2,5}), 1.48 (t, *J*= 6.9 Hz, 2H, CH$_2$^{15}), 1.52-1.60 (m, 2H, CH$_2$^{8}), 1.88 (dd, *J* = 14.1, 7.4 Hz, 2H, CH$_2$^{21}), 2.47 – 2.67 (m, 4H, CH$_2$^{7,22}), 2.88 – 3.07 (m, 2H, CH^{3,4}), 3.15 (q, *J* = 6.8 Hz, 2H, CH$_2$^{16}), 4.14 (t, *J* = 6.4 Hz, 2H, CH$_2$^{20}), 4.74 (br, d, 1H, NH^{17}) ppm.
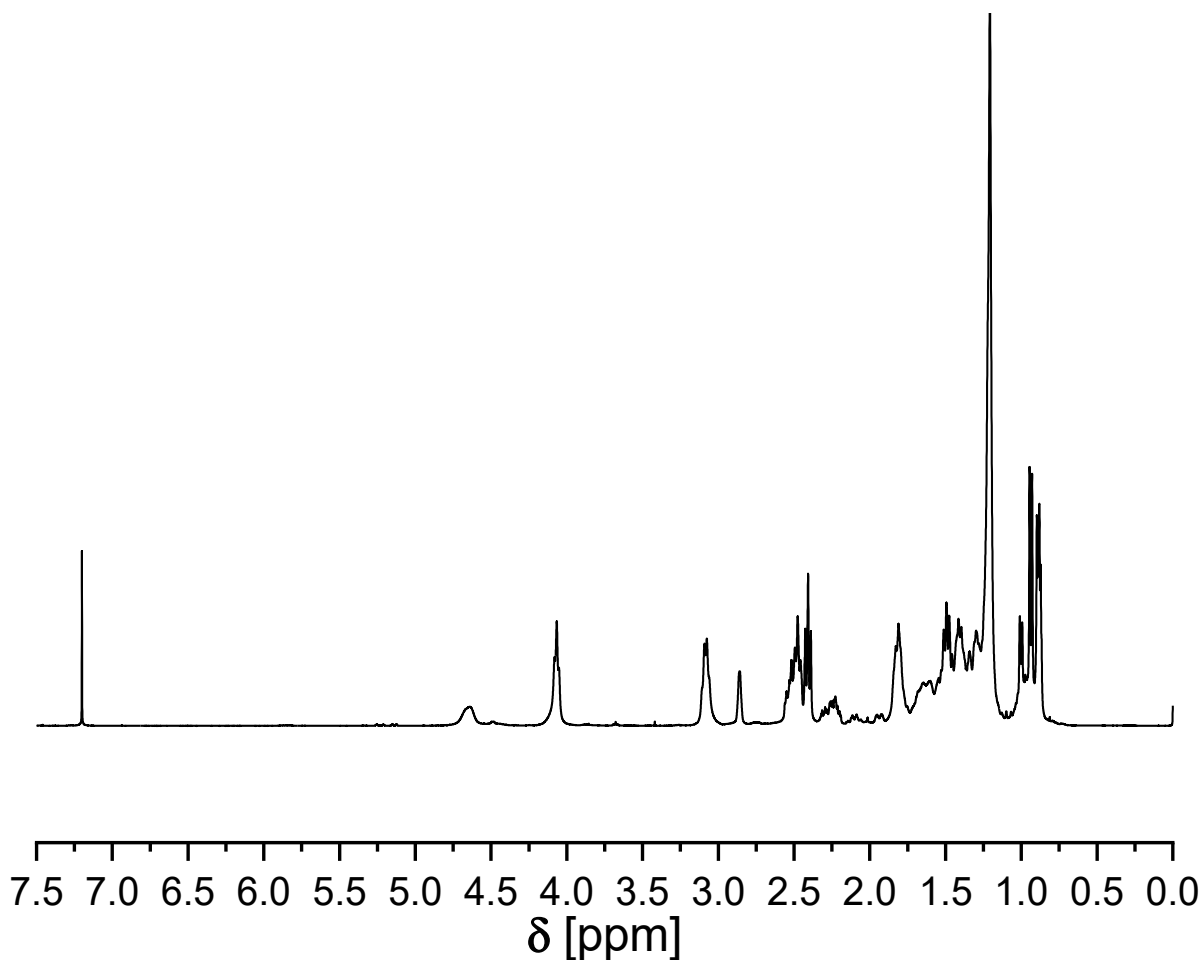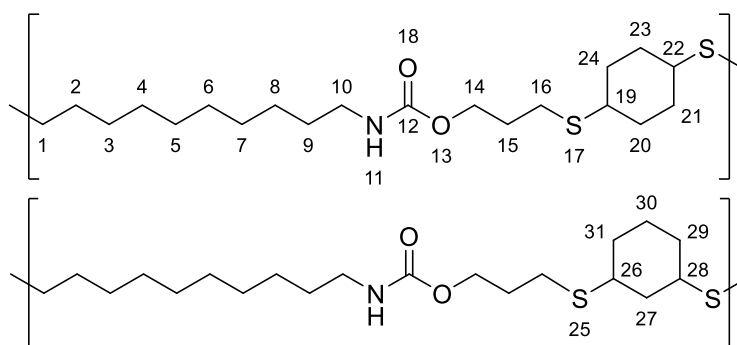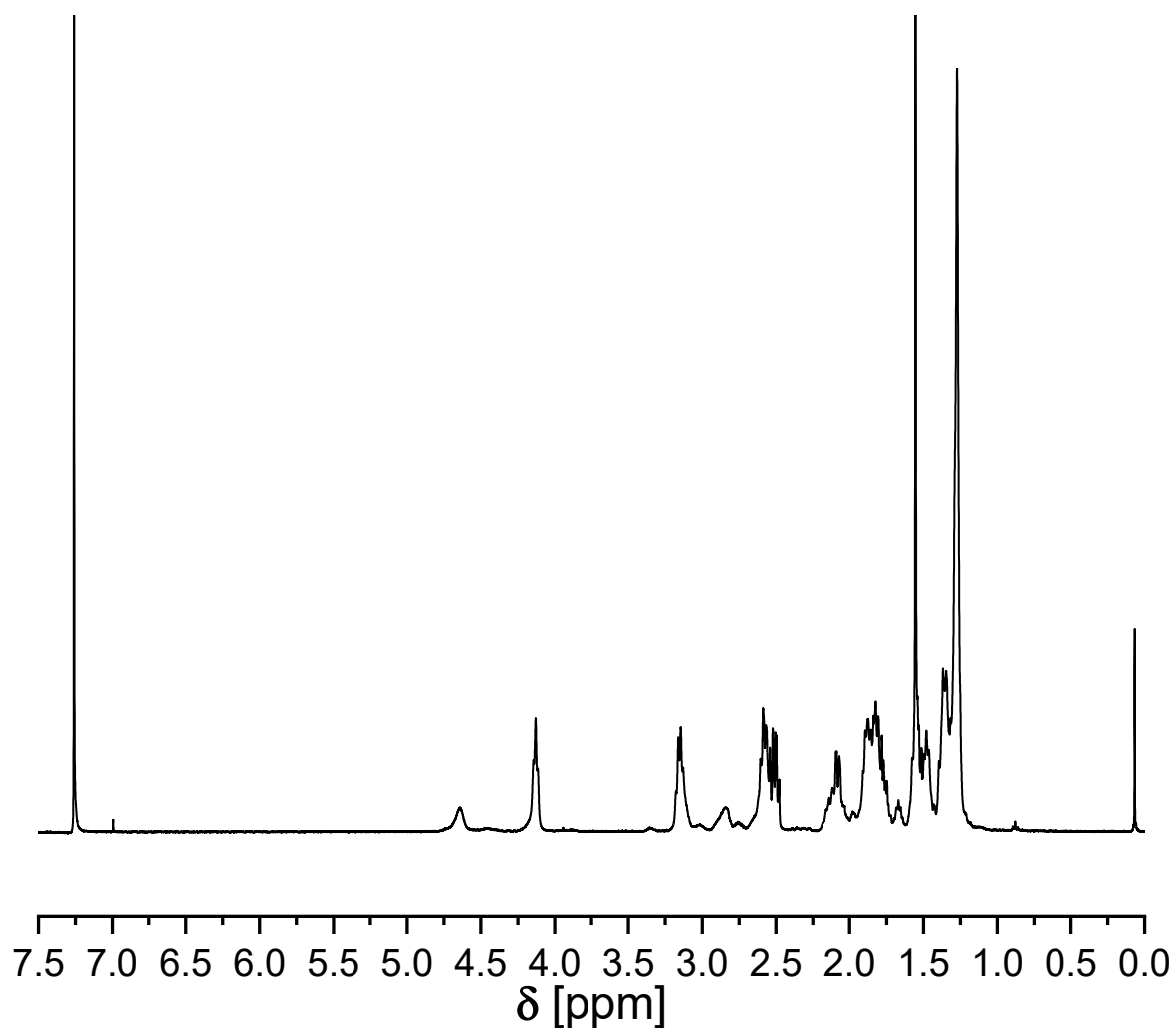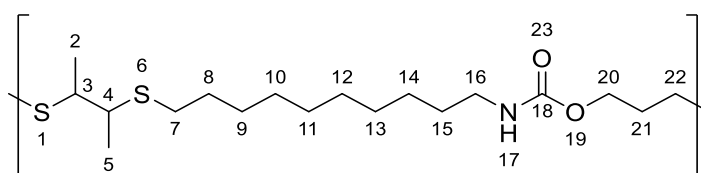
IR (ATR) ṽ = 3332.2, 2922.9, 2852.9, 1696.9 (amide), 1524.2, 1446.0, 1372.0, 1242.4, 1135.4, 1100.4, 1042.9, 1024.3, 954.4, 775.5, 722.0 cm^{-1}.
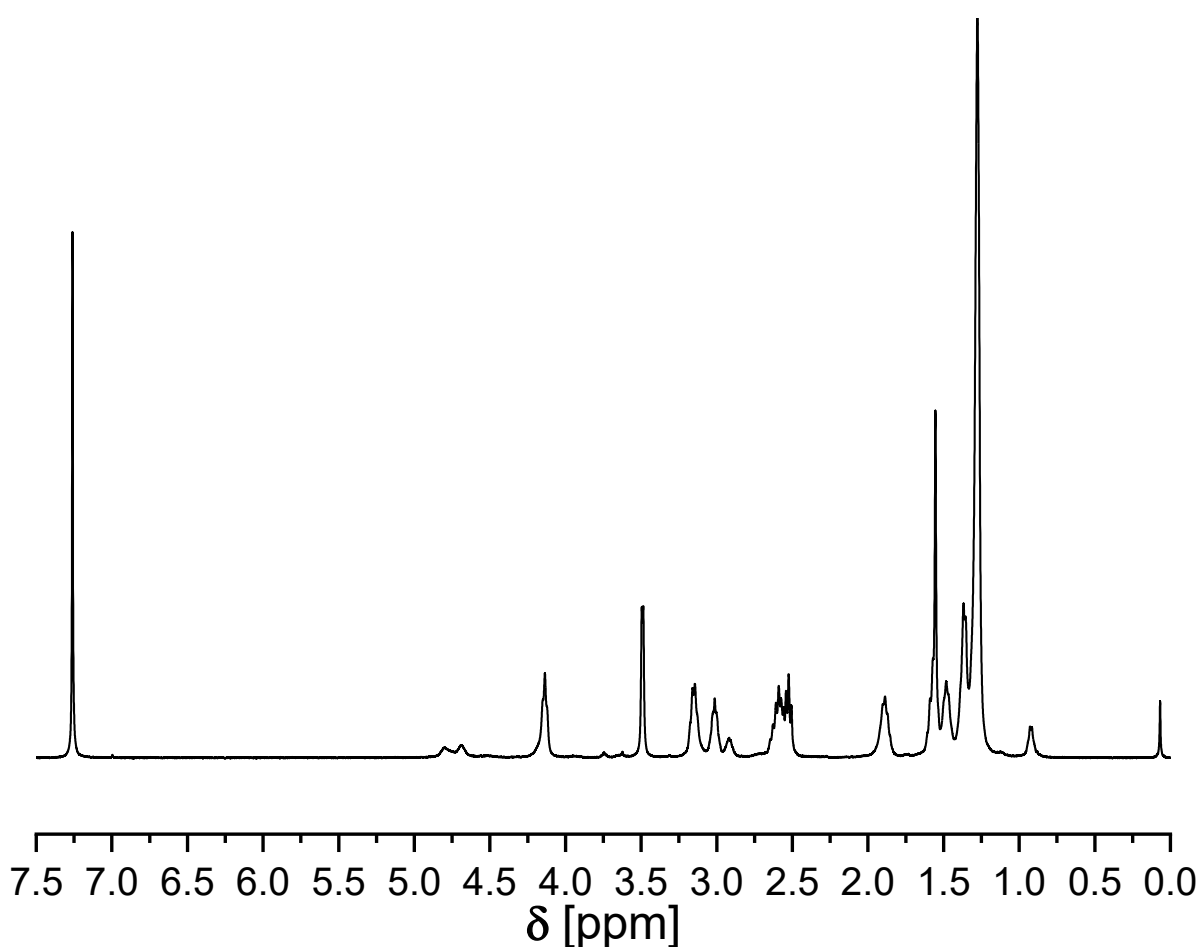
Figure 114 ^{1}H NMR spectrum of **P9** (400 MHz, CDCl$_3$). The impurity at 3.49 ppm derives from residual methanol.

P10
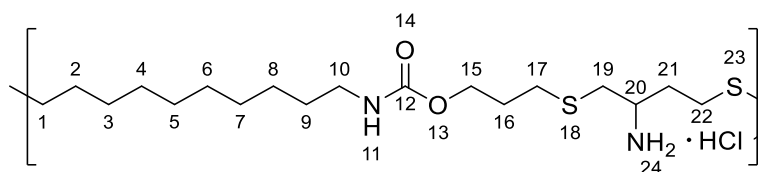
The thiol-ene polymerization of allyl dec-9-enyl carbamate **4** and 2-amino-1,4-butanedithiol hydrochloride led to the formation of **P10** as a colorless solid (81%).

^{1}H NMR (DMSO-d_6, 400 MHz) δ=1.15 − 1.43 (m, 12H, CH_2^{3-9}), 1.51 (t, J = 6.8 Hz, 2H, CH_2^2), 1.80 (q, J = 6.6 Hz, 2H, CH_2^{16}), 1.85 − 1.97 (m, 2H, CH_2^{21}), 2.44 − 2.70 (m, 8H, $CH_2^{1,17,19a,22}$), 2.72 − 2.84 (m, 2H, CH^{20}, CH_2^{19b}) 2.93 (q, J = 6.6 Hz, 2H, CH_2^{10}), 3.98 (t, J = 5.3 Hz, 2H, CH_2^{15}), 7.08 (s, 1H, NH^{11}), 8.24 (br, s, 4H, ammonium NH_3^+) ppm.

IR (ATR) ṽ = 3305.5, 2922.9, 2852.9, 2620.5, 1703.1 (amide), 1614.7, 1528.3, 1435.7, 1415.2, 1376.1, 1248.5, 1137.5, 1016.1, 952.3, 703.5 cm^{-1}.
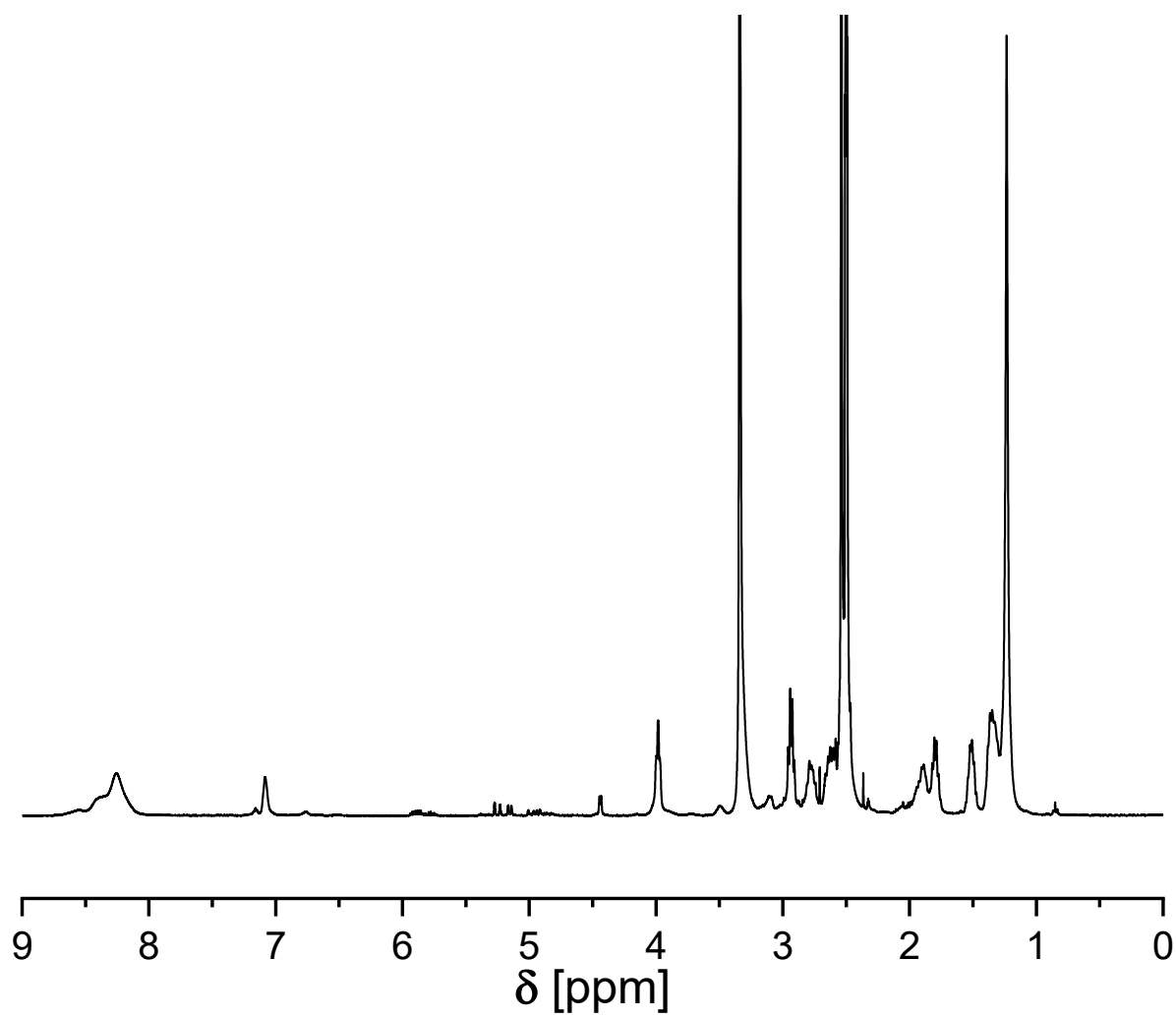
Figure 115 ^{1}H NMR spectrum of **P10** (400 MHz, DMSO-d$_6$).

P11
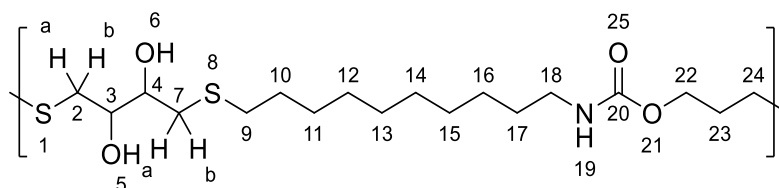
The thiol-ene polymerization of allyl dec-9-enyl carbamate **4** (1.00 eq.) and dithioerythritol (1.00 eq.) led to the formation of **P11** as a colorless solid (85%).

¹H NMR (CDCl$_3$, 400 MHz) δ= 1.14 − 1.41 (m, 12H, CH$_2^{11-16,}$), 1.47 (p, J = 7.2, 6.2 Hz, CH$_2^{17}$), 1.58 (p, J = 7.6, 7.0 Hz, 2H CH$_2^{10}$), 1.89 (p, J = 7.0, 5.7 Hz, 2H, CH$_2^{26}$), 2.13 (br, s, 2H, OH^{5,6}), 2.53 (t, J = 7.2 Hz, 2H, CH$_2^9$), 2.62 (t, J=7.2 Hz, 4H, CH$_2^{2a,7a,24}$) 2.82 − 2.95 (m, 2H, CH$_2^{2b,7b}$), 3.14 (q, J = 7.0 Hz, 2H, CH$_2^{18}$), 3.67 (br, s, 2H, CH^{3,4}), 4.15 (t, J = 6.1 Hz, 2H, CH$_2^{22}$), 5.01 (br, d, 1H, NH^{19}) ppm.

IR (ATR) ṽ = 3332.2, 2920.8, 2850.9, 1682.6 (amide), 1536.5, 1468.6, 1435.7, 1417.2, 1337.0, 1244.4, 1145.7, 1049.0, 981.1, 779.6, 719.9 cm^{-1}.
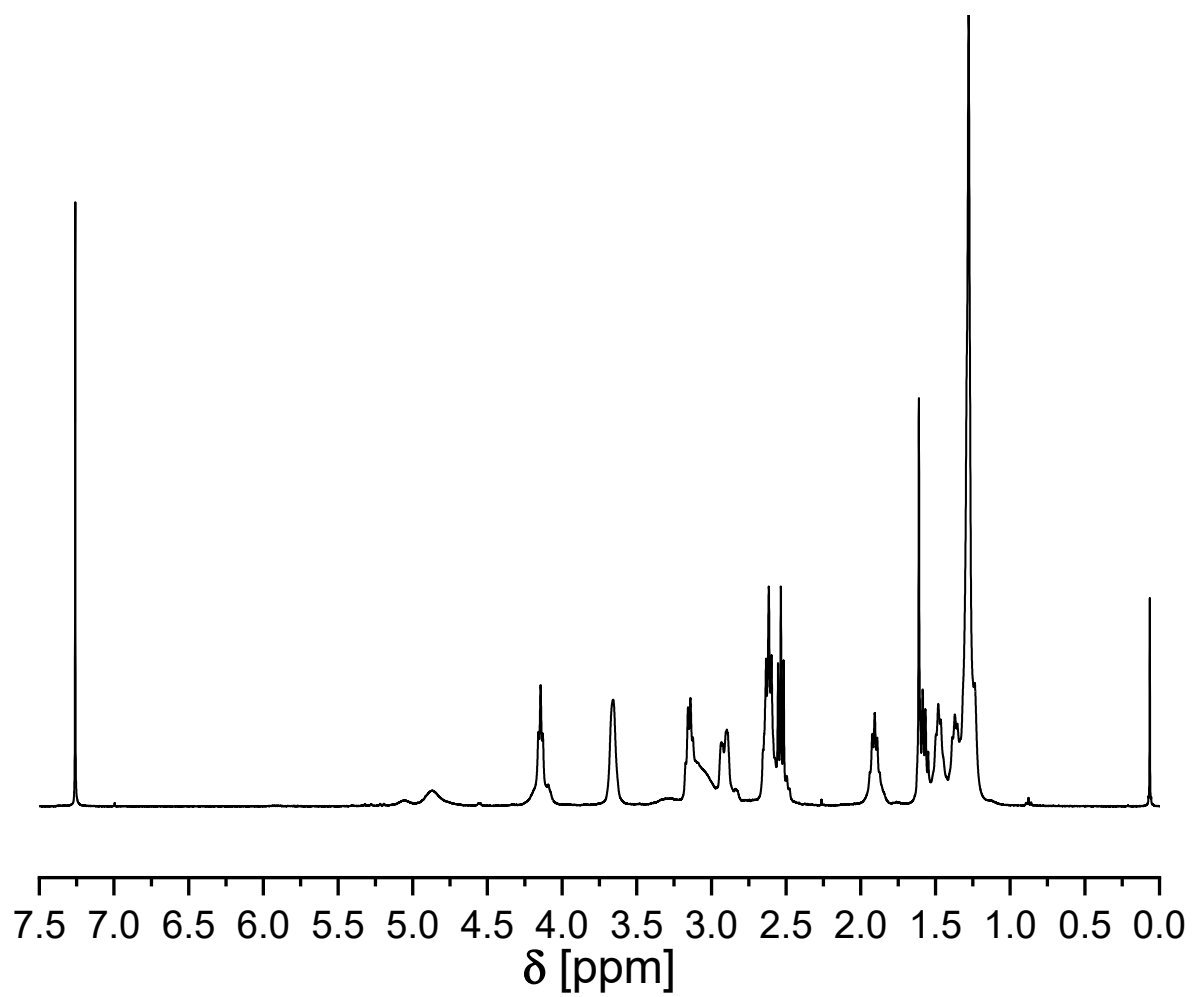
Figure 116 ^{1}H NMR spectrum of **P11** (400 MHz, CDCl$_3$).

P13
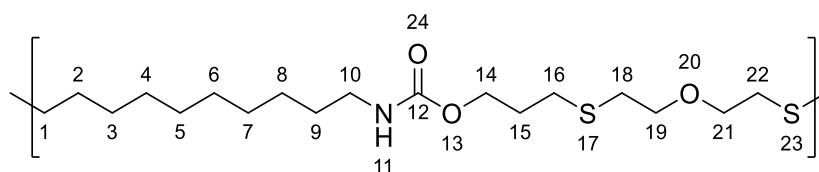
The thiol-ene polymerization of allyl dec-9-enyl carbamate **4** (1.00 eq.) and 2,2′-oxybis (ethane-1-thiol) (1.00 eq.) led to the formation of **P13** as a colorless solid (89%).

^{1}H NMR (CDCl$_3$, 400 MHz) δ= 1.20 – 1.42 (m, 12H, CH$_2$$^{3-8}$), 1.47 (q, J = 6.9 Hz, 2H, CH$_2$^{2}), 1.57 (m, 2H, CH$_2$^{9}), 1.89 (p, J = 6.8 Hz, 2H, CH$_2$^{15}), 2.54 (t, J = 7.5 Hz, 2H, CH$_2$^{1}), 2.62 (t, J = 7.3 Hz, 2H, CH$_2$^{16}), 2.70 (td, J = 6.8, 2.7 Hz, 4H, CH$_2$^{18,22}), 3.15 (q, J = 6.8 Hz, 2H, CH$_2$^{10}), 3.62 (td, J = 6.7, 2.9 Hz, 4H, CH$_2$^{19,21}), 4.13 (t, J = 6.3 Hz, 2H, CH$_2$^{14}), 4.70 (br, s, 1H, NH^{11}) ppm.

IR (ATR) ṽ = 3324.0, 2918.8, 2850.9, 1682.6 (amide), 1536.5, 1468.6, 1437.8, 1355.5, 1289.7, 1265.0, 1246.5, 1143.6, 1100.4, 1038.3, 1018.2, 779.6, 719.9 cm^{-1}.

Figure 117 ^{1}H NMR spectrum of **P13** (400 MHz, CDCl$_3$).

P14

The thiol-ene polymerization of allyl dec-9-enyl carbamate **4** (1.00 eq.) and 3,6-oxa-1,8-octanedithiol (1.00 eq.) led to the formation of **P14** as a colorless solid (82%).

^{1}H NMR (CDCl$_3$, 400 MHz) δ= 1.20 – 1.42 (m, 12H, CH$_2$$^{13-18,}$), 1.48 (p, J = 7.7, 7.5, 6.4 Hz, 2H, CH$_2$^{19}), 1.52 – 1.60 (m, 2H, CH$_2$^{12}), 1.89 (p, J = 6.9 Hz, 2H,CH$_2$^{25}), 2.54 (t, J= 7.6 Hz, 2H, CH$_2$^{11}), 2.61 (t, J= 7.4 Hz, 2H, CH$_2$^{26}), 2.71 (td, J= 6.9, 2.3 Hz, 4H, CH$_2$^{2,9}), 3.15 (q, J = 6.8 Hz, 2H, CH$_2$^{20}), 3.69–3.58 (m, 8H, CH$_2$^{3,5,6,8}), 4.13 (t, J = 6.3 Hz, 2H, CH$_2$^{24}), 4.71 (br, s, 1H, NH^{21}) ppm.
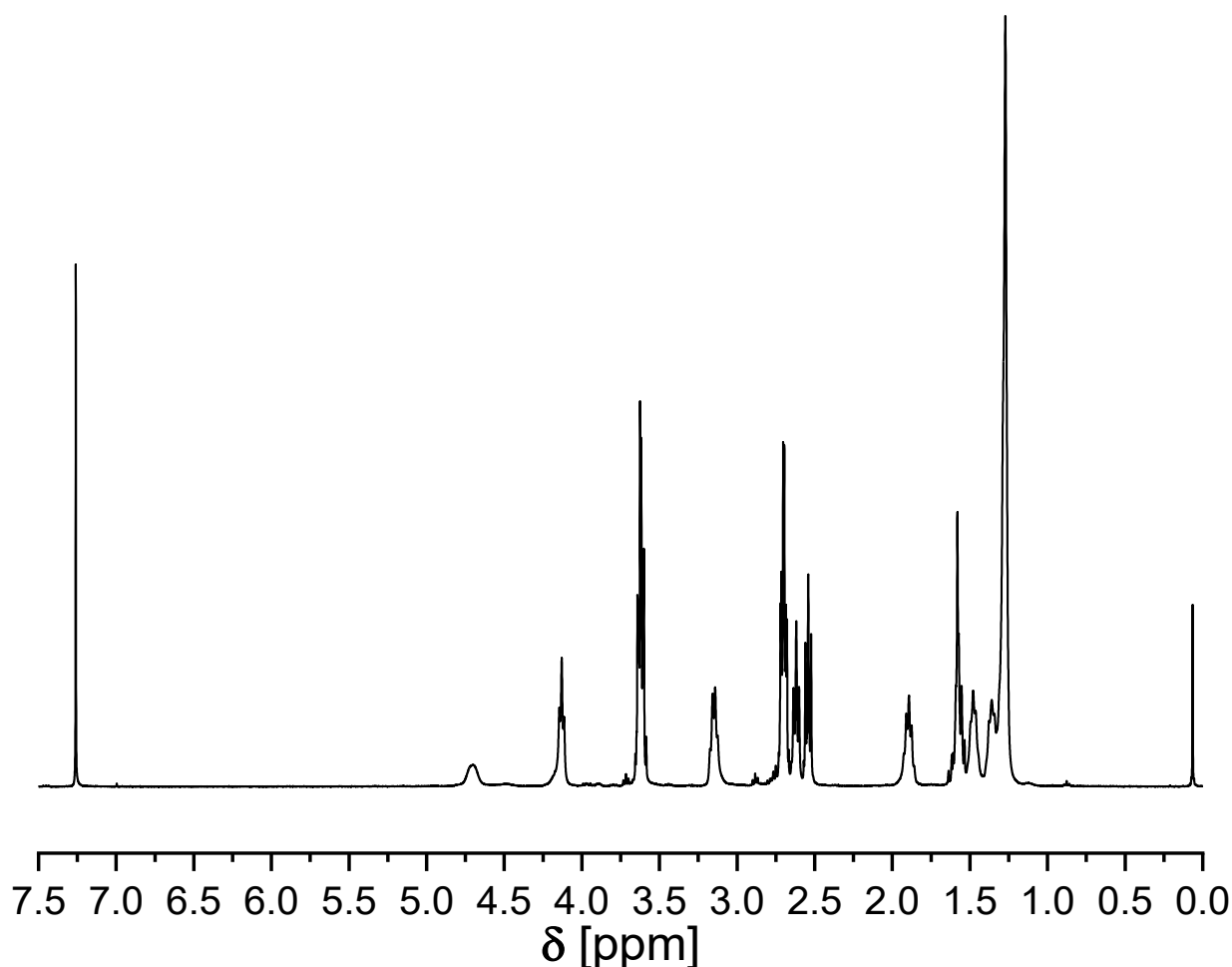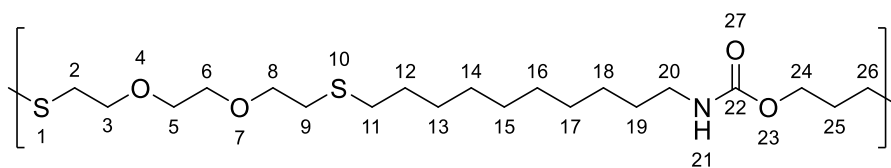
IR (ATR) ṽ = 3311.6, 2916.7, 2898.2, 2848.8, 1682.5, 1540.6, 1466.6, 1439.8, 1417.2, 1351.4, 1320.5, 1279.4, 1246.5, 1127.2, 1110.7, 1036.7, 975.0, 946.2, 888.6, 781.6, 736.4, 722.0 cm^{-1}.
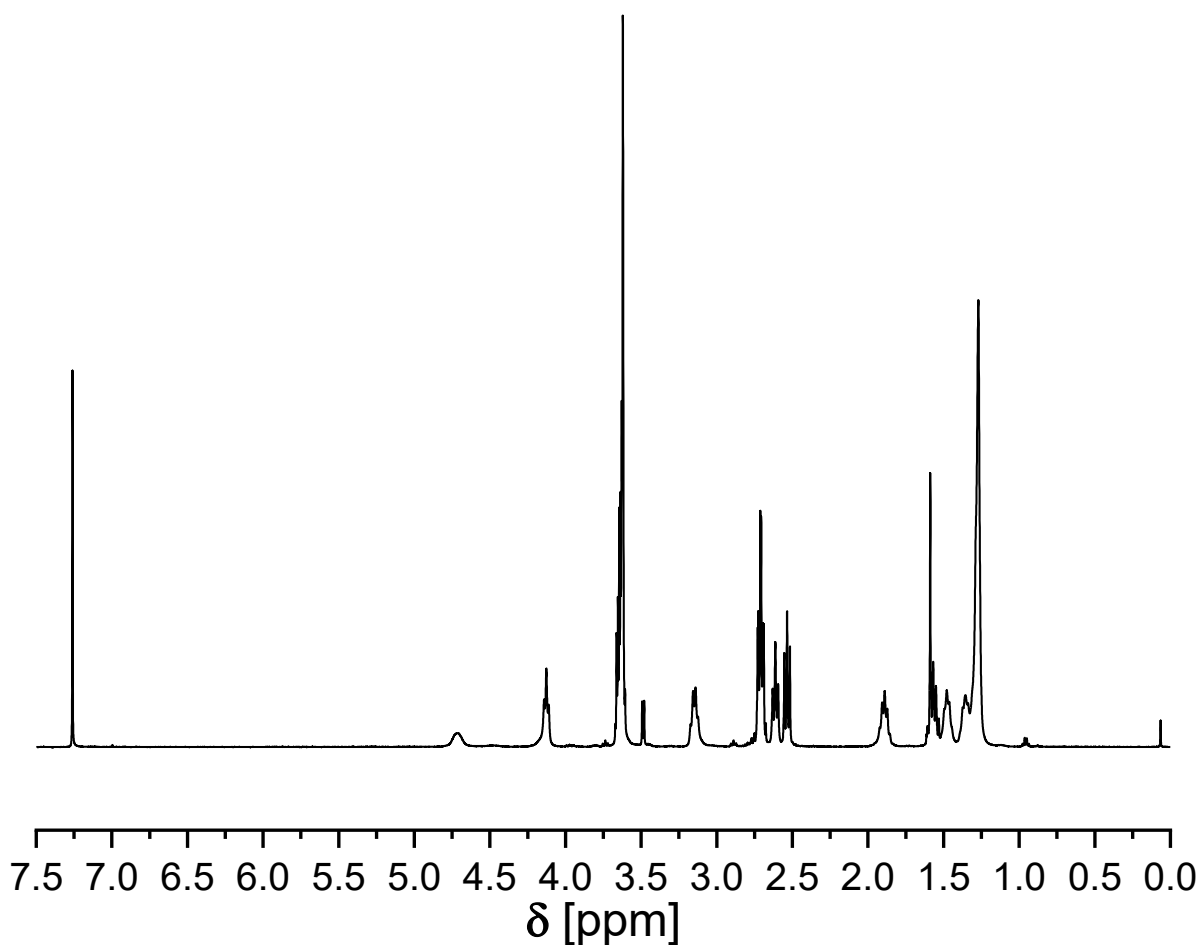
Figure 118 ^{1}H-NMR spectrum of **P14** (400 MHz, CDCl$_3$).

P15
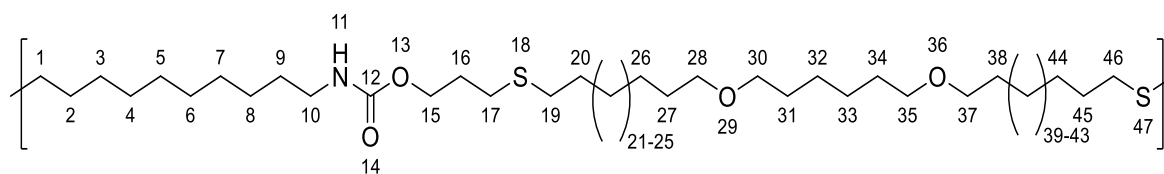
The thiol-ene polymerization of allyl dec-9-enyl carbamate **4** (1.00 eq.) and 10,10'-(hexane-1,6-diylbis(oxy))bis(decane-1-thiol) (1.00 eq.) led to the formation of **P15** as a colorless solid (95%).

^{1}H NMR (CDCl$_3$, 400 MHz) δ= 1.20 – 1.42 (m, 40H, CH$_2$[3-8,21-26,32,33,39-44]), 1.44-1.51 (m, 2H, CH$_2$[9]), 1.52 – 1.62 (m, 14H, CH$_2$[2,20,27,31,34,38,45]), 1.89 (p, J = 8.0, 6.7 Hz, 2H,CH$_2$[16]), 2.50 (td, J= 7.5, 2.6 Hz, 6H, CH$_2$[1,19,46]), 2.56 (t, J= 7.3 Hz, 2H, CH$_2$[17]), 3.15 (q, J = 6.6, 6.1 Hz, 2H, CH$_2$[10]), 3.39 (td, J= 6.7, 2.9 Hz, 8H, CH$_2$[28,30,35,37]), 4.14 (t, J= 6.2 Hz, 2H, CH$_2$[15]), 4.65 (br, s, 1H, NH[11]) ppm.

IR (ATR) ṽ = 3334.2, 2918.8, 2850.9, 1688.7 (amide), 1534.5, 1485.1, 1468.6, 1376.1, 1283.5, 1242.4, 1114.8, 1053.1, 1036.7, 1022.3, 719.9 cm^{-1}.
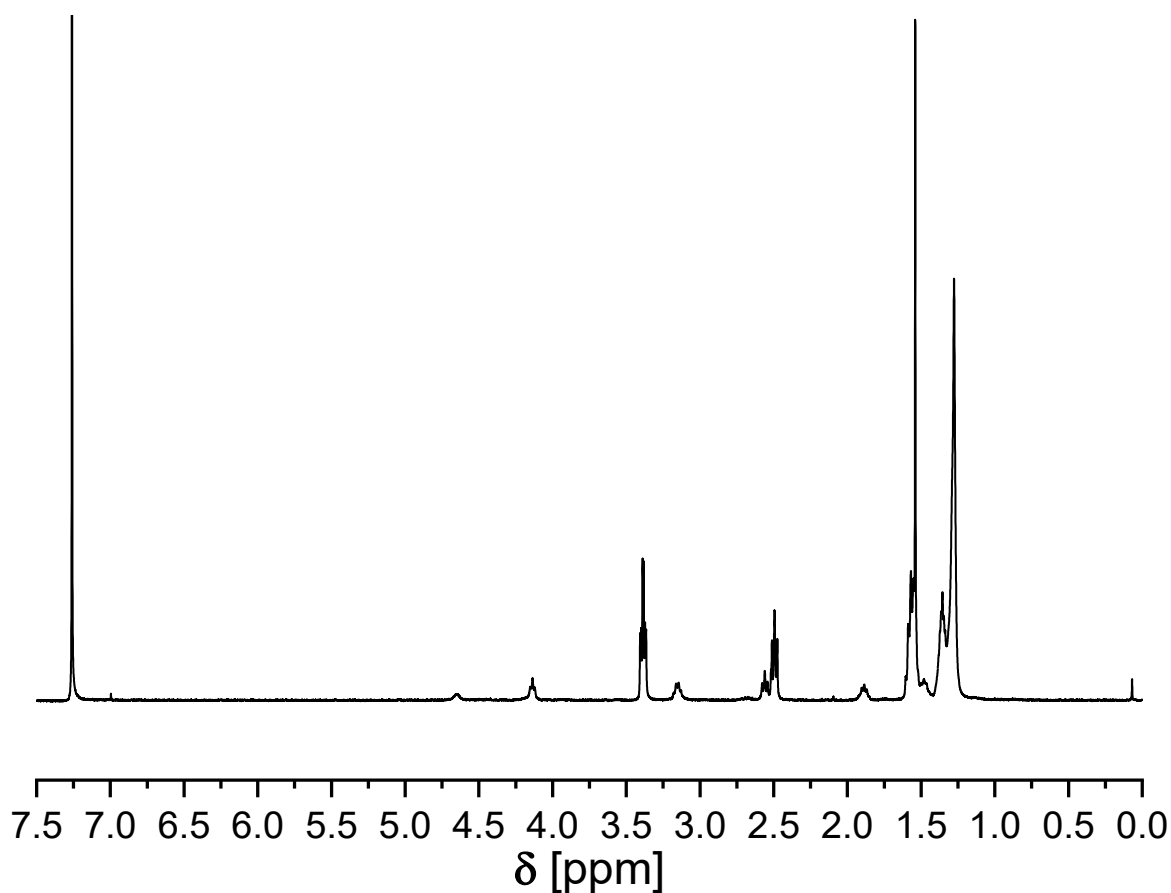
Figure 119 ^{1}H NMR spectrum of **P15** (400 MHz, CDCl$_3$).

P16
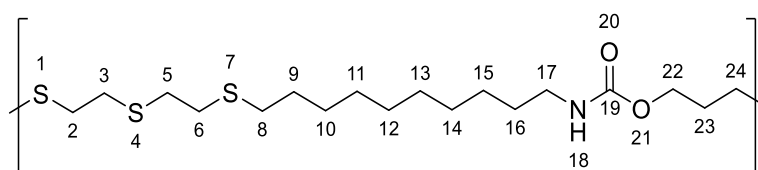
The thiol-ene polymerization of allyl dec-9-enyl carbamate **4** (1.00 eq.) and 2,2′-thiobis (ethane-1-thiol) (1.00 eq.) led to the formation of **P16** as a colorless solid (80%).

¹H NMR (CDCl$_3$, 400 MHz) δ= 1.19 – 1.42 (m, 12H, CH$_2$$^{10-15}$), 1.48 (p, *J* = 7.3 Hz, 2H, CH$_2$^{16}), 1.58 (m, *J* = 7.7, 6.8 Hz, 2H, CH$_2$^{9}), 1.89 (p, *J* = 6.6 Hz, 2H, CH$_2$^{23}), 2.53 (t, *J* = 7.4 Hz, 2H, CH$_2$^{8}), 2.60 (t, *J* = 7.3 Hz, 2H, CH$_2$^{24}), 2.67 – 2.82 (m, 8H, CH$_2$^{2,3,5,6}), 3.15 (q, *J* = 6.8 Hz, 2H, CH$_2$^{17}), 4.13 (t, *J* = 6.2 Hz, 2H, CH$_2$^{22}), 4.72(br, s, 1H, NH^{18}) ppm.

IR (ATR) ṽ = 3330.1, 2920.8, 2848.8, 1682.6 (amide), 1534.5, 1468.6, 1423.4, 1293.8, 1267.1, 1246.5, 1188.9, 1135.4, 1014.1, 779.6, 722.0, 707.6 cm^{-1}.

Figure 120 ¹H NMR spectrum of **P16** (400 MHz, CDCl$_3$).

P17

The thiol-ene polymerization of allyl dec-9-enyl carbamate **4** (1.00 eq.) and 1,4-Butanediol bis(thioglycolate) (1.00 eq.) led to the formation of **P17** as a colorless solid (87%).

¹H NMR (CDCl₃, 400 MHz) δ= 1.41 – 1.19 (m, 12H, CH_2^{3-8}), 1.48 (p, J = 7.0, 6.5 Hz, 2H, CH_2^9), 1.59 (p, J = 7.7, 6.9 Hz, 2H, CH_2^2), 1.75 (hept, J = 2.9 Hz, 4H, $CH_2^{22,23}$), 1.91 (p, J = 6.8 Hz, 2H, CH_2^{15}), 2.61 (t, J = 7.3 Hz, 2H, CH_2^1), 2.70 (t, J = 7.3 Hz, 2H, CH_2^{16}), 3.15 (q, J = 6.8 Hz, 2H, CH_2^{10}), 3.21 (d, J = 3.2 Hz, 4H, $CH_2^{18,27}$), 4.24 – 4.09 (m, 6H, $CH_2^{14,21,24}$), 4.74 (br, s, 1H, NH^{11}) ppm.

IR (ATR) ṽ = 3321.9, 2920.8, 2850.9, 1725.7 (ester), 1680.5 (amide), 1536.5, 1468.6, 1411.0, 1386.4, 1265.0, 1246.5 (sulfone), 1168.3, 1129.2 (sulfone), 1079.9, 1034.6, 954.4, 886.5, 779.6, 719.9 cm⁻¹.

Figure 121 ¹H NMR spectrum of **P17** (400 MHz, CDCl₃).

P18

The thiol-ene polymerization of allyl dec-9-enyl carbamate **4** and ethane-1,2-diyl bis(3-mercaptopropanoate) led to the formation of **P18** as a colorless solid (86%).

^{1}H NMR (CDCl$_3$, 400 MHz) δ= 1.21 – 1.41 (m, 12H, CH$_2$$^{17-22}$), 1.47 (q, J = 7.1 Hz, 2H, CH$_2$^{23}), 1.58 (p, J = 7.7, 7.2 Hz, 2H CH$_2$^{16}), 1.89 (p, J = 6.7 Hz, 2H, CH$_2$^{30}), 2.53 (t, J = 7.5 Hz, 2H, CH$_2$^{15}), 2.55 – 2.67 (m, 6H, CH$_2$^{3,12,31}), 2.78 (td, J = 7.1, 4.5 Hz, 4H, CH$_2$^{2,13}), 3.15 (q, J = 6.8 Hz, 2H, CH$_2$^{24}), 4.14 (t, J = 6.3 Hz, 2H, CH$_2$^{29}), 4.31 (s, 4H, CH$_2$^{7,8}), 4.75 (br, s, 1H, NH^{25}) ppm.
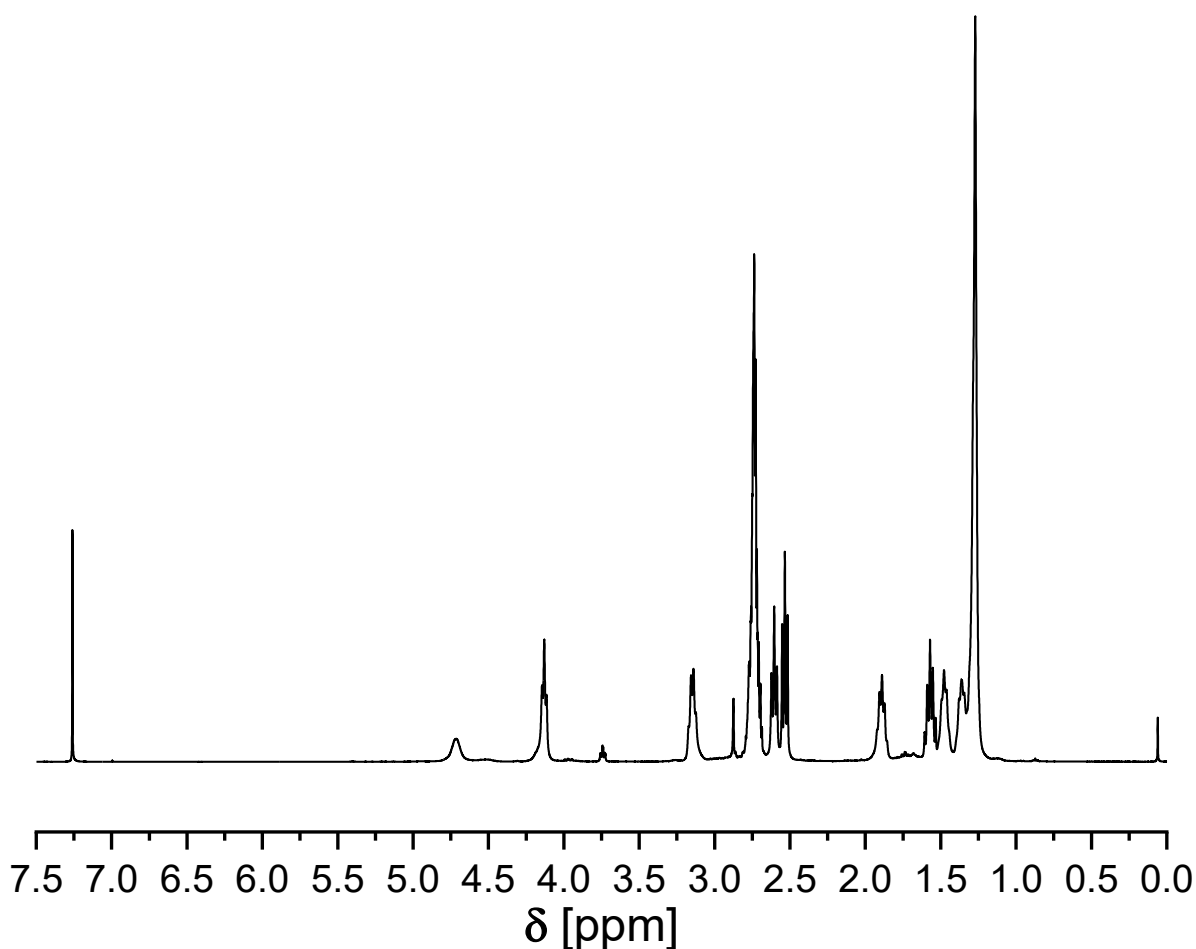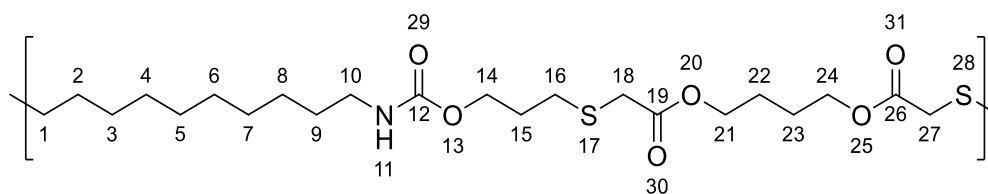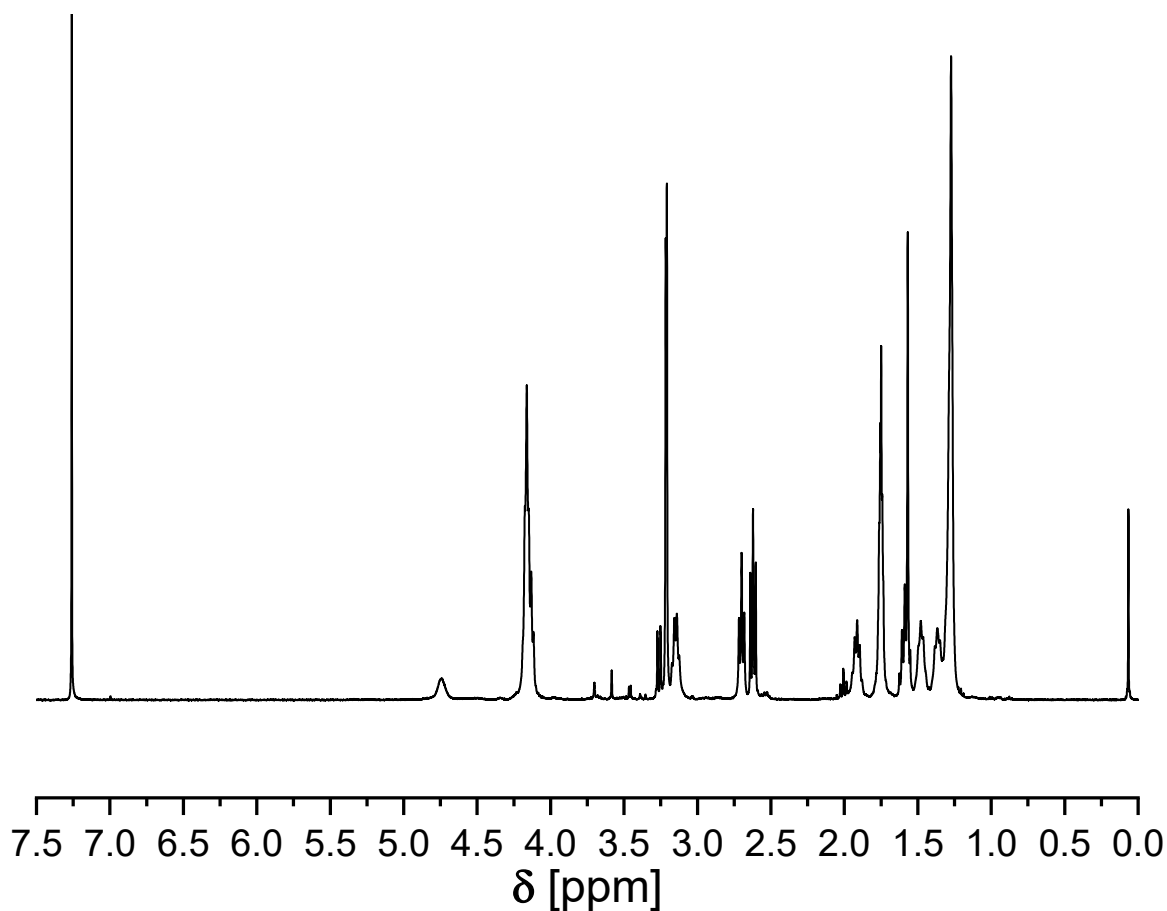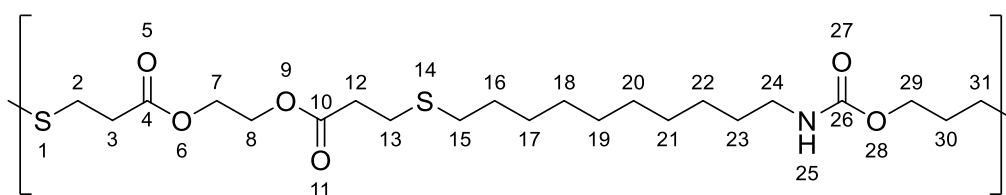
IR (ATR) ṽ = 3324.0, 2918.8, 2848.8, 1729.9 (ester), 1717.5, 1682.6 (amide), 1532.4, 1468.6, 1456.3, 1437.8, 1423.4, 1415.2, 1374.0, 1341.1, 1242.4, 1137.5, 1038.7, 981.1, 952.3, 777.5 cm^{-1}.
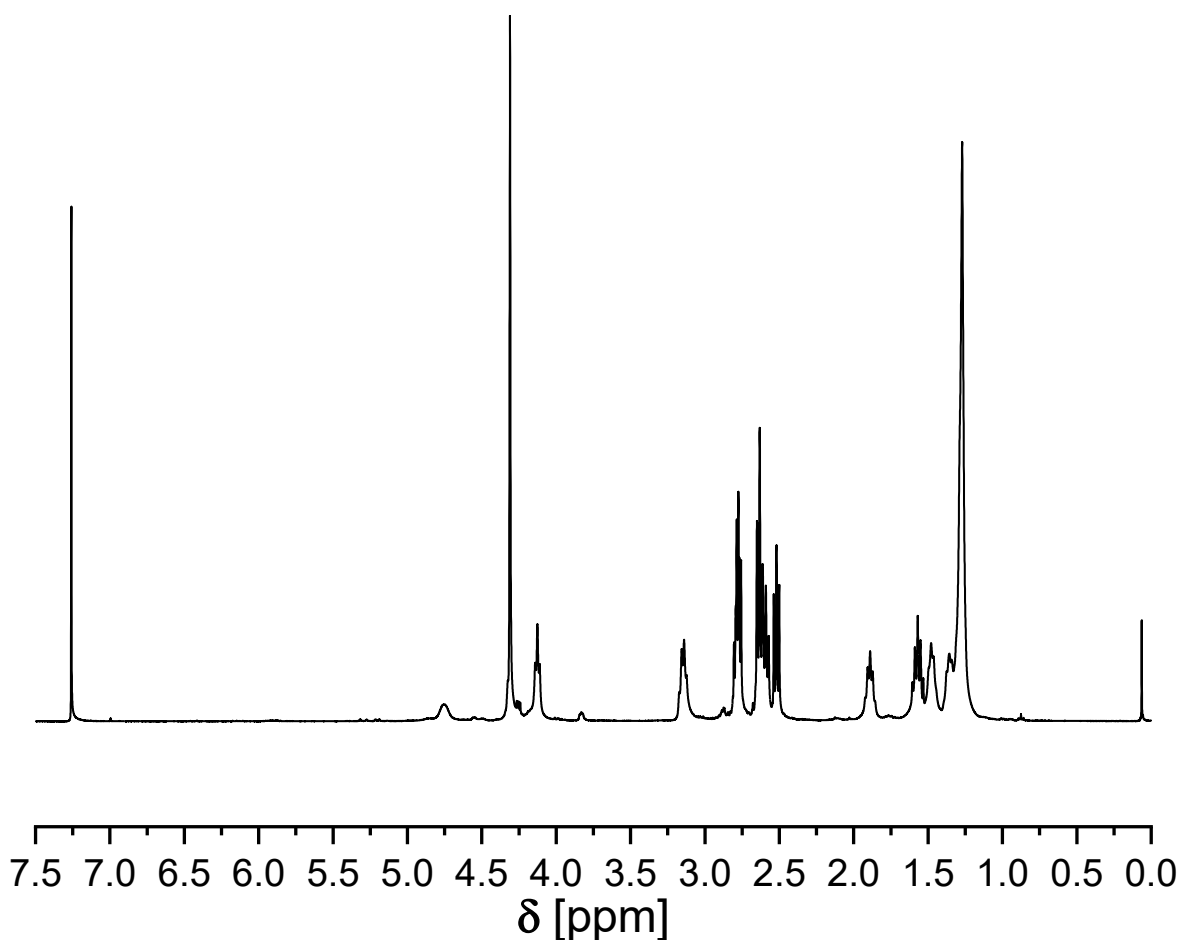
Figure 122 ^{1}H NMR spectrum of **P18** (400 MHz, CDCl$_3$).

P19
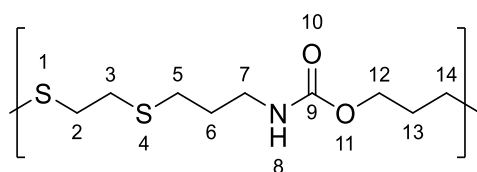
The thiol-ene polymerization of allyl allyl carbamate **3** (1.00 eq.) and 1,2-ethanedithiol (1.00 eq.) led to the formation of **P19** as a colorless solid (84%).

^{1}H NMR (CDCl$_3$, 400 MHz) δ= 1.81 (p, *J* = 7.1 Hz, 2H, CH$_2$^{6}), 1.90 (p, *J* = 6.7 Hz, 2H, CH$_2$^{13}), 2.60 (q, *J* = 7.5 Hz, 4H, CH$_2$^{5,14}), 2.73 (s, 4H, CH$_2$^{2,3}), 3.28 (q, *J* = 7.5 Hz, 2H, CH$_2$^{7}), 4.14 (t, *J* = 7.5 Hz, 2H, CH$_2$^{12}), 5.08 (br, s, 1H, NH^{11}) ppm.

IR (ATR) ṽ = 3321.9, 2953.7, 2922.9, 2852.9, 1682.6 (amide), 1536.5, 1437.8, 1423.4, 1297.9, 1246.5, 1201.2, 1137.5, 1075.8, 1014.1, 777.5 cm^{-1}.
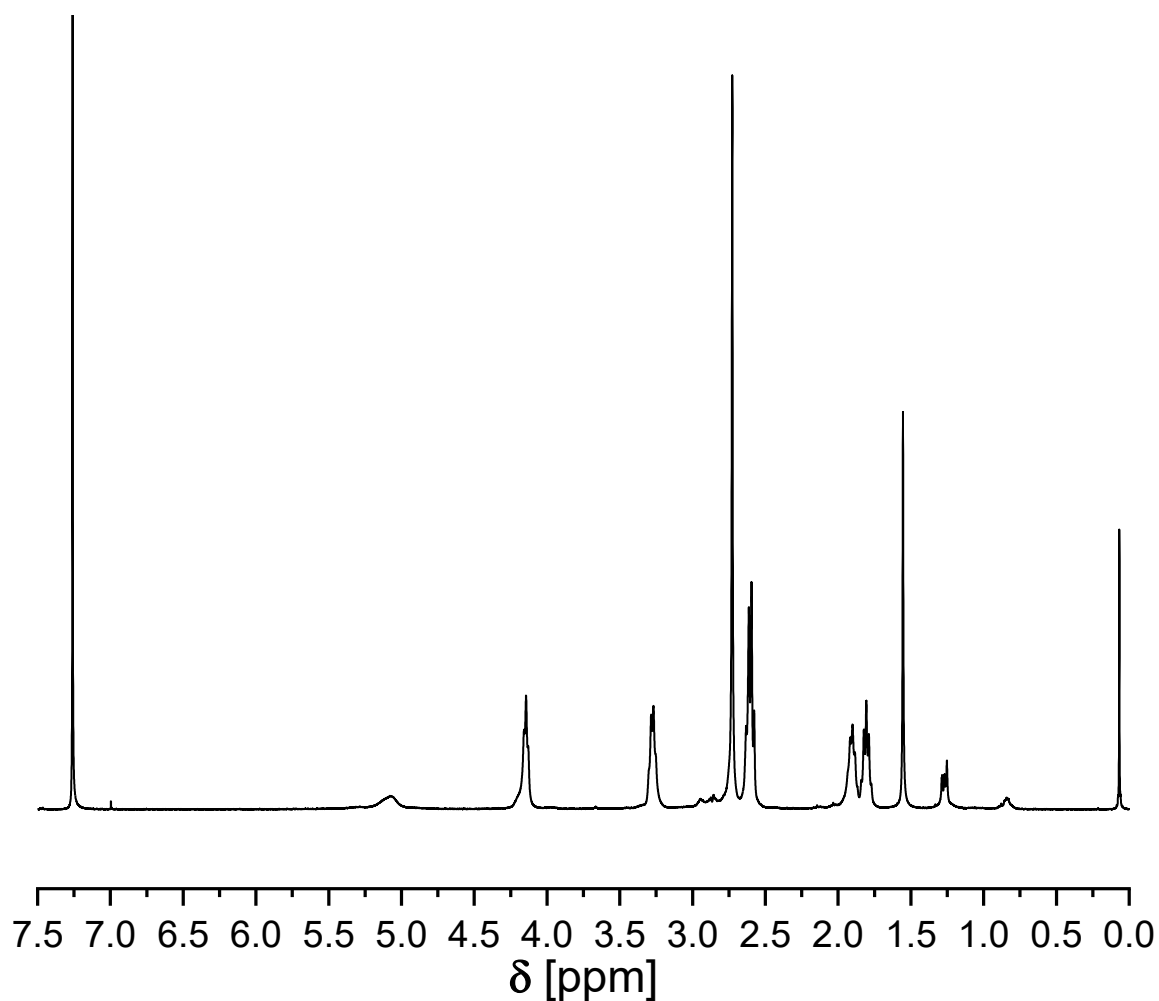
Figure 123 ^{1}H NMR spectrum of **P19** (400 MHz, CDCl$_3$).

P20
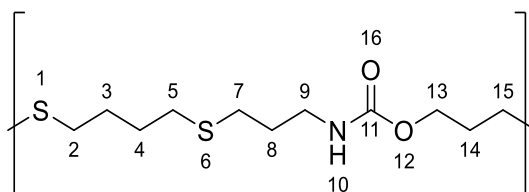
The thiol-ene polymerization of allyl allyl carbamate **x** (1.00 eq.) and 1,4-butanedithiol (1.00 eq.) led to the formation of **P20** as a colorless solid (90%).

^{1}H NMR (CDCl$_3$, 400 MHz) δ= 1.68 (dd, J = 10.6, 3.3 Hz, 4H, CH$_2^{3,4}$), 1.79 (p, J = 7.0 Hz, 2H CH$_2^8$), 1.88 (p, J = 6.9 Hz, 2H, CH$_2^{14}$), 2.49 − 2.60 (m, 8H, CH$_2^{2,5,7,15}$), 3.27 (q, J = 6.5 Hz, 2H, CH$_2^9$), 4.14 (q, J = 6.3, 5.7 Hz, 2H, CH$_2^{13}$), 4.96 (br, s, 1H, NH^{10}) ppm.

IR (ATR) ṽ = 3315.7, 2935.2, 2918.8, 2855.0, 1678.4 (amide), 1536.5, 1470.7, 1431.6, 1326.7, 1310.3, 1254.7, 1193.0, 1137.5, 1077.8, 1042.9, 1009.9, 798.1, 779.6, 746.7, 732.2 cm^{-1}.
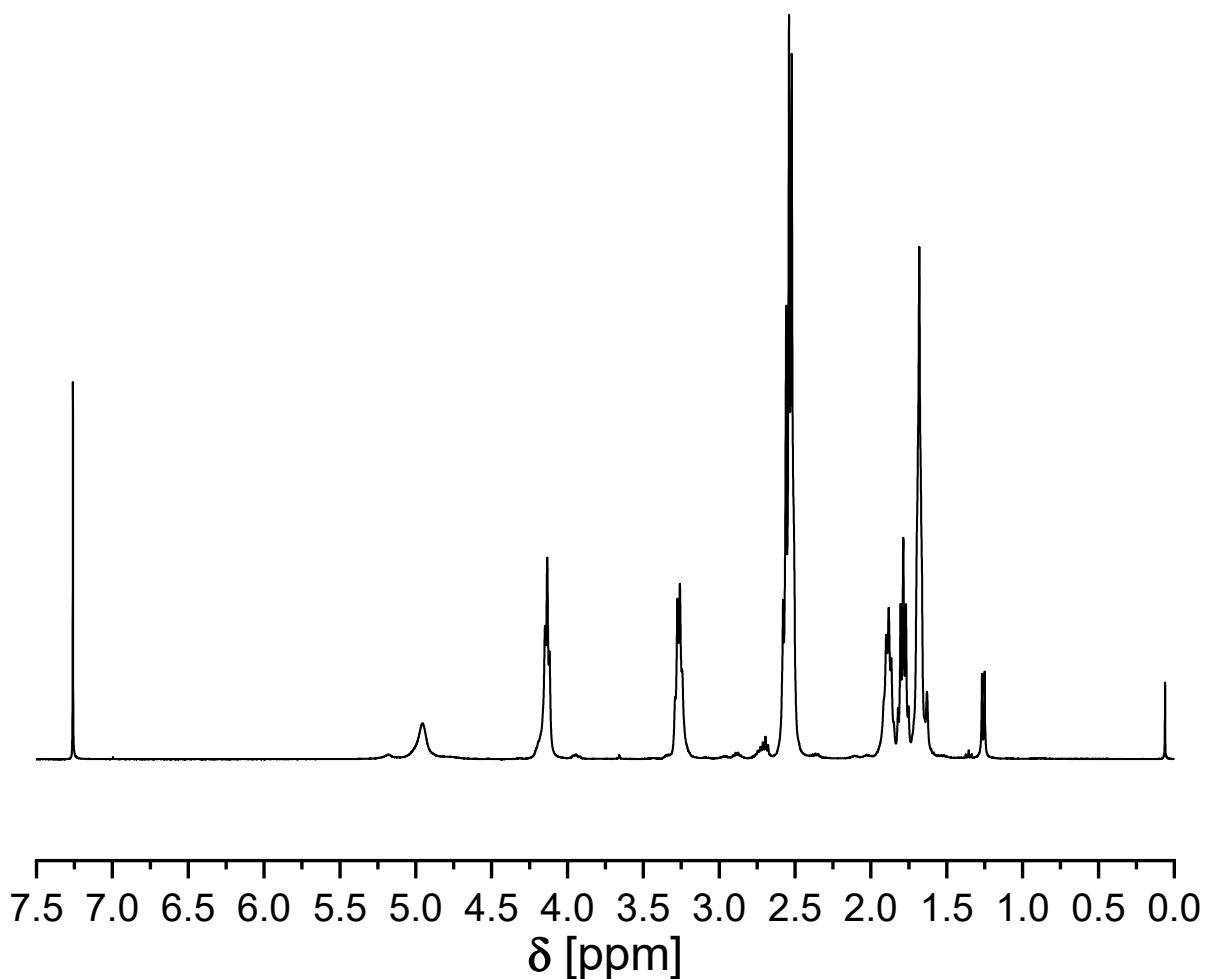
Figure 124 ^{1}H NMR spectrum of **P20** (400 MHz, CDCl$_3$). The contamination at 1.25 ppm could not be identified or removed through multiple precipitation steps.

P21
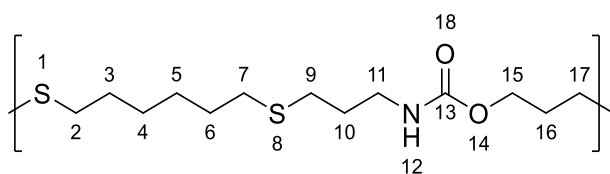
The thiol-ene polymerization of allyl allyl carbamate **3** (1.00 eq.) and 1,6-hexanedithiol (1.00 eq.) led to the formation of **P21** as a colorless solid (90%).

¹H NMR (CDCl₃, 400 MHz) δ= 1.39 (dq, *J* = 10.0, 6.3, 4.8 Hz, 4H, CH₂⁴ˏ⁵), 1.52 − 1.63 (m, 4H, CH₂³ˏ⁶), 1.79 (p, *J* = 7.0 Hz, 2H, CH₂¹⁰), 1.88 (p, *J* = 5.6 Hz, 2H, CH₂¹⁶), 2.41 − 2.61 (m, 8H, CH₂²ˏ⁷ˏ⁹ˏ¹⁷), 3.27 (q, *J* = 6.8 Hz, 2H, CH₂¹¹), 4.14 (t, *J* = 5.9 Hz, 2H, CH₂¹⁵), 4.89 (br, s, 1H, NH¹²) ppm.

IR (ATR) ṽ = 3315.7, 2920.8, 2850.9, 1678.4 (amide), 1538.6, 1470.7, 1460.4, 1450.1, 1431.6, 1326.7, 1252.7, 1221.8, 1188.9, 1141.6, 1075.8, 1047.0, 1012.0, 775.5, 746.7, 726.1 cm⁻¹.
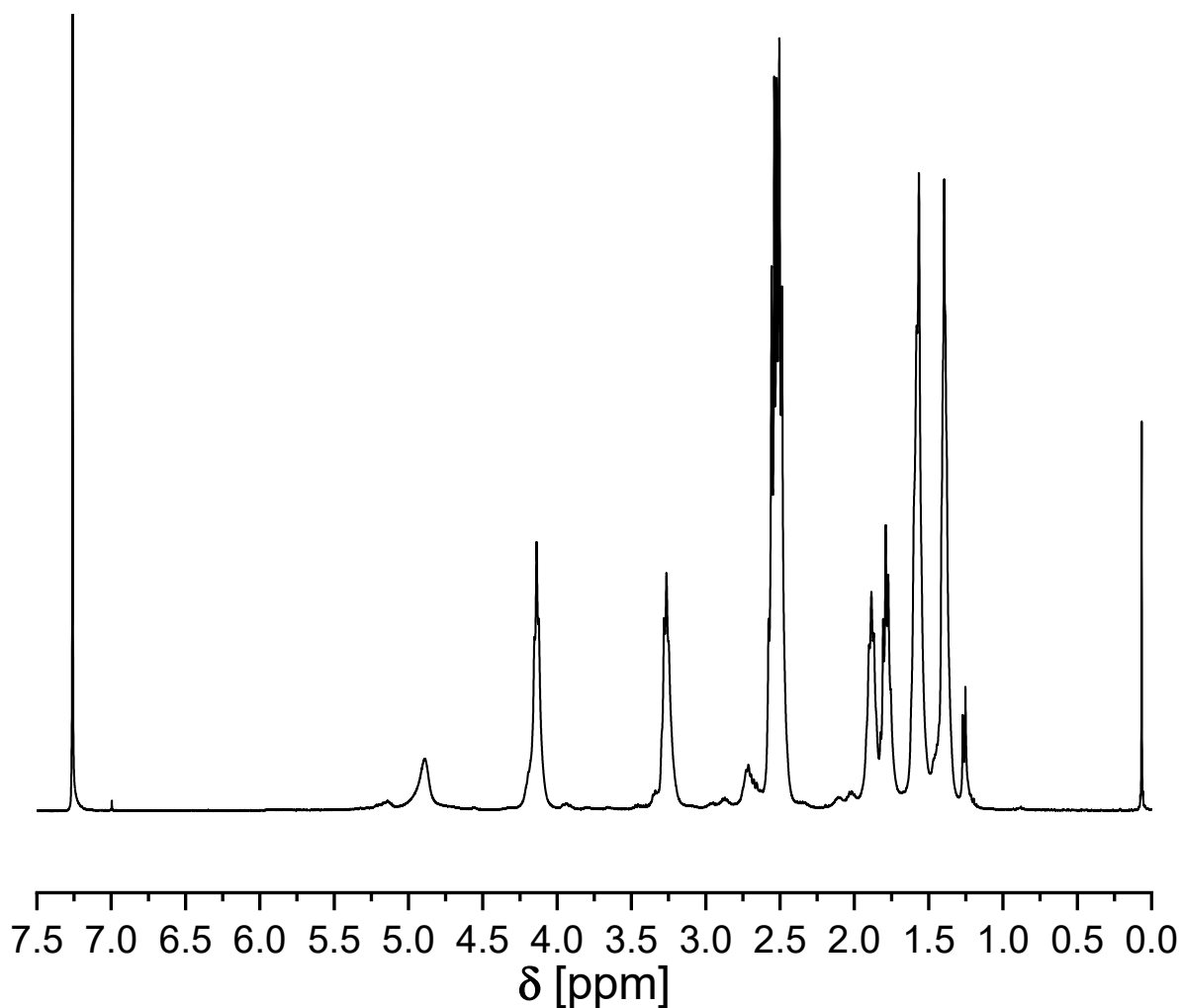
Figure 125 ¹H NMR spectrum of **P21** (400 MHz, CDCl₃).

P22
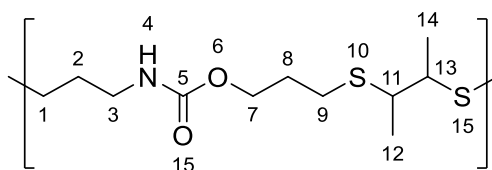
The thiol-ene polymerization of allyl allyl carbamate **3** (1.00 eq.) and 2,3-butanedithiol (1.00 eq.) led to the formation of **P22** as a transparent viscous substance (85%).

¹H NMR (CDCl₃, 400 MHz) δ= 1.27 − 1.40 (m, 6H, $CH_3^{12,14}$), 1.79 (p, J = 7.8, 6.9 Hz, 2H, CH_2^2), 1.88 (p, J = 6.2, 4.7 Hz, 2H, CH_2^8), 2.47 − 2.68 (m, 4H, $CH_2^{1,9}$), 2.89 − 3.06 (m, 2H, $CH^{11,13}$), 3.20 (q, J = 7.2, 7.2, 5.2 Hz, 2H, CH_2^3), 4.14 (t, J = 6.2 Hz, 2H, CH_2^7), 5.12 (s, 1H, NH^4) ppm.

IR (ATR) ṽ = 3326.0, 2961.9, 2924.9, 1692.8 (amide), 1522.1, 1443.9, 1372.0, 1316.4, 1242.4, 1176.6, 1135.4, 1102.5, 1073.7, 1036.7, 1009.9, 954.4, 775.5 cm⁻¹.
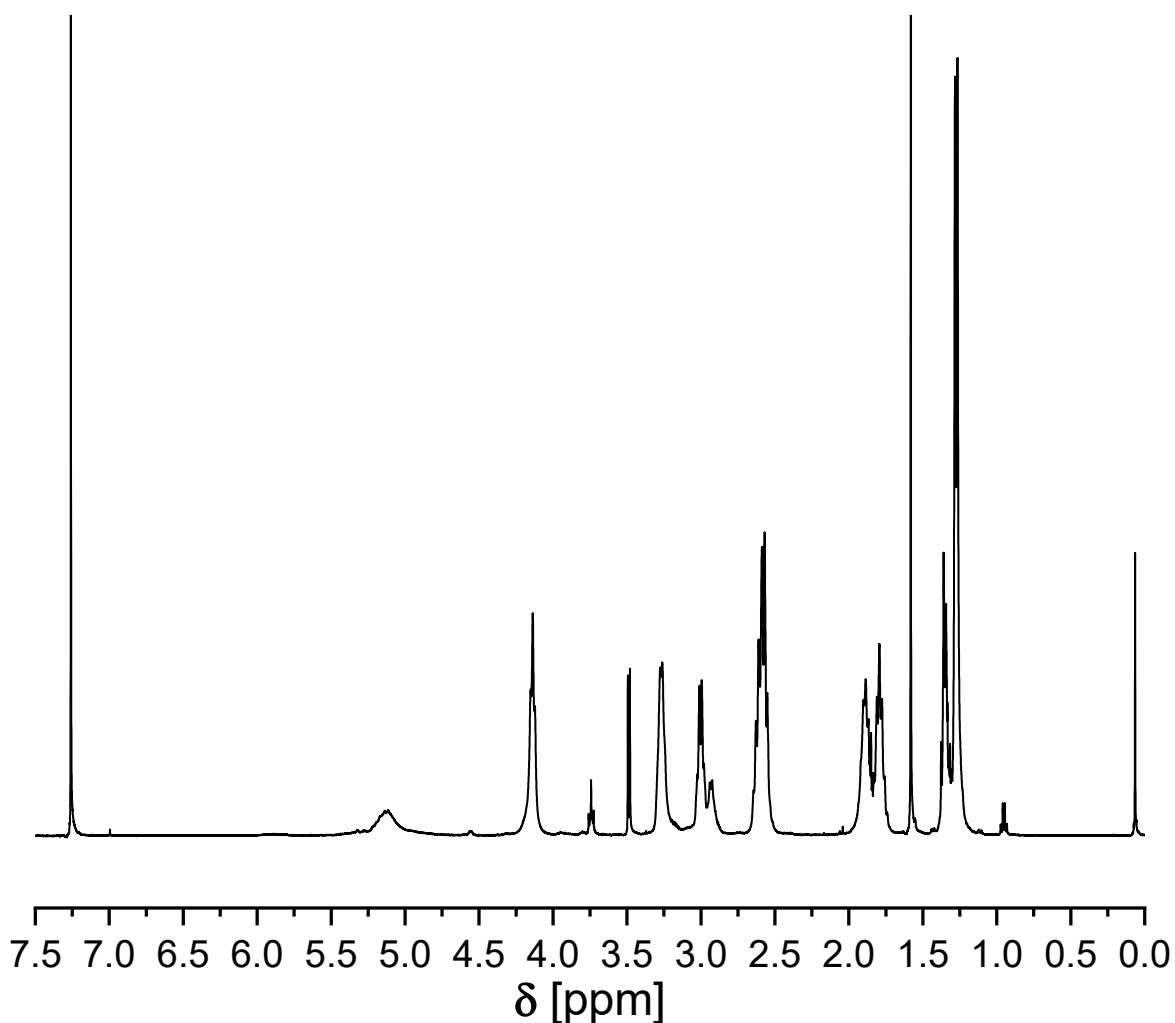
Figure 126 ¹H NMR spectrum of **P22** (400 MHz, CDCl₃). The impurity at 3.49 ppm belongs to residual methanol.

286

P23
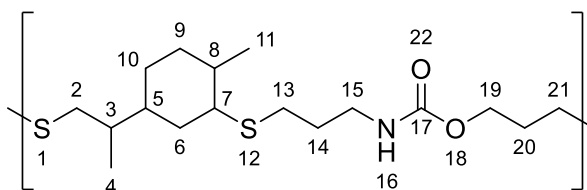
The thiol-ene polymerization of allyl allyl carbamate **3** (1.00 eq.) and limonene dithiol (1.00 eq.) led to the formation of **P23** as a transparent viscous substance (90%).

^{1}H NMR (CDCl$_3$, 400 MHz) δ= 0.99 (m, CH^3, CH$_3$^{4,11}), 1.55 (m, 1H, CH^8), 1.70 – 1.75 (m, CH$_2$^{6,10}, CH^8), 1.79 (p, J = 7.0 Hz, 2H, CH$_2$^{14}), 1.88 (p, J = 6.9 Hz, 2H, CH$_2$^{20}), 2.49 – 2.62 (m, CH^{3,5,7}, CH$_2$^{2,13,21}), 2.93 (br, s, CH^7), 3.27 (q, J = 6.7, 6.3, 5.5 Hz, 2H, CH$_2$^{15}), 4.14 (t, J = 6.4 Hz, 2H, CH$_2$^{19}), 4.99 (br, s, 1H, NH^{16}) ppm.

IR (ATR) ṽ = 3326.0, 2953.7, 2918.8, 2867.3, 2850.9, 1694.9 (amide), 1524.2, 1446.0, 1374.0, 1318.5, 1244.4, 1135.4, 1075.8, 1014.1, 913.3, 775.5, 730.2 cm^{-1}.
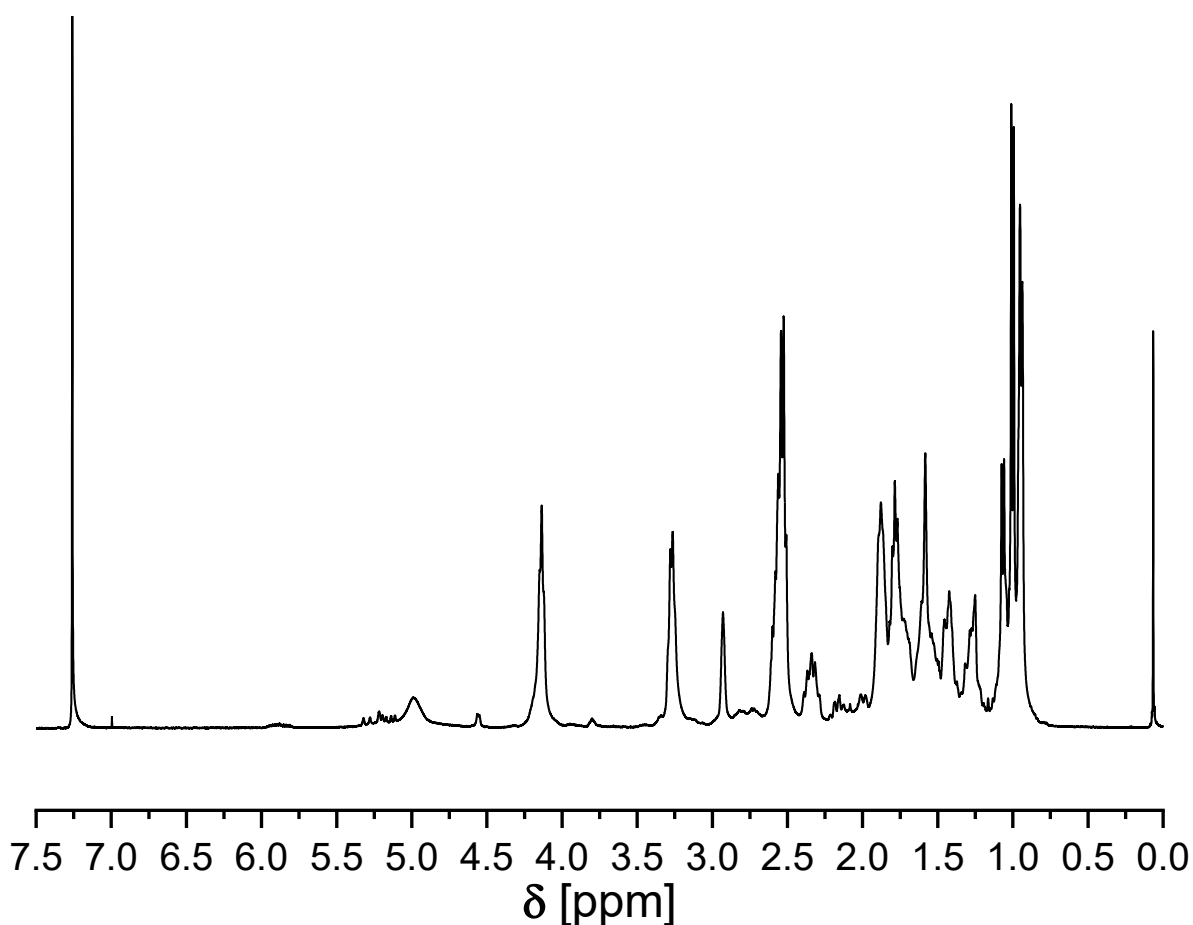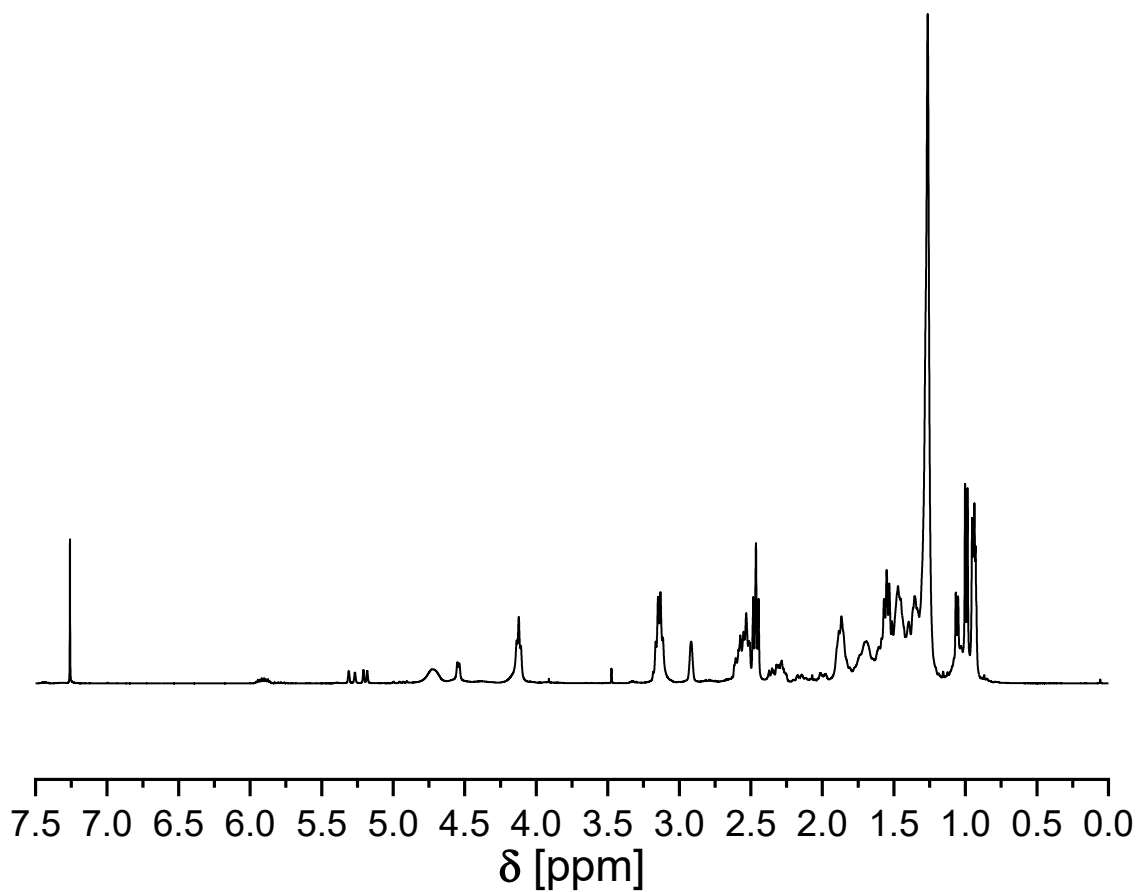

Figure 127 ^{1}H NMR spectrum of **P23** (400 MHz, CDCl$_3$).

P24
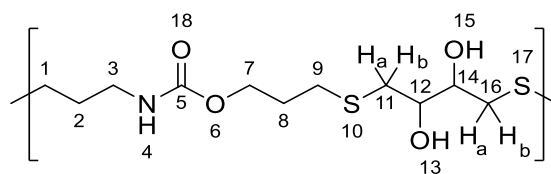
The thiol-ene polymerization of allyl allyl carbamate **3** (1.00 eq.) and dithioerythritol (1.00 eq.) led to the formation of **P24** as a colorless solid (83%).

^{1}H NMR (DMSO-d_6, 400 MHz) δ= 1.64 (p, J = 7.1 Hz, 2H, CH$_2^2$), 1.79 (p, J = 6.7 Hz, 2H, CH$_2^8$), 2.43 − 2.52 (m, 2H, CH$_2^{11b,16b}$), 2.56 (t, J = 7.2 Hz, 6H, CH$_2^{1,9,11b,16b}$), 2.70 − 2.83 (m, 2H, CH$_2^{11a,16a}$), 3.04 (q, J = 6.5 Hz, 2H, CH$_2^3$),3.37 − 3.47 (m, 2H, CH^{12,14}), 4.00 (q, J = 6.6 Hz, 2H, CH$_2^7$), 4.86 (ddt, J = 8.1, 5.7, 4.1 Hz, 2H, OH^{13,15}), 7.12 (t, J = 5.7 Hz, 1H, NH^4) ppm.

IR (ATR) ṽ = 3330.1, 2920.8, 2896.1, 1680.5 (amide), 1536.5, 1470.7, 1435.7, 1417.2, 1334.9, 1248.5, 1139.5, 1049.0, 977.0, 777.5 cm^{-1}.
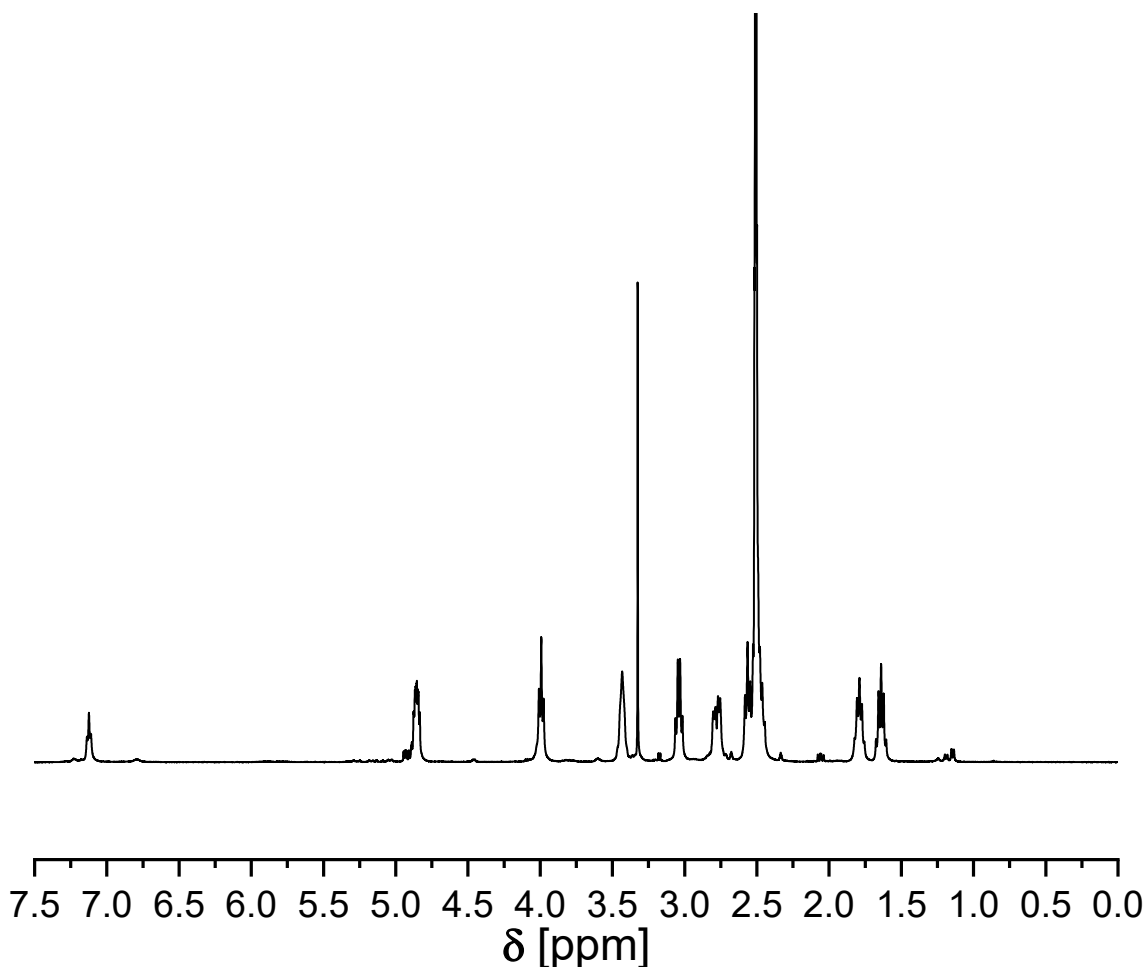
Figure 128 ^{1}H NMR spectrum of **P24** (400 MHz, DMSO-d_6). The impurity at 3.3 ppm derives from residual water in the deuterated solvent.

P25
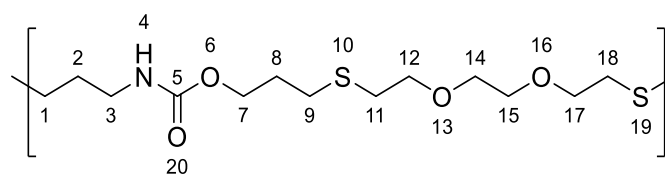
The thiol-ene polymerization of allyl allyl carbamate **3** (1.00 eq.) and 3,6-oxa-1,8-octanedithiol (1.00 eq.) led to the formation of **P25** as a colorless solid (79%).

^{1}H NMR (CDCl$_3$, 400 MHz) δ= 1.80 (p, J = 7.0 Hz, 2H, CH$_2^2$), 1.89 (t, J = 7.1 Hz, 2H, CH$_2^8$), 2.55 – 2.66 (m, 4H, CH$_2^{1,9}$), 2.71 (td, J = 6.8, 1.7 Hz, 4H, CH$_2^{11,18}$), 3.27 (q, J = 6.6 Hz, 2H, CH$_2^3$), 3.58 – 3.71 (m, 8H, CH$_2^{12,14,15,17}$), 4.13 (t, J = 6.2 Hz, 2H, CH$_2^7$), 5.01 (s, 1H, NH^4) ppm.

IR (ATR) ṽ = 3330.1, 2916.7, 2863.2, 1696.9 (amide), 1526.2, 1470.7, 1441.9, 1351.4, 1320.5, 1244.4, 1098.4, 1038.7, 1003.8, 775.5 cm^{-1}.
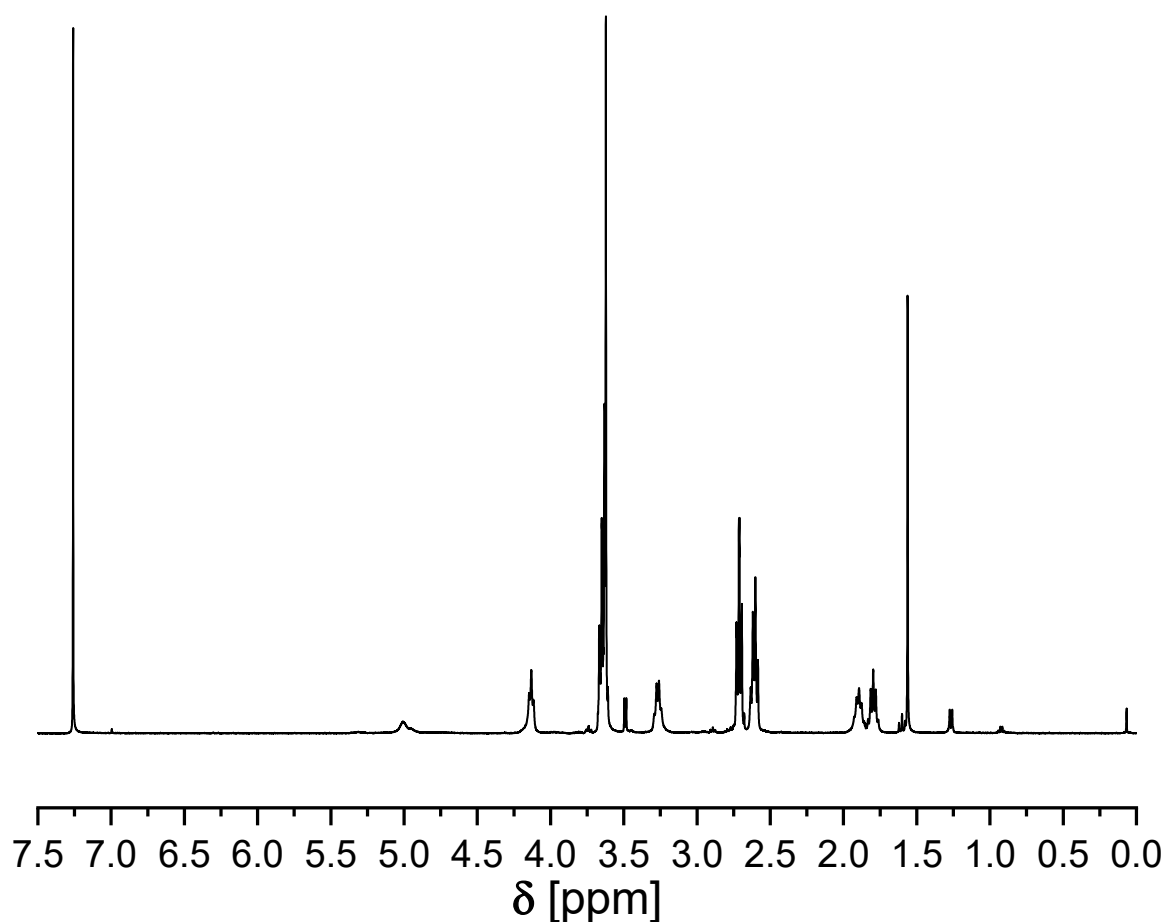
Figure 129 ^{1}H NMR spectrum of **P25** (400 MHz, CDCl$_3$).

P26
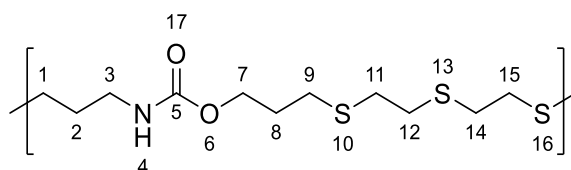
The thiol-ene polymerization of allyl allyl carbamate **3** (1.00 eq.) and 2,2′-thiobis (ethane-1-thiol) (1.00 eq.) led to the formation of **P26** as a colorless solid (84%).

^{1}H NMR (CDCl$_3$, 400 MHz) δ= 1.80 (p, J = 6.9 Hz, 2H, CH$_2$^{2}), 1.90 (h, J = 6.8, 6.2 Hz, 2H, CH$_2$^{8}), 2.60 (q, J = 7.3 Hz, 4H, CH$_2$^{1,9}), 2.75 (tt, J = 7.3, 3.5 Hz, 8H, CH$_2$^{11,12,14,15}), 3.27 (q, J = 6.6 Hz, 2H, CH$_2$^{3}), 4.14 (t, J = 6.1 Hz, 2H, CH$_2$^{7}), 4.99 (br, s, 1H, NH^4) ppm.

IR (ATR) ṽ = 3321.9, 2953.7, 2924.9, 1682.6 (amide), 1536.5, 1468.6, 1437.8, 1423.4, 1250.6, 1193.0, 1137.5, 1073.7, 1038.7, 1016.1, 777.5 cm^{-1}.

Figure 130 ^{1}H NMR spectrum of **P26** (400 MHz, CDCl$_3$).

P27
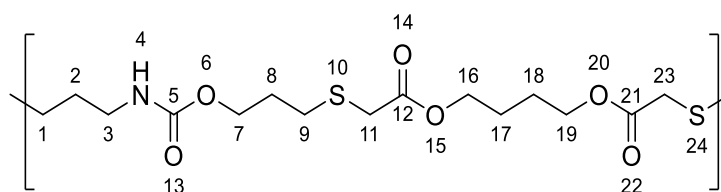
The thiol-ene polymerization of allyl allyl carbamate **3** (1.00 eq.) and 1,4-Butanediol bis(thioglycolate) (1.00 eq.) led to the formation of **P27** as a colorless solid (88%).

¹H NMR (CDCl$_3$,400 MHz) δ = 1.75 (dq, J = 5.9, 2.8 Hz, 4H, CH$_2$^{17,18}), 1.89 – 1.79 (m, 2H, CH$_2$$^{2'}$), 1.92 (q, J = 6.7 Hz, 2H, CH$_2$^{8}), 2.75 – 2.63 (m, 4H, CH$_2$^{1,9}), 3.22 (s, 4H, CH$_2$^{11,23}), 3.32 – 3.24 (m, 2H, CH$_2$^{3}), 4.15 (dt, J = 16.1, 5.4 Hz, 6H, CH$_2$^{7,14,19}), 5.05 (s, 1H, NH^4) ppm.

IR (ATR) ṽ = 3350.7, 2955.8, 1715.5 (ester, amide), 1524.2, 1468.6, 1446.0, 1411.0, 1265.0, 1246.5, 1127.2, 1065.5, 1026.4, 960.6, 775.5 cm^{-1}.

Figure 131 ¹H NMR spectrum of **P27** (400 MHz, CDCl$_3$). The impurities at 1.85 and 3.73 ppm derive from residual THF.

P28

The thiol-ene polymerization of diallyl butane-1,4-diyldicarbamate **6** (1.00 eq.) and 1,4-butanedithiol (1.00 eq.) led to the formation of **P28** as a colorless solid (90%).

¹H NMR (DMSO-d_6, 400 MHz) δ= 1.28 – 1.42 (m, 4H, CH$_2$[8,9]), 1.59 (hept, J = 3.5, 3.4, 2.8, 2.6 Hz, 4H, CH$_2$[19,20]), 1.78 (p, J = 6.9, 6.5, 6.3 Hz, 4H, CH$_2$[2,15]), 2.40 – 2.63 (m, 8H, CH$_2$[1,16,18,21]), 2.95 (q, J = 5.7, 5.3, 5.0 Hz, 4H, CH$_2$[7,10]), 3.98 (t, J = 6.3 Hz, 4H, CH$_2$[3,14]), 7.07 (s, 2H, NH[6,11]) ppm.

IR (ATR) ṽ = 3313.7, 2949.6, 2935.2, 2914.6, 1680.5 (amide), 1534.5, 1478.9, 1435.7, 1406.9, 1279.4, 1236.2, 1141.6, 1028.5, 952.3, 744.6 cm^{-1}.

Figure 132 ¹H NMR spectrum of **P28** (400 MHz, DMSO-d$_6$).

P29

The thiol-ene polymerization of diallyl butane-1,4-diyldicarbamate **6** (1.00 eq.) and limonene dithiol **11** (1.00 eq.) led to the formation of **P29** as a colorless solid (91%).

^{1}H NMR (DMSO-d_6, 400 MHz) δ= 0.84 – 0.92 (m, 4H, $CH_3^{24,25}$), 0.94 (d, J = 6.6 Hz, 2H, CH_3^{24}), 1.01 (d, J = 6.4 Hz, 2H), 1.24 (s, 4H), 1.36 (s, 6H, $CH_2^{8,9}$), 1.67 – 1.89 (m, 7H, CH^{23}, $CH_2^{2,15}$), 2.29 (p, J = 1.7 Hz, 1H), 2.33 (p, J = 1.8 Hz, 6H), 2.43 – 2.55 (m, 6H, $CH_2^{1,16}$), 2.94 (q, J = 5.7, 5.4, 4.9 Hz, 5H, CH^{18}, $CH_2^{7,10}$), 3.98 (t, J = 6.2 Hz, 4H, $CH_2^{3,14}$), 7.05 (s, 2H, $NH^{6,11}$) ppm.

IR (ATR) ṽ =3323.2, 2922.1, 1694.4 (amide), 1532.0, 1447.7, 1375.5, 1253.6, 1141.0, 1024.1, 753.4, 636.4 cm^{-1}.

Figure 133 ^{1}H NMR spectrum of **P29** (400 MHz, DMSO-d_6). Chloroform was also employed for the solubilization (8.32 ppm).

P30

The thiol-ene polymerization of diallyl butane-1,4-diyldicarbamate **6** (1.00 eq.) and 2,3-butanedithiol (1.00 eq.) led to the formation of **P30** as a colorless solid (87%).

¹H NMR (CDCl₃, 400 MHz) δ= 1.20 − 1.40 (m, 4H; CH₂^{8,9}), 1.75 − 2.00 (m, 4H, CH^{22,15}), 2.45 − 2.73 (m, 4H, CH₂^{1,16}), 3.01 (q, J = 6.1 Hz, 2H, CH^{18,19}), 3.18 (s, 4H, CH₂^{7,10}), 3.49 (d, J = 5.1 Hz, 2H, CH^{18,19}), 4.13 (t, J = 6.3 Hz, 2H, CH₂^{3,14}), 5.14 (d, J = 63.1 Hz, 2H, NH^{6,11}) ppm.

IR (ATR) ṽ = 3330.1, 2957.8, 2931.1, 2869.4, 1692.8 (amide), 1524.2, 1446.0, 1374.0, 1244.4, 1137.5, 1100.4, 1022.3, 777.5 cm⁻¹.

Figure 134 ¹H NMR spectrum of **P30** (400 MHz, DMSO-d_6).

P31

The thiol-ene polymerization of diallyl butane-1,4-diyldicarbamate **6** (1.00 eq.) and 1,4-Butanediol bis(thioglycolate) (1.00 eq.) led to the formation of **P31** as a colorless solid (92%).

^{1}H NMR (DMSO-d_6, 400 MHz) δ= 1.36 (p, J = 3.1 Hz, 4H, CH$_2^{8,9}$), 1.66 (dd, J = 5.5, 3.0 Hz, 4H, CH$_2^{22,23}$), 1.80 (p, J = 6.8 Hz, 4H, CH$_2^{2,15}$), 2.62 (t, J = 7.2 Hz, 4H, CH$_2^{1,16}$), 2.95 (q, J = 6.4, 5.9 Hz, 4H, CH$_2^{7,10}$), 3.34 (s, 4H, CH$_2^{18,27}$), 3.98 (t, J = 6.4 Hz, 4H, CH$_2^{3,14}$), 4.08 (q, J = 3.7 Hz, 4H, CH$_2^{21,24}$), 7.07 (t, J = 5.1 Hz, 2H, NH^{6,11}) ppm.

IR (ATR) ṽ = 3313.7, 2951.7, 2922.9, 1725.7 (ester), 1682.6 (amide), 1532.4, 1472.7, 1439.8, 1411.0, 1386.4, 1277.3, 1258.8, 1236.2, 1168.3, 1131.3, 1079.9, 1030.5, 954.4, 886.5, 779.6, 744.6 cm^{-1}.

Figure 135 ^{1}H NMR spectrum of **P31** (400 MHz, DMSO-d_6).

P32

The thiol-ene polymerization of diallyl butane-1,4-diyldicarbamate **6** (1.00 eq.) and 10,10'-(hexane-1,6-diylbis(oxy))bis(decane-1-thiol) (1.00 eq.) led to the formation of **P32** as a colorless solid (95%).

^{1}H NMR (DMSO-d_6, 400 MHz) δ= 1.19 – 1.43 (m, 28H, CH$_2^{20-25,31.32,38-43}$), 1.46 – 1.65 (m, 16H, CH$_2^{8,9,19,26,30,33,37,44}$), 1.90 (dp, J = 13.5, 6.8 Hz, 3H, CH$_2^{2,15}$), 2.41 – 2.61 (m, 8H, CH$_2^{1,16,18,45}$), 3.09 – 3.25 (m, 12H, CH$_2^{7,10,27,29,34,36}$), 4.16 (t, J = 6.2 Hz, 4H, CH$_2^{3,14}$), 4.77 (s, 2H, NH^{6,11}) ppm.

IR (ATR) ṽ = 3315.7, 2918.8, 2850.9, 1682.6 (amide), 1534.5, 1468.6, 1376.1, 1281.5, 1236.2, 1141.6, 1114.8, 1034.6, 968.8, 783.7, 719.9 cm^{-1}.

Figure 136 ^{1}H NMR spectrum of **P32** (400 MHz, CDCl$_3$).

P33

The thiol-ene polymerization of 1,3-di(dec-9-en-1-yl)urea **9** (1.00 eq.) and 1,2-ethanedithiol (1.00 eq.) led to the formation of **P33** as a colorless solid (68%).

IR (ATR) ṽ = 3336.3, 2918.8, 2848.8, 1614.7 (amide), 1577.6, 1476.9, 1464,.5, 1411.0, 1285.6, 1260.9, 1236.2, 1193.0, 1182.7, 724.0 cm^{-1}.

Figure 137 IR spectrum of **P33**.

P34

The thiol-ene polymerization of 1,3-di(dec-9-en-1-yl)urea **9** (1.00 eq.) and 1,4-butanedithiol (1.00 eq.) led to the formation of **P34** as a colorless solid (66%).

Unfortunately, the polymer was insoluble in all common deuterated solvents.

IR (ATR) ṽ = 3335.3, 2921.2, 2849.1, 1613.5 (amide), 1572.7, 1461.7, 1214.8, 750.3, 666.7, 613.5cm⁻¹.

Figure 138 IR spectrum of **P34**.

P35

The thiol-ene polymerization of 1,3-di(dec-9-en-1-yl)urea **9** (1.00 eq.) and 1,6-hexanedithiol (1.00 eq.) led to the formation of **P35** as a colorless solid (71%).

Unfortunately, the polymer was insoluble in all common deuterated solvents.

IR (ATR) ṽ = 3334.2, 2920.8, 2848.8, 1612.6, 1569.4, 1509.8, 1476.9, 1462.5, 1429.6, 1285.6, 1267.1, 1232.1, 1077.8, 773.4, 724.0 cm^{-1}.

Figure 139 IR spectrum of **P35**.

P36

The thiol-ene polymerization of 1,3-di(dec-9-en-1-yl)urea **9** (1.00 eq.) and 1,10-decanedithiol (1.00 eq.) led to the formation of **P36** as a colorless solid (73%).

Unfortunately, the polymer was insoluble in all common deuterated solvents.

IR (ATR) $\tilde{v}$ = 3336.3, 2918.8, 2848.8, 1614.7 (amide), 1571.5, 1462.5, 1285.6, 1258.8, 1230.0, 724.0 cm^{-1}.

Figure 140 IR spectrum of **P36**.

P37

The thiol-ene polymerization of 1,3-di(dec-9-en-1-yl)urea **9** (1.00 eq.) and limonene dithiol (1.00 eq.) led to the formation of **P37** as a colorless solid (58%).

^{1}H NMR (CDCl$_3$, 400 MHz) δ= 0.85 − 1.02 (m, CH^{33}, CH$_2$^{28}, CH$_3$^{24,26}), 1.11 − 1.33 (m, 26H, CH$_2$$^{3-8,16-21,26,28,29}$), 1.33 − 1.44 (m, 4H, CH$_2$^{9,15}), 1.49 (p, *J* = 7.6 Hz, 4H, CH$_2$^{2,22}), 1.59 − 2.35 (m, CH^{25,27}, CH$_2$^{16,28,29}), 2.41 (ddt, *J* = 9.6, 7.3, 2.8 Hz, 4H, CH$_2$^{1,23}), 2.52 (m, 4H, CH$_2$^{34}), 2.88 (q, *J* = 3.7 Hz, CH^{30}), 3.07 (t, *J* = 6.0 Hz, 4H, CH$_2$^{10,14}), 5.01 (br, s, 2H, NH^{11,13}) ppm.
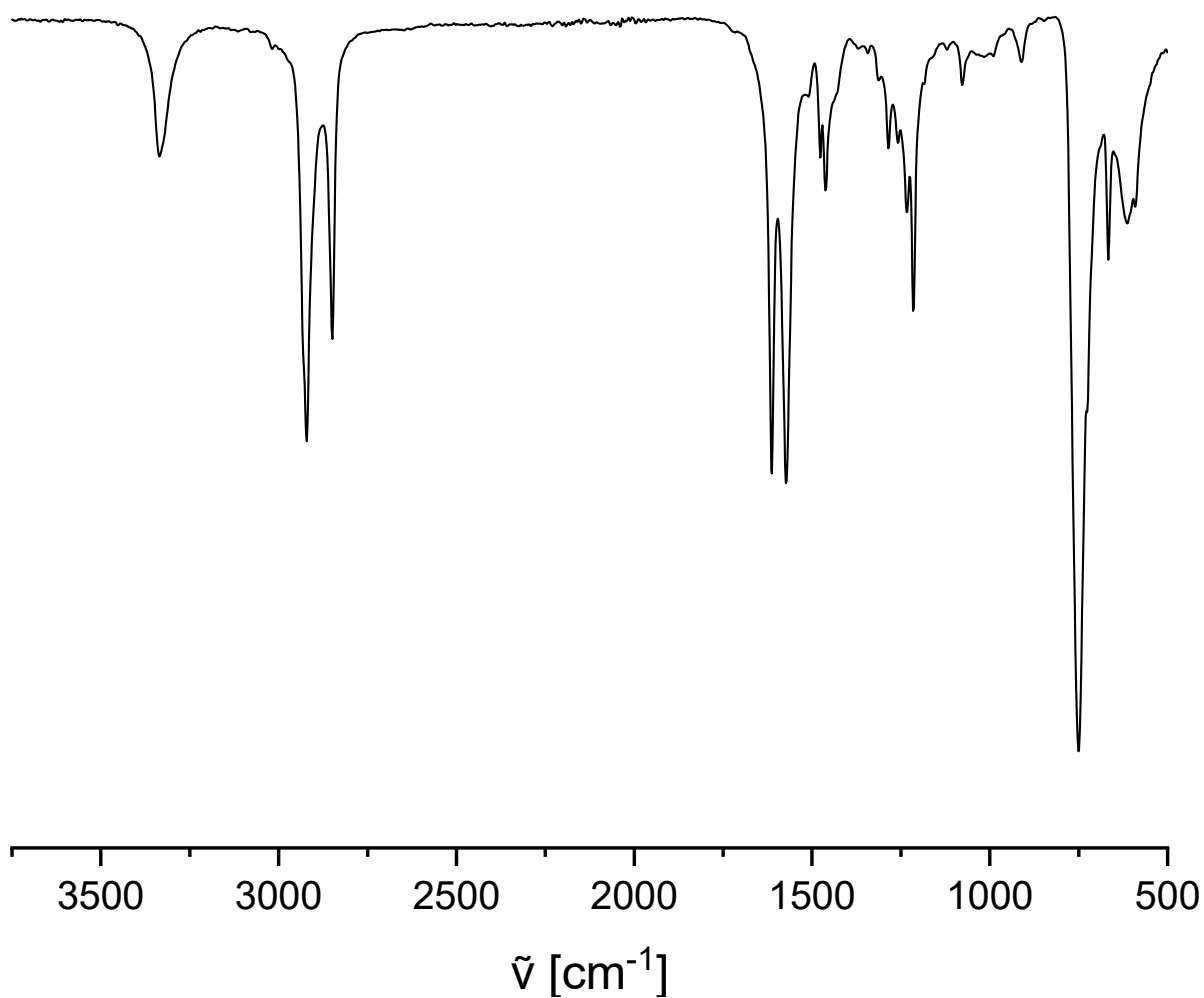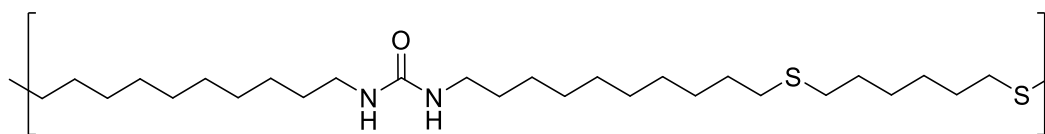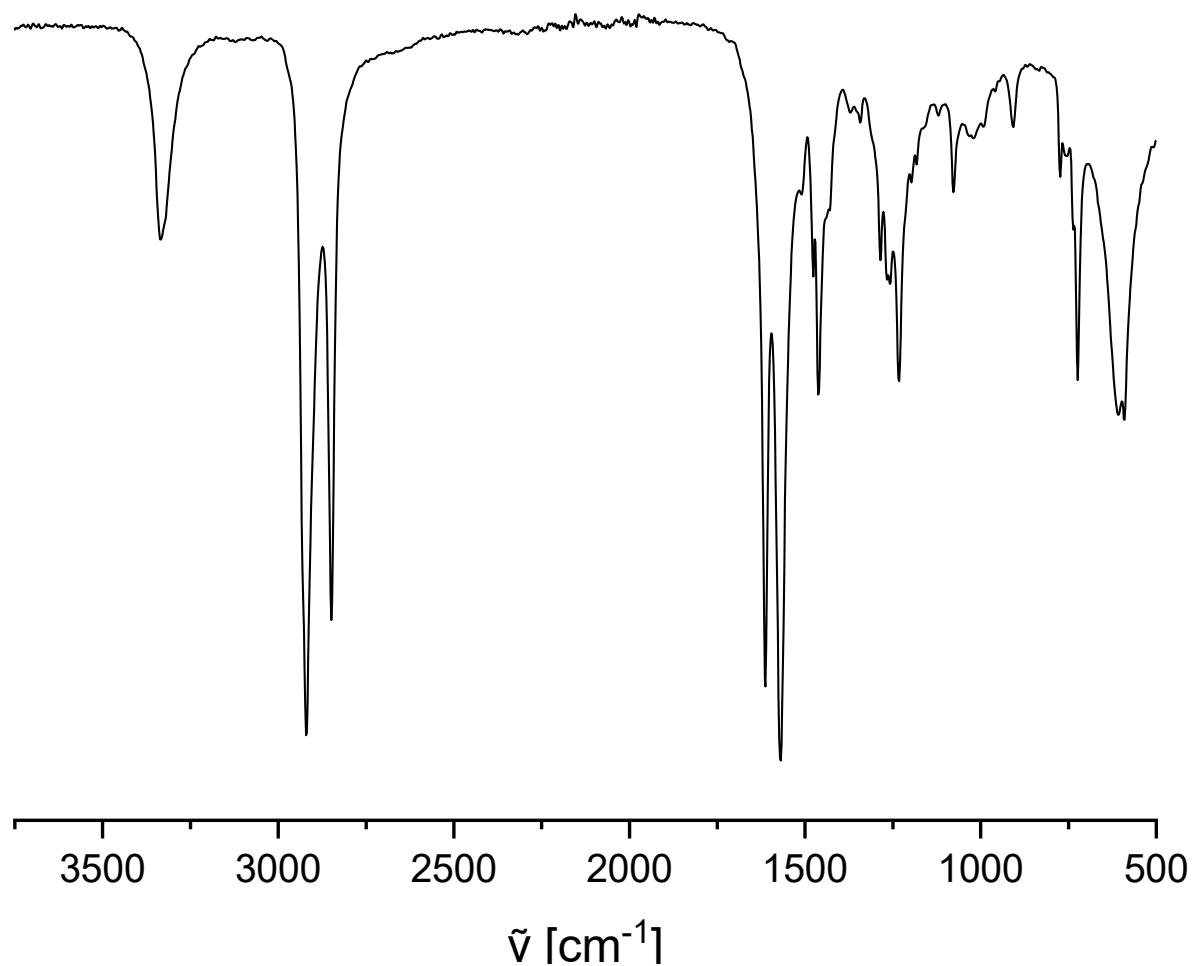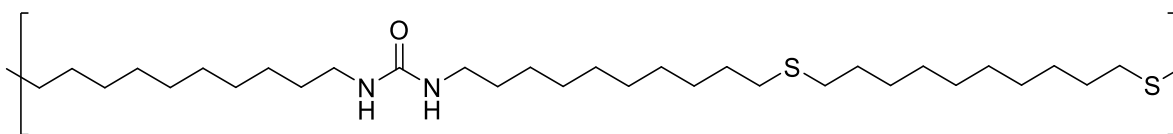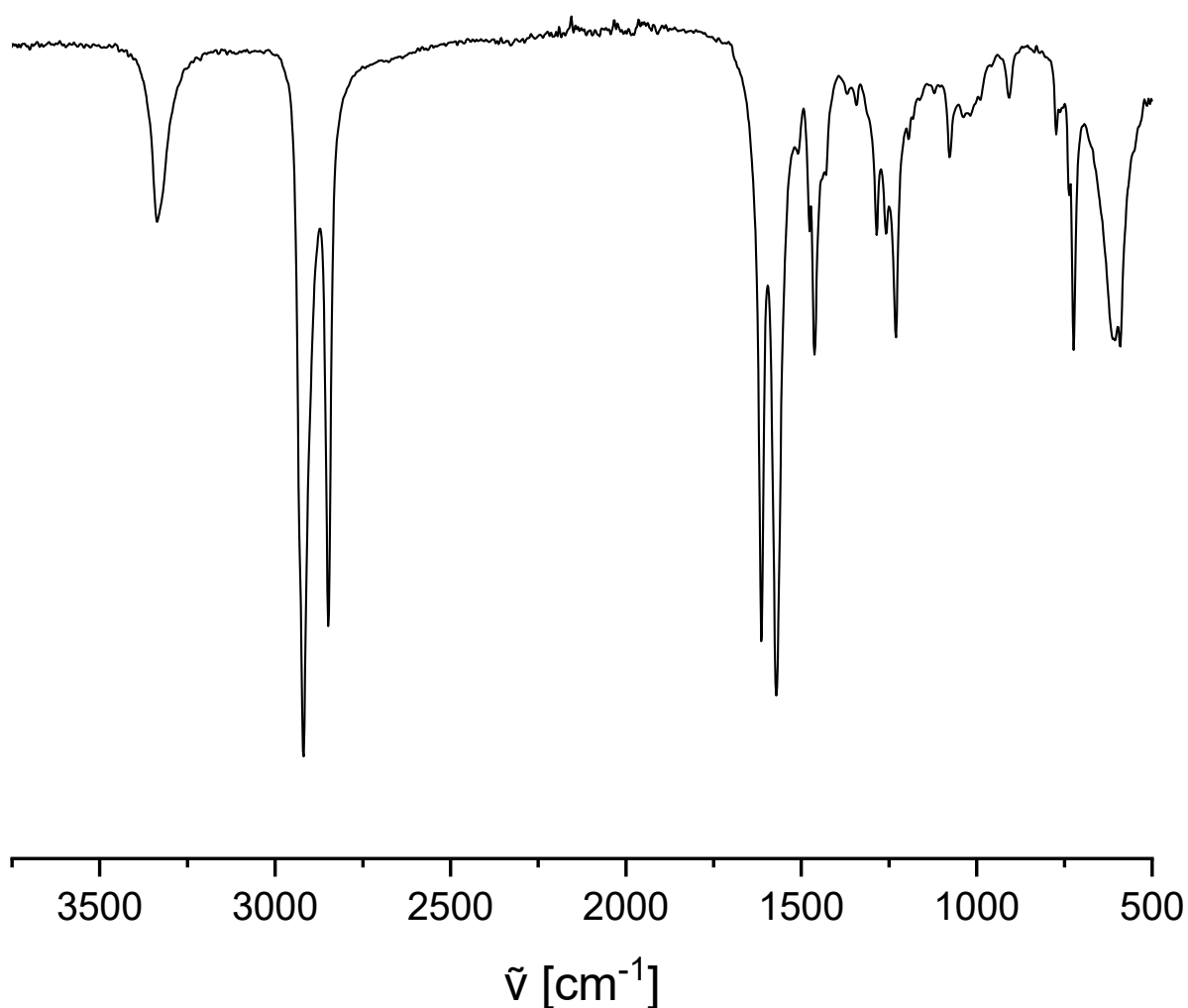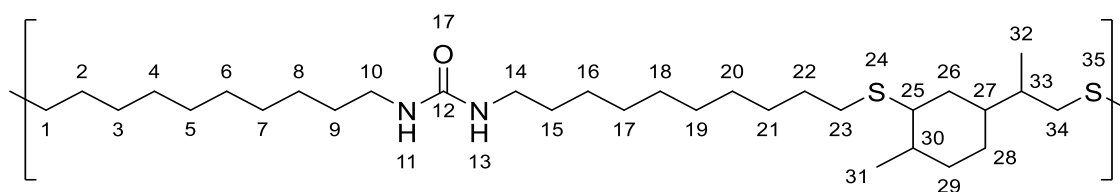
IR (ATR) ṽ = 3321.6, 2918.9, 2848.9, 1616.4 (amide), 1571.9, 1464.9, 1374.1, 1234.8, 721.6, 616.6 cm^{-1}.
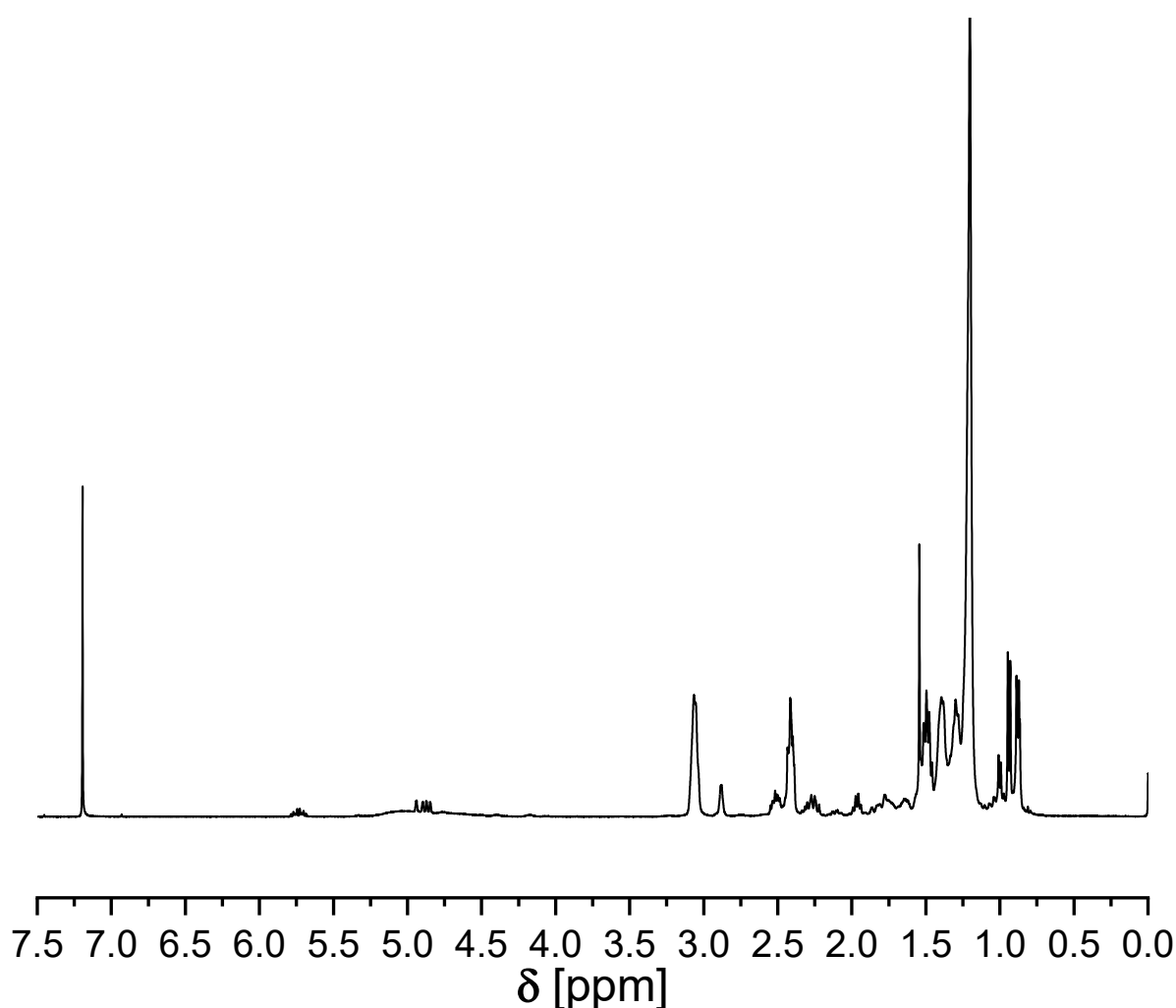
Figure 141 ^{1}H NMR spectrum of **P34** (400 MHz, CDCl$_3$).

P38
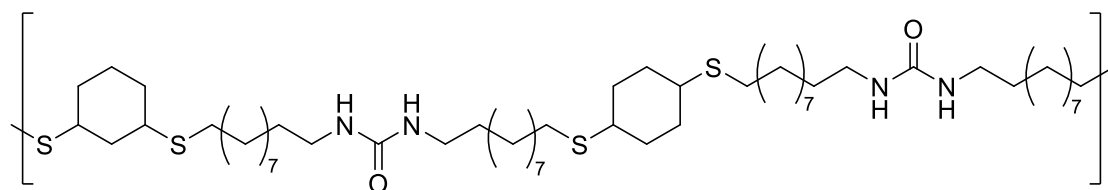
The thiol-ene polymerization of 1,3-di(dec-9-en-1-yl)urea **9** (1.00 eq.) and a mixture of 1,3- and 1,4-cyclohexanedithiol (1.00 eq.) led to the formation of **P38** as a colorless solid (44%).

Unfortunately, the polymer was insoluble in all common deuterated solvents.

IR (ATR) ṽ = 3341.7, 2919.8, 2849.2, 1618.3 (amide), 1568.8, 1466.0, 1443.6, 1341.0, 1261.4, 1233.8, 1027.9, 994.9, 895.4, 721.6, 618.2 cm^{-1}.
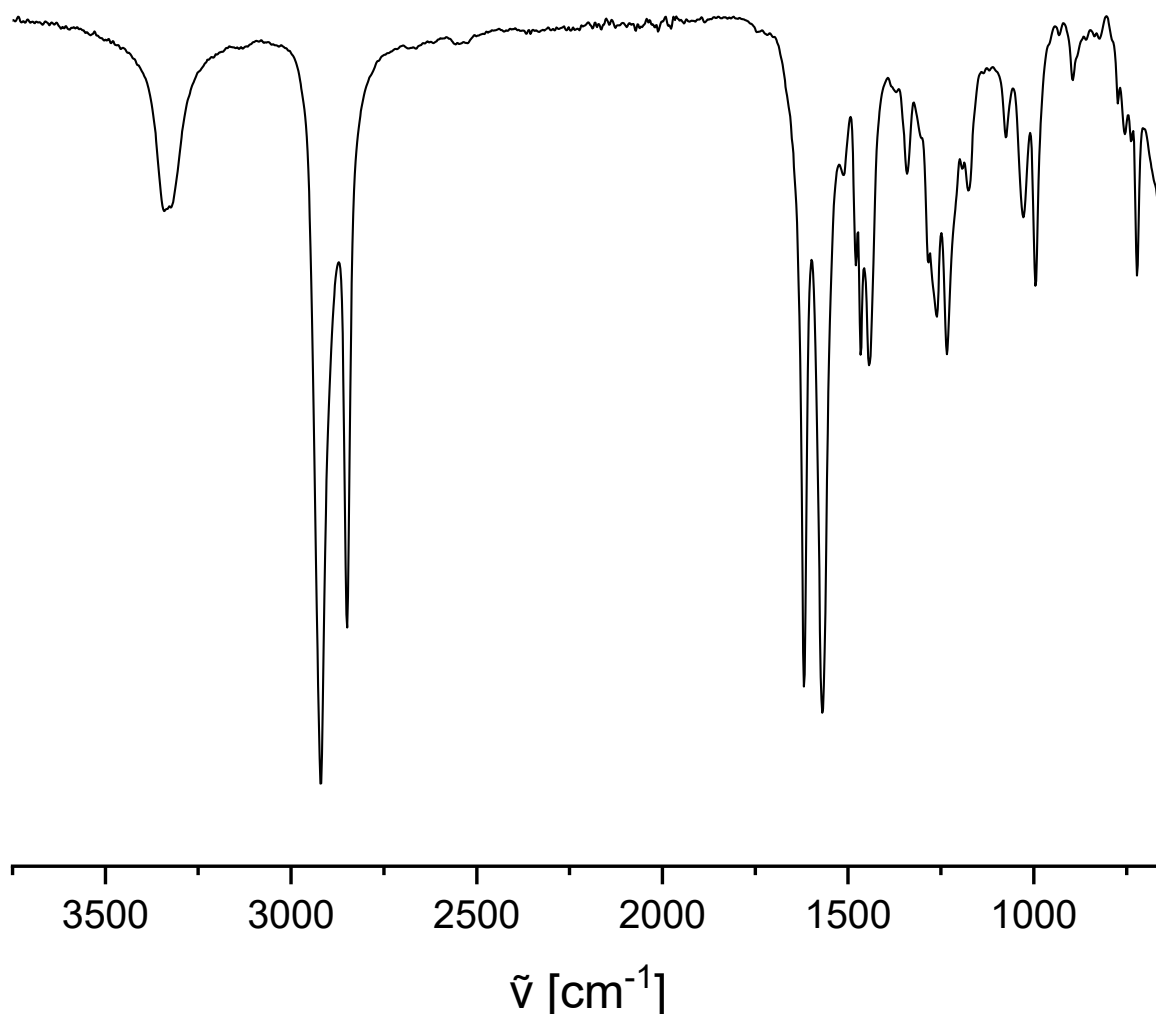
Figure 142 IR spectrum of **P38**.

P39
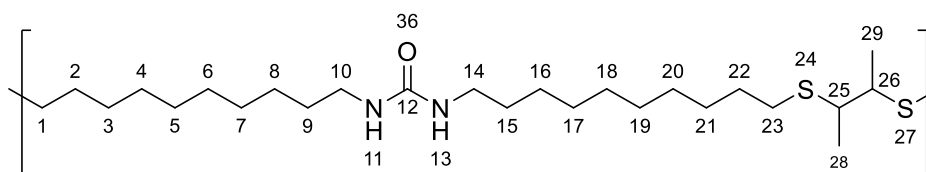
The thiol-ene polymerization of 1,3-di(dec-9-en-1-yl)urea **9** (1.00 eq.) and 2,3-butanedithiol (1.00 eq.) led to the formation of **P39** as a colorless solid (59%).

¹H NMR (CDCl₃,400 MHz) δ= 1.09 – 1.41 (m, 30H, CH₃²⁸,²⁹, CH₂³⁻⁸,¹⁶⁻²¹), 1.47 (m, 4H, CH₂⁹,¹⁵), 1.57 (d, *J* = 4.9 Hz, 4H, CH₂²,²²), 2.39 – 2.65 (m, 4H, CH₂¹,²³), 3.03 (tdd, *J* = 8.7, 7.0, 2.9 Hz, 2H, CH²⁵,²⁶), 3.14 (d, *J* = 8.5 Hz, 4H, CH₂¹⁰,¹⁴), 5.19 (br, s, 2H, NH¹¹,¹³) ppm.

IR (ATR) ṽ = 3332.2, 2920.8, 2848.8, 1616.7 (amide), 1573.5, 1478.9, 1464.5, 1372.0, 1283.5, 1258.8, 1236.2, 1036.7, 722.0 cm⁻¹.
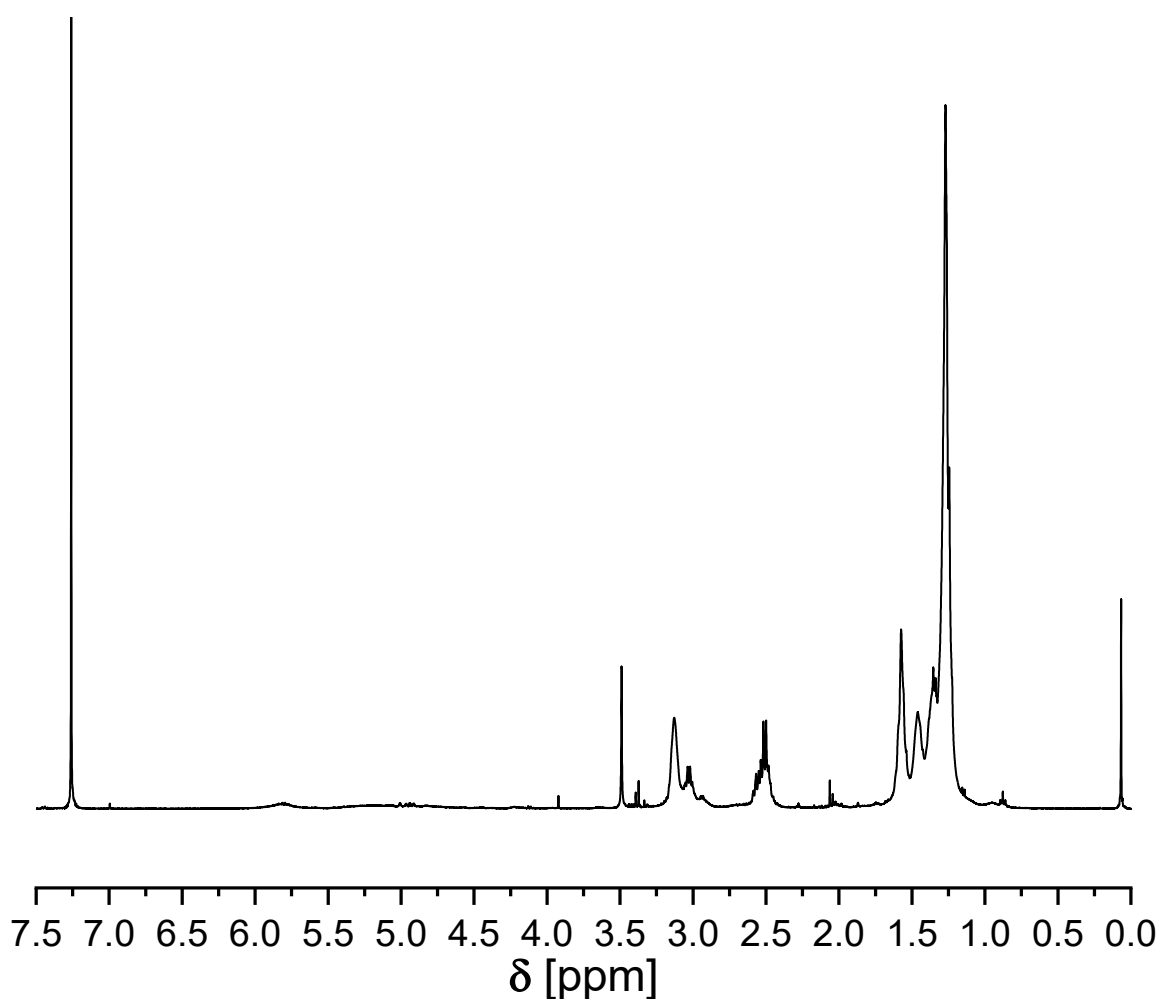
Figure 143 ¹H NMR spectrum of **P39** (400 MHz, CDCl₃). The impurity at 3.49 ppm derives from residual MeOH.
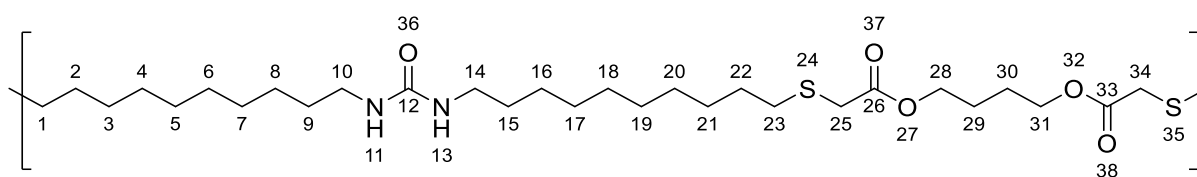
P40

The thiol-ene polymerization of 1,3-di(dec-9-en-1-yl)urea **9** (1.00 eq.) and 1,4-Butanediol bis(thioglycolate) led to the formation of **P40** as a colorless solid (65%).

^{1}H NMR (CDCl$_3$, 400 MHz) δ= 1.19 − 1.42 (m, 24H, CH$_2^{3-8,16-21}$), 1.43 (m, 4H, CH$_2^{9,15}$), 1.58 (p, J = 7.7, 7.0 Hz, 4H, CH$_2^{2,22}$), 1.76 (hept, J = 3.2 Hz, 4H, CH$_2^{29,30}$), 2.62 (t, J = 7.4 Hz, 4H, CH$_2^{1,23}$), 3.14 (q, J = 7.0 Hz, 4H, CH$_2^{10,14}$), 3.21 (s, 4H CH$_2^{25,34}$), 4.08 − 4.22 (m, 4H, CH$_2^{28,31}$), 4.75 (br, s, 2H, NH^{11,13}) ppm.

IR (ATR) ṽ = 3332.2, 2920.8, 2848.8, 1727.8 (ester), 1612.6 (amide), 1577.6, 1476.9, 1460.4, 1384.3, 1295.9, 1260.9, 1234.1, 1164.2, 1133.4, 1075.8, 1044.9, 954.4, 750.8, 724.0 cm^{-1}.
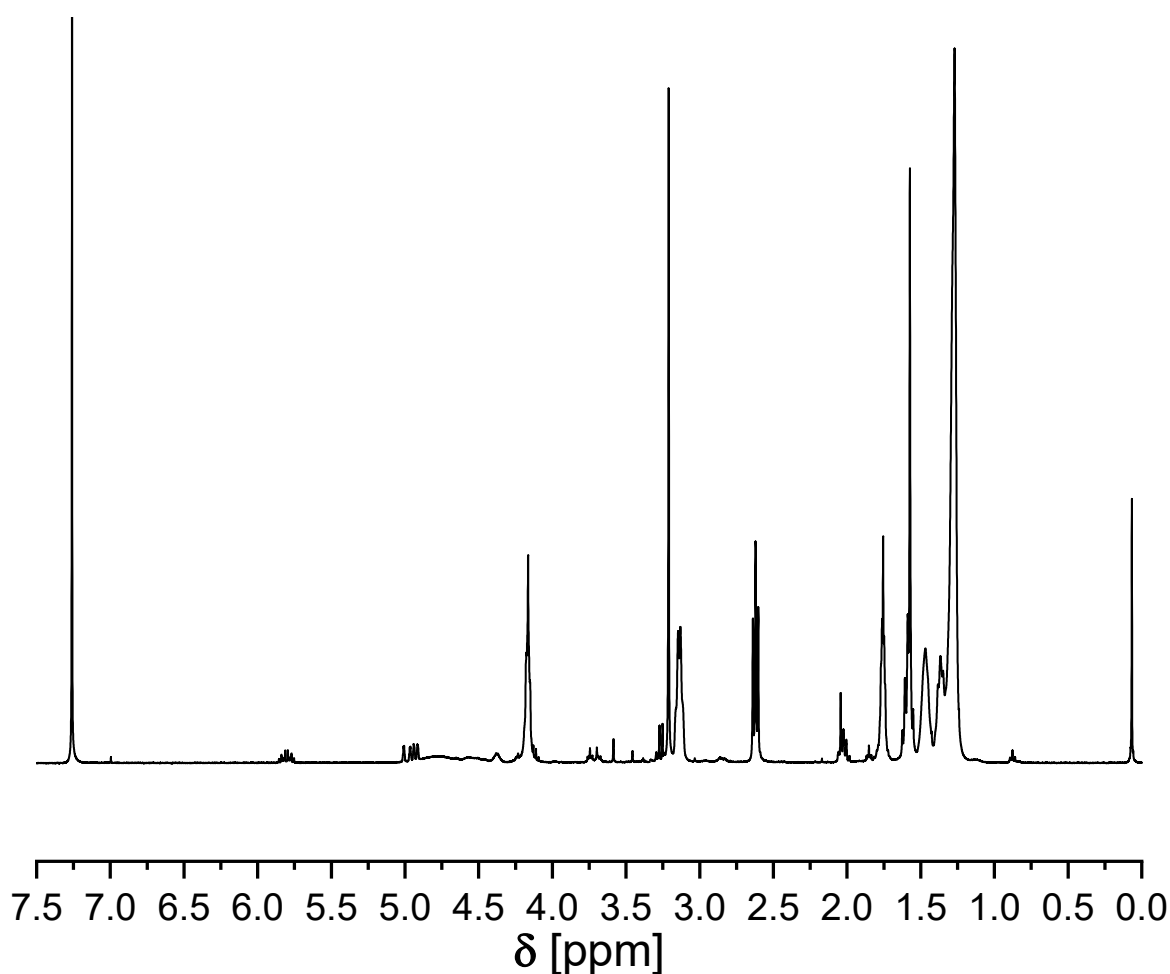
Figure 144 ^{1}H NMR spectrum of **P40** (400 MHz, CDCl$_3$).

P41
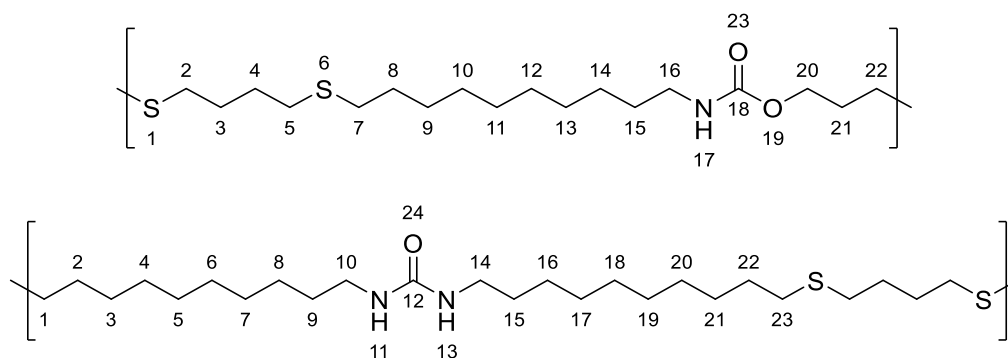
The thiol-ene polymerization of **4** (0.90 eq.) and **9** (0.10 eq.) and 1,4-butanedithiol (1.00 eq) led to the formation of **P41** as colorless solid (89%).

^{1}H NMR (CDCl$_3$, 400 MHz) δ= 1.22 − 1.40 (m, 12H, **4**-CH$_2$$^{9-14}$, **9**-CH$_2$$^{3-8,16-21}$), 1.47 (p, *J* = 7.8, 6.8 Hz, 2H, **4**-CH$_2$^{15}, **9**-CH$_2$^{9,15}), 1.55 (p, *J* = 7.8, 7.3, 6.9 Hz, 2H, **4**-CH$_2$^{8}, **9**-CH$_2$^{2,22}), 1.70 (dt, *J* = 6.6, 3.1 Hz, 4H, **4**-CH$_2$^{3,4}), 1.89 (p, *J* = 6.7 Hz, 2H, **4**-CH$_2$^{21}), 2.45. − 2.59 (m, 8H, **4**-CH$_2$^{2,5,7,22}, **9**-CH$_2$^{1,23}), 3.14 (t, *J* = 6.7 Hz, 2H, **4**-CH$_2$^{16}, **9**-CH$_2$^{10,14}), 4.14 (t, *J* = 6.3 Hz, 2H, **4**-CH$_2$^{20}), 4.69 (br, s, 1H, **4**-NH^{17}, **9**-NH^{11,13}) ppm.

IR (ATR) ṽ = 3329.5, 2919.2, 2850.5, 1685.5 (amide), 1532.1, 1468.4, 1242.5, 1140.4, 1019.7, 778.6, 721.0, 629.5 cm^{-1}.
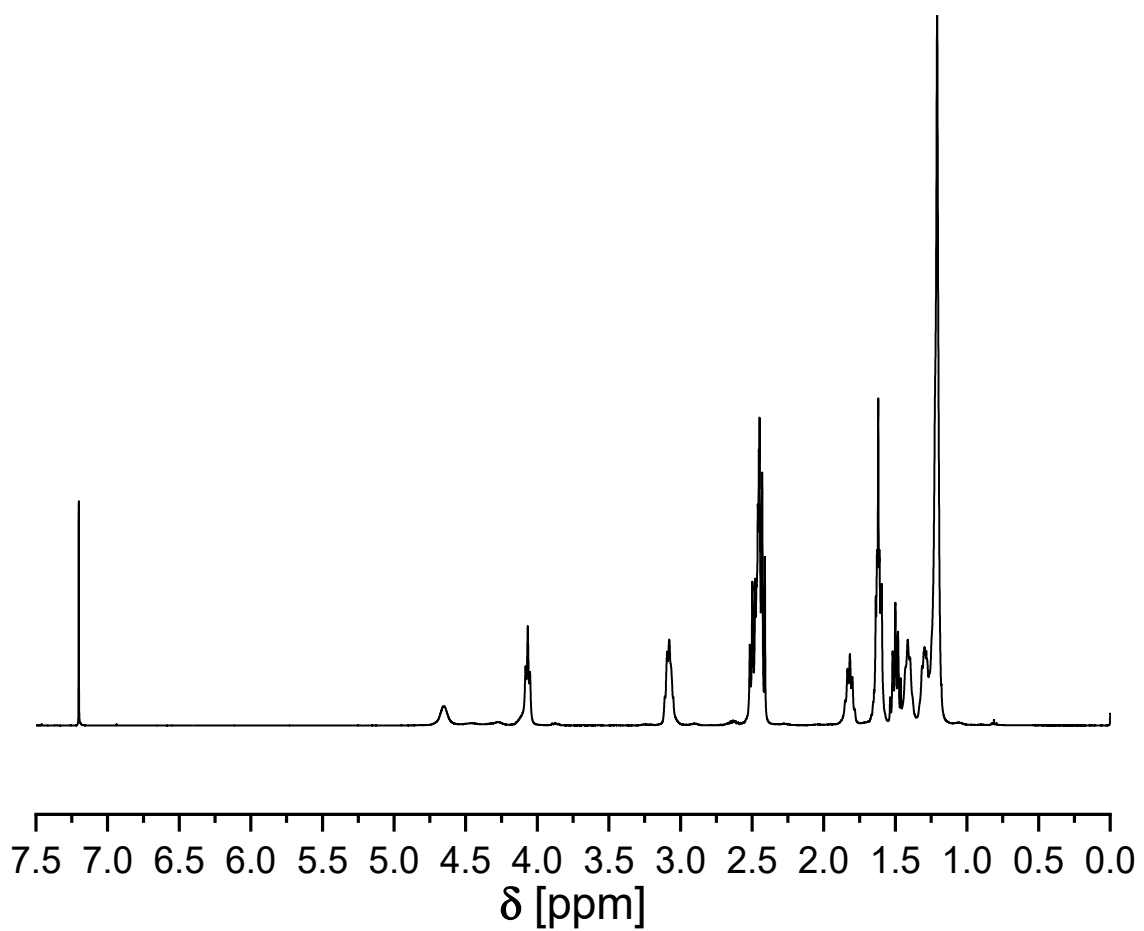
Figure 145 ^{1}H NMR spectrum of **P41** (400 MHz, CDCl$_3$).

P42
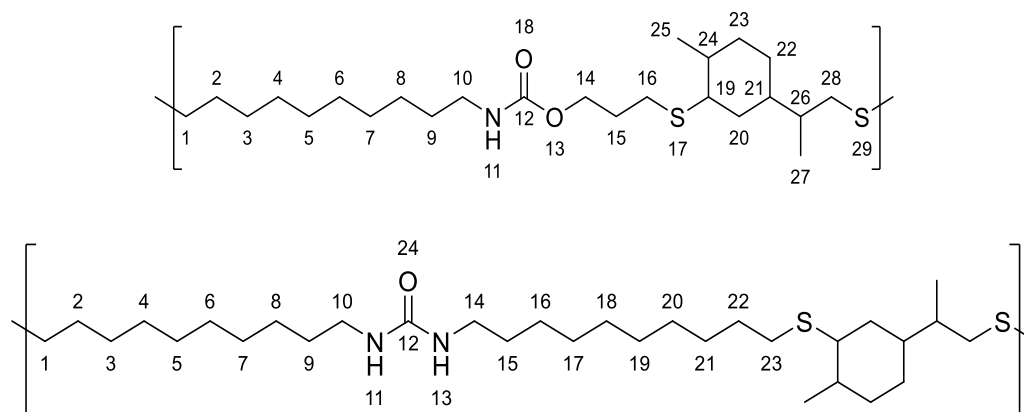
The thiol-ene polymerization of **4** (0.90 eq.) and **9** (0.10 eq.) and limonene dithiol **11** led to the formation of the random copolymer **P42** as an opaque solid (87%).

¹H NMR (CDCl₃, 400 MHz) δ= 0.91 − 1.12 (m, **4**-CH^{26},CH$_2$^{22},CH$_3$^{25,27}), 1.22 − 1.80 (m, **4**-CH$_2$$^{2-9,20-22,23}$, CH^{21,24}, **9**-CH$_2$$^{2-9,15-22}$), 1.89 (m, 2H, **4**-CH$_2$^{15}), 1.96 − 2.42 (m, **4**-CH$_2$^{23}, CH^{21,19}), 2.48 (t, *J* = 7.5 Hz, **4**-CH$_2$^{16}), 2.51 − 2.64 (m, **4**-CH$_2$^{1,28}, **9**-CH$_2$^{1,23}), 2.93 (br, s, **4**-CH^{19}), 3.14 (q, *J* = 6.9, 6.2 Hz, **4**-CH$_2$^{10}, **9**-CH$_2$^{10,14}), 4.14 (t, *J* = 6.1, 5.4 Hz, **4**-CH$_2$^{14}), 4.71 (br, s, **4**-NH^{11}, **9**-NH^{11,13}) ppm.

IR (ATR) ṽ = 2923.1, 2852.6, 1704.5 (amide), 1519.0, 1453.8, 1241.1, 1136.5, 750.3, 665.6 cm^{-1}.

Figure 146 ^{1}H NMR spectrum of **P42** (400 MHz, CDCl$_3$).

P43
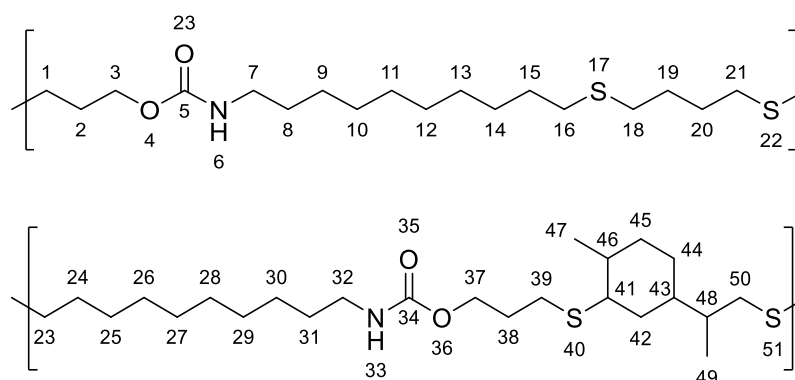
The thiol-ene polymerization of allyl dec-9-enyl carbamate **4** (1.00 eq.) with 1,4-butanedithiol (0.50 eq.) and limonene dithiol **11** (0.50 eq.) led to the formation of the random copolymer **P43** as a colorless solid (90%).

¹H NMR (CDCl₃, 400 MHz) δ= 0.84 – 1.17 (m, CH$_3$^{47,49}, CH^{48}), 1.16 – 1.41 (m, CH$_2$$^{9-14,25-30}$), 1.47 (q, J = 6.8 Hz, 3H, CH$_2$^{8,31}), 1.55 (q, J = 7.2, 6.6 Hz, CH$_2$^{15,24}), 1.70 (p, J = 3.4 Hz, 4H, CH$_2$^{19,20}), 1.88 (p, J = 7.1, 6.3 Hz, CH$_2$^{2,38}), 2.41 – 2.67 (m, 7H, CH$_2$^{16,18,21,23,39}), 3.15 (q, J = 6.8 Hz, 2H, CH$_2$^{7,32}), 4.13 (t, J = 6.3 Hz, 2H, CH$_2$^{3,37}), 4.70 (br, s, 1H, NH^{6,33}) ppm.

IR (ATR) ṽ = 3338.4, 2918.8, 2850.9, 1686.7 (amide), 1530.3, 1466.6, 1456.3, 1372.0, 1289.7, 1242.4, 1137.5, 1020.2, 777.5, 722.0 cm⁻¹.

Figure 147 ^{1}H-NMR spectrum of **P43** (400 MHz, CDCl$_3$).

P44

The thiol-ene polymerization of allyl dec-9-enyl carbamate **4** (1.00 eq.) with 1,4-butanedithiol (0.50 eq.) and 2,3-butanedithiol (0.50 eq.) led to the formation of the random copolymer **P44** as a colorless solid (89%).

^{1}H NMR (CDCl$_3$, 400 MHz) δ= 1.16 – 1.42 (m, CH$_2$$^{9-14,31-36}$, CH$_3$^{24,27}), 1.47 (q, J = 7.1 Hz, CH$_2$^{15,37}), 1.51 – 1.59 (m, CH$_2$^{8,30}), 1.62 – 1.73 (m, CH$_2$^{3,4}), 1.88 (p, J = 6.9 Hz, CH$_2$^{21,44}), 2.42 – 2.68 (m, CH$_2$^{2,5,7,22,29,45}), 3.01 (tt, J = 6.7, 4.1 Hz, CH$_2$^{25,26}), 3.14 (p, J = 8.7, 7.6 Hz, CH$_2$^{16,38}), 4.13 (t, J = 6.3 Hz, CH$_2$^{20,43}), 4.74 (br, s, NH^{17,39}) ppm.
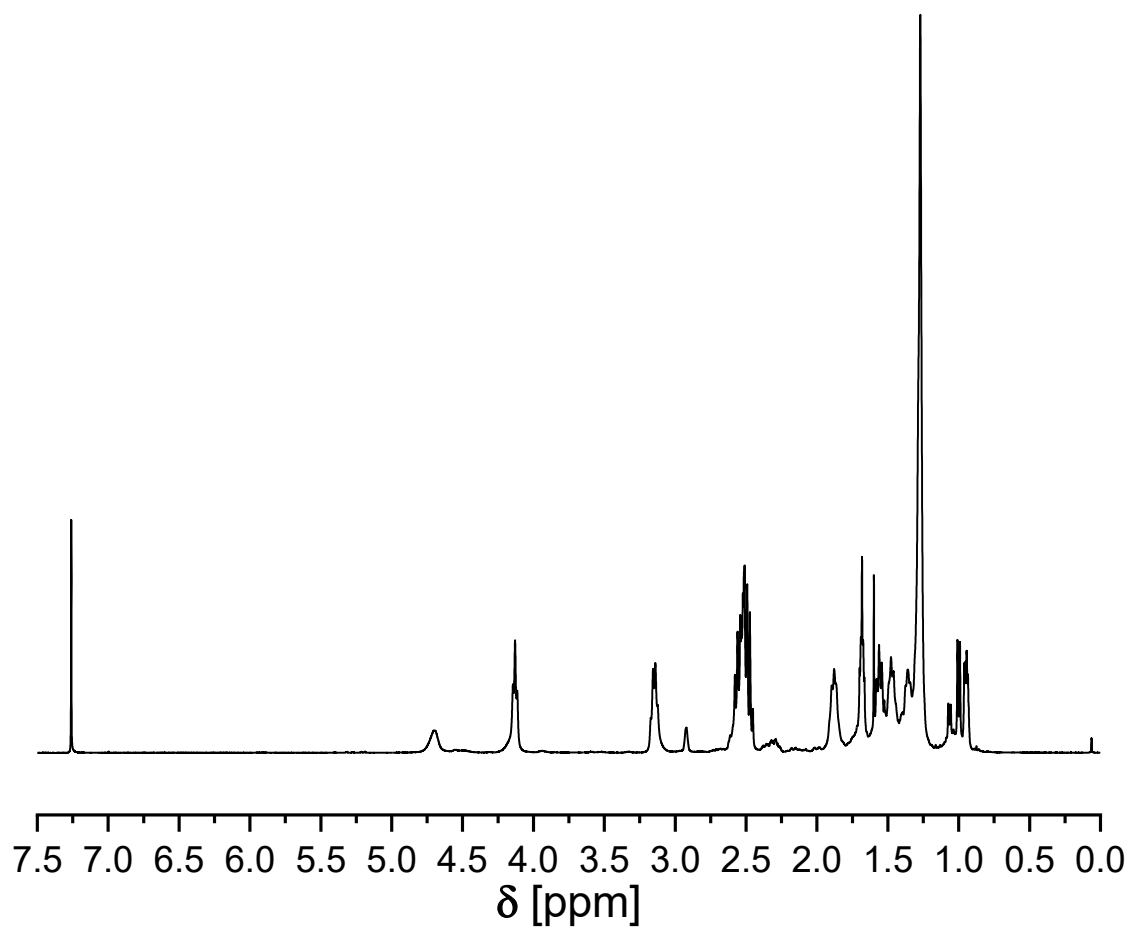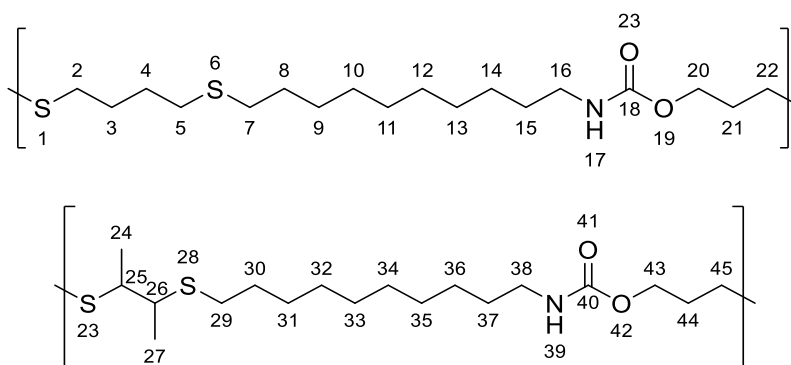
IR (ATR) ṽ = 3336.3, 2918.8, 2850.9, 1684.6 (amide), 1530.3, 1468.7, 1456.3, 1372.0, 1289.7, 1242.4, 1137.5, 1040.8, 1020.2, 777.5, 722.0 cm^{-1}.
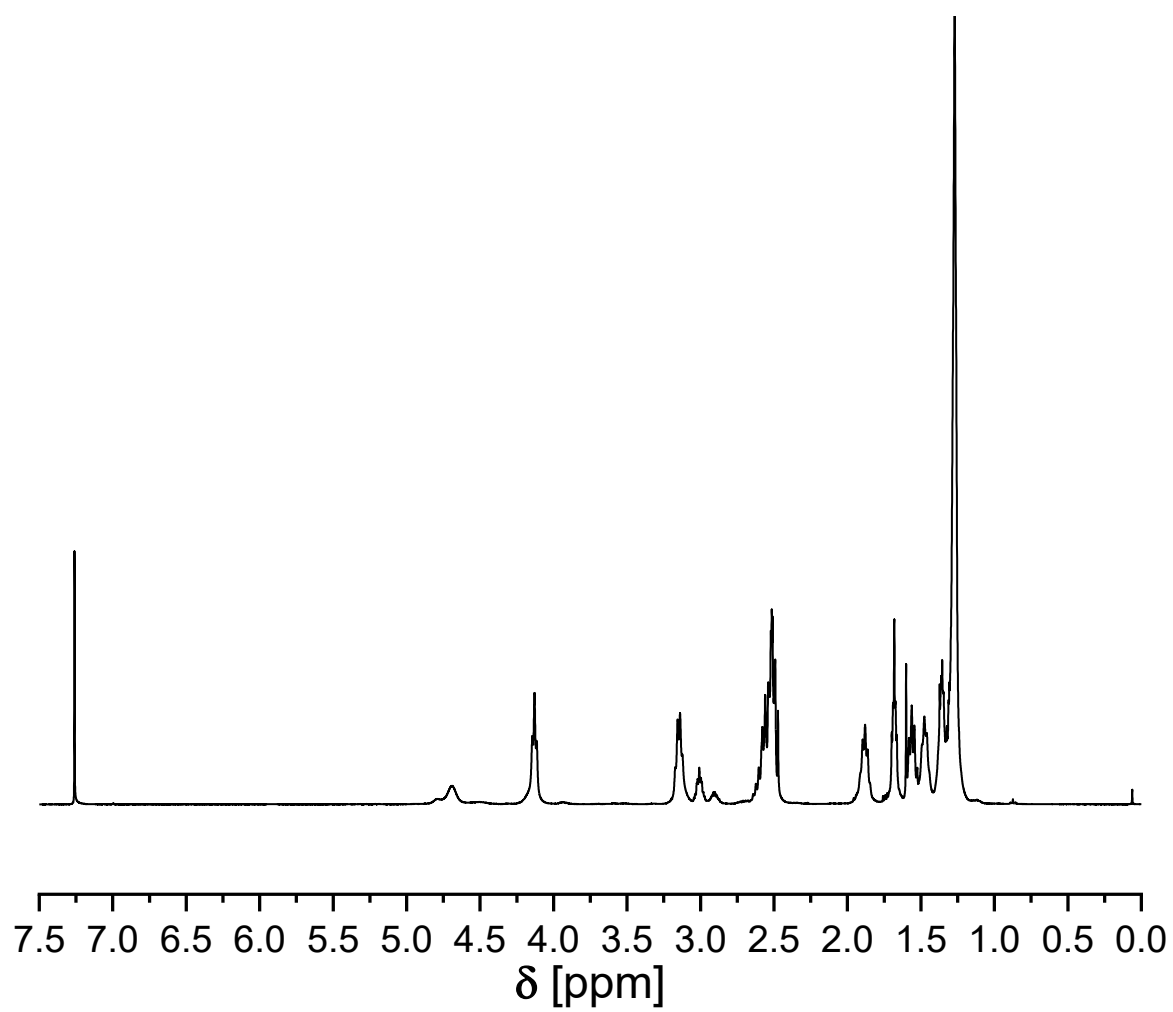
Figure 148 ^{1}H NMR spectrum of **P44** (400 MHz, CDCl$_3$).

P45
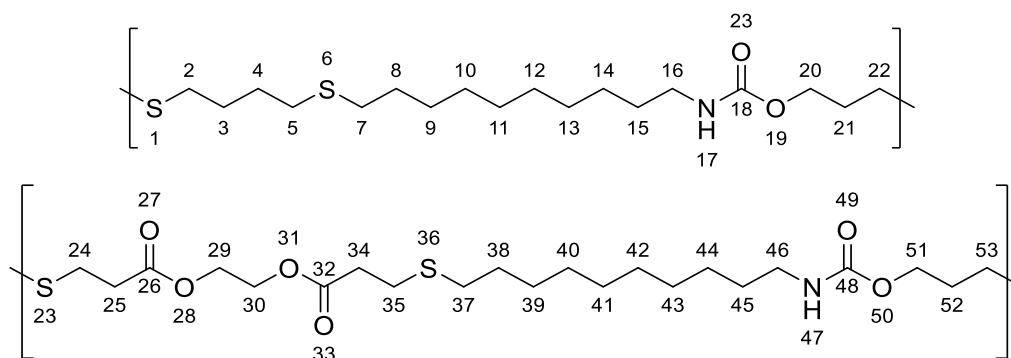
The thiol-ene polymerization of allyl dec-9-enyl carbamate **4** (1.00 eq.) with ethane-1,2-diyl bis(3-mercaptopropanoate) (0.50 eq.) and limonene dithiol **11** (0.50 eq.) led to the formation of the random copolymer **P45** as a colorless solid (86%).

^{1}H NMR (CDCl$_3$, 400 MHz) δ= 1.18 − 1.41 (m, CH$_2^{9-14,39-44}$), 1.46 (q, J = 6.5 Hz, CH$_2^{15,45}$), 1.52-1.61 (m, CH$_2^{8,38}$), 1.68 (hept, J = 5.1, 3.3, 2.8 Hz, CH$_2^{3,4}$), 1.88 (h, J = 7.2, 6.6, 6.0, 2.9 Hz, CH$_2^{21,52}$), 2.45 − 2.68 (m, CH$_2^{2,5,7,22,24,34,37,53}$), 2.72 − 2.83 (m, CH$_2^{24,35}$), 3.15 (q, J = 6.8 Hz, CH$_2^{16,46}$), 4.13 (t, J = 6.4 Hz, CH$_2^{20,51}$), 4.31 (t, J = 1.0 Hz, CH$_2^{29,30}$), 4.71 (br, s, NH^{17,47}) ppm.

IR (ATR) ṽ = 3330.1, 2920.8, 2850.9, 1731.9 (ester), 1682.6 (amide), 1532.4, 1468.6, 1456.3, 1437.8, 1376.1, 1345.2, 1322.6, 1289.7, 1262.9, 1242.4, 1139.5, 1077.8, 1055.2, 1040.8, 1022.3, 779.6, 722.0 cm^{-1}.
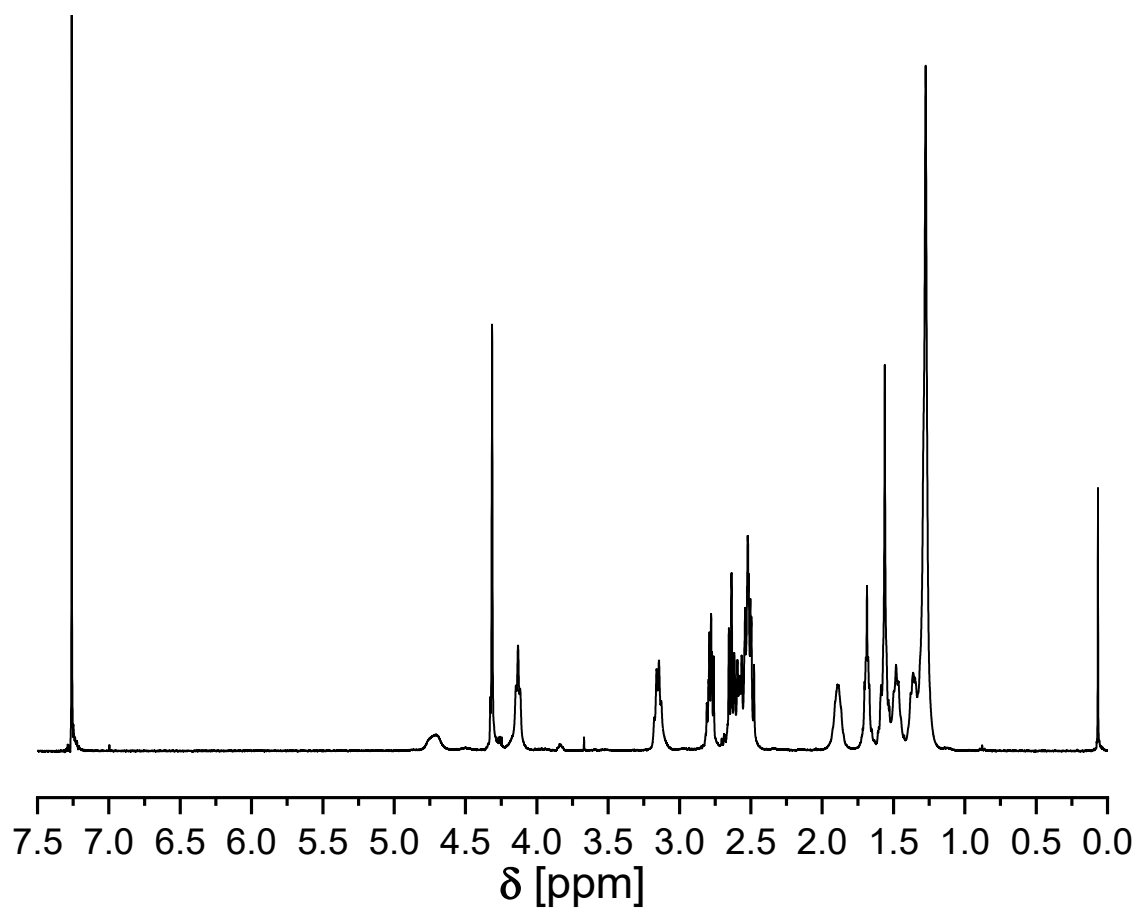
Figure 149 ^{1}H NMR spectrum of **P45** (400 MHz, CDCl3).

P46
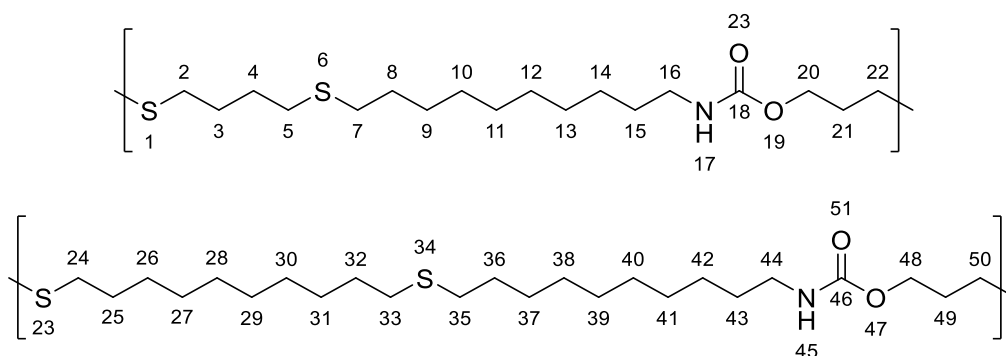
The thiol-ene polymerization of allyl dec-9-enyl carbamate **4** (1.00 eq.) with 1,4-butanedithiol (0.50 eq.) and 1,10-decanedithiol (0.50 eq.) led to the formation of the random copolymer **P46** as a colorless solid (83%).

^{1}H NMR (CDCl$_3$, 400 MHz) δ= 1.21 – 1.41 (m, CH$_2$$^{9-14,26-31,37-42}$), 1.47 (p, *J* = 7.1, 6.5 Hz, CH$_2$^{15,43}), 1.57 (p, *J* = 7.6, 6.9 Hz, CH$_2$^{,8,25,32,36}), 1.69 (p, *J* = 3.5 Hz, CH$_2$^{3,4}), 1.89 (p, *J* = 7.0, 6.5, 6.5 Hz, CH$_2$^{21,49}), 2.44 – 2.60 (m, CH$_2$^{2,5,7,22,24,33,35,50}), 3.15 (q, *J* = 6.4, 5.9 Hz, CH$_2$^{16,44}), 4.14 (t, *J* = 6.3 Hz, CH$_2$^{20,48}), 4.67 (br, s, NH^{17,45}) ppm.

IR (ATR) ṽ = 3327.1, 2919.2, 2850.3, 1684.2 (amide), 1535.3, 1648.4, 1345.1, 1288.9, 1244.5, 1140.6, 1020.6, 778.7, 720.0, 635.9 cm^{-1}.

Figure 150 ^{1}H NMR spectrum of **P46** (400 MHz, CDCl$_3$).

P47

The thiol-ene polymerization of allyl allyl carbamate **3** (1.00 eq.) with 1,4-butanedithiol (0.50 eq.) and limonene dithiol **11** (0.50 eq.) led to the formation of the random copolymer **P47** as a colorless solid (89%).

^{1}H NMR (CDCl$_3$, 400 MHz) δ= 0.87 − 1.15 (m, CH$_3$^{32,34}, CH^{33}, CH$_2$^{29}), 1.17 − 1.46 (m, CH$_2$^{27,29,30}), 1.55 (m, CH^{31}), 1.63 − 1.73 (m, CH^{31,33}, CH$_2$^{27,29,30}), 1.73 − 1.84 (m, CH$_2$^{2,17}), 1.84 − 1.98 (m, CH$_2$^{8,23}), 2.46 − 2.65 (m, CH$_2$^{1,9,11,14,16,24,35}), 2.93 (br, s, CH^{26}), 3.27 (q, J = 6.6 Hz, CH$_2$^{3,18}), 4.14 (t, J = 6.4 Hz, CH$_2$^{7,22}), 4.96 (s, NH^{4,19}) ppm.

IR (ATR) ṽ = 3328.1, 2916.7, 2865.3, 2852.9, 1692.8 (amide), 1524.2, 1441.9, 1242.4, 1135.4, 1067.5, 1009.9, 775.5 cm^{-1}.

Figure 151 ^{1}H NMR spectrum of **P47** (400 MHz, CDCl$_3$).

P48

The thiol-ene polymerization of allyl dec-9-enyl carbamate **4** (1.00 eq.) with 1,2-ethanedithiol (0.50 eq.) and limonene dithiol **11** (0.50 eq.) led to the formation of the random copolymer **P48** as a colorless solid (85%).

¹H NMR (CDCl$_3$, 400 MHz) δ= 0.84 – 1.11 (m, CH^{26}, CH$_2$^{22}, CH$_3$^{25,27}), 1.17 – 1.42 (m, CH$_2$$^{3-8,20,22,32-37}$, CH^{24}), 1.46 (p, J = 6.3, 5.8 Hz, CH$_2$^{9,38}), 1.62-1.53 (m, CH$_2$^{2,31}), 1.90 (t, J = 7.1 Hz, CH$_2$^{15,45}), 2.48 (t, J = 7.4 Hz, CH$_2$^{23}, CH^{19,21}), 2.54 (t, J = 7.4 Hz, CH$_2$^{1,28,30,46}, CH), 2.61 (t, J = 7.4 Hz, CH$_2$^{16}), 2.72 (d, J = 2.1 Hz, CH$_2$^{48,49}), 2.93 (br, s, CH^{19}), 3.16 (p, J = 6.7 Hz, CH$_2$^{10,39}), 4.14 (t, J = 6.4 Hz, CH$_2$^{14,44}), 4.69 (br, s, NH^{11,40}) ppm.
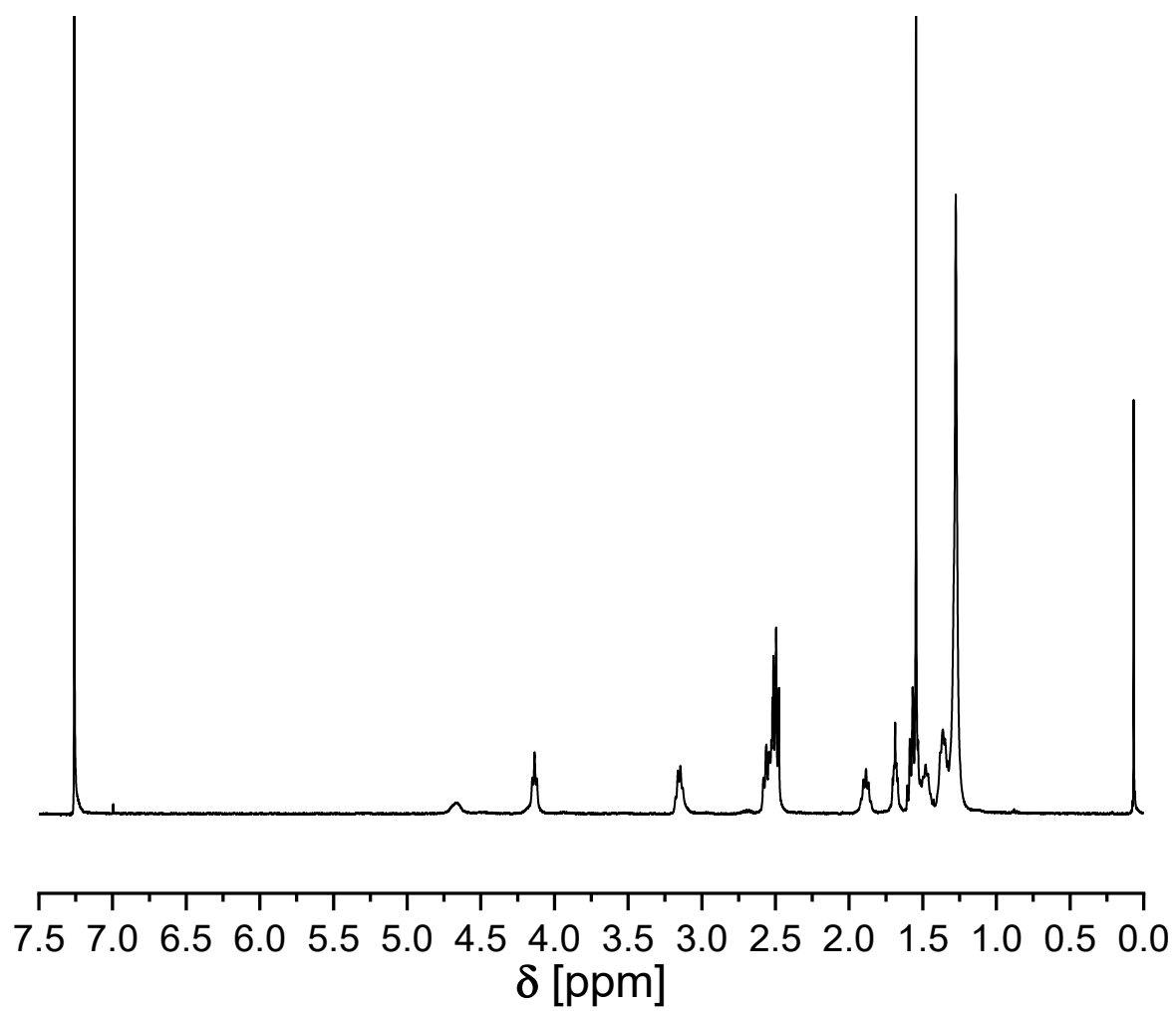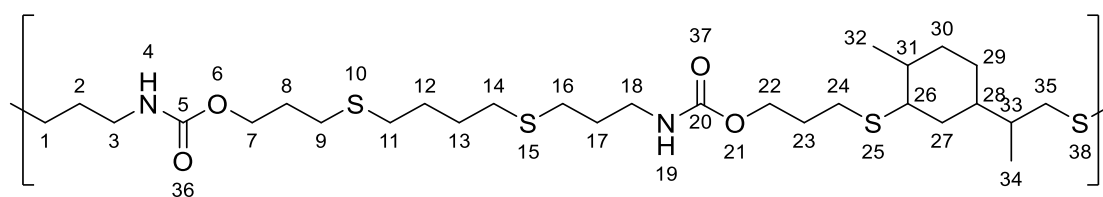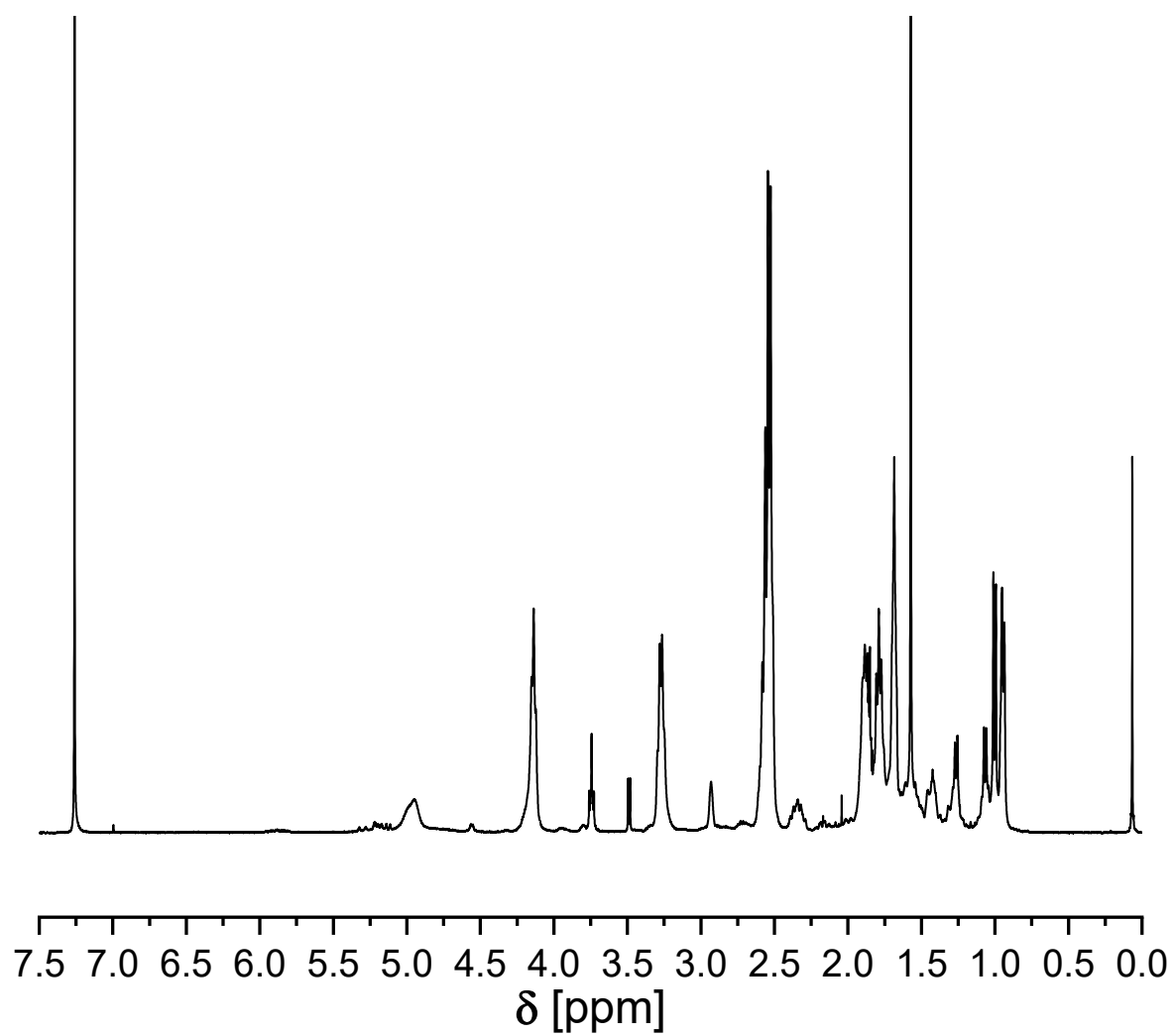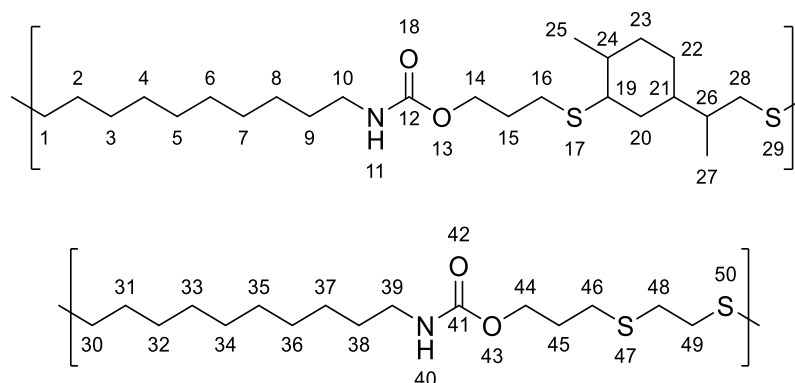
IR (ATR) ṽ = 3318.1, 2917.0, 2850.2, 1683.7 (amide), 1535.6, 1466.3, 1375.3, 1246.8, 1207.3, 1143.5, 1025.7, 935.2, 722.0, 688.4, 645.8 cm^{-1}.
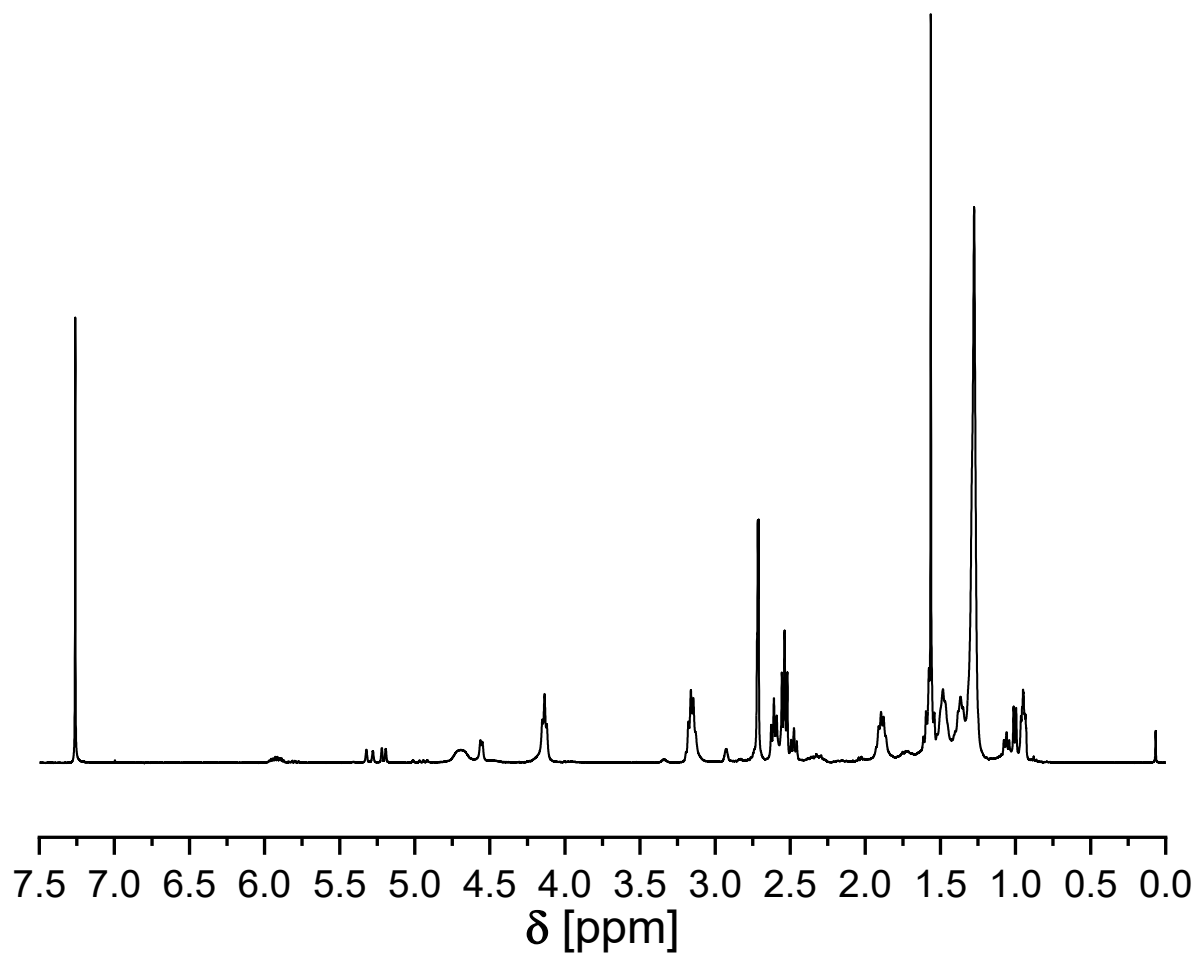
Figure 152 ^{1}H NMR spectrum of **P48** (400 MHz, CDCl$_3$).

P49
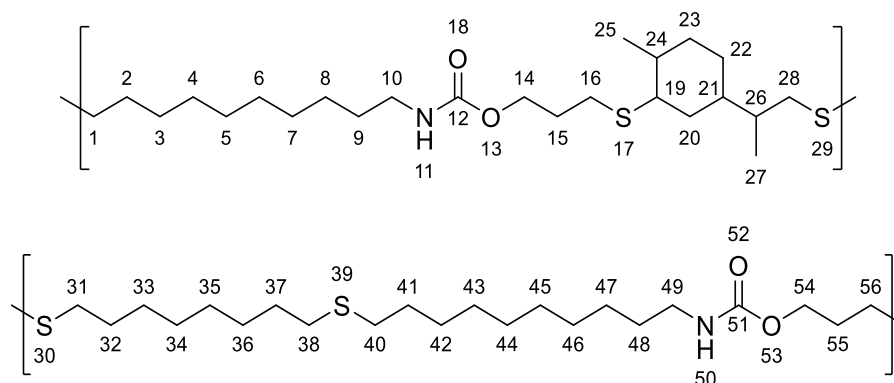
The thiol-ene polymerization of allyl dec-9-enyl carbamate **4** (1.00 eq.) with 1,8-octanedithiol (0.50 eq.) and limonene dithiol **11** (0.50 eq.) led to the formation of the random copolymer **P49** as a colorless solid (89%).

^{1}H NMR (CDCl$_3$, 400 MHz) δ = 0.90 − 1.12 (m, CH^{26}, CH$_2$^{22}, CH$_3$^{25,27}), 1.16 − 1.41 (m, CH$_2$$^{3\text{-}8,33\text{-}36,42\text{-}47}$), 1.47 (p, J = 7.9 Hz, CH$_2$^{9,48}), 1.52-1.60 (m, CH$_2$^{2,32,37,41}), 1.80 − 1.98 (m, CH$_2$^{15,55}), 1.94-2.40 (m, CH$_2$^{23}, CH^{21,19}), 2.41 − 2.65 (m, 3H, CH$_2$^{1,16,28,31,38,40,56}), 3.16 (p, J = 6.8 Hz, CH$_2$^{10,49}), 4.13 (t, J = 6.4 Hz, CH$_2$^{14,54}), 4.68 (br, s, NH^{11,50}) ppm.

IR (ATR) ṽ =3334, 2918, 2850, 1685 (amide), 1530, 1467, 1289, 1263, 1241, 1139, 1022, 923, 778, 720 cm^{-1}.
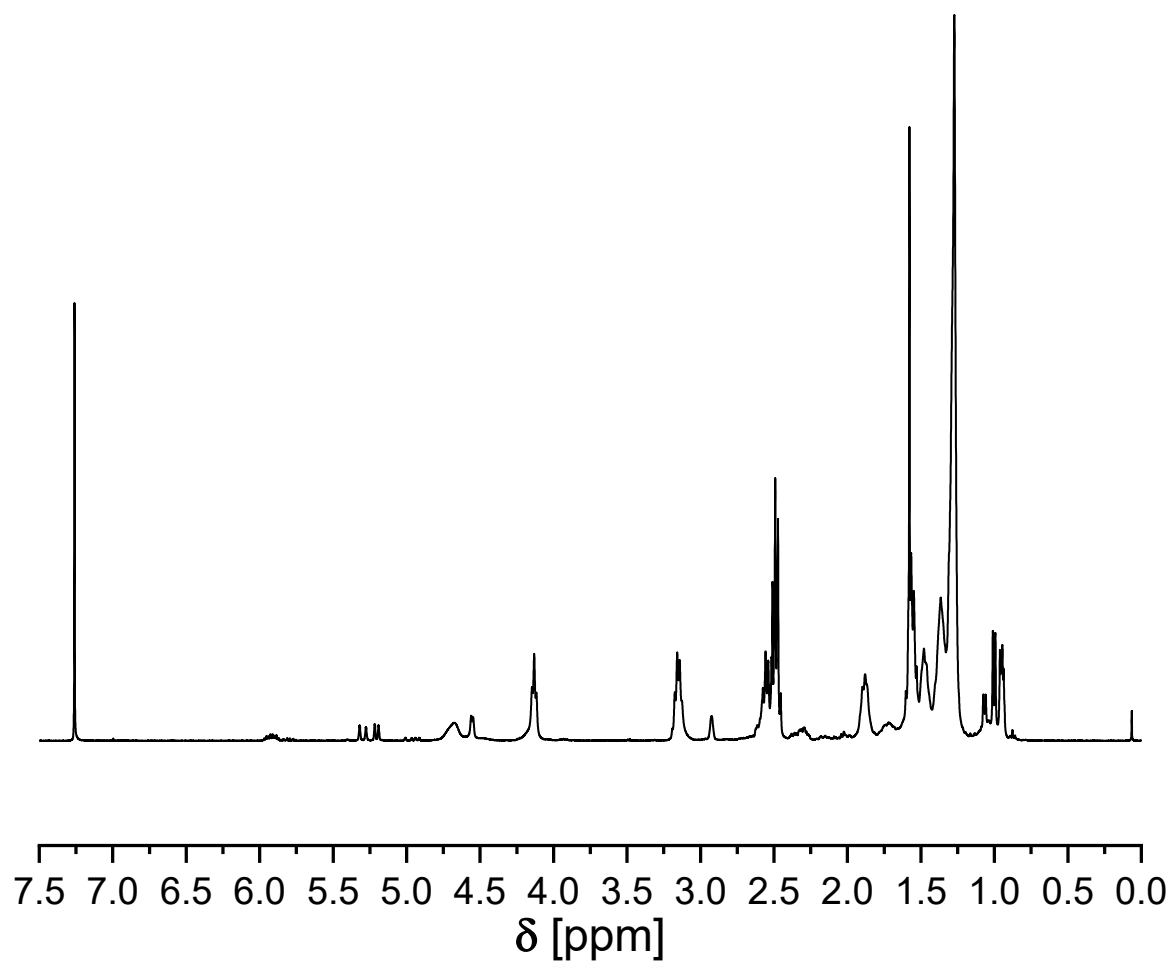
Figure 153 ^{1}H NMR spectrum of **P49** (400 MHz, CDCl$_3$).

P50
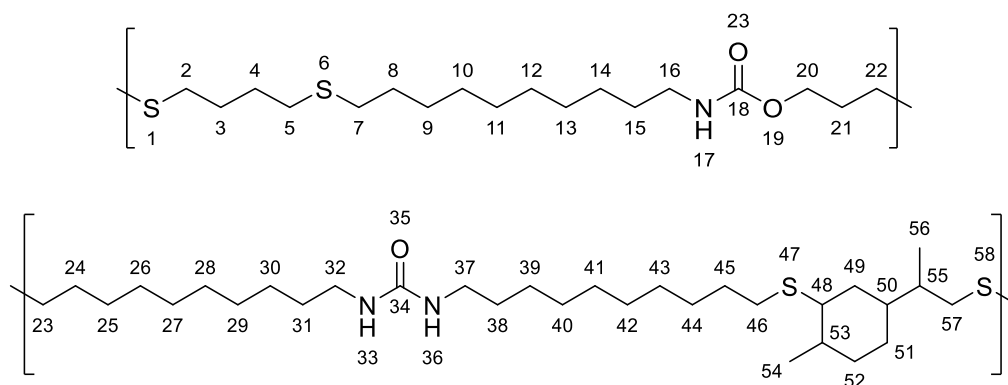
The thiol-ene polymerization of allyl dec-9-enyl carbamate **4** (0.90 eq.) and 1,3-di(dec-9-en-1-yl)urea **9** (0.10 eq.) with 1,4-butanedithiol (0.50 eq.) and limonene dithiol **11** (0.50 eq.) led to the formation of the random copolymer **P50** as a colorless solid (89%).

^{1}H NMR (CDCl$_3$, 400 MHz) δ = 0.89 – 1.11 (m, 2H, CH^{55}, CH$_3{}^{54,56}$), 1.19 – 1.41 (m, CH$_2{}^{9\text{-}14,25\text{-}30,39\text{-}44,}$), 1.47 (q, *J* = 6.8 Hz, CH$_2{}^{15,31,38}$), 1.55 (q, *J* = 7.7, 6.9 Hz, CH$_2{}^{8,22,23,46}$), 1.68 (h, *J* = 7.2 Hz, 2H), 1.80 – 1.94 (m, 1H, CH$_2{}^{21}$), 2.43 – 2.64 (m, CH$_2{}^{2,5,7,23,46}$), 3.05 – 3.21 (m, CH$_2{}^{16,32,37}$), 4.13 (t, *J* = 6.3 Hz, CH$_2{}^{20}$), 4.70 (br, s, NH^{17,33,36}) ppm.

IR (ATR) ṽ = 3335.2, 2919.4, 2850.1, 1685.1 (amide, carbamate), 1614.5 (amide, urea), 1531.9, 1468.4, 1372.6, 1289.2, 1262.2, 1243.7, 1140.1, 1021.0, 779.8, 722.5, 627.1 cm^{-1}.
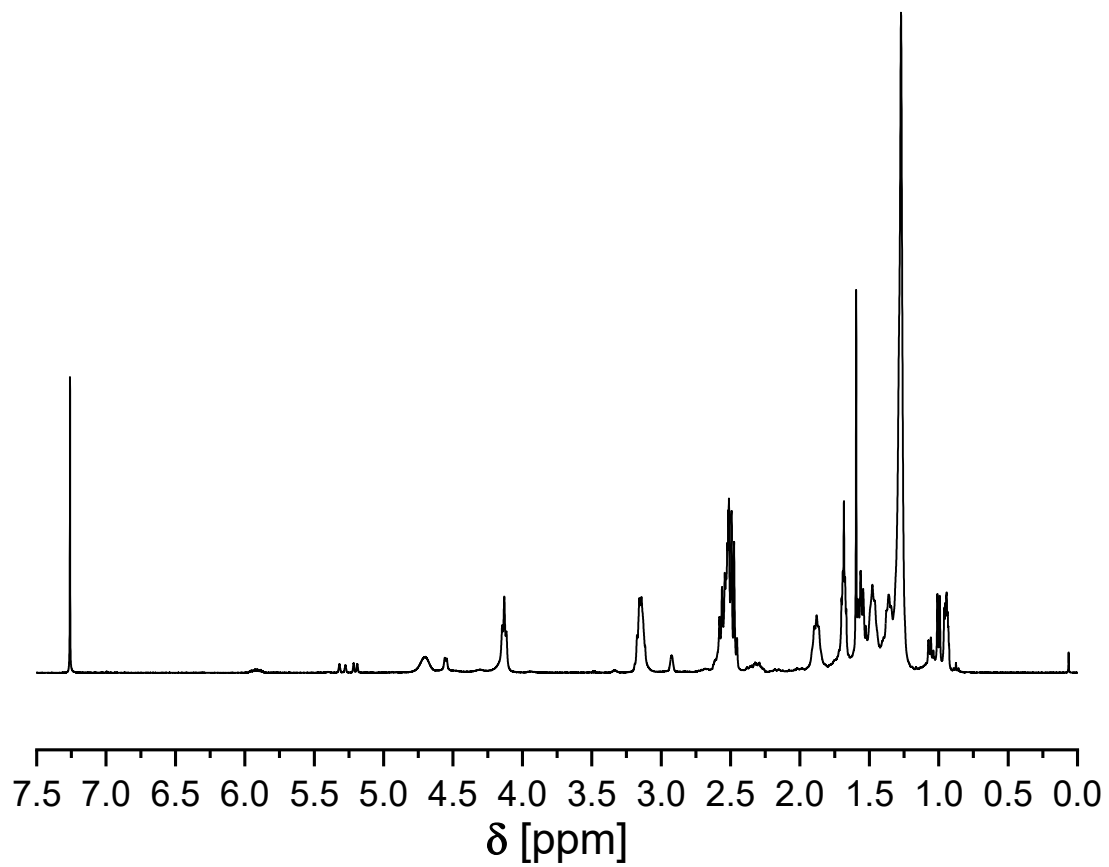
Figure 154 ^{1}H NMR spectrum of **P50** (400 MHz, CDCl$_3$).

5.3.4 General procedure for the preparation of block copolymers

Each block is firstly prepared in the same fashion as in the previous section (**chapter 5.3.3**). Without further purification, excess of one monomer type is added to each prepolymer (e.g. excess dithiol to prepolymer 1 and excess diene to prepolymer 2), and the mixtures are left stirring for 16 h at r.t. under UV irradiation (DMPA, 365 nm). Afterwards, the end group-functionalized NIPUs are purified by precipitation in methanol and dried under vacuum overnight. The two prepolymers are then mixed together in a THF solution and stirred for 24 h at r.t under UV irradiation (DMPA, 365 nm), followed by purification *via* precipitation in methanol and subsequent drying *in vacuo*. The prepolymers and the block copolymers are analyzed by SEC, NMR (proton and DOSY) and DSC.

5.3.5 General procedure for the oxidation of polysulfides to polysulfones

The polymers were dissolved in THF at room temperature, followed by the addition of H_2O_2 (5.00 eq., 30 wt% in H_2O). The reaction mixture was then heated to 65 °C for 24 h. Afterwards, the oxidized polymers were precipitated in a water/methanol (30:70) mixture and dried *in vacuo* overnight. The successful conversion from sulfide to sulfone was determined *via* IR spectroscopy. The yields cannot be precisely calculated without a determined DS and were therefore neglected.
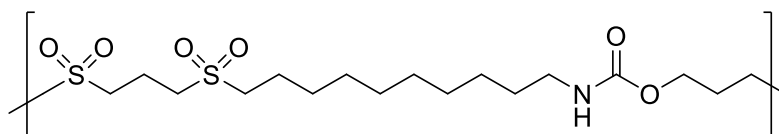
P2 ox.

The oxidation of **P2** with H_2O_2 in THF led to the formation of **P2 ox.** as a colorless solid.

Unfortunately, the polymer was insoluble in all common deuterated solvents.

IR (ATR) ṽ = 3346.6, 3299.3, 2920.8, 2850.9, 1676.4 (amide), 1540.6, 1464.5, 1450.1, 1413.1, 1318.5, 1289.7, 1262.9, 1230.0 (sulfone), 1123.1 (sulfone), 1077.8, 1040.8, 1026.4, 775.5, 736.4 cm^{-1}.
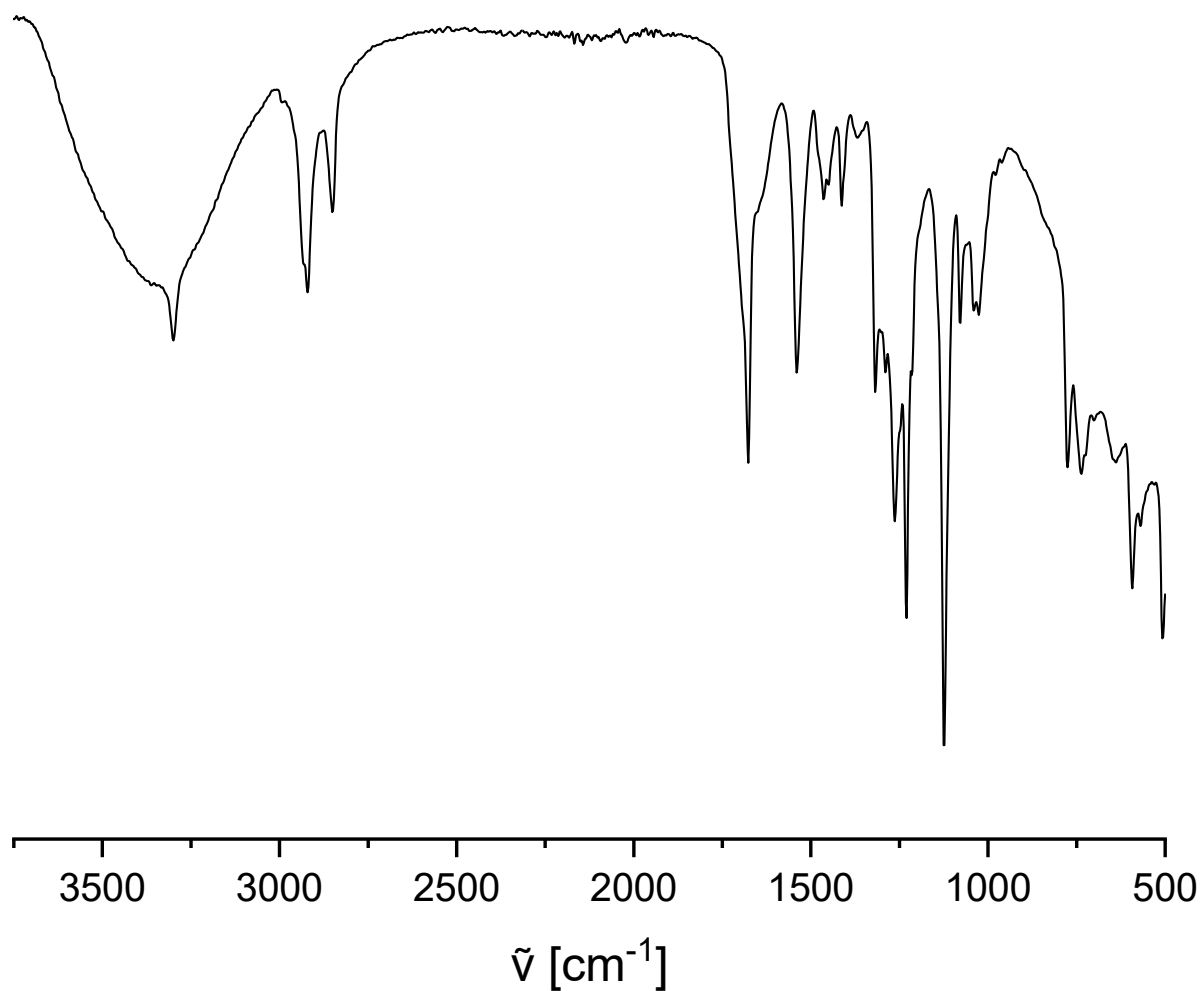
Figure 155 IR spectrum of **P2 ox**.

P3 ox.
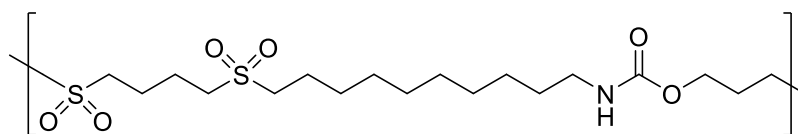
The oxidation of **P3** with H_2O_2 in THF led to the formation of **P3 ox.** as a colorless solid. Unfortunately, the polymer was insoluble in all common deuterated solvents.

IR (ATR) $\tilde{v}$ = 3301.3, 2920.8, 2850.9, 1676.4 (amide), 1538.6, 1466.6, 1450.1, 1411.0, 1324.6, 1250.6 (sulfone), 1225.9, 1211.5, 1121.0 (sulfone), 1077.8, 1038.7, 1005.8, 979.1, 763.1, 736.4 cm^{-1}.
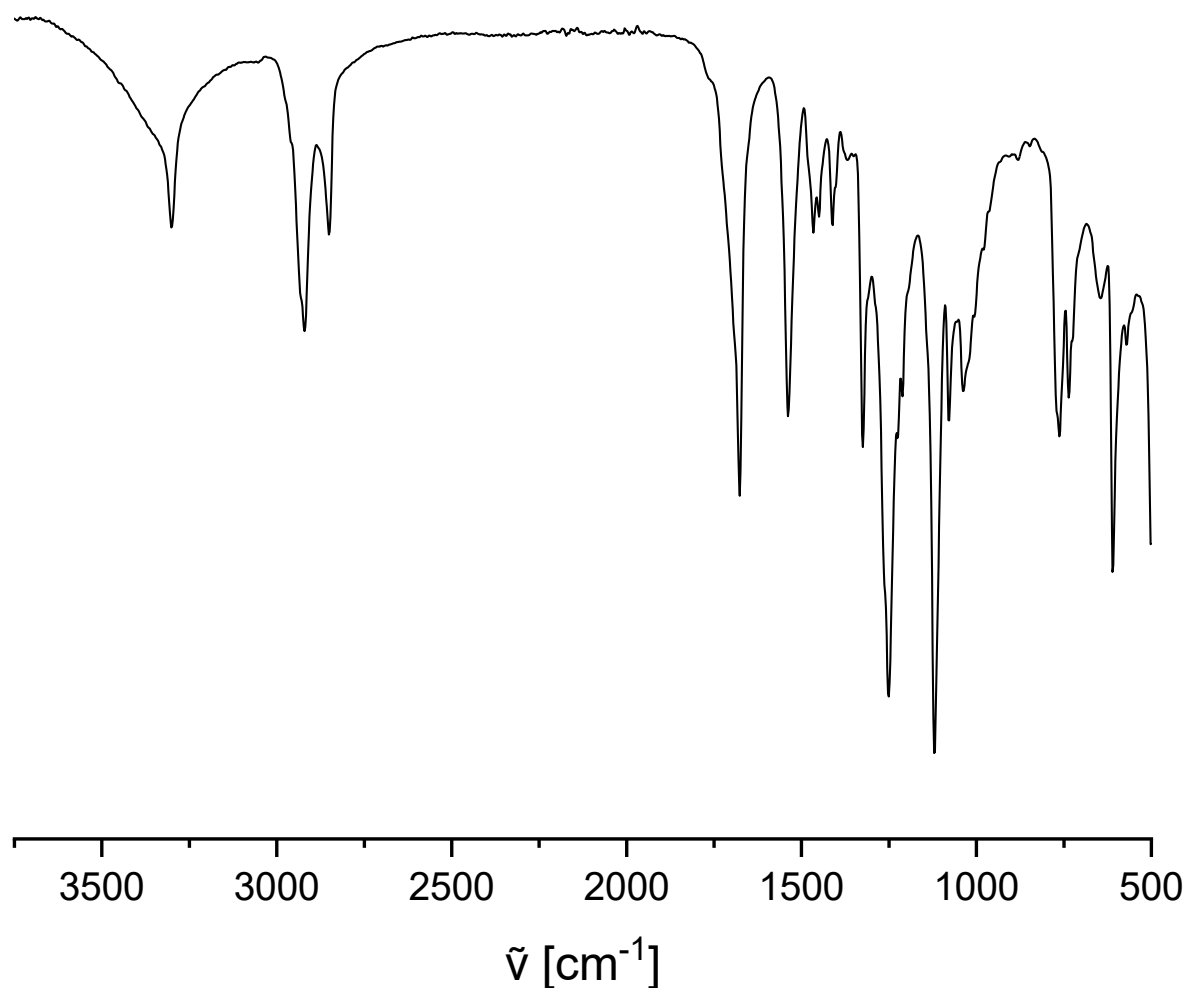
Figure 156 IR spectrum of **P3 ox**.
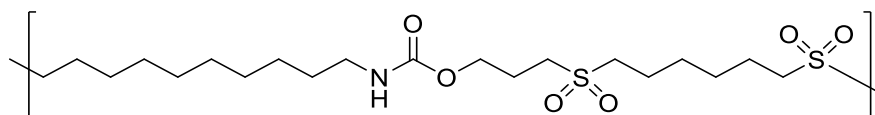
P4 ox.

The oxidation of **P4** with H_2O_2 in THF led to the formation of **P4 ox.** as a colorless solid. Unfortunately, the polymer was insoluble in all common deuterated solvents.

IR (ATR) $\tilde{v}$ = 3299.3, 2920.8, 2850.9, 1676.4 (amide), 1538.6, 1466.6, 1456.3, 1411.0, 1324.6, 1289.7, 1262.9, 1240.3 (sulfone), 1201.2, 1121.0 (sulfone), 1079.9, 1038.7, 991.4, 962.6, 905.0, 851.6, 771.3, 728.1 cm^{-1}.
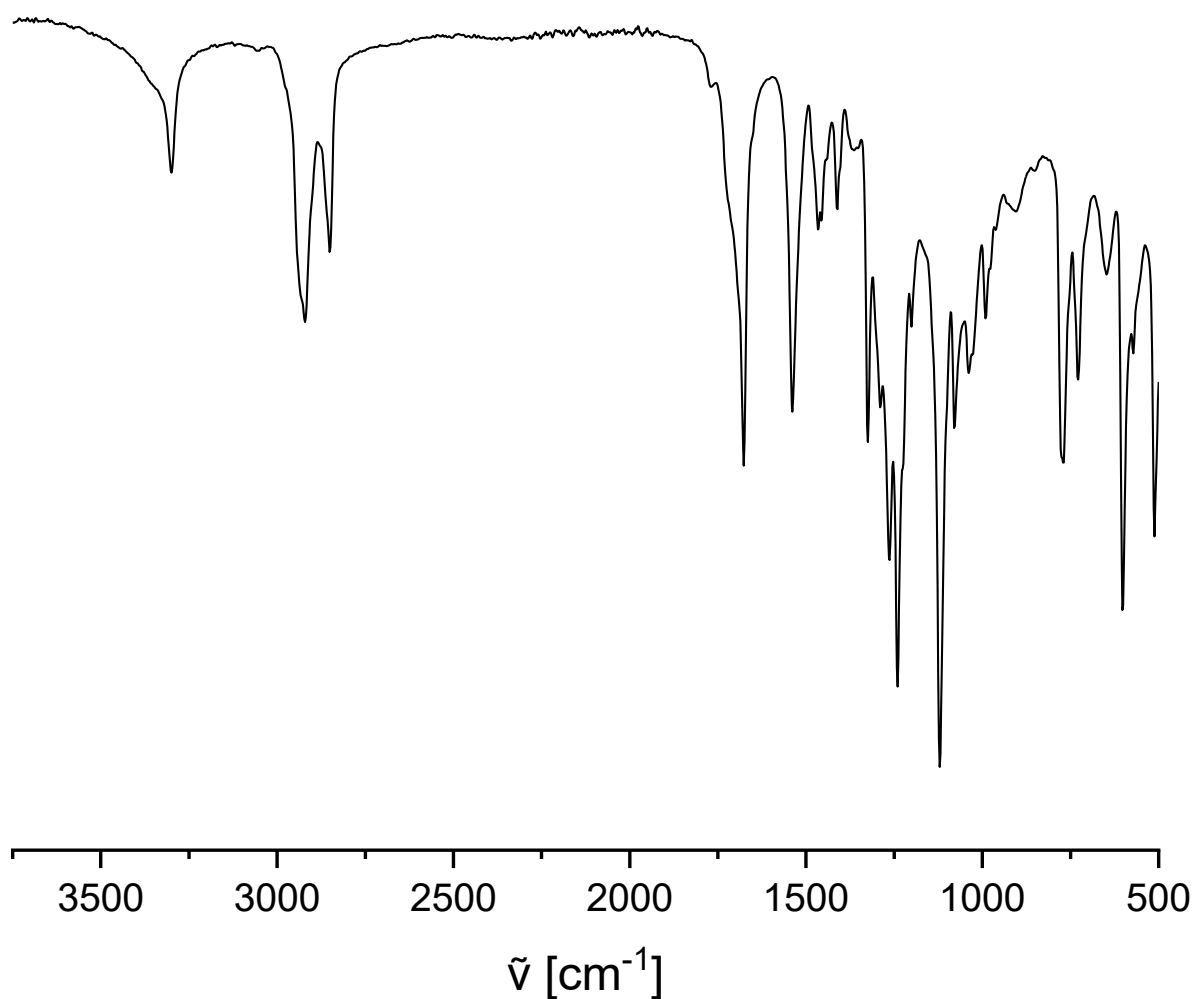
Figure 157 IR spectrum of **P4 ox**.

P7 ox.
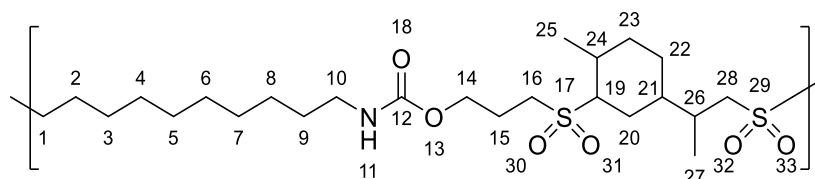
The oxidation of **P7** with H_2O_2 in THF led to the formation of **P7 ox.** as a colorless solid.

The polymer was scarcely soluble in CHCl₃, thus the intensities in HSQC and COSY were insufficient for an exact attribution of all proton signals. Worth mentioning is the shift of the CH₂ groups **1, 16, 28** and the CH group **19** towards lower field (from 2.4 in the unoxidized polymer to 3.1 ppm), while the CH₂ group **14** remained at around 4.2 ppm (**Chapter 4.2.13**).

IR (ATR) ṽ = 3361.0, 2924.9, 2855.0, 1707.2 (amide), 1530.3, 1460.4, 1411.0, 1273.2, 1248.5 (sulfone), 1125.1 (sulfone), 1063.4, 1032.6, 905.0, 868.0, 847.4, 777.5, 750.8, 722.0 cm⁻¹.
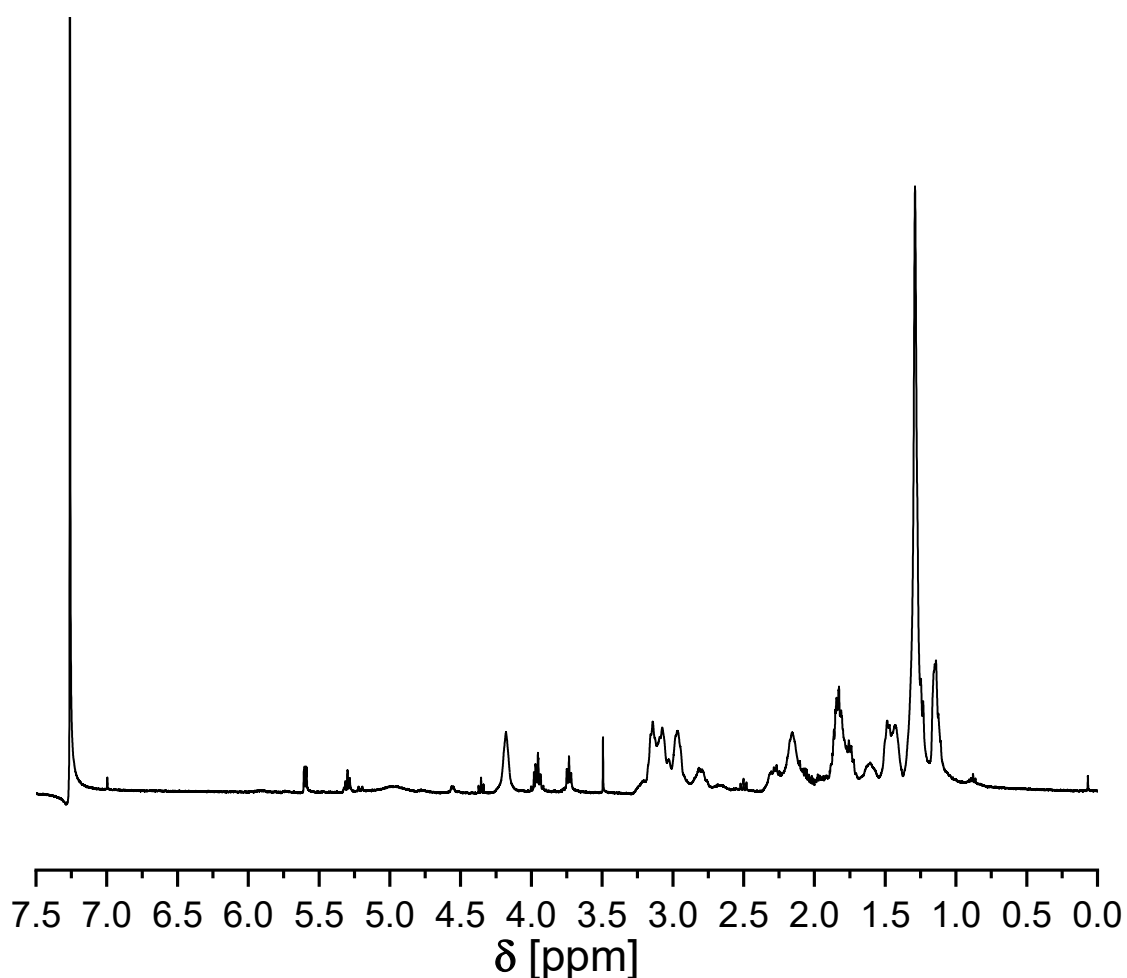
Figure 158 ¹H NMR spectrum of **P7 ox.** (400 MHz, CDCl₃).
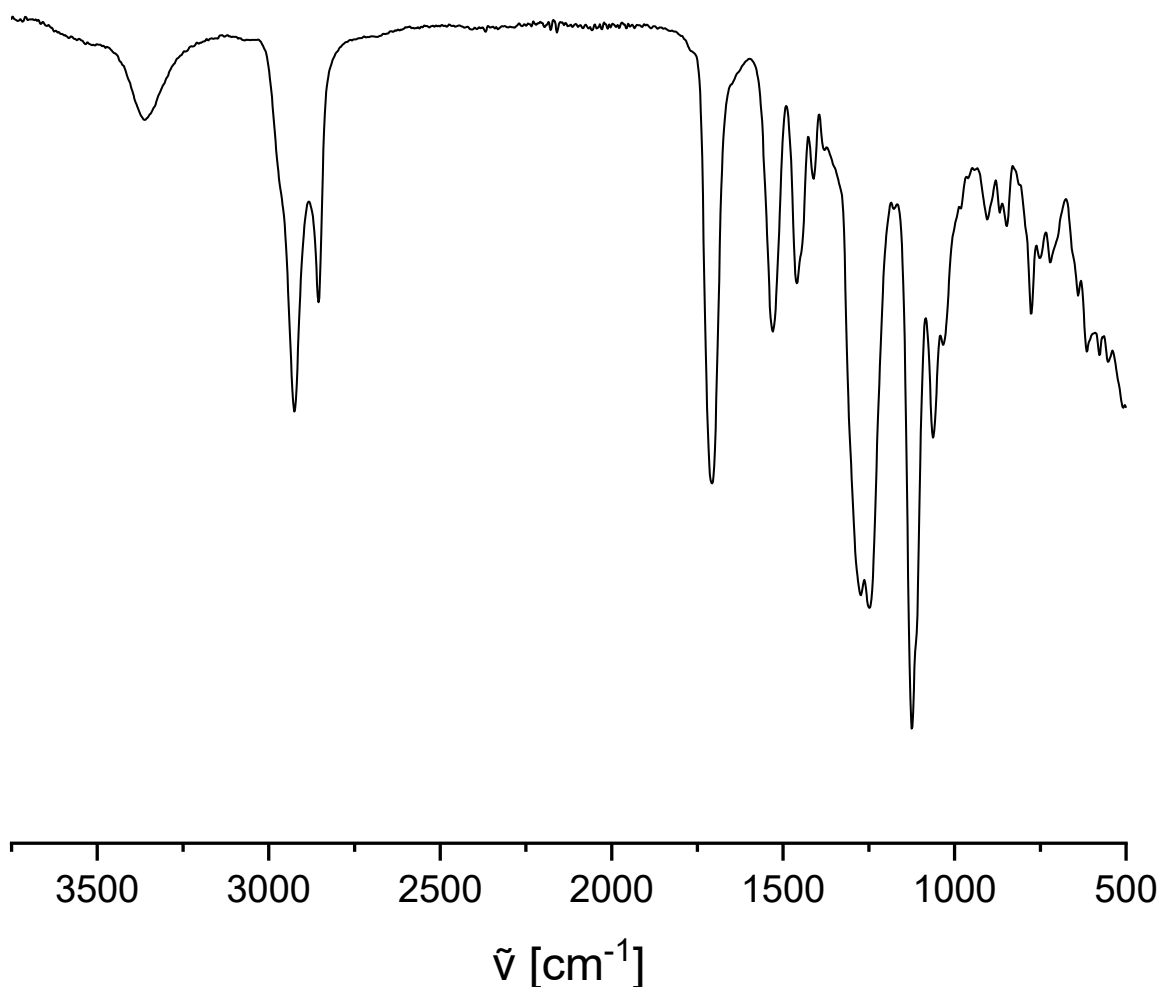
Figure 159 IR spectrum of **P7 ox**.

P9 ox.
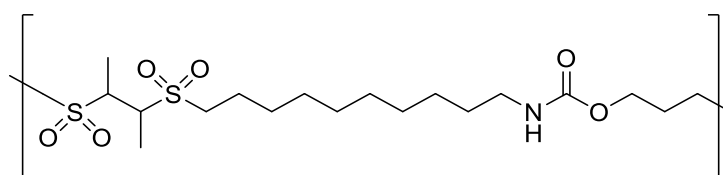
The oxidation of **P9** with H_2O_2 in THF led to the formation of **P9 ox.** as a colorless solid. Unfortunately, the polymer was insoluble in all common deuterated solvents.

IR (ATR) $\tilde{v}$ = 3367.2, 2924.9, 2855.0, 1697.0 (amide), 1532.4, 1460.4, 1411.0, 1357.6, 1289.7, 1260.9 (sulfone), 1131.3, 1114.8 (sulfone), 1053.1, 1024.3, 835.1, 775.5, 722.0 cm^{-1}.
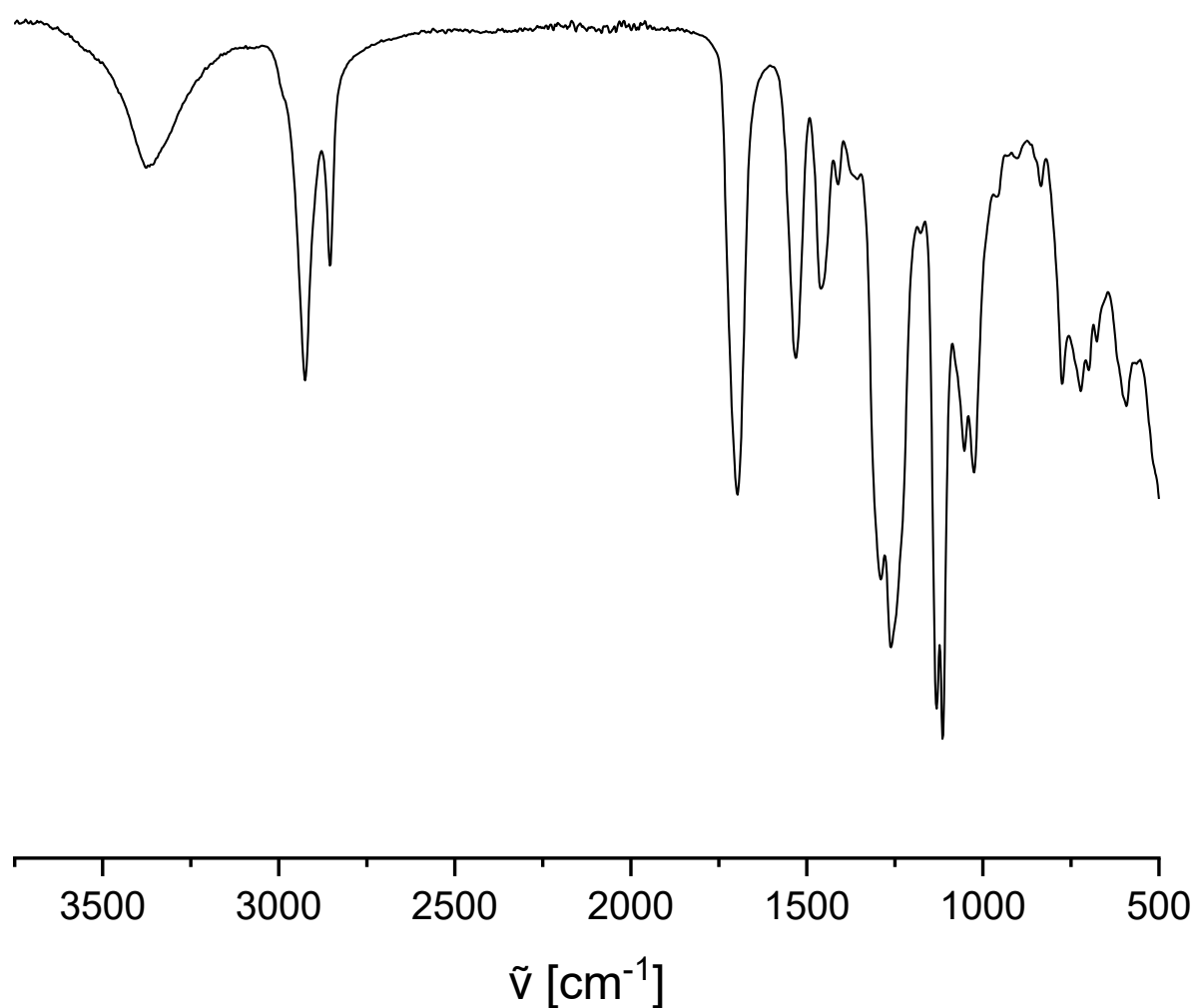
Figure 160 IR spectrum of **P9 ox**.

Experimental section

P14 ox.
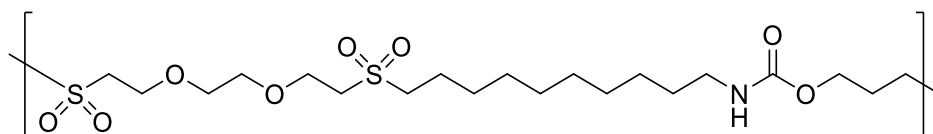
The oxidation of **P14** with H_2O_2 in THF led to the formation of **P14 ox.** as a colorless solid. Unfortunately, the polymer was insoluble in all common deuterated solvents.

IR (ATR) ṽ = 3307.5, 2920.8, 2852.9, 1678.4 (amide), 1538.6, 1466.6, 1406.9, 1394.6, 1374.0, 1357.6, 1316.4, 1289.7, 1262.9 (sulfone), 1248.5, 1188.9, 1121.0 (sulfone), 1079.9, 1036.7, 997.6, 968.8, 925.6, 820.7, 804.3, 779.6, 763.1, 750.8, 717.9 cm^{-1}.
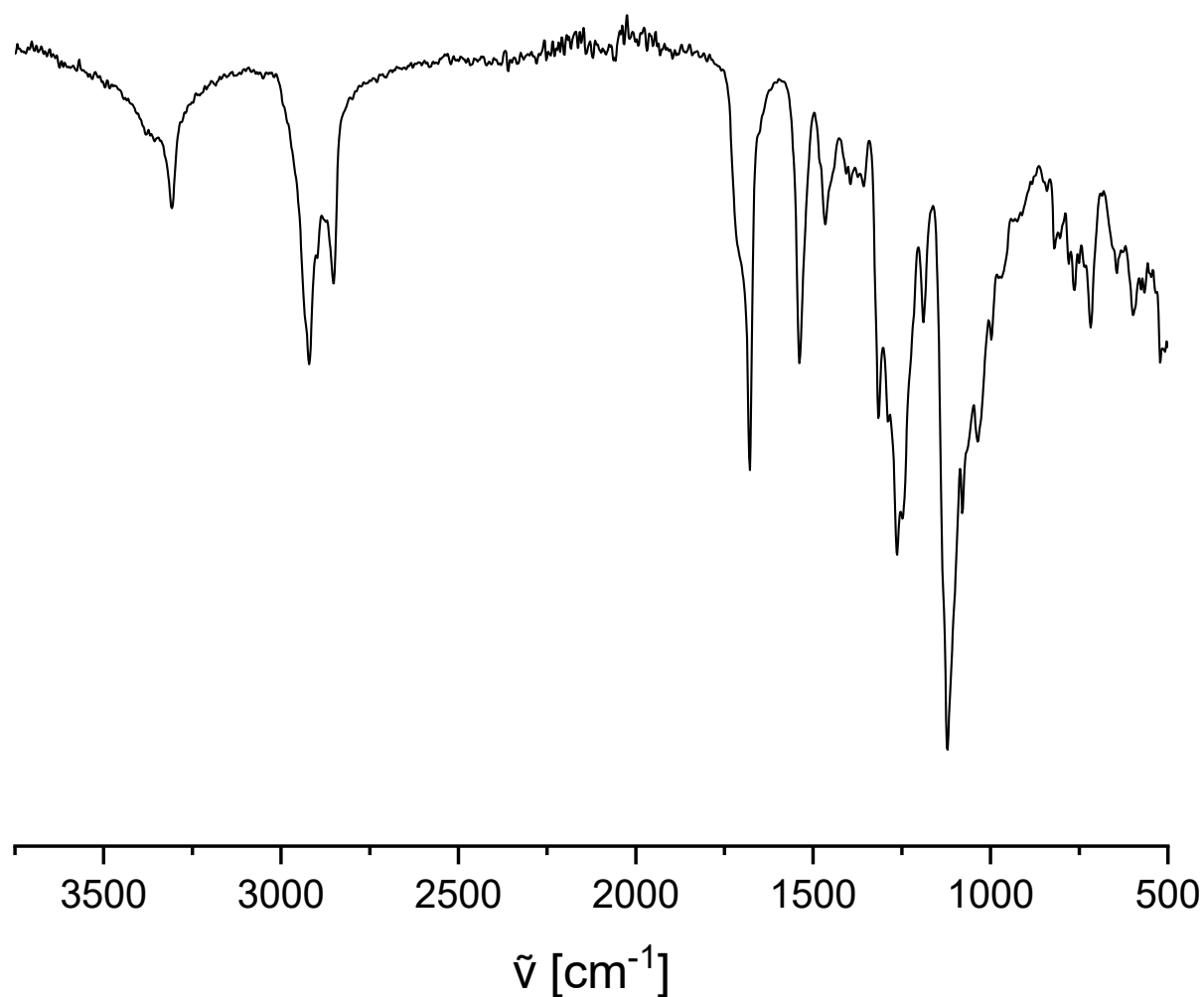
Figure 161 IR spectrum of **P14 ox**.

P15 ox.
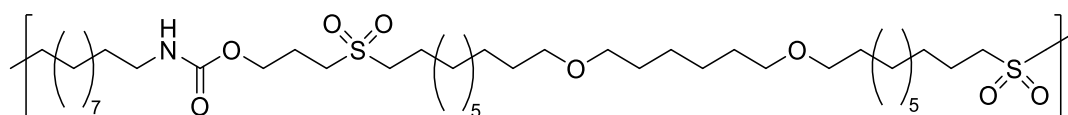
The oxidation of **P15** with H_2O_2 in THF led to the formation of **P15 ox.** as a colorless solid.

Unfortunately, the polymer was insoluble in all common deuterated solvents.

IR (ATR) ṽ = 3299.7, 2916.7, 2848.8, 1676.4 (amide), 1538.6, 1464.5, 1324.6, 1289.7, 1265.0, 1250.6 (sulfone), 1223.9, 1116.9 (sulfone), 1079.9, 1051.1, 1026.4, 773.4, 724.0 cm^{-1}.
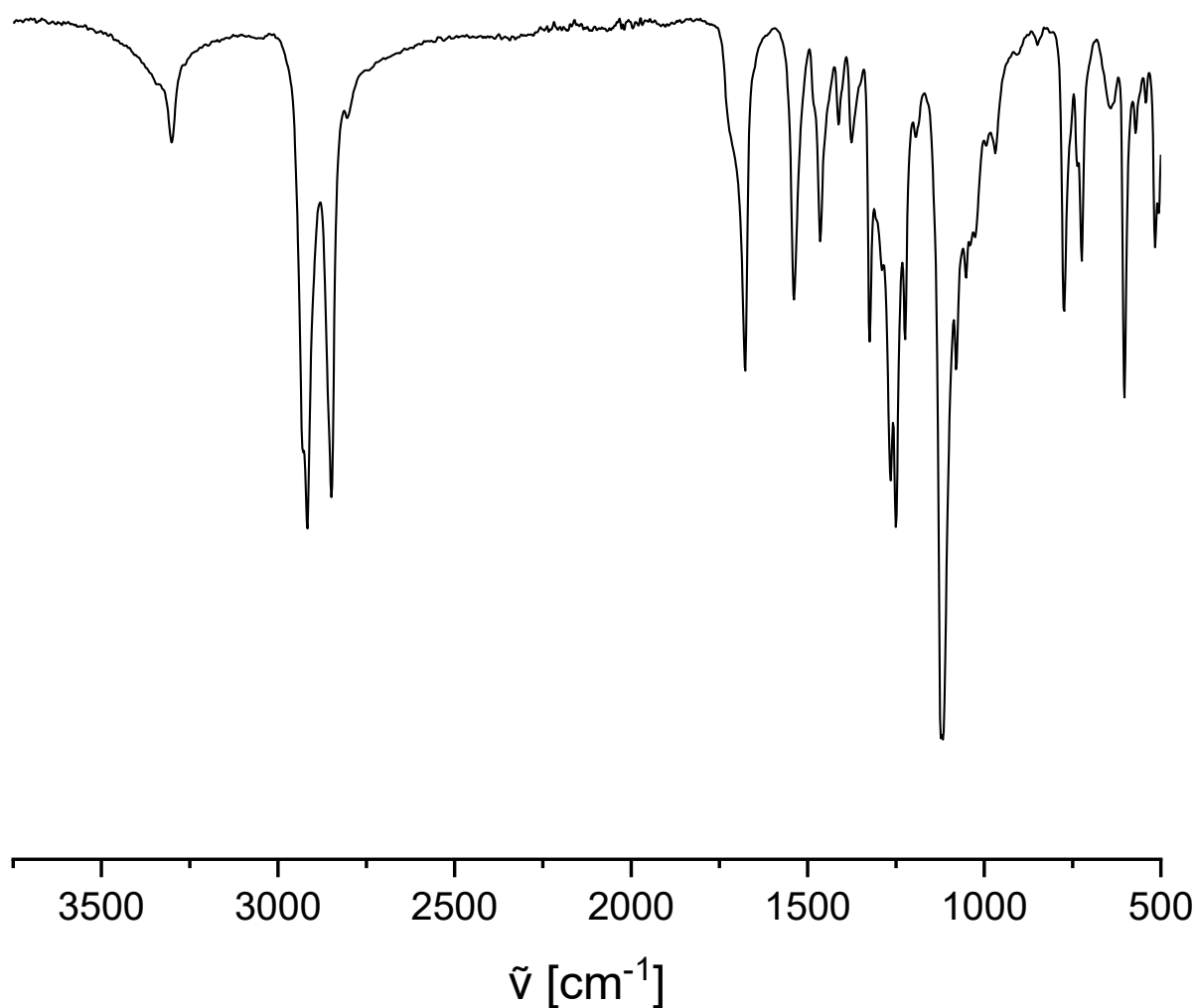
Figure 162 IR spectrum of **P15 ox**.
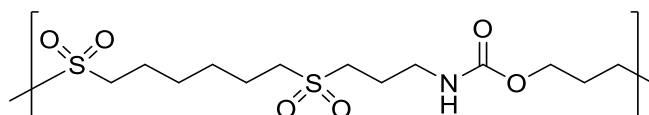
P21 ox.

The oxidation of **P21** with H_2O_2 in THF led to the formation of **P21 ox.** as a colorless solid. Unfortunately, the polymer was insoluble in all common deuterated solvents.

IR (ATR) $\tilde{v}$ = 3313.7, 2943.4, 2931.1, 1676.4 (amide), 1538.6, 1470.7, 1456.3, 1411.0, 1324.6, 1297.9, 1289.7, 1260.9 (sulfone), 1240.3, 1201.2, 1180.7, 1164.2 (sulfone), 1119.0, 1084.0, 1073.7, 1038.7, 1012.0, 989.4, 929.7, 911.2, 851.6, 771.3, 750.8, 730.2, 711.7, 637.6 cm^{-1}.
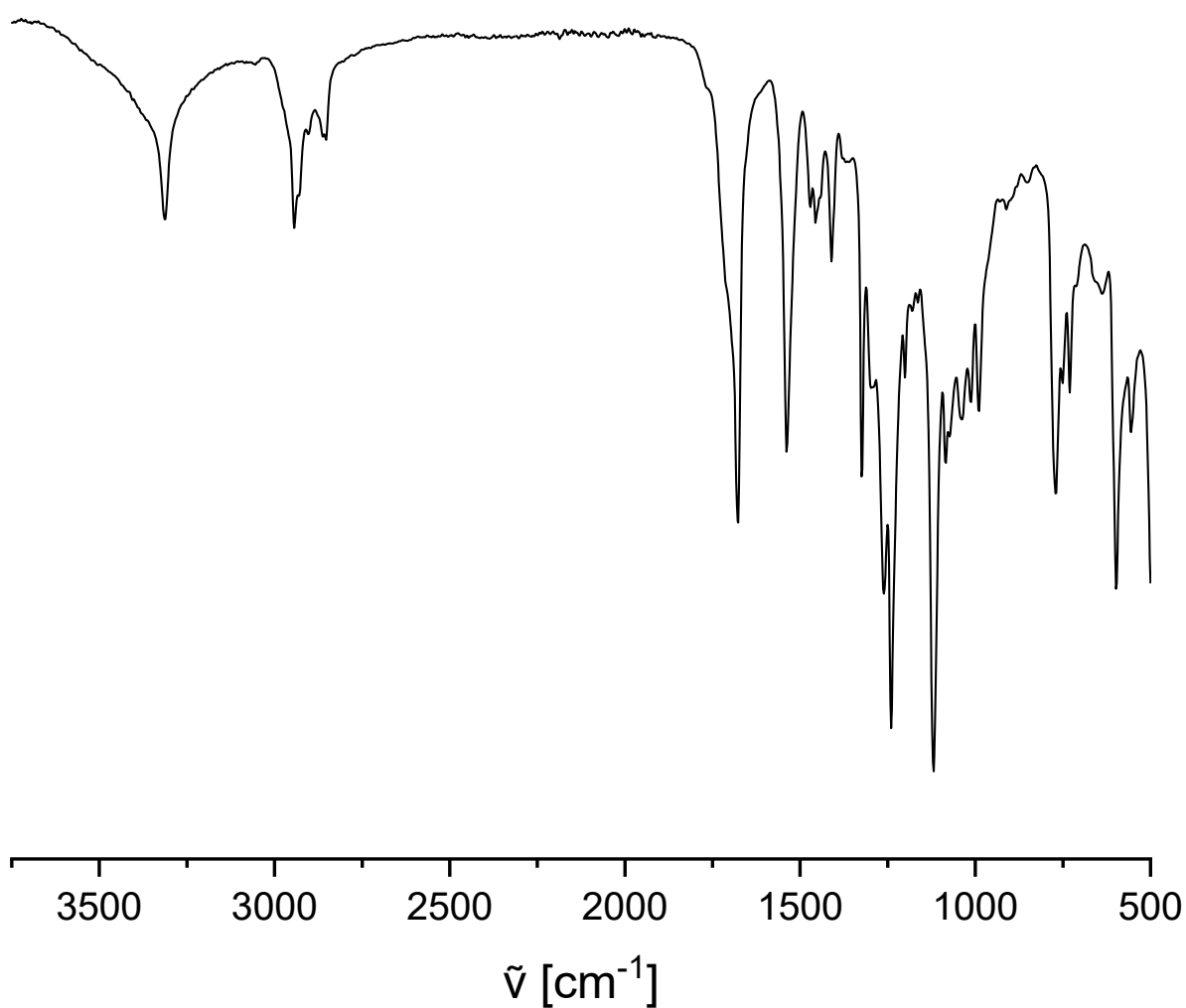
Figure 163 IR spectrum of **P21 ox**.

P35 ox.
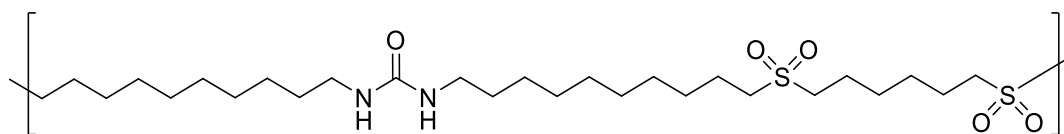
The oxidation of **P35** with H_2O_2 in THF led to the formation of **P35 ox.** as a colorless solid.

Unfortunately, the polymer was insoluble in all common deuterated solvents.

IR (ATR) $\tilde{v}$ = 3336.3, 2920.8, 2848.8, 1614.7 (amide), 1571.5, 1509.8, 1476.9, 1462.5, 1413.1, 1318.5, 1285.6, 1275.3 (sulfone), 1236.2, 1182.7, 1162.2, 1125.1 (sulfone), 1077.8, 1032.6, 993.5, 773.4, 724.0 cm^{-1}.
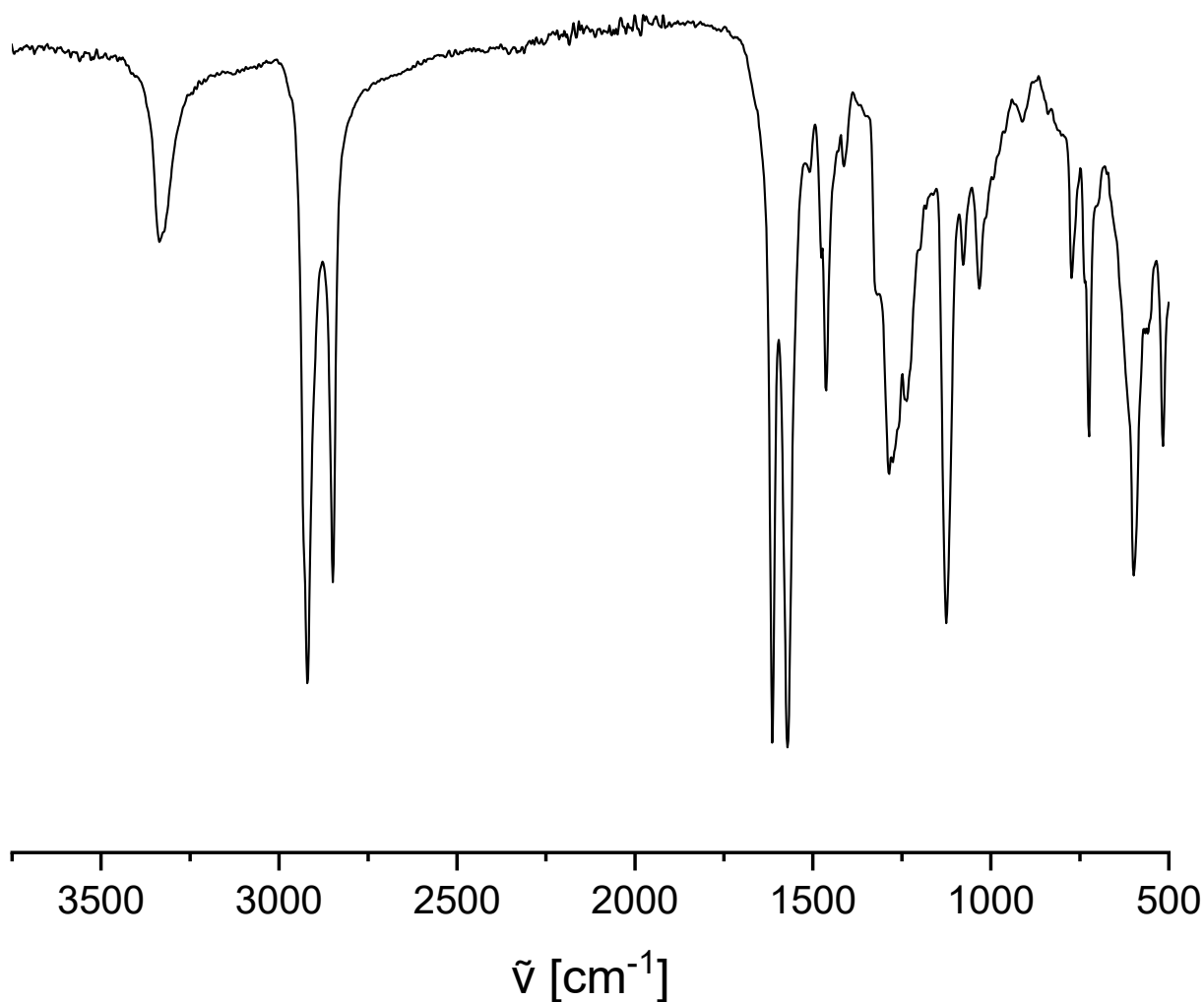
Figure 164 IR spectrum of **P35 ox.**
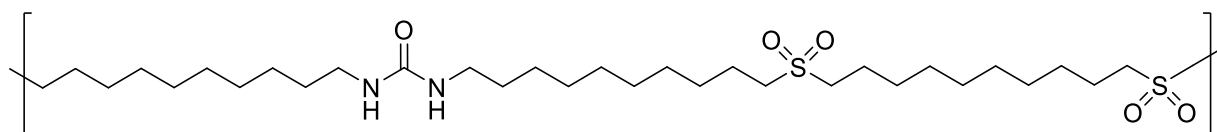
P36 ox.

The oxidation of **P36** with H_2O_2 in THF led to the formation of **P36 ox.** as a colorless solid. Unfortunately, the polymer was insoluble in all common deuterated solvents.

IR (ATR) ṽ = 3336.3, 2918.8, 2848.8, 1614.7 (amide), 1571.5, 1509.8, 1476.9, 1464.5, 1322.6, 1285.6, 1265.0, 1230.0 (sulfone), 1195.1, 1180.7, 1166.3, 1127.2 (sulfone), 1077.8, 1036.7, 1014.1, 771.3, 736.4, 724.0 cm^{-1}.
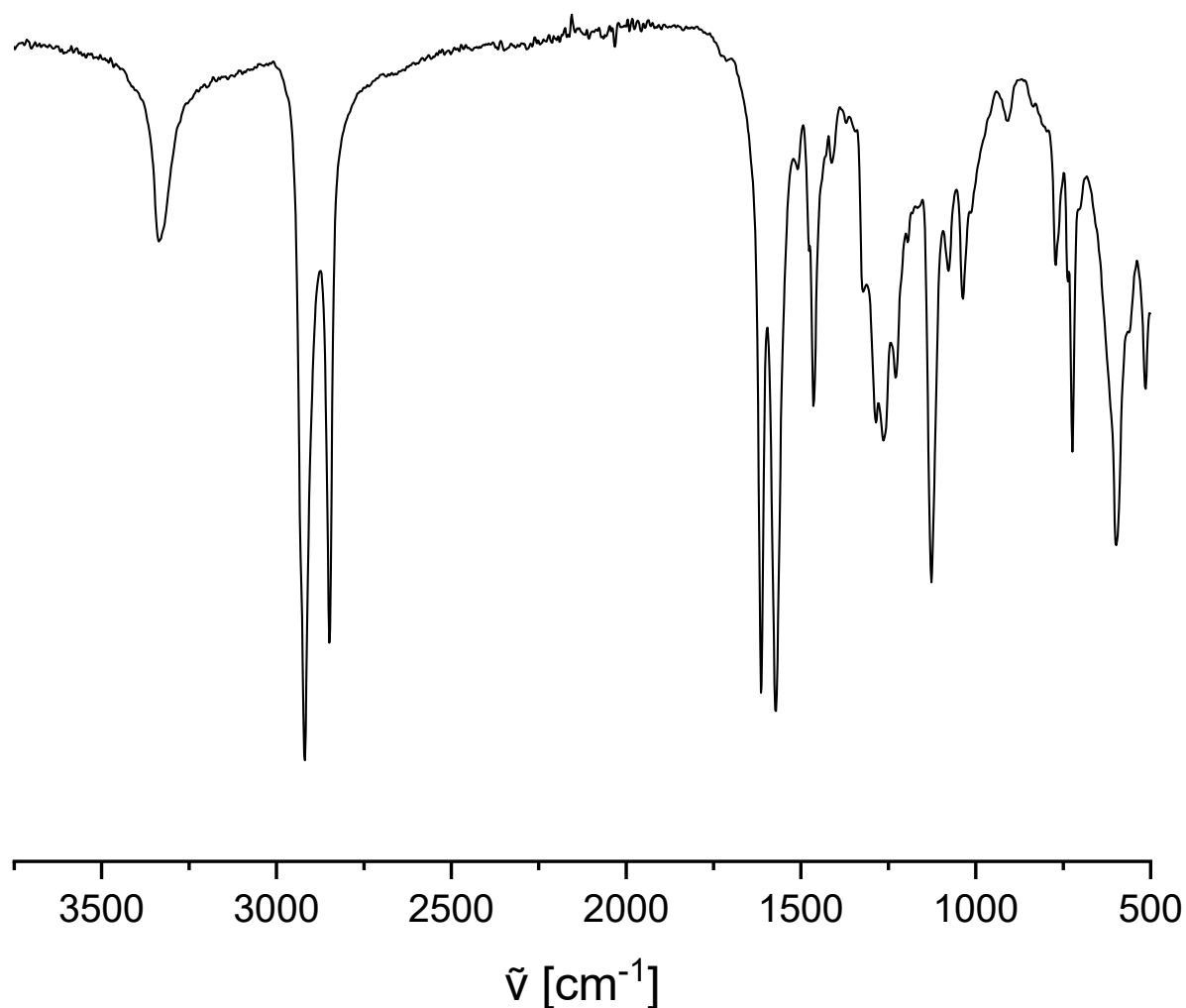
Figure 165 IR spectrum of **P36 ox**.

P37 ox.
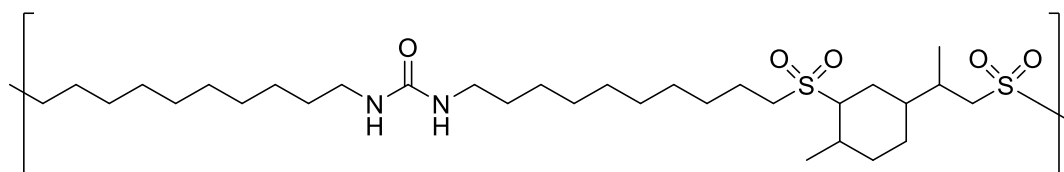
The oxidation of **P37** with H_2O_2 in THF led to the formation of **P37 ox.** as a colorless solid. Unfortunately, the polymer was insoluble in all common deuterated solvents.

IR (ATR) $\tilde{v}$ = 3326.0, 2918.8, 2850.9, 1618.8 (amide), 1573.5, 1464.5, 1277.3 (sulfone), 1127.2 (sulfone), 1077.8, 1012.0, 738.4, 722.0 cm^{-1}.
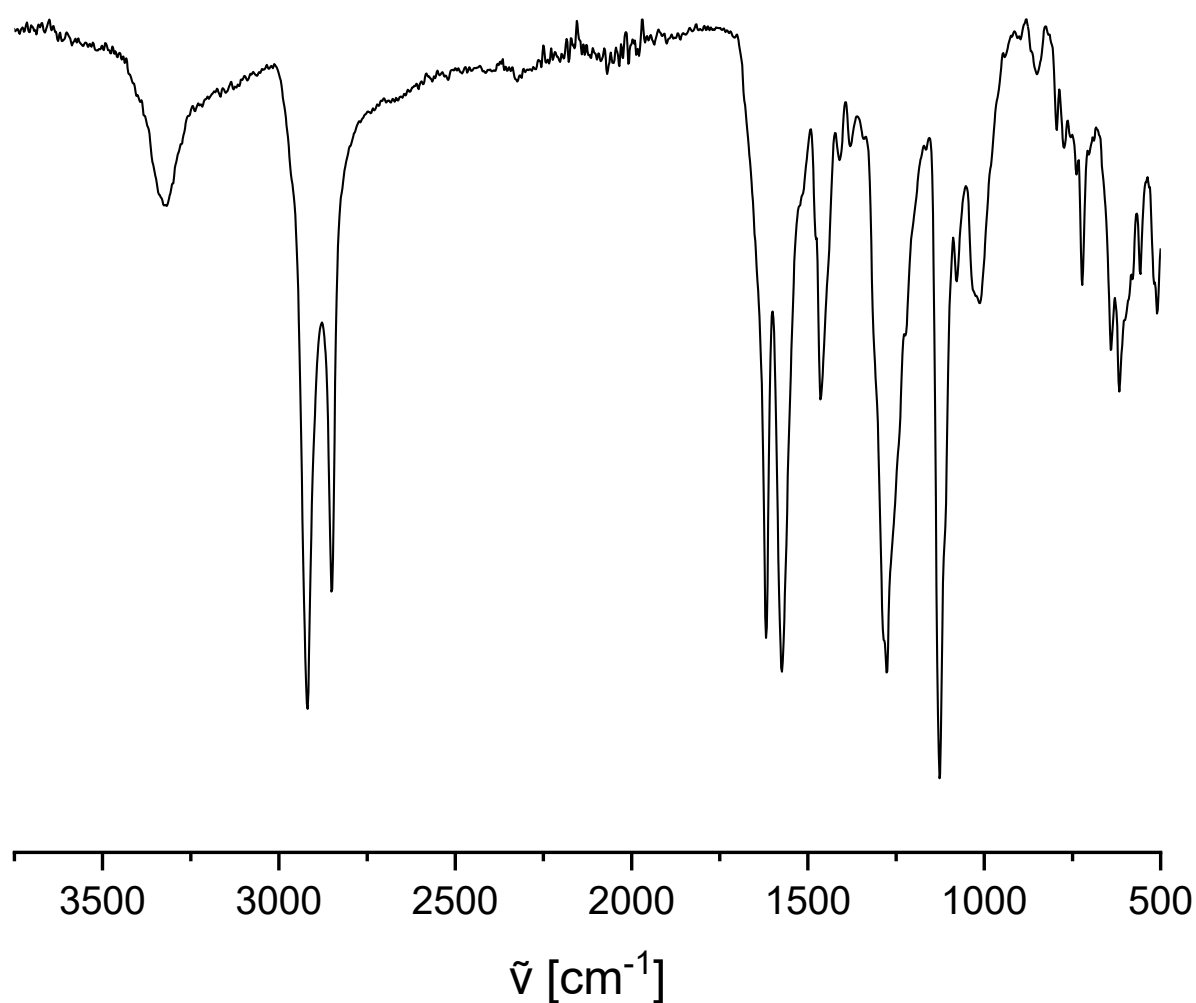
Figure 166 IR spectrum of **P37 ox**.
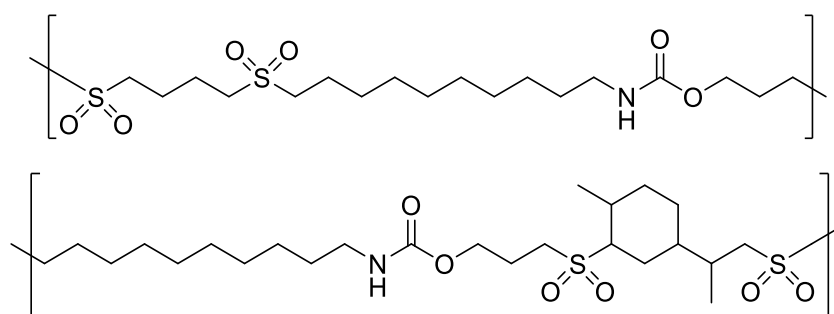
P43 ox.

The oxidation of **P43** with H$_2$O$_2$ in THF led to the formation of **P43 ox.** as a colorless solid. Unfortunately, the polymer was insoluble in all common deuterated solvents.

IR (ATR) ṽ = 3303.4, 2918.8, 2850.9, 1688.7 (amide), 1536.5, 1324.6, 1250.6 (sulfone), 1121.0 (sulfone), 1077.8, 1036.7, 1024.3, 771.3, 763.1 cm^{-1}.
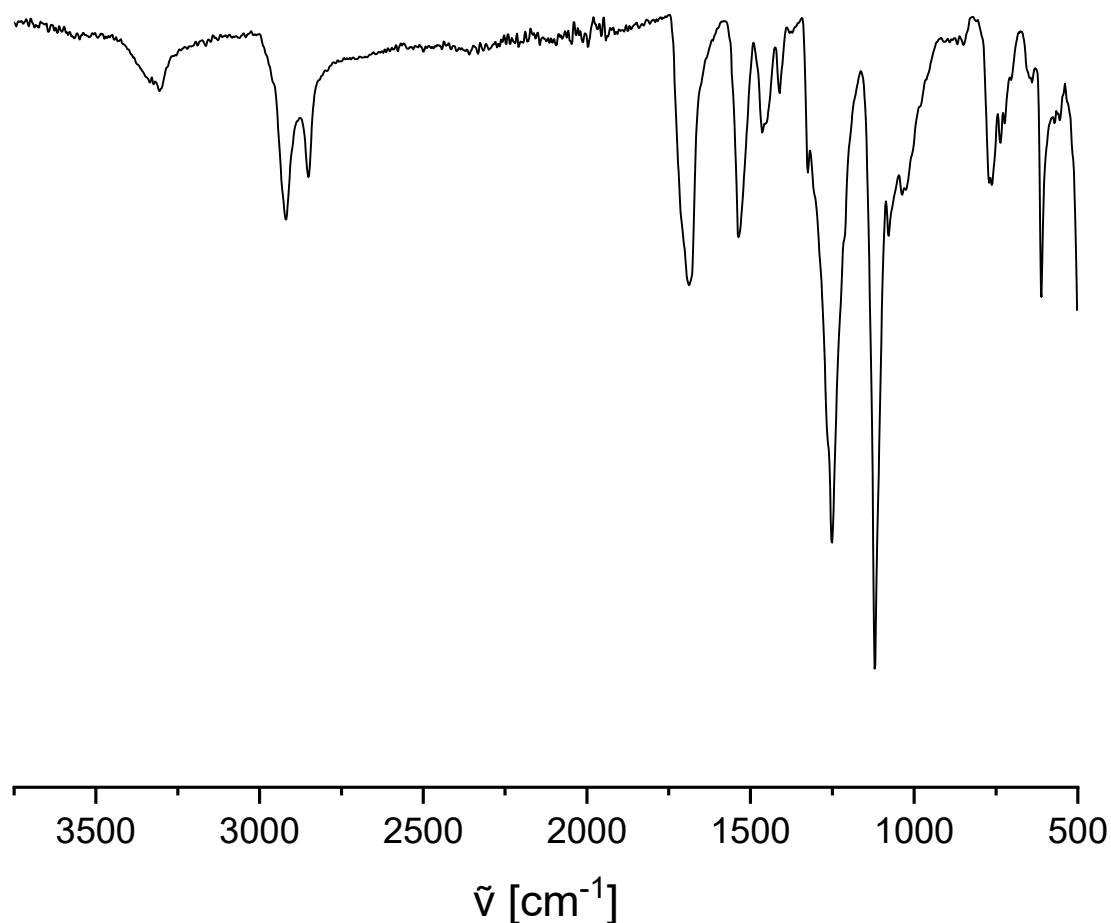
Figure 167 IR spectrum of **P43 ox.**

P44 ox.
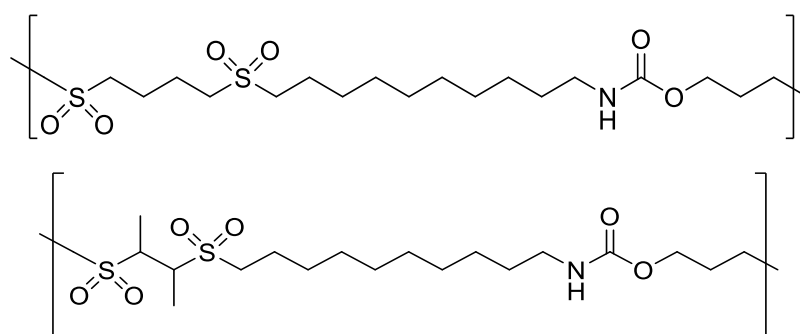
The oxidation of **P44** with H_2O_2 in THF led to the formation of **P44 ox.** as a colorless solid. Unfortunately, the polymer was insoluble in all common deuterated solvents.

IR (ATR) ṽ = 3305.5, 2920.8, 2850.9, 1680.5 (amide), 1538.6, 1466.6, 1452.2, 1324.6, 1252.7 (sulfone), 1119.0 (sulfone), 1077.8, 1036.7, 771.3, 763.1, 736.4, 724.0 cm^{-1}.
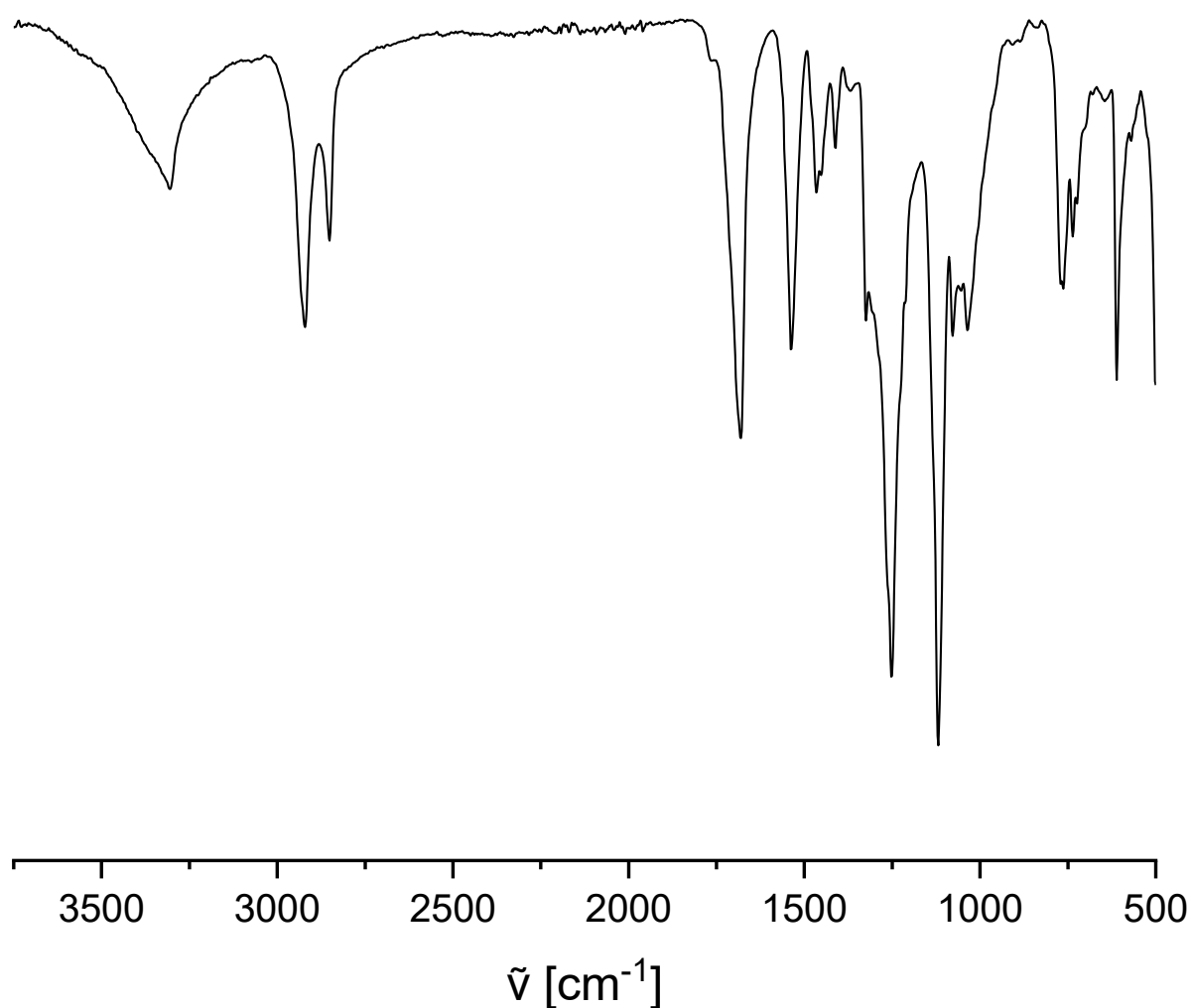
Figure 168 IR spectrum of **P44 ox.**

P45 ox.
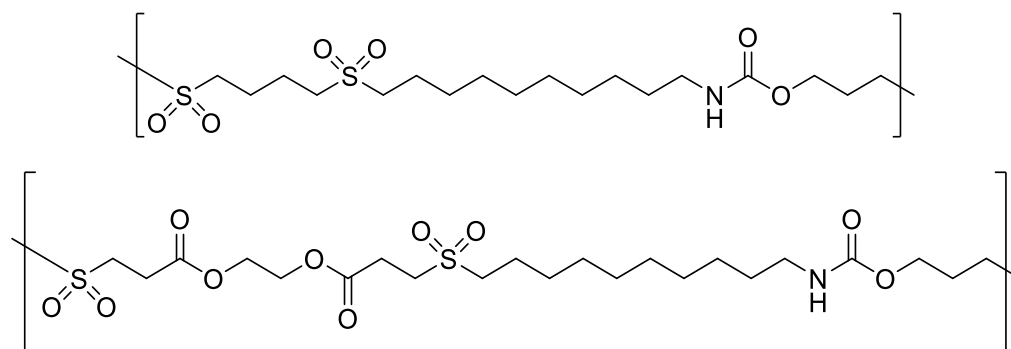
The oxidation of **P45** with H_2O_2 in THF led to the formation of **P45 ox.** as a colorless solid (x%). Unfortunately, the polymer was insoluble in all common deuterated solvents.

IR (ATR) ṽ = 3307.5, 2918.8, 2848.8, 1727.8 (ester), 1680.5 (amide), 1538.6, 1468.6, 1413.1, 1322.6, 1306.1, 1250.6 (sulfone), 1225.9, 1186.8 (sulfone), 1119.0, 1077.8, 1038.7, 769.3, 736.4, 724.0 cm^{-1}.
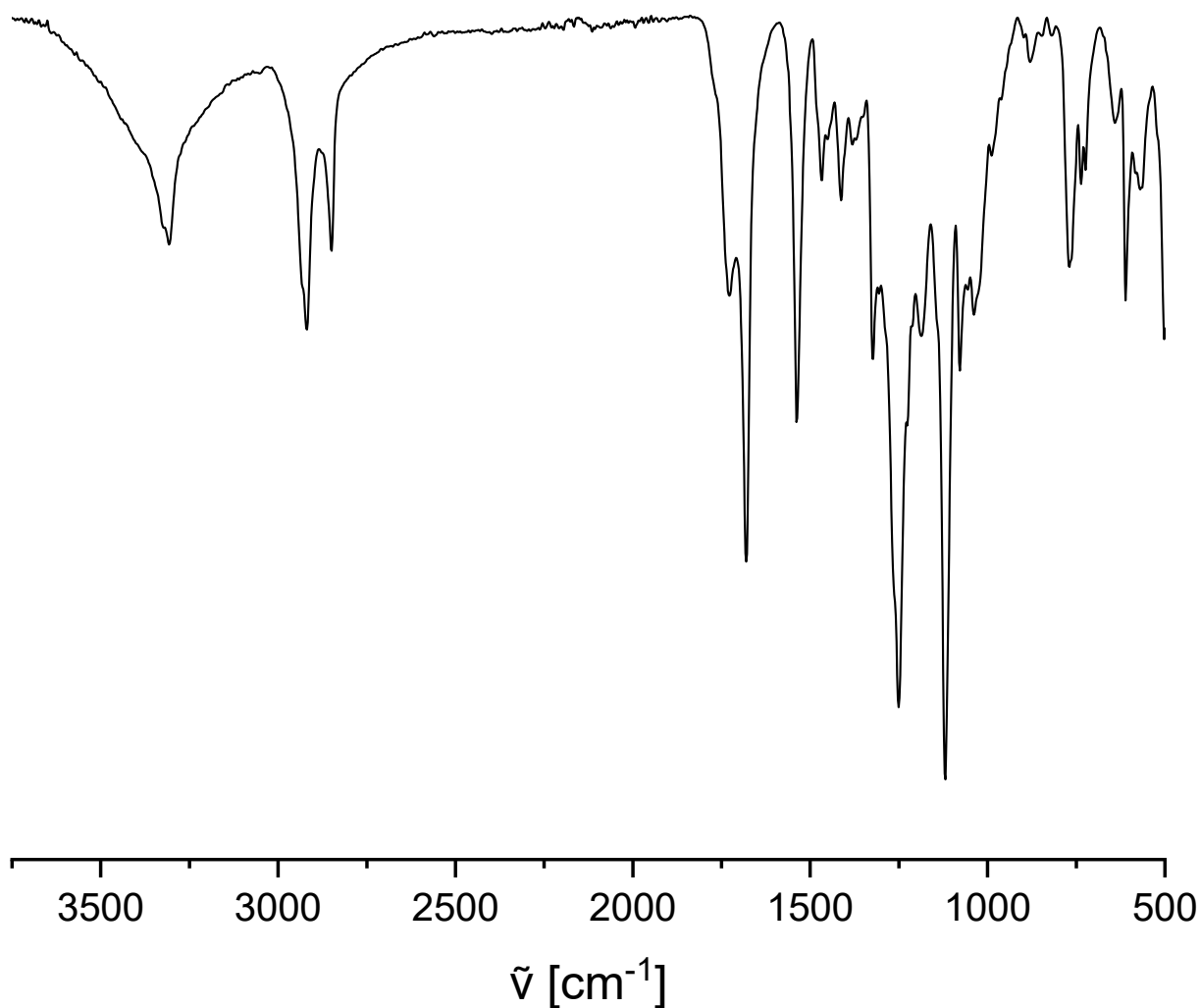
Figure 169 IR spectrum of **P45 ox.**

6 <u>Appendix</u>

6.1 List of abbreviations

ADMET	acyclic diene metathesis
AIBN	Azobisisobutyronitrile
ASAP	atmospheric solids analysis probe
ATRP	atom transfer radical polymerization
Cat.	catalyst
CHD	cyclohexadiene
CH	cyclohexane
$CHCl_3$	chloroform
CNCs	cellulose nanocrystals
COSY	Correlated spectroscopy
cyrene	Dihydrolevoglucosenone
$Đ_M$	dispersity
DABCO	1,4-diazabicyclo[2.2.2]octane
DBU	1,8-diazabicyclo[5.4.0]undec-7-ene
DBN	1,5-Diazabicyclo(4.3.0)non-5-ene
DAC	diallyl carbonate
DCM	dichloromethane
DMC	dimethyl carbonate
DMF	dimenthylformamide
DMPA	2,2-Dimethoxy-2-phenylacetophenone
DMSO	dimethylsulfoxide
DOSY	diffusion oriented spectroscopy
DPC	diphenyl carbonate
DSC	differential scanning calorimetry
e.g.	example given
EA	ethyl acetate
EI-MS	electron impact ionization-mass spectrometry
eq.	equivalents

ESBO	epoxidized soyabean oil
ESI-MS	electrospray ionization-mass spectrometry
Et_2O	diethyl ether
EWGs	electron withdrawing groups
FAB-MS	fast atom bombardment-mass spectrometry
GBL	γ-butyrolactone
GC	gas chromatography
GC-MS	gas chromatography mass spectrometry
GVL	γ-valerolactone
H_2O_2	hydrogen peroxide
HFIP	hexafluoroisopropanol
HIV	human immunodeficiency virus
HOSO	high oleic sunflower oil
HSQC	Heteronuclear single quantum correlation
i.e.	id est
I_{corr}	corrosion current density
IR	infrared
IS	internal standard
K_2CO_3	potassium carbonate
MeCN	acetonitrile
Me-THF	2-methyl tetrahydrofuran
M_n	number average molar mass
MS	mass spectrometry
NIPU	non-isocyanate poly(urethane)
NMP	nitroxide-mediated radical polymerization
NMR	nuclear magnetic resonance
p.a.	per annum
PEG	poly(ethylene glycol)
PMMA	Poly(methyl methacrylate)
Polarclean®	methyl-5-(dimethylamido)-2-methyl-5-oxopentanoate
ppm	parts per million
PU	poly(urethane)

PHU	poly(hydroxy urethane)
r.t.	room temperature
RAFT	reversible addition-fragmentation chain transfer polymerization
ROP	ring opening polymerization
R_f	retention factor
SAXS	Small angle X-ray spectroscopy
$_{sc}CO_2$	supercritical CO_2
SEC	size exclusion chromatography
T	temperature
T_g	glass transition temperature
T_m	melting temperature
TEA	triethylamine
THF	tetrahydrofuran
TLC	thin layer chromatography
UV	ultraviolet
WAXS	Wide angle X-ray spectroscopy
wt%	weight percent

6.2 List of publications

[1] Filippi, L., Meier, M. A. R., *Macromol. Rapid Commun.* **2021**, 42, 2000440. https://doi.org/10.1002/marc.202000440.

7   List of figures, schemes and tables

7.1 List of figures

Bilbiography

Figure 104 ¹H NMR spectrum of **11** (400 MHz, CDCl₃). 258

Figure 105 ¹H NMR spectrum of **12** (400 MHz, CDCl₃). 260

Figure 106 ¹H NMR spectrum of **P1** (400 MHz, CDCl₃). 263

Figure 107 ¹H NMR spectrum of **P2** (400 MHz, CDCl₃). 264

Figure 108 ¹H NMR spectrum of **P3** (400 MHz, CDCl₃). 265

Figure 109 ¹H NMR spectrum of **P4** (400 MHz, CDCl₃). The impurity at 3.49 ppm derives from residual methanol. 267

Figure 110 ¹H NMR spectrum of **P5** (400 MHz, CDCl₃). 268

Figure 111 ¹H NMR spectrum of **P6** (400 MHz, CDCl₃). 269

Figure 112 ¹H NMR spectrum of **P7** (400 MHz, CDCl₃). 270

Figure 113 ¹H-NMR spectrum of **P8** (400 MHz, CDCl₃).. 271

Figure 114 ¹H NMR spectrum of **P9** (400 MHz, CDCl₃). The impurity at 3.49 ppm derives from residual methanol. 272

Figure 115 ¹H NMR spectrum of **P10** (400 MHz, DMSO-d₆)... 274

Figure 116 ¹H NMR spectrum of **P11** (400 MHz, CDCl₃). 276

Figure 117 ¹H NMR spectrum of **P13** (400 MHz, CDCl₃). 277

Figure 118 ¹H-NMR spectrum of **P14** (400 MHz, CDCl₃)... 278

Figure 119 ¹H NMR spectrum of **P15** (400 MHz, CDCl₃). 279

Figure 120 ¹H NMR spectrum of **P16** (400 MHz, CDCl₃). 280

Figure 121 ¹H NMR spectrum of **P17** (400 MHz, CDCl₃). 281

Figure 122 ¹H NMR spectrum of **P18** (400 MHz, CDCl₃). 282

Figure 123 ¹H NMR spectrum of **P19** (400 MHz, CDCl₃). 283

Figure 124 ¹H NMR spectrum of **P20** (400 MHz, CDCl₃). The contamination at 1.25 ppm could not be identified or removed through multiple precipitation steps. 284

Figure 125 ¹H NMR spectrum of **P21** (400 MHz, CDCl₃). 285

Figure 126 ¹H NMR spectrum of **P22** (400 MHz, CDCl₃). The impurity at 3.49 ppm belongs to residual methanol. 286

Figure 127 ¹H NMR spectrum of **P23** (400 MHz, CDCl₃). 287

Figure 128 ¹H NMR spectrum of **P24** (400 MHz, DMSO-d₆). The impurity at 3.3 ppm derives from residual water in the deuterated solvent.. 288

Figure 129 ¹H NMR spectrum of **P25** (400 MHz, CDCl₃). 289

Figure 130 ¹H NMR spectrum of **P26** (400 MHz, CDCl₃). 290

Figure 131 ¹H NMR spectrum of **P27** (400 MHz, CDCl₃). The impurities at 1.85 and 3.73 ppm derive from residual THF.. 291

Figure 132 ¹H NMR spectrum of **P28** (400 MHz, DMSO-d₆).. 292

7.2 List of schemes

7.3 List of tables

Bilbiography

8 <u>Bibliography</u>

[1]   N. Stern, C. Taylor, *Science* **2007**, *317*, 203-204.

[2]   P. T. Anastas, J. C. Warner, *Green Chemistry: Theory and Practice*, Oxford University Press, **1998**.

[3]   A. Demirbas, in *Biofuels: Securing the Planet's Future Energy Needs* (Ed.: A. Demirbas), Springer London, London, **2009**, 45-85.

[4]   T. Kuramochi, A. Ramírez, W. Turkenburg, A. Faaij, *Progress in Energy and Combustion Science* **2012**, *38*, 87-112.

[5]   S. J. Poland, D. J. Darensbourg, *Green Chemistry* **2017**, *19*, 4990-5011.

[6]   J. O. Akindoyo, M. D. H. Beg, S. Ghazali, M. R. Islam, N. Jeyaratnam, A. R. Yuvaraj, *RSC Advances* **2016**, *6*, 114453-114482.

[7]   C. Six, F. Richter, *Isocyanates, Organic* in *Ullmann's Encyclopedia of Industrial Chemistry*.

[8]   A. Cornille, R. Auvergne, O. Figovsky, B. Boutevin, S. Caillol, *European Polymer Journal* **2017**, *87*, 535-552.

[9]   C. Wulf, M. Reckers, A. Perechodjuk, T. Werner, *ACS Sustainable Chemistry & Engineering* **2020**, *8*, 1651-1658.

[10]   A. P. Aizebeokhai, *International journal of physical sciences* **2009**, *4*, 868-879.

[11]   K. O. Yoro, M. O. Daramola, in *Advances in Carbon Capture* (Eds.: M. R. Rahimpour, M. Farsi, M. A. Makarem), Woodhead Publishing, **2020**, 3-28.

[12]   IPCC climate change fourth assessment report 2007 Chapter 2, https://archive.ipcc.ch/publications_and_data/ar2004/wg2001/en/ch2002s2002-2003.html#2002-2003-2001. (Accessed 12.08.2021).

[13]   The NOAA Annual Greenhouse Gas Index (AGGI). https://gml.noaa.gov/aggi/aggi.html (Accessed 12.08.2021).

[14]   A. R. Kristinsdóttir, P. Stoll, A. Nilsson, N. Brandt, KTH Royal Institute of Technology, **2013**.

[15]   N. W. Arnell, J. A. Lowe, A. J. Challinor, T. J. Osborn, *Climatic Change* **2019**, *155*, 377-391.

[16]   a) T. M. Wigley, S. C. Raper, *Science* **2001**, *293*, 451-454.
        b) J. M. Murphy, D. M. Sexton, D. N. Barnett, G. S. Jones, M. J. Webb, M. Collins, D. A. Stainforth, *Nature* **2004**, *430*, 768-772.

[17]   I. C. Prentice, Farquhar, G.D., Fasham, M.J.R., Goulden, M.L., Heimann, M., Jaramillo V.J., Kheshgi H.S. ,Le Quéré, C., , R. J. Scholes, Wallace, D.W.R. , *The Carbon Cycle and Atmospheric Carbon Dioxide Content* in *Working Group I: The Scientific Basis* (Ed.: A. Ramirez Rojas, L. Pitelka), IPCC, **2001**.

Bibliography

[18]   a) J. Chirac, *Deforestation and Desertification*, Foundation Chirac, **2007**.

b) K. L. Denman, G. Brasseur, A. Chidthaisong, P. Ciais, P.M. Cox, R.E. Dickinson, D. Hauglustaine, C. Heinze, E. Holland, D. Jacob, U. Lohmann, S Ramachandran, P.L. da Silva Dias, S.C. Wofsy and X. Zhang, *Couplings Between Changes in the Climate System and Biogeochemistry* in *Climate Change 2007: The Physical Science Basis*, Cambridge University Press, Cambridge, United Kingdom and New York, NY, USA, **2007**.

[19]   W. D. Nordhaus, *The economics of hurricanes in the United States*, National Bureau of Economic Research Cambridge, Mass., USA, **2006**.

[20]   R. García-Herrera, J. Díaz, R. M. Trigo, J. Luterbacher, E. M. Fischer, *Critical Reviews in Environmental Science and Technology* **2010**, *40*, 267-306.

[21]   R. Steeneveldt, B. Berger, T. A. Torp, *Chemical Engineering Research and Design* **2006**, *84*, 739-763.

[22]   a) N. MacDowell, N. Florin, A. Buchard, J. Hallett, A. Galindo, G. Jackson, C. S. Adjiman, C. K. Williams, N. Shah, P. Fennell, *Energy & Environmental Science* **2010**, *3*, 1645-1669.

b) D. M. D'Alessandro, B. Smit, J. R. Long, *Angewandte Chemie International Edition* **2010**, *49*, 6058-6082.

[23]   L. He, J. Wang, J.-L. Wang, *Pure and Applied Chemistry* **2009**, *81*, 2069-2080.

[24]   J. B. H.Herzog, J. Gale, B. Kane, S. Plasynski, *CO₂ Capture and Storage (CCS)* in *9ᵗʰ international Conference on Greenhouse Gas Control Technologies*, Washington, D.C., USA, **2008**.

[25]   M. C. Cann*, ATOM ECONOMY: A Measure of the Efficiency of a Reaction*, **2000**. https://www.scranton.edu/faculty/cannm/green-chemistry/english/organicmodule.shtml (Accessed 23.03.2020).

[26]   N. D. Anastas, J. C. Warner, *Chemical Health and Safety* **2005**, *12*, 9-13.

[27]   P. J. Dunn, *Chemical Society Reviews* **2012**, *41*, 1452-1461.

[28]   R. A. Sheldon, *Chemical Communications* **2008**, 3352-3365.

[29]   M. Poliakoff, P. Licence, *Nature* **2007**, *450*, 810-812.

[30]   R. A. Sheldon, *Chem. Ind.* **1992**, 903-906

[31]   V. G. Zuin, I. Eilks, M. Elschami, K. Kümmerer, *Green Chemistry* **2021**, *23*, 1594-1608.

[32]   E. A. Spindler, *The History of Sustainability The Origins and Effects of a Popular Concept* in *Sustainability in Tourism: A Multidisciplinary Approach* (Eds.: I. Jenkins, R. Schröder), Springer Fachmedien Wiesbaden, Wiesbaden, **2013**, 9-31.

[33]   C. Park, M. Allaby, "*renewable resource*", Oxford University Press, **2017**.

[34]   M. Balat, G. Ayar, *Energy Sources* **2005**, *27*, 931-940.

[35]   "Renewable resources", National Geographic Society **2019**, https://www.nationalgeographic.org/encyclopedia/renewable-resources/

(Accessed 09.08.2021).

[36]   R. A. Sheldon, *Green Chemistry* **2014**, *16*, 950-963.

[37]   D. Klemm, B. Heublein, H.-P. Fink, A. Bohn, *Angewandte Chemie International Edition* **2005**, *44*, 3358-3393.

[38]   M. Dusselier, M. Mascal, B. Sels, *Topics in current chemistry* **2014**, *353*, 1-40.

[39]   E. M. Rubin, *Nature* **2008**, *454*, 841-845.

[40]   a) J. Clark, F. Deswarte, in *Introduction to Chemicals from Biomass*, **2015**, 1-29.

b) P. Daoutidis, A. Kelloway, W. A. Marvin, S. Rangarajan, A. I. Torres, *Current Opinion in Chemical Engineering* **2013**, *2*, 442-447.

[41]   A. Brandt, J. Gräsvik, J. P. Hallett, T. Welton, *Green Chemistry* **2013**, *15*, 550-583.

[42]   D. Tian, R. P. Chandra, J.-S. Lee, C. Lu, J. N. Saddler, *Biotechnology for Biofuels* **2017**, *10*, 157.

[43]   G. Centi, P. Lanzafame, S. Perathoner, *Catalysis Today* **2011**, *167*, 14-30.

[44]   C.-H. Zhou, X. Xia, C.-X. Lin, D.-S. Tong, J. Beltramini, *Chemical Society Reviews* **2011**, *40*, 5588–5617.

[45]   H. Kobayashi, A. Fukuoka, *Green Chemistry* **2013**, *15*, 1740–1763.

[46]   M. S. Ganewatta, H. N. Lokupitiya, C. Tang, *Polymers* **2019**, *11*, 1176.

[47]   *Structure and Characteristics of Lignin* in *Lignin Chemistry and Applications* (Eds.: J. Huang, S. Fu, L. Gan), Elsevier, **2019**, 25-50.

[48]   X. Wang, R. Rinaldi, *Angewandte Chemie International Edition* **2013**, *52*, 11499-11503.

[49]   K.-E. L. Eriksson, R. A. Blanchette, P. Ander, *Biodegradation of Lignin* in *Microbial and Enzymatic Degradation of Wood and Wood Components* (Eds.: K.-E. L. Eriksson, R. A. Blanchette, P. Ander), Springer Berlin Heidelberg, Berlin, Heidelberg, **1990**, 225-333.

[50]   C. H. Vane, S. C. Martin, C. E. Snape, G. D. Abbott, *Journal of Agricultural and Food Chemistry* **2001**, *49*, 2709-2716.

[51]   a) R. A. Zabel, J. J. Morrell, in *Wood Microbiology (Second Edition)* (Eds.: R. A. Zabel, J. J. Morrell), Academic Press, San Diego, **2020**, 215-244.

b) T. K. Kirk, W. J. Connors, J. G. Zeikus, *Advances in Understanding the Microbiological Degradation of Lignin* in *The Structure, Biosynthesis, and Degradation of Wood* (Eds.: F. A. Loewus, V. C. Runeckles), Springer US, Boston, MA, **1977**, 369-394.

[52]   Kirk, T. & Chang, H. , *Wood research and Technology*, *29*(2), 56-64.

[53]   M. Pfeuffer, A. Jaudszus, *Advances in Nutrition* **2016**, *7*, 730-734.

[54]   "*Oilseeds: World Markets and Trade*", United States Department of Agriculture, ForeignAgricultural Service, **June 2021**. https://usda.library.cornell.edu/concern/publications/tx31qh68h?locale=en (Accessed 08.08.2021).

Bibliography

[55]   *Animal Fats and Oils* in *Fats and Oils Handbook* (Ed.: M. Bockisch), AOCS Press, **1998**, 121-173.

[56]   C. J. Forde, M. Meaney, J. B. Carrigan, C. Mills, S. Boland, A. Hernon, *Biobased Fats (Lipids) and Oils from Biomass as a Source of Bioenergy* in *Bioenergy Research: Advances and Applications* (Eds.: V. K. Gupta, M. G. Tuohy, C. P. Kubicek, J. Saddler, F. Xu), Elsevier, Amsterdam, **2014**, 185-201.

[57]   a) J. W. King, R. L. Holliday, G. R. List, *Green Chemistry* **1999**, *1*, 261-264.
         b) F. O. Nitbani, P. J. P. Tjitda, B. A. Nurohmah, H. E. Wogo, *Journal of Oleo Science* **2020**, *69*, 277-295.

[58]   J. M. Encinar, J. F. González, A. Rodríguez-Reinares, *Fuel Processing Technology* **2007**, *88*, 513-522.

[59]   P. G. Jessop, S. M. Mercer, D. J. Heldebrant, *Energy & Environmental Science* **2012**, *5*, 7240-7253.

[60]   P. G. Jessop, W. Leitner, *Supercritical Fluids as Media for Chemical Reactions* in *Chemical Synthesis Using Supercritical Fluids*, Wiley-VCH Verlag GmbH, **2007**, 1-36.

[61]   B. Subramaniam, Busch, D. H., *CO_2 Conversion and Utilization*, American Chemical Society, Washington, **2002**, 364-386.

[62]   P. G. Jessop, D. J. Heldebrant, X. Li, C. A. Eckert, C. L. Liotta, *Nature* **2005**, *436*, 1102.

[63]   a) E. R. Pérez, R. H. A. Santos, M. T. P. Gambardella, L. G. M. de Macedo, U. P. Rodrigues-Filho, J.-C. Launay, D. W. Franco, *The Journal of Organic Chemistry* **2004**, *69*, 8005-8011.
         b) D. J. Heldebrant, P. G. Jessop, C. A. Thomas, C. A. Eckert, C. L. Liotta, *The Journal of Organic Chemistry* **2005**, *70*, 5335-5338.

[64]   P. Munshi, A. D. Main, J. C. Linehan, C. C. Tai, P. G. Jessop, *Journal of the American Chemical Society* **2002**, *124*, 7963-7971.

[65]   D. J. Heldebrant, C. R. Yonker, P. G. Jessop, L. Phan, *Energy & Environmental Science* **2008**, *1*, 487-493.

[66]   B. Lv, B. Guo, Z. Zhou, G. Jing, *Environmental Science & Technology* **2015**, *49*, 10728-10735.

[67]   a) E. Privalova, M. Nurmi, M. S. Marañón, E. V. Murzina, P. Mäki-Arvela, K. Eränen, D. Y. Murzin, J. P. Mikkola, *Separation and Purification Technology* **2012**, *97*, 42-50.
         b) E. Privalova, M. Nurmi, M. S. Marañón, E. V. Murzina, P. Mäki-Arvela, K. Eränen, D. Yu Murzin, J. P. Mikkola, *Separation and Purification Technology* **2013**, *107*, 340.

[68]   D. J. Heldebrant, P. K. Koech, M. T. C. Ang, C. Liang, J. E. Rainbolt, C. R. Yonker, P. G. Jessop, *Green Chemistry* **2010**, *12*, 713-721.

[69]   T. Yamada, P. J. Lukac, M. George, R. G. Weiss, *Chemistry of Materials* **2007**, *19*, 967-969.

[70]   W. H. Brown, T. Poon, *Einführung in die Organische Chemie*, Wiley, **2020**.

[71] L. Phan, J. R. Andreatta, L. K. Horvey, C. F. Edie, A.-L. Luco, A. Mirchandani, D. J. Darensbourg, P. G. Jessop, *The Journal of Organic Chemistry* **2008**, *73*, 127-132.

[72] E. Vessally, K. Didehban, M. Babazadeh, A. Hosseinian, L. Edjlali, *Journal of CO$_2$ Utilization* **2017**, *21*, 480-490.

[73] L. Phan, D. Chiu, D. J. Heldebrant, H. Huttenhower, E. John, X. Li, P. Pollet, R. Wang, C. A. Eckert, C. L. Liotta, P. G. Jessop, *Industrial & Engineering Chemistry Research* **2008**, *47*, 539-545.

[74] a) R. Hart, P. Pollet, D. J. Hahne, E. John, V. Llopis-Mestre, V. Blasucci, H. Huttenhower, W. Leitner, C. A. Eckert, C. L. Liotta, *Tetrahedron* **2010**, *66*, 1082-1090.

b) V. M. Blasucci, R. Hart, P. Pollet, C. L. Liotta, C. A. Eckert, *Fluid Phase Equilibria* **2010**, *294*, 1-6.

[75] C. Samori, C. Torri, G. Samori, D. Fabbri, P. Galletti, F. Guerrini, R. Pistocchi, E. Tagliavini, *Bioresource technology* **2010**, *101*, 3274-3279.

[76] L. Phan, H. Brown, J. White, A. Hodgson, P. G. Jessop, *Green Chemistry* **2009**, *11*, 53-59.

[77] Z. Yuan, B. Chen, G. Sin, R. Gani, *AIChE Journal* **2012**, *58*, 1640-1659.

[78] R. J. Hickey, A. E. Pelling, *Frontiers in Bioengineering and Biotechnology* **2019**, *7, 45*.

[79] S. Virtanen, R. Talja, S. Vuoti, *Carbohydrate Polymers* **2017**, *177*, 105-115.

[80] a) R. P. Swatloski, S. K. Spear, J. D. Holbrey, R. D. Rogers, *Ionic liquids: New solvents for nonderivitized cellulose dissolution,* American Chemical Society, **2002**, IEC-076.

b) R. P. Swatloski, R. D. Rogers, J. D. Holbrey, The University of Alabama, USA; Pg Research Foundation, Inc. . **2003**, WO2003029329A2.

c) L. Feng, Z.-l. Chen, *Journal of Molecular Liquids* **2008**, *142*, 1-5.

[81] H. Xie, X. Yu, Y. Yang, Z. K. Zhao, *Green Chemistry* **2014**, *16*, 2422-2427.

[82] Q. Zhang, N. S. Oztekin, J. Barrault, K. De Oliveira Vigier, F. Jerome, *ChemSusChem* **2013**, *6*, 593-596.

[83] Y. Yang, L. Song, C. Peng, E. Liu, H. Xie, *Green Chemistry* **2015**, *17*, 2758-2763.

[84] D. L. Sackett, J. Wolff, *Analytical Biochemistry* **1987**, *167*, 228-234.

[85] P. G. Jessop, L. Phan, A. Carrier, S. Robinson, C. J. Dürr, J. R. Harjani, *Green Chemistry* **2010**, *12*, 809-814.

[86] A. R. Boyd, P. Champagne, P. J. McGinn, K. M. MacDougall, J. E. Melanson, P. G. Jessop, *Bioresource technology* **2012**, *118*, 628-632.

[87] P. G. Jessop, L. Kozycz, Z. G. Rahami, D. Schoenmakers, A. R. Boyd, D. Wechsler, A. M. Holland, *Green Chemistry* **2011**, *13*, 619-623.

[88] Y. Kohno, H. Arai, H. Ohno, *Chemical Communications* **2011**, *47*, 4772-4774.

[89] J. S. Chickos, W. E. A. Jr., *Journal of Physical and Chemical Reference Data* **2003**, *32*, 519-878.

Bibliography

[90]   A. M. Hyde, S. L. Zultanski, J. H. Waldman, Y.-L. Zhong, M. Shevlin, F. Peng, *Organic Process Research & Development* **2017**, *21*, 1355-1370.

[91]   S. M. Mercer, P. G. Jessop, *ChemSusChem* **2010**, *3*, 467-470.

[92]   "Catalysis", https://courses.lumenlearning.com/boundless-chemistry/chapter/catalysis/ (Accessed 04.08.2021).

[93]   A. B. Andreetta, G; Gregorio, G, *Chimica Industriale* **1978**, *60*, 887-891.

[94]   S. L. Desset, D. J. Cole-Hamilton, *Angewandte Chemie International Edition* **2009**, *48*, 1472-1474.

[95]   F. I. B. König, *Zeitschrift für Naturforschung , Teil B* **2009**, 1053-1056.

[96]   a) E. Aramendia, M. J. Barandiaran, J. Grade, T. Blease, J. M. Asua, *Langmuir* **2005**, *21*, 1428-1435.

 b) N. Shirakbari, M. Ebrahimi, H. Salehi-Mobarakeh, M. Khorasani, *Journal of Macromolecular Science, Part B* **2014**, *53*, 1286-1292.

[97]   Q. Zhang, G. Yu, W.-J. Wang, H. Yuan, B.-G. Li, S. Zhu, *Langmuir* **2012**, *28*, 5940-5946.

[98]   P. Brown, C. P. Butts, J. Eastoe, *Soft Matter* **2013**, *9*, 2365-2374.

[99]   a) C. B. Minkenberg, L. Florusse, R. Eelkema, G. J. M. Koper, J. H. van Esch, *Journal of the American Chemical Society* **2009**, *131*, 11274-11275.

 b) F. Tu, D. Lee, *Journal of the American Chemical Society* **2014**, *136*, 9999-10006.

[100] M.-a. Morikawa, K. Murata, K. Yamada, N. Kimizuka, *Chemistry Letters* **2013**, *42*, 501-503.

[101] a) K. Sakai, R. Yamazaki, Y. Imaizumi, T. Endo, H. Sakai, M. Abe, *Colloids and Surfaces A: Physicochemical and Engineering Aspects* **2012**, *410*, 119-124.

 b) P. Mirarefi, C. T. Lee, *Biochimica et Biophysica Acta (BBA) - Proteins and Proteomics* **2010**, *1804*, 106-114.

[102] C. I. Fowler, P. G. Jessop, M. F. Cunningham, *Macromolecules* **2012**, *45*, 2955-2962.

[103] a) X. Su, C. Fowler, C. O'Neill, J. Pinaud, E. Kowal, P. Jessop, M. Cunningham, *Macromolecular Symposia* **2013**, *333*, 93-101.

 b) M. Mihara, P. Jessop, M. Cunningham, *Macromolecules* **2011**, *44*, 3688-3693.

[104] a) M. Chai, Z. Zheng, L. Bao, W. Qiao, *Journal of Surfactants and Detergents* **2014**, *17*, 383-390; b) W. Qiao, Z. Zheng, Q. Shi, *Journal of Surfactants and Detergents* **2012**, *15*, 533-539.

[105] Y. Ding, S. Chen, H. Xu, Z. Wang, X. Zhang, T. H. Ngo, M. Smet, *Langmuir* **2010**, *26*, 16667-16671.

[106] L. M. Scott, T. Robert, J. R. Harjani, P. G. Jessop, *RSC Advances* **2012**, *2*, 4925-4931.

[107] A. Darabi, P. G. Jessop, M. F. Cunningham, *Chemical Society Reviews* **2016**, *45*, 4391-4436.

[108] a) S. Dai, P. Ravi, K. C. Tam, *Soft Matter* **2008**, *4*, 435-449.

 b) R. B. Karabacak, *Journal of Applied Polymer Science* **2016**, *133*.

[109]   A. Darabi, A. R. Shirin-Abadi, J. Pinaud, P. G. Jessop, M. F. Cunningham, *Polymer Chemistry* **2014**, *5*, 6163-6170.

[110]   a) N. Che, S. Yang, H. Kang, R. Liu, Z. Li, Z. Liu, P. Li, X. Qu, Y. Huang, *Polymer Chemistry* **2014**, *5*, 7109-7120.

b) Q. Zhang, W.-J. Wang, Y. Lu, B.-G. Li, S. Zhu, *Macromolecules* **2011**, *44*, 6539-6545.

[111]   a) Q. Zhang, S. Zhu, *ACS Macro Letters* **2014**, *3*, 743-746.

b) B.-w. Liu, H. Zhou, S.-t. Zhou, H.-j. Zhang, A.-C. Feng, C.-m. Jian, J. Hu, W.-p. Gao, J.-y. Yuan, *Macromolecules* **2014**, *47*, 2938-2946.

c) H. Chen, Y. Wang, X. Li, B. Liang, S. Dong, T. You, P. Yin, *RSC Advances* **2018**, *8*, 22177-22181.

d) J. Arredondo, P. G. Jessop, P. Champagne, J. Bouchard, M. F. Cunningham, *Green Chemistry* **2017**, *19*, 4141-4152.

[112]   a) M. Zeng, M. Huo, Y. Feng, J. Yuan, *Macromolecular Rapid Communications* **2018**, *39*, 1800291.

b) X. Jiang, F. Chun, G. Lu, H. Xiaoyu, *Polymer Chemistry* **2017**, *8*, 1163-1176.

c) A. Feng, C. Zhan, Q. Yan, B. Liu, J. Yuan, *Chemical Communications* **2014**, *50*, 8958-8961.

d) H. Liu, Z. Guo, S. He, H. Yin, C. Fei, Y. Feng, *Polymer Chemistry* **2014**, *5*, 4756-4763.

[113]   a) J. Glasing, J. Bouchard, P. G. Jessop, P. Champagne, M. F. Cunningham, *Polymer Chemistry* **2017**, *8*, 6000-6012.

b) O. Garcia-Valdez, T. Brescacin, J. Arredondo, J. Bouchard, P. G. Jessop, P. Champagne, M. F. Cunningham, *Polymer Chemistry* **2017**, *8*, 4124-4131.

c) A. Darabi, A. R. Shirin-Abadi, P. G. Jessop, M. F. Cunningham, *Macromolecules* **2015**, *48*, 72-80.

[114]   a) Z. Guo, Y. Feng, Y. Wang, J. Wang, Y. Wu, Y. Zhang, *Chemical Communications* **2011**, *47*, 9348-9350.

b) Z. Guo, Y. Feng, S. He, M. Qu, H. Chen, H. Liu, Y. Wu, Y. Wang, *Advanced Materials* **2013**, *25*, 584-590.

c) P. Schattling, F. D. Jochum, P. Theato, *Polymer Chemistry* **2014**, *5*, 25-36.

d) J. Y. Quek, P. J. Roth, R. A. Evans, T. P. Davis, A. B. Lowe, *Journal of Polymer Science Part A: Polymer Chemistry* **2013**, *51*, 394-404.

[115]   S. Kumar, X. Tong, Y. L. Dory, M. Lepage, Y. Zhao, *Chemical Communications* **2013**, *49*, 90-92.

[116]   J. Zhang, D. Han, H. Zhang, M. Chaker, Y. Zhao, D. Ma, *Chemical Communications* **2012**, *48*, 11510-11512.

[117]   H. Che, M. Huo, L. Peng, Q. Ye, J. Guo, K. Wang, Y. Wei, J. Yuan, *Polymer Chemistry* **2015**, *6*, 2319-2326.

[118]   National Library of Medicine, *The Medical Letter on Drugs and Therapeutics* **2000**, *42*, 83-92.

Bibliography

[119]   J. A. Witjes, *Drugs* **1997**, *53*, 404-414.

[120]   S. Rossi, A. Vitry, G. Gabb, E. Hurley, *Australian Medicines Handbook. Adelaide*, **2000**.

[121]   D. W. Northfelt, *Drugs* **1994**, *48*, 569-582.

[122]   S. Pocoví-Martínez, L. Francés-Soriano, E. Zaballos-García, J. C. Scaiano, M. González-Béjar, J. Pérez-Prieto, *RSC Advances* **2013**, *3*, 4867-4871.

[123]   H. Kim, T. S. Lee, *Molecular Crystals and Liquid Crystals* **2019**, *685*, 78-86.

[124]   J. Tang, X. Zhou, S. Cao, L. Zhu, L. Xi, J. Wang, *ACS Applied Materials & Interfaces* **2019**, *11*, 16156-16163.

[125]   S. Guo, Y. Zhang, *Colloids and Surfaces A: Physicochemical and Engineering Aspects* **2019**, *562*, 119-126.

[126]   Z. Li, R. V. Linares, S. Sarp, G. Amy, *Direct and Indirect Seawater Desalination by Forward Osmosis* in *Membrane-Based Salinity Gradient Processes for Water Treatment and Power Generation* (Eds.: S. Sarp, N. Hilal), Elsevier, **2018**, 245-272.

[127]   P.G. Jessop, S.M. Mercer, T. Robert, R.S. Brown, T.J. Clark, B.E. Mariapillai, R. Resendes, D. Wechsler, *Systems and methods for use of water with switchable ionic strength*, **2012,** US2014/0076810A1.

[128]   Y. Cai, W. Shen, R. Wang, W. B. Krantz, A. G. Fane, X. Hu, *Chemical Communications* **2013**, *49*, 8377-8379.

[129]   H. Jiang, E. Wang, J. Wang, *RSC Advances* **2015**, *5*, 35622-35630.

[130]   R. D. Athey, Jr., *European Coating Journal* **1998**, 146-149.

[131]   X. Su, P. G. Jessop, M. F. Cunningham, *Macromolecules* **2012**, *45*, 666-670.

[132]   Y. Wang, L. Zhao, A. Otto, M. Robinius, D. Stolten, *Energy Procedia* **2017**, *114*, 650-665.

[133]   L. Q. Xu, B. Zhang, M. Sun, L. Hong, K.-G. Neoh, E.-T. Kang, G. D. Fu, *Journal of Materials Chemistry A* **2013**, *1*, 1207-1212.

[134]   a) Y. Furusho, T. Endo, *Journal of Polymer Science Part A: Polymer Chemistry* **2013**, *51*, 3404-3411.

    b) Y. Ma, L.-Y. L. Yung, *Analytical Chemistry* **2014**, *86*, 2429-2435.

[135]   J. Zhang, I. Kutnyakov, P. K. Koech, A. Zwoster, C. Howard, F. Zheng, C. J. Freeman, D. J. Heldebrant, *Energy Procedia* **2013**, *37*, 285-291.

[136]   J. E. Rainbolt, P. K. Koech, C. R. Yonker, F. Zheng, D. Main, M. L. Weaver, J. C. Linehan, D. J. Heldebrant, *Energy & Environmental Science* **2011**, *4*, 480-484.

[137]   H. Lossen, *Justus Liebigs Annalen der Chemie* **1869**, *150*, 314-322.

[138]   J. M. Altenburger, C. Mioskowski, H. d'Orchymont, D. Schirlin, C. Schalk, C. Tarnus, *Tetrahedron Letters* **1992**, *33*, 5055-5058.

[139]   A. S. Reddy, M. S. Kumar, G. R. Reddy, *Tetrahedron Letters* **2000**, *41*, 6285-6288.

366

[140] E. Adiguzel, F. Yilmaz, M. Emirik, M. Ozil, *Journal of Molecular Structure* **2017**, *1127*, 403-412.

[141] Sanallah, M. **(2016)**. *Lossen Rearrangement reaction of Aromatic and Aliphatic Hydroxamates* (Master Thesis, Carleton University, Ottawa, Ontario, Canada). Retrieved from https://curve.carleton.ca/system/files/etd/85614a10-f9f3-49d3-a13b-3b377e826967/etd_pdf/715dbcd1474541a3a0e269d41dc5cb65/sanaallah-lossenrearrangementreactionofaromaticandaliphatic.pdf (Accessed 12.08.2021).

[142] E. Farkas, P. Buglyó, *Metal Ions in Life Sciences*, **2017**, *17*, 201-240.

[143] D. Al Shaer, O. Al Musaimi, B. G. de la Torre, F. Albericio, *European Journal of Medicinal Chemistry* **2020**, *208*, 112791.

[144] R. C. Hider, X. Kong, *Natural Product Reports* **2010**, *27*, 637-657.

[145] M. J. Miller, *Chemical Reviews* **1989**, *89*, 1563-1579.

[146] H. J. Rogers, I*ron Transport in Microbes, Plants and Animals*, Winkelmann, G., van der Helm, D., Neilands, J. B., Eds.; VCH: Weinheim, New York, **1987**; Chapter 13.

[147] M. J. Miller, *Accounts of Chemical Research* **1986**, *19*, 49-56.

[148] M. Miethke, M. A. Marahiel, *Microbiology and Molecular Biology Reviews : MMBR* **2007**, *71*, 413-451.

[149] W. Lossen, *Justus Liebigs Annalen der Chemie* **1872**, *161*, 347-362.

[150] D. Dell, D. R. Boreham, B. K. Martin, *Journal of Pharmaceutical Sciences* **1971**, *60*, 1368-1370.

[151] P. Dubé, N. F. F. Nathel, M. Vetelino, M. Couturier, C. L. Aboussafy, S. Pichette, M. L. Jorgensen, M. Hardink, *Organic Letters* **2009**, *11*, 5622-5625.

[152] O. Kreye, S. Wald, M. A. R. Meier, *Advanced Synthesis & Catalysis* **2013**, *355*, 81-86.

[153] D. K. Yadav, A. K. Yadav, V. P. Srivastava, G. Watal, L. D. S. Yadav, *Tetrahedron Letters* **2012**, *53*, 2890-2893.

[154] M. A. Stolberg, R. C. Tweit, G. M. Steinberg, T. Wagner-Jauregg, *Journal of the American Chemical Society* **1955**, *77*, 765-767.

[155] H. L. Yale, *Chemical Reviews* **1943**, *33*, 209-256.

[156] N. Ohtsuka, M. Okuno, Y. Hoshino, K. Honda, *Organic & Biomolecular Chemistry* **2016**, *14*, 9046-9054.

[157] J. Bruffaerts, N. von Wolff, Y. Diskin-Posner, Y. Ben-David, D. Milstein, *Journal of the American Chemical Society* **2019**, *141*, 16486-16493.

[158] H. Ulrich, *Chemistry and Technology of Isocyanates*, Wiley, Chichester, **1996**.

[159] F. Paul, *Coordination Chemistry Reviews* **2000**, *203*, 269-323.

[160] H. V. Le, B. Ganem, *Organic Letters* **2011**, *13*, 2584-2585.

[161] J. A. Jones, J. R. Starkey, A. Kleinhofs, *Mutation Research/Genetic Toxicology* **1980**, *77*, 293-299.

Bibliography

[162]   Chemical & Engineering News (14 Mar 1994) Vol. 1972, No. 1911, 1994.

[163]   R. M. J. Withers, F. P. Lees, *Journal of Hazardous Materials* **1986**, *13*, 279-299.

[164]   E. A. Castro, R. B. Moodie, P. J. Sansom, *Journal of the Chemical Society, Perkin Transactions 2* **1985**, 737-742.

[165]   Y. Hoshino, M. Okuno, E. Kawamura, K. Honda, S. Inoue, *Chemical communications* **2009**, 2281-2283.

[166]   T. R. Fukuto, *Environmental Health Perspectives* **1990**, *87*, 245-254.

[167]   National Pesticide Information Center **2015**, *Insect Growth Regulators*. Retreived from http://npic.orst.edu/ingred/ptype/igr.html. (Accessed 08.08.2021)

[168]   R. C. Gupta, *Handbook of Toxicology of Chemical Warfare Agents*, Elsevier Science, **2015**.

[169]   M. Popovska-Gorevski, M. L. Dubocovich, R. V. Rajnarayanan, *Chemical research in toxicology* **2017**, *30*, 574-582.

[170]   a) Z. Zhang, P. R. Schreiner, *Chemical Society Reviews* **2009**, *38*, 1187-1198.
        b) A. G. Doyle, E. N. Jacobsen, *Chemical Reviews* **2007**, *107*, 5713-5743.
        c) P. R. Schreiner, A. Wittkopp, *Organic Letters* **2002**, *4*, 217-220.

[171]   P. K. Gupta, *Herbicides and fungicides* in *Biomarkers in Toxicology* (Ed.: R. C. Gupta), Academic Press, Boston, **2014**, 409-431.

[172]   E. Möller, J. F. McIntosh, D. D. Van Slyke, *The Journal of clinical investigation* **1928**, *6*, 427-465.

[173]   P. C. Withers, *Clinical and Experimental Pharmacology and Physiology* **1998**, *25*, 722-727.

[174]   a) L. Huan-Qiu, L. Peng-Cheng, Y. Tao, Z. Hai-Liang, *Anti-Cancer Agents in Medicinal Chemistry* **2009**, *9*, 471-480.
        b) J. Wu, Y. Huang, Q. Xie, J. Zhang, Z. Zhan, *Anti-Cancer Drugs* **2020**, *31*, 500-506.

[175]   J.-H. Shi, K.-L. Zhou, Y.-Y. Lou, D.-Q. Pan, *Spectrochimica Acta Part A: Molecular and Biomolecular Spectroscopy* **2018**, *188*, 362-371.

[176]   Kummerlöwe C., Endres HJ., Susoff M., *Synthese von Makromolekülen, Polyreaktionen*. In: *Makromolekulare Chemie.* (**2020**) (eds) Lechner, Gehrke, Nordmeier, Springer Spektrum, Berlin, Heidelberg.

[177]   L. W. Jones, L. Neuffer, *Journal of the American Chemical Society* **1917**, *39*, 659-668.

[178]   L. W. Jones, D. H. Powers, *Journal of the American Chemical Society* **1924**, *46*, 2518-2533.

[179]   C. Gastaldi, Longiave, M., Sircana, F., *Gazzetta chimica italiana* **1926**, *56*, 550.

[180]   H. F. Whalen, L. W. Jones, *Journal of the American Chemical Society* **1925**, *47*, 1353-1357.

[181]   C. D. Hurd, L. U. Spence, *Journal of the American Chemical Society* **1927**, *49*, 266-274.

[182]   F. Tiemann, *Berichte der Deutschen Chemie Gesellschaft B* **1939 (1889)**, *22*.

[183]   L. Cambi, *Atti accademici Lincei [5]* **1909**, *18*, 687.

[184]   O. Bayer, *Angewandte Chemie* **1947**, *59*, 257-272.
368

[185]   R. B. Seymour, G. B. Kauffman, *Journal of Chemical Education* **1992**, *69*, 909.

[186]   Z. S. Petrović, J. Ferguson, *Progress in Polymer Science* **1991**, *16*, 695-836.

[187]   *Bio-based Polyurethane Market Size, Share & Trends Analysis Report by Product, by End use, by Region (North America, Europe, Asia Pacific, RoW) and Segment Forecasts. 2015-2020*, **2015**, retrieved from https://www.grandviewresearch.com/industry-analysis/bio-based-polyurethane-industry, (Accessed 08.08.2021).

[188]   B. Claeys, A. Vervaeck, X. K. D. Hillewaere, S. Possemiers, L. Hansen, T. De Beer, J. P. Remon, C. Vervaet, *European Journal of Pharmaceutics and Biopharmaceutics* **2015**, *90*, 44-52.

[189]   G. Brereton, R. M. Emanuel Jr, R. Lomax, K. Pennington, T. Ryan, H. Tebbe, M. Timm, P. Ware, K. Winkler, T. Yuan, Z. Zhu, N. Adam, G. Avar, H. Blankenheim, W. Friederichs, M. Giersig, E. Weigand, M. Halfmann, F.-W. Wittbecker, D.-R. Larimer, U. Maier, S. Meyer-Ahrens, K.-L. Noble, H.-G. Wussow, *Polyurethanes* in *Ullmann's Encyclopedia of Industrial Chemistry*, 1-76.

[190]   N. V. Gama, A. Ferreira, A. Barros-Timmons, *Materials* **2018**, *11*, 1841.

[191]   K. Polaczek, M. Kurańska, M. Auguścik-Królikowska, A. Prociak, J. Ryszkowska, *Journal of Cleaner Production* **2021**, *290*, 125875.

[192]   W.-Y. Jang, A. M. Kraynik, S. Kyriakides, *International Journal of Solids and Structures* **2008**, *45*, 1845-1875.

[193]   K. Yasunaga, R. Neff, X. Zhang, C. Macosko, *Journal of Cellular Plastics* **1996**, *32*, 427-448.

[194]   N. J. Mills, *Air flow in open-cell foams* in *Polymer Foams Handbook* **2007**, 177-203.

[195]   A. H. Baferani, R. Keshavarz, M. Asadi, A. R. Ohadi, *Advances in Polymer Technology* **2018**, *37*, 71-83.

[196]   A. Kairyte, A. Kremensas, G. Balčiūnas, S. Członka, A. Strąkowska, *Materials* **2020**, *13*, 1438.

[197]   A. Demharter, *Cryogenics* **1998**, *38*, 113-117.

[198]   S. M. Kang, S. H. Kwon, J. H. Park, B. K. Kim, *Polymer Bulletin* **2013**, *70*, 885-893.

[199]   C. Zhang, M. R. Kessler, *ACS Sustainable Chemistry & Engineering* **2015**, *3*, 743-749.

[200]   L. Thiele, *Acta Polymerica* **1979**, *30*, 323-342.

[201]   S. T. McKenna, T. R. Hull, *Fire Science Reviews* **2016**, *5*, 3.

[202]   B. P. Thapliyal, R. Chandra, *Progress in Polymer Science* **1990**, *15*, 735-750.

[203]   E. Sharmin, F. Zafar, *Polyurethane: An Introduction* in *InTech* **2012**.

[204]   D. Webster, *Progress in Organic Coatings* **2002**, *44*, 319-319.

[205]   R. L. Gray, R. E. Lee, *Scorch inhibitors for flexible polyurethanes* in *Plastics Additives: An A-Z reference* (Ed.: G. Pritchard), Springer Netherlands, Dordrecht, **1998**, 567-575.

[206]   K. Ashida, *Polyurethane and related foams : chemistry and technology* **2007**, Boca Raton, FL, CRC/Taylor & Francis.

[207]   A.W. Hofmann, *Jahresberichte* **1858**: 349.

Bibliography

[208]   L. Nicholas, G. T. Gmitter, *Journal of Cellular Plastics* **1965**, *1*, 85-90.

[209]   I. Rotaru, M. Ionescu, D. Donescu, M. Vuluga, *Materiale Plastice* **2008**, *45*, 23.

[210]   K. Frisch, K. Patel, R. Marsh, *Journal of Cellular Plastics* **1970**, *6*, 203-214.

[211]   G. W. Ball, G. A. Haggis, R. Hurd, J. F. Wood, *Journal of Cellular Plastics* **1968**, *4*, 248-261.

[212]   R. Samborska-Skowron, A. Balas, *Polymers for Advanced Technologies* **2002**, *13*, 653-662.

[213]   a) M. Malik, R. Kaur, *Polymer Engineering & Science* **2017**, *58*.

         b) M. Corcuera, L. Rueda, A. Saralegi, L. Martin, B. Bidegain, I. Mondragon, A. Eceiza, *Journal of Applied Polymer Science* **2011**, *122*, 3677-3685.

[214]   A. Das, P. Mahanwar, *Advanced Industrial and Engineering Polymer Research* **2020**, *3*, 93-101.

[215]   M. Ionescu, *Chemistry and Technology of Polyols for Polyurethanes*, Rapra Limited, **2005**.

[216]   a) M. M. Velencoso, M. J. Ramos, J. C. Garcia-Martinez, A. De Lucas, J. F. Rodriguez, *Journal of Macromolecular Science, Part A* **2013**, *50*, 905-913.

         b) L. C. Bailosky, L. M. Bender, D. Bode, R. A. Choudhery, G. P. Craun, K. J. Gardner, C. R. Michalski, J. T. Rademacher, G. J. Stella, D. J. Telford, *Progress in Organic Coatings* **2013**, *76*, 1712-1719.

[217]   D. Allan, J. H. Daly, J. J. Liggat, *Polymer Degradation and Stability* **2019**, *161*, 57-73.

[218]   L. Nguyen Dang, S. Le Hoang, M. Malin, J. Weisser, T. Walter, M. Schnabelrauch, J. Seppälä, *European Polymer Journal* **2016**, *81*, 129-137.

[219]   a) D. Pangersic, U. Primozic, *Kovine, Zlitine, Tehnol.* **1997**, *31*, 441-443.

         b) M. Kunaver, A. Krzan, V. Tisler, Biotehniska Fakulteta, Oddelek za Lesarstvo, Slovenia; Kemijski Institut . **2006**, 6.

[220]   J. K. Stille, *Journal of Chemical Education* **1981**, *58*, 862.

[221]   C. Xie, *Method for preparing polycaprolactone polyol,* Qingdao University of Science and Technology, Peop. Rep. China . **2020**, 6, *CN111995736A*.

[222]   K. Gorna, S. Polowinski, S. Gogolewski, *Journal of Polymer Science Part A: Polymer Chemistry* **2002**, *40*, 156-170.

[223]   a) M. DeBolt, A. Kiziltas, D. Mielewski, S. Waddington, M. J. Nagridge, *Journal of Applied Polymer Science* **2016**, *133*.

         b) N. Patil, S. Bhoopathi, V. Chidara, N. Hadjichristidis, Y. Gnanou, X. Feng, *ChemSusChem* **2020**, *13*, 5080-5087.

[224]   P. Alagi, R. Ghorpade, Y. J. Choi, U. Patil, I. Kim, J. H. Baik, S. C. Hong, *ACS Sustainable Chemistry & Engineering* **2017**, *5*, 3871-3881.

[225]   W.F. Su, *Step Polymerization* in *Principles of Polymer Design and Synthesis* (Ed.: W.-F. Su), Springer Berlin Heidelberg, Berlin, Heidelberg, **2013**, 111-136.

[226] a) Z. Miao, *Polyurethane foamed plastic for processing of raw material storage box,* Anhui Meishijia New Material Co., Ltd., Peop. Rep. China . **2020**, p. 8pp, *CN210590192U*.

b) T. Hasegawa, O. Wakisaka, *Nonflammable polyurethane foam thermal insulator construction materials with excellent heat resistance and no formaldehyde release,* Tokai Rubber Industries, Ltd., Japan . **2006**, p. 10pp, *JP2006326943A*.

c) V. F. Smokin, O. L. Figovskii, *Polyester and Polyurethane Resins in Construction*, Budivel'nik, **1974**.

d) M. Winter, *Construction material for wall structures*, Farbenkrauth und Co., Chemische Werke und Tackfabrik . **1970**, p. 4 pp, *DE1912444A*.

[227] a) D. Cai, J. Gu, *Preparation method of low-VOC (volatile organic compound) polyurethane adhesive for flexible package*, Nanjing Xuansi New Material Co., Ltd., Peop. Rep. China . **2020**, p. 12pp; *CN111171775A*.

b) J. R. Gouveia, R. R. de Sousa Junior, A. O. Ribeiro, S. A. Saraiva, D. J. dos Santos, *European Polymer Journal* **2020**, *131*, Ahead of Print.

c) E. K. Leitsch, W. H. Heath, J. M. Torkelson, *International Journal of Adhesion and Adhesives* **2016**, *64*, 1-8.

d) M. M. Aung, Z. Yaakob, S. Kamarudin, L. C. Abdullah, *Industrial Crops and Products* **2014**, *60*, 177-185.

[228] a) B. Bruchmann, D. Schoenfelder, J. Ferbitz, A. Eisenhardt, *Highly elastic flexible polyurethane foams based on highly branched polyethers for use in mattresses, furniture and vehicle sits,* BASF SE, Germany . **2010**, p. 30pp, *WO2010079155A1*.

b) S. Triouleyre, S. Meyer-Ahrens, A. Mosbach-Rosenberger, *Polyether polyol composition for viscoelastic polyurethane foam useful in furniture, pillows, shoe soles and safety clothing,* Bayer Materialscience A.-G., Germany . **2009**, p. 30pp, *WO2009080202A1.*

c) P. Wang, *Environmentally friendly coating for furniture,* Sichuan Aiyijia Furniture Co., Ltd., Peop. Rep. China . **2018**, p. 4pp, *CN109021827A*.

d) S. D. Rajput, D. G. Hundiwale, P. P. Mahulikar, V. V. Gite, *Progress in Organic Coatings* **2014**, *77*, 1360-1368.

[229] a) Z. Liu, Y. Gao, K. Zhao, H. Wang, P. Li, *Preparing method and application of polyurethane hard foam plastic composite*, Qingdao Haier Joint Stock Co., Ltd., Peop. Rep. China . **2018**, p. 12pp, *CN108659194A*.

b) H. Zhuang, Peop. Rep. China . **2016**, p. 9pp; cJ. Qiang, Peop. Rep. China . **2010**, 7.

[230] C. Reeb-Whitaker, S. G. Whittaker, D. M. Ceballos, E. C. Weiland, S. L. Flack, K. W. Fent, J. M. Thomasen, L. G. Trelles Gaines, L. A. Nylander-French, *Journal of Occupational and Environmental Hygiene* **2012**, *9*, 329-339.

Bibliography

[231] D. Bello, C. A. Herrick, T. J. Smith, S. R. Woskie, R. P. Streicher, M. R. Cullen, Y. Liu, C. A. Redlich, *Environmental Health Perspectives* **2007**, *115*, 328-335.

[232] T. C. Nicholson-Roberts, *J R Army Med Corps* **2019**, *165*, 183-187.

[233] a) A. Vaish, S. Consul, A. Agrawal, S. Chaudhary, M. Gutch, N. Jain, M. Singh, *Journal of Emergencies, Trauma, and Shock* **2013**, *6*, 271-275.
b) J. Borak, W. Diller, *Journal of occupational and environmental medicine / American College of Occupational and Environmental Medicine* **2001**, *43*, 110-119.

[234] a) O. Kreye, H. Mutlu, M. A. R. Meier, *Green Chemistry* **2013**, *15*, 1431-1455.
b) A. Llevot, M. Meier, *Polymer International* **2019**, *68*, 826-831.
c) A. Cornille, R. Auvergne, O. Figovsky, B. Boutevin, S. Caillol, *Eur. Polym. J.* **2017**, *87*, 535-552.
d) S. Matsumura, Y. Soeda, K. Toshima, *Appl. Microbiol. Biotechnol.* **2006**, *70*, 12-20.

[235] P. W. Morgan, *Journal of Polymer Science Part C: Polymer Symposia* **1963**, *4*, 1075-1096.

[236] M. Pozo, V. Gotor, *Tetrahedron: Asymmetry* **1995**, *6*, 2797-2802.

[237] G. Rokicki, A. Piotrowska, *Polymer* **2002**, *43*, 2927-2935.

[238] M. Unverferth, O. Kreye, A. Prohammer, M. A. R. Meier, *Macromolecular Rapid Communications* **2013**, *34*, 1569-1574.

[239] M. Firdaus, M. A. R. Meier, *Green Chemistry* **2013**, *15*, 370-380.

[240] M. Firdaus, L. Montero de Espinosa, M. A. R. Meier, *Macromolecules* **2011**, *44*, 7253-7262.

[241] a) J. Kušan, H. Keul, H. Höcker, *Macromolecules* **2001**, *34*, 389-395.
b) S. Neffgen, H. Keul, H. Höcker, *Macromolecular Chemistry and Physics* **1998**, *199*, 197-206.

[242] a) O. Ihata, Y. Kayaki, T. Ikariya, *Angewandte Chemie International Edition* **2004**, *43*, 717-719.
b) K. Soga, W.-Y. Chiang, S. Ikeda, *Journal of Polymer Science: Polymer Chemistry Edition* **1974**, *12*, 121-131.

[243] S. Neffgen, H. Keul, H. Höcker, *Macromolecules* **1997**, *30*, 1289-1297.

[244] H. K. Hall, A. K. Schneider, *Journal of the American Chemical Society* **1958**, *80*, 6409-6412.

[245] U. Steuerle, R. Feuerhake, in *Ullmann's Encyclopedia of Industrial Chemistry*.

[246] A. Heggelund, K. Undheim, *Synthetic Communications* **2009**, *39*, 1903-1913.

[247] a) A. S. More, B. Gadenne, C. Alfos, H. Cramail, *Polymer Chemistry* **2012**, *3*, 1594-1605.
b) C. N. D. Neumann, W. D. Bulach, M. Rehahn, R. Klein, *Macromolecular Rapid Communications* **2011**, *32*, 1373-1378.
c) D. V. Palaskar, A. Boyer, E. Cloutet, C. Alfos, H. Cramail, *Biomacromolecules* **2010**, *11*, 1202-1211.

[248] a) O. Figovsky, A. Leykin, L. Shapovalov, *Alternative Energy and Ecology* **2016**, 95-108.
b) M. Helou, J.-F. Carpentier, S. M. Guillaume, *Green Chemistry* **2011**, *13*, 266-271.
c) C. D. Diakoumakos, D. L. Kotzev, *Macromolecular Symposia* **2004**, *216*, 37-46.

[249]   S. Benyahya, J.-P. Habas, R. Auvergne, V. Lapinte, S. Caillol, *Polymer International* **2012**, *61*, 1666-1674.

[250]   C. Carré, H. Zoccheddu, S. Delalande, P. Pichon, L. Avérous, *European Polymer Journal* **2016**, *84*, 759-769.

[251]   A. Boyer, E. Cloutet, T. Tassaing, B. Gadenne, C. Alfos, H. Cramail, *Green Chemistry* **2010**, *12*, 2205-2213.

[252]   K. M. Tomczyk, P. A. Guńka, P. G. Parzuchowski, J. Zachara, G. Rokicki, *Green Chemistry* **2012**, *14*, 1749-1758.

[253]   S. Schmidt, F. J. Gatti, M. Luitz, B. S. Ritter, B. Bruchmann, R. Mülhaupt, *Macromolecules* **2017**, *50*, 2296-2303.

[254]   P.-K. Dannecker, M. A. R. Meier, *Scientific Reports* **2019**, *9*, 9858.

[255]   L. Maisonneuve, O. Lamarzelle, E. Rix, E. Grau, H. Cramail, *Chemical Reviews* **2015**, *115*, 12407-12439.

[256]   J. L. J. van Velthoven, L. Gootjes, D. S. van Es, B. A. J. Noordover, J. Meuldijk, *European Polymer Journal* **2015**, *70*, 125-135.

[257]   a) H. Tomita, F. Sanda, T. Endo, *Journal of Polymer Science Part A: Polymer Chemistry* **2001**, *39*, 3678-3685.

b) H. Tomita, F. Sanda, T. Endo, *Journal of Polymer Science Part A: Polymer Chemistry* **2001**, *39*, 851-859.

[258]   A. Steblyanko, W. Choi, F. Sanda, T. Endo, *Journal of Polymer Science Part A: Polymer Chemistry* **2000**, *38*, 2375-2380.

[259]   A. Cornille, M. Blain, R. Auvergne, B. Andrioletti, B. Boutevin, S. Caillol, *Polymer Chemistry* **2017**, *8*, 592-604.

[260]   J. De Gaspari, *Mechanical Engineering Magazine (ASME),* June **1999**.

[261]   Brandrup, J., Bittner, M., Michaeli, W. and Menges, G., *Recycling and Recovery of Plastics* **1996**, Carl Hanser Verlag, Munich and New York.

[262]   K. M. Zia, H. N. Bhatti, I. Ahmad Bhatti, *Reactive and Functional Polymers* **2007**, *67*, 675-692.

[263]   J. Troitzsch, *International plastics flammability handbook, T/C PUBLIC., P. O. BOX 842, EL SEGUNDO, CA 90245, USA.* **1983**.

[264]   H. C. Kolb, M. G. Finn, K. B. Sharpless, *Angewandte Chemie International Edition* **2001**, *40*, 2004-2021.

[265]   D. K. Mandal, *Pericyclic Reactions: Introduction, Classification and the Woodward-Hoffmann Rules* in *Pericyclic Chemistry* (Ed.: D. K. Mandal), Elsevier, **2018**, 63-106.

[266]   R. Huisgen, *Angewandte Chemie International Edition in English* **1963**, *2*, 565-598.

Bibliography

[267] A. T. Francesco Fringuelli, *Diels–Alder Reaction: General Remarks* in *The Diels–Alder Reaction*, **2001**, 1-28.

[268] R. Akhtar, S. A. R. Naqvi, A. F. Zahoor, S. Saleem, *Molecular Diversity* **2018**, *22*, 447-501.

[269] M. Fallah-Mehrjardi, A. R. Kiasat, K. Niknam, *Journal of the Iranian Chemical Society* **2018**, *15*, 2033-2081.

[270] F. A. Carey, R. J. Sundberg, in *Advanced Organic Chemistry: Part B: Reactions and Synthesis* (Eds.: F. A. Carey, R. J. Sundberg), Springer US, Boston, MA, **1977**, 73-127.

[271] J. E. M. N. Klein, G. Knizia, H. S. Rzepa, *ChemistryOpen* **2019**, *8*, 1244-1250.

[272] T. T. Bui, H.-K. Kim, *Synlett* **2020**, *31*, 997-1002.

[273] A. Leggio, E. L. Belsito, G. De Luca, M. L. Di Gioia, V. Leotta, E. Romio, C. Siciliano, A. Liguori, *RSC Advances* **2016**, *6*, 34468-34475.

[274] M. O. Lozinskii, A. F. Shivanyuk, P. S. Pel'kis, *Chemistry of Heterocyclic Compounds* **1971**, *7*, 439-442.

[275] C. E. Hoyle, C. N. Bowman, *Angewandte Chemie International Edition* **2010**, *49*, 1540-1573.

[276] T. Posner, *Berichte der deutschen chemischen Gesellschaft* **1905**, *38*, 646-657.

[277] M. J. Kade, D. J. Burke, C. J. Hawker, *Journal of Polymer Science Part A: Polymer Chemistry* **2010**, *48*, 743-750.

[278] A. B. Lowe, *Polymer Chemistry* **2010**, *1*, 17-36.

[279] C. E. Hoyle, T. Y. Lee, T. Roper, *Journal of Polymer Science Part A: Polymer Chemistry* **2004**, *42*, 5301-5338.

[280] K. W. E. Sy Piecco, A. M. Aboelenen, J. R. Pyle, J. R. Vicente, D. Gautam, J. Chen, *ACS Omega* **2018**, *3*, 14327-14332.

[281] K. Long, X. Zhang, S. Huang, J. Sinha, M. Podgorski, C. Bowman, *Kinetic differences between primary, secondary, and tertiary alkyl thiols in thiol-ene reactions* in *ABSTRACTS OF PAPERS OF THE AMERICAN CHEMICAL SOCIETY, Vol. 255*, AMER CHEMICAL SOC 1155 16TH ST, NW, WASHINGTON, DC 20036 USA, **2018**.

[282] F. Dénès, M. Pichowicz, G. Povie, P. Renaud, *Chemical Reviews* **2014**, *114*, 2587-2693.

[283] K. Griesbaum, *Angewandte Chemie International Edition* **1970**, *9*, 273-287.

[284] B. H. Northrop, R. N. Coffey, *Journal of the American Chemical Society* **2012**, *134*, 13804-13817.

[285] a) J. P. Fouassier, J. F. RABEK, *Radiation Curing in Polymer Science and Technology: Fundamentals and methods*, Springer Netherlands, **1993**.

b) S. K. Reddy, N. B. Cramer, C. N. Bowman, *Macromolecules* **2006**, *39*, 3673-3680.

[286] C. F. H. Allen, J. O. Fournier, W. J. Humphlett, *Canadian Journal of Chemistry* **1964**, *42*, 2616-2620.

[287] D. P. Nair, M. Podgórski, S. Chatani, T. Gong, W. Xi, C. R. Fenoli, C. N. Bowman, *Chemistry of Materials* **2014**, *26*, 724-744.

[288] S. Gao, T. Tzeng, M. N. V. Sastry, C.-M. Chu, J.-T. Liu, C. Lin, C.-F. Yao, *Tetrahedron Letters* **2006**, *47*, 1889-1893.

[289] R. Alleti, W. S. Oh, M. Perambuduru, C. V. Ramana, V. Prakash Reddy, *Tetrahedron Letters* **2008**, *49*, 3466-3470.

[290] F. M. Moghaddam, G. R. Bardajee, R. O. Chadorneshine Veranlou, *Synthetic Communications* **2005**, *35*, 2427-2433.

[291] W. Xi, C. Wang, C. J. Kloxin, C. N. Bowman, *ACS Macro Letters* **2012**, *1*, 811-814.

[292] C. E. Hoyle, A. B. Lowe, C. N. Bowman, *Chemical Society Reviews* **2010**, *39*, 1355-1387.

[293] R. J. Pounder, M. J. Stanford, P. Brooks, S. P. Richards, A. P. Dove, *Chemical Communications* **2008**, 5158-5160.

[294] V. S. Khire, T. Y. Lee, C. N. Bowman, *Macromolecules* **2008**, *41*, 7440-7447.

[295] B. Yu, J. W. Chan, C. E. Hoyle, A. B. Lowe, *Journal of Polymer Science Part A: Polymer Chemistry* **2009**, *47*, 3544-3557.

[296] a) Y. Wang, D. Huang, X. Wang, F. Yang, H. Shen, D. Wu, *Biomaterials Science* **2019**, *7*, 3238-3248.

b) K. L. Killops, L. M. Campos, C. J. Hawker, *Journal of the American Chemical Society* **2008**, *130*, 5062-5064.

c) G. Franc, A. K. Kakkar, *Chemical Society Reviews* **2010**, *39*, 1536-1544.

d) M. I. Montañez, L. M. Campos, P. Antoni, Y. Hed, M. V. Walter, B. T. Krull, A. Khan, A. Hult, C. J. Hawker, M. Malkoch, *Macromolecules* **2010**, *43*, 6004-6013.

[297] M. Ghirardello, K. Öberg, S. Staderini, O. Renaudet, N. Berthet, P. Dumy, Y. Hed, A. Marra, M. Malkoch, A. Dondoni, *Journal of Polymer Science Part A: Polymer Chemistry* **2014**, *52*, 2422-2433.

[298] D. Guzmán, A. Serra, X. Ramis, X. Fernández-Francos, S. De la Flor, *Reactive and Functional Polymers* **2019**, *136*, 153-166.

[299] N. Simpson, M. Takwa, K. Hult, M. Johansson, M. Martinelle, E. Malmström, *Macromolecules* **2008**, *41*, 3613-3619.

[300] O. D. McNair, A. P. Janisse, D. E. Krzeminski, D. E. Brent, T. E. Gould, J. W. Rawlins, D. A. Savin, *ACS Applied Materials & Interfaces* **2013**, *5*, 11004-11013.

[301] A. F. Senyurt, C. E. Hoyle, H. Wei, S. G. Piland, T. E. Gould, *Macromolecules* **2007**, *40*, 3174-3182.

[302] O. D. McNair, T. E. Gould, S. G. Piland, D. A. Savin, *Journal of Applied Polymer Science* **2014**, *131*.

Bibliography

[303]   H. Lu, J. A. Carioscia, J. W. Stansbury, C. N. Bowman, *Dental materials : official publication of the Academy of Dental Materials* **2005**, *21*, 1129-1136.

[304]   R. Schwalm, *UV Coatings: Basics, Recent Developments and New Applications* , Elsevier, **2007**.

[305]   O. Llorente, A. Agirre, I. Calvo, M. Olaso, R. Tomovska, H. Sardon, *Polymer Journal* **2021**.

[306]   B. J. Sparks, E. F. T. Hoff, L. P. Hayes, D. L. Patton, *Chemistry of Materials* **2012**, *24*, 3633-3642.

[307]   B. R. Donovan, J. S. Cobb, E. F. T. Hoff, D. L. Patton, *RSC Advances* **2014**, *4*, 61927-61935.

[308]   L. Shen, J. Cheng, J. Zhang, *European Polymer Journal* **2020**, *137*, 109927.

[309]   U. Y. Lau, E. M. Pelegri-O'Day, H. D. Maynard, *Macromolecular Rapid Communications* **2018**, *39*, 1700652.

[310]   R. A. Ortiz, A. E. Garcia Valdéz, M. G. Martinez Aguilar, M. L. Berlanga Duarte, *Carbohydrate Polymers* **2009**, *78*, 282-286.

[311]   E. Passaglia, F. Donati, *Polymer* **2007**, *48*, 35-42.

[312]   C. N. Salinas, K. S. Anseth, *Macromolecules* **2008**, *41*, 6019-6026.

[313]   B. D. Fairbanks, M. P. Schwartz, A. E. Halevi, C. R. Nuttelman, C. N. Bowman, K. S. Anseth, *Advanced materials* **2009**, *21*, 5005-5010.

[314]   S. Wittrock, T. Becker, H. Kunz, *Angewandte Chemie International Edition* **2007**, *46*, 5226-5230.

[315]   L. You, H. Schlaad, *Journal of the American Chemical Society* **2006**, *128*, 13336-13337.

[316]   a) G. Chen, S. Amajjahe, M. H. Stenzel, *Chemical Communications* **2009**, 1198-1200.
b)K. Neumann, A. Conde-González, M. Owens, A. Venturato, Y. Zhang, J. Geng, M. Bradley, *Macromolecules* **2017**, *50*, 6026-6031.

[317]   I. J. Goldstein, C. E. Hayes, in *Advances in Carbohydrate Chemistry and Biochemistry, Vol. 35* (Eds.: R. S. Tipson, D. Horton), Academic Press, **1978**, 127-340.

[318]   Y. E. Gao, A. ; Kakehi, K. ; Lee, Yuan C., *Organic Letters* **2004**, *6*, 3457-3460.

[319]   D. L. Elbert, A. B. Pratt, M. P. Lutolf, S. Halstenberg, J. A. Hubbell, *Journal of controlled release: official journal of the Controlled Release Society* **2001**, *76*, 11-25.

[320]   P. van de Wetering, A. T. Metters, R. G. Schoenmakers, J. A. Hubbell, *Journal of controlled release: official journal of the Controlled Release Society* **2005**, *102*, 619-627.

[321]   G. Pitarresi, G. Tripodo, R. Calabrese, E. F. Craparo, M. Licciardi, G. Giammona, *Macromolecular bioscience* **2008**, *8*, 891-902.

[322]   V. S. Wadi, K. K. Jena, K. Halique, Brigita Rožič, L. Cmok, V. Tzitzios, S. M. Alhassan, *Scientific Reports* **2020**, *10*, 14924.

[323]   M. D. Alim, S. Mavila, D. B. Miller, S. Huang, M. Podgórski, L. M. Cox, A. C. Sullivan, R. R. McLeod, C. N. Bowman, *ACS Materials Letters* **2019**, *1*, 582-588.

[324]   K. Matsumoto, E. A. Costner, I. Nishimura, M. Ueda, C. G. Willson, *Macromolecules* **2008**, *41*, 5674-5680.

[325]   a) J. M. Ziebarth, M. D. McGehee, *Journal of Applied Physics* **2005**, *97*, 064502,
        b) Y.-H. Lin, H. Ren, Y.-H. Fan, Y.-H. Wu, S.-T. Wu, *Journal of Applied Physics* **2005**, *98*, 043112.

[326]   I. C. Khoo, Y. Z. Williams, B. Lewis, T. Mallouk, *Molecular Crystals and Liquid Crystals* **2006**, *446*, 233-244.

[327]   M. J. Ventura, C. Bullen, M. Gu, *Optics Express* **2007**, *15*, 1817-1822.

[328]   J. H. Y. Young Jin Lim, Hyesun Yoo, Seong Min Song, Ramesh Manda, Srinivas Pagidi, Myong-Hoon Lee, Jae-Min Myoung, and Seung Hee Lee, *Optical Materials Express* **2018**, *8*, 3698-3707.

[329]   S. K. Manohar, C. Fafadia, N. Saran, R. Rao, *Journal of Applied Physics* **2008**, *103*, 094501.

[330]   K. S. Lee, H. L. T. Lee, R. J. Ram, *Lab on a Chip* **2007**, *7*, 1539-1545.

[331]   a) J.-H. Park, I. C. Khoo, *Applied Physics Letters* **2005**, *87*, 091110.
        b) S.-H. Nam, J.-W. Kang, J.-J. Kim, *Optics Communications* **2006**, *266*, 332-335.
        c) N. H. Mack, J. W. Wackerly, V. Malyarchuk, J. A. Rogers, J. S. Moore, R. G. Nuzzo, *Nano Letters* **2007**, *7*, 733-737.

[332]   A. Ganeshpurkar, D. Kumar, S. K. Singh, *Current Organic Synthesis* **2018**, *15*, 154-165.

[333]   C. R. Hauser, S. W. Kantor, *Journal of the American Chemical Society* **1950**, *72*, 4284-4285.

[334]   L. Bauer, O. Exner, *Angewandte Chemie International Edition in English* **1974**, *13*, 376-384.

[335]   G. B. Quistad, N. Zhang, S. E. Sparks, J. E. Casida, *Chem Res Toxicol* **2000**, *13*, 652-657.

[336]   M. Thomas, J. Alsarraf, N. Araji, I. Tranoy-Opalinski, B. Renoux, S. Papot, *Organic & Biomolecular Chemistry* **2019**, *17*, 5420-5427.

[337]   a) E. Gómez-Sánchez, J. Marco-Contelles, *Tetrahedron* **2005**, *61*, 1207-1219.
        b) A. Yoshimura, M. W. Luedtke, V. V. Zhdankin, *The Journal of Organic Chemistry* **2012**, *77*, 2087-2091.
        c) S. Yoganathan, S. J. Miller, *Organic Letters* **2013**, *15*, 602-605.

[338]   F. Brock, *The Journal of Organic Chemistry* **1959**, *24*, 1802-1804.

[339]   M. R. Sahasrabudhe, *Journal of the American Oil Chemists' Society* **1977**, *54*, 323-324.

[340]   F. Vernon, J. H. Khorassani, *Talanta* **1978**, *25*, 410-412.

[341]   I. W. G. o. M. o. Analysis, *Flavour and Fragrance Journal* **2011**, *26*, 297-299.

[342]   F. Falaki (April 2nd 2019). *Sample Preparation Techniques for Gas Chromatography, Gas Chromatography - Derivatization, Sample Preparation, Application*, Peter Kusch, IntechOpen, DOI: 10.5772/intechopen.84259.
        Available from: https://www.intechopen.com/chapters/6651

[343]   S. Oprea, *Polymer Degradation and Stability* **2002**, *75*, 9-15.

[344]   L. W. Dittert, T. Higuchi, *Journal of Pharmaceutical Sciences* **1963**, *52*, 852-857.

[345]   R. D. Bright, C. R. Hauser, *Journal of the American Chemical Society* **1939**, *61*, 618-629.

[346]   D. Berndt, H. Shechter, *The Journal of Organic Chemistry* **1964**, *29*, 916-918.

Bibliography

[347] E. R. Pérez, M. O. da Silva, V. C. Costa, U. P. Rodrigues-Filho, D. W. Franco, *Tetrahedron Letters* **2002**, *43*, 4091-4093.

[348] K. N. Onwukamike, T. Tassaing, S. Grelier, E. Grau, H. Cramail, M. A. R. Meier, *ACS Sustainable Chemistry & Engineering* **2018**, *6*, 1496-1503.

[349] B. Husár, R. Liska, *Chemical Society Reviews* **2012**, *41*, 2395-2405.

[350] F. Biedermann, E. A. Appel, J. del Barrio, T. Gruendling, C. Barner-Kowollik, O. A. Scherman, *Macromolecules* **2011**, *44*, 4828-4835.

[351] H. Mutlu, L. M. de Espinosa, M. A. R. Meier, *Chemical Society Reviews* **2011**, *40*, 1404-1445.

[352] H. Weychardt, H. Plenio, *Organometallics* **2008**, *27*, 1479-1485.

[353] B. Vasantha, H. P. Hemantha, V. V. Sureshbabu, *Synthesis* **2010**, *2010*, 2990-2996.

[354] M. Firdaus, M. A. R. Meier, U. Biermann, J. O. Metzger, *European Journal of Lipid Science and Technology* **2014**, *116*, 31-36.

[355] H. Mutlu, R. Hofsäß, R. E. Montenegro, M. A. R. Meier, *RSC Advances* **2013**, *3*, 4927-4934.

[356] L. Lascialfari, G. Pescitelli, A. Brandi, M. Mannini, D. Berti, S. Cicchi, *Soft Matter* **2015**, *11*, 8333-8341.

[357] 2,2'-Azobis(2-Methylpropionitrile) 98%: Sigma-Aldrich. Retrieved from https://www.sigmaaldrich.com/DE/en/product/aldrich/441090?%C441092%AEion=US. (Accessed 30.08.2021)

[358] R. Kitamura, L. Pilon, M. Jonasz, *Appl. Opt.* **2007**, *46*, 8118-8133.

[359] V. Mucci, C. Vallo, *Journal of Applied Polymer Science* **2012**, *123*, 418-425.

[360] P. J. Flory, *Principles of Polymer Chemistry*, Cornell University Press, **1953**.

[361] D. Joshi, N. Adhikari, *Journal of Pharmaceutical Research International* **2019**, 1-18.

[362] a) A.-G. Sicaire, M. Vian, A. Filly, Y. Li, A. Bily, F. Chemat, *2-Methyltetrahydrofuran: Main Properties, Production Processes, and Application in Extraction of Natural Products* in *Alternative Solvents for Natural Products Extraction.* Green Chemistry and Sustainable Technology, **2014**, 253-268. Springer, Berlin, Heidelberg. https://doi.org/10.1007/978-3-662-43628-8_12.
b) H. Singh, N. Iyengar, R. Yadav, A. Rai, A. K. Sinha, *Sustainable Energy & Fuels* **2018**, *2*, 1699-1706.

[363] Y. Shen, J.-K. Sun, Y.-X. Yi, B. Wang, F. Xu, R.-C. Sun, *Bioresource technology* **2015**, *192*, 812-816.

[364] V. Antonucci, J. Coleman, J. B. Ferry, N. Johnson, M. Mathe, J. P. Scott, J. Xu, *Organic Process Research & Development* **2011**, *15*, 939-941.

[365] J. Sherwood, M. De bruyn, A. Constantinou, L. Moity, C. R. McElroy, T. J. Farmer, T. Duncan, W. Raverty, A. J. Hunt, J. H. Clark, *Chemical Communications* **2014**, *50*, 9650-9652.

[366]   a) K.-M. Roy, *Sulfones and Sulfoxides* in *Ullmann's Encyclopedia of Industrial Chemistry* **2000**.
         b) C. B. Kreutzberger, *Chloroformates and Carbonates* in *Kirk-Othmer Encyclopedia of Chemical Technology* **2001**.

[367]   Solvay,   "Rhodiasolv   Polarclean",
         chema.scc.kit.edu/page/substance/inventoryPage.html?vs=6, retrieved 04.08.2021.

[368]   National Center for Biotechnology Information (2021). PubChem Patent Summary for CA-2302591-C, *High service temperature polyurethane elastomers*. Retrieved August 2302530, 2302021 from https://pubchem.ncbi.nlm.nih.gov/patent/CA-2302591-C.

[369]   R. Gogoi, M. Alam, R. Khandal, *International Journal of Basic and Applied Sciences* **2014**, *3*, 6.

[370]   K. Balani, V. Verma, A. Agarwal, R. Narayan, *Physical, Thermal, and Mechanical Properties of Polymers* in *Biosurfaces*, **2014**, 329-344.

[371]   N. S. Vrandečić, M. Erceg, M. Jakić, I. Klarić, *Thermochimica Acta* **2010**, *498*, 71-80.

[372]   J.-L. Sormana, S. Chattopadhyay, J. C. Meredith, *Journal of Nanomaterials* **2008**, *2008*, 869354.

[373]   S. Michael, Structure–Property Relations in Polyurethanes in *Szycher's Handbook of Polyurethanes*, CRC Press, **2012**.

[374]   Y. Xiao, L. Jiang, Z. Liu, Y. Yuan, P. Yan, C. Zhou, J. Lei, *Polymer Testing* **2017**, *60*, 160-165.

[375]   R. Huo, R. Wehrens, J. v. Duynhoven, L. M. C. Buydens, *Analytica Chimica Acta* **2003**, *490*, 231-251.

[376]   M. E. Brown, P. K. Gallagher, *Handbook of thermal analysis and calorimetry: recent advances, techniques and applications* **2011**.

[377]   Y. Ye, J.-H. Choi, K. I. Winey, Y. A. Elabd, *Macromolecules* **2012**, *45*, 7027-7035.

[378]   A. K. Riau, D. Mondal, G. H. F. Yam, M. Setiawan, B. Liedberg, S. S. Venkatraman, J. S. Mehta, *ACS Applied Materials & Interfaces* **2015**, *7*, 21690-21702.

[379]   W. Zhang, W. Lu, S. Wang, H. Zhou, *Polymer Journal* **2003**, *35*, 470-475.

[380]   U. Siemann, in *Scattering Methods and the Properties of Polymer Materials* (Eds.: N. Stribeck, B. Smarsly), Springer Berlin Heidelberg, Berlin, Heidelberg, **2005**, 1-14.

[381]   J. R. Davis, *Tensile Testing, 2nd Edition*, ASM International, **2004**.

[382]   H. Cho, S. Mayer, E. Pöselt, M. Susoff, P. J. in 't Veld, G. C. Rutledge, M. C. Boyce, *Polymer* **2017**, *128*, 87-99.

[383]   H. M. Jeong, B. K. Kim, Y. J. Choi, *Polymer* **2000**, *41*, 1849-1855.

[384]   E. J. Mittemeijer, *Mechanical strength of Materials* in *Fundamentals of Materials Science: The Microstructure–Property Relationship Using Metals as Model Systems*, Springer Berlin Heidelberg, Berlin, Heidelberg, **2011**, 497-581.

Bibliography

[385]   V. Khoshkava, M. R. Kamal, *ACS Applied Materials & Interfaces* **2014**, *6*, 8146-8157.

[386]   J. C. Wierman, *Percolation Tresholds, Exact* in *Encyclopedia of Complexity and Systems Science* (Ed.: R. A. Meyers), Springer New York, New York, NY, **2009**, 6579-6587.

[387]   a) E. Vatansever, D. Arslan, D. S. Sarul, Y. Kahraman, G. Gunes, A. Durmus, M. Nofar, *Journal of Materials Science* **2020**, *55*, 15523-15537
        b) J. M. Jardin, Z. Zhang, G. Hu, K. C. Tam, T. H. Mekonnen, *International Journal of Biological Macromolecules* **2020**, *152*, 428-436.

[388]   K. N. Onwukamike, S. Grelier, E. Grau, H. Cramail, M. A. R. Meier, *ACS Sustainable Chemistry & Engineering* **2018**, *6*, 8826-8835.

[389]   C. Vaca-Garcia, M. E. Borredon, A. Gaseta, *Cellulose* **2001**, *8*, 225-231.

[390]   P. Uschanov, L.-S. Johansson, S. L. Maunu, J. Laine, *Cellulose* **2011**, *18*, 393-404.

[391]   H. Abushammala, *Polymers* **2019**, *11*, 1164.

[392]   Kusmono, R. F. Listyanda, M. W. Wildan, M. N. Ilman, *Heliyon* **2020**, *6*, e05486.

[393]   a) O. V. Surov, E. O. Lebedeva, N. V. Rubleva, M. I. Voronova, A. G. Zakharov, *Russian Journal of General Chemistry* **2021**, *91*, 864-869
         b) X. Cao, H. Dong, C. M. Li, *Biomacromolecules* **2007**, *8*, 899-904
         c) M. S. Peresin, Y. Habibi, J. O. Zoppe, J. J. Pawlak, O. J. Rojas, *Biomacromolecules* **2010**, *11*, 674-681.

[394]   Y. Suzuki, T. Higashihara, S. Ando, M. Ueda, *European Polymer Journal* **2010**, *46*, 34-41.